THE UNIVERSITY
of EDINBURGH

Immunomodulatory proteins in *Heligmosomoides polygyrus* excretory/secretory products.

Andrea M. Kemter

Thesis submitted for the degree of Doctor of Philosophy

The University of Edinburgh

2016

Abstract

Infections with parasitic helminths are counted as neglected tropical diseases; they infect millions of people worldwide, causing high morbidity and economic loss. Many parasites establish long lasting infections in the host by blocking immune recognition, activation and effector pathways. To allow in depth research on their modes of immune evasion, several mouse models for parasitic helminth infections have been established. *Heligmosomoides polygyrus* for example is a gastrointestinal nematode of rodents exhibiting a wide spectrum of immunomodulatory effects, mediated in part by soluble molecules released by adult worms in vitro, the excretory/secretory products (HES). HES is a potent inhibitor of dendritic cell (DC) activation by Toll-like receptor (TLR) ligands, completely abolishing LPS induced IL-12 production and reducing the upregulation of cell surface activation markers. As of now, neither the modulatory molecule nor its mechanism of action are known.

Here, the effect of HES on TLR ligand induced DC maturation was characterized in considerably more detail compared to previous publications. It could be shown to inhibit DC maturation induced by various TLR ligands, on both protein and mRNA levels. These effects were comparable in both C57BL/6 and BALB/c derived cells; in contrast to this HES differentially affected alternative activation of BMDC from these two mouse strains.

Although for most of the experiments GM-CSF differentiated BMDC were used, HES also inhibited LPS induced activation of splenic $CD11c^+$ cells as well as the activation of all three populations described in Flt3-L differentiated BMDC - pDCs, $CD11b^+$ cDCs and $CD24^+$ cDCs. Furthermore, it could be shown here that HES also inhibits LPS induced maturation in human monocyte derived DCs.

In the search for the component in HES responsible for its inhibition of TLR ligand induced DC maturation, exosome depleted HES rather than exosomes was inhibitory, and the effect was heat labile. This lead to the conclusion that the modulatory molecule has a protein component which is indispensable for its effect; following this reasoning HES was subjected

to fractionation, with subsequent analysis of the fraction protein contents by mass spectrometry. The top nine candidate proteins were expressed recombinantly; however, the recombinants were not able to inhibit LPS induced DC activation.

In parallel, experiments to elucidate the mechanism by which HES inhibits TLR ligand induced DC maturation were performed. This led to the conclusion that HES induces changes in the cells that, while not affecting the induction of signalling downstream of TLRs, do impair its maintenance.

As a complement to these experiments, the transcriptomes of LPS and LPS+HES treated cells eight hours after LPS stimulation were compared. This revealed that transcripts encoding a number of transcription factors inducing the expression of activation markers after TLR ligation were reduced upon treatment of cells with HES, as were the transcript levels of IRAK2, a kinase necessary for persistent signalling. In addition, HES increased the transcript levels for several factors known to negatively regulate DC maturation, including ATF3.

Furthermore, this analysis revealed changes in transcript levels of factors like HIF-1α, indicating an even greater reliance on aerobic glycolysis if cells were treated with HES, in addition to hints at increased ER and oxidative stress.

In conclusion, this work narrows down the list of potential DC modulators in HES, gives a first insight into changes in DC metabolism induced by HES and sheds light on the role of a number of signalling pathways with important roles in DC activation as targets of DC inhibition by HES.

Lay Summary

Parasitic helminths infect millions of people worldwide, and can cause severe symptoms; infections of animals are equally problematic, as they cause great economic loss. These worms have developed a number of ways to avoid the immune response of their hosts, including inhibiting the activation of the cells responsible for recognizing infectious agents and activating specific immune reactions. This effect is mediated by factors the parasites produce and secrete. Finding the specific component in these parasite products and how it affects immune cells was the aim here, as it could be exploited for the development of treatment strategies for a number of different conditions.

To find the component in question, methods to identify specific proteins were used, and the most promising candidates produced in the laboratory. These top candidates did not reproduce the effect, but a number of further possibilities are yet to be tested.

In addition, by analysing changes within the cells that lead to their activation, insights into how the parasite affects these cells could be gained as well.

Finally, these effects could not only be seen in mouse, but also in human cells, showing that this research could indeed be useful for drug development.

Declaration

I declare that this thesis has been composed by myself, describes my own work and that the work has not been submitted towards any other degree.

The experiments using exosomes and exosome depleted HES have been carried out in collaboration with Gillian Coakley.

Selected figures from reviews published by other researchers have been used where appropriate; the authors and source are indicated in each case.

Andrea Kemter
May 2016

Acknowledgements

And with this, almost four years in Edinburgh come to an end - and I have to say, I will be sad to leave, it has been a great four(ish) years!

Many people have contributed to making sure of that:

First of all: Rick - thank you so much for being the best supervisor I could have wished for, helping me to get here in the first place and then giving me loads of freedom to develop my project while always being there with advice and guidance, sending me to great conferences (just saying, Hydra!), and giving me the freedom to pursue my sport too, which took quite a few hours out of my week! And finally, thank you so much for all your help in the last year or so, making sure I could finish my PhD without (too much) panic, and making me actually get a Postdoc position long before I would have even started thinking about it.

Then the whole rest of the lab - lab-mama Yvonne, who has saved me countless of times; Danielle and Henry, who've worked with me on/helped me with quite a few experiments (and gave me cat-time!); Gillian, for letting me play with exosomes, and my office desk and lab-bench neighbour Xuhang, both of you were great conference mates!; as well as Janice, Kara, James, Katie, Lisa, Stephie, Elaine, Chris and David Dresser - all of you taught me so much, be it methods or discussing science, and have made the lab a great place to work in! Also, thanks to Yvonne and Henry for your help proofreading Material and Methods / the candidate protein chapter!

In general, the people in Ashworth Labs, I really enjoyed the very collegial atmosphere; special mention here has to go to a few people who helped me immeasurably, like Martin Waterfall, who helped me out so many times when I ran into FACS trouble; Thomas Tan for teaching me a lot about cell signalling; Al Ivens for help with the array and answering bioinformatics questions Henry and I were clueless about; the Allen and Taylor labs especially, sharing labs and offices - and quite a few times reagents - with us, and especially Sharon for many chats and discussions.

Andrew MacDonald for inviting me to Manchester to learn/try out the FLDCs and human moDCs, and his lab, especially Alex Phythian-Adams who organized my visit there and taught me how to make FLDCs - I've also learned so many new things about flow cytometry! - and Cecilia Forss and James Crooks for the moDCs.

And finally: my friends and family. There's way too much to write it all, so just: THANK YOU! One thing to mention here though: thank you, Johannes, for giving me your UoE PhD thesis LaTeX template, it probably saved me hours (or days?) of trying to get the layout right!

Meinen Eltern: ich kann gar nicht beschreiben wie dankbar ich bin, euch zu haben - ihr seid immer für mich da wenn ich Unterstützung oder gutes Zureden brauche, erinnert mich, ab und zu auch mal Pausen einzulegen, und seid überhaupt die besten Eltern die ich mir wünschen könnte! Danke!

Contents

Table of Contents ix

List of Figures xiii

List of Tables xv

1 Introduction 1
- 1.1 Helminths . . . 1
  - 1.1.1 Helminths infecting humans and their animal models . . . 4
    - 1.1.1.1 *Heligmosomoides polygyrus* . . . 6
- 1.2 Immune responses to helminths . . . 9
- 1.3 Dendritic cells . . . 14
  - 1.3.1 Signalling pathways in DC activation . . . 17
  - 1.3.2 Metabolism . . . 23
  - 1.3.3 Mechanisms to control DC activation . . . 26
    - 1.3.3.1 TLRs and ligand binding . . . 27
    - 1.3.3.2 Interference with induction of signalling . . . 27
    - 1.3.3.3 Inhibition of the downstream signalling cascade . . . 28
    - 1.3.3.4 Inhibition of transcription factor activation or activity . . . 30
    - 1.3.3.5 Post-transcriptional regulation of target genes and signalling mediators . . . 31
  - 1.3.4 DC modulation by helminths . . . 32
    - 1.3.4.1 Cestodes . . . 32
    - 1.3.4.2 Trematodes . . . 33
    - 1.3.4.3 Filaria . . . 36
    - 1.3.4.4 *Trichinella spiralis* . . . 37
    - 1.3.4.5 Soil transmitted helminths . . . 37
      - Heligmosomoides polygyrus . . . 38
- 1.4 Objectives . . . 41

2 Material and Methods 43
- 2.1 Material . . . 43
- 2.2 Methods . . . 48
  - 2.2.1 Animals . . . 48
  - 2.2.2 Cell isolation and culture . . . 48
    - 2.2.2.1 Bone marrow derived dendritic cells . . . 48
      - Extraction and culture . . . 48
      - Stimulation . . . 48
    - 2.2.2.2 Spleen cell isolation and culture . . . 49
      - Extraction . . . 49
      - Stimulation . . . 49

2.2.2.3 Human monocyte derived DCs . . . 49
PBMC preparation and culture . . . 49
Stimulation . . . 50
2.2.2.4 MACS . . . 50
2.2.3 Analysis of cytokine production by ELISA . . . 50
2.2.4 Analysis of cytokine production by CBA . . . 51
2.2.5 Analysis of cells by flow cytometry . . . 51
2.2.5.1 Basic staining protocol . . . 51
2.2.5.2 Fixation . . . 51
2.2.6 Gene expression analysis . . . 53
2.2.6.1 RNA extraction . . . 53
2.2.6.2 Reverse transcription of RNA . . . 53
2.2.6.3 Real time PCR . . . 53
2.2.6.4 Microarray . . . 54
2.2.7 HES production and fractionation . . . 54
2.2.7.1 Fractionations . . . 54
2.2.7.2 SDS-PAGE and silver stain of HES fractions . . . 55
2.2.7.3 Mass spectrometric analysis of HES fractions . . . 55
2.2.8 Cloning and expression of recombinant proteins . . . 56
2.2.8.1 Cloning of target genes . . . 56
2.2.8.2 Transfection into HEK-293 cells . . . 56
2.2.8.3 Purification of recombinant proteins . . . 57
2.2.9 Software and statistics . . . 57

3 Dendritic cell modulation by *Heligmosomoides polygyrus* excretory/secretory products. 59
3.1 Introduction . . . 60
3.2 Results . . . 62
3.2.1 HES inhibits activation of BMDC by various TLR ligands. . . . 62
3.2.2 HES inhibition of LPS-induced DC activation. . . . 65
3.2.3 HES differentially affects alternative activation of BMDC from C57BL/6 and BALB/c mice. . . . 68
3.2.4 The soluble fraction of HES, not exosomes, inhibits LPS induced DC activation. . . . 71
3.2.5 HES inhibits activation of multiple DC subsets. . . . 73
3.2.6 HES inhibits activation of human DCs . . . 75
3.3 Discussion . . . 78

4 Identification of potential dendritic cell modulators in HES 85
4.1 Introduction . . . 86
4.2 Results . . . 88
4.2.1 Comparison of protein contents of active size exclusion and anion exchange fractions fails to identify any candidate proteins 88
4.2.1.1 Size exclusion fractionation of HES . . . 89
4.2.1.2 Anion exchange fractionation of HES . . . 92
4.2.1.3 Proteomics analysis of active fractions . . . 92

4.2.2 Proteomics analysis of HES sequential fractions identifies five candidates that do not modulate DC activation . . . 96
4.2.2.1 Sequential fractionation of HES . . . 97
4.2.2.2 Proteomics analysis of sequential fractions . . . 99
4.2.2.3 Expression and test of candidate proteins . . . 107
4.2.3 Proteomics analysis of size exclusion, sequential and anion exchange fractions leads to identification of four further candidates, but not the DC modulator . . . 110
4.2.3.1 HES fractionations . . . 110
4.2.3.2 Proteomics analysis of all fractions . . . 113
4.2.3.3 Expression and test of candidate proteins . . . 123
4.2.3.4 Abundance profiles of previously described candidates or modulators . . . 126
4.3 Discussion . . . 129

5 Effects of HES on LPS induced signalling pathways and DC metabolism 133
5.1 Introduction . . . 134
5.2 Results . . . 138
5.2.1 HES increases ERK1/2 phosphorylation, but inhibition of BMDC activation is independent of ERK. . . . 138
5.2.2 HES inhibits p38 and JNK phosphorylation only after the immediate-early phase of BMDC activation. . . . 140
5.2.3 HES inhibits phosphorylation of IκBα and reduces A20 expression in LPS-stimulated BMDC. . . . 143
5.2.4 Differential dynamics of cytokine and activation marker expression and their inhibition by HES. . . . 146
5.2.5 HES inhibits cytokine secretion and activation marker expression even if added hours after LPS. . . . 150
5.2.6 HES affects mRNA levels of signalling pathway components, transcription factors and enzymes involved in cell metabolism in BMDC eight hours post LPS stimulation. . . . 152
5.3 Discussion . . . 162

6 Final Discussion 175

References 181

Appendices 221

A Scripts written for data analysis 223
A.1 Sorting flow cytometry data . . . 223
A.2 Sorting ELISA data . . . 228
A.3 Comparing fraction protein content . . . 230
A.4 Extraction of emPAI values . . . 235
A.5 Comparing protein emPAI peaks . . . 238

B Supplementary material for the proteomics analysis of HES **243**
B.1 Mass spectrometry results for active size exclusion and anion exchange fractions from the first round of fractionations 243
B.2 Mass spectrometry and content comparison of sequential fractions . . . 252
B.3 Mass spectrometry and analysis of all fractions 290

C Supplementary material for BMDC signalling and metabolism changes **317**

List of Figures

1.1 Proportion of children (1-14 years of age) in the country requiring preventative chemotherapy (PC) for soil-transmitted helminthiases, worldwide, 2014 . . . 2
1.2 Rough classification of major helminths according to phylogeny and mode of infection . . . 5
1.3 Life cycle of *H. polygyrus* . . . 7
1.4 Helminths induce type 2 immunity . . . 9
1.5 Modulation of DC functions by Th2 cell-skewing stimuli . . . 16
1.6 Signalling pathways in LPS induced DC activation. . . . 19
1.7 Cellular energy metabolism . . . 24
1.8 Toll-like receptor signalling integrates endoplasmic reticulum stress and changes in metabolism to support activation . . . 25

2.1 Gating strategies used to identify DCs . . . 52

3.1 HES inhibits secretion of pro-inflammatory cytokines in response to various TLR ligands . . . 63
3.2 HES inhibits DC activation by various TLR ligands . . . 64
3.3 HES inhibition of LPS induced DC activation is dose dependent and heat labile . . . 66
3.4 HES inhibits LPS induced DC activation at both the mRNA and intracellular protein level . . . 67
3.5 Pre-incubation of BMDC with HES impairs LPS induced activation . . . 69
3.6 HES differentially affects alternative activation of BMDC from C57BL/6 and BALB/c mice . . . 70
3.7 The soluble fraction of HES, not exosomes, inhibits LPS induced DC activation . . . 72
3.8 HES inhibits activation of CD115 depleted BMDC and ex vivo DCs . . . 74
3.9 HES inhibits activation of FLDC . . . 76
3.10 HES inhibits activation of human monocyte derived DCs . . . 77

4.1 Schematic of workflow to identify the first round of candidate proteins . 88
4.2 Size exclusion fractionation of HES resulted in two fractions completely inhibiting IL-12p70 production by LPS-stimulated GM-CSF BMDC . . . 90
4.3 TGM inhibits LPS-induced DC activation, but not to the same extent as HES . . . 91
4.4 Anion exchange fractionation of HES resulted in two fractions completely inhibiting IL-12p70 production by LPS-stimulated GM-CSF BMDC . . . 93
4.5 Number of proteins found in the four active fractions . . . 94
4.6 Schematic of workflow to identify the second round of candidate proteins 96

4.7 Size exclusion fractionation of HES resulted in two fractions completely inhibiting IL-12p70 production by LPS-stimulated GM-CSF BMDC . . . 97
4.8 Sequential fractionation of HES resulted in three fractions completely inhibiting IL-12p70 production by LPS-stimulated GM-CSF BMDC . . . 98
4.9 Examples for proteins peaking in the active sequential fractions and an overall poor or good fit of abundance profile to activity profile 100
4.10 Top candidates from sequential fractionation 106
4.11 Sequences, predicted molecular weights and conserved domains of the first five candidate proteins 108
4.12 Cloning and expression of the first five candidate proteins 109
4.13 None of the five candidates from the sequential fractionation inhibit LPS-induced DC activation 110
4.14 Schematic of workflow of third round to identify further candidate proteins 111
4.15 Anion exchange fractionation of HES resulted in one fraction completely inhibiting IL-12p70 production by LPS-stimulated GM-CSF BMDC 112
4.16 Number of proteins with emPAI values peaking in active fractions of size exclusion, sequential and anion exchange fractionations 114
4.17 Comparison of protein composition of several fractionation approaches resulted in the identification of four new candidate proteins 122
4.18 Sequences and conserved domains of the four candidate proteins identified by comparing size exclusion fractionation, sequential fractionation and anion exchange fractionation data 123
4.19 Cloning and expression of candidate proteins from the third round of fractionations 124
4.20 None of the four candidates identified in the third round inhibit LPS induced DC activation 125
4.21 Abundance profiles of second round candidates in all three fractionation approaches 127
4.22 Abundance profiles of cystatin 128
4.23 Abundance profiles of TGM 128

5.1 Signalling pathways in LPS-induced DC activation 135
5.2 HES increases ERK1/2 phosphorylation, but inhibition of DC activation is independent of ERK 139
5.3 HES does not alter p38 phosphorylation during the early phase of LPS-induced BMDC maturation but reduces it at later time points 141
5.4 HES does not alter JNK phosphorylation during the early phase of LPS-induced BMDC maturation but reduces it at later time points 142
5.5 HES reduces phosphorylation of IκBα in the intermediate and late phase of LPS-induced BMDC maturation 144
5.6 HES does not alter A20 expression during the early phase of LPS-induced BMDC maturation but reduces it at later time points 145
5.7 Differential dynamics of cytokine and activation marker expression and their inhibition by HES 148
5.8 Differential dynamics of cytokine expression and their inhibition by HES 149

5.9 HES inhibits cytokine secretion and activation marker expression even if added hours after LPS . . . 151
5.10 HES affects DC mRNA levels at 8h after stimulation . . . 153
5.11 Activation marker mRNA levels are regulated by HES at 8h after stimulation . . . 154
5.12 HES affects mRNA levels of some proteins relevant in DC activation signalling pathways at 8h after stimulation . . . 156
5.13 HES affects mRNA levels of some transcription factors relevant for DC activation at 8h after stimulation . . . 158
5.14 HES affects mRNA levels of proteins relevant for DC metabolism at 8h after stimulation . . . 161
5.15 Schematic detailing changes in signalling and metabolism between LPS- and LPS+HES-treated BMDC . . . 162

B.1 Rejected candidates from the sequential fractionation . . . 289
B.2 Rejected candidates from third round of candidate protein identification 316

List of Tables

1 Abbreviations xix

2.1 Buffers and Media 43
2.2 Antibodies used for flow cytometry, MACS and ELISA. 46
2.3 Substances used for stimulation of dendritic cells 49

4.1 Proteins shared in all four active fractions of the first round of fractionations 95
4.2 Longlist of 18 candidate proteins for DC modulatory activity with their emPAI values across the sequential fractions 101
4.3 Further analysis of 18 longlisted proteins listed in Table 4.2, considering conserved domains, top named blastx result and peptide coverage from mass spectrometry 102
4.4 Final step of selection of shortlisted proteins considering designations and ranks in egg release material (ERM), L4 larvae ES (L4ES) and HES according to the in-house proteomics analysis 105
4.5 Size exclusion fractionation emPAI values of proteins peaking in active fractions of all fractionation approaches 115
4.6 Sequential fractionation emPAI values of proteins peaking in active fractions of all fractionation approaches 115
4.7 Anion exchange fractionation emPAI values of proteins peaking in active fractions of all fractionation approaches 116
4.8 Size exclusion fractionation emPAI values of proteins peaking in active fractions of size exclusion and sequential fractionation 116
4.9 Sequential fractionation emPAI values of proteins peaking in active fractions of size exclusion and sequential fractionation 118
4.10 Further selection of eight shortlisted proteins considering conserved domains, top named blastx result and peptide coverage from mass spectrometry 119
4.11 Candidates for expression including names and ranks in egg release material (ERM), L4 larvae ES (L4ES) and HES according to the in house proteomics analysis 121

B.1 Proteins identified in fraction 14 of the first size exclusion fractionation of HES 243
B.2 Proteins identified in fraction 15 of the first size exclusion fractionation of HES 244
B.3 Proteins identified in fraction 39 of the first anion exchange fractionation of HES 246
B.4 Proteins identified in fraction 40 of the first anion exchange fractionation of HES 248
B.5 Proteins identified in fraction 28 of the sequential fractionation of HES . 252

B.6 Proteins identified in fraction 29 of the sequential fractionation of HES . 261
B.7 Proteins identified in fraction 30 of the sequential fractionation of HES . 270
B.8 Proteins with emPAI values peaking in active sequential fractions 28-30 with their emPAI values across the fractions 278
B.9 Proteins identified in fraction 14 of the second size exclusion fractionation of HES 290
B.10 Proteins identified in fraction 15 of the second size exclusion fractionation of HES 298
B.11 Proteins identified in the active fraction 25 of the second anion exchange fractionation of HES 302
B.12 Proteins with emPAI values peaking in size exclusion fractions 14 or 15 . 312
B.13 Proteins with emPAI values peaking in anion exchange fraction 25 . . . 314

C.1 Transcripts up-regulated in LPS+HES treated compared to LPS stimulated BMDC 318
C.2 Transcripts down-regulated in LPS+HES treated compared to LPS stimulated BMDC 330

Abbreviations

Table 1: Abbreviations used throughout the thesis in alphabetical order.

APC	antigen presenting cell
AAM	alternatively activated macrophage
ABIN	TNFAIP3 (A20)-interacting protein 1
AP-1	activator protein 1
Arg1	arginase 1
Ass1	argininosuccinate synthetase
ATF	activating transcription factor
ATP	adenosine triphosphate
BATF	basic leucine zipper transcription factor, ATF-like
BMDC	bone marrow derived dendritic cell
bp	base pairs
BSA	bovine serum albumin
C	Celsius
C/EBPβ	CCAAT-enhancer-binding proteins beta
CBA	cytometric bead array
CBP	CREB-binding protein
CCL	chemokine (CC motif) ligand
CCR	chemokine (CC motif) receptor
CD	cluster of differentiation
cDC	conventional dendritic cell
CISH	cytokine-inducible SH2-containing protein
CLR	C-type lectin receptor
CpG	Cytosin-phosphat-Guanin
CREB	cAMP response element-binding protein
DAMP	danger associated molecular pattern
DC	dendritic cell
DC-SIGN	DC-specific intercellular adhesion molecule-3-grabbing non-integrin
Ddit4	DNA-damage-inducible transcript 4 protein
DMSO	dimethyl sulphoxide
DNA	desoxyribonucleic acid
dNTP	2′-desoxynucleosidtriphosphate
DTR	diphteria toxin receptor
DUSP	dual specificity phosphatase
EAE	experimental autoimmune encephalitis
EC	epithelial cell
EDTA	ethylenediaminetetraacetic acid
ELISA	enzyme linked immunosorbent assay
ER	endoplasmatic reticulum

Table 1: Abbreviations (continued).

ERK	Extracellular-signal-regulated kinases
ERM	egg release material (*H. polygyrus*)
ERP	egg release protein
ES	excretory/secretory products
ETC	electron transport chain
ETS	E26 transformation-specific transcription factor
FACS	Fluorescence-activated cell sorting
FCS	fetal calf serum
FITC	fluorescein isothiocyanate
FLDC	BMDC differentiated with Flt3-L
GM-CSF	granulocyte-macrophage colony-stimulating factor
GSK-3	glycogen synthase kinase 3
h	hour
HES	*H. polygyrus* ES
HIF	hypoxia induced factor
HK	hexokinase
HO	heme oxygenase
HRP	horseradish peroxidase
IκB	NF-κB inhibitor
Idh1	isocitrate dehydrogenase
IFN	interferon
Ig	immunoglobulin
IKK	NF-κB inhibitor kinase
IL	interleukin
ILC	innate lymphoid cell
iNOS	inducible nitric oxide synthase
IP_3	inositol 1,4,5-trisphosphate
IRAK	interleukin-1 receptor-associated kinases
IRF	interferon regulatory factor
ITAM	immunoreceptor tyrosine-based activation motif
ITIM	immunoreceptor tyrosine-based inhibition motif
JAK	Janus kinase
JNK	c-Jun N-terminal kinases
KLH	keyhole limpet hemocyanin
l	litre
L4ES	ES from *H. polygyrus* L4 larvae
LBP	LPS-binding protein
LDHA	lactate dehydrogenase A
LN	lymph node
LPS	lipopolysaccharide
LSP	larval secreted protein

Table 1: Abbreviations (continued).

M	molar
mAb	monoclonal antibody
MACS	magnetic-activated cell sorting
MAPK	mitogen-activated protein kinase
March1	membrane-associated RING finger protein 1
MEK	mitogen-activated protein kinase kinase
MHC	major histocompatibility complex
min	minute
Mknk2	MAPK-interacting serine/threonine-protein kinase 2
mLN	mesenteric lymph node
moDC	monocyte derived dendritic cells
MR	mannose receptor
MyD88	myeloid differentiation factor 88
NAD^+ / NADH	nicotinamide adenine dinucleotide
NASP	nuclear autoantigenic sperm protein
NES	*N. brasiliensis* ES
NF-κB	nuclear factor κ-light-chain-enhancer of activated B cells
NFAT	nuclear factor of activated T-cells
NLR	Nod-like receptors
NO	nitric oxide
NOD	nucleotide-binding oligomerization domain-containing protein
NSP	novel secreted protein
OVA	ovalbumin
OXPHOS	oxidative phosphorylation
Pa	*Propionibacterium acnes*
PAMP	pathogen associated molecular pattern
PBMC	peripheral blood monocytes
PBS	phosphate buffered saline
PCR	polymerase chain reaction
pDC	plasmacytoid dendritic cell
PDH	pyruvate dehydrogenase
PDK	pyruvate dehydrogenase kinase
PDK1	3-phosphoinositide dependent protein kinase-1
PE	phycoerythrin
PI3K	phosphatidylinositide 3-kinase
PIP_2	phosphorylates phosphatidylinositol (4,5)-bisphosphate
PIP_3	phosphatidylinositol (3,4,5)-triphosphate
PKB	protein kinase B (also called Akt)
PLC	phospholipase C
Poly(I:C)	polyriboinosinic polyribocytidylic acid
PPP	pentose phosphate pathway

Table 1: Abbreviations (continued).

PRR	pattern recognition receptor
Rab7b	Ras-related protein 7b
RBC	red blood cell
RELM	resistin-like molecule
RIG	retinoic acid-inducible gene 1
RIP	receptor-interacting serine/threonine-protein kinase
RLR	RIG-like receptor
ROS	reactive oxygen species
rpm	revolutions per minute
SA	streptavidin
SCP	sperm coating protein
SDS-PAGE	sodium dodecyl dulphate polyacrylamide gel electrophoresis
SEA	*Schistosoma* soluble egg antigen
SFK	Src family kinases
ShK	*Stichodactyla helianthus* toxin
Slc	solute carrier
SOCS	suppressor of cytokine signalling
STAT	signal transducers and activators of transcription proteins
Syk	spleen tyrosine kinase
T_{reg}	regulatory T cell
T_H	T helper cell
TAB	TAK1-interacting protein
TAK1	mitogen-activated protein kinase kinase kinase 7
TBK1	TANK-binding kinase 1
TCA	tricarboxylic acid
TCR	T cell receptor
TGF	transforming growth factor
TGM	TGF-β mimic (*H. polygyrus*)
TIR	Toll-interleukin 1 receptor
TIRAP	TIR-domain containing adaptor protein
TLR	Toll-like receptor
TNF	tumour necrosis factor
TRAF	tumour necrosis factor receptor associated factor
TRAM	TRIF-related adaptor molecule
TRIF	TIR-domain-containing adapter-inducing IFN-β
TSLP	thymic stromal lymphopoietin
TTR-10	transthyretin-like protein 10
UPR	unfolded protein response
VAL	venom allergen-like protein

CHAPTER 1

Introduction

1.1 Helminths

Infections with helminths are a major health problem worldwide. They are counted as neglected tropical diseases as they affect large numbers of people mostly in the developing countries and living in extreme poverty. Fig. 1.1 is a map produced by the World Health Organization for the year 2014, showing the proportion of children in a given country needing to receive preventative chemotherapy for soil-transmitted helminthiases (STH) alone, which indicates the disease burdens in these countries. According to the WHO, more than 1.5 billion people worldwide are infected with STH, which is over 20% of the world's population (WHO fact sheet: http://www.who.int/mediacentre/factsheets/fs366/en/, as of April 2016).

Helminths, rather than causing the death of their hosts, usually lead to long lasting, chronic infections. The high morbidity is due to the effects of this long term infection, especially if a person is infected by a large number of parasites. STH for example can cause severe anaemia and malnutrition, as they feed on host tissues or blood in the intestine, causing intestinal bleeding and malabsorption of nutrients (Crompton and Nesheim, 2002). In pregnant women, helminth infections decrease the birth weight of infants and increase neonatal mortality (Christian et al., 2004). Chronic infections in children were shown to impair their physical and intellectual development, leading to a reduced performance in school. In general, helminth infections decrease worker productivity, leading to massive economic losses (Crompton and Nesheim, 2002).

In addition to their effects on humans, helminths also infect livestock. This leads to increased costs in treatment of infected animals or to prevent infections, and decreased productivity in addition to increased mortality of livestock (Miller and Horohov, 2006).

These direct effects are not the only problem caused by helminths, as these

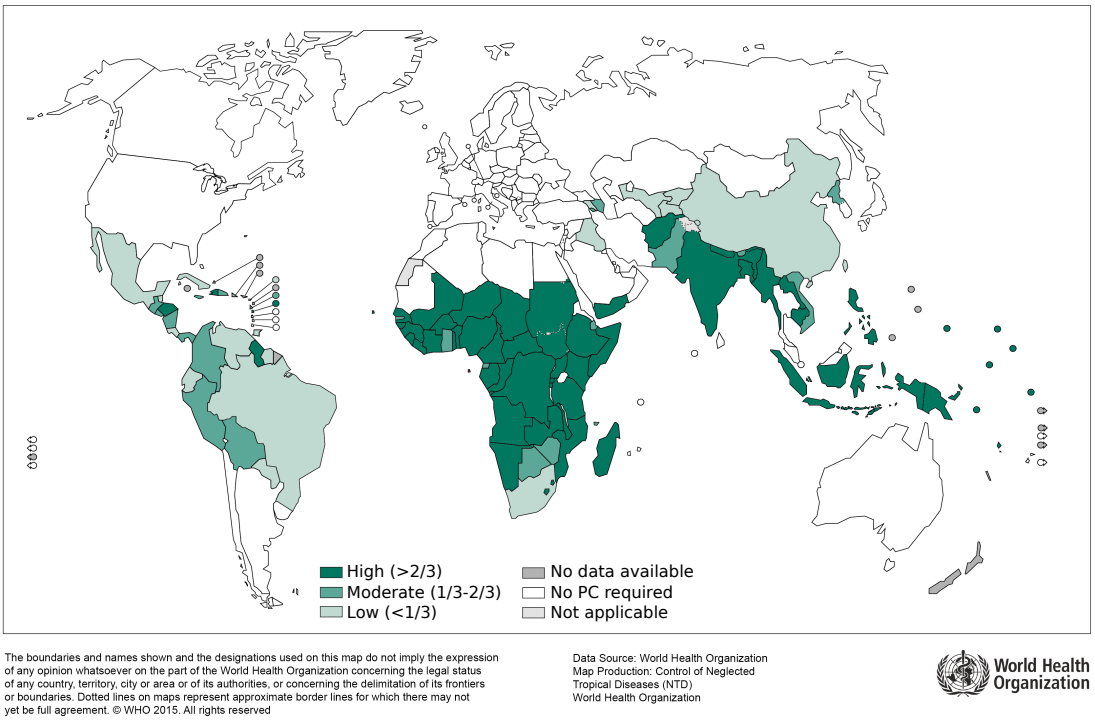

Figure 1.1: Proportion of children (1-14 years of age) in the country requiring preventative chemotherapy (PC) for soil-transmitted helminthiases, worldwide, 2014. Indicated are countries where less than a third (low), between one and two thirds (moderate) and more than two thirds of children (high) needed to receive PC in the year 2014. Adapted from the WHO map gallery: http://gamapserver.who.int/mapLibrary/Files/Maps/STH_2014.png (as of April 2016)

parasites also alter immune responses to other agents. The geographical distribution of diseases like tuberculosis (TB), malaria and HIV for example overlaps significantly with that of helminth infections (Salgame et al., 2013). In tuberculosis infected individuals, co-infection with helminths impairs IFNγ production, probably in a Treg dependent manner, and exacerbates disease (Resende Co et al., 2006; Wammes et al., 2010). Additionally, infection with helminths might increase the risk of contracting TB upon exposure and for it to progress to active disease, due to the impaired TB specific immune responses (Babu et al., 2009; George et al., 2013; Salgame et al., 2013; Verhagen et al., 2012). In co-infections with *Plasmodium* species, the intensity of helminth infection seemed to generally positively correlate with increased *Plasmodium* parasitemia (Degarege et al., 2009; Mulu et al., 2013a). Their effects on malaria pathology however seem to vary, with some reports demonstrating a positive correlation between helminth burden and severity of malaria (Le Hesran et al., 2004)

but others showing helminths to alleviate malaria pathogenesis (Degarege et al., 2009; Lyke et al., 2005). The effects of helminth infection on HIV seem to be two-sided as well, as they can both impair HIV progression in the early stages of infection thanks to their effects on innate immune cells (Salgame et al., 2013), but also contribute to higher infection risks (Downs et al., 2011; Jourdan et al., 2011; Kjetland et al., 2006) and increased viral load in the later stages of infection (Mulu et al., 2013b; Wolday et al., 2002).

Furthermore, helminth infections hamper disease prevention efforts, as they interfere with vaccination. This has been shown for example in children infected with *Ascaris lumbricoides* who received an oral cholera vaccine (Cooper et al., 2000), in study subjects infected with *Schistosoma mansoni* before vaccination using tetanus toxoid (Sabin et al., 1996) or in people generally infected with intestinal helminths that received the BCG vaccination against tuberculosis (Elias et al., 2001). In each of these studies, the resulting vaccine specific immune reactions were impaired by the helminth infection. This applies to livestock as well; a study on pigs infected with *Ascaris suum* came to the same conclusion after vaccination against *Mycoplasma hyopneumoniae* (Steenhard et al., 2009).

The range of extensive effects of nematode infections in humans exemplifies how important it is to implement effective treatment and prevention strategies. However, the rate of re-infection following anthelminthic treatment is high and the funding going into research to develop better treatment regimes is comparatively low; although work on the development of vaccines has been underway for many years, efficient vaccines against helminth infections have yet to be realised (Hewitson and Maizels, 2014; Hotez et al., 2008).

The eradication of helminth infections due to improved hygiene and medicine especially in the developed world may have brought other, unexpected, health consequences. In fact, helminth infection rates inversely correlate with the incidence of autoimmune conditions and allergy, afflictions that are dramatically gaining importance especially in the first-world countries. This is recognized by an updated formulation of the "hygiene hypothesis", which first postulated that microbial infections protect against allergy (Strachan, 1989). A more recent view suggests that our immune system evolved in the presence of helminth infections and removing these leads to a shift in the balance of immune inhibition and effector mechanisms resulting in an increased incidence of conditions characterized by an overactive immune response (Maizels et al., 2014; Wilson and Maizels, 2004; Yazdanbakhsh et al., 2002). A number of studies support this theory. Children living in rural areas were less prone to asthma than their urban counterparts (Yemaneberhan et al., 1997), and an upbringing on a farm resulted in decreased risk to develop allergic reactions in

adulthood (Leynaert et al., 2001; Mutius and Vercelli, 2010). Also getting in contact with infectious agents via other children in early childhood, for example in case of larger families or by an early entry into day nurseries was associated with protection from allergy (Krämer et al., 1999).

The immunological response of children treated with anti-helminthics also shows that these parasites may alleviate allergy. Worm clearance, while decreasing total serum IgE and IL-4 levels, led to an increase in serum IgE against environmental allergens and immediate-hypersensitivity skin-test reactivity to allergens, indicating that there is a causal link between active infection with helminths and suppression of allergy (Biggelaar et al., 2004; Lynch et al., 1993).

Remarkably, it was reported that adventitiously-acquired helminth infection significantly inhibited progression of multiple sclerosis in a cohort of 12 patient in Argentina (Correale and Farez, 2007). Infection and remission were associated with an increase in Tregs as well as an increase in IL-10 and TGF-β secreting and a decrease in IL-12 and IFNγ producing cells. After just over five years, some of these patients had to be treated with anti-helminthics. Three months later the number of IL-10 and TGF-β secreting cells as well as Tregs decreased, while the number of IL-12 and IFNγ secreting cells increased; MS symptoms in these patients returned as well (Correale and Farez, 2007; Correale and Farez, 2011).

Considering this, it is not surprising that a number of clinical trials are currently underway, mostly using infection with *Trichuris suis* to treat various autoimmune diseases as well as allergy and asthma (`http://www.niaid.nih.gov/topics/tropicaldiseases/Pages/helminthDatabase.aspx`, as of 16. March 2016)); however, recent analyses have reported mixed, or even disappointing, outcomes to these trials (Fleming and Weinstock, 2015).

Both the development of new treatments and vaccines for helminth infections and the development of treatments based on helminth infection therefore still require an immense amount of research. For this, the use of animal models is crucial. The next section covers helminth species relevant as human pathogens and commonly used animal models.

1.1.1 Helminths infecting humans and their animal models

Helminths are parasitic worms that belong to the two phyla Nematoda and Platyhelminthes (see Fig. 1.2).

Platyhelminthes, which are also called flatworms, can be subdivided into two classes, Trematoda (flukes) and Cestoda (tapeworms). Among the Trematoda, blood and liver flukes are the main groups infecting humans and contain for example

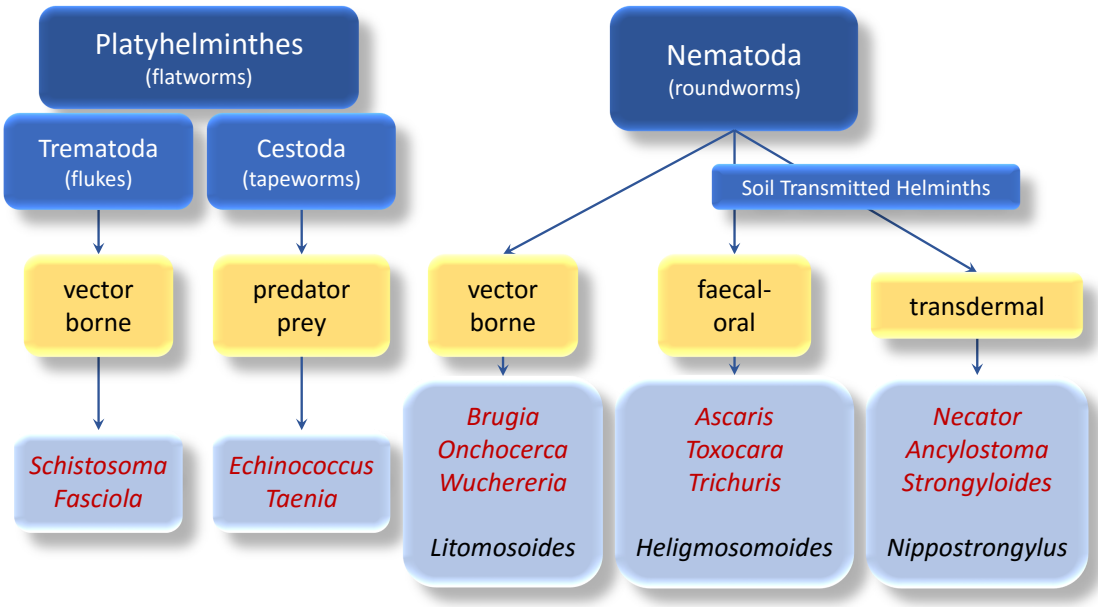

Figure 1.2: Rough classification of major helminths according to phylogeny and mode of infection. Top line: taxonomic grouping; Second line: mode of transmission; Third line: species, human parasites in red and animal models in black. Adapted from Hewitson and Maizels, 2014

Schistosoma and *Fasciola* species. Helminths of both of these genera are also used as animal models, as *Schistosoma mansoni* and *Fasciola hepatica* infect mice as well as humans. Flukes have complex life cycles involving snails as intermediate hosts, which is why their mode of transmission is defined as vector-borne. Most notable among the Cestoda are *Echinococcus* and *Taenia* species. Again, the life cycles of these species involve intermediate hosts, here definitive hosts are infected by ingesting encysted larvae within their food, the intermediate hosts. Hence, they fall under the predator-prey category of transmission modes. While for *Taenia* species humans are definitive hosts, this is not the case for *Echinococcus*, for which dogs act in this capacity and humans count as aberrant intermediate hosts when infected by ingesting eggs from the environment.

Nematodes contain a considerable number of different groups of parasites beyond those listed in Fig. 1.2, including pin-worms (Oxyurida, e.g. *Enterobius vermicularis*) and guinea worms (Camallanida, *Dracunculus medinensis*). Of the three major sets of nematode parasites shown in Fig. 1.2, the filarial worms (Spirurida, including *Onchocerca, Wuchereria* and *Brugia*) are vector-borne parasites, as they are

transmitted by mosquitoes or flies feeding on the definitive host's blood. *Litomosoides sigmodontis* as well as *Acanthocheilonema viteae* are mouse models used to study filariae. Parasites of the remaining two groups shown in Fig. 1.2 are soil-transmitted helminths, as eggs are passed into the environment via faeces and develop there into infectious third stage larvae. Some whip-worms (Trichocephalida) like *Trichura* species have a faecal-oral mode of transmission just like round-worms (Ascaridida) like *Toxocara* and *Ascaris* species, with the eggs or L3 larvae taken up orally through contaminated drinking water or food. Hookworms (Strongylida, *Necator* and *Ancylostoma*) and some threadworms (Rhabditida, *Strongyloides*) have a transdermal mode of infection; free living infectious larvae borrow through the skin of a new host. The adult stages of all these parasites live in the hosts intestine, although some life cycles include a pulmonary migration step (for example the hookworms or *Ascaris*) while others directly infect the gut, like *Trichuris*. Widely used model organisms for STH are *Nippostrongylus brasiliensis* which is a skin penetrating parasite that migrates to the intestinal tract via the lungs of its host, and *Heligmosomoides polygyrus*. As this is the parasite used here, it will be described in more detail in the next section.

1.1.1.1 *Heligmosomoides polygyrus*

The threadworm *H. polygyrus* (first described as *Nematospiroides dubius* Baylis, 1926) is a natural parasite of rodents; infections with this nematode are common amongst wild mice. Its life cycle was first described in 1954 (Ehrenford, 1954), and it has since been found to be relatively easy to maintain in the laboratory, making it an invaluable model for intestinal helminth infections (Behnke et al., 2009). Fig. 1.3 gives an overview over the life cycle of this parasite as it is being kept in the laboratory.

H. polygyrus eggs are contained in the faeces of infected mice; within about one week they develop into infective L3 larvae. These are taken up orally by mice (in the laboratory setting by gavaging), invade the duodenal mucosa after approximately 24 hours and encyst between the muscle layer and the serosa. There they moult twice before they re-emerge into the lumen of the intestine as adults, about eight days post infection. The adult worms coil around the villi in the small intestine, where they were shown to feed on the epithelial cell layer (Bansemir and Sukhedo, 1994), although recent intravital imaging microscopy analyses cast doubt on this finding, as there was no evidence of *H. polygyrus* feeding on host tissue (J. Hewitson, personal communication). About ten days post infection and after mating, adult worms start producing eggs. The *H. polygyrus* parasites are used to induce chronic infections in experimental studies. In primary infections, different mouse strains were found to differ in their abilities to expel the worms, ranging from resistant strains that cleared

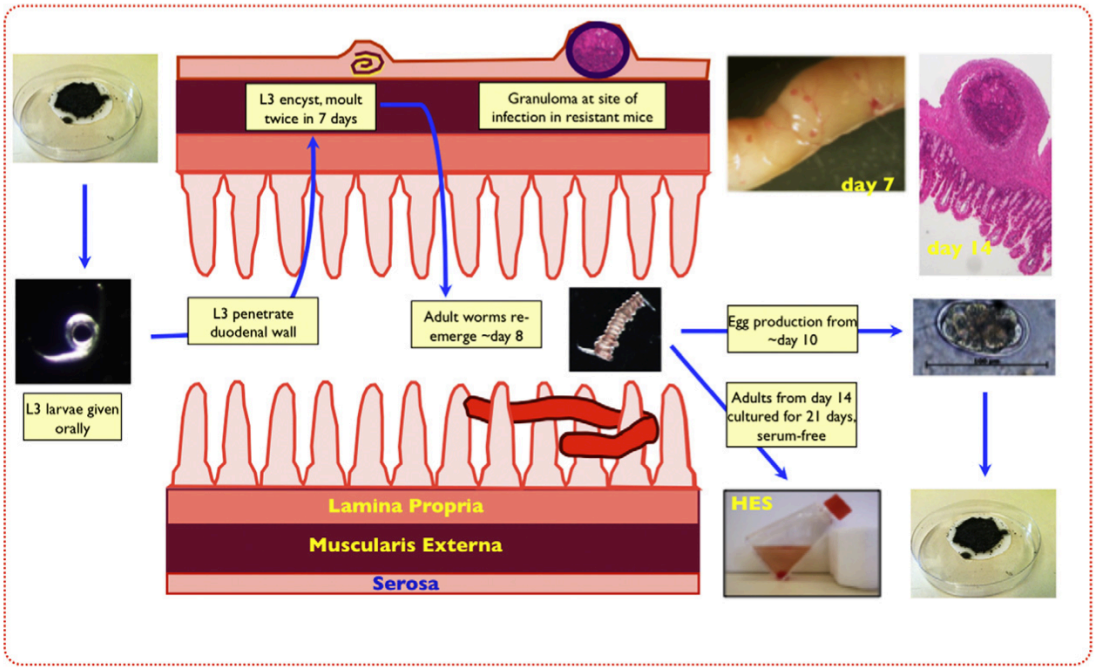

Figure 1.3: Life cycle of *H. polygyrus*. Infectious L3 larvae can be obtained by culture of the egg containing faeces of infected mice. As infection occurs orally, mice can be infected by gavage; larvae then invade the mucosa of the duodenum, where they encyst and mature into adult worms. Eight days post infections, adults emerge into the gut lumen, where they coil around villi. In the lumen, adults mate and start producing eggs around day ten post infection. Adult worms can be cultured in vitro for at least three weeks in tissue culture medium; this way their excretory/secretory products can easily be collected. From Maizels et al., 2012.

the infection within a week to susceptible strains that were not able to fight infection (Behnke et al., 2009; Filbey et al., 2014). If mice were treated with anti-helminthics before being infected a second time however, all strains were resistant to infection indicating the development of a protective immune response (Behnke et al., 2009).

Adult *H. polygyrus* is known to strongly repress immune responses. As reviewed in ibid., it was found early on that adult worms suppressed mouse immune responses and that they did so via their excretory/secretory products. Since then, numerous studies have been published demonstrating the protective effect of infection with this parasite or treatment with its products (called HES) in a variety of diseases. It has been shown for example that infected mice are protected from EAE as well as allergy (Wilson et al., 2010) and colitis (Hang et al., 2010). HES has been demonstrated to protect mice from allergic airway inflammation (McSorley et al., 2014; McSorley et al.,

2015; McSorley et al., 2012).

HES can be obtained by culturing *H. polygyrus* in vitro, as the worms survive in tissue culture medium for at least three weeks. The culture medium can be collected and concentrated down to enrich the parasite products (Johnston et al., 2015). The original proteomics analysis of HES identified 374 proteins (Hewitson et al., 2011b), and as techniques become more sensitive and fractions are submitted for analysis, many more components are being found (Buck et al., 2014). Within the total HES, three dominant protein families have been identified, namely the venom allergen-like (VAL) proteins, ShK-like proteins and the Sushi protein family. However, an extensive number of proteases and protease inhibitors, as well as apyrases, chitinases and a large number of proteins with unknown functions were found as well. This analysis also showed that there are many similarities in the products contained in HES and those in the ES of related helminths, including the hookworm *Ancylostoma caninum*, demonstrating the value of *H. polygyrus* as a model for soil-transmitted helminth infections (Hewitson et al., 2011b).

1.2 Immune responses to helminths

Infection with nematodes typically induces a type 2 immune response and involves a large number of different cell types and mediators (Figure 1.4).

Epithelial cells (ECs) provide a barrier between host tissues and environmental factors, including commensal bacteria and inhaled or ingested antigens. In steady state, they produce TGF-β and promote a tolerogenic phenotype in DCs sampling

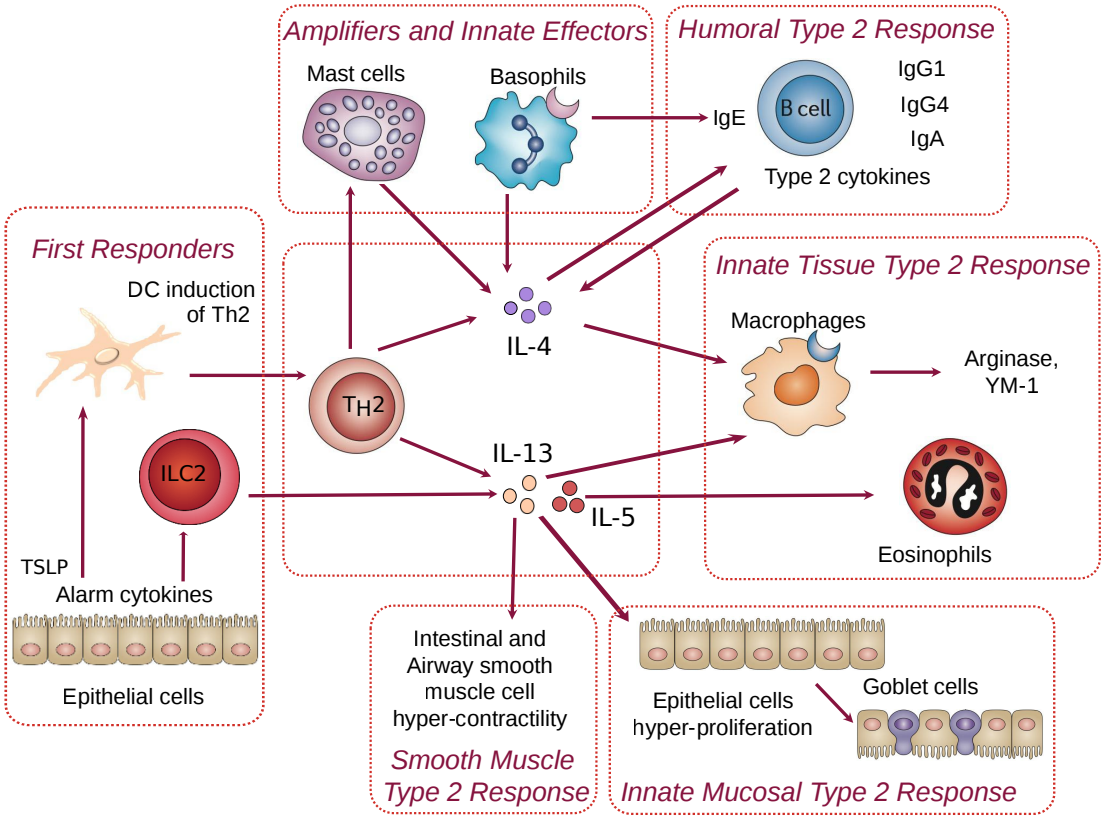

Figure 1.4: Helminths induce type 2 immunity. After infection with nematodes, the immune system is activated and dendritic cells induce the differentiation of naive T cells into T_H2 cells. During the following type 2 immune response, several cell types are activated. These include mast cells, eosinophils, basophils and macrophages, which differentiate into alternatively activated macrophages. In B cells, the class switch to IgG1, IgG4 or IgE is induced. Furthermore, the mucosa and the smooth muscles of the intestines and the airways are activated to help expel the parasites. DC, dendritic cell; Ig, immunoglobulin; IL, interleukin; ILC2, innate lymphoid cell type 2; T_H2, T helper 2; TSLP, thymic stromal lymphopoietin; YM-1, chitinase-like secreted protein (adapted from Allen and Maizels, 2011).

antigens from lungs or gut (Iliev et al., 2009; Wang et al., 2009). They are however also the first cell type that comes into contact with pathogens invading these organs, including helminths. ECs can recognize these via a number of different mechanisms. They express pattern recognition receptors (PRRs) such as Toll-like receptors (TLRs) (Abreu, 2010; Hammad et al., 2009), enabling them to respond directly to pathogen associated molecular patterns (PAMPs). They can also respond to proteases produced by helminths to gain entry into host tissues thanks to their expression of protease-activated receptors (PARs) (Chiu et al., 2007; Park et al., 2011). Upon activation, ECs start producing cytokines to alert the immune system to infection. Among these are TSLP, IL-25 and IL-33 (Hammad et al., 2009; Hara et al., 2014) but also danger associated molecular patterns (DAMPs) like ATP (O'Grady et al., 2013), HMGB1 (Ullah et al., 2014) or uric acid (Kool et al., 2011) and chemokines like CCL17 or CCL22 (Chen and Chiang, 2016; Hammad and Lambrecht, 2015). All these factors are involved in the activation and recruitment of immune cells contributing to the type 2 response (reviewed in Hammad and Lambrecht, 2015 and Perrigoue et al., 2008).

One of the affected cell types are DCs. In addition to recognizing PAMPs themselves, which they can sample either directly by extending dendrites into the gut lumen or which can be delivered to them by so called microfold (M) cells (Artis, 2008), they are also further activated by the factors secreted by ECs. These factors help ensure that activated DCs drive T_H2 rather than T_H1 responses (Hammad and Lambrecht, 2015). Upon activation, costimulatory molecules like CD80, CD86 and CD40 on DCs are upregulated to provide the so called signal 2 in addition to antigen processing and presentation as MHC:peptide complexes (signal 1) and secretion of cytokines to direct T cell differentiation (Banchereau et al., 2000)

While the mechanisms behind T_H1 or T_H17 induction are well known, it is less clear what leads to the differentiation of $CD4^+$ T cells into T_H2 cells. DCs generally do not produce IL-4; while it is now known that deletion of IL-4 does not affect T_H2 differentiation (Panhuys et al., 2008), earlier indications had been that this cytokine induces T_H2 responses (reviewed in Hammad and Lambrecht, 2015 and (Paul, 2010)).

For a while it was thought that the mere lack of T_H1 inducing cytokines was responsible for T_H2 induction, with DCs inducing T_H2 differentiation by default unless they also secrete cytokines that lead to the differentiation of other helper cell subsets (Pulendran et al., 2010; Sher et al., 2003). This default hypothesis has since then been disproved; instead, cytokines produced by different cells in the environment, expression of a different set of costimulatory molecules like OX40L on the DC and a weak interaction between T cell and DC - for example by low expression of MHC II or costimulatory molecules - have been shown to contribute (Haan et al., 2014; Paul and Zhu, 2010).

That DCs are critical for the induction of T_H2 responses has been demonstrated in experiments depleting $CD11c^+$ cells from CD11c-diphteria toxin (DTx) receptor transgenic mice. These mice were protected from the development of allergic asthma if DTx was administered before antigen challenge, which was reversed by the transfer of DCs (Rijt et al., 2005). Furthermore, in infections with both *S. mansoni* or *H. polygyrus*, $CD11c^+$ cell depletion by daily injection of DTx resulted in impaired T_H2 responses (Phythian-Adams et al., 2010; Smith et al., 2011), while basophil depletion had no effect, confirming the pivotal role of DCs.

Another cell type activated by the factors secreted by ECs during helminth infection are type 2 innate lymphoid cells (ILC2s). In the past also called nuocytes, ILC2s are innate bone marrow-derived cells and are similar to their helper T cell counterparts in their transcription factor usage and cytokine profile (Walker et al., 2013). ILC2s have been discovered as cells expanding due to IL-25 and IL-33, and have been shown to be crucial for the induction of type 2 immune responses, producing IL-5 and IL-13 long before T_H2 cells do so (Fallon et al., 2006). However, it has been shown that ILC2 and T_H2 cells have to work together for optimal induction of type 2 responses and helminth expulsion (Oliphant et al., 2014).

The production of IL-4, IL-5 and IL-13 by ILC2s and T_H2 cells mediates subsequent effects. IL-13 for example causes hypercontractility of the smooth musculature; together with its effects on goblet cells, including their increased production of mucins this results in the so called weep and sweep response that aids in expulsion of parasites (Allen and Maizels, 2011). Goblet cells also produce mediators like RELMβ, which has been shown to directly impair the function of a nematode's chemosensory apparatus (Artis et al., 2004).

T_H2 cells and the type 2 cytokines produced by T_H2 cells are integral to the induction of the antibody class switch to IgE, IgG1 and, in humans, IgG4 in B cells (Xu et al., 2012). After their activation, $CD4^+$ T cells migrate to the B cell zones of lymphoid tissues. There, B cells which recognize an antigen - expressing B cell receptors that can bind to an epitope of the antigen - get activated and act like other antigen presenting cells by upregulation of costimulatory molecules and processing of the antigen to present its peptides as MHC II:peptide complexes. These activated B cells can interact with the activated helper T cells if they present the peptide for which the T cells are specific; this interaction and cytokines secreted by the T cells, here IL-4 and IL-5, induce the proliferation and class switching of the B cells (Garside et al., 1998; Xu et al., 2012).

Class switched antibodies are important in a number of effector mechanisms. IgE for example is central to the activation of mast cells and basophils by antigens or allergens which crosslink IgE bound to their cell surface FcεR1, the high affinity

IgE receptors (Brunner et al., 1993; Urb and Sheppard, 2012; Weller et al., 2011). In mast cells, this leads to degranulation and release of effectors such as histamine and proteases. These molecules aid nematode expulsion in some models; amongst other functions they enhance mucus production and act on smooth muscle cells to contribute to the induction of the weep and sweep response (Allen and Maizels, 2011; Urb and Sheppard, 2012). In helminth infections, mast cells have also been shown to be activated by IgE independent mechanisms, which has been hypothesized to be due to their expression of a range of PRRs (Urb and Sheppard, 2012; Weller et al., 2011). Basophils on the other hand have been shown to additionally be activated by the cytokines secreted by ECs upon parasite recognition, specifically IL-33 and TSLP (Hammad and Lambrecht, 2015). Their role in type 2 responses is controversial. They have been reported to promote worm expulsion in secondary but not primary infection with *N. brasiliensis* and *H. polygyrus* (Herbst et al., 2012; Schwartz et al., 2014), and their depletion did not impair T_H2 responses to these two models (Phythian-Adams et al., 2010; Smith et al., 2011). On the other hand, in primary infection with *T. muris* they were necessary for T_H2 induction, as they were major producers of IL-4 and could act as APCs (Perrigoue et al., 2009). As discussed in Finkelman, 2009, the exact contribution of basophils to the development if T_H2 responses might depend on the model used, as they might be dispensable in models with strong T_H2 induction but play a necessary support role in infections or stimulation with weak T_H2 inducers.

IgG1 is the prevalent isotype induced by infection with *H. polygyrus* and has been demonstrated to be induced by vaccination with HES, which induced immunity in normally susceptible mice (Hewitson et al., 2015; Hewitson et al., 2011a). Both IgG1 and IgG2a/c have been reported to be important for the immobilization and trapping of tissue-migrating *H. polygyrus* larvae (Esser-von Bieren et al., 2015; Hewitson et al., 2015). A cell type crucial for this effect are alternatively activated macrophages (AAMs). These cells are induced by activation of macrophages in the presence of IL-4 and IL-13 rather than IFNγ, which has been demonstrated to be provided by memory T_H2 cells in secondary infection (Anthony et al., 2006). They have been shown to accumulate around the larvae and contribute to their immobilization (Esser-von Bieren et al., 2013, 2015).

In contrast to classically activated macrophages, which express iNOS and produce high levels of NO using L-Arginine as a substrate, AAMs need this amino acid as a substrate for Arg1. Furthermore, AAMs highly express YM1 and RELMα. While the degradation products of L-Arginine via Arg1 play roles in wound healing (Witte and Barbul, 2003) and, with L-ornithine impairing larval motility, play a role in the AAM mediated larvae trapping mentioned above (Esser-von Bieren et al., 2013), the function of both YM-1 and RELMα is less clear. RELMα appears to be a

mediator used to keep T_H2 responses in check, as Retnla$^{-/-}$ mice showed exacerbated lung inflammation after both challenge with *S. mansoni* eggs and in infection with *N. brasiliensis*. In the latter case this was accompanied by improved parasite clearance, but also increased mortality (Chen et al., 2016; Nair et al., 2009). The function of YM1 on the other hand is more elusive; it has been speculated to support wound healing, as it is able to bind to the extracellular matrix (Sutherland et al., 2009). More recently however, it has been shown to induce IL-17 production by $\gamma\delta$ T cells in response to infection with *N. brasiliensis*, recruiting neutrophils which on the one hand exacerbate lung damage but on the other hand also limit parasite survival (Sutherland et al., 2014). In addition to these effects, AAMs have been shown to be important in primary responses to helminth infections, as their depletion impaired the weep and sweep response and helminth expulsion (Filbey et al., 2014; Zhao et al., 2008).

Another cell type which has been implicated in binding to and acting against tissue-migrating helminth larvae are eosinophils. Generation of these cells from bone-marrow precursors is induced by IL-5, they are activated by IL-5 and degranulation can be induced by binding of antibodies and complement (Coffman et al., 1989; Kita et al., 1992; Klion and Nutman, 2004). This leads to release of molecules contributing to the killing of larvae from at least some helminth species (amongst others cationic proteins, ROS, leukotrienes, platelet-activating factor, lysosomal hydrolases and peroxidase), but on the other hand also contributing to host tissue damage (Klion and Nutman, 2004). In eosinophil-deficient mice that were infected with *N. brasiliensis*, secondary immune responses, specifically those acting on larvae migrating to the lung, were impaired (Knott et al., 2007). Another important role of eosinophils however seems to be as producers of type 2 cytokines and chemokines like CCL17 or CCL7 to contribute to recruitment of immune cells to the site of infection, as shown in allergic inflammation models (Jacobsen et al., 2008; Walsh et al., 2008).

Finally, the cell type investigated in this thesis are the dendritic cells. As such, these will be described in more detail in the next section.

1.3 Dendritic cells

Dendritic cells are the most important type of antigen presenting cells. They were originally discovered as a previously unknown cell type in mouse spleen that was clearly distinguishable by its unique morphology; these new cells were quite large and featured a variable number of pseudopods, giving them their distinct shape and resulting in them being named dendritic cells (Steinman and Cohn, 1973). They were later shown to be the professional antigen presenting cells leading to activation of the adaptive immune response. The first indication of this was the fact that they were potent inducers of the mixed leukocyte reaction, and were in fact the main cell type in mouse spleens inducing this reaction (Steinman and Witmer, 1978). In naive mice, DCs were mainly localized between splenic red and white pulp, where they could sample the blood filtered through the spleen for antigen. Indeed, they were found to process soluble antigen effectively. Upon injection of mice with LPS however, DCs became activated and expressed elevated levels of CD80. This was accompanied by an increase in their ability to stimulate T cells and a decrease in their antigen processing capability. They also were found mainly in the T cell areas of the spleen only six hours after LPS injection, showing that maturation was accompanied by migration (De Smedt et al., 1996). DCs were also found to be able to secrete IL-12 and therefore induce T_H1 differentiation in the T cells they activate (Macatonia et al., 1995).

A number of different DC subsets have been identified in mice. DCs arise from bone marrow precursors. A subset called plasmacytoid DCs, thanks to their plasma cell-like morphology, terminally differentiates in the bone marrow and migrates through the blood stream to lymphoid organs and tissues in the body. These pDCs are important for recognition of and defence against viruses, as they express TLR7, TLR9 and cytosolic sensors to bind to RNA and DNA PAMPs. They are the most important producers of type I IFNs and can also act as APCs. TLR ligation causes their maturation, but not their migration to draining lymph nodes, unlike in steady state conditions where they constantly migrate to the lymph nodes. They have in fact been shown to play important roles in tolerance induction both in airway and oral response settings (Lombardi and Khaiboullina, 2014; Schraml and Reis e Sousa, 2015).

The precursors giving rise to pDCs in the bone marrow, the common DC precursors (CDP) also give rise to so called pre-DC or pre-cDC. These cells exit the bone marrow and terminally differentiate in the tissues into the different subsets belonging to the conventional DCs which express high levels of CD11c, in contrast to pDCs (Schraml and Reis e Sousa, 2015). In the spleen, two types of cDCs have been described, $CD11b^+$ $CD8^-$cDC and $CD11c^-CD8^+$ cDCs (Pulendran et al., 1997).

In a number of reports, these two subsets have been shown to have different properties when it comes to induction of T cell responses. While KLH loaded $CD8^+$ cDCs can induce T_H1 cells, the $CD11b^+$ subset was shown to induce a T_H2 response instead (Maldonado-López et al., 1999). However, both cell types exhibited the same gradient of T_H2 to T_H1 induction in experiments with rising concentrations of OVA (Boonstra et al., 2003), demonstrating that the previously mentioned preference is by no means fixed. Indeed, there seem to be a number of different stimuli that induce DCs to support T_H2 rather than the T_H1 differentiation that is induced by most TLR ligands for example, summarized in Fig. 1.5 from Na et al., 2016.

As can be seen in this figure, not only the dosage of the antigen or TLR ligands - low doses of inhaled LPS have for example been shown to induce T_H2 differentiation, unlike high levels of LPS in the same model (Eisenbarth et al., 2002) - but also the type of TLR ligand determines subsequent T cell polarization. LPS from *P. gingivalis* induced T_H2 responses while LPS from *E. coli* induced the expected T_H1 response, both of which were TLR4 dependent (Pulendran et al., 2001), and the TLR2 ligand Pam-3-cys lead to T_H2 development via activation of ERK which inhibited IL-12 production. A number of the mechanisms mentioned in the previous section are also shown in Fig. 1.5, with helminths for example stimulating ECs to secrete TSLP, IL-25 and IL-33 that act on DCs; DAMPs released by tissue damage like uric acid or ATP as well as glycans contained in allergens like house dust mite particles, but also in helminth products activating DCs; these DCs finally inducing T_H2 responses by expression of costimulatory molecules like OX40L or low expression of CD80 and CD86, and by recruitment of basophils that produce high levels of IL-4 and can act as APCs themselves, supporting the DCs. One additional mechanism of particular interest, described below in more detail, is the effect of helminth secreted products such as ω-1 from *S. mansoni* on DCs (Na et al., 2016).

DC subsets in the gut differ from those in the spleen or lymph nodes. Here, four different subsets are found. They can be distinguished by their expression of CD103 and CD11b, with $CD103^+$ $CD11b^+$ cells being related to the splenic or LN $CD11b^+$ subset and $CD103^+$ $CD11b^-$DCs related to the $CD8^+$ cells. In addition, there is a third, less abundant subset expressing neither marker and finally, a subset expressing CD11b but not CD103 (reviewed in Bekiaris et al., 2014). These subsets have been shown to take up antigen from the gut lumen and migrate to the draining lymph nodes in steady state conditions to induce tolerance, as do pDCs. Upon activation, cDCs have been shown to mature and migrate to the draining lymph nodes where they activate T cells (Cerovic et al., 2013; Schulz et al., 2009). $CCR7^{-/-}$ mice, which are deficient in the chemokine receptor necessary for migration of DCs to draining lymph nodes, do not develop $CD8^+$ T cell responses to oral antigens (Johansson-Lindbom

et al., 2005). Similarly, the induction of oral tolerance was abrogated in these mice (Worbs, 2006).

To study DCs in vitro, methods to generate them from bone marrow have been developed. Mice injected with GM-CSF showed an expansion of the $CD11b^{+}$ $CD8^{-}$cDC subset (Pulendran et al., 1999) and in vitro stimulation with GM-CSF has been a widely adopted technique to generate DCs from bone marrow (Inaba et al., 1992). However, this method also generates macrophages, which, like GM-CSF BMDC, express CD11c and CD11b (Helft et al., 2015). Indeed, publications using these

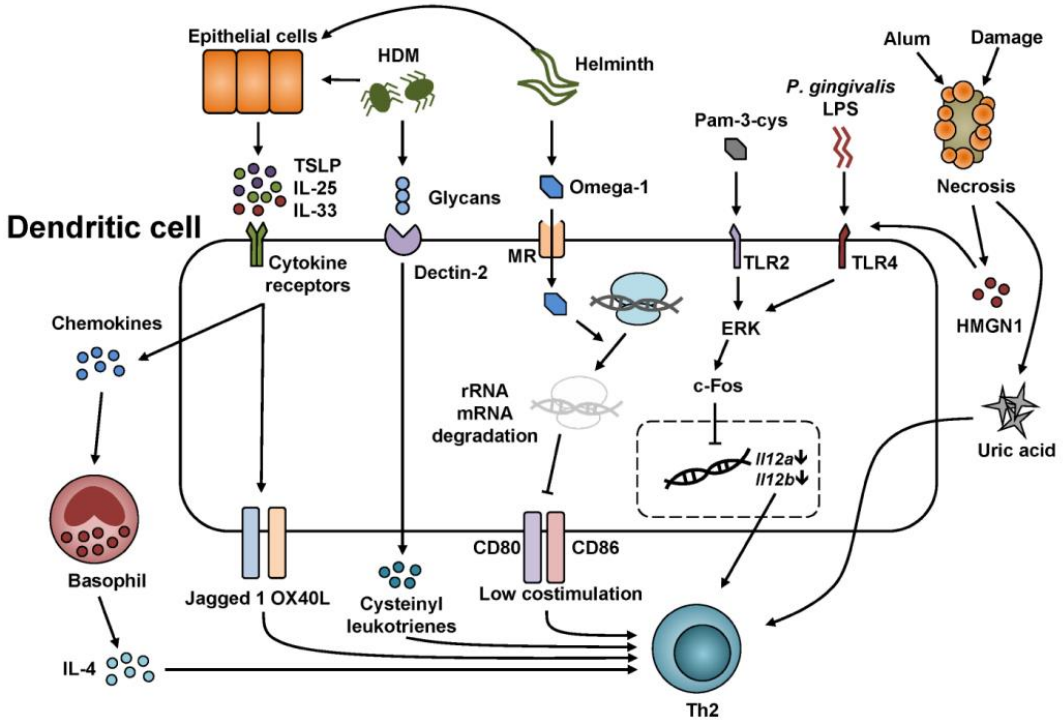

Figure 1.5: Modulation of DC functions by Th2 cell-skewing stimuli. A number of different factors can stimulate DCs to induce T_H2 responses, amongst others PAMPs including some TLR ligands like Pam-3-cys or LPS from *P. gingivalis* or glycans acting via CLRs. ECs activated by helminths secrete alarmins like IL-33, IL-25 or TSLP, and tissue damage releases DAMPs like ATP or uric acid which also activate DCs to induce T_H2 differentiation. Helminths can secrete further products affecting DC maturation, like for example ω-1. All of these factors can activate DCs to express OX40L and low levels of CD80 or CD86, and recruit basophils to support T_H2 induction by secretion of IL-4. Figure taken from Na et al., 2016.

cells usually do not distinguish these two reported subpopulations. Injection of mice with Flt3-L on the other hand leads to expansion of both $CD11b^+$ and $CD8^+$ cDC subsets (Pulendran et al., 1997), and differentiation of bone marrow cells with Flt3-L generates populations equivalent to these two subsets in addition to cells equivalent to pDCs (Naik et al., 2005).

Using these models, a substantial amount of knowledge on mechanisms underlying DC maturation has been gathered. In the following sections, signalling pathways involved in DC activation and necessary changes to DC metabolism during this process are described.

1.3.1 Signalling pathways in DC activation

Dendritic cells express a number of receptors that recognise a wide range of molecules associated with infections, tissue damage or inflammation. Most of these are pattern recognition receptors (van Vliet et al., 2007), but DCs also express cytokine receptors (such as the receptor for TNF) and can be activated by reverse signalling, for example via CD40 ligation (Kikuchi et al., 2003).

Among the PRRs are transmembrane receptors such as TLRs and CLRs, and different types of cytosolic sensors such as NLRs (van Vliet et al., 2007). TLRs can roughly be divided into extracellular receptors mostly recognizing bacterial molecules and endosomal receptors mainly recognizing viral ones. Among the TLRs that are localized on the cell surface are TLR1, 2, 4, 5 and 6 (Takeda et al., 2003). TLR2 forms heterodimers with either TLR1 or TLR6, the former recognizing triacyl glycopeptides like Pam3SCK4 (Takeuchi et al., 2002) while the latter binds diacyl glycopeptides like MALP-2 (Takeuchi et al., 2001). TLR2 can also cooperate with non-TLRs as it was shown to recognize zymosan in cooperation with dectin-1 (Gantner et al., 2003), and it is able to bind peptidoglycans as well (Takeuchi et al., 1999). TLR4 is well known to recognize LPS (Hoshino et al., 1999), but it has also been shown to bind to viral envelope proteins, and TLR5 binds to bacterial flagellin (Hayashi et al., 2001). The endosomal TLRs on the other hand mainly bind to nucleic acids; while TLR3 recognizes double stranded RNA (dsRNA) and signalling through it can be induced using poly(I:C) (Alexopoulou et al., 2001), TLR7 and TLR8 recognize single stranded RNAs; a synthetic compound, R848, induces signalling through both receptors in human cells, although in mice this is restricted to TLR7 (Diebold et al., 2004; Heil et al., 2004; Hemmi et al., 2002). Finally, TLR9 recognizes unmethylated CpG DNA from bacteria as well as viruses (Hemmi et al., 2000).

While all TLRs lead to activation of nuclear factor κ-light-chain-enhancer of activated B cells (NF-κB) and the mitogen-activated protein kinase (MAPK)

cascade, the involvement of specific signalling molecules differs. Therefore signalling pathways induced in LPS stimulated cells will be described first (also see Fig. 1.6), followed by a short description of the differences in the other pathways.

Extracellular LPS is first bound by the LPS binding Protein (LBP), then by CD14 on the cell surface of DCs (Muta and Takeshige, 2001). CD14 forms a complex with TLR4 and MD-2 (Shimazu et al., 1999). TLR4 signals via two intracellular adapter proteins: Myeloid differentiation primary response gene 88 (MyD88) (Wesche et al., 1997) and Toll/Interleukin-1 receptor (TIR)-domain-containing adapter-inducing interferon-β (TRIF) (Yamamoto et al., 2003a). The MyD88 dependent signalling pathway was first described for IL-1 receptor signalling, but then shown to be involved in LPS induced TLR signalling as well (Zhang et al., 1999).

Once MyD88 is recruited, at least 7 steps occur in succession to transduce the activation signal to the nucleus: (I) together with toll-interleukin 1 receptor domain containing adaptor protein (TIRAP) (Yamamoto et al., 2002), MyD88 interacts with Interleukin-1 receptor-associated kinases (IRAK) leading to autophosphorylation of IRAK4; (II) IRAK4 subsequently phosphorylates and therefore activates IRAK1 and IRAK2 (Fitzgerald et al., 2001; Li et al., 2002). (III) These kinases in turn activate a protein complex containing tumour necrosis factor receptor associated factor (TRAF) 6 (Cao et al., 1996; Kawagoe et al., 2008). (IV) The poly-ubiquitinated active TRAF6 then activates a complex containing mitogen-activated protein kinase kinase kinase 7, also called TAK1 and mitogen-activated protein kinase kinase kinase 7-interacting proteins 1, 2 and 3, also called TAB1-3. (V) This complex then activates the canonical NF-κB inhibitor (IκB) kinases (IKK) (Wang et al., 2001), which have been shown to induce the phosphorylation of IκBs (DiDonato et al., 1997; Mercurio et al., 1997). (VI) The phosphorylation if IκBs leads to their ubiquitination and subsequent proteasomal degradation (Chen et al., 1995; DiDonato et al., 1996), unmasking the nuclear translocation signal of NF-κB; (VII) NF-κB is then free to translocate into the nucleus and induce transcription of its target genes (Beg et al., 1992; Ganchi et al., 1992; Zabel et al., 1993). The NF-κB subunits activated in this pathway are p50/p65, as opposed to for example p52/RelB which are induced after ligation of CD40 (Kaisho and Tanaka, 2008).

In addition to this central NF-κB mediated signalling pathway, TAK1-TAB1/2/3 also activate the MAPK cascade leading to activation of several MAP kinase kinases (MKKs) and the MAP kinase families p38 mitogen-activated protein kinases, c-Jun N-terminal kinases (JNK) and extracellular-signal-regulated kinases (ERK) (Wang et al., 2001). Among the targets of these kinases are proteins like c-Jun, c-Fos, phosphorylation of which leads to the formation of the transcription factor activator protein 1 (AP-1). Another two transcription factors that are activated in the MyD88

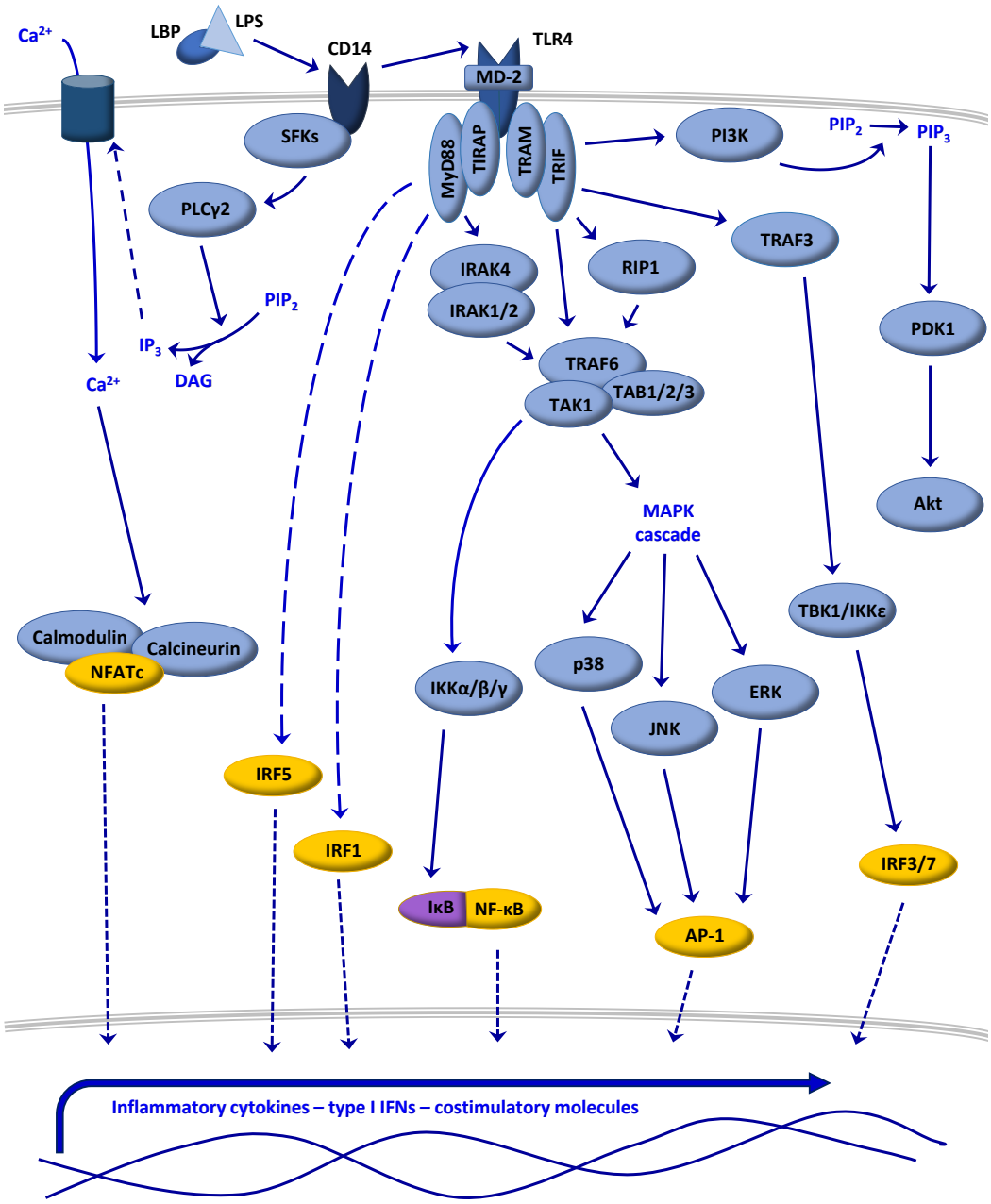

Figure 1.6: Signalling pathways in LPS induced DC activation. LPS is recognized by CD14 and TLR4; TLR4 ligation induces MyD88 and TRIF dependent signalling pathways leading to the activation of canonical and noncanonical NF-κB cascades and the MAP kinase cascades. It further activates PI3K signalling, and leads to the activation of further IRF transcription factors including IRF1 and IRF5. CD14 also induces a signalling cascade, leading to influx of calcium and activation of the calcium dependent calcineurin and calmodulin, which activate NFATc. The activated transcription factors translocate into the nucleus and induce the expression of their target genes.

dependent pathway are interferon regulatory factor (IRF) 1 (Negishi et al., 2006) and IRF5 (Takaoka et al., 2005). This branch of the TLR4 mediated response has been shown to be initiated at the plasma membrane, and activation can therefore be seen very soon after stimulation (Plociennikowska et al., 2015).

A key role is also played by the TLR4 adaptor protein TRIF, which, together with TRIF-related adaptor molecule (TRAM) acting as a bridge between TLR4 and TRIF (Fitzgerald et al., 2003; Yamamoto et al., 2003a,b), activates the receptor-interacting serine/threonine-protein kinase (RIP) 1 (Cusson-Hermance et al., 2005). TRIF also directly binds both TRAF3 (Häcker et al., 2006) and TRAF6 (Jiang et al., 2004). RIP1 and TRAF6 cooperatively activate the TAK1-TAB1/2/3 complex and subsequent NF-κB and MAPK signalling as described above (Jiang et al., 2004; Wang et al., 2001). Furthermore, TRAF3 activates non-canonical NF-κB signalling; the IKKs activated here are TANK-binding kinase 1 (TBK1) and IKKε, which in turn activate both IRF3 and IRF7 (Oganesyan et al., 2006). This leads to the production of the type I interferon IFNβ, which upregulates IRF7 in an autocrine fashion via JAK-STAT signalling involving STAT1 and STAT2 (Hoshino et al., 2002; Lee and Kim, 2007), hence creating a feed-forward amplification of the type I IFN response.

An important distinction is that activation of the TRIF dependent branch of TLR4 signalling is delayed compared to the MyD88 dependent pathway, due to the fact that it is only induced after TLR4 is internalized (Kagan et al., 2008; Plociennikowska et al., 2015). This internalization seems to be mediated by CD14 via Syk and PLCγ2 (Zanoni et al., 2011), and has been shown to also be important for both termination of signals through the internalized receptors and processing of antigens associated with the internalized LPS (Husebye et al., 2006).

Another mediator induced by LPS binding to TLR4 is phosphatidylinositide 3-kinase (PI3K), which phosphorylates phosphatidylinositol (4,5)-bisphosphate (PIP_2) to phosphatidylinositol (3,4,5)-triphosphate (PIP_3) (Hazeki et al., 2007). PIP_3 in turn activates protein kinase B (PKB), also known as Akt, through 3-phosphoinositide dependent protein kinase-1 (PDK1) (Alessi et al., 1997). This pathway plays an important role in the regulation of DC metabolism, as discussed below. On the other hand the PKB/Akt pathway is implicated in negative regulation of TLR signalling in DCs (Fukao et al., 2002). In this setting, Akt may inhibit GSK3 and therefore stop its inhibitory activity towards the transcription factor CREB. Once CREB is activated, it interacts with CBP, inducing the transcription of factors like IL-10. Interestingly, CBP is also needed as a co-activator for the NF-κB member p65, so the increased activity of CREB competitively inhibits the formation of p65-CBP and transcription of genes encoding pro-inflammatory factors like IL-12, TNF or IL-6 (Guha and Mackman, 2002; Martin et al., 2003; Martin et al., 2005; Ohtani et al., 2008).

In recent years it has also been reported that CD14 signals via the nuclear factor of activated T-cells (NFAT) pathway (Zanoni et al., 2009). Upon LPS binding, CD14 recruits Src family kinases that activate phospholipase C (PLC) $\gamma 2$. This enzyme cleaves PIP_2 to inositol 1,4,5-trisphosphate (IP_3) and diacylglycerol (DAG). IP_3 then induces influx of extracellular Ca^{2+}, which activates calcium-modulated protein (calmodulin) and the protein phosphatase calcineurin. Calcineurin then dephosphorylates the calcium dependent members of the NFAT transcription factor family (NFATc), which subsequently translocate to the nucleus and induce transcription of target genes in cooperation with other transcription factors like AP-1 (reviewed in Zanoni and Granucci, 2012). One member of this transcription factor family, NFAT5, is not calcium dependent; instead it has been shown that - at least in macrophages - the expression of this transcription factor is increased by NF-κB after stimulation and that it contributes to the expression of inflammatory mediators dependent on antigen dose (Buxadé et al., 2012).

JAK-STAT signalling also plays a role in LPS induced DC maturation. $JAK2^{-/-}$ DC are impaired in their production of pro-inflammatory cytokines, and it was demonstrated that this was independent of NF-κB signalling. Instead, the JAK2 deficiency led to a decrease in the phosphorylation of STAT3, 4, 5 and 6, of which STAT5 and STAT6 subsequently were shown to be the downstream mediators in this context (Zhong et al., 2010). STAT1 and STAT2 are involved in the positive feedback loop induced by type I IFNs that are produced after TLR4 ligation; $STAT1^{-/-}$ BMDC stimulated with LPS were impaired in their upregulation of CD40 and production of IFNβ as well as IFN inducible genes (Hoshino et al., 2002). In addition, STAT3 and STAT4 have been shown to have regulatory function in TLR induced signalling, which will be discussed further below.

While TLR4 represents the broad TLR family apart from TLR3 in activating the MyD88 pathway in DCs, there are key differences in the downstream events following ligation of each TLR family member. TLR3 uses TRIF as adaptor protein and signals via TRAF3 and via RIP1 as described above for TLR4, it does however not require TRAM (Fitzgerald et al., 2003; Yamamoto et al., 2003a,b). One difference between MyD88 dependent signalling downstream of TLR4 and that downstream of TLR7 and TLR9 is that the latter also signal through TRAF3 to induce the production of type I IFNs, like TLR3. Furthermore, TLR7 and 9 are highly expressed in pDCs; these cells also constitutively express IRF7, which therefore does not have to be induced first via IRF3, contributing to their ability to quickly produce large amounts of type I IFNs. TLR2 has been shown to differ from the other TLRs too, in that its ligation can induce prolonged activation of ERK; the increased levels of activated c-FOS lead to an increased production of IL-10 and therefore a shift towards T_H2 induction (Dillon

et al., 2004). TLR2 is also the only receptor other than TLR4 to be dependent on TIRAP as has been demonstrated using TIRAP deficient mice (Horng et al., 2002; Yamamoto et al., 2002) CD14 has been shown to interact with TLRs other than TLR4 as well, as it has been demonstrated to enhance TLR3 mediated macrophage activation (Lee et al., 2006) as well as that induced by TLR2/6 stimulation (Jiang et al., 2005).

A completely separate pattern recognition pathway that activates DCs ensues following binding of glycosylated products to C-type lectin receptors (CLRs) like dendritic cell-specific intercellular adhesion molecule-3-grabbing non-integrin (DC-SIGN), dectin-1 and dectin-2. Binding of Dectin-1 to its ligands leads to the phosphorylation of its cytoplasmatic tail and recruitment of Syk. On the one hand this leads to the recruitment of a number of proteins including Card9, Bcl10 and Malt1, forming a complex that activates the canonical NF-κB signalling pathway described above for MyD88 dependent signalling (i.e. the one involving IKKα, IKKβ and IKKγ) through an unknown mechanism (Gross et al., 2006); on the other hand it activates non-canonical NF-κB signalling (i.e. the pathway involving actication of IKKε and TBK1) as well (Gringhuis et al., 2009). The signalling pathways triggered by dectin-2 ligation are thought to be similar to the ones downstream of dectin-1 (Geijtenbeek and Gringhuis, 2009). Dectin-1 has also been shown to induce NFAT signaling via the same pathway as CD14 (Xu et al., 2009; Zanoni and Granucci, 2012). Activation of both DC-SIGN and dectin-1 also induces the activation of RAF1, which phosphorylates p65, making it a target for acetylation by CBP and p300. The binding of acetylated p65 to IκB is impaired, resulting in prolonged activity of this NF-κB member in a way that increases IL-10 production (Gringhuis et al., 2007, 2009). This is therefore a mechanism to limit inflammation. In addition to this a group of CLRs contain ITIMs and associate with phosphatases; if they are triggered at the same time as activating receptors they modulate cell activation (Geijtenbeek and Gringhuis, 2009).

Two further families of important PRRs are cytoplasmic PRRs: the NOD like receptors (NLRs) and the RIG-I like receptors (RLRs). RLRs are receptors for double stranded RNA and therefore play an important role in immune reactions against viruses (Andrejeva et al., 2004; Yoneyama et al., 2004). They share their role as RNA sensors with TLR7 and TLR9, with pDCs relying on the latter while all other cell types utilize the RLRs (Kato et al., 2005). Two RLRs are known that are able to bind to ligands, RIG-I and MDA5, both of which need IPS-1, a third RLR that is unable to bind RNAs, for signalling. They signal through TBK1 and IKKε to activate IRF3 and induce type I IFN production. In addition, they have been reported to activate a complex containing TRAF6 and RIP1 which leads to NF-κB activation (Kawai et al., 2005; Lee and Kim, 2007).

NLRs on the other hand recognise a variety of PAMPs and DAMPs and are

subdivided into several families. Among the members of the NOD subfamily are NOD1 and 2, which bind peptidoglycan fragments (Lee and Kim, 2007); they activate RIP2 which leads to NF-κB activation, probably via IKKγ, TAK1 and TRAF6 amongst others (Abbott et al., 2004). There also are reports of NOD1 leading to activation of the MAPK JNK (Girardin et al., 2001), while NOD2 has been shown to activate p38 and ERK instead (Kobayashi et al., 2005). The other subfamilies are important components of the so called inflammasomes. These react to numerous different molecules including PAMPs and DAMPs and mediate the proteolytic cleavage and therefore activation of IL-1 and IL-18. Mutations in NLRs have been reported to cause a number of autoimmune diseases, showing their important role in regulating immune responses (Hammer and Ma, 2013).

All of these signalling pathways lead to the activation of numerous transcription factors and the induction of expression of the proteins that mark DC maturation, in particular cytokines and costimulatory molecules. One of the genes whose expression is upregulated in LPS stimulated DCs is IL-12, the cytokine inducing the shift to T_H1 cells in $CD4^+$ T cells (Brunda, 1994; Schoenhaut et al., 1992; Trinchieri et al., 1992). The two subunits IL-12p35 and IL-12p40 form the active heterodimer IL-12p70 and their expression is regulated by a number of transcription factors. Involved are for example NF-κB (Murphy et al., 1995) and AP-1 (Ma et al., 2004), as well as IRF3 (Goriely et al., 2006), IRF1 (Negishi et al., 2006) and 8 (Zhu et al., 2003), STAT1 (Gautier et al., 2005) and NFAT (Elloumi et al., 2012).

1.3.2 Metabolism

With this increase in the production of new proteins, the metabolism of DCs is under pressure to provide both energy and metabolic intermediates. This results in a drastic change in DC metabolism (see Fig. 1.7 and 1.8 for an overview over the cell's energy metabolism and its change in DC activation, taken from Pearce and Everts, 2015).

Resting DCs, while using glycolysis to some extent, rely mostly on β-oxidation of fatty acids followed by oxidative phosphorylation (OXPHOS) to meet their energy demands (Fig. 1.7). Upon stimulation, the activation of the non-canonical IKKs TBK1 and IKKε leads to phosphorylation and therefore activation of Akt, which in turn increases the activity of the hexokinase 2 and more generally, glycolysis. This leads to an increase in pyruvate and therefore more acetyl-CoA that can be fed into the TCA cycle, which means the cells can spare intermediates of the TCA cycle, specifically citrate, for other purposes. Indeed, citrate is exported from the mitochondria again and converted back to acetyl-CoA, which is used to increase de novo fatty acid synthesis. To provide the necessary NADPH for this process, the activity of the

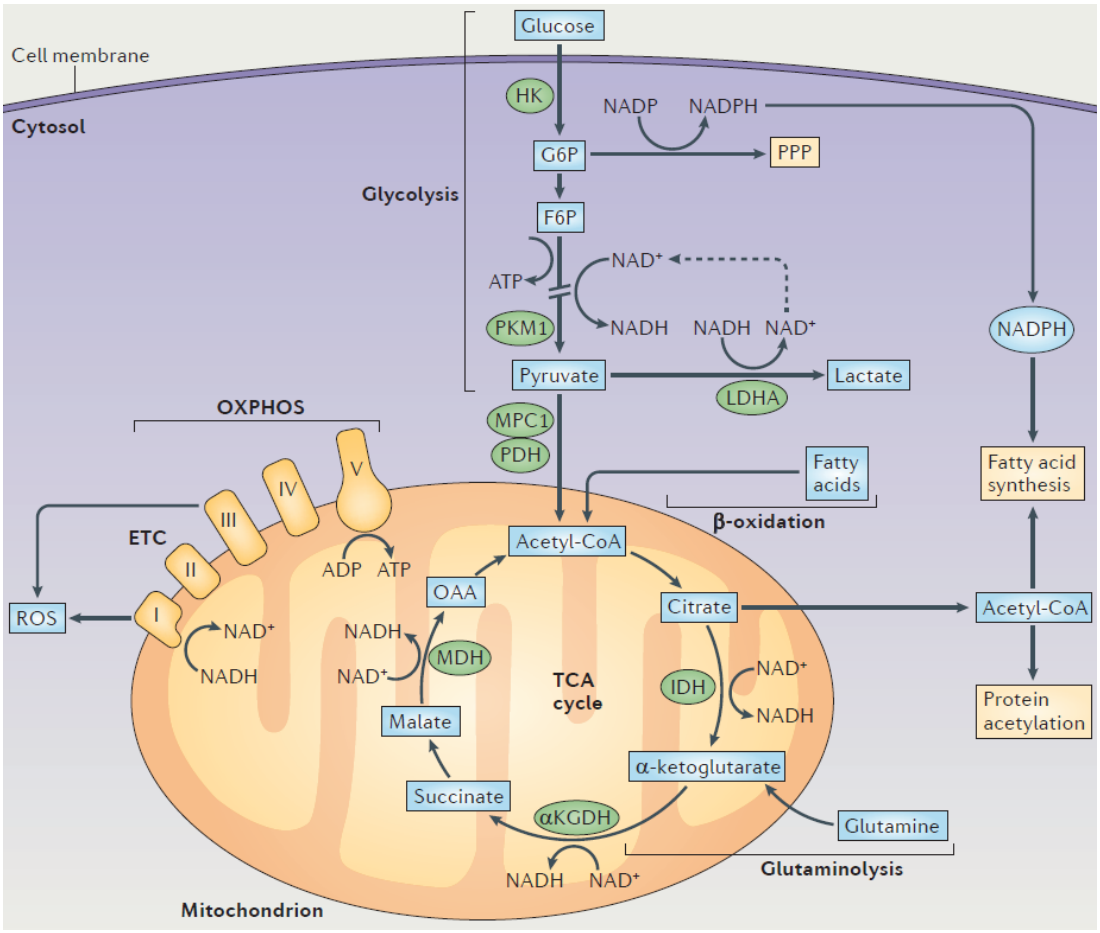

Figure 1.7: Cellular energy metabolism. Glucose is imported into the cell cytoplasm and phosphorylated to glucose-6-phosphate (G6P) by the enzyme hexokinase (HK). G6P can either be further used for glycolysis to generate pyruvate and ATP or used to generate NADPH in the pentose phosphate pathway (PPP). Pyruvate can either be converted to lactate by lactate dehydrogenase (LDHA) to regenerate NAD^+, or transported into the mitochondria to be converted into acetyl-CoA by the pyruvate dehydrogenase (PDH) and used in the tricarboxylic acid (TCA) cycle. Acetyl-CoA can also be provided by fatty acid β-oxidation. The TCA cycle on the one hand provides NADH that can be used as substrate in the electron transport chain (ETC) to ultimately produce ATP by oxidative phosphorylation (OXPHOS), which requires oxygen and leads to the production of reactive oxygen species (ROS). On the other hand, the produced citrate can be exported from the mitochondria into the cytoplasm, converted back into acetyl-CoA and used for the de novo synthesis of fatty acids. Figure taken from Pearce and Everts, 2015.

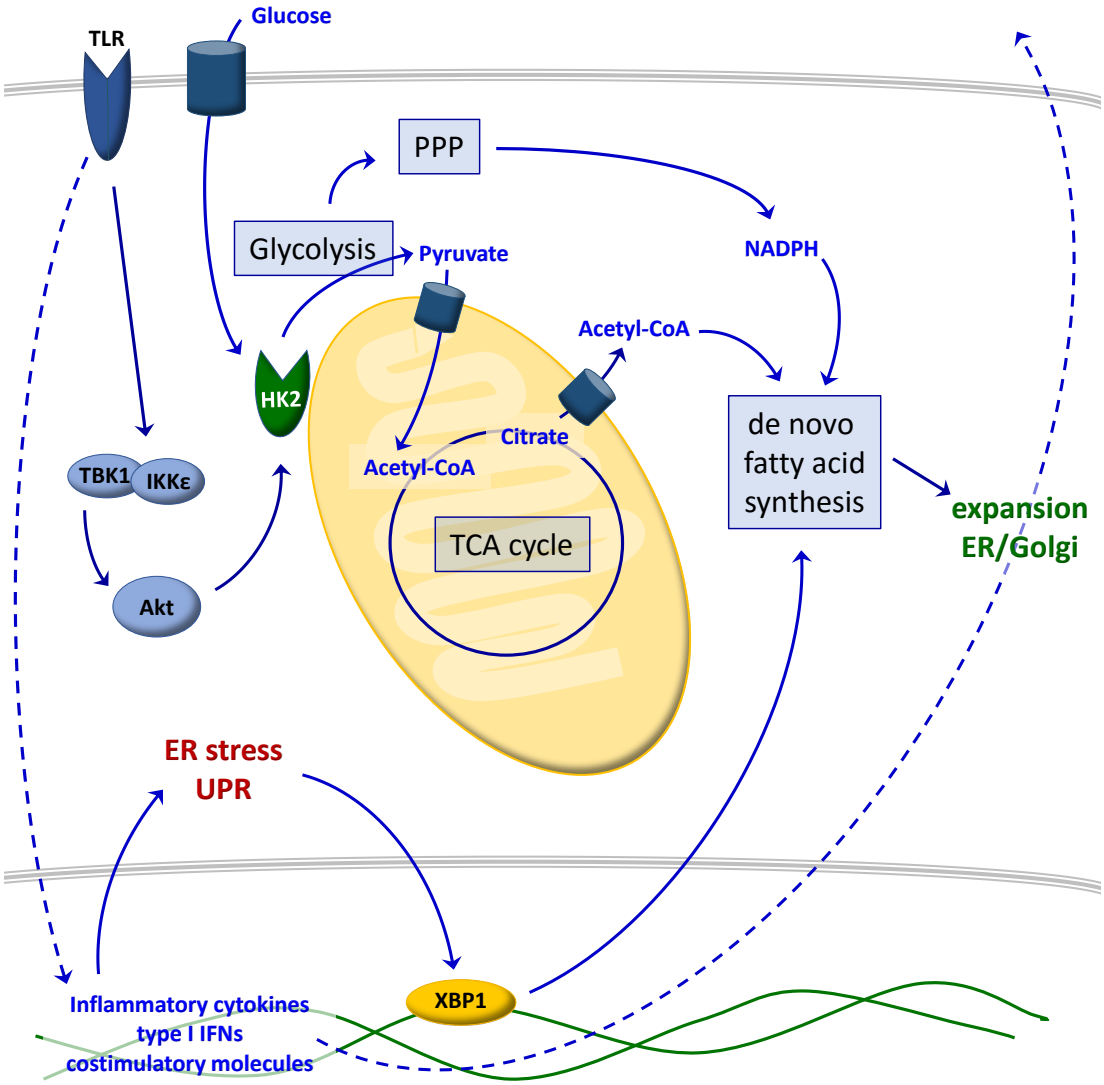

Figure 1.8: Toll-like receptor signalling integrates endoplasmic reticulum stress and changes in metabolism to support activation. Upon TLR ligation, DCs start to produce a large amount of proteins destined for secretion or expression on the cell surface. This leads to ER stress and an increased unfolded protein response (UPR), which activates the transcription factor XBP1. XBP1 in turn induces transcription of fatty acid synthesis enzymes. Signalling induced by TLR ligation also leads to activation of the non-canonical IKKs TBK1 and IKKε and activation of Akt, which increases the activity of the hexokinase 2 (HK2), thereby increasing glycolytic flux. On the one hand that provides the pentose phosphate pathway (PPP) with more substrate to generate NADPH, on the other hand more pyruvate can be fed into the TCA cycle; an increased amount of citrate can therefore be exported from the mitochondria for de novo fatty acid synthesis. This increased synthesis of fatty acids allows expansion of ER and Golgi apparatus, which can now support the increased production and secretion of DC effector molecules. Figure adapted from Pearce and Everts, 2015.

pentose phosphate pathway is increased as well. Another factor driving the increase in de novo fatty acid production is ER stress. When DCs get activated, their ER and Golgi are overwhelmed by the increase in protein production, leading to an increase in misfolded proteins and the induction of the unfolded protein response (UPR). This in turn activates XBP1, a transcription factor inducing expression of fatty acid synthesis proteins. The result of these changes in metabolism is an increase in the size of the cell's ER and Golgi apparatus, which can now support the increased protein production. If any step in this process is interfered with, for example by providing 2-deoxy-D-glucose (2-DG) which can not be used for glycolysis, by impeding the transport of pyruvate into the mitochondrion for use in the TCA cycle, or by inhibiting fatty acid synthesis, production of costimulatory molecules and pro-inflammatory cytokines is impaired even though their mRNA levels remain the same as in untreated stimulated cells (Everts et al., 2014).

Later during stimulation, the NO produced by the cells inhibits the electron transport chain, so that OXPHOS is no longer possible (Everts et al., 2012b). This forces the cells to adopt a different means to generate ATP and leads to their commitment to aerobic glycolysis. Expression of glycolytic enzymes is increased in these cells, as is their glucose consumption and their production of lactate, as the conversion of pyruvate to lactate is used to regenerate NAD^+ for further ATP generation through glycolysis; β-oxidation of fatty acids and O_2 consumption are reduced. Again, interference with this process, for example by adding 2-DG instead of glucose, inhibits DC maturation, demonstrating the reliance of the cells on glycolysis. This switch to aerobic glycolysis is dependent on PI3K signalling via Akt (Krawczyk et al., 2010). The mammalian target of rapamycin (mTOR) is a downstream target of these signalling molecules, and in turn induces hypoxia inducible factor-1 which increases expression of glycolysis enzymes (Pearce and Everts, 2015).

In contrast to inflammatory DCs, tolerogenic DCs have been reported to express higher levels of OXPHOS proteins; Everts and Pearce hypothesized that if any parallels can be drawn between alternatively activated macrophages (AAMs) and DCs then it is likely that tolerogenic DCs, just like AAMs rely on β-oxidation of fatty acids and OXPHOS rather than the aerobic glycolysis of their classically activated counterparts (Everts and Pearce, 2014).

1.3.3 Mechanisms to control DC activation

Considering the dangers of an over-active immune response, as indeed seen in many autoimmune conditions, in allergies or in a number of diseases where the pathology stems from the body's reaction to the pathogen rather than the pathogen

itself, it comes as no surprise that there are numerous mechanisms in place to regulate immune responses. For TLR signalling specifically, many regulators have been identified which suppress activation or terminate the cell's response or even to fine tune it. These regulators act on components of each different stage of the DC activation process described above, interfering with PRR ligand binding, modulating signalling pathways or transcription initiation, and inhibiting the expression of specific inflammatory mediators.

1.3.3.1 TLRs and ligand binding

First described in macrophages and for TLR4 (Iwami et al., 2000), splice variants of TLRs exist that are secreted by cells and compete with cell surface TLRs for their ligands. In that study, the production of soluble TLR4 was induced by LPS and inhibited LPS induced production of TNF and NF-κB activation, indicating this is - at least in macrophages - a physiological negative feedback regulator for LPS activated cells. In human cells, a splice variant for the MD-2 protein which co-complexes with CD14 and TLR4 has been described. This shorter form competes with the full length MD-2 for binding to TLR4, and while it binds both the receptor and LPS, it does not induce signalling (Gray et al., 2010).

In addition, levels of surface TLR4 are finely regulated. In macrophages, Rab7b has been identified to promote lysosomal degradation of TLR4, thereby attenuating LPS induced response pathways and production of pro-inflammatory cytokines (Wang et al., 2007). Rab7b, which also promotes degradation of TLR9 (Yao et al., 2009), is now known to be expressed and promote TLR4 degradation in DCs too (Klaver et al., 2015a).

1.3.3.2 Interference with induction of signalling

A significant range of inhibitory factors act to interfere with the binding of adaptor proteins to TLRs. The TLR4-binding protein TIRAP for example, once phosphorylated, is targeted by suppressor of cytokine signalling (SOCS)-1 leading to its ubiquitination and proteasomal degradation (Mansell et al., 2006). TRAM is another protein with a splice variant, TAG; this variant competes with TRAM for binding of TRIF which as a consequence is not recruited to TLR4 (Palsson-McDermott et al., 2009). Another inhibitory protein interacting with TRIF and probably also MyD88 is Sterile α and Armadillo-motif-containing protein (SARM), which inhibits activation of signalling cascades downstream of TLR3 and TLR4 (Carty et al., 2006; Peng et al., 2010). Calcineurin and calmodulin, components of the NFAT signalling pathway described above, have been reported to inhibit TLR mediated signalling;

calcineurin has been demonstrated to be associated with MyD88, TRIF, TLR2 and TLR4, but the exact mechanism of this inhibition is not yet known (Kang et al., 2007). A protein identified due to its interaction with TRIF is a disintegrin and metalloprotease (ADAM)-15, which inhibits TRIF signalling by mediating its proteolytic cleavage (Ahmed et al., 2013). TRIM38 has only recently been shown to induce proteasomal degradation of TRIF (Hu et al., 2015).

Several factors are known that interfere with MyD88 binding of downstream signalling components. MyD88 itself is another protein with a dominant negative splice variant, MyD88s, which is inducible by LPS in monocytes (Janssens et al., 2002). It lacks the domain necessary for recruitment of IRAK4 to the so called myddosome, the MyD88-dependent signalling complex formed after TLR4 ligation, so while it still recruits IRAK1, this kinase is not phosphorylated (Burns et al., 2003). This results in an inhibition of NF-κB, but not MAPK signalling (Janssens et al., 2003). Another protein interacting with MyD88 is IRF5; this binding is competitively inhibited by IRF4, which is induced by TLR ligation (Negishi et al., 2005).

1.3.3.3 Inhibition of the downstream signalling cascade

Not only the initiation of activation is subject to strict regulation, but also the progression of signalling through the complex pathways described above is carefully controlled.

An additional IRAK family member, IRAK-M is for example induced by TLR stimulation and inhibits both the phosphorylation and the dissociation of the activating IRAKs from MyD88, thus impairing pro-inflammatory signalling (Kobayashi et al., 2002). IRAK2 as well has been shown to have two inhibitory splice variants, which lack domains important for their functions (Hardy and O'Neill, 2004). Another protein inhibiting IRAK is Tollip, which associates with both TLR2 and TLR4 and is a substrate of IRAK itself (Zhang and Ghosh, 2002). The phosphatase SHP-1 on the other hand directly binds to IRAK1 and inhibits its activation (An et al., 2008).

TRAF6, as an important signalling molecule shared by both MyD88 and TRIF dependent pathways in TLR4 signalling, is the target of a number of inhibitors. One of these is A20, which inhibits TRAF6 - as well as RIP1 and TRAF2 - by removing their activating poly-ubiquitin chains (Heyninck and Beyaert, 1999; Turer et al., 2008; Wertz et al., 2004). TAX1BP1 has been demonstrated to be necessary to recruit A20 to both TRAF6 and RIP1 (Iha et al., 2008), as well as to proteins interacting with and activating TRAF6 like Ubc13 (Shembade et al., 2010). The transcription of this protein is negatively regulated by STAT3, thus limiting TRAF6 activation (Zhang et al., 2014). In addition, NLR3 limits the activating poly-ubiquitination of TRAF6 (Schneider et

al., 2012), as do β-arrestin (Wang et al., 2006), TANK (Kawagoe et al., 2009) and the nuclear receptor SHP (Yuk et al., 2011). Another protein demonstrated to be able to remove poly-ubiquitin chains from TRAF6, as well as TRAF2, was USP4 (Xiao et al., 2012; Zhou et al., 2012). TRAF3 too is regulated by deubiquitination, as DUBA has been reported to bind ubiquitinated TRAF3, removing the poly-ubiquitin chain and therefore inducing the dissociation from TBK1 and limiting type I IFN production (Kayagaki et al., 2007). In TLR2 stimulated cells the expression of CYLD was induced, which subsequently inhibited both TRAF6 and TRAF7 activation, probably by deubiquitination as well (Yoshida et al., 2005a). SOCS-3 has been shown to inhibit poly-ubiquitination of TRAF6 too, which specifically impairs the activation of TAK1 (Frobøse et al., 2006). SOCS-2 on the other hand induces poly-ubiquitination and proteasomal degradation of TRAF6 (McBerry et al., 2012). This mechanism is also used by the negative feedback regulator TRIM38 (Zhao et al., 2012).

As demonstrated in TNF or IL-1 treated cells, TRIM38 additionally mediates ubiquitin independent lysosomal degradation of TAB2 and TAB3, thereby inhibiting TAK1 activity (Hu et al., 2014; Hu et al., 2015); TRIM30α likewise induces lysosomal TAB2/3 degradation (Shi et al., 2008).

The kinase PDK1 that is activated by the PI3K product PIP_3 as described above, has recently been shown to interact with TAK1, inhibiting the formation of the TRAF6/TAK1/TAB complex and poly-ubiquitination and therefore activation of its components (Moon et al., 2015).

Deubiquitination of proteins downstream of TRAF6 also plays an important role in signalling regulation; USP4 has been shown to deubiquitinate and therefore inactivate TAK1 in addition to TRAF6 and 2 (Fan et al., 2011).

The A20 interacting proteins ABIN1, 2 and 3, recognize poly-ubiquitin chains in IKKγ; ABIN-1 has been shown to be necessary for recruitment of A20 to IKKγ, which is followed by its deubiquitination and therefore inhibition of NF-κB activation (Mauro et al., 2006). In addition, the ABIN proteins and A20 can also inhibit NF-κB activation independently from any deubiquitinating activity, as they can compete with activating proteins for their binding to IKKs (Heyninck et al., 2003; Skaug et al., 2011; Verstrepen et al., 2009; Wagner et al., 2008; Wullaert et al., 2007). TBK1 is regulated as well, as association of SHP-2 with this kinase blocks its activation and TRIF dependent cytokine production (An et al., 2006).

Components of the MAPK cascade are subject to a number of specific regulatory mechanisms. The PI3K pathway component Akt for example has been shown to target the MAP kinase kinase kinase apoptosis signal-regulating kinase 1 (ASK1), impairing its activation of the JNK and p38 cascades (Kim et al., 2001). Dual specificity phosphatases are a family of proteins that are very important in the

dephosphorylation of MAPKs. For example the MAPK phosphatase MKP-1 (also known as DUSP1), is rapidly induced after LPS stimulation, and terminates activation of p38 and JNK by dephosphorylating these kinases (Chi et al., 2006; Zhao et al., 2005, 2006). DUSP2 is also inducible by LPS, but targets ERK and p38 rather than JNK in vitro (Jeffrey et al., 2006; Zhang et al., 2005). A number of additional DUSPs exist that target one or more of the MAPKs, although most are not inducible by stimulation (for a review see Patterson et al., 2009). The activation of ERK is regulated by Dok1 and Dok2 as well; these are activated by phosphorylation after LPS stimulation to limit the activation of ERK and subsequent production of inflammatory mediators by macrophages (Shinohara et al., 2005).

1.3.3.4 Inhibition of transcription factor activation or activity

No less important targets of cellular inhibition have been found to be the transcription factors themselves.

The activation of the NF-κB member c-Rel for example is inhibited upon binding of activated STAT3, which impairs its nuclear translocation (Nefedova et al., 2005). Tristetraprolin (TTP) is another protein that impairs nuclear translocation of c-Rel, in addition to p65 (Gu et al., 2013). Furthermore, the termination of NF-κB activity is important as well. IκBNS for example has been described as an IκB protein that is induced after LPS stimulation and binds to nuclear NF-κB, terminating NF-κB activation (Kuwata et al., 2006) and the ubiquitin ligase PDLIM2 terminates p65 activity by inducing its proteasomal degradation (Tanaka et al., 2007). The latter mechanism also requires HSP-70, as this protein surprisingly translocates to the nucleus, binds to complexes containing p65 and PDLIM2 and promotes their transport to the proteasome (Tanaka et al., 2014).

IRF proteins are subject to regulation as well. As mentioned before, the activation of IRF5 is inhibited by IRF4. IRF4 has also been described to compete with IRF1 for binding to promoter regions, but in contrast to the activating IRF1 it represses target gene transcription of pro-inflammatory factors (Yoshida et al., 2005b); on the other hand it induces transcription of IL-10 and IL-33, which promotes T_H2 differentiation (Williams et al., 2013). Activation of IRF3 and IRF7 is limited by their regulation through the ubiquitin ligase RAUL, which initiates their proteasomal degradation and therefore termination of the signal (Yu and Hayward, 2010). Phosphorylated IRF3 is additionally recognized by another ubiquitin ligase, Pin1 (Saitoh et al., 2006).

Mechanisms involving epigenetic regulation of gene transcription are receiving increasing attention. On the one hand, epigenetic mechanisms are involved in shaping DC responses; DCs deficient in the methyl-CpG-binding domain protein Mbd2 for

example have been shown to be impaired in their ability to induce T_H2 responses, while the induction of T_H1 responses was unaffected. On the other hand, epigenetic regulation of gene expression has been described to be a mechanism to limit DC activation. The transcription factor ATF3 for example is induced by LPS stimulation; its binding to target genes leads to the recruitment of HDACs, specifically HDAC1, which mediates deacetylation of histones followed by condensation of chromatin. ATF3 binding sites are often closely associated with p65 binding sites in gene promoters, as for example in the promoters for IL-6 and IL-12p40. ATF3 was therefore described as a negative feedback regulator, inhibiting transcription of NF-κB target genes (Gilchrist et al., 2006; Whitmore et al., 2007).

1.3.3.5 Post-transcriptional regulation of target genes and signalling mediators

There are a number of mechanisms at work that regulate the expression of molecules such as pro-inflammatory cytokines or costimulatory molecules after transcription has been induced. Regnase for example has been demonstrated to destabilize a set of mRNAs including the ones for IL-6 and IL-12p40 (Matsushita et al., 2009). The accessibility of surface molecules can be regulated by their internalization. This mechanism has been described for CD40, which is internalized following its ligation. This was dependent on the scaffold protein JNK-associated leucine-zipper protein (JLP), which is expressed upon CD40 ligation (Wang et al., 2013). In addition, protein expression can be regulated by targeting them for degradation. This is for example the case for CD86, which is ubiquitinated by MARCH1, followed by its proteasomal degradation (Baravalle et al., 2011; Corcoran et al., 2011).

More recently it has become clear that microRNAs can very efficiently regulate TLR signalling pathways. Specifically two molecules, miR-155 and miR-223, have been found in DCs to target multiple signalling components (reviewed in O'Neill et al., 2011). Among the targets of miR-223 are for example IKKα (Li et al., 2010) and the transcription factor C/EBPβ (Zhou et al., 2015), while targets of miR-155 include MyD88 (Tang et al., 2010), TAB2 (Ceppi et al., 2009) and IKKε (Tili et al., 2007). O'Neill et al. propose that miRNAs may be just as important as transcription factors in the regulation of gene expression, as they can co-ordinately down-modulate several signalling pathways at the same time and shorten the half-life of transcripts encoding signalling molecules, which therefore could not be replenished once degraded (O'Neill et al., 2011). In addition, miRNAs can also target effector mRNAs. miR-10a and miR-107 were found to be expressed in intestinal DCs; while miR-10a targeted IL-12/IL-23p40 (Wu et al., 2015; Xue et al., 2011), miR-107 restricted the expression of IL-23p19 (Xue et al., 2014).

All these mechanisms are essential to regulate immune responses and avoid damage to the host, but they also present numerous targets that can be exploited by pathogens to evade immune responses. This is discussed further in the next section.

1.3.4 DC modulation by helminths

To evade the immune system of the host, helminths have evolved a spectrum of sophisticated mechanisms to inhibit immune reactions (Maizels et al., 2004; Maizels and Yazdanbakhsh, 2003). To date, most inhibitory pathways have been attributed to secreted proteins, but detailed knowledge of individual immunomodulatory proteins and their mechanisms of action is sparse. Nevertheless, there is now a substantial body of literature describing the modulation of DC maturation not only in the course of helminth infection, but also by treatment of animals or cells with helminth products. These findings are described below for each of the major groups of helminth parasites.

1.3.4.1 Cestodes

A common thread among studies of helminth effects on DCs has been the inhibition of pro-inflammatory responses to TLR ligation. For example, ES of the cestode *Taenia crassiceps* impairs LPS induced DC maturation in susceptible BALB/c mice and in human DCs, inhibiting the upregulation of the costimulatory molecules CD40, CD80 and CD86 and production of the inflammatory cytokines IL-12 and TNF (Reyes et al., 2009; Terrazas et al., 2010; Terrazas et al., 2011). Priming of DO11.10 T cells with ES treated OVA pulsed DCs also impaired production of IFNγ while increasing IL-4 secretion, thereby shifting the response from T_H1 to T_H2 (Terrazas et al., 2010). In human DCs, treatment with TcES induced the production of IL-10 and increased expression of the CLR macrophage galactose/N-acetylgalactosamine-specific C-type lectin (MGL), while it decreased the expression of DC-SIGN (Terrazas et al., 2011). MGL was later shown to be one of the receptors through which TcES acts, in addition to the mannose receptor (MR) and TLR2, to induce phosphorylation of c-RAF and interfere with the LPS induced activation of p65 and p38 (Terrazas et al., 2013).

Members of another cestode genus, *Echinococcus multilocularis* and *E. granulosus*, have been demonstrated to impair TLR ligand induced DC maturation as well. The larvae of these worms form hydatid cyst in the intermediate host (including humans), and cyst proteins have been investigated as potential immunomodulators. Two proteins from cysts formed by *E. granulosus*, AgB and SHF, have been found to alter human DC subsets, giving rise to cells that are less responsive to TLR ligation. These cells, while initially expressing more CD86, show a reduced upregulation of CD80, CD83 and CD86 and produce less IL-12, TNF and IL-6 after

LPS stimulation. Treatment of normally differentiated DCs with these two proteins leads to phosphorylation of IRAK1 and the activation of NF-κB, specifically p65 and p50, and induces them to prime T_H2 responses. This was even true for LPS stimulated DCs, which again showed an impaired upregulation of costimulatory molecules and inflammatory cytokines (Riganò et al., 2007). Later, another study demonstrated that *E. granulosus* ES inhibits the maturation of CpG activated OVA pulsed DCs, which subsequently induced the development of DO11.10 T cells into FoxP3$^+$ Tregs (Wang et al., 2015).

E. multilocularis has also been demonstrated to alter DCs, increasing the number of DCs in the peritoneum of mice following larval infection; these DCs had elevated levels of TGF-β mRNA and expressed lower levels of CD40, CD80 and CD86, although the responsiveness to TLR ligands was not tested in this study. However, it was found that infection decreased the mRNA levels of a number of proteins involved in the expression of MHC II, indicating an impairment of the antigen presentation pathway; in addition, DCs from infected mice were shown to inhibit the proliferation of ConA stimulated T cells (Mejri et al., 2011). A second study investigated the effects of ES from different life cycle stages, and found that ES from the early and intermediate stages (primary cells and metacestodes) was able to suppress LPS induced DC maturation, in addition to inducing apoptosis of BMDC (Nono et al., 2012). So far, no underlying mechanism has been described for these effects.

1.3.4.2 Trematodes

The liver fluke *Fasciola hepatica* has been shown to contain molecules inhibiting DC maturation whether evaluated as tegumental coat antigen (Teg), ES or worm extracts. Teg was demonstrated to inhibit the production of cytokines like IL-12p70, IL-6 and TNF and the upregulation of CD40, CD80 and CD86 after stimulation with various TLR ligands and even post PMA treatment (Falcon et al., 2010; Hamilton et al., 2009). Teg was even able to inhibit DC maturation if given 2.5 hours before or after LPS stimulation. Teg treatment was shown to inhibit the activation of multiple signalling pathways, including their components p65 (Hamilton et al., 2009), p38, ERK and JNK (Vukman et al., 2013). Inhibitor studies mentioned - but not shown - in the earlier study were thought to exclude the MAP kinases as mediators of Teg's effects; more specifically, Vukman et al. found the expression of SOCS-3 to be increased in Teg treated DCs exposed to LPS stimulation. Teg treatment of DCs also alters their ability to prime T cell responses. Hamilton et al. described that Teg suppresses phagocytosis by DCs, and they could show that if Teg treated OVA pulsed DCs were transferred into DO11.10 mice, the cells from the draining lymph nodes produced lower levels of IFNγ

upon restimulation with OVA (Hamilton et al., 2009). Similar results were obtained in another study, coculturing splenocytes with irradiated DCs that had been stimulated with LPS and ES, as ES treatment of the DCs inhibited splenocyte proliferation and IFNγ production. Interestingly, in this study DCs treated with ES were able to induce IL-4, IL-5, IL-10 and TGF-β production on cocultured T cells, indicating the priming of T_H2 and regulatory T cells (Falcon et al., 2010).

In addition, the extracts of adult worms had DC inhibitory activity that was shown to be contained in the fraction containing proteins of less than 10 kDa. A Kunitz type protease inhibitor was then identified in this fraction, and the recombinantly expressed protein shown to partially reproduce the inhibitory function (Falcon et al., 2014). Another study demonstrated the importance of glycoproteins in worm extracts, as oxidation of glycans partially inhibited LPS induced DC maturation (Rodriguez et al., 2015). The requirement for specific glycosylation patterns could potentially explain the less distinct inhibition of LPS induced DC activation by the recombinant Kunitz type protease compared to total worm extracts that was found in the first study.

Worms of the genus *Schistosoma*, the blood flukes, have been well studied, especially the soluble egg antigen from *S. mansoni* (SEA) that has proved to be an archetypal Type 2-inducing stimulus which can drive the differentiation of T cells into T_H2 cells (MacDonald et al., 2002). In part, this may be due to its route of uptake and subsequent compartmentalization within DCs, which differs from that associated with Type 1 driving antigens such as the bacterial *Proprionobacter acnes* (Pa); DCs copulsed with SEA and Pa could even induce distinct Pa specific T_H1 and SEA specific T_H2 responses, provided the concentration of Pa was not too high (Cervi and MacDonald, 2004). While Pa was taken up via clathrin mediated endocytosis and localized in LAMP2$^+$ lysosomes in this study, SEA was later demonstrated to be bound by CLRs, specifically DC-SIGN, MGL and MR and trafficked through early endosomal compartments to LAMP-1$^+$ lysosomes, where it colocalized with MHC II (van Liempt et al., 2007).

Three distinct DC2-inducing molecules within SEA have so far been described. The first, glycan lacto-N-fucopentaose III (LNFPIII), has been shown to induce T_H2 differentiation via DC2s, inducing ERK phosphorylation via TLR4. Its fucose group has been shown to be crucial for this function (Thomas et al., 2003). Subsequently, the signalling induced by LNFPIII was compared to that induced by LPS, and it was found that while LPS induced persisting NF-κB activation, which was crucial for the production of pro-inflammatory mediators, LNFPIII only induced a transient activation of that transcription factor. This transient activation was not accompanied by a degradation of IκB, but a rapid accumulation of p50 indicated the induction of p105 cleavage (Thomas et al., 2005). A second molecule is the schistosome-specific

phosphatidylserine found to act via TLR2 on DCs to induce T_H2 skewing and IL-10 producing regulatory T cells (Van der Kleij et al., 2002)), in contrast to the more general dampening of TLR-mediated responses by SEA discussed below. Thirdly, the glycoprotein ω-1 has been found to be another molecule acting on DCs to induce T_H2 responses (Everts et al., 2009; Steinfelder et al., 2009). The effects of ω-1 include inhibition of LPS induced DC activation, which was not mediated via MyD88 or TRIF (Steinfelder et al., 2009). This glycoprotein was internalized via MR, explaining the necessity of its glycans for its activity on DCs, but then acted as a ribonuclease to degrade RNAs. It was found to generally inhibit protein synthesis by degrading both mRNAs and rRNAs (Everts et al., 2012b).

As mentioned above, SEA inhibits TLR ligand induced DC maturation (Kane et al., 2004; van Liempt et al., 2007). Kane et al. showed that stimulation by various TLR ligands as well as heat killed bacteria was affected, and that while IL-10 was induced by SEA, the inhibition of DC maturation was independent of this cytokine. They also demonstrated that, at least in IL-10 deficient cells, activation of all three MAP kinases as well as NF-κB was inhibited early after stimulation (Kane et al., 2004). Later, they further added that this effect was not mediated via TLR2 or TLR4 and was independent of MyD88 as well (Kane et al., 2008).

A different picture emerged from studies of Correale et al. in peripheral blood DCs and moDCs of human multiple sclerosis patients, in which the inhibition of LPS-induced upregulation of costimulatory molecules by SEA was MyD88 independent, but siRNA induced knockdown of MyD88 showed that suppression of cytokine secretion by SEA was dependent on this signalling mediator. Both effects were mediated by TLR2 signalling as demonstrated by knockdown of this receptor, and SEA was found to induce ERK activation in this study, which induced the expression of IL-10 (Correale and Farez, 2009). IL-10 was shown to be crucial for the induction of regulatory T cells; in addition, SEA was found to induce retinoic acid production on DCs. This metabolite was found to synergize with SEA - in a TLR2 dependent manner - to induce the expression of SOCS-3 in DCs, which was necessary for the inhibition of pro-inflammatory cytokine production (Correale and Farez, 2013). Only recently a study found that glycans in SEA, internalized via MR, induce SOCS-1 and SHP-1 as well (Klaver et al., 2015b); hence several inhibitory proteins (SOCS-1, SOCS-3 and SHP-1) are implicated in the inhibition of DC activation, and each appears to require small molecule or glycan interactions for their activity.

Although less well studied, *Schistosoma haematobium* has also been shown to inhibit DC activation, as myeloid DCs from infected patients secreted less IL-12, IL-6 and TNF after stimulation with R848 and showed a reduced upregulation of CD80 after stimulation with several TLR ligands. Compared to DCs from non-

infected individuals, the ratio of phosphorylated ERK to p38 early after activation was increased in infected patients; the ability of these cells to prime T cell responses was reduced as well (Everts et al., 2010).

1.3.4.3 Filaria

Several reports describe the effects of *Brugia malayi* on DC function. These nematodes infect their host by invading the skin during a vector's blood meal; their infective L3 larvae have been shown to induce migration of Langerhans cells, simultaneously impairing their ability to process and present antigens (Semnani et al., 2004). Microfilariae (Mf), the stage found in the host's blood, were shown to induce apoptosis of DCs, and although they induced the expression of cytokines like TNF and IL-1, they suppressed IL-12 and IL-10 production by DC and inhibited priming of both T_H1 and T_H2 responses. These effects were replicated by treatment of DCs with ES, although this was slightly less potent (Semnani et al., 2003). The induction of apoptosis in DCs was later shown to be mediated by the increased TNF as well as an increase in expression of TRAIL; Mf induced the expression and cleavage of BH3-interacting domain death agonist (Bid), leading to cytochrome c release from the mitochondria followed by caspase 9 activation, resulting in apoptosis (Semnani et al., 2008b). The relevance of this mechanism in vivo is unclear however, as it was found that the number of circulating DCs is actually increased in *Brugia* infected patients (Semnani et al., 2010). In addition, Mf have been shown to inhibit the activation of DCs by both LPS and poly(I:C). Semnani et al. found that treatment of DCs with live Mf reduced the mRNA levels of MyD88 and impaired the activation of NF-κB, specifically p65. Furthermore, the expression of SOCS-3 was induced by Mf (Semnani et al., 2008a). Moreover, DCs from filaria infected humans showed reduced expression of IL-12 as well as several chemokines in response to malaria antigens, while again demonstrating the increased expression of TNF, but also IL-1, IL-6 and IL-10. The expression of the transcription factors IRF1, IRF2 and IRF3 was reduced by Mf as well, and knockdown of IRF1 with siRNA could reduce the expression of IL-12p35 (Metenou et al., 2012).

The ES of another filarial nematode, *Acanthocheilonema viteae*, has been shown to predominantly contain one phosphorylcholine (PC) containing protein, ES-62 (Harnett et al., 1989). This protein has, since its discovery, been demonstrated to affect various immune cells, amongst others also DCs (reviewed in Al-Riyami and Harnett, 2012). While DCs primed with ES-62 showed a low level of activation and prime T_H2 responses, subsequent stimulation with LPS failed to activate them further (Goodridge et al., 2004; Whelan et al., 2000). The effect of ES-62 was shown to be

dependent on TLR4 and MyD88 (Goodridge et al., 2005b), and could be replicated by using a PC-Ova conjugate; the contribution of the protein component could not be ascertained, as the lack of the PC moiety altered its conformation (Goodridge et al., 2007). In this study, while ES-62 or PC-Ova alone did not induce the activation of ERK or p38, they inhibited Akt phosphorylation. The effects of ES-62 in LPS induced signalling have been investigated in more detail in macrophages, where LPS+IFNγ induced activation of p38 and JNK was inhibited by ES-62, while ERK phosphorylation was increased (Goodridge et al., 2005a; Goodridge et al., 2003).

1.3.4.4 *Trichinella spiralis*

The ES from muscle encysted *Trichinella spiralis* has been demonstrated to inhibit LPS induced DC activation as well, although it has been shown that this is specific for TLR4 ligation and not all forms of LPS (Aranzamendi et al., 2012; Kuijk et al., 2012; Langelaar et al., 2009). TspES has also been demonstrated to suppress the expression of a number of components of the signalling pathways induced by TLR4, including transcription factors like NF-κB and IRF1; this has been hypothesized to be responsible for the inhibition but the specific mechanism has not been identified yet (Aranzamendi et al., 2012).

1.3.4.5 Soil transmitted helminths

A number of soil transmitted nematodes that parasitise the gastrointestinal tract have been investigated for their ability to modulate DC responses; these include two of the most prevalent taxa of human parasite, Ascaris and Trichuris, as well as model rodent species..

Both *Ascaris lumbricoides* (a parasite of humans) and *Ascaris suum* (of swine) have been demonstrated to contain molecules affecting TLR induced DC activation. Adult parasites are sufficiently large to make it possible to isolate pseudocoelomic fluid (PCF) from the body of the worm. While *A. lumbricoides* PCF alone did induce production of IL-6 and IL-12p40 in murine BMDC, the cells did not increase their expression of costimulatory molecules; the production of IL-6 and IL-12p40 was inhibited by treatment with the MEK1/2 inhibitor U0126, indicating an involvement of ERK. In LPS stimulated cells, pre-treatment with PCF inhibited IL-12p70 production but did not affect IL-6 or IL-12p40 levels (Dowling et al., 2011). Pretreatment with PCF from *A. suum* similarly inhibited IL-12 production by LPS stimulated BMDC, in addition to their upregulation of CD40 and CD86 (McConchie et al., 2006). The high-molecular-weight components of these worms were shown to inhibit the activation of $CD11c^+$ LN cells in mice immunized with OVA, and inhibit T cell priming in an

IL-10 dependent mechanism (Silva et al., 2006). They were later shown to inhibit the activation of BMDC by LPS, poly(I:C) and Pam3CSK4, and actually reduced the baseline expression of CD40, CD80 and CD86, while at the same time inducing the expression of low levels of IL-6 and IL-10 (Favoretto et al., 2014).

Trichuris suis has been tested in a number of clinical trials of live helminth therapy against diseases such as multiple sclerosis, but also asthma and allergy (Fleming and Weinstock, 2015 and http://www.niaid.nih.gov/topics/tropicaldiseases/Pages/helminthDatabase.aspx, as of 16. March 2016). *T. suis* ES has been shown to protect mice from EAE, and to inhibit LPS induced TNF and IL-12 production in human DCs (Kuijk et al., 2012). In addition, it inhibited the LPS induced production of a number of chemokines. This inhibition was shown to be at least partially due to glycans, probably mannose binding to MR and DC-SIGN (Klaver et al., 2013). Analysing changes in DCs upon treatment with ES in addition to LPS, it was later shown that ES inhibits both MyD88 and TRIF dependent pathways; the mRNA levels of signalling components and transcription factors like MyD88, IRAK2, c-Jun, p65 and IRF8 were lower in ES+LPS compared to LPS treated cells. In addition, ES inhibited the LPS induced phosphorylation of IRAK1. In this study, expression of STAT4 and Rab7b was discovered to be increased by ES. Consistent with the studies described above on Rab7b, it was shown to reduce the surface levels of TLR4 at the later time points after *T. suis* ES administration, thereby contributing to the inhibition of TLR4 signalling. Interestingly, in this study ES was able to inhibit LPS induced DC activation even if it was added some time after the stimulation, with a trend towards inhibition still being evident if it was added four hours later (Klaver et al., 2015a).

One of the more widely-used model nematode species in *Nippostrongylus brasiliensis*, a rat parasite related to the human hookworms. *N. brasiliensis* ES too was shown to induce DCs to prime T_H2 responses, activating them to express elevated levels of OX40L and CD86 as well as IL-6 and IL-12p40, but not CD80 or IL-12p70. In addition, it inhibited LPS induced IL-12p70 production, but did not affect IL-6 secretion (Balic et al., 2004). In vivo, infection with this parasite reduced the number of migratory, lamina-propria derived $CD8^{int}CD11b^{-}$DCs in the draining lymph nodes; after LPS stimulation $CD11c^{+}$ mLN cells from infected mice were slightly impaired in their production of IL-12 and TNF, but again not IL-6 (Balic et al., 2009).

Heligmosomoides polygyrus

As mentioned above, *H. polygyrus* is a much used mouse model for intestinal helminth infections. Its influence on the ability of DCs to activate immune responses was first described in 2005, when it was found that co-infection of mice with *Plasmodium chabaudi* AS and *H. polygyrus* severely exacerbated malaria, with lower

serum levels of IFNγ and elevated TGFβ compared to mice infected with *P. chabaudi* AS alone. Helminth infection was found to impair the ability of splenic DCs to induce proliferation of T cells (Su et al., 2005). Subsequently, the same group showed that ES but not worm extracts inhibited BMDC activation, both in response to LPS and CpG, but not the TLR independent activation induced by PMA. The activation of OVA pulsed BMDC was impaired as well, although uptake and processing of ovalbumin protein was not affected, and upon transfer into DO11.10 mice these HES treated OVA pulsed DCs did not induce OVA specific antibody responses. In in vitro co-cultures, HES treatment of BMDC impaired the production of IFNγ and IL-4 by T cells, but increased IL-10 secretion (Segura et al., 2007).

In addition, in a mouse model of colitis, infection with *H. polygyrus* was shown to protect and reverse disease pathology, with lamina propria DCs of these mice expressing lower levels of CD80 and CD86 as well as secreting less IL-12 (Hang et al., 2010). Subsequently, these DCs were subsequently shown to inhibit the production of IFNγ and IL-17 by T cells, as well as protecting from colitis upon adoptive transfer into mice (Blum et al., 2012).

Furthermore, infection of mice has been shown to alter DC populations in vivo. The loss of the $CD8^{int}CD11b^{-}$population of $CD11c^{+}$ cells in the draining lymph nodes was even more pronounced than in *N. brasiliensis* infected mice (Balic et al., 2009), and a population of $CD11c^{lo}$ DCs was shown to expand upon infection. This population induced Tregs rather than effector T cells, in contrast to the $CD11c^{+}$ DC population, even though the latter expressed lower levels of CD40, CD80 and CD86 in *H. polygyrus* infected mice (Li et al., 2011; Smith et al., 2011). In a follow up study, *H. polygyrus* induced T_H2 responses were abrogated in mice depleted of $CD11c^{+}$ cells and could be induced by adoptive transfer of DCs pulsed with HES (Smith et al., 2012).

The identification of molecular components from H. polygyrus that may interact with DCs has led to analyses of the ES antigens (HES) from this parasite. So far, two proteins have been identified that act on DCs. Calreticulin has been identified in HES, and subsequently shown to induce a T_H2 response upon immunization. It was also shown to be bound by scavenger receptor A on DCs and be internalized by them, although the exact effect calreticulin has on DCs was not investigated (Rzepecka et al., 2009). Another protein contained in HES is cystatin; this protein too was expressed recombinantly and tested on DCs. If DCs were exposed to this protein during their differentiation, subsequent activation by CpG was impaired. This was also the case if DCs were preincubated with cystatin before stimulation; LPS induced DC maturation however was barely affected. Cystatin was shown to be an active protease inhibitor, acting on the cathepsins involved in antigen processing and presentation on MHC II (Sun et al., 2013).

Further and so far unpublished data on the effects of HES on DC activation were collected by John Grainger and Blaise Dayer during their time in the Maizels laboratory.

John Grainger found that, while HES alone did not induce classical activation of DCs, HES pulsed BMDC did induce a HES specific T_H2 response upon transfer into mice, even if the DCs were co-pulsed with Pa. While these cells still induced a Pa specific T_H1 response, demonstrating the intact separation between both pathways, this response was impaired compared to the one induced by BMDC that were pulsed with Pa alone. This induction of a T_H2 response by HES was heat stable, in contrast to the inhibition of LPS or Pa induced DC maturation which he could show was heat labile. This inhibition only lasted for a short period, as if BMDCs were stimulated one day after HES treatment, the inhibitory effect was lost, and even reversed if the cells were stimulated three days post HES treatment. Furthermore, he could show that HES did not impair antigen uptake by DCs (Grainger, 2009).

Blaise Dayer expanded on these findings, again showing a dose dependent inhibition of LPS induced DC maturation that was lost upon heat treatment of HES, but additionally demonstrating that HES could inhibit IL-12p70 production even if it was added up to eight hours after LPS treatment. He also excluded both calreticulin and TGFβ as the inhibitory factors, as recombinant calreticulin did not show any inhibitory function, and inhibition of TGFβ signalling did not abrogate DC modulation by HES. He also performed a size exclusion fractionation of HES, showing that the inhibitory activity of HES could be pinpointed to only a few fractions. Furthermore, he investigated the contribution of several signalling pathways. As described above, signalling through CLRs has been reported to negatively regulate TLR induced DC activation, and several helminths do indeed use this mechanism. This was therefore one option considered, but treating cells with antibodies to block dectin-1 or dectin-2 or using cells from dectin-$1^{-/-}$ mice did not abolish the inhibitory effect of HES. Blocking the activity of Syk, a kinase downstream of a number of CLRs, also had no effect on HES modulation of DC activation. Additionally, he investigated the possibility that HES might utilize the PI3K signalling pathway; cells were therefore treated with a PI3K inhibitor, which also did not impair DC modulation by HES. To investigate if HES induces signalling through TLRs that might lead to the observed effects, something that also has been described in other helminths, cells from mice deficient in MyD88 and TRIF were used. Again, HES was able to inhibit DC maturation, which in double knock out mice was induced by ligation of CD40 (Dayer, 2011).

1.4 Objectives

As described in the previous section, HES has been demonstrated to modulate DC activation, but neither the component responsible for this effect, nor the mechanism through which modulation takes place, is known so far. The aim of this project was to shed light on these questions.

First, a more detailed description of the phenotype of HES treated DCs was established, to be able to better draw comparisons to effects described in different models and to be able to draw conclusions as to the underlying mechanism.

Secondly, the fractionation strategy was refined with the aim to identify the molecule responsible for the inhibition of DC maturation. Both size exclusion fractionation and anion exchange fractionation were used in several combinations, followed by mass spectrometry analysis of the fractions. Proteins contained in the active fractions were identified, the most promising candidates expressed in HEK293 cells and tested on BMDCs.

Thirdly, the work on identifying the mechanism underlying the inhibition of DC maturation by HES was extended. The effect of HES on the two main pathways involved in TLR ligand induced DC activation, NF-κB and MAPK signalling, was investigated, and a timeline of the inhibitory effect of HES established. With this knowledge, a transcriptomics analysis comparing BMDC stimulated with LPS and LPS+HES was performed and interpreted to identify possible causes for the observed effects.

CHAPTER 2

Material and Methods

2.1 Material

Following are lists of buffers and media used (Table 2.1), and antibodies used for flow cytometry, MACS and ELISA (Table 2.2). Reagents are from Sigma if not otherwise specified.

Table 2.1: Buffers and Media in alphabetical order.

Anion exchange elution buffer	20mM Tris-HCl 1M NaCl (Fisher Chemical) in dH_2O pH 8
Anion exchange starting buffer	20mM Tris-HCl in dH_2O pH 8
Carbonate Buffer for ELISA	45.3ml sol. A (8.5g $NaHCO_3$ in 100ml dH_2O) 18.2ml sol. B (10.6g $NaCO_3$ in 100ml dH_2O) 936.5ml dH_2O pH 9.6 10μl 10% sodium azide
cRPMI	500ml RPMI (Gibco) 50ml FCS (Gibco) 5ml L-Glutamine (Gibco) 5ml Penicillin/Streptavidin (Gibco)

Table 2.1: Buffers and Media (continued).

ELISA blocking buffer	TBS 0.05% Tween® 20 10% FCS
ELISA Washing Buffer	5l TBS 2.5ml Tween® 20
FACS buffer	PBS 0.5% BSA
HEK cell growth medium	500ml DMEM 50ml FCS 5ml L-Glutamine 5ml Penicillin/Streptomycin
HEK cell SFM medium	1l serum free medium (Gibco) 10ml L-Glutamine 10ml Penicillin/Streptomycin
HIS binding buffer (8x)	1168.8g NaCl 13.6g Imidazole 126g Tris-HCl fill up to 5l with dH_2O pH 7.9
HIS elution buffer (8x)	58.4g NaCl 136.15g Imidazole 6.3g Tris-HCl fill up to 500ml with dH_2O pH 7.9
HiTrap column charge buffer (8x)	15.52g $NiSO_4$ fill up to 100ml with dH_2O
HiTrap column strip buffer (4x)	14.61g EDTA 14.61g NaCl 1.58g Tris-HCl fill up to 250ml with dH_2O pH 7.9

Table 2.1: Buffers and Media (continued).

MACS-Buffer	500ml PBS 2.5ml BSA 2ml 2mM EDTA
Silver Stain Developing	6.25g Sodium carbonate 0.05ml Formaldehyde (37%) fill up to 250ml with dH_2O
Silver Stain Fixation	100ml Ethanol 25ml Acetic acid fill up to 250ml with dH_2O
Silver Stain Sensitizing	75ml Ethanol 0.5g Sodium thiosulfate 17g Sodium acetate fill up to 250ml with dH_2O
Silver Stain silver reaction reagent	0.1g Silver nitrate 40ml dH_2O
Silver Stain Stop solution	3.65g EDTA $Na_2.2H_2O$ fill up to 250ml with dH_2O
Western Blot blocking buffer	TBS 0.1% Tween® 20 % BSA
Western Blot washing buffer	TBS 0.1% Tween® 20

Table 2.2: Antibodies used for flow cytometry, MACS and ELISA.

Specificity	Flourochrome	Clone	Isotype	Dilution
A20 (TNFAIP3)	AF488	EPR2663 (abcam)	Rabbit IgG	1/200
Arginase 1	PE	(R&D Systems)	Sheep IgG	1/200
B220	PerCP	RA3-6B2 (BioLegend)	Rat IgG2a, κ	1/200
CD11b	Biotin	M1/70 (BioLegend)	Rat IgG2b, κ	1/200
	FITC	M1/70 (BioLegend)	Rat IgG2b, κ	1/200
	PB	M1/70 (BioLegend)	Rat IgG2b, κ	1/200
CD11c	Biotin	N418 (eBioscience)	Hamster IgG	1/200
	eFluor 450	N418 (eBioscience)	Hamster IgG	1/200
	APC	N418 (BioLegend)	Armenian Hamster IgG	1/200
CD24	PE-Cy7	M1/69 (BioLegend)	Rat IgG2b, κ	1/400
CD40	PE	3/23 (BD Biosciences)	Rat IgG2a, κ	1/200
CD80	APC	16-10A1 (Biolegend)	Hamster IgG	1/200
CD86	AF488	GL-1 (BioLegend)	Rat IgG2a, κ	1/200
	BV650	GL-1 (BioLegend)	Rat IgG2a, κ	1/1600 - 1/2000
CD115	APC	AFS98 (eBioscience)	Rat IgG2a, κ	1/200
	Biotin	AFS98 (eBioscience)	Rat IgG2a, κ	1/200
IL-6	-	MP5-20F3 (BD Biosciences)	Rat IgG1	1/250
	Biotin	MP5-32C11 (BD Biosciences)	Rat IgG2a	1/1000
IL-12p40/70	APC	C15.6 (BD Biosciences)	Rat IgG1	1/200
	Biotin	C17.8 (BD Biosciences)	Rat IgG2a	1/1000
IL-12p70	-	(BD Biosciences)		1/125

Table 2.2: Antibodies used for flow cytometry, MACS and ELISA (continued).

Specificity	Flourochrome	Clone	Isotype	Dilution
MHC II (I-A/I-E)	PerCP	M5/114.15.2 (Biolegend)	Rat IgG2b, κ	1/400
	APC-Cy7	M5/114.15.2 (Biolegend)	Rat IgG2b, κ	1/1600
OX40L	PE-Cy7	RM134L (BioLegend)	Rat IgG2b, κ	1/100
pERK (Thr202/Tyr204)	-	D13.14.4E (Cell Signaling Technology)	Rabbit IgG	1/400
pIκBa (S32/S36)	eF660	RILYB3R (eBioscience)	Mouse IgG2b	1/20
pJNK (T183/Y185)	-	81E11 (Cell Signaling Technology)	Rabbit IgG	1/400
pp38 (T180/Y182)	-	D3F9 (Cell Signaling Technology)	Rabbit IgG	1/400
Relmα	-	(PeproTech)	Rabbit IgG	1/100
Streptavidin	PerCP	(BD)	-	1/200
	PE-Cy7	(BioLegend)	-	1/200
TNF	-	TN3-19 (eBioscience)	Hamster IgG	1/250
	Biotin	Polyclonal (eBioscience)	Rabbit IgG	1/250
Zenon AF488 rabbit IgG labeling reagent	AF488	(life technologies)	-	1/200

2.2 Methods

2.2.1 Animals

For this work both male and female C57BL/6 mice and Balb/c mice aged 6-8 weeks were used; these were bred in-house.

2.2.2 Cell isolation and culture

2.2.2.1 Bone marrow derived dendritic cells

Extraction and culture
Bone marrow was extracted from femurs and tibiae of the hind legs, homogenised using PBS and a 23ga needle and filtered through a 100μm nylon cell strainer. For generation of GM-CSF BMDCs, cells were then plated at 2x10^6 cells per bacteriological petri dish in 10ml cRPMI plus 20ng/ml GM-CSF (PeproTech) and incubated at 37°Cwith 5% CO_2. A further 10ml medium was added on day 3 and replaced on days 6 and 8 of culture. Non-adherent cells were harvested gently on day 10 and directly used for stimulation or depleted of $CD115^+$ cells by MACS as described below. For generation of FLDC, red blood cells were lysed (Sigma RBC lysis buffer, 5ml, 4min) before resuspension of cells at 1.5x10^6 cells/ml in cRPMI and addition of 200ng/ml Flt3L. They were then incubated in tissue culture flasks for eight days at 37°C, 5% CO_2 and used for stimulation on day 8.

Stimulation
Cells were stimulated in 96, 48 or 24 well plates according to the experiment. Stimulation reagents were used in cRPMI with 5ng/ml instead of 20ng/ml GM-CSF or 50ng/ml instead of 200ng/ml Flt3L as shown in Table 2.3. HES was used at concentrations between 1-20μg/ml as indicated and added before, with or after the stimulation reagents as indicated. The MEK1/2 inhibitor U0126 (Cell Signaling Technology) was used at 10μM, cells were pre-incubated with medium alone, DMSO or U0126 for 60-90min before stimulation. For analysis by flow cytometry, GM-CSF BMDC were used at 2x10^5 cells/well in 200μl/well in 96 well round bottom plates, for RNA extraction at 2x10^6 cells/well in 1ml/well in 24 well plates. The FL-DC were used at 2x10^6 cells/ml in 24 well plates (1ml/well) or 48 well plates (500ml/well).

Table 2.3: Substances used for stimulation of dendritic cells

ligand	amount used	receptor triggered
CpG	10μg/ml	TLR9
LPS	100ng/ml or 1μg/ml	TLR4
Pam3CSK4	100ng/ml	TLR1/2
Poly(I:C)	580μg/ml	TLR3
R848	1μg/ml	TLR7

2.2.2.2 Spleen cell isolation and culture

Extraction
Splenocytes were extracted by mashing spleens through 70 or 100μm nylon cell strainers followed by red blood cell lysis (5ml red blood cell lysis buffer (Sigma), 5min, on ice). To enrich the target population, cells were then MACS sorted for $CD11c^+$ cells as described below.

Stimulation
Splenic $CD11c^+$ cells were stimulated in 24 well plates according to the same protocol as BMDC, without the addition of GM-CSF or FLT3L to the stimulation medium. They were harvested after 18h.

2.2.2.3 Human monocyte derived DCs

PBMC preparation and culture
Apheresis cones were collected from a blood bank, the blood contents extracted in a sterile hood, diluted in PBS and layered over Percoll in 50ml falcon tubes. PBMCs were separated by gradient centrifugation, 40min, 400g at room temperature, the PBMC layer collected in new tubes, washed and cells counted. $CD14^+$ cells were then enriched by MACS as described below. After the MACS sort, $0.5x10^6$/ml were seeded per well in a 24 well plate with 25ng/ml IL-4 and GM-CSF in cRPMI. Cells were incubated at 37°C, 5% CO_2 for six days, with a medium exchange at day three.

Stimulation
On day six, cells were gently aspirated to only collect non-adherent cells and resuspended at 0.5x10^6/ml with half old and half fresh medium (cRPMI); to this mixture another 25ng/ml IL-4 and GM-CSF were added. 500μl of this cell suspension were added per well on a 48 well plate and treated with 100ng/ml LPS and/or 10μg/ml HES. Cells were then incubated at 37°C for 18 hours.

2.2.2.4 MACS

Magnetic activated cell sorting was used for either positive or negative selection of cell populations. For both approaches, a maximum of 10^8 cells/ml in MACS buffer were incubated with a biotinylated primary mAB as appropriate for 20min on ice, before incubation with SA-beads diluted 1/10 in MACS buffer for 15min on ice.MACS® Separation Columns (Miltenyi Biotec) were prepared and used according to the manufacturers instructions, using LD columns and collecting the flow through for negative and LS columns collecting the eluent for positive selection.

2.2.3 Analysis of cytokine production by ELISA

To measure levels of secreted cytokines in culture supernatants, enzyme-linked immunosorbent assay (ELISA) was performed. Nunc plates were coated over night at 4°Cwith 50μl coating buffer and unlabelled mAB as appropriate (see Table 2.2 for concentrations). On day 1, wells were blocked with 150μl ELISA blocking buffer per well for 2 hours at 37°C, followed by incubation with standards and samples over night at 4°C. For TNFα and IL-6 ELISAs of BMDC supernatants, samples were diluted 1/10 in medium. On day 2, ELISA plates were developed by sequential incubations (1h, RT) with biotinylated detection antibodies (concentrations see Table 2.2) and extravidin alkaline phosphatase (1/10000) in 50μl blocking buffer per well, followed by incubation with 100μl SIGMAFAST™ p-Nitrophenyl phosphate Tablets (Sigma) made up according to the manufacturers instructions, until colour development allowed measurement to take place. Between each incubation step, plates were washed 4-6 times using ELISA wash buffer, followed by two washes with distilled water before addition of the pNPP. ELISA plates were then read using an Emax precision microplate reader (Molecular Devices) and concentrations calculated using the SoftMax®Pro software (Molecular Devices).

2.2.4 Analysis of cytokine production by CBA

Concentrations of cytokines secreted by human monocyte derived DCs were measured by CBA (BD Bioscience). In brief, 50µl sample supernatant diluted as appropriate or a mixture of the appropriate standards were incubated for 2h, RT with 50µl each of capture beads and detection beads made up in bead or assay diluent. After washing off unbound beads, cytokine concentrations were measured on a BD FACS Verse.

2.2.5 Analysis of cells by flow cytometry

Flow cytometry was used for analysis of expression of cell surface markers, intracellular proteins or phosphorylation status of cell signalling molecules. If only surface markers were investigated, cells were used fresh; for intracellular stainings cells were fixed as described.

Instruments used for acquisition were the FACS Canto II, LSR II or Fortessa (all BD), and FlowJo (FlowJo, LLC) used for data analysis. The gating strategies used for identification of DCs are shown in Fig. 2.1.

2.2.5.1 Basic staining protocol

Staining was performed in the 96 well plates the cells were stimulated in after collection of supernatants for ELISA. For live/dead stain, cells were washed in PBS prior to staining and then incubated with 200μl/well live/dead® Fixable Aqua Dead Cell Stain (molecular probes, life technologies) diluted 1/1000 in PBS before the blocking step. Otherwise, cells were washed in FACS buffer prior to staining and directly blocked for 10min using rat IgG diluted 1/50 in FACS buffer. Staining was performed using the appropriate antibodies diluted in 20μl/well FACS buffer (see Table 2.2) for 20min at 4°C. If a secondary staining step was necessary cells were washed with FACS buffer and stained with the secondary antibodies or SA diluted in 20μl/well FACS buffer.

2.2.5.2 Fixation

To preserve phosphorylation state, formaldehyde was added directly into the stimulation wells at the appropriate time points for an end concentration of 2% formaldehyde and incubated for 10min, RT. Cells were then pelleted (1500rpm, 5min), formaldehyde removed and the cell pellet resuspended in prewarmed phosflow fix/lyse buffer (BD Bioscience) followed by incubation for 10min at 37°C. After a wash in PBS, cells were washed and then incubated in BD phosflow perm buffer for 15min at

room temperature. Following this fixation and permeabilization, cells were incubated with the extra- and intracellular primary antibodies in perm buffer over night at 4°C. The next day, cells were washed in perm buffer and incubated for 1h, RT with the appropriate secondary antibodies in perm buffer. Following another washing step in perm buffer, cells were resuspended in FACS buffer and acquired.

Staining was performed in 96 well plates.

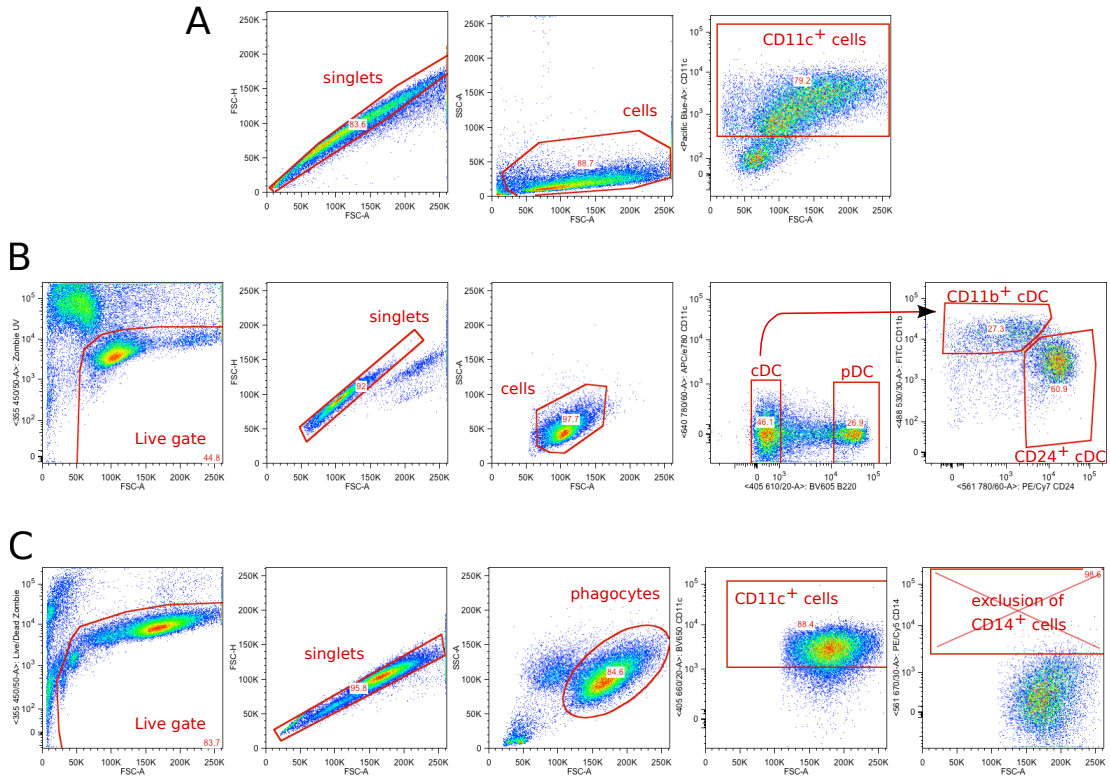

Figure 2.1: Gating strategies used to identify DCs. (A) For GM-CSF BMDC, singlets were gated first, followed by gating the population of live cells. Lastly, $CD11c^+$ cells were selected. **(B)** For FLDC, the first step was the identification of live cells, followed by gating singlets and another step of specifically gating the cell population. Then, cDC and pDC were distinguished by their expression of B220, followed by separation of $CD11b^+$ and $CD24^+$ cells according to (Naik et al., 2005). **(C)** Human PBMC similarly were first gated for live cells, followed by gating of singlets and the phagocyte population. They then were gated for the $CD11c^+$ population, followed by exclusion of $CD14^+$ cells.

2.2.6 Gene expression analysis

2.2.6.1 RNA extraction

RNA was extracted from BMDC stimulated in 24 well plates at various time points after stimulation. After removal of supernatants, cells were resuspended in 1ml Trizol. After transfer into an RNase free 2ml tube, 200μl chloroform was added and samples were vortexed for 15s. Following centrifugation (13000rpm, 15min, 4°C), the aqueous phase was transferred into a new RNase free 1.5ml tube, mixed with 500μl isopropanol, incubated 10min at room temperature and spun down (10min, 13000rpm, 4°C). After washing with 1ml ethanol, pellets were left to dry followed by resuspension in 30μl RNase free water.

For analysis by microarray, RNA was cleaned further using the RNeasy® Mini Kit (Qiagen) instead of resuspension in Water.

2.2.6.2 Reverse transcription of RNA

RNA concentrations were measured using a NanoDrop 2000 (Thermo Scientific) and quality assessed by gel electrophoresis. For the reverse transcription, 1μl oligo-dT Primer was added to 1μg RNA in 16μl RNase free water and incubated for 10min at 70°C, followed by addition of 8μl of master mix (all reagents from Promega). The reaction was performed in a thermocycler with the following program.

MasterMix		Protocol	
5x M-MLV reaction buffer	5μl	42°C	60min
dNTPs	1.25μl	70°C	10min
RNasin ribonuclease inhibitor (40U/μl)	0.75μl	4°C	hold
M-MLV reverse transcriptase (200U/μl)	1μl		

2.2.6.3 Real time PCR

cDNA was diluted 1/5 and a few μl of each sample pooled for use as top standard. Standards were serially diluted 1/5 to obtain six standard concentrations. 2μl of sample or standard and 4μl of master mix (see below) were added to each well. Samples and standards were used in duplicate for each primer; experiments were performed using 384 well plates and the Lightcycler 480 II (Roche).

MASTERMIX	
AgilentSYBR	3μl
ddH_2O	0.4μl
each Primer	0.3μl

2.2.6.4 Microarray

For analysis by microarray, RNA was extracted, its quality ensured, and then transcribed into cDNA as described above. For the preliminary microarray, cDNA was biotinylated using the Illumina® TotalPrep™ RNA Amplification Kit (life technologies) according to the manufacturers instructions. The microarray was then analysed at the Edinburgh Clinical Research Facility, using the MouseWG-6 v2.0 Expression BeadChip (Illumina). Statistical analysis was performed by Dr. Alasdair Ivens.

2.2.7 HES production and fractionation

H. polygyrus and HES were obtained as described in Johnston et al., 2015. In brief, F1 mice were infected orally with 400 L3 larvae and 14 days later adult *H. polygyrus* were harvested, washed and transferred into medium in tissue culture flasks. Twice weekly the medium was exchanged, the old medium collected and subsequently concentrated using an Amicon® system with Ultracel® 3kDa Ultrafiltration discs (Merck Millipore).

2.2.7.1 Fractionations

HES was fractionated using an ÄKTApurifier™ (GE Healthcare) and either the Superdex 200 10/300 GL for size exclusion fractionation or the Mono Q™ 5/50 GL for anion exchange fractionation. Between 500μl and 1ml of HES were directly injected using a sample loop of the appropriate size and the partial filling method. 0.5ml or 1ml fractions were collected in 96 well Masterblock®(greiner bio-one).

For size exclusion fractionation, the buffer used was PBS and the flow rate was 0.5ml/min. For anion exchange fractionation, HES was first dialysed into anion exchange starting buffer. For the first fractionation, the flow rate was 2ml/min and the gradient used was as following:

GRADIENT	LENGTH OF GRADIENT
0-40% anion elution buffer	40 column volumes
40-100% anion elution buffer	5 column volumes
100% anion elution buffer	5 column volumes

For the sequential fractionation of active size exclusion fractions by anion exchange fractionation, the fractions were collected in 0.5ml volumes again with a flow rate of 2ml/min and the following gradient:

GRADIENT	LENGTH OF GRADIENT
0-50% anion elution buffer	12.5 column volumes
50-100% anion elution buffer	5 column volumes
100% anion elution buffer	5 column volumes

For the second anion exchange fractionation of HES the protocol used was the same as for the sequential fractionation anion exchange, but fractions were collected in 1ml volumes.

2.2.7.2 SDS-PAGE and silver stain of HES fractions

To visualize protein content in the first size exclusion and anion exchange fractionations, all fractions were subjected to SDS-PAGE using NuPAGE®4-12% Bis-Tris Gels and NuPAGE®MES SDS Running Buffer (novex®, life technologies), followed by silver staining of the gels. For this, gels were fixed for 1-2 hours, followed by 30min of sensitization. After 3x5min washes with dH_2O the gels were treated with silver nitrate solution for 20min in the dark. After two 1min washes with dH_2O, gels were incubated for 2-5min in the developing solution until the protein bands were clearly visible, at which point the reaction was stopped.

2.2.7.3 Mass spectrometric analysis of HES fractions

Size exclusion fractions 14 and 15 and anion exchange fractions 39 and 40 were first analysed by Suzanne Eadie at the Sir Henry Wellcome Functional Genomics Facility, Institute of Infection, Immunity and Inflammation of the University of Glasgow. All other HES fractions were analysed by Lisa Imrie at Synthsys, University of Edinburgh. 5μg of each fraction were submitted to a trypsin digest, analysed using an Orbitrap mass spectrometer and then compared to an in house *H. polygyrus* transciptomics database (Harcus, manuscript in preparation) using Mascot. The significance threshold for consideration of proteins was p=0.05. In the facility in Glasgow, no minimum cutoff score was set, while in the analysis in Edinburgh, proteins with a score below 20 were not considered.

Scripts written in Python 2.7 were used to analyse the mass spectrometry results.

2.2.8 Cloning and expression of recombinant proteins

2.2.8.1 Cloning of target genes

The coding sequences for the target proteins were extracted from the *H. polygyrus* database, open reading frames identified using the ExPASy Translate tool (http://web.expasy.org/translate/) and signal peptides predicted using SignalP 4.1 software (http://www.cbs.dtu.dk/services/SignalP/). After removal of the signal peptides, sequences were codon optimized for expression in HEK-293 cells, outfitted with restriction sites using the GeneArt GeneOptimizer® tool (ThermoFisher Scientific) and synthesized by GeneArt. Inserts were extracted by restriction digests using AscI and XhoI according to the following protocol at 37°Cover night.

AscI + XhoI digest	
dH_2O	14μl
DNA	10μl
CutSmart Buffer	3μl
restriction enzymes	1.5μl

The expression vector pSecTag2a was digested using the same protocol; digest products were purified using gel electrophoresis and the QIAquick® Gel Extraction Kit, and ligated over night at 4°C. The ligation products were used to transform JM109 cells, followed by selection of positive clones using ampicillin-containing LB agar plates and colony screen PCR using T7 and BGH primers, DNA extraction and sequence verification. Clones containing the verified insert were grown up in 100ml LB medium containing ampicillin and DNA extracted using the QIAfilter™ Plasmid Midi Kit (Qiagen); this DNA was used for transfection of HEK-293 cells.

2.2.8.2 Transfection into HEK-293 cells

One day before transfection, HEK-293 cells were plated out at 8x10^5 cells per 10ml tissue culture dish. Three hours before the transfection, media in the plates was replaced. For each construct, 5 plates of cells were transfected. Per plate, 20μg DNA were mixed with 62μl 2M $CaCl_2$ and brought to a final volume of 500μl with dH_2O. This mixture was added dropwise to 500μl 2x HEPES buffered saline (Sigma) per plate while vortexing gently. After 30min incubation at room temperature, the mixture was vortexed shortly and 1ml added dropwise to each plate. Cells were then incubated at 37°Cfor one day before washing them twice and replacing the medium with fresh HEK cell medium. On day three after the transfection, cells were transferred into

tissue culture flasks with selection medium (HEK cell medium containing 100μg/ml Zeocin™ (invitrogen)). Selection for cells that were successfully transfected was performed for three to four weeks, with biweekly medium exchange, after which cells were used in serum free medium to produce recombinant proteins for purification.

2.2.8.3 Purification of recombinant proteins

Supernatants of stably transfected cells in serum free medium were collected, filtered using Thermo Scientific™ Nalgene™ Rapid-Flow™ 75mm Filter Unit (0.2μm) and dialysed into His binding buffer using SnakeSkin® Dialysis Tubing (10kDa MWCO, Thermo Scientific). Dialysed product was loaded onto a 1ml HiTrap™ Chelating HP column (GE Healthcare) using a Minipuls 2 peristaltic pump (Anachem) and then eluted over a gradient from 0-100% His Elution Buffer in 20 column volumes using the ÄKTApurifier™ (GE Healthcare) together with the UNICORN software. 1ml Fractions were collected. Protein content of the fractions was analysed by SDS-PAGE using NuPAGE® 4-12% Bis-Tris Gels and NuPAGE® MES SDS Running Buffer (novex®, life technologies), with one gel being directly stained using InstantBlue™ (expedeon). The other gel was used for western blot transfer onto a nitrocellulose membrane (Bio-Rad), the membrane blocked with 2% BSA in TBSt and protein detected using anti-Penta-His HRP Conjugate (Qiagen). Bands were visualized with a FluorChem™ SP (Alpha Innotech).

Fractions containing recombinant protein and little FCS contamination were pooled and dialysed into PBS using Slide-A-Lyzer Dialysis Cassettes (Thermo Scientific) and protein concentrations determined with a BCA assay (Thermo Scientific) according to the manufacturers instructions. If concentrations were too low, proteins were concentrated using Vivapin® columns (Sartorius).

2.2.9 Software and statistics

Software used for data acquisition and analysis of raw data is mentioned in the respective sections above. Python scripts used for data parsing can be found in Appendix A. Statistical analysis was performed using GraphPad Prism 6. Depending on the data set, multiple t-tests, one or two-way ANOVAs were used, with significance thresholds of: $* : p \leq 0.05$; $** : p \leq 0.01$; $*** : p \leq 0.001$.

CHAPTER 3

Dendritic cell modulation by *Heligmosomoides polygyrus* excretory/secretory products.

ABSTRACT

Dendritic cells (DCs) are the professional antigen-presenting cells responsible for recognition of pathogens and induction of appropriate adaptive immune responses. There are several reports of modulation of DC activation by helminths, including *Heligmosomoides polygyrus*. Here, the phenotype of DCs treated with this nematode's excretory/secretory products (HES) is described. HES is able to suppress secretion of the pro-inflammatory cytokines IL-12p70, TNF and IL-6 and the upregulation of costimulatory molecules in response to various Toll-like receptor (TLR) ligands. Its effect in LPS induced DC activation is heat-labile, dose-dependent and could be observed on both intracellular protein and mRNA levels. In addition, pre-treatment of BMDCs with HES inhibited subsequent LPS-induced activation. Exosomes present in HES were not able to inhibit DC activation, while HES depleted of exosomes was as efficient as total HES. Modulation of alternative activation differed between mouse strains. In BMDCs from BALB/c mice, which are fairly resistant to infection, HES increased the expression of OX40L and arginase 1 independent of stimulation. RELMα production after IL-4 treatment was not impaired in BMDC from these mice, in contrast to BMDC from susceptible C57BL/6 mice. These findings indicate profound changes in the maturation process of DCs upon HES treatment, likely induced by a protein or protein complex, and provide necessary information for the elucidation of both inhibitory molecule and mechanism of action.

3.1 Introduction

Dendritic cells (DCs) are the professional antigen-presenting cells activating and shaping adaptive immune responses. If they encounter pathogens, DCs are activated by pathogen associated molecular patterns (PAMPs) binding to pattern recognition receptors (PRRs) such as the Toll-like receptors (TLRs). This leads to uptake and processing of the antigen, followed by presentation as MHC:peptide complexes to T cells in the draining lymph nodes. This is accompanied by an upregulation of surface molecules like CD40, CD80 and CD86, which are costimulatory molecules needed for activation of T cells. Together with a cytokine response appropriate to the pathogen, this shapes the subsequent T cell response. One example for such cytokines is IL-12p70, which induces T_H1 responses after stimuli such as LPS (reviewed in Pulendran, 2005). There are a number of reports describing the modulatory effects helminth species have on DCs, impacting on this important step in the development of immune reactions to the helminth itself, but also to bystander antigens or co-infections.

One prominent example is omega-1, the ribonuclease responsible for some of the immune modulatory effect of the soluble egg antigens from *Shistosoma mansoni* (SEA). This protein could be shown to induce a T_H2 response upon injection into naive mice, and to inhibit LPS induced upregulation of CD86 and production of IL-12p70 by human monocyte derived DCs. This was dependent on both its glycosylation and its activity as an RNase, as it is bound and internalized by the mannose receptor on moDC and subsequently non-specifically degrades both rRNA and mRNA, effectively inhibiting protein synthesis by DCs (Everts et al., 2012a; Steinfelder et al., 2009). Glycoconjugates play important roles in the immunomodulation exhibited by other parasites as well. Another trematode, *Fasciola hepatica*, contains glycoconjugates in its ES that induce a "semi-mature" state in DCs, reducing their IL-12p40 and IL-6 production and leading to what the authors called a modified T_H2 response, with increased production of IL-4 and IL-10 but reduced secretion of IFNγ (Rodriguez et al., 2015). Glycoproteins also play an important role in immunomodulation by the filarial nematode *Acanthocheilonema viteae*. More specifically, the major component of this parasite's ES is a phosphorylcholine containing protein called ES-62. While inducing low expression of IL-12p40 and TNF in BMDC, it then inhibits any further production of those cytokines after stimulation with LPS. BMDC derived from bone marrow extracted from mice that had received physiological amounts of ES-62 for two weeks via an osmotic pump exhibited the same reduced responsiveness to LPS stimulation and in addition an increased production of IL-10 (Goodridge et al., 2004). In another nematode, *Ascaris suum*, the worm extracts proved to have a regulatory effect on DCs,

as they inhibited TLR ligand induced upregulation of costimulatory molecules and secretion of pro-inflammatory cytokines by BMDC and in vivo lead to low expression of CD40, CD80 and CD86 on lymph node cells of OVA immunized mice (Favoretto et al., 2014). A rodent parasite used as a model organism for hookworm infections, *Nippostrongylus brasiliensis*, has also been shown to secrete products that modulate DC activation. NES induced BMDCs to upregulate CD86 and OX40L and, upon transfer into naive mice, induce a T_H2 response. Furthermore, pre-treatment of BMDC with NES for two hours inhibited subsequent LPS induced IL-12p70 but not IL-6 production (Balic et al., 2004).

It should come as no surprise that *H. polygyrus* has an effect on DC activation as well. Segura et al., 2007 found that BMDCs treated with HES but not those treated with worm extracts showed reduced expression of costimulatory molecules and proinflammatory cytokines after stimulation with CpG and LPS, and that this effect of HES was not detectable in PMA activated BMDC. Furthermore, they could show that BMDC treated with HES inhibited both IL-4 and IFNγ production in co-cultured OT-II cells in the presence of pOVA, but induced the secretion of IL-10. In vivo, HES treated pOVA pulsed DCs lead to reduced antibody responses compared to DCs that were stimulated without HES. That this effect is induced on DCs in vivo by infection with *H. polygyrus* was indicated by findings that DCs in the lamina propria of infected mice showed reduced expression of costimulatory molecules, were less able to induce production of IFNγ and IL-17 upon co-culture with T cells, and had a protective effect in the T cell transfer model of colitis (Blum et al., 2012; Hang et al., 2013, 2010).

These findings of DC modulation by HES have also been corroborated in our laboratory. In his PhD Thesis, John Grainger demonstrated that while HES alone did not induce maturation of BMDCs, it did inhibit both LPS- and *P. acnes* extract (Pa)-induced DC maturation. Upon transfer of BMDC pulsed with HES and Pa, HES inhibited Pa-specific T_H1 responses as measured by secretion of IFNγ by restimulated splenocytes of the recipient mice. Furthermore, he could show in these experiments that BMDC pulsed with HES alone induced HES specific T_H2 responses and that these, in contrast to the heat labile inhibition of DC activation and T_H1 induction, could also be found with heat inactivated HES (Grainger, 2009).

With these findings in mind, characterizing the effects of HES on DCs further was a first step towards identifying both the modulatory molecule and its mechanism of action. Therefore, the effect of HES on the maturation of GM-CSF BMDC from two mouse strains with different levels of susceptibility to infection with *H. polygyrus*, the susceptible C57BL/6 mice and the relatively resistant BALB/c mice induced with various stimuli was investigated.

3.2 Results

3.2.1 HES inhibits activation of BMDC by various TLR ligands.

As there are different reports on the ability of HES to inhibit activation of BMDCs by various TLR ligands, this was the first aspect of DC modulation by HES to be tested. Bone marrow cells from C57BL/6 or BALB/c mice were differentiated with GM-CSF for ten days before stimulation with CpG (TLR9), LPS (TLR4), Pam3CSK4 (TLR1/2), Poly(I:C) (TLR3) and R848 (TLR7/8) for 18h. As can be seen in Fig. 3.1A, IL-12p70 was induced by CpG, LPS, R848 and to a very small extent by Pam3CSK4. In C57BL/6 cells, HES completely inhibited this induction. This was also true for LPS- and Pam3CSK4-induced IL-12p70 in BALB/c DCs, although Pam3CSK4 barely induced measurable levels of this cytokine. IL-12p70 secretion by CpG- or R848-stimulated BALB/c BMDC was, although not completely abolished, still very significantly inhibited. TNF was induced by all TLR ligands in DCs of both mouse strains, and in all cases HES was able to inhibit the secretion of this cytokine. IL-6 on the other hand was barely induced by Poly(I:C), and its secretion by R848-stimulated C57BL/6 BMDC did not seem to be inhibited by HES. In contrast, IL-6 production by R848 stimulated BALB/c BMDC was very significantly inhibited. Secretion of this cytokine after CpG, LPS and Pam3CSK4 stimulation was inhibited in both mouse strains, although the latter did not reach significance in BALB/c cells.

To ensure that these effects are not due to HES interfering with the ELISA itself, recombinant IL-12, TNF or IL-6 were diluted in cRPMI with or without 10μg of HES and analysed by ELISA. HES did not interfere with any of the ELISA reactions, as the ODs for the colour reaction were not significantly different for any of the three cytokines between samples with and without HES (3.1B).

In addition to analysing cytokine secretion, the expression of costimulatory molecules on BMDC of both mouse strains stimulated with the TLR ligands was measured by flow cytometry (Fig 3.2). Both CD40 and CD80 were upregulated on $CD11c^+$ cells upon stimulation, albeit to varying degrees. HES inhibited this upregulation of CD40 and CD80 in both mouse strains and with all of the tested stimuli.

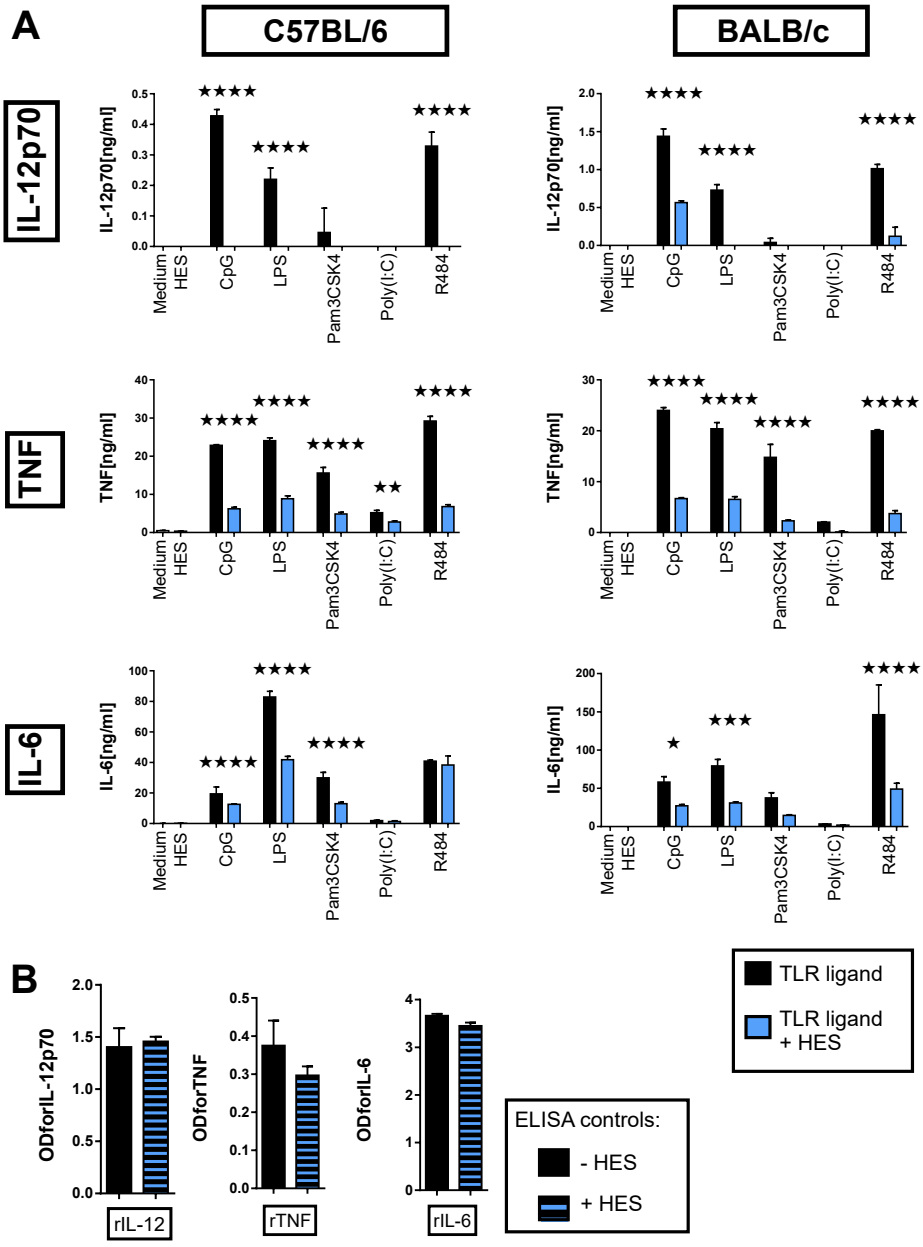

Figure 3.1: HES inhibits secretion of pro-inflammatory cytokines in response to various TLR ligands. BMDC of C57BL/6 and BALB/c mice were differentiated with GM-CSF for ten days before incubation with TLR ligands and HES as indicated for 18h. **(A)** Secretion of IL-12p70, TNF and IL-6 by BMDC stimulated as indicated was measured by ELISA. **(B)** To control for potential interference of HES with the ELISA itself, concentrations of IL-12p70, TNF and IL-6 were determined in cRPMI with recombinant cytokines with or without addition of HES as indicated. Data are representative of at least 3 independent experiments with C57BL/6 BMDC, BALB/c BMDC were tested once. Data represent mean ± SD, n = 3; Results from 1way ANOVA and Sidak's multiple comparison test are indicated as $* : p \leq 0.05$; $** : p \leq 0.01$; $*** : p \leq 0.001$; $**** : p \leq 0.0001$.

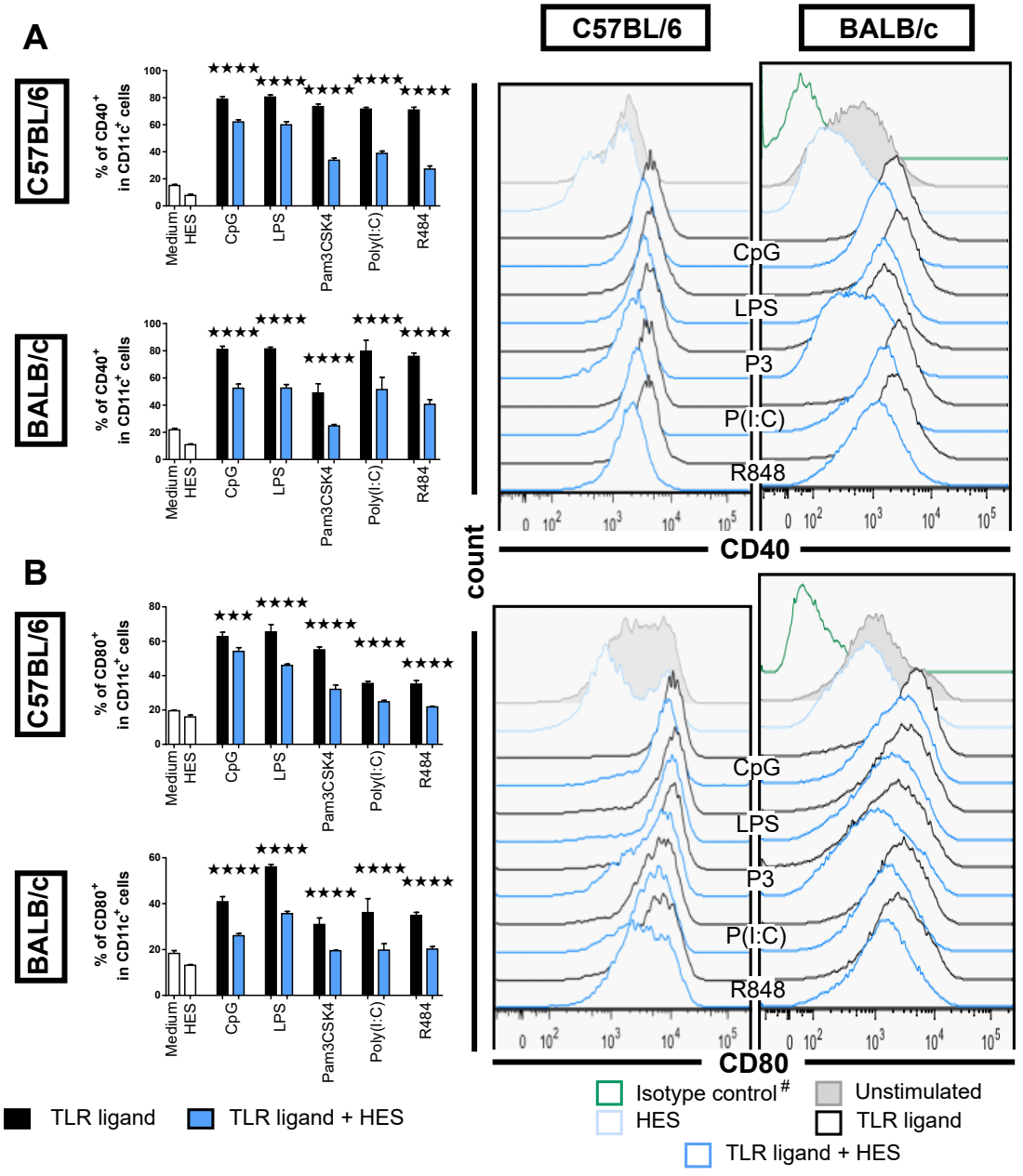

Figure 3.2: HES inhibits DC activation by various TLR ligands. BMDC of C57BL/6 and BALB/c mice were differentiated with GM-CSF for ten days before incubation with TLR ligands and HES as indicated for 18h. **(A)** CD40 and **(B)** CD80 on CD11c$^+$ cells was determined by flow cytometry. Left: percentages of CD40$^+$ or CD80$^+$ cells; Right: histograms of CD40 and CD80 expression on CD11c$^+$ cells - # isotype control not in all panels. Data are representative of at least 3 independent experiments with C57BL/6 BMDC, BALB/c BMDC were tested once. Data represent mean ± SD, n = 3; Results from 1way ANOVA and Sidak's multiple comparison test are indicated as $*$: $p \leq 0.05$; $**$: $p \leq 0.01$; $***$: $p \leq 0.001$; $****$: $p \leq 0.0001$; P3: Pam3CSK4; P(I:C): Poly(I:C).

3.2.2 HES inhibition of LPS-induced DC activation.

Following this, the inhibitory effect of HES on LPS-stimulated BMDC was investigated further. Before, HES was always used at 10μg/ml; to determine if it will be more or less effective in different concentrations LPS stimulated BMDC were incubated with 20, 10 or 1μg/ml of HES. As shown in Fig. 3.3A, HES does indeed inhibit LPS-induced secretion of IL-12p70, TNF and IL-6 in a dose dependent manner, although with different efficiency in C57BL/6 and BALB/c DCs. While 1μg/ml of HES on C57BL/6 cells was still able to potently suppress secretion of all three cytokines, even though not to the same extent as the previously used 10μg/ml, in BALB/c DCs, it only slightly reduced the concentration of secreted IL-12p70 and TNF and was not able to inhibit IL-6 production. Both the 10μg/ml and 20μg/ml treatments had the same significant effects on cells from both mouse strains.

When comparing expression of costimulatory molecules, similar results could be observed. Here shown is the expression of CD80 on BMDC of both mouse strains (Fig. 3.3B). In contrast to the cytokines tested, CD80 expression on DCs of both mouse strains followed similar dose response patterns, with a slight inhibition by 1μg/ml and increasing suppression of CD80 upregulation with increasing concentration of HES.

Interestingly, when HES was heat-treated for five minutes at 95°C it lost its ability to inhibit DC activation. BMDC of C57BL/6 mice treated with LPS and heat-inactivated HES secreted comparable amounts of IL-12p70, TNF and IL-6, while untreated HES of the same batch showed the expected ability to inhibit these responses (Fig. 3.3C).

To further check at which level HES inhibits the activation of DCs, BMDC from C57BL/6 and BALB/c mice were stimulated with LPS and HES and their expression of IL-12 determined by intracellular flow cytometry. Upon stimulation with LPS, the percentage of IL-12$^+$ BMDCs of both mouse strains increased as expected. In BMDC treated with both LPS and HES, the percentage of IL-12$^+$ BMDC did increase as well, but a marked reduction compared to LPS-treated BMDC was visible (Fig. 3.4A). Following this finding, levels of mRNAs for both subunits of IL-12, p35 and p40, as well as TNF and IL-6 in BMDC of C57BL/6 mice treated with LPS and HES were measured by real time PCR. As shown in Fig. 3.4B, HES did indeed significantly reduce the LPS-induced increase in the mRNA levels of all three cytokines. This was, however, not due to general RNA degradation, as, in addition to the fact that cytokine mRNA levels were normalized with housekeeping transcript levels, both RNA quality and concentrations were comparable in all samples (data not shown).

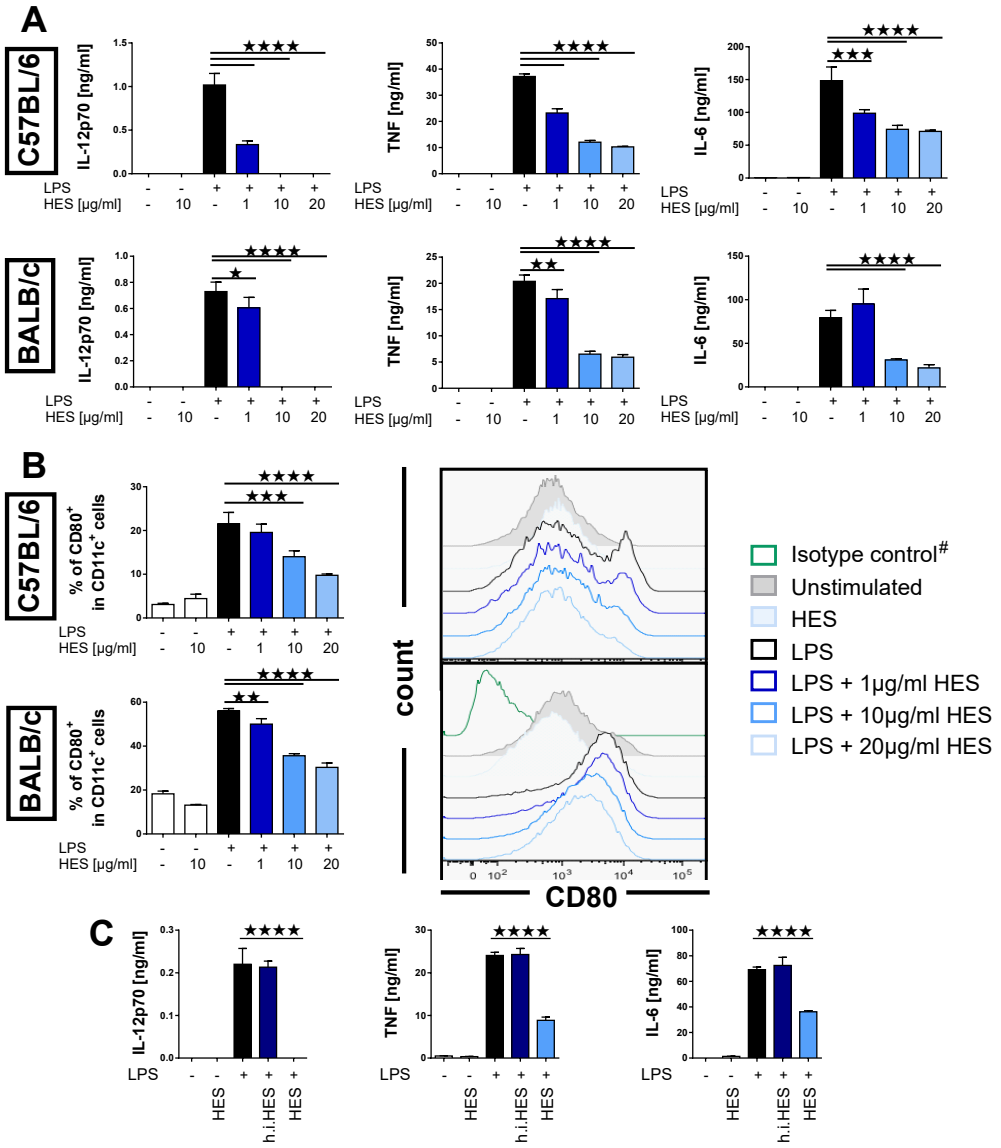

Figure 3.3: HES inhibition of LPS induced DC activation is dose dependent and heat labile. BMDC of C57BL/6 and BALB/c mice were differentiated with GM-CSF for ten days before incubation with LPS and HES as indicated for 18h. **(A)** Secretion of IL-12p70, TNF and IL-6 was measured by ELISA. **(B)** Expression of CD80 on $CD11c^+$ cells was determined by flow cytometry. Left: percentages of $CD80^+$ cells; Right: histograms of CD80 expression on $CD11c^+$ cells - # isotype control not in all panels. **(C)** To assess the heat stability of the inhibitory effect, LPS stimulated BMDC of C57BL/6 mice were treated with $10\mu g/ml$ of HES and heat inactivated (h.i.) HES as indicated and secretion of IL-12p70, TNF and IL-6 measured by ELISA. Data are representative of at least two independent experiments with C57BL/6 BMDC, BALB/c BMDC were tested once. Data represent mean $\pm$ SD, n = 3; Results from 1way ANOVA and Dunnett's multiple comparison test are indicated as $* : p \leq 0.05$; $** : p \leq 0.01$; $*** : p \leq 0.001$; $**** : p \leq 0.0001$.

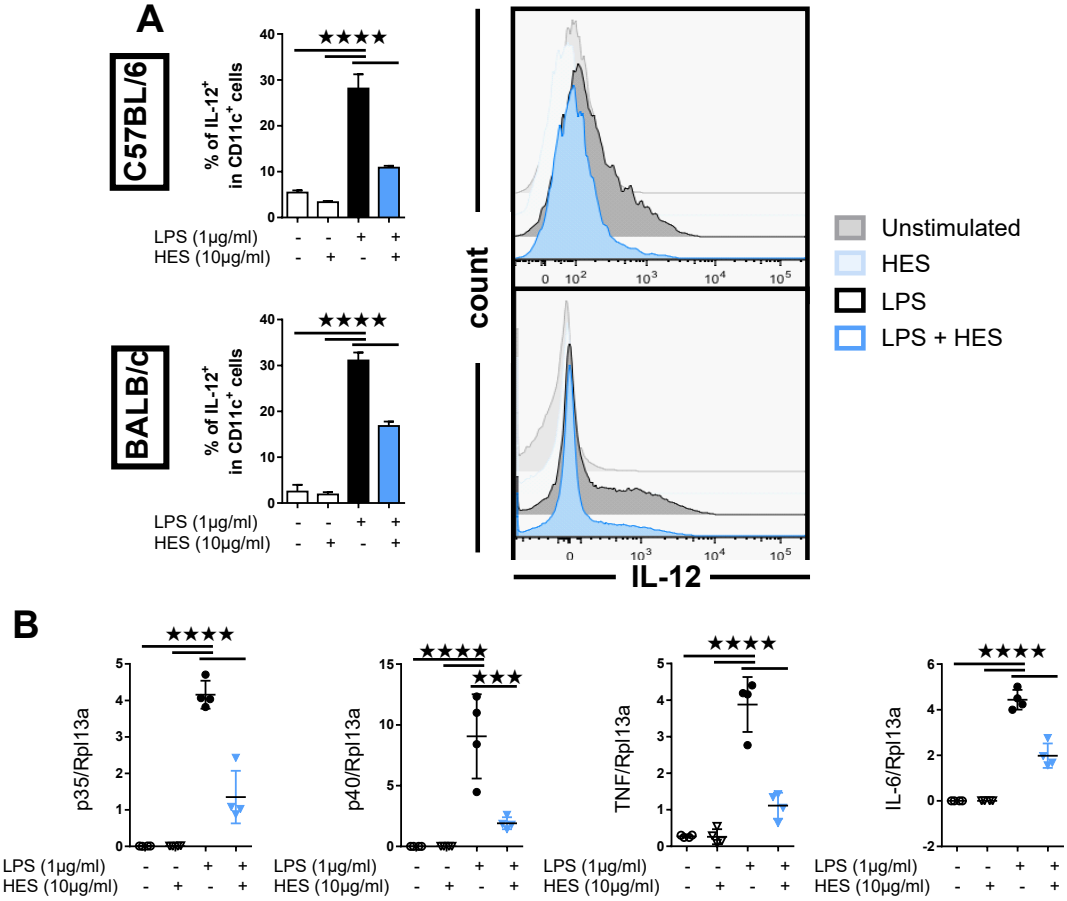

Figure 3.4: HES inhibits LPS induced DC activation at both the mRNA and intracellular protein level. BMDC of C57BL/6 and BALB/c mice were differentiated with GM-CSF for ten days before incubation with LPS and HES as indicated. **(A)** Intracellular IL-12p40/p70 protein in $CD11c^+$ cells of both mouse strains was determined by flow cytometry after 18h of stimulation. Left: percentages of $IL\text{-}12^+$ cells; Right: histograms of IL-12 expression on $CD11c^+$ cells. n = 3. **(B)** Levels of IL-12, TNF and IL-6 mRNA in C57BL/6 BMDC were measured by real time PCR at 8h after stimulation and normalized to Rpl13a mRNA levels. n = 4. IL-12 data are representative of 3 independent experiments with C57BL/6 BMDC, IL-6 and TNF mRNA levels in C57BL/6 BMDC and intracellular IL-12 in BALB/c BMDC were tested in two independent experiments. Data represent mean ± SD; Results from 1way ANOVA and Dunnett's multiple comparison test are indicated as $* : p \leq 0.05$; $** : p \leq 0.01$; $*** : p \leq 0.001$; $**** : p \leq 0.0001$.

To confirm that HES is indeed acting on the cells themselves to alter their response to TLR ligands, BMDCs of C57BL/6 mice were incubated for one hour in cRPMI with or without 10μg/ml of HES. After a washing step, cells were then stimulated as usual with LPS and HES (see Fig. 3.5A for a schematic of the workflow).

As can be seen in the top panel of Fig. 3.5B, pre-incubation of BMDC with HES for only one hour completely abolished the subsequent production of IL-12p70 by cells that were then incubated with LPS for 18h even without the addition of HES after the washing step. As shown before, incubation of cells with LPS and HES for 18h did completely inhibit IL-12p70 production; pre-incubation with HES did not change this outcome. In the bottom panels TNF and IL-6 secretion by BMDCs are shown. Production of both of these cytokines is highly reduced when comparing LPS-treated BMDC that were pre-incubated with HES-containing medium (striped bars and marked with ⊕) with those that were pre-incubated with medium alone (black bars). If BMDC that had been pre-incubated with HES for one hour were then treated with LPS and HES for 18h after the washing step, secretion of TNF and IL-6 was further reduced (striped bars marked with ⊕). The concentrations of these cytokines in the supernatants of cells treated with LPS+HES were comparable in samples pre-incubated with or without HES (light blue bars).

3.2.3 HES differentially affects alternative activation of BMDC from C57BL/6 and BALB/c mice.

DCs have, like macrophages, been found to display an alternatively activated phenotype, expressing for example RELMα (Cook et al., 2012). Hence, RELMα expression in DCs was analysed to investigate whether HES does either induce or modulate alternative activation of DCs. As before, BMDC from C57BL/6 and BALB/c mice were differentiated for ten days with GM-CSF before stimulation for 18h. In addition to LPS, IL-4 was added as a potent inducer of alternative activation.

Fig. 3.6A shows the expression profiles of RELMα. In cells treated with neither LPS nor IL-4, HES did not induce RELMα secretion or its production in CD11c$^+$ cells. The same was true for cells stimulated with LPS and LPS + HES. IL-4 on the other hand induced RELMα expression in CD11c$^+$ cells and its secretion into the supernatant. Interestingly, while the inhibition of LPS-induced IL-12 production in CD11c$^+$ cells from both mouse strains again was comparable, IL-4 stimulated cells from C57BL/6 mice show a different response to HES compared to cells from BALB/c mice. While supernatants of the latter contained comparable concentrations of RELMα in IL-4- and IL-4+HES-treated samples, HES inhibited both its secretion and reduced the percentage of RELMα^+ cells in the CD11c$^+$ population of C57BL/6 mice. Following

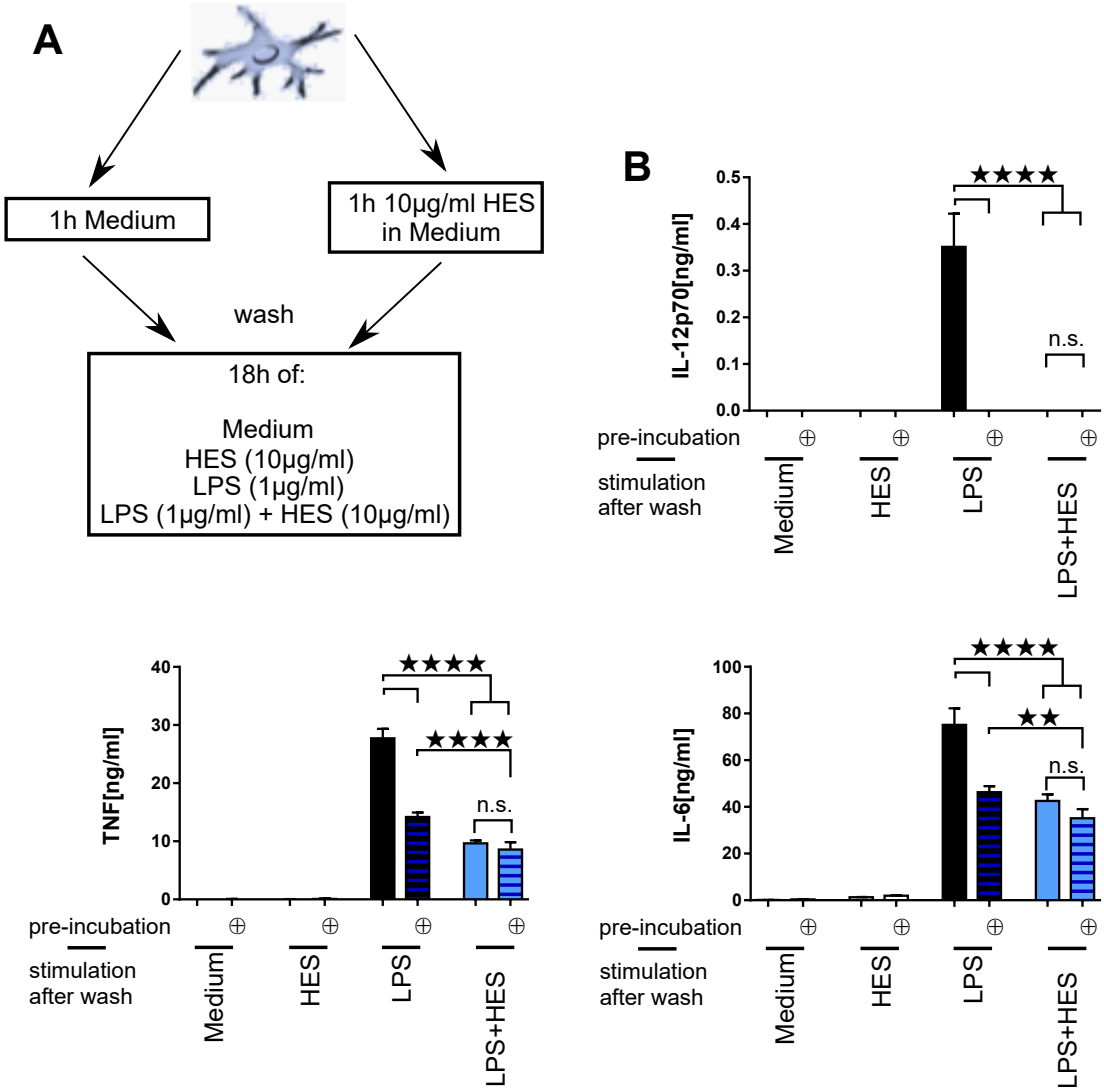

Figure 3.5: Pre-incubation of BMDC with HES impairs LPS induced activation. BMDC of C57BL/6 mice were differentiated with GM-CSF for ten days before treatment as indicated. **(A)** Schematic of the experimental setup. d10 BMDC were incubated with medium alone of 10μg/ml HES in medium for 1h at 37°C before washing and treatment with LPS and HES as indicated. **(B)** Secretion of IL-12, TNF and IL-6 was measured by ELISA. Samples pre-treated with HES are marked with a ⊕, stimulation after the washing step is indicated below the lines. IL-12p70 and TNF secretion were analysed in two independent experiments, IL-6 once. Data represent mean ± SD, n = 3; Results from 1way ANOVA and Tukey's multiple comparison test are indicated as $* : p \leq 0.05$; $** : p \leq 0.01$; $*** : p \leq 0.001$; $**** : p \leq 0.0001$.

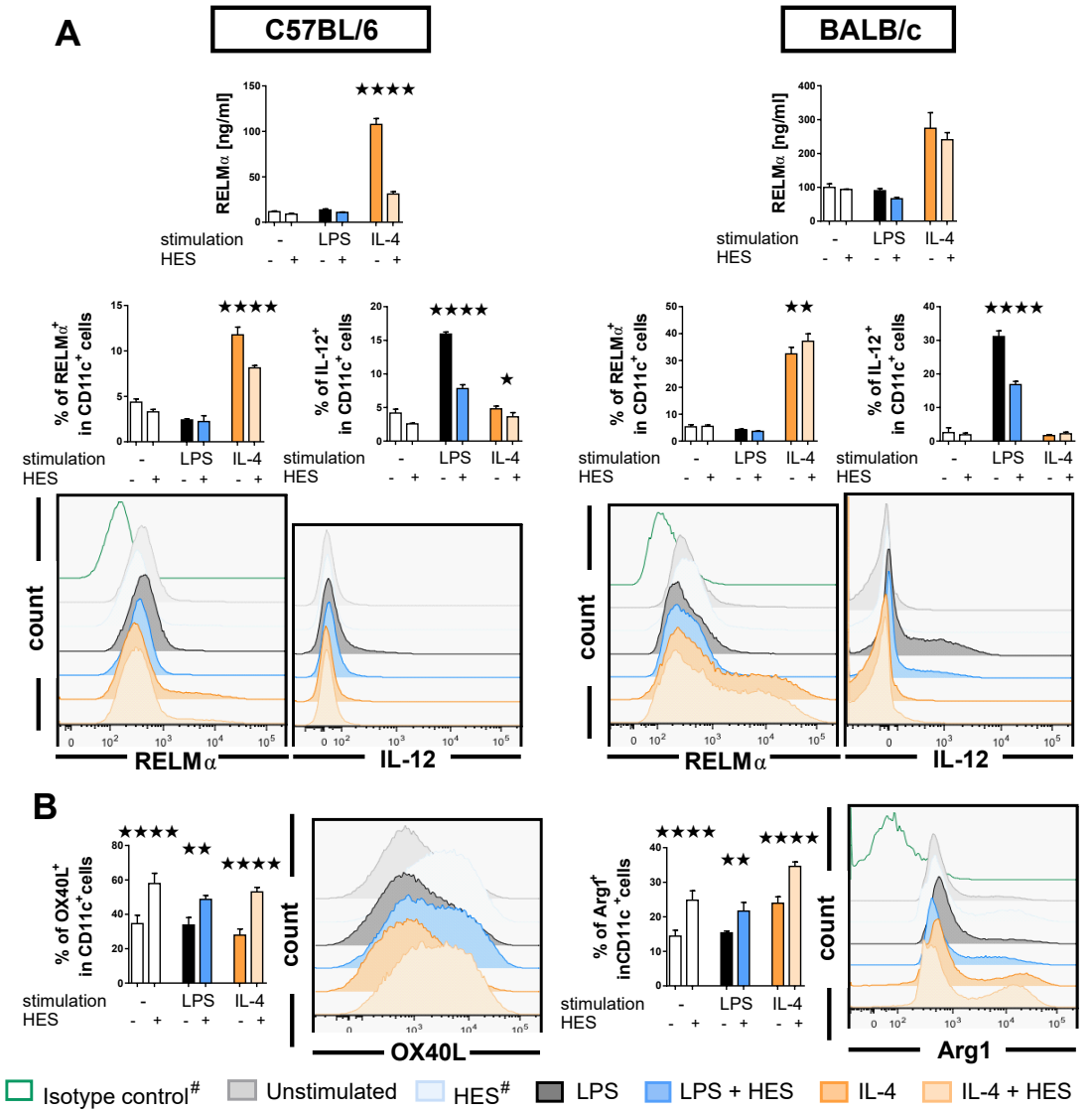

Figure 3.6: HES differentially affects alternative activation of BMDC from C57BL/6 and BALB/c mice. BMDC of C57BL/6 and BALB/c mice were differentiated with GM-CSF for ten days before stimulation with LPS, IL-4 and HES as indicated. **(A)** RELMα concentrations in supernatants of C57BL/6 and BALB/c BMDC as measured by ELISA (top) and percentages of RELMα^+ and IL-12$^+$ cells in the CD11c$^+$ population (middle) as determined by intracellular flow cytometry. Histograms of RELMα and IL-12 in CD11c$^+$ cells in bottom panels. **(B)** Expression of OX40L and Arg1 by BALB/c BMDC was determined by flow cytometry. Left: percentages of OX40L$^+$ or Arg$^+$ cells within the CD11c$^+$ population; Right: histograms of OX40L and Arg1 expression on CD11c$^+$ cells - # isotype control and HES alone not in all panels. Data are representative of two independent experiments, except for RELMα ELISA data and OX40L expression on BALB/c BMDC, which were tested once. Data represent mean $\pm$ SD, n = 3; Results from 1way ANOVA and Sidak's multiple comparison test are indicated as $* : p \leq 0.05$; $** : p \leq 0.01$; $*** : p \leq 0.001$; $**** : p \leq 0.0001$.

this lack of modulation in BALB/c BMDCs, the expression of two more markers for alternative activation, OX40L and Arg1 was investigated. Interestingly, while IL-4 alone did not induce an increase in the percentage of $OX40L^+$ BMDC, HES did so irrespective of the presence of other ligands. In contrast, in the case of Arg1 both HES and IL-4 increased the percentage of $CD11c^+$ cells producing Arg1 compared to either the unstimulated or the LPS-treated BMDCs, and the effect appeared additive in the presence of both HES and IL-4 (Fig 3.6B).

3.2.4 The soluble fraction of HES, not exosomes, inhibits LPS induced DC activation.

In recent years it has become increasingly clear that parasites influence their hosts by secretion of small vesicles containing proteins and miRNAs, called exosomes (Coakley et al., 2015). Indeed, it has been shown that *H. polygyrus* does produce exosomes and that those contain immunomodulatory molecules including miRNAs acting on endothelial cells (Buck et al., 2014). These exosome vesicles can be separated from the soluble portion of HES by ultracentrifugation, and were also shown to inhibit LPS induced activation of bone marrow derived macrophages (Coakley et al., manuscript in preparation). To test if the effect of HES on BMDCs stems from exosomes or from products in the soluble fraction of HES, these were provided by Gillian Coakley and tested on LPS-stimulated day ten BMDC from C57BL/6 mice. In contrast to the effects on macrophages, exosomes did not inhibit LPS-induced DC activation. The concentrations of IL-12p70, TNF or IL-6 in supernatants of LPS-stimulated BMDC treated with exosomes were comparable to those treated with LPS alone, while HES depleted of exosomes retained the inhibitory activity (Fig. 3.7A). This was true for costimulatory molecules as well, as demonstrated in Fig. 3.7B for the expression of CD80 by $CD11c^+$ cells.

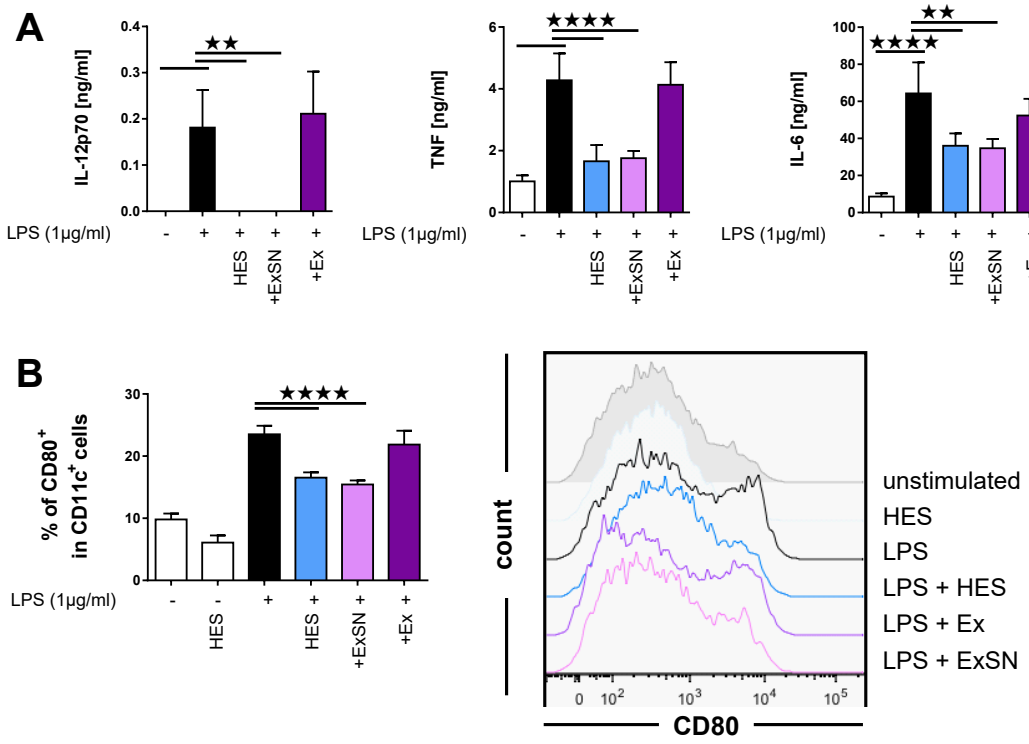

Figure 3.7: The soluble fraction of HES, not exosomes, inhibits LPS induced DC activation. GM-CSF BMDC of C57BL/6 mice were treated with LPS, HES, exosomes and exosome-depleted HES for 18h as indicated. HES, exosomes and exosome depleted HES were provided by Gillian Coakley. **(A)** Secretion of IL-12p70, TNF and IL-6 was measured by ELISA. **(B)** Expression of CD80 on $CD11c^+$ cells was determined by flow cytometry. Left: percentages of $CD80^+$ cells within the $CD11c^+$ population; Right: histograms of CD80 expression on $CD11c^+$ cells. Data are representative of at least two independent experiments. Data represent mean ± SD, n = 4 mice, in duplicates; Results from 1way ANOVA and Dunnett's multiple comparison test are indicated as $* : p \leq 0.05$; $** : p \leq 0.01$; $*** : p \leq 0.001$; $**** : p \leq 0.0001$; ExSN: exosome depleted HES; Ex: exosomes.

3.2.5 HES inhibits activation of multiple DC subsets.

It was recently described that BMDC differentiated with GM-CSF actually consist of two different populations (Helft et al., 2015). One of these populations was classified as macrophage like cells, while the other population showed more similarity to classically-defined DCs. These authors suggested that to distinguish between the two populations, CD115 could be used as a marker, as this is only expressed on the macrophage like population. As the expression of CD115 on GM-CSF-differentiated bone marrow cells decreases after stimulation (data not shown), it was not a feasible marker to separate both populations after treatment. Instead, BMDC were depleted of $CD115^+$ cells by MACS before stimulation, to increase the ratio of DC to macrophage-like cells in the cultures. Both total GM-CSF BMDC and CD115-depleted cells were stimulated with LPS and HES for 18h (see Fig. 3.8A). Both total and CD115-depleted BMDC cultures did secrete IL-12p70, IL-6 and TNF upon stimulation. As seen before, IL-12p70 production by total BMDC was completely abolished by HES, and this effect was also observed in CD115-depleted cultures. The inhibition of TNF secretion too was inhibited to a similar extent in both total and CD115-depleted BMDC. IL-6 on the other hand seemed to be induced to a slightly lesser extent in the CD115-depleted BMDC than in total cells, and while it was still significantly suppressed by HES, the difference was less marked (Fig. 3.8B). However, although depletion of $CD115^+$ cells by MACS resulted in a reduction of cell numbers by 50%, the percentage of $CD115^+$ cells in the culture seemed to only be reduced from about 65% to around 50% (data not shown). As such, it was not sufficient as proof that it is the DC population that is affected by HES.

As a second approach to ascertain the inhibitory effect of HES on DCs, splenocytes were enriched for $CD11c^+$ cells by MACS and stimulated for 18h with LPS and HES (Fig. 3.8C). While the expression of costimulatory molecules on the $CD11c^+$ cells was not inhibited by HES (data not shown), secretion of TNF and IL-6 was (Fig. 3.8D). IL-12p70 could not be detected in the culture supernatants.

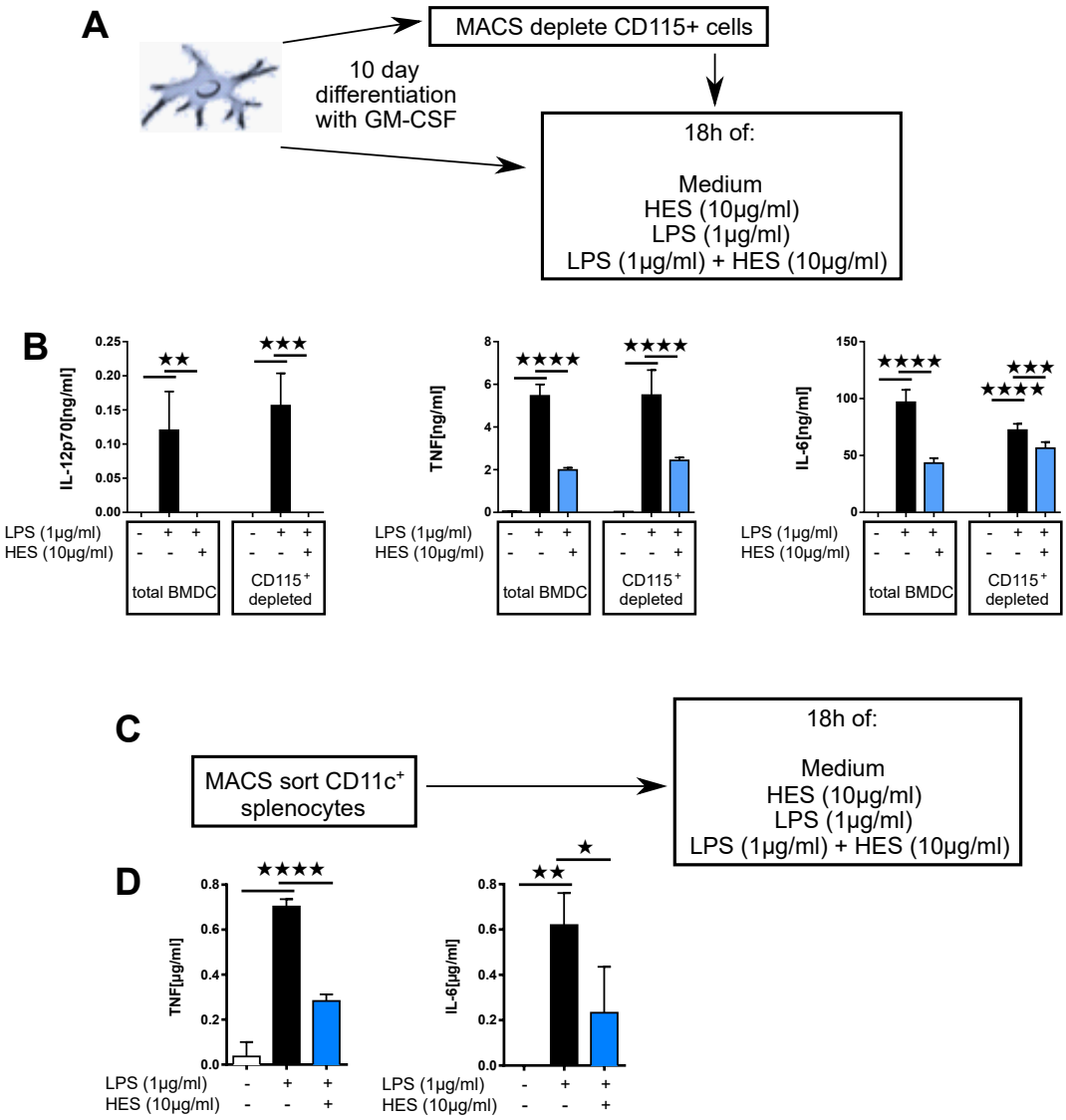

Figure 3.8: HES inhibits activation of CD115 depleted BMDC and ex vivo DCs. **(A)** BMDC were differentiated with GM-CSF for ten days and either stimulated as usual, or depleted of $CD115^+$ cells by MACS before stimulation as indicated. This experiment was done once. **(B)** Secretion of IL-12p70, TNF and IL-6 by total GM-CSF BMDC or CD115-depleted BMDC was measured by ELISA. **(C)** Spleen cells were enriched in $CD11c^+$ cells by MACS and incubated with LPS and HES for 18h as indicated. **(D)** The secretion of TNF and IL-6 by splenic CD11c-enriched cells was measured by ELISA. TNF data is representative of 4 independent experiments, IL-6 of one. Data represent mean ± SD, n = 3; Results from 1way ANOVA and Sidak's multiple comparison test are indicated as *: $p \leq 0.05$; **: $p \leq 0.01$; ***: $p \leq 0.001$; ****: $p \leq 0.0001$

BMDC differentiated with Flt3-L instead of GM-CSF have been described as cells that more closely reproduce DC subsets found in vivo. Namely, cultures of these cells result in the production of $B220^+$ $CD11c^+$ cells that were considered pDCs, and $B220^-CD11c^+$ cells that resembled cDCs. These latter cells could be further subdivided into $CD11b^+$ cells and $CD24^+$ cells, the former corresponding to $CD11b^+$ cDCs and the latter to $CD8^+$ cDCs *in vivo* (Naik et al., 2005). As such, these FLDCs constituted a more sophisticated system to investigate the effect HES has on different subsets of DCs.

Bone marrow cells were differentiated with Flt3-L for eight days before stimulation with LPS and HES for 18h; the experiment shown was performed in Prof. Andrew MacDonald's laboratory at the University of Manchester with help of Dr. Alexander Phythian-Adams. Just as described for GM-CSF BMDC, LPS stimulation induced secretion of IL-12p70, TNF and IL-6 by FLDCs. Again, IL-12p70 production was completely inhibited by HES. TNF and IL-6 concentrations in supernatants were dramatically reduced as well (Fig. 3.9A). In addition to that, the three subsets present in these cultures were analysed for their expression of costimulatory molecules. CD40 was chosen as one that was highly induced in all subsets. As shown in Fig. 3.9B, HES inhibited the upregulation of CD40 to varying degrees but significantly in all three subsets. According to these data, pDCs seem to be affected the strongest, while $CD24^+$ cDCs only showed a slight inhibition by HES.

3.2.6 HES inhibits activation of human DCs

A broader question of key interest was whether HES is also able to suppress activation of human dendritic cells, which would indicate that the parasite is targeting a conserved pathway in the mammalian host. To examine this question, human peripheral blood monocytes were differentiated into monocyte derived DCs (moDCs) with GM-CSF and IL-4 for seven days before stimulation with LPS and HES for 18h; the experiment again was performed in Prof. Andrew MacDonald's laboratory, with help from Dr. James Crooks and Cecilia Forss. Concentrations of IL-12p40, IL-6, IL-8 and TNF in the culture supernatants were determined by CBA. Cells from different donors displayed a high variability in the strength of their cytokine response; nevertheless, HES significantly inhibited the secretion of IL-12p40, IL-6 and IL-8 by LPS-stimulated moDCs (Fig. 3.10B). The expression of costimulatory molecules on $CD14^-CD11c^+$ cells however was not affected by HES, as is shown in Fig. 3.10B for CD80. This was also found to be the case for CD40, CD83 and CD86 (data not shown).

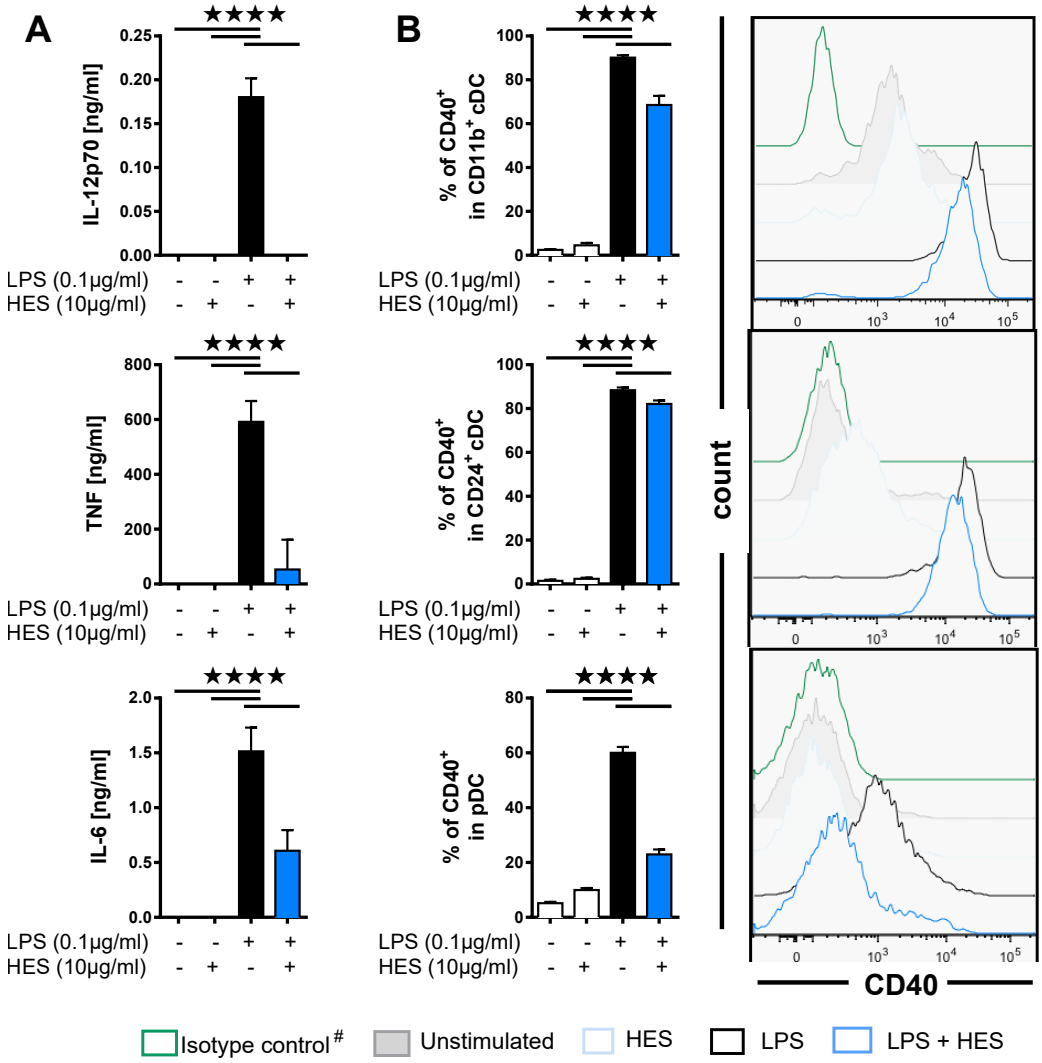

Figure 3.9: HES inhibits activation of FLDC. BMDC were differentiated with Flt3-L for eight days before incubation with LPS and HES for 18h as indicated. **(A)** Concentrations of IL-12p70, TNF and IL-6 in the supernatants of total FLDC were measured by ELISA. **(B)** FLDC were analysed by flow cytometry to distinguish between different subsets and determine their expression of activation markers. pDC were defined as $CD11c^+$ $B220^+$ cells, while $CD11c^+$ $B220^-$cells were labelled cDC. Those were further divided into $CD11b^+$ and $CD24^+$ populations (according to Naik et al., 2005). Left: percentages of $CD40^+$ cells within the subsets; Right: histograms of CD80 expression on $CD11c^+$ cells. Data are representative of 2 independent experiments, shown are the results from the experiment performed in Prof. Andrew MacDonald's laboratory with help of Dr. Alexander Phythian-Adams. Data represent mean ± SD, n = 3 mice, in duplicates; Results from 1way ANOVA and Sidak's multiple comparison test are indicated as $* : p \leq 0.05$; $** : p \leq 0.01$; $*** : p \leq 0.001$; $**** : p \leq 0.0001$.

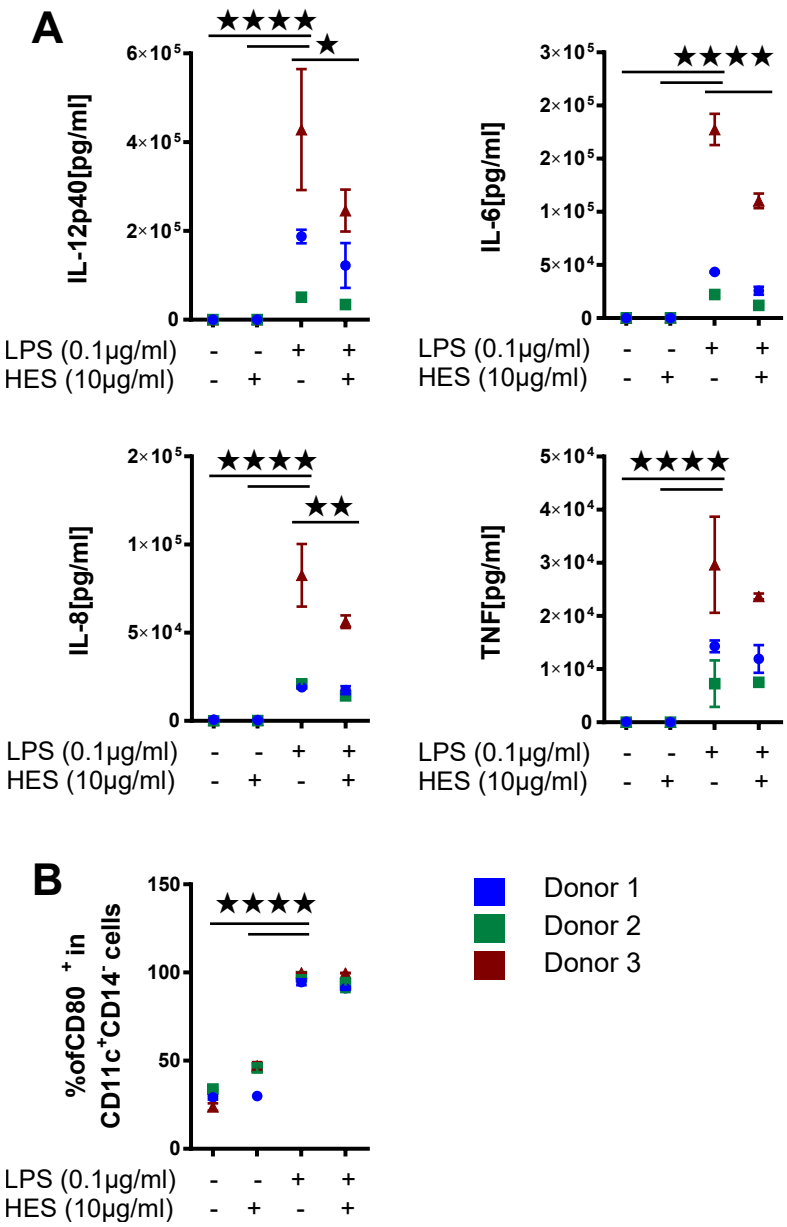

Figure 3.10: HES inhibits activation of human monocyte derived DCs. Human PBMC were differentiated to moDC with GM-CSF and IL-4 for six days before incubation with LPS and HES for 18h as indicated. **(A)** Concentrations of IL-12p40, IL-6, IL-8 and TNF in culture supernatants were analysed by CBA. **(B)** Expression of CD80 on $CD14^{-}CD11c^{+}$ cells was measured by flow cytometry. The experiment was performed once, in Prof. Andrew MacDonald's laboratory with help from Dr. James Crooks and Cecilia Forss. Data represent mean ± SD, n = 3 donors, in duplicates; Results from 2way ANOVA and Dunnett's multiple comparison test, comparing row means, are indicated as $* : p \leq 0.05$; $** : p \leq 0.01$; $*** : p \leq 0.001$; $**** : p \leq 0.0001$.

3.3 Discussion

To better understand the effect of HES on the maturation process of DCs, it was important to characterize it in considerably greater detail. To date, only a small number of publications describe DC modulation by HES. It is known that GM-CSF BMDC pre-treated with HES were impaired in their responses to CpG and LPS (Segura et al., 2007) and DCs co-pulsed with Pa and HES were inhibited in their activation and induced weaker T_H1 responses compared to DCs pulsed with Pa alone (Grainger, 2009). In mice infected with *H. polygyrus*, lamina propria DCs show an inhibited phenotype and are protective in a T cell transfer colitis model (Blum et al., 2012; Hang et al., 2013, 2010). DCs extracted from mLNs of *H. polygyrus*-infected mice showed reduced expression of IL-12 but interestingly increased TNF expression upon ex vivo stimulation with LPS (Balic et al., 2009); in addition, a decrease in the numbers of $CD11c^+$ DCs inducing effector T cells and an expansion of $CD11c^{lo}$ DCs that induce regulatory T cells further skew immune responses (Balic et al., 2009; Smith et al., 2011).

Here, the first question addressed was if HES specifically inhibits DC activation by certain stimuli but not others. To this end, BMDCs were stimulated with ligands for TLR1/2, 3, 4, 7 and 9 and the effect of concomitant treatment with HES on the expression of costimulatory molecules and secretion of pro-inflammatory cytokines analysed. As expected after the above-mentioned reports, HES was found to inhibit DC activation after LPS and CpG stimulation. In addition, it was also able to inhibit activation induced with the three other TLR ligands. In most cases, the upregulation of CD40, CD80 and CD86 and the secretion of IL-12p70, TNF and IL-6 were inhibited, and that was true for C57BL/6 as well as BALB/c BMDC (Fig. 3.1, 3.2). This widespread effect of HES did not come as a total surprise, as in previous experiments in our group BMDCs from wild type C57BL/6 and $MyD88^{-/-}TRIF^{-/-}$ mice were stimulated by ligation of CD40, which was inhibited by HES as well (Dayer, 2011).

Another significant finding is that if BMDC are briefly pre-treated with HES, subsequent LPS-induced maturation is impaired. This impairment is not quite as strong as with concomitant treatment of DCs with LPS and HES; TNF and IL-6 secretion were slightly elevated in LPS-stimulated DCs pre-treated with HES compared to the LPS+HES-stimulated pre-treated group, and the effects on costimulatory molecule expression were less pronounced as well (Fig. 3.5). While it is possible that this effect is due to endotoxin tolerance induced by low levels of LPS in HES, this is unlikely. For the experiments reported in this thesis, every batch of HES was tested for its content of LPS, and only very clean batches ($< 0.1 U/\mu g$ protein) were used for these experiments. Furthermore, the intact inhibition of DC activation

upon simultaneous treatment of DCs with LPS and HES, especially the fact that this inhibition was dose dependent (Fig. 3.3), and the inhibition of maturation induced by other TLR ligands does argue against this. Therefore, the impairment of DC activation by pre-treatment with HES gives another insight into the changes induced by HES in those cells. Interestingly, these changes were only fairly shortlived, as an 18h pre-treatment with HES reduced IL-12p70 secretion in BMDC that were stimulated with LPS directly following the pre-treatment, but if these cells were stimulated one day later the inhibitory effect was lost, and three days later cells pre-treated with HES even produced elevated levels of IL-12p70 (Grainger, 2009).

These findings led us to believe that the mechanism by which HES acts probably targets some component of the DC activation machinery far enough downstream to be shared in the signalling cascades induced by all of those stimuli.

Furthermore, it is clear that HES can impact in the intracellular protein levels of at least some of the regulated proteins, as the percentage of IL-12^{+} BMDCs was decreased in LPS-stimulated samples upon addition of HES. Even more interesting, this reduction could also be observed measuring the levels of the mRNAs for IL-12, TNF and IL-6 at eight hours after stimulation (Fig. 3.4). This could either indicate a reduction in gene transcription or indeed in RNA stability. One example for the latter pathway for down-regulation of DC activation is the degradation of RNAs by the ribonuclease omega-1 that was found in SEA (Everts et al., 2012a). General degradation of RNAs is unlikely in this case, however, as RNA concentrations were comparable between DCs treated with LPS and LPS+HES, and RNA quality did not change with the addition of HES. Further experiments to determine the mechanism behind the inhibition of DC maturation by HES can be found in Chapter 5.

Another interesting question is the identity of the component or molecule in HES responsible for the modulatory effect. A new perspective was introduced by the discovery of small extracellular vesicles from parasites, containing both proteins and micro-RNAs and possibly influencing host cells, specifically in the context of immune modulation (reviewed in Coakley et al., 2015). In the case of *H. polygyrus* secreted exosomes were shown to alleviate allergic airway inflammation, and inhibit the expression of Dusp1 and IL-33R in mouse epithelial cells. The identified miRNAs were further demonstrated to be able to suppress the expression of Dusp1 in a reporter gene assay (Buck et al., 2014). In addition to this, exosomes were also shown to inhibit LPS induced activation of BM-macrophages (Coakley et al., manuscript in preparation).

To see if exosomes played any role in the observed inhibition of DC activation, HES, exosomes and HES depleted of exosomes were provided by Gillian Coakley and tested for their ability to inhibit LPS-induced DC maturation. In contrast to their

effects on epithelial cells and macrophages, exosomes did not appear to modulate DC maturation (Fig. 3.7). While macrophages internalize exosomes through phagocytosis, it might be that DCs do not, and therefore escape the immune modulation induced by their contents. To shed light on this difference, uptake experiments with labelled exosomes in both cell types could be performed. By analysing the cells with confocal microscopy it could further be investigated if, in case DCs also internalize exosomes, these might subsequently localize to different compartments in each cell type. Overall, exosomes were found not to exert an effect on DCs, while exosome-depleted HES retained the inhibitory activity. This together with the fact that the inhibitory activity of HES is heat-labile (Fig. 3.3) indicates the presence of a soluble protein or protein complex acting on DCs, which will be further investigated in Chapter 4.

The results so far indicate an impressive ability of HES to suppress DC activation to bystander antigens. This does make sense, as *H. polygyrus* damages the intestinal wall, which could lead to exposure of DCs to commensal bacteria. It could be argued that the profound inhibition of DC activation to bystander antigens is a mechanism developed by the parasite to protect the host from a potentially deadly response to the intestinal microflora. In addition to this, it was important to see what influence HES would have on DC activation in a type 2 setting. DCs play an important role in the induction of T_H2 responses during *H. polygyrus* infection; depletion of $CD11c^+$ cells lead to a significant decrease in IL-4 producing $CD4^+$ T cells in mLNs of infected mice and in restimulation experiments both IL-5 and IL-13 secretion were impaired as well (Smith et al., 2012). Furthermore, HES pulsed BMDC were able to induce HES specific T_H2 responses upon adoptive transfer into naive recipients, even if they were co-pulsed with Pa (Grainger, 2009).

A molecule expressed on DCs that has been shown to be quite important in the induction of T_H2 responses is OX40L (Ekkens et al., 2003; Jenkins et al., 2007). After adoptive transfer of SEA pulsed DCs, restimulated splenocytes secreted significantly reduced levels of T_H2 cytokines if the transferred DCs were from $OX40L^{-/-}$ mice (Jenkins et al., 2007). During the primary response of *H. polygyrus* infected BALB/c mice, OX40L deficiency resulted in a reduction in IL-4 and serum IgE levels and an increased egg count at day 12 post infection. Interestingly, both egg counts and worm burden were increased in the setting of secondary infection which is normally rapidly cleared, indicating an impairment of the memory response as well (Ekkens et al., 2003). As shown in Fig 3.6B, BMDCs from the more resistant BALB/c strain treated with HES increase their expression of OX40L independent of other stimuli. It would be interesting to test if this is a key step in their activation for induction of HES-specific T_H2 responses.

Two further molecules associated with type 2 immune responses that have been

shown to play important roles in anti-helminth responses are arginase 1 (Esser-von Bieren et al., 2013) and RELMα (Chen et al., 2016; Cook et al., 2012; Pesce et al., 2009b). In a comparison of four mouse strains with different susceptibilities to infection with *H. polygyrus*, the expression of both RELMα and Arg1 positively correlated with resistance to infection (Filbey et al., 2014). While Arg1 has indeed been found to be an important component of the protective immune response against secondary infection with *H. polygyrus* (Esser-von Bieren et al., 2013), albeit reported to be produced by macrophages in this study, RELMα seems to limit both IL-4 production in T cells and development of pathology. In infections with *Nippostrongylus brasiliensis*, mice deficient in RELMα produced elevated levels of IL-4 and showed a reduced egg burden and increased worm clearance, but that came at the cost of increased lung inflammation and mortality (Chen et al., 2016; Pesce et al., 2009b). This elevated production of IL-4 by T cells could be replicated in co-culture experiments with BMDCs from mice deficient in RELMα, in addition to a complete loss of IL-10 production (Cook et al., 2012).These authors also demonstrated that DCs express Relmα after stimulation with IL-4; IL-4 was therefore chosen as the stimulus to analyse the influence of HES on alternative activation of DCs.

In the experiments reported here, IL-4 did indeed increase the expression of both RELMα and Arg1 in both C57BL/6 and BALB/c BMDC. Mirroring the findings by Filbey et al., 2014, HES did not inhibit RELMα production and even increased the expression of Arg1 in BMDCs from BALB/c mice, which is a fairly resistant strain, but inhibited the expression of RELMα in BMDCs from the susceptible C57BL/6 mice (Fig. 3.6). The relevance of this will have to be demonstrated in future experiments, especially considering the counter-intuitive downregulation of RELMα by HES in C57BL/6 BMDC. It would be interesting to see if mice deficient in this molecule show a similar reaction to infection with *H. polygyrus* as with *N. brasiliensis*, and if so, if it is indeed RELMα produced by DCs that is limiting T_H2 responses.

The relevance of the induction of Arg1 also remains to be seen, especially in the light of reports demonstrating that Arg1 production by macrophages actually suppresses T_H2 responses (Pesce et al., 2009a) and, produced by DCs, induces FoxP3$^+$ T_{reg} cells (Chang et al., 2013). This could easily be tested by employing Arg1 inhibitors, either in direct co-culture experiments of HES pulsed DCs with T cells, or by injection of Arg1 inhibitors at the same time as adoptive transfer of HES pulsed BMDC into recipient mice and analysis of T cell cytokine production in experiments similar to those described above.

All the work described above has been performed in GM-CSF differentiated BMDCs. Alarmingly, a recent publication demonstrated the presence of a strong macrophage like population in these cultures, responding to stimulation in a distinct

way (Helft et al., 2015). Especially in the light of the differential effects of HES components on GM-CSF BMDCs and M-CSF differentiated macrophages, it was therefore important to ascertain that the described effects were indeed due to regulation of DC responses. The authors describe CD115 as a marker that can be used to distinguish between the populations they termed GM-Macs (expressing CD115) and GM-DCs ($CD115^-$). Unfortunately cells lose the expression of this marker after stimulation, so it does not distinguish the two populations once activated. Instead, $CD115^+$ cells were depleted before stimulation; activation of the remaining cells, enriched for the "GM-DCs", was still inhibited (Fig. 3.8A). Interestingly, IL-6 production by the CD115-depleted cells was reduced compared to total GM-CSF BMDC, and the inhibition by HES, while significant, was less distinct. IL-6 also showed different patterns of modulation by HES on splenic cells stimulated with LPS. While IL-6 production was inhibited in splenic cells enriched for $CD11c^+$ cells by positive selection (Fig. 3.8B), in spleen cell cultures depleted of B and T cells HES was not able to influence the production of this cytokine (data not shown). TNF on the other hand, was inhibited in both approaches. This does indicate different effects of HES on cell populations still present after these rather crude methods of sorting, and is a reminder that in mixed cell cultures interactions between different cell types are often important in determining the overall response. An important new method of generating DCs from mouse bone marrow uses Flt3-L as differentiation factor. With this method three populations of cells are created, which have been characterized and correspond to splenic DC populations. Distinguishable are $CD11c^+$ $B220^+$ cells (pDCs) and two populations of $CD11c^+$ $B220^-$cDCs, the $CD24^+$ cells corresponding to $CD8^+$ cDCs and the $CD11b^+$ cells corresponding to the $CD11b^+$ cDC population in the spleen (Naik et al., 2005). Upon treatment with HES, LPS-induced maturation of all three of these subsets was inhibited, confirming that HES is indeed modulating DC responses, including the inhibition of IL-6 production (Fig. 3.9).

Considering the importance of DCs in the induction and shaping of immune responses, the demonstrated ability of HES to modulate DC responses could potentially be exploited in drug development. As such, it was important to see if HES also had an effect on human DCs. While it did not modulate the expression of costimulatory molecules on LPS activated human moDCs, their secretion of pro-inflammatory cytokines was significantly inhibited (Fig. 3.10). This might either indicate less efficient inhibition due to the differences in the targeted molecules or pathways between mice and humans, or indeed that several different mechanisms of DC modulation are being employed by HES and only some are effective on human DCs. In future experiments it would be interesting to see which gel filtration fraction(s) of HES inhibit human moDC activation and if the TGFβ mimic produced

by HES, TGM, has an effect. This protein has been shown to be effective on human cells as well as mouse cells, and as can be seen in the next chapter, it does partially inhibit LPS induced mouse DC activation.

In conclusion, the work presented in this chapter expands on previous knowledge about the modulation of DC maturation by HES. It forms an important basis for both experiments to elucidate the mechanism - or indeed mechanisms - employed by HES to inhibit TLR ligand induced DC maturation as well as experiments to find the molecule (or molecules) in HES that is responsible for this effect. The following Chapters will cover these questions in further detail.

CHAPTER 4

Identification of potential dendritic cell modulators in HES

ABSTRACT

With several clinical trials of live helminth infections currently underway, the search for specific immunomodulatory molecules produced by helminths is a logical step in the development of new treatments for a number of diseases. Here, the aim was finding the molecule in HES that modulates DC activation. As shown in the previous chapter, this DC modulatory effect was heat-labile, indicating a protein component. Therefore, HES was fractionated using size exclusion and anion exchange fractionation approaches, with each fraction tested for inhibitory activity and analysed by mass spectrometry. Comparison of the fraction protein contents and protein abundance profiles resulted in the identification of nine candidate proteins. These were expressed in HEK-293 cells. However, treatment of LPS-activated GM-CSF BMDC with these recombinant proteins revealed that none of them had an effect on DC activation. It remains possible that the protein in question has not yet been identified, or that key post-translational modifications are required for one of the existing candidates to replicate the function of the native molecule. Hence further experiments and a refinement of the approach will be necessary to identify the molecule responsible for the effect HES has on dendritic cells.

4.1 Introduction

While researchers are currently attempting to exploit the immunomodulatory effects of helminth infections for treatment of various diseases and conditions like multiple sclerosis, IBD, allergies and asthma in clinical trials infecting patients with live worms (http://www.niaid.nih.gov/topics/tropicaldiseases/Pages/helminthDatabase.aspx, as of 16. March 2016), doing so is a rather crude approach to treatment. Aside from the fact that patients might object to being infected with live parasites, they would also be exposed to a mixture of parasite derived products with various and mostly unknown functions, some of which could even exacerbate disease. Taking *H. polygyrus* as an example, the ES of this nematode contains at least 374 proteins. Among these are a number of enzymes including proteases, apyrases and chitinases, in addition to protease inhibitors, proteoglycans and lectins and numerous proteins with unknown functions (Hewitson et al., 2011b).

This mixture of proteins has been shown to modulate multiple aspects of immune responses in a number of different disease models. Amongst others, it has been shown to suppress allergic airway inflammation (McSorley et al., 2014; McSorley et al., 2015; McSorley et al., 2012) and produce a TGFβ mimic that induces regulatory T cells which are active in suppressing pathology in asthma models (Grainger et al., 2010). The proteins responsible for these two effects of HES, the alarmin release inhibitor (ARI) suppressing allergic airway inflammation and the TGFβ mimic TGM have recently been identified (Osbourne et al., manuscript in preparation; Johnston et al., manuscript in preparation).

Especially of note for the importance of the dendritic cell modulation in disease settings are the findings by Hang et al., 2010, as they could demonstrate that DCs in the lamina propria of RAG$^{-/-}$ mice infected with *H. polygyrus* showed a reduced expression of CD80 and CD86, produced less IL-12 and were less efficient at inducing IFNγ and IL-17 production upon coculture with OT-II cells in the presence of OVA. They expanded on that finding by demonstrating the role of these inhibited DCs in protecting mice from colitis, as transferring lamina propria DCs from mice infected with *H. polygyrus* protected Rag$^{-/-}$ mice in a T cell transfer model of colitis (Blum et al., 2012).

With this in mind, it would be an important step for the development of more targeted treatment regimes based on helminth products to identify the molecule responsible for the modulation of dendritic cell responses by *H. polygyrus*. One such protein in HES has previously been described. This protein, cystatin, was expressed and tested on BMDCs. As expected it acted as a protease inhibitor, inhibiting a variety

of cathepsins important in antigen processing by DCs. It also modulated CpG induced DC activation, however LPS induced DC activation was barely affected. The authors proposed that the inhibition of cathepsins resulted in an impairment of signalling pathways activated by CpG, but not LPS (Sun et al., 2013). Considering the more profound effects of total HES described in the previous chapter, it is likely that there is indeed at least one other molecule contained in HES that modulates DC activation.

Finding this molecule was the aim of the work described in this chapter. To this end, three rounds of analyses with increasing complexity were carried out:

- Separate fractionation by size exclusion and anion exchange fractionation, mass spectrometry on active fractions only followed by comparison of protein contents
- Sequential fractionation (size exclusion fractionation followed by anion exchange fractionation of active fractions), mass spectrometry on all sequential fractions followed by identification of proteins with abundance profiles peaking in active fractions
- Size exclusion, sequential and anion exchange fractionation, mass spectrometry on all fractions followed by identification of shared proteins with abundance profiles peaking in active fractions

These are described in more detail in their specific sections.

4.2 Results

As described earlier, the inhibitory effect of HES on DC maturation is heat-labile (Fig. 3.3), which indicates that a protein component present in HES is responsible for this effect. With this in mind, one approach to identify this modulatory molecule was to fractionate HES to create smaller pools of candidate molecules, and to identify the proteins common to fractions that retain inhibitory activity.

4.2.1 Comparison of protein contents of active size exclusion and anion exchange fractions fails to identify any candidate proteins

In a first attempt to find potential candidate proteins for DC modulatory activity, HES was fractionated by both size exclusion fractionation (otherwise called gel filtration) and anion exchange fractionation. The fractions were analysed for their inhibitory activity on GM-CSF BMDC and protein contents of active fractions determined by mass spectrometry (see schematic in Fig 4.1).

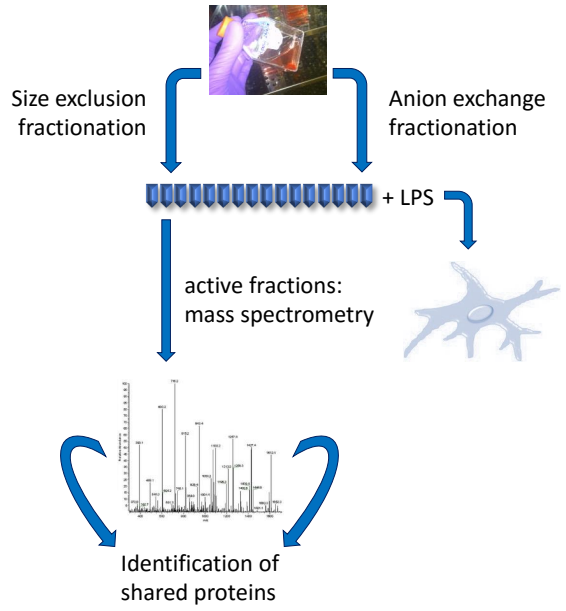

Figure 4.1: Schematic of workflow to identify the first round of candidate proteins. HES was fractionated by either size exclusion or anion exchange fractionation and fractions tested for DC inhibitory activity. Active fractions were analysed by mass spectrometry and protein contents compared to identify proteins shared by active fractions.

4.2.1.1 Size exclusion fractionation of HES

Size exclusion fractionation of HES (0.476mg) was the first method of fractionation chosen. Using this method, proteins of a higher molecular weight are eluted earlier than smaller proteins, with protein and nucleic acid contents recorded over time resulting in a distinctive fractionation profile (see Fig. 4.2A). As shown by Kara Filbey (previous Maizels group PhD student), fractionation profiles obtained with this method are highly reproducible. This also appeared to be the case for the protein contents as visualized by SDS-PAGE and subsequent silver stain of the gels, as the profile obtained from the gel filtration here (see Fig. 4.2B) reproduces those from earlier fractionations (Filbey, 2013).

To determine the activity of the current fractions on DCs, day ten GM-CSF BMDC were treated with LPS and fractions as indicated in Fig. 4.2C. Only two fractions, number 14 and 15, were able to replicate the effect of total HES and completely abolish IL-12p70 production.

Interestingly, there is also a notable effect on IL-12p70 secretion visible around fraction 9, which has been shown to contain the TGF-β mimic (TGM) present in HES. This protein has recently been identified and expressed in our laboratory (Johnston et al., manuscript in preparation), and could replicate the effect of fraction 9 when added to LPS stimulated GM-CSF BMDC. As shown in Fig. 4.3A, treatment of LPS-stimulated BMDC with TGM resulted in an inhibition of IL-12p70, TNF and IL-6 secretion. However, compared to the effect HES has on these cells, TGM clearly was less effective. This was also apparent when analysing costimulatory molecule expression on LPS-stimulated BMDC treated with HES or TGM. LPS-induced CD80 upregulation was slightly impaired with TGM, but again the effect of HES on the expression of this activation marker was a lot more profound. The expression of the other costimulatory molecules tested, with CD40 expression shown here as an example, was even comparable between LPS and LPS+TGM treated groups, unlike the inhibition observed upon HES treatment of cells (Fig. 4.3B). Together with the distinct separation of the TGM-containing size exclusion fractions and the active fractions 14 and 15, the conclusion was that although TGM modulates DC activation somewhat, it is not the only DC inhibitor in HES.

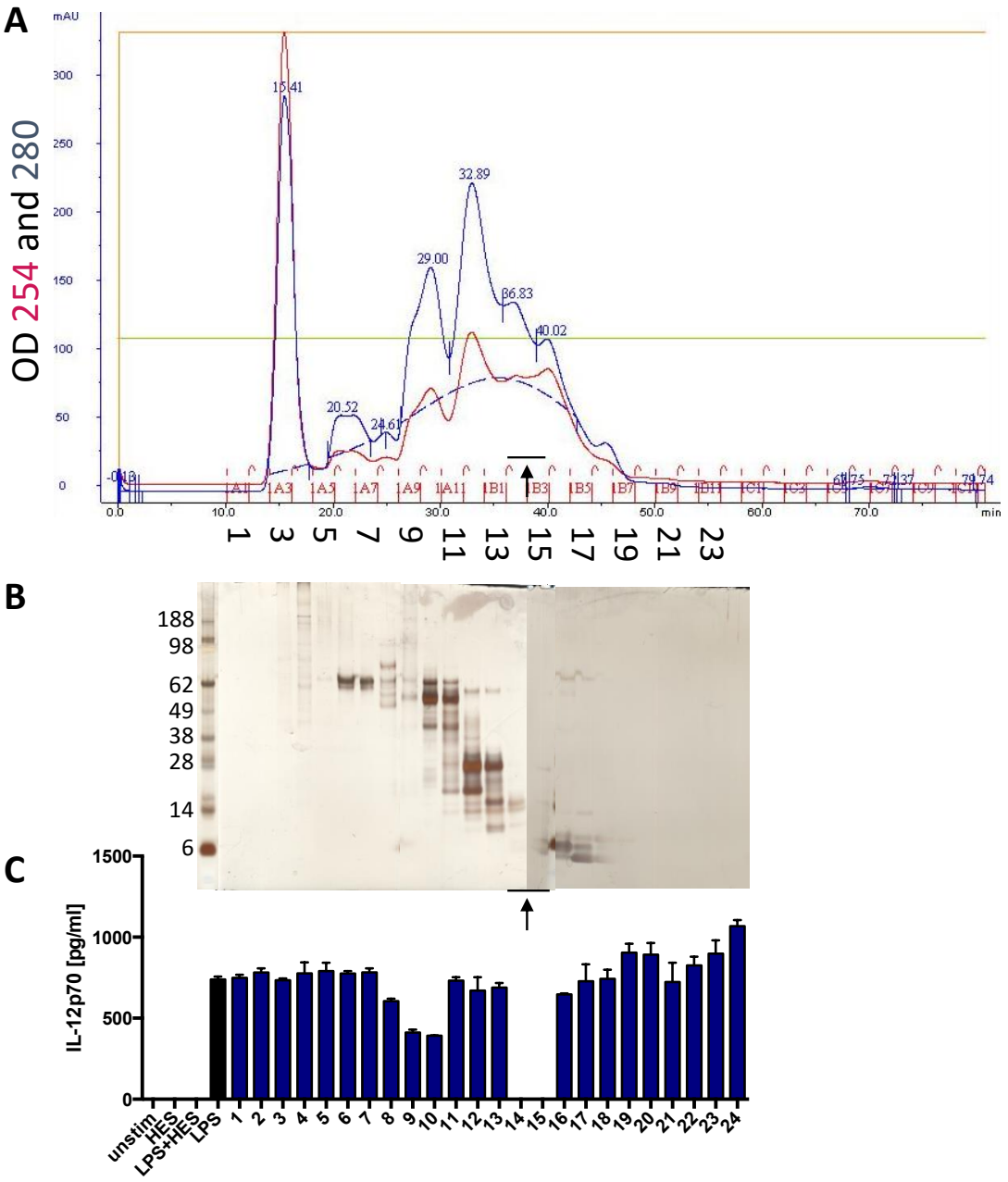

Figure 4.2: Size exclusion fractionation of HES resulted in two fractions completely inhibiting IL-12p70 production by LPS-stimulated GM-CSF BMDC. (A) HES was fractionated by size exclusion fractionation using a Superdex 200 10/300 GL column on an ÄktaPurifier system. **(B)** Protein content in the fractions was visualized by SDS-PAGE followed by silver stain of the gels. **(C)** Fractions were tested for their ability to inhibit LPS-induced IL-12p70 production by BMDC differentiated with GM-CSF. Arrows indicate active fractions.

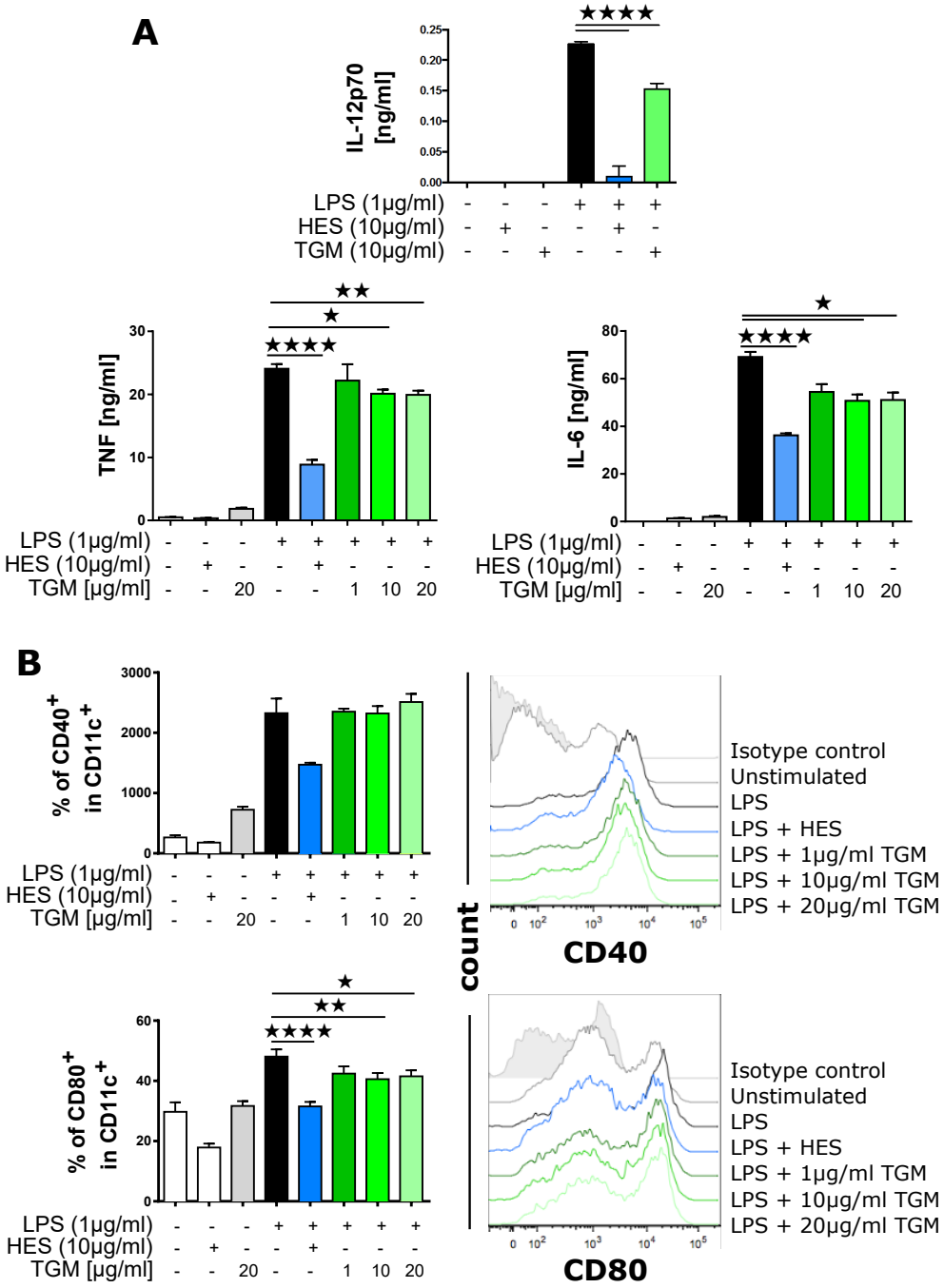

Figure 4.3: TGM inhibits LPS-induced DC activation, but not to the same extent as HES. GM-CSF BMDC were incubated with LPS, HES and TGM as indicated for 18h. **(A)** IL-12p70, TNF and IL-6 concentrations in the supernatants as measured by ELISA. **(B)** Expression of CD40 and CD80 on BMDC with flow cytometry histograms on the left. Data are representative of at least 3 independent experiments except IL-6, which was measured twice. Data represent mean ± SD, n = 3; Results from 1way ANOVA and Sidak's (flow) or Dunnett's (ELISA) multiple comparison test are indicated as $*$: $p \leq 0.05$; $**$: $p \leq 0.01$; $***$: $p \leq 0.001$; $****$: $p \leq 0.0001$.

4.2.1.2 Anion exchange fractionation of HES

As a second approach to fractionate HES, anion exchange fractionation was chosen to separate proteins in HES according to their overall negative charge. In this approach, positively charged and uncharged components are eluted first, with increasingly negatively charged proteins being eluted with the increasing salt concentration in the buffer. For this fractionation of 0.751mg HES, the salt concentration was increased from zero to 0.4M NaCl over the course of 40 column volumes (CV), followed by an increase to 1M NaCl within the next 5CV, finally washing any remaining proteins off the column with 1M NaCl for another 5CV (see Fig. 4.4A). Protein contents of all 61 fractions were visualized by SDS-PAGE followed by silver stain of the gels (Fig. 4.4B); as indicated by the fractionation profile the fractions five to 35 did not contain any detectable protein. Most of the protein contents in HES were eluted between fractions 36 and 46. To test the activity of these fractions on DCs, LPS stimulated day ten GM-CSF BMDC were treated with HES or fractions. As before, only two fractions, fractions 39 and 40, were able to completely inhibit IL-12p70 production (Fig. 4.4C).

4.2.1.3 Proteomics analysis of active fractions

Since the DC inhibitory effect in both fractionation approaches was very distinctively localized in two fractions each, protein contents of these four active fractions were determined by mass spectrometry. According to these analyses - which can be found in Appendix A.5 and used a significance threshold for consideration of proteins of $p<0.05$ and no minimum cutoff Mascot score - size fraction 14 contained only 26 proteins (Tab. B.1), size fraction 15 slightly more with 38 proteins (Tab. B.2), anion exchange fraction 39 (Tab. B.3) 70 proteins and fraction 40 (Tab. B.4) 105 proteins.

Using a script written in Python 2.7 (see Appendix A.3), fraction contents were compared and four proteins present in all four active fractions identified (see Fig. 4.5 for numbers of proteins shared between specific fractions). The four proteins found in all active fractions were cross checked against our in house proteomics database of adult HES, ES from the L4 larval stage of *H. polygyrus* (L4ES) and egg release material, identifying one of the proteins as a myoglobin (Hp_I21133_IG13077_L683) and a second as a sperm protein (Hp_I05325_IG00908_L1903), leading to their exclusion as housekeeping proteins. The third protein, Hp_I05364_IG00921_L2082 had been identified falsely; the peptides found by mass spectrometry and attributed to this

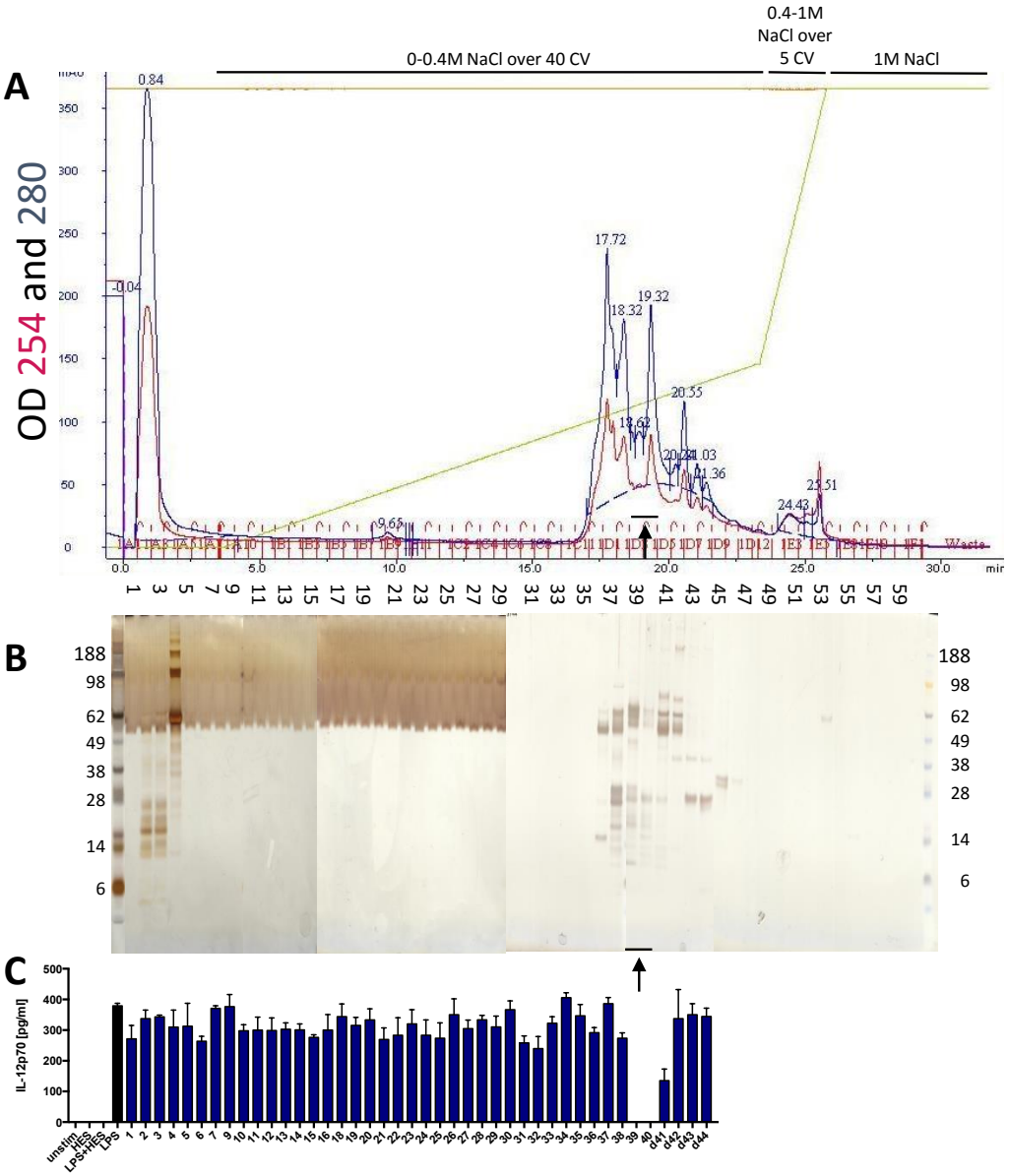

Figure 4.4: Anion exchange fractionation of HES resulted in two fractions completely inhibiting IL-12p70 production by LPS-stimulated GM-CSF BMDC. (A) HES was fractionated by anion exchange fractionation using a MonoQ™ 5/50 GL column on an ÄktaPurifier. **(B)** Protein content in the fractions was visualized by SDS-PAGE followed by silver stain of the gels. Pictures of gels were stretched to increase visibility of bands. **(C)** Fractions were tested for their ability to inhibit LPS-induced IL-12p70 production by BMDC differentiated with GM-CSF. Arrows indicate active fractions.

protein when analysed using Mascot and the in-house transcriptomics database did not match the protein sequence obtained by translating the nucleotide sequence, possibly owing to faulty assembly of the entry in our database. The fourth protein, Legumain (Hp_I02849_IG00289_L1962), appeared promising; however, when cross referencing the proteins found here with those in fraction 9, which was subjected to mass spectrometry by Kara Filbey to identify TGM (Filbey, 2013), and which as explained above is distinct from the DC modulatory activity investigated here, Legumain had to be excluded as well as it was one of the more common proteins identified in fraction 9 (Tab. 4.1).

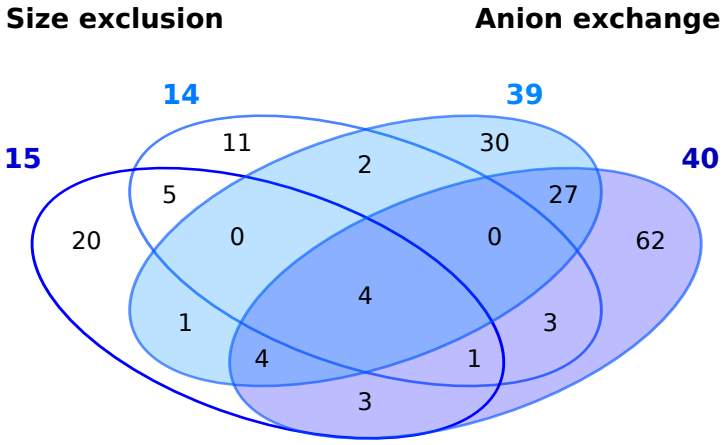

Figure 4.5: Number of proteins found in the four active fractions. HES was fractionated by size exclusion fractionation (Fig. 4.2) and anion exchange fractionation (Fig. 4.4) and fractions tested for inhibitory activity on GM-CSF differentiated BMDC. Active fractions were analysed by mass spectrometry in the facility in Glasgow, using an Orbitrap mass spectrometer and analysed using Mascot and an in-house *H. polygyrus* transcriptomics database. The significance threshold for consideration of proteins was $p<0.05$; no minimum cutoff score was set. Proteins shared amongst active fractions were identified; shown are the number of proteins shared between the indicated fractions.

Table 4.1: Proteins shared in all four active fractions of the first round of fractionations. HES was fractionated by size exclusion fractionation (Fig 4.2) and anion exchange fractionation (Fig 4.4) and fractions tested for inhibitory activity on GM-CSF differentiated BMDC. Active fractions were analysed by mass spectrometry in the facility in Glasgow, using an Orbitrap mass spectrometer and analysed using Mascot and an in-house *H. polygyrus* transcriptomics database. The significance threshold for consideration of proteins was $p<0.05$; no minimum cutoff score was set. Proteins shared in all active fractions were identified and their accession numbers compared to an in-house database of proteins identified in HES in addition to a previous mass spectrometric analysis of size exclusion fraction 9, performed by Kara Filbey. Sequences were further used to predict the molecular weight of the proteins and subjected to blastx and conserved domain search. Lastly, it was checked if the proteins had been identified by more than one peptide in the mass spectrometry analysis, and if the peptides listed matched the protein sequence. Blue text: proteins excluded as being housekeeping proteins.

	Predicted molecular weight	**Domain search**	**Top named blastx hit**	**More than one peptide in MS?**	**Fraction 9**
Hp_I21133_IG13077_L683	19.871 kDa	Myoglobin like family	99% to Myoglobin [Heligmosomoides polygyrus]; 77% query cover	Yes	Yes
Hp_I05364_IG00921_L2082	64.94 kDa	P-loop NTPase super family	45% to CELE_F08F12.1 [Caenorhabditis elegans]; 70% query cover	No - no peptide hit in sequence!	No
Hp_I02849_IG00289_L1962	49.795 kDa	Peptidase C13 family	56% to Peptidase C13 fam. protein [Ancylostoma ceylanicum]; 62% query cover	Yes	Yes
Hp_I05325_IG00908_L1903	55.585 kDa	Tetratricopeptide repeat domain	68% to Tetratricopeptide repeat protein [Necator americanus]; 37% query cover	Yes	No

4.2.2 Proteomics analysis of HES sequential fractions identifies five candidates that do not modulate DC activation

Since comparing fraction protein contents after subjecting HES to gel filtration and anion exchange fractionation separately did not lead to identification of any plausible candidate proteins for expression, the method had to be refined. Next, HES was first fractionated by gel filtration as described above and fractions tested for activity; the active ones then further underwent anion exchange fractionation and all sequential fractions were analysed by mass spectrometry (see schematic in Fig. 4.6).

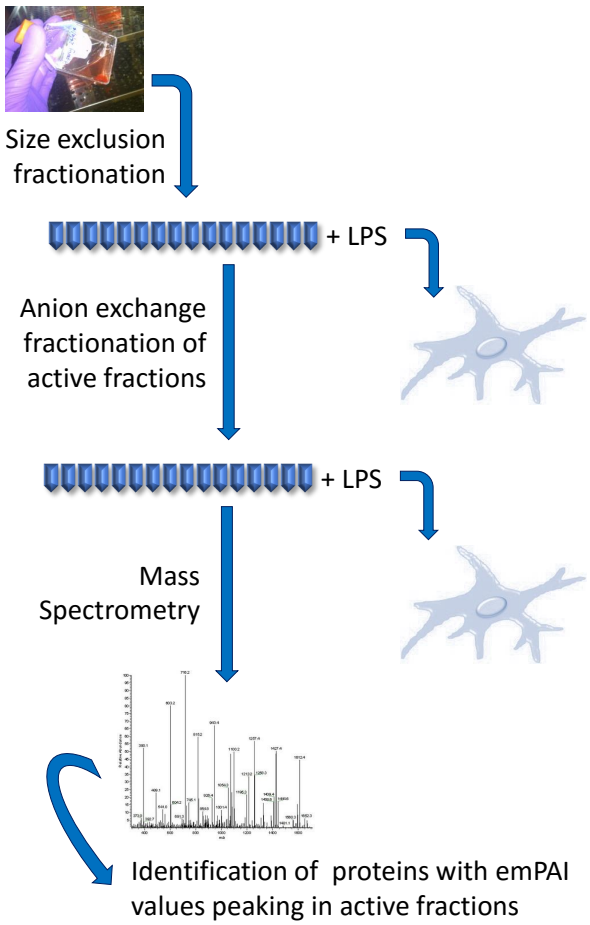

Figure 4.6: Schematic of workflow to identify the second round of candidate proteins. HES was fractionated by size exclusion fractionation and fractions tested for DC inhibitory activity. Active fractions were pooled and further fractionated by anion exchange fractionation. All sequential fractionation fractions were analysed by mass spectrometry and protein contents and abundance distributions compared.

4.2.2.1 Sequential fractionation of HES

Using the same protocol as before but with a higher input amount of HES (1.244mg) due to the planned subsequent fractionation, HES was fractionated by gel filtration and fractions tested for their ability to inhibit LPS induced activation of day ten GM-CSF BMDC. As before, fractions 14 and 15 completely inhibited IL-12p70 production, in addition to an almost complete inhibition by fraction 16 (Fig 4.7). Fractions 14 and 15 were pooled and further fractionated by anion exchange fractionation. To improve the fractionation resolution, the gradient was adjusted. This time, the salt gradient increased from 0-0.5M NaCl within 12.5CV, then to 1M NaCl within another 5CV, followed by 5CV with 1M NaCl; fractions were collected in volumes of 0.5ml instead of 1ml. For activity testing and mass spectrometry, only fractions containing detectable amounts of protein were used, which were fractions 19-35. Of those, three showed the ability to completely inhibit IL-12p70 production by LPS-stimulated GM-CSF BMDC (Fig. 4.8), sequential fractions 28, 29 and 30 (see tables B.5, B.6 and B.7 in the appendix for lists of the proteins identified in those fractions).

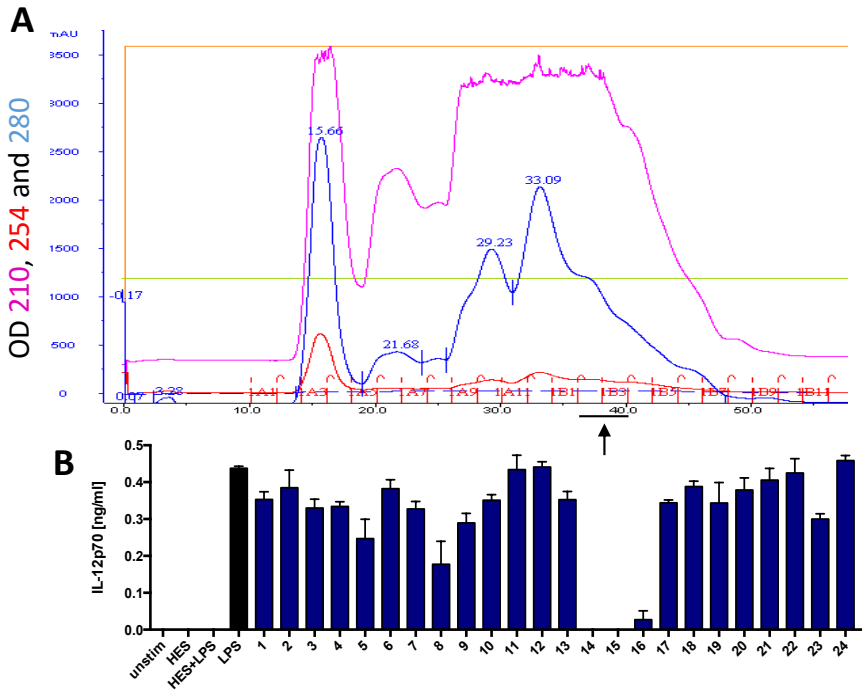

Figure 4.7: Size exclusion fractionation of HES resulted in two fractions completely inhibiting IL-12p70 production by LPS-stimulated GM-CSF BMDC. HES was fractionated by size exclusion fractionation and fractions tested for their ability to inhibit LPS-induced IL-12p70 production by BMDC differentiated with GM-CSF. **(A)** Äkta profile of size exclusion fractionation. **(B)** IL-12p70 concentrations in supernatants of GM-CSF BMDC treated with LPS and HES or fractions as indicated.

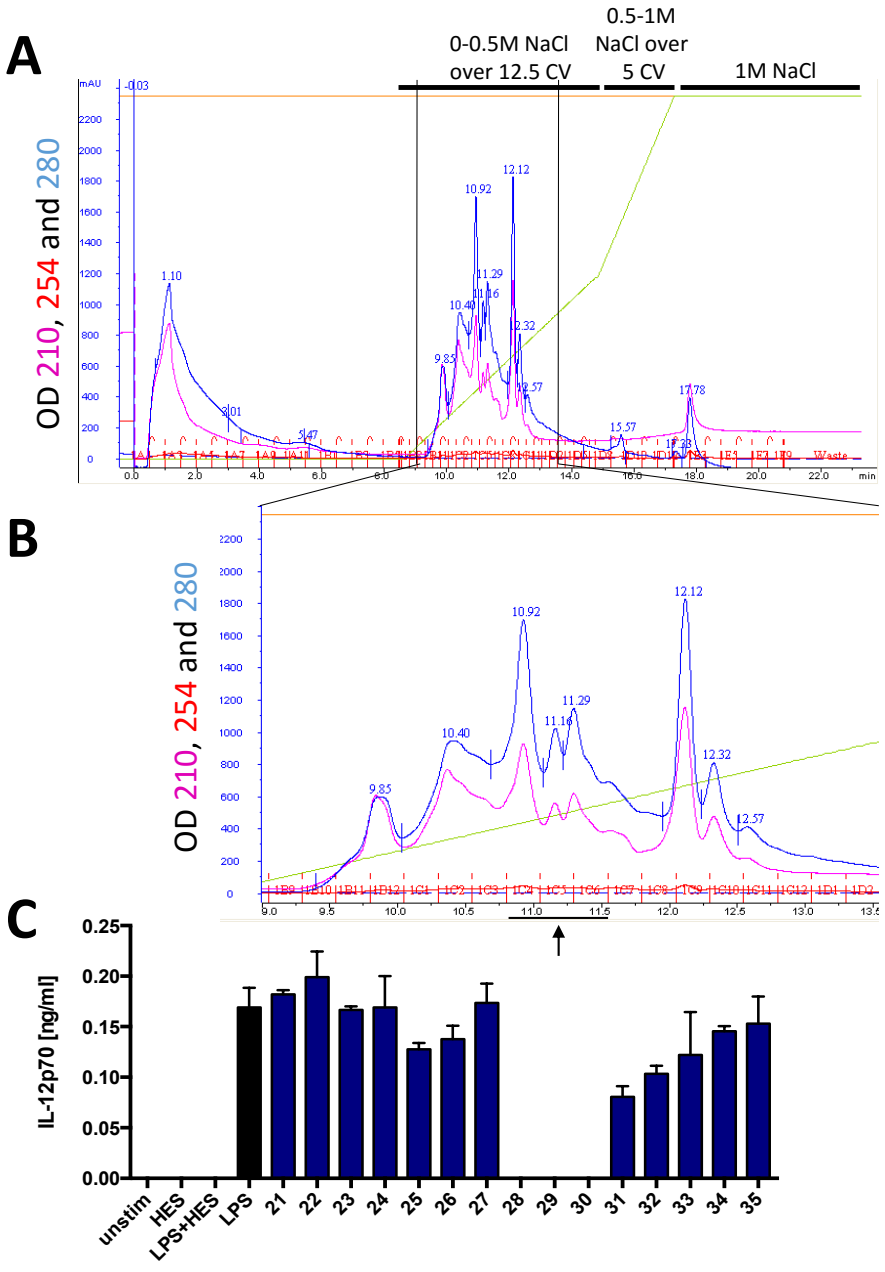

Figure 4.8: Sequential fractionation of HES resulted in three fractions completely inhibiting IL-12p70 production by LPS-stimulated GM-CSF BMDC. The two active size exclusion fractionation fractions 14 and 15 were pooled and further fractionated by anion exchange fractionation. Fractions were tested for their ability to inhibit LPS-induced IL-12p70 production by BMDC differentiated with GM-CSF. **(A)** Äkta profile of the sequential fractionation. **(B)** Magnification of the area of the fractionation profile with fractions containing protein. **(C)** IL-12p70 concentrations in supernatants of GM-CSF BMDC treated with LPS and HES or fractions as indicated. Arrow indicates active fractions.

4.2.2.2 Proteomics analysis of sequential fractions

In contrast to the previous round, mass spectrometric analysis of the sequential fractions was performed in the facility in Edinburgh, again using an Orbitrap mass spectrometer and using Mascot and the in-house *H. polygyrus* transcriptomics database. The significance threshold for consideration of proteins again was $p<0.05$, but a minimum cutoff score of 20 was set in addition. Mass spectrometry of fractions 28, 29 and 30 produced no fewer than 311, 306 and 277 identities respectively. To narrow the field of likely candidates, the 12 other fractions devoid of activity (21-27 and 31-35) were also subjected to mass spectrometry on the same instrument. The abundance profiles of each protein identified in the 15 analysed fractions were then calculated. A measurement for protein abundance in mass spectrometry is the exponentially modified protein abundance index, the emPAI (Ishihama et al., 2005). This value is dependent on the properties of the peptides and therefore not strictly comparable between different proteins, but is a valid measure when comparing emPAI values of the same protein.

To enable compilation of emPAI profiles, these values were extracted from the mass spectrometry results files using another script written in Python (Appendix A.4). Then those proteins with emPAI values peaking in any of the active fractions were identified (see Tab. B.8 in the appendix), from this list, proteins with emPAI profiles fitting the activity profile of the fractions were selected by hand. Fig. 4.9 shows one example of a protein that was considered as having a poor fit between activation and abundancy profiles and therefore was discounted (Fig. 4.9A), and NSP-42, a protein with a good fit (Fig. 4.9B).

The resulting list of potential candidate proteins is shown in Tab. 4.2. Of the 18 proteins thus identified, seven were excluded as they were either falsely identified with the found peptides not actually matching the protein sequence, or identified by only one peptide. Another protein was excluded as being a housekeeping protein, as it belonged to the chaperonin family of proteins (Tab. 4.3). To further reduce the number of potential candidate proteins, they were compared to our in house proteomics database. According to this, another five proteins could be excluded as being specific egg or larval stage proteins (Tab. 4.4). The abundance profiles of the proteins thus rejected from the list of proteins with top priority for expression can be found in the appendix (Fig. B.1). This selection resulted in a list of five remaining proteins with good fits of their abundance profiles to the activity profile of the sequential fractions (Fig. 4.10).

The five remaining candidate proteins have mostly unknown functions. One of them was VAL-4 (Hpb-VAL-4), a protein belonging to one of the most abundant

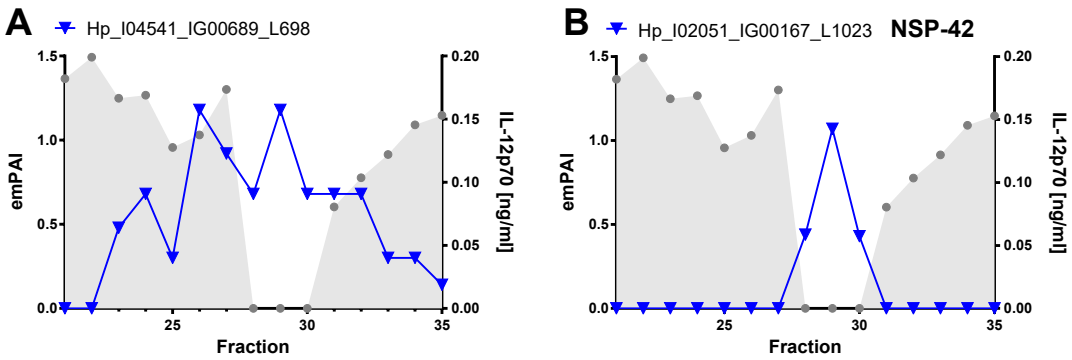

Figure 4.9: Examples for proteins peaking in the active sequential fractions and an overall (A) poor or (B) good fit of abundance profile to activity profile. HES was fractionated by size exclusion fractionation (Fig 4.7) followed by fractionation of the DC inhibitory fractions by anion exchange (Fig 4.8). All sequential fractions were analysed by mass spectrometry and results compared to identify proteins with emPAI values peaking in the active fractions 28-30 (see Tab. B.8 for all 221 proteins). To further narrow down the list of potential candidates, proteins with abundance profiles with good fits to the fraction activities were selected, resulting in a list of 18 proteins (see Tab. 4.2). Shown here are **(A)** one example of a protein with emPAI values peaking in the active fractions but with an overall bad fit to the activity profile and **(B)** one example of a protein with a good fit.

protein families in HES, the venom allergen-like protein family. Another protein, Hp_I20539_IG12483_L707, was found to contain an ShK-like domain, and therefore belongs to another abundant protein family. This specific protein was however not identified before and has for this work been given the name ShK-707. Two of the proteins were novel secreted proteins, NSP-4 (Hp_I24607_IG16551_L570) and NSP-42 (Hp_I02051_IG00167_L1023). These proteins are defined by their lack of any conserved domain or sequence similarity to proteins in other organisms and their functions in *H. polygyrus* are unknown. The last protein, Hp_I26188_IG18132_L529, had not been found before and did not show any conserved domains either and was therefore named L529 according to its length.

Table 4.2: Longlist of 18 candidate proteins for DC modulatory activity with their emPAI values across the sequential fractions. HES was fractionated by size exclusion fractionation (Fig 4.7) followed by fractionation of the DC inhibitory fractions by anion exchange (Fig 4.8). All sequential fractions were analysed by mass spectrometry in the facility in Edinburgh. The significance threshold for consideration of proteins was $p<0.05$; a minimum cutoff score of 20 was set. Results were compared to identify proteins with emPAI values peaking in the active fractions 28-30 (see Tab. B.8 for all 221 proteins), followed by selection of the 18 proteins with abundance profiles best fitting the fraction activities (see Fig. 4.9 for examples of poor and good fits). Blue shading: Active fractions completely inhibiting IL-12p70 production by LPS-activated GM-CSF BMDC. Red text: final five proteins chosen for expression.

	21	22	23	24	25	26	27	28	29	30	31	32	33	34	35
HELDS7W07IETUG_length=224	0	0	0	0	0	0	0	0.47	0.47	0.47	0	0	0	0	0
Hp_I00806_IG00050_L1112	0	0	0	0	0	0	0.18	0.09	0.18	0.18	0	0	0	0	0
Hp_I02051_IG00167_L1023	0	0	0	0	0	0	0	0.44	1.07	0.43	0	0	0	0	0
Hp_I05999_IG01134_L555	0	0	0	0	0	0	0	0	0.18	0.64	0.39	0.39	0	0	0.18
Hp_I13066_IG05010_L1961	0	0	0	0	0	0	0.1	0	0.1	0.05	0.05	0.05	0	0	0
Hp_I14250_IG06194_L1431	0	0	0	0	0	0	0	0.07	0.14	0.07	0.07	0	0	0	0
Hp_I15760_IG07704_L1122	0	0	0	0	0	0	0	0.09	0.18	0.18	0.09	0.09	0	0	0
Hp_I20539_IG12483_L707	0	0	0	0	0	0	0	0.47	0.29	0.14	0	0	0	0	0
Hp_I20654_IG12598_L702	0	0	0	0	0	0	0.14	0.47	0.29	0.29	0	0	0	0	0
Hp_I23863_IG15807_L590	0	0	0	0	0	0	0	0	0.83	0.16	0	0.17	0	0	0
Hp_I24607_IG16551_L570	0	0	0	0	0	0	0	1.56	1.99	0.17	0	0	0	0	0
Hp_I26188_IG18132_L529	0	0	0	0	0	0	0	2.74	2.17	0.64	0	0	0	0	0
Hp_I29394_IG21338_L484	0	0	0	0	0	0	0	0.21	1.61	1.15	1.15	0.21	0	0	0
Hp_I32194_IG24138_L452	0	0	0	0	0	0	0.22	0.48	0.22	0.48	0.22	0	0	0	0
Hp_I38698_IG30642_L388	0	0	0	0	0	0	0	0.59	0.59	1	0.59	0.26	0	0	0
Hp_I43851_IG35795_L337	0	0	0	0	0	0	0	0.29	12.13	1.8	0	0	0	0	0
Hp_I54277_IG46221_L174	0	0	0	0	0	0	0	1.74	0.66	0.66	0	0	0	0	0
Hpb-VAL-4	0	0	0	0	0	0	0	0.32	1.66	2.06	0.15	0	0	0	0

Table 4.3: Further analysis of 18 longlisted proteins listed in Table 4.2, considering conserved domains, top named blastx result and peptide coverage from mass spectrometry. After sequential fractionation of HES by size exclusion fractionation (Fig 4.7) and anion exchange fractionation (Fig 4.8) and mass spectrometry analysis of all sequential fractions, the sequences of the 18 proteins with the best fit of their emPAI values in the fractions to their inhibitory activity (see Fig 4.10 and Suppl Fig B.1) were further analysed to identify those proteins with only one peptide identified or inconsistent peptide identifications. Furthermore, sequences were subjected to blastx and conserved domain searches. Blue text: protein excluded as being a housekeeping protein; Red text: final five candidates chosen for expression.

	Domain search	**top named blastx hit**	**more than one peptide in MS?**
HELDS7W07IETUG_length=224	none	85% to putative T-complex protein 1, epsilon subunit [Ancylostoma ceylanicum]; 25% query cover	No - no peptide hit in sequence!
Hp_I00806_IG00050_L1112	Zn dependent Metalloprotease (astacin like)	67% to metalloprotease 1 precursor [Ancylostoma ceylanicum]; 95% query cover	mostly mismatched
Hp_I02051_IG00167_L1023	none	none	Yes
Hp_I05999_IG01134_L555	Transthyretin-like family	53% to transthyretin-like family protein [Necator americanus]; 70% query cover	No
Hp_I13066_IG05010_L1961	Chaperonin family	93% to Chaperonin Cpn60 TCP-1 domain containing protein [Haemonchus contortus]; 82% query cover	Yes

Table 4.3: Further analysis of 18 longlisted proteins listed in Table 4.2, considering conserved domains, top named blastx result and peptide coverage from mass spectrometry (continued).

	Domain search	**top named blastx hit**	**more than one peptide in MS?**
Hp_I14250_IG06194_L1431	Hyaluronan / mRNA binding family, SAM dependent methyltransferase class I, von Willebrand factor A superfamily	83% to hyaluronan / mRNA binding family protein [Necator americanus]; 40% query cover	No
Hp_I15760_IG07704_L1122	Ashwin superfamily, FCP1 C-term, chromatin assembly factor complex 1 p60	44% to unnamed protein [Haemonchus contortus]; 23% query cover	No - no peptide hit in sequence!
Hp_I20539_IG12483_L707	ShK superfamily	43% to ShTK domain containing protein [Brugia malayi]; 17% query cover	Yes
Hp_I20654_IG12598_L702	none	46% to chondroitin proteoglycan 3 [Haemonchus contortus]; 61% query cover	Yes
Hp_I23863_IG15807_L590	none	none	Yes
Hp_I24607_IG16551_L570	none	100% NSP-4 [H. polygyrus]	Yes
Hp_I26188_IG18132_L529	none	42% to trypsin inhibitor like cysteine rich domain protein [Oesophagostomum dentatum]; 30% query cover	Yes

Table 4.3: Further analysis of 18 longlisted proteins listed in Table 4.2, considering conserved domains, top named blastx result and peptide coverage from mass spectrometry (continued).

	Domain search	**top named blastx hit**	**more than one peptide in MS?**
Hp_I29394_IG21338_L484	none	33% to protein CELE_ZC412.3 [Caenorhabditis elegans]; 59% query cover	Yes
Hp_I32194_IG24138_L452	none	none	variants of one peptide
Hp_I38698_IG30642_L388	none	none	Yes
Hp_I43851_IG35795_L337	none	30% to uncharacterized protein [Caenorhabditis elegans]; 56% query cover	Yes
Hp_I54277_IG46221_L174	Translation elongation factor	98% to elongation factor 2 [Oesophagostomum dentatum]	No
Hpb-VAL-4	SCP superfamily	100% VAL-4 [H. polygyrus]	Yes

Table 4.4: Final step of selection of shortlisted proteins considering designations and ranks in egg release material (ERM), L4 larvae ES (L4ES) and HES according to the in-house proteomics analysis. After sequential fractionation of HES by size exclusion fractionation and anion exchange fractionation and mass spectrometry analysis of all sequential fractions, proteins with the best fit of their emPAI values in the fractions to their inhibitory activity were selected (see Fig 4.10 and Suppl Fig B.1). These 18 proteins were further narrowed down to this shortlist of 10 proteins by exclusion of housekeeping proteins and those with only one peptide identified or inconsistent peptide identifications. In a final selection step, names and ranks in egg release material, L4ES and HES for the shortlisted proteins were taken from an in house database. ERP: egg release protein; LSP: larval specific protein; NSP: novel secreted protein; VAL: venom allergen-like protein

	Name	ERM	L4ES	HES
Hp_I02051_IG00167_L1023	NSP-42	-	62	307
Hp_I20539_IG12483_L707	ShK-707	-	-	-
Hp_I20654_IG12598_L702	L702	149	-	304
Hp_I23863_IG15807_L590	LSP-11	-	169	-
Hp_I24607_IG16551_L570	NSP-4	-	128	39
Hp_I26188_IG18132_L529	L529	-	-	-
Hp_I29394_IG21338_L484	ERP-13	120	-	-
Hp_I38698_IG30642_L388	LSP-04	-	65	-
Hp_I43851_IG35795_L337	ERP-18	102	-	-
Hpb-VAL-4	VAL-4	-	133	17

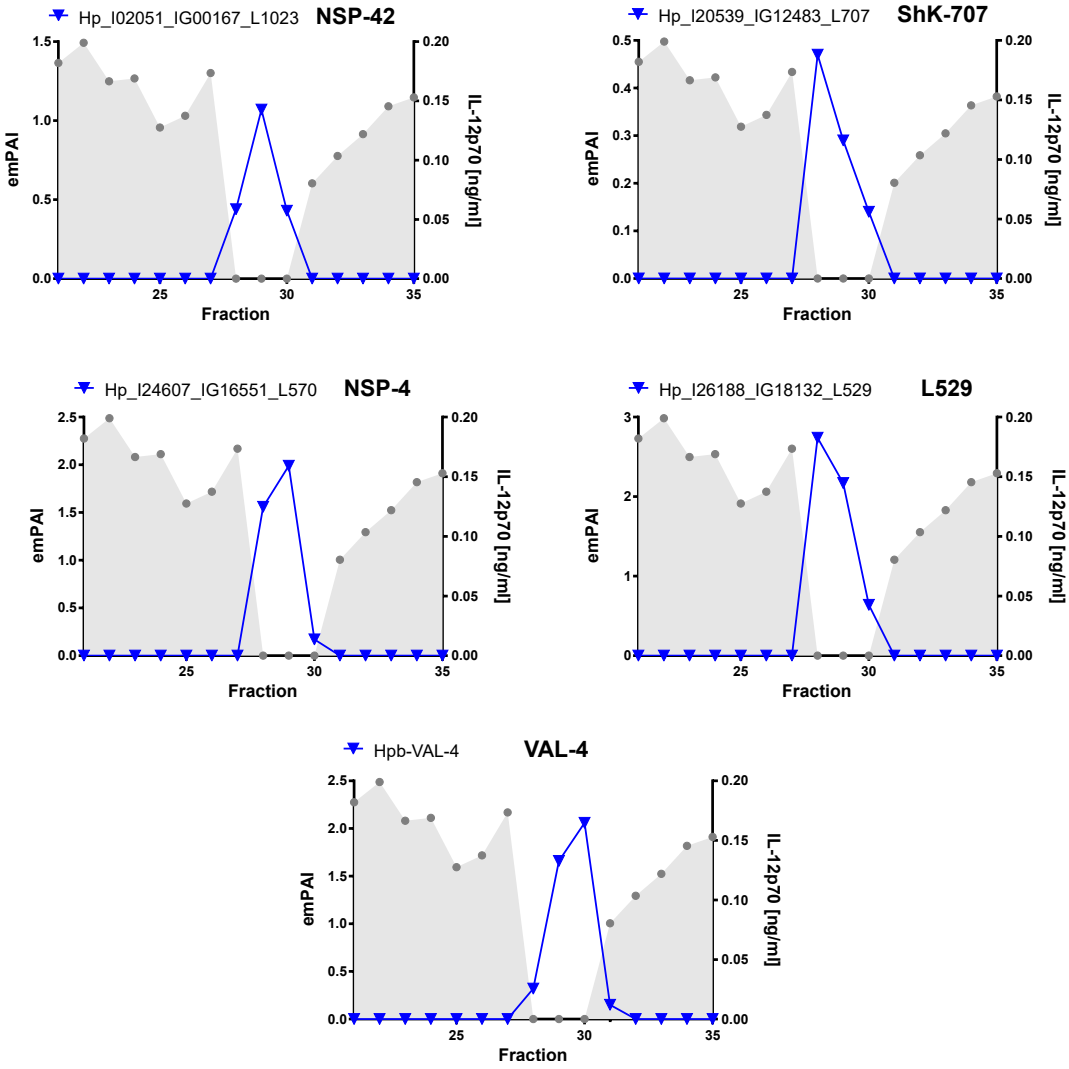

Figure 4.10: Top candidates from sequential fractionation. HES was fractionated using size exclusion fractionation (Fig 4.7) followed by anion exchange fractionation of the active fractions (Fig 4.8). All sequential fractions were analysed by mass spectrometry. Proteins with emPAI values peaking in the active fractions were subjected to further selection comparing their emPAI profiles to activity across the fractions, excluding housekeeping, egg or larval stage proteins and those that have been identified falsely or with only one peptide (see tables B.8, 4.3 and 4.4). This resulted in the shown five proteins as final candidates for expression. Shown are their names, the emPAI values across the fractions on the left y axis and the concentration of IL-12p70 produced by GM-CSF BMDC treated with LPS (1µg/ml) and the respective fraction on the right y axis.

4.2.2.3 Expression and test of candidate proteins

To be able to test those candidate proteins for inhibitory activities, signal peptides were identified and removed from their sequences (see Fig. 4.11), and sequences codon optimized, restriction sites for ligation into pSecTag2a as expression vector added and DNA synthesized by GeneArt. The sequence was inserted into pSeqTag2a so that it would be expressed under the vector's promoter with the vector's signal peptide, but with a stop codon immediately after the 6xHis-Tag as shown in Fig. 4.12A. HEK-293 cells were transfected with those plasmids and after four weeks of selection with Zeocin containing medium, the supernatants of stable cell lines secreting the recombinant proteins collected, dialysed into HIS-Binding buffer and purified using nickel-charged 1ml HiTrap™ Chelating HP columns. The Äkta profiles of those purifications can be seen in Fig. 4.12B, left hand panels. Protein contents of the fractions were visualized by SDS-PAGE and Western Blot (right hand panels). Comparing the sizes of the constructs according to the western blots with the predicted sizes of the proteins (see Fig. 4.11), only the NSP-42 fractions contained proteins that were of the predicted size of around 14 kDa, in addition to much larger proteins of around 50 kDa. The size of ShK-707 was predicted to be almost 18 kDa, but the recombinant protein produced a band between 40 to 45 kDa. Similarly, NSP-4 was predicted to have a size of 16 kDa but ran at around 30 kDa. The recombinant L529 was around double the predicted size as well, with a predicted size of around ten and an actual size of around 20 kDa. VAL-4 was predicted to be around 22 kDa but came to an actual size of 30 to 35 kDa.

For further use, the fractions containing the recombinant proteins with as little contamination as possible were pooled (per protein), dialysed into PBS and concentrated using VivaSpin columns.

To see if any of the recombinant proteins had DC inhibitory activity, day ten GM-CSF BMDC were incubated for 18h with LPS, HES or the proteins as indicated. None of the proteins were able to inhibit LPS-induced IL-12p70 production (Fig. 4.13).

NSP-42

14.17 kDa

MLSTYLTAVC ALLTSAGIGA NSVRSCSDVT DTVKDTIIRT VEAEVPTLEW
NEVFFPYAQQ YGINGKKPHP EENYIYLKKK GEFVGNATLD EMATTVLDSV
TEETKQALRS NPGNRIYACV AIHCDKTEHT PISLEVACIS TVATMQN

ShK-707

17.65 kDa

ShK-like domain

MLLVFLLLIV VVSGKPLSEG EPQICEDKST DCDTQMDVCH DPMWERAMRR
YCAKTCGFCR AEVTTTTTTM TAPPTTSKPH QKPQQQQQQQ SLIILFFQPE
RCHRLFEQVC RWIVTYGQFP NLIRIPYYNT AQLQRSEASD SDRESNSIPV
LGPENDRIFT RPNDSSPTKE SD

NSP-4

15.78 kDa

MIRFVVSVLS MTHFVSLERI NCHGSGGDWQ LGMYESYHEN LSWYLTLDCD
IVGEAIAANE FELKNPNEPQ RFLNSTKYCR YSNVLHKDTI GIGGGDVTTL
LNGLPREQIK RTLWKLGETT FGCSAHNYRY PAFADHTHVK LICLYRKQHA
EPTCI

L529

10.03 kDa

MLCKLFVLTA LICAVASDDE DKGCGPNEKY YEEECAPMET CWSMRVLTRC
DKGRCGCKDG YLWGYDGCQL FGTPGCTKED RLHYSYHTHH RKRREAFRFG
NH

VAL-4

21.83 kDa

MSTLPTVSFL VVLVALGKAE FGCDGTLEQN DTTREVFLRF HNDVRKFIAL
GIYPNKVGVL GPAKNMYQLK WSCDLEEEAH ESIYSCSYNP LLLHPQSYSK
SCP-like domain
LLSVDLPDTD VVGATLEMWT EFMRIYGVNT KTNSYNPSFS QFANMAYSKN
TKVGCSYKKC GGDTLVTCVY ELGVKLPSHP QMWENGPTCV CVAYTDSICN
DNNLCEYAPT SAR

Figure 4.11: Sequences, predicted molecular weights and conserved domains of the first five candidate proteins. After mass spectrometry analysis of HES sequentially fractionated by size exclusion fractionation and anion exchange fractionation and several steps of selection of probable candidates for DC modulatory activity, the shown five proteins were selected for expression. Red: Signal peptide (not cloned); Green: peptides identified by mass spectrometry; Underlined with blue description: conserved domains.

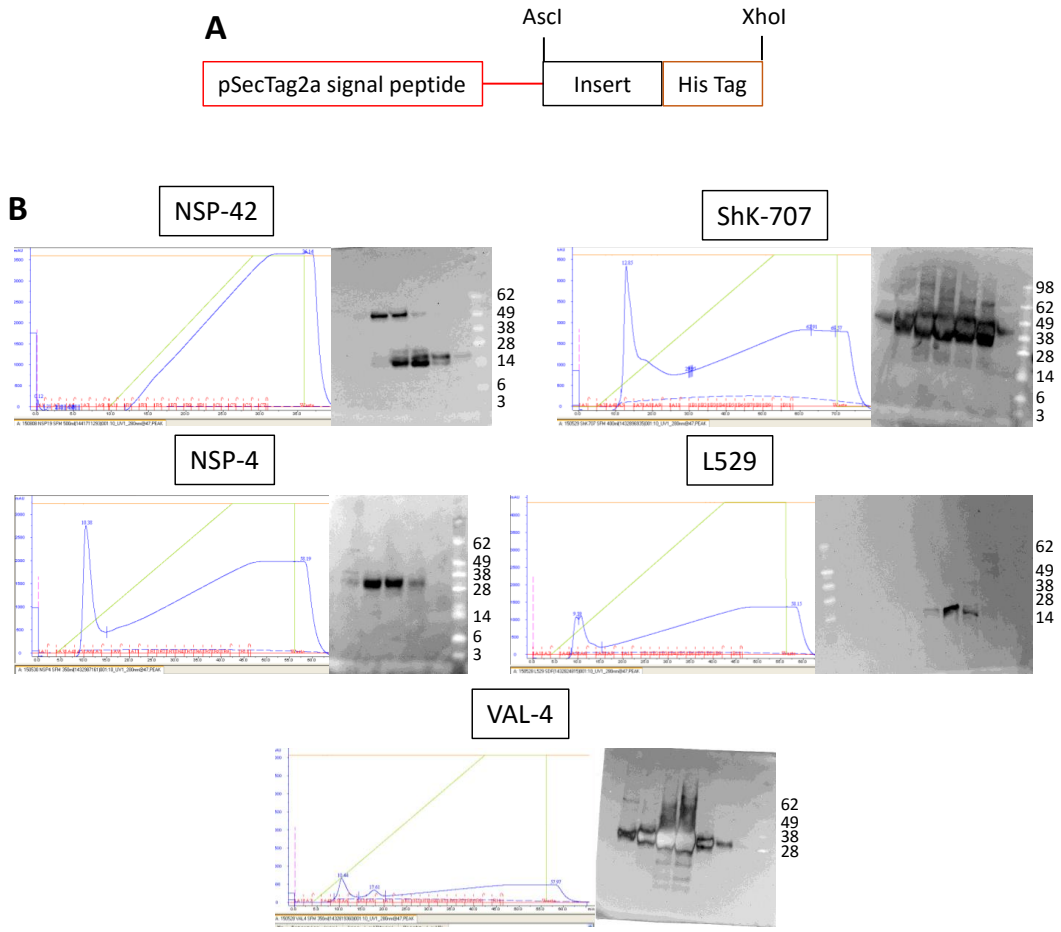

Figure 4.12: Cloning and expression of the first five candidate proteins. Sequences were codon optimized for expression in human cells, ordered from GeneArt, digested with the appropriate restriction enzymes and inserts purified by gel electrophoresis and gel extraction and ligated into the expression vector pSecTag2a. **(A)** Schematic of the proteins produced, with vector sequences in red and restriction sites used indicated (not drawn to scale). **(B)** After transfection into HEK293 cells, supernatants were collected and purified (Akta profiles in the left panels). Candidate protein content in the fractions was visualized with SDS-PAGE and Western Blot detecting the His-tag (right panels).

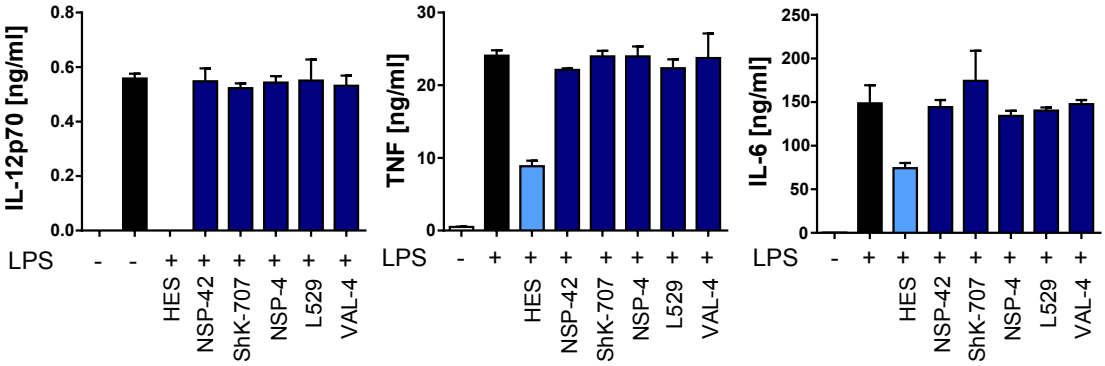

Figure 4.13: None of the five candidates from the sequential fractionation inhibit LPS-induced DC activation. BMDC were differentiated with GM-CSF for ten days before stimulation with LPS and 10µg/ml of either HES or candidate proteins as indicated. IL-12p70, TNF and IL-6 concentrations in supernatants were measured by ELISA. This experiment was performed twice using the same batch of proteins.

4.2.3 Proteomics analysis of size exclusion, sequential and anion exchange fractions leads to identification of four further candidates, but not the DC modulator

To reduce the amount of subjective manual selection of proteins with abundance profiles fitting the activity profiles of the fractions, more parameters were included. As shown in the schematic in Fig. 4.14, fractions from size exclusion, anion exchange and sequential fractionation of HES were obtained, analysed for DC modulatory activity and subjected to mass spectrometry for comparison of their protein contents.

4.2.3.1 HES fractionations

In addition to the already performed mass spectrometric analysis of the sequential fractions, the size exclusion fractions acquired in the first step of generating the sequential fractions were analysed by mass spectrometry as well, again in the facility in Edinburgh and with a minimum Mascot score of 20. For a list of proteins identified in the active fractions 14 and 15, see tables B.9 and B.10 in the appendix. Interestingly, while there are overlaps to the previous analysis of size fractions 14 and 15, which

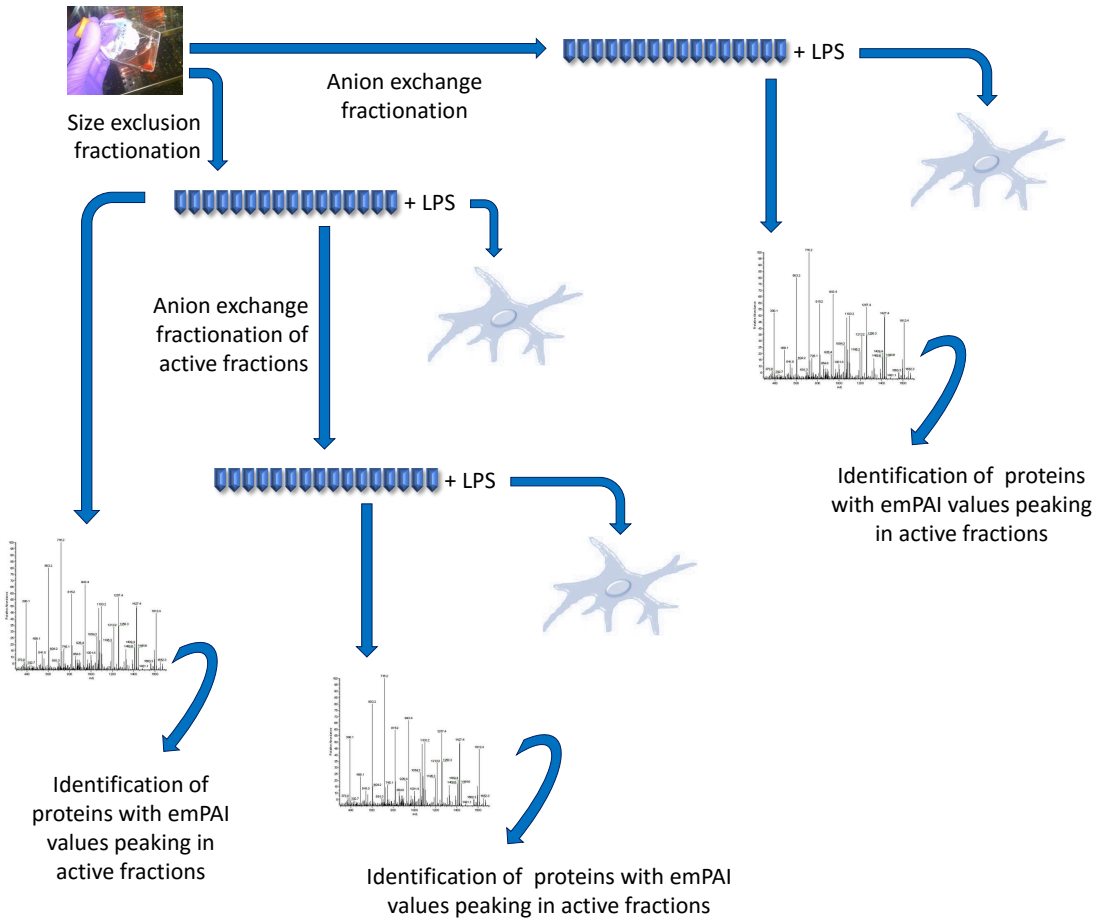

Figure 4.14: Schematic of workflow of third round to identify further candidate proteins. HES was fractionated by either size exclusion fractionation or anion exchange fractionation and fractions tested for DC inhibitory activity. Active size fractions were further fractionated by anion exchange fractionation (as described above). All fractions were analysed by mass spectrometry and protein contents and abundance distributions compared.

was performed in the facility in Glasgow, there are also notable differences. Firstly, the number of proteins identified by this later analysis greatly exceeded the number identified in the first, with 206 compared to 26 proteins in fraction 14 and 105 compared to 38 proteins in fraction 15. The proteins identified in both of the respective fractions are coloured in green in tables B.1, B.2, B.9 and B.10, with the ranks in the other fractionation mentioned as well. More than half of the proteins identified in the first fractionation have not been found in the second, and the ranks of the proteins

that have been found again were very different.

In addition to the analysis of the size exclusion fractions, HES (1mg) was also subjected to anion exchange fractionation using the same gradient as for the pooled size fractions 14 and 15 before, but collecting 1ml fractions this time. Here, fraction 25 completely inhibited IL-12p70 production by LPS-stimulated GM-CSF BMDC. The difference to the neighbouring fractions was not quite as clear cut as before, with fractions 24, 26 and 27 also showing partial inhibitory activity (Fig. 4.15). This was not due to lower total protein concentrations in these fractions, as those were comparable between fractions 24-26 (data not shown).

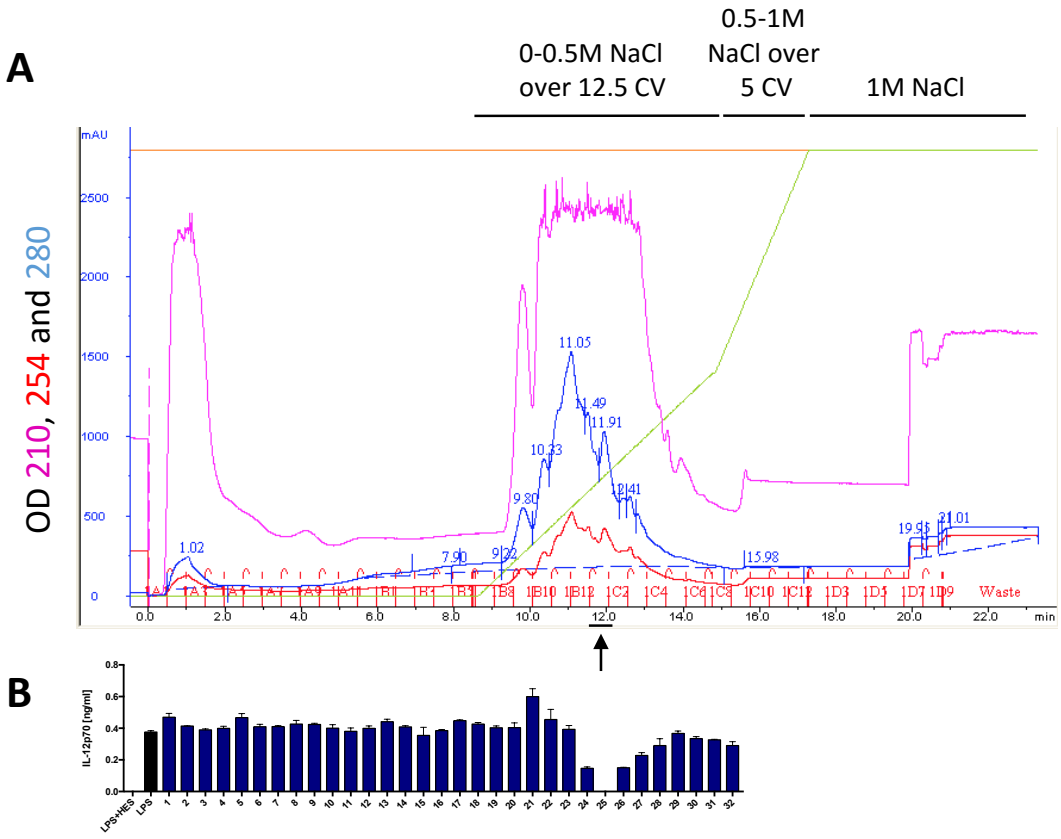

Figure 4.15: Anion exchange fractionation of HES resulted in one fraction completely inhibiting IL-12p70 production by LPS-stimulated GM-CSF BMDC. 1mg of HES was fractionated by anion exchange fractionation and fractions tested for their ability to inhibit LPS-induced IL-12p70 production by BMDC differentiated with GM-CSF. **(A)** Akta profile of anion exchange fractionation. **(B)** IL-12p70 concentrations in supernatants of GM-CSF BMDC treated with LPS and HES or fractions as indicated. Arrow indicates active fraction.

Again, all fractions were analysed by mass spectrometry in the Edinburgh facility, using the minimum cutoff Mascot score of 20; the list of proteins found in anion exchange fraction 25 can be found in Tab. B.11. Again, this list was compared to the lists of proteins found previously in the active fractions 39 (Tab. B.3) and 40 (Tab. B.4), with shared proteins being coloured green and the ranks in the other fractionation approach indicated. Overlap between the fractionations seemed slightly better here, with many proteins found in fractions 39 and 40 also being identified in fraction 25. However, the ranks of proteins found in both fractionations were very different, and the number of proteins identified in fraction 25 again greatly exceeded the number of proteins identified in the previous fractionation, with 256 proteins in fraction 25 compared to the 70 in fraction 39 and 105 in fraction 40.

4.2.3.2 Proteomics analysis of all fractions

As before, the first step for compiling a list of potentially interesting proteins was to extract the proteins' emPAI values and identify those proteins with emPAI values peaking in the active fractions for each fractionation (see Tab. B.8, B.12 and B.13 for lists of these). Using another Python script (Appendix A.5), these lists were compared to identify proteins shared between fractionations. The numbers of proteins with emPAI values peaking in the active fractions of any combination of the three fractionation approaches can be seen in Fig. 4.16.

The emPAI values of the four proteins with emPAI peaks in the active fractions of all three fractionation approaches are given in Tab. 4.5, 4.6 and 4.7. Considering only four proteins peaked in the active fractions of all fractionation approaches and the lack of a clear cut activity profile of the anion exchange fractionation, proteins with peaks in the active fractions of the size and sequential fractionations but not the anion exchange fractionation were considered as well (Tab. 4.8 and 4.9).

This increased the number of initially shortlisted proteins to 29. Again, proteins with abundance profiles too different from the activity profiles of the fractions were excluded by hand, leaving only 8 proteins for further consideration (see Fig. 4.17 and B.2). Of those, three had to be excluded as they were identified falsely or with only one peptide. Another protein was excluded as a housekeeping protein after blastx and conserved domain searches identified it as a phosphoenolpyruvate carboxykinase (Tab. 4.10). With this, only four proteins were left and chosen for expression. Among those were a previously identified ShK domain containing protein, SXCL4, and with NSP-19 another novel secreted protein. The other two proteins identified were one

containing a transthyretin-like domain, TTR-10, and another completely novel protein without any sequence similarities, named L452 according to the length of its sequence in the in house transcriptomics database (Tab. 4.11). Their emPAI profiles against the fraction activity profiles can be found in Fig. 4.17.

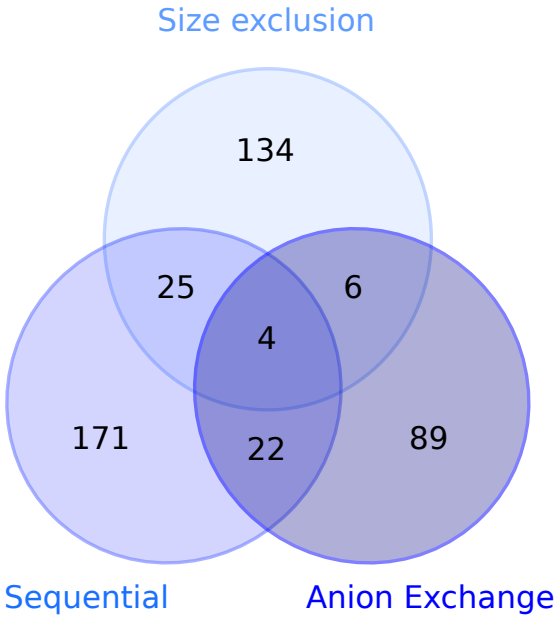

Figure 4.16: Number of proteins with emPAI values peaking in active fractions of size exclusion, sequential and anion exchange fractionations. HES was fractionated by size exclusion fractionation (see Fig. 4.7), sequentially by anion exchange fractionation of the two active size fractions (see Fig. 4.8) and anion exchange fractionation of HES (Fig. 4.15) and fractions tested for inhibitory activity on GM-CSF differentiated BMDC. All fractions were analysed by mass spectrometry in the facility in Edinburgh, using an Orbitrap mass spectrometer and using Mascot and the in-house *H. polygyrus* transcriptomic database. The significance threshold for consideration of proteins was $p<0.05$; a minimum cutoff score of 20 was set. The emPAI values across all fractions were compared to find proteins with abundance profiles peaking in active DC inhibitory fractions of all fractionation approaches. Shown are the number of proteins sharing emPAI peaks between the active fractions of the indicated fractionations.

Table 4.5: Size exclusion fractionation emPAI values of proteins peaking in active fractions of all fractionation approaches. HES was fractionated by size exclusion (Fig. 4.7), anion exchange (Fig. 4.15) and sequential fractionation (Fig. 4.8) and all fractions analysed by mass spectrometry. The emPAI values across all fractions were compared to find proteins with emPAI values peaking in active DC inhibitory fractions of all fractionation approaches. Shown here are proteins with emPAI peaks in the active fractions of all three fractionation approaches with their emPAI values across the size exclusion fractions. Blue shading: Fractions that completely abolished IL-12p70 secretion by LPS activated BMDC. Red text: Expressed proteins.

	3	4	5	6	7	8	9	10	11	12	13	14	15	16	17	18	19
GNK0QLK03GQOZO_length=396	0	0	0	0	0	0	0	0	0	0	0.25	1.41	0.55	0	0	0	0
Hp_I12776_IG04720_L2202	0	0	0	0	0	0	0	0	0.04	0	0	0.09	0	0	0	0	0
Hp_I19958_IG11902_L735	0	0	0	0	0	0	0	0	0	0	0.13	0.13	0	0	0	0	0
Hp_I29394_IG21338_L484	0	0	0	0	0	0	0	0	0	0	0.21	0.47	0	0	0	0	0

Table 4.6: Sequential fractionation emPAI values of proteins peaking in active fractions of all fractionation approaches. HES was fractionated by size exclusion (Fig. 4.7), anion exchange (Fig. 4.15) and sequential fractionation (Fig. 4.8) and all fractions analysed by mass spectrometry. The emPAI values across all fractions were compared to find proteins with emPAI values peaking in active DC inhibitory fractions of all fractionation approaches. Shown here are proteins with emPAI peaks in the active fractions of all three fractionation approaches with their emPAI values across the sequential fractions. Blue shading: Fractions that completely abolished IL-12p70 secretion by LPS activated BMDC. Red text: Expressed proteins.

	21	22	23	24	25	26	27	28	29	30	31	32	33	34	35
GNK0QLK03GQOZO_length=396	0	0	0	0	0.25	0.25	0.25	1.41	2.74	2.74	1.41	1.41	0.55	0.25	0.55
Hp_I12776_IG04720_L2202	0	0	0	0.09	0	0	0.09	0.13	0.04	0.13	0.04	0	0	0	0
Hp_I19958_IG11902_L735	0	0	0	0	0	0	0	0	0.28	0.28	0.13	0	0	0	0
Hp_I29394_IG21338_L484	0	0	0	0	0	0	0	0.21	1.61	1.15	1.15	0.21	0	0	0

Table 4.7: Anion exchange fractionation emPAI values of proteins peaking in active fractions of all fractionation approaches. HES was fractionated by size exclusion (Fig. 4.7), anion exchange (Fig. 4.15) and sequential fractionation (Fig. 4.8) and all fractions analysed by mass spectrometry. The emPAI values across all fractions were compared to find proteins with emPAI values peaking in active DC inhibitory fractions of all fractionation approaches. Shown here are proteins with emPAI peaks in the active fractions of all three fractionation approaches with their emPAI values across the anion exchange fractions. Blue shading: Fractions that completely abolished IL-12p70 secretion; Grey shading: Fractions that partially inhibited IL-12p70 secretion by LPS activated BMDC. Red text: Expressed proteins.

	19	20	21	22	23	24	25	26	27	28	29	30	31	32
GNK0QLK03GQOZO_length=396	0	0	0	0	0	0	0.55	0	0	0	0	0	0	0
Hp_I12776_IG04720_L2202	0	0	0	0	0	0	0.04	0	0	0	0	0	0	0
Hp_I19958_IG11902_L735	0	0	0	0	0	0	0.13	0	0	0	0	0	0	0
Hp_I29394_IG21338_L484	0	0	0	0	0	0	0.21	0	0	0	0	0	0	0

Table 4.8: Size exclusion fractionation emPAI values of proteins peaking in active fractions of size exclusion and sequential fractionation. HES was fractionated by size exclusion (Fig. 4.7), anion exchange (Fig. 4.15) and sequential fractionation (Fig. 4.8) and all fractions analysed by mass spectrometry. The emPAI values across all fractions were compared to find proteins with emPAI values peaking in active DC inhibitory fractions of size exclusion and sequential fractionation approaches. These are shown here with their emPAI values across the size exclusion fractions. Blue shading: Fractions that completely abolished IL-12p70 secretion by LPS activated BMDC. Red text: Expressed proteins.

	3	4	5	6	7	8	9	10	11	12	13	14	15	16	17	18	19
GS66ZV203DB0T9_length=193	0	0	0	0	0	0	0	0	0.55	0.55	0	0.55	0	0	0	0	0
HICN8C105F7BX8_length=227	0	0	0	0	0	0	0	0	0	0.47	0	0.47	0	0	0	0	0
HICN8C106HP9PI_length=274	0	0	0	0	0	0	0	0	0	0	0.82	2.31	0.35	0.82	0	0.35	0

Table 4.8: Size exclusion fractionation emPAI values of proteins peaking in active fractions of size exclusion and sequential fractionation (continued).

	3	4	5	6	7	8	9	10	11	12	13	14	15	16	17	18	19
Hp_I00695_IG00044_L591	0	0	0	0	0	0	0	0	0	0	0	0.16	0.16	0	0	0	0
Hp_I03228_IG00366_L2337	0	0	0	0	0	0	0	0	0	0	0	0.04	0	0	0	0	0
Hp_I05407_IG00935_L1040	0	0	0.09	0.09	0.09	0.09	0	0	0	0	0.09	0.09	0	0	0	0	0
Hp_I05827_IG01076_L1116	0	0	0	0	0	0	0	0	0	0	0	0.38	0.08	0	0.08	0.08	0
Hp_I05999_IG01134_L555	0	0	0	0	0	0	0	0	0	0	0	0.18	0	0	0	0	0
Hp_I07334_IG01751_L2741	0	0	0	0	0	0	0	0	0	0	0	0.04	0	0	0	0	0
Hp_I14584_IG06528_L1336	0	0	0	0	0	0	0	0	0	0.07	0.07	0.07	0.07	0	0	0	0
Hp_I15760_IG07704_L1122	0	0	0	0	0	0	0	0	0	0	0	0.09	0	0	0	0	0
Hp_I15783_IG07727_L1116	0	0	0	0	0	0	0	0	0	0	0	0.09	0	0	0	0	0
Hp_I19989_IG11933_L735	0	0	0	0	0	0	0	0	0	0	0.29	1.46	0	0	0	0	0
Hp_I21313_IG13257_L675	0	0	0	0	0	0	0	0	0	0	0.48	2.69	0	0.14	0	0	0
Hp_I22350_IG14294_L635	0	0	0	0	0	0	0	0	0	0	0.15	0.15	0	0	0	0	0
Hp_I23863_IG15807_L590	0	0	0	0	0	0	0	0	0	0	0.16	0.16	0	0	0	0	0
Hp_I24096_IG16040_L584	0	0	0	0	0	0	0	0	0	0	0.38	0.38	0	0	0	0	0
Hp_I24512_IG16456_L570	0	0	0	0	0	0	0	0	0	0.37	0.61	0.89	0	0	0	0	0
Hp_I26601_IG18545_L528	0	0	0	0	0	0	0	0	0	0	6.31	6.31	0.44	0.2	0	0	0
Hp_I30585_IG22529_L470	0	0	0	0	0	0	0	0	0	0	0.21	0.21	0	0	0	0	0
Hp_I32194_IG24138_L452	0	0	0	0	0	0	0	0	0	0	0	0.48	0	0	0	0	0
Hp_I34646_IG26590_L427	0	0	0	0	0	0	0	0	0	0	0.53	4.47	0	0	0	0	0
Hp_I38850_IG30794_L366	0	0	0	0	0	0	0	0	0	0	0	0.65	0	0	0	0	0
Hp_I38988_IG30932_L386	0	0	0	0	0	0	0	0	0	0	0	0.98	0	0	0	0	0
Hp_I40999_IG32943_L364	0	0	0	0	0	0	0	0	0	0	0.28	0.28	0	0	0	0	0

Table 4.9: Sequential fractionation emPAI values of proteins peaking in active fractions of size exclusion and sequential fractionation. HES was fractionated by size exclusion (Fig. 4.7), anion exchange (Fig. 4.15) and sequential fractionation (Fig. 4.8) and all fractions analysed by mass spectrometry. The emPAI values across all fractions were compared to find proteins with emPAI values peaking in active DC inhibitory fractions of size exclusion and sequential fractionation approaches. These are shown here with their emPAI values across the sequential fractions. Blue shading: Fractions that completely abolished IL-12p70 secretion by LPS activated BMDC. Red text: Expressed proteins.

	21	22	23	24	25	26	27	28	29	30	31	32	33	34	35
GS66ZV203DB0T9_length=193	0	0	0	0	0	0.55	0.55	0	0	0.55	0	0	0	0	0
HICN8C105F7BX8_length=227	0	0	0	0	0	0	0	0	0	0.47	0	0	0	0	0
HICN8C106HP9PI_length=274	0	0	0.35	0	0.35	1.45	0.82	3.46	12.66	8.85	6.11	8.85	7.11	5.01	8.85
Hp_I00695_IG00044_L591	0	0	0.35	0.35	0	0.16	0.16	0.16	0.35	0	0	0	0	0	0
Hp_I03228_IG00366_L2337	0	0	0	0	0	0	0	0.04	0	0	0	0	0	0	0
Hp_I05407_IG00935_L1040	0	0	0	0	0	0	0.09	0.09	0	0.09	0	0	0	0	0
Hp_I05827_IG01076_L1116	0	0	0.18	0.52	0.18	0.38	0.38	0.5	0.4	0.52	0.27	0.18	0.18	0.27	0.18
Hp_I05999_IG01134_L555	0	0	0	0	0	0	0	0	0.18	0.64	0.39	0.39	0	0	0.18
Hp_I07334_IG01751_L2741	0	0	0	0	0	0	0	0.04	0.04	0.04	0	0	0	0	0
Hp_I14584_IG06528_L1336	0	0	0	0	0	0	0.07	0	0.15	0	0	0	0.07	0	0
Hp_I15760_IG07704_L1122	0	0	0	0	0	0	0	0.09	0.18	0.18	0.09	0.09	0	0	0
Hp_I15783_IG07727_L1116	0	0	0	0	0.09	0	0.09	0.09	0	0	0	0	0	0	0
Hp_I19989_IG11933_L735	0	0	0	0.14	0	0	0	0	0	0.14	0	0	0	0	0
Hp_I21313_IG13257_L675	0	0	0.14	0.15	0.3	0.69	2.24	4.47	2.24	2.24	2.69	0.92	0.48	0.3	0.69
Hp_I22350_IG14294_L635	0	0	0	0	0	0	0.32	0.32	0.15	0	0	0	0	0.15	0
Hp_I23863_IG15807_L590	0	0	0	0	0	0	0	0	0.83	0.16	0	0.17	0	0	0
Hp_I24096_IG16040_L584	0	0	0	0.18	0.18	0.18	0.18	0	0	0.18	0	0	0	0	0
Hp_I24512_IG16456_L570	0	0	0	0.37	0.61	0.37	2.57	2.04	1.6	3.18	0.89	0.37	0	0	0

Table 4.9: Sequential fractionation emPAI values of proteins peaking in active fractions of size exclusion and sequential fractionation (continued).

	21	22	23	24	25	26	27	28	29	30	31	32	33	34	35
Hp_I26601_IG18545_L528	0	0	0.2	0.72	1.47	0.72	1.06	0	0.44	1.96	0.72	0.44	0	0	0
Hp_I30585_IG22529_L470	0	0	0.21	0.21	0	0	0.21	0.21	0.21	0.21	0	0	0	0	0
Hp_I32194_IG24138_L452	0	0	0	0	0	0	0.22	0.48	0.22	0.48	0.22	0	0	0	0
Hp_I34646_IG26590_L427	0	0	0.53	0.53	0.89	0.53	0.89	0.24	0.53	0.89	0.24	0.53	0	0	0.24
Hp_I38850_IG30794_L366	0	0	0.28	0	0	0	0.28	0.28	0	0	0	0	0	0	0
Hp_I38988_IG30932_L386	0	0	2.12	1.49	0.98	0.98	0.58	0.58	2.12	0.58	0.98	0.58	0.26	0.58	0.58
Hp_I40999_IG32943_L364	0	0	0.65	1.71	0.65	2.48	1.11	0.65	2.48	1.71	0.28	0	0	0.28	0.28

Table 4.10: Further selection of eight shortlisted proteins considering conserved domains, top named blastx result and peptide coverage from mass spectrometry. After comparing emPAI profiles of proteins identified in size exclusion (Fig. 4.7), sequential (Fig. 4.8) and anion exchange fractionation of HES (Fig. 4.15) and identifying the 29 proteins that peak in active fractions of all three fractionations or size exclusion and sequential fractionation, the sequences of the eight proteins with the best fit of their emPAI values in the fractions to their inhibitory activity (see Fig. 4.17 and Suppl. Fig. B.2) were further analysed to identify those proteins with only one peptide identified or inconsistent peptide identifications. Furthermore, sequences were subjected to blastx and conserved domain searches. Blue text: protein excluded as being a housekeeping protein; Red text: final five candidates chosen for expression.

	Domain search	top named blastx hit	more than one peptide in MS?
GNK0QLK03GQOZO_length=396	ShK superfamily	44% to shTK domain protein [Oesophagostomum dentatum]; 45% query cover	Yes

Table 4.10: Further selection of eight shortlisted proteins considering conserved domains, top named blastx result and peptide coverage from mass spectrometry (continued).

	Domain search	top named blastx hit	more than one peptide in MS?
Hp_I12776_IG04720_L2202	Phosphoenolpyruvate carboxykinase (GTP)	93% to phosphoenolpyruvate carboxykinase domain containing protein [Haemonchus contortus]; 89% query cover	Yes
Hp_I19958_IG11902_L735	Transthyretin-like family	89% to Transthyretin-like family protein [Necator americanus]; 53% query cover	Yes
HICN8C105F7BX8_length=227	none	none	No
Hp_I03228_IG00366_L2337	-	-	no peptide hit in sequence
Hp_I07334_IG01751_L2741	cell division protein ZipA like domain	81% to oxidoreductase, short chain dehydrogenase/reductase family protein [Necator americanus]; 66% query cover	No
Hp_I21313_IG13257_L675	none	46% to unnamed protein product [Haemonchus contortus]; 56% query cover	Yes
Hp_I32194_IG24138_L452	none	none	Yes

Table 4.11: Candidates for expression including names and ranks in egg release material (ERM), L4 larvae ES (L4ES) and HES according to the in house proteomics analysis. After comparing emPAI profiles of proteins identified in size exclusion, sequential and anion exchange fractionation of HES and identifying the 29 proteins that peak in active fractions of all three fractionation approaches or size exclusion and sequential fractionation, the eight proteins with the best fit of their emPAI values in the fractions to their inhibitory activity were selected (see Fig. 4.17 and Suppl. Fig. B.2). These were further narrowed down to this list of four top priority proteins by exclusion of housekeeping proteins and those with only one peptide identified or inconsistent peptide identifications. Names and ranks in egg release material, L4ES and HES for the listed proteins were taken from an in-house database. TTR: Transthyrethin; NSP: novel secreted protein

	Name	ERM	L4ES	HES
GNK0QLK03GQOZO_length=396	SXCL4	112	68	-
Hp_I19958_IG11902_L735	TTR-10	-	182	206
Hp_I21313_IG13257_L675	NSP-19	150	-	124
Hp_I32194_IG24138_L452	L452	-	-	-

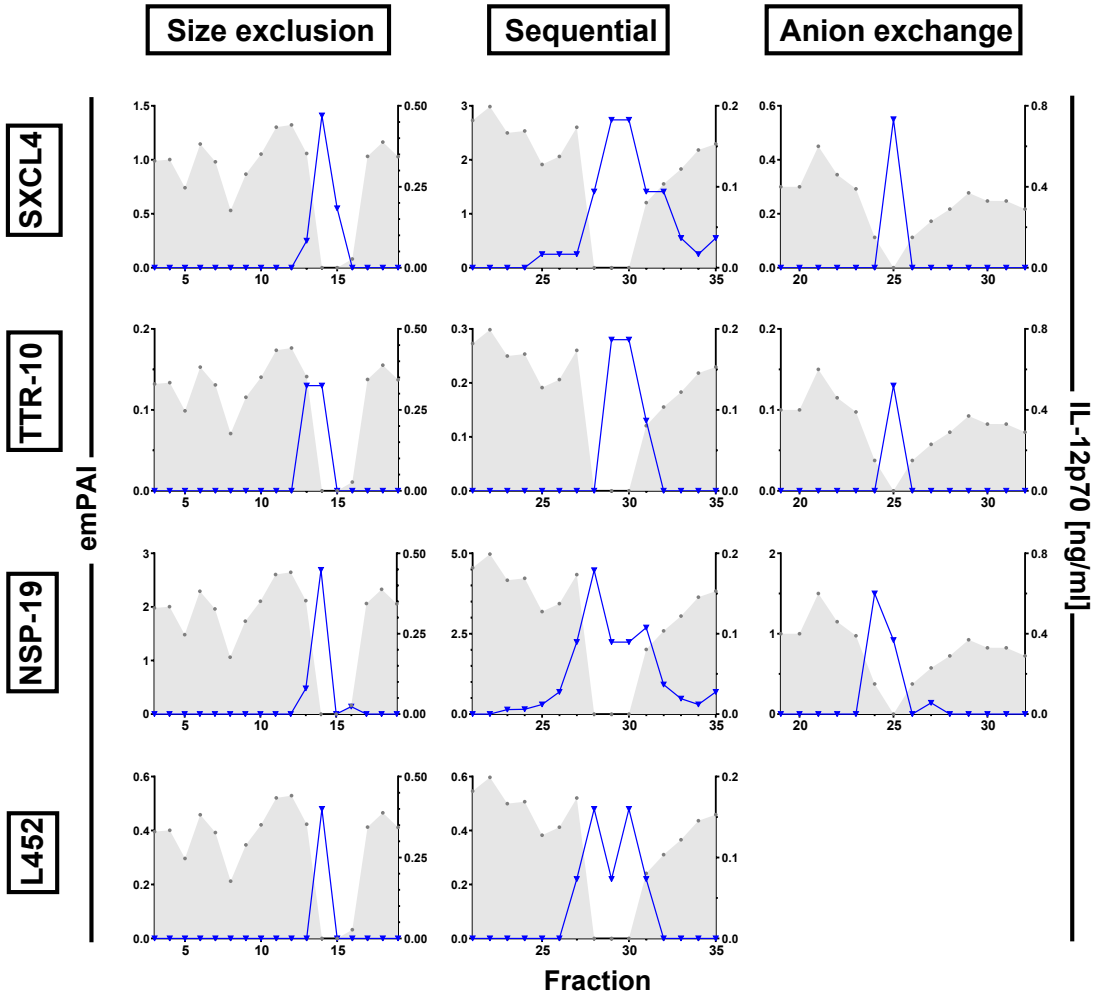

Figure 4.17: Comparison of protein composition of several fractionation approaches resulted in the identification of four new candidate proteins. HES was fractionated by size exclusion (Fig. 4.7), sequential (Fig. 4.8) and anion exchange fractionation (Fig. 4.15), all fractions were analysed by mass spectrometry and their inhibitory activity tested on LPS-activated GM-CSF BMDC. Lists of proteins with emPAI values peaking in the active fractions were compiled for each fractionation approach and compared to identify shared proteins. These were subjected to further selection comparing their abundance profiles (emPAI values over the fractions) to activity (inhibition of IL-12p70 production in LPS-activated BMDC) across the fractions and excluding housekeeping proteins and those that have been identified falsely or with only one peptide (see tables 4.5-4.10) . This resulted in the shown four proteins as final candidates for expression. Shown are their names, the emPAI values across the fractions on the left y axis and the concentration of IL-12p70 produced by GM-CSF BMDC treated with LPS (1µg/ml) and the respective fraction on the right y axis for all three fractionation approaches.

4.2.3.3 Expression and test of candidate proteins

As with the previous set of proteins, the signal peptides were removed from the sequences (Fig. 4.18) before codon optimization and addition of restriction sites. The modified DNA sequences were again synthesized by GeneArt.

As before, pSecTag2a was chosen as expression vector. Fig. 4.19A shows a schematic of the expressed proteins in pSecTag2a, again including the pSecTag2a signal peptide, but this time only NSP-19 was designed with a stop codon after the 6xHIS-tag. The remaining three proteins, designed by Dr. Henry McSorley, now

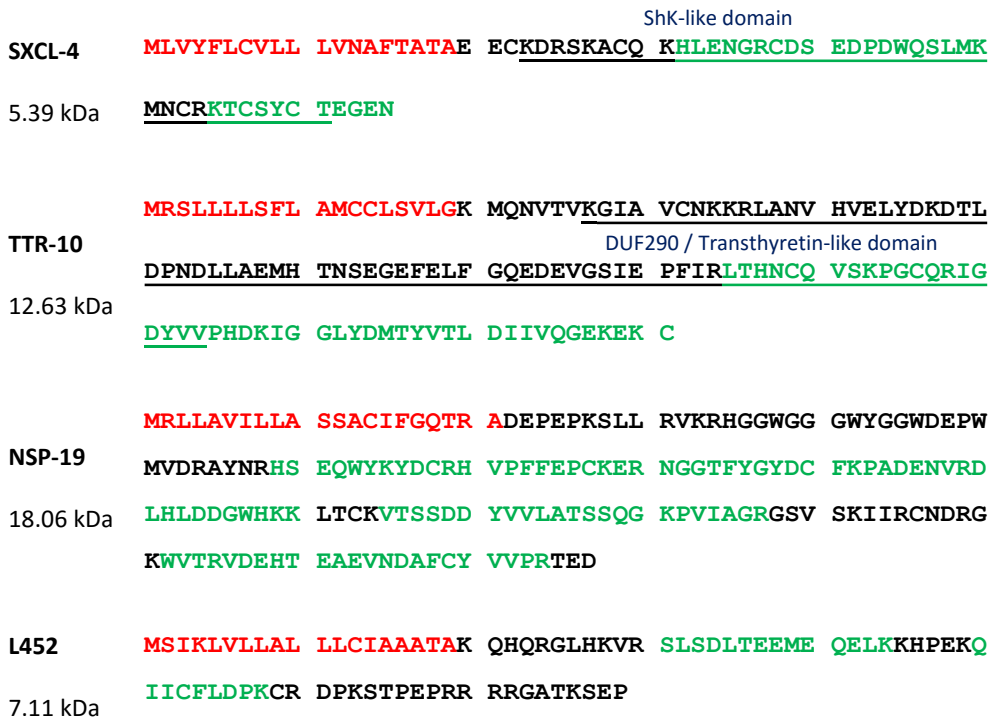

Figure 4.18: Sequences and conserved domains of the four candidate proteins identified by comparing size exclusion fractionation, sequential fractionation and anion exchange fractionation data. After mass spectrometry analysis of HES fractionated by size exclusion, sequential and anion exchange fractionation and several steps of selection of probable candidates for DC modulatory activity, the shown four proteins were selected for expression. Red: Signal peptide (not cloned); Green: peptides identified by mass spectrometry; Underlined with blue label: conserved protein domains.

inserted into pSecTag2a in a way to also include a short stretch of vector sequence and the vector's myc and 6xHIS-tags. HEK-293 cells were transfected with the insert containing vectors, stable cell lines produced and supernatants collected, dialysed into His-Binding buffer and purified using the Äkta purifier (Fig. 4.19B, left hand panels). Protein content across the fractions and their purity again was determined by SDS-PAGE and Western Blot (Fig. 4.19B, right hand panels).

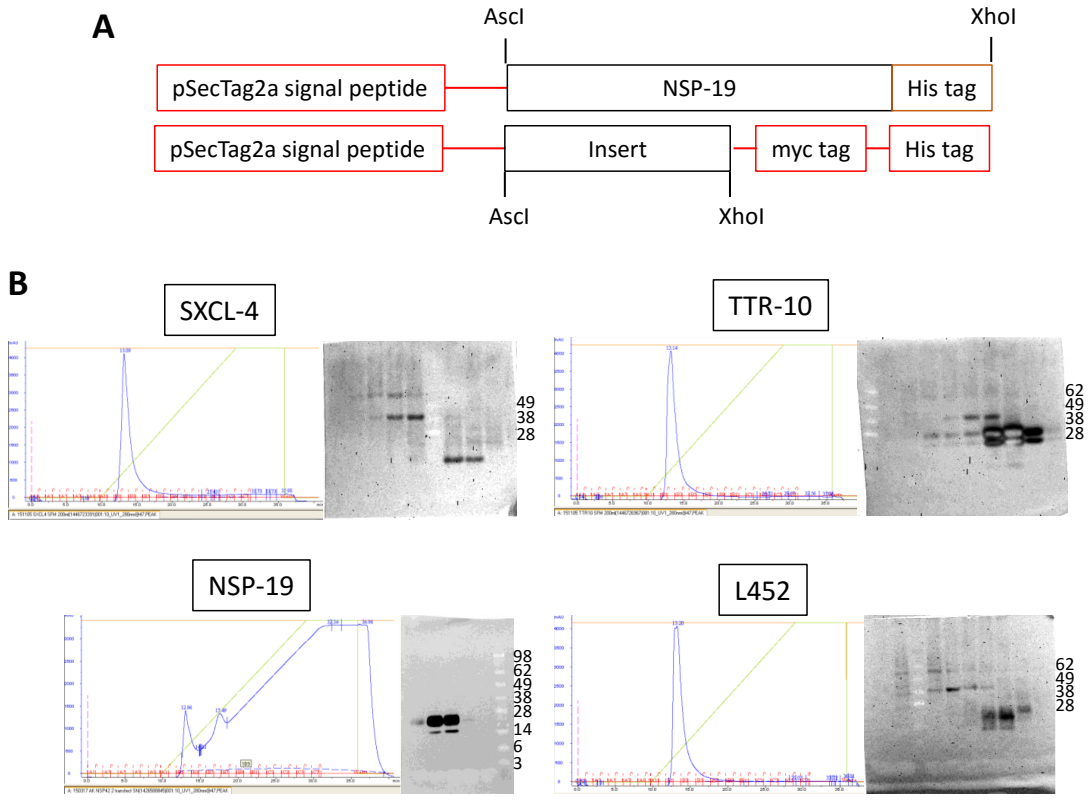

Figure 4.19: Cloning and expression of candidate proteins from the third round of fractionations. Sequences were codon optimized for expression in human cells, ordered from GeneArt, digested with the appropriate restriction enzymes and inserts purified by gel electrophoresis and gel extraction and ligated into the expression vector pSecTag2a. **(A)** Schematic of the proteins produced, with vector sequences in red and restriction sites used indicated (not drawn to scale). **(B)** After transfection into HEK293 cells, supernatants were collected and purified (Akta profiles in the left panels). Candidate protein content in the fractions was visualized with SDS-PAGE and Western Blot detecting the His-tag (right panels).

Similar to the first proteins expressed, none of recombinant proteins were of the predicted size, even allowing for the extra vector sequences. SXCL-4 was predicted to be between 5-6 kDa; the western blot showed proteins at three different heights, the ones eluting first only resulting in a faint band at around 60 kDa, followed by stronger bands at around 40 kDa. The smallest eluted last, with an estimated size of about 15 kDa. The predicted size of TTR-10 was just below 13 kDa; again the recombinant protein produced several bands, in this case between 20-40 kDa. NSP-19 was predicted to have a size of 18 kDa, and a faint band can be found with this size. The majority of this recombinant protein appeared to be around 25 kDa. The last of these candidates, L452, was predicted to be only slightly larger than SXCL-4 with only 7 kDa. The recombinant L452 produced bands at around 25, 40 and 60 kDa.

Again as before, protein containing fractions of reasonable purity were pooled, dialysed into PBS and concentrated down using VivaSpin columns before test on BMDC. For this, day ten GM-CSF BMDC were treated for 18h with LPS, HES and proteins as indicated, and again none of the proteins were able to inhibit IL-12p70 production (Fig. 4.20).

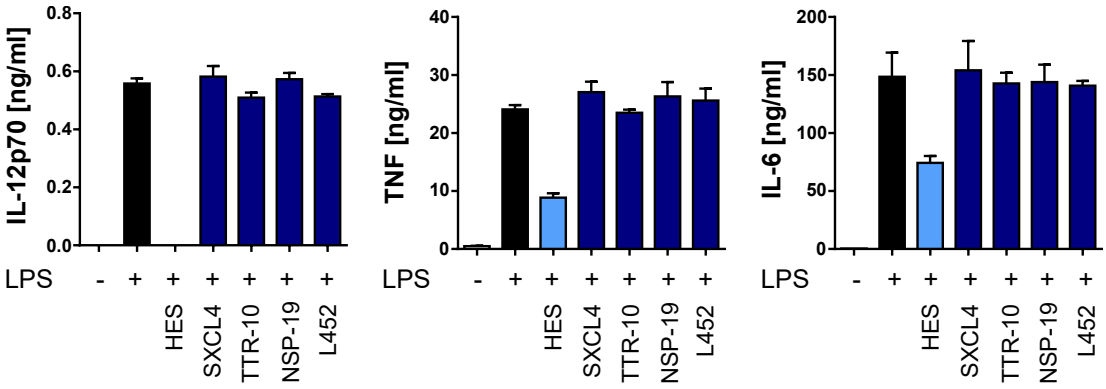

Figure 4.20: None of the four candidates identified in the third round inhibit LPS induced DC activation. BMDC were differentiated with GM-CSF for ten days before stimulation with LPS and 10µg/ml of HES or candidate proteins as indicated. IL-12p70, TNF and IL-6 concentrations in supernatants were measured by ELISA. This experiment was performed twice using the same batch of proteins.

4.2.3.4 Abundance profiles of previously described candidates or modulators

With the abundance profiles in the three fractionation approaches available, the distribution of the second-round candidates in the size exclusion and in the anion exchange fractions could easily be checked as well (Fig. 4.21).

L529 was not found in the size exclusion fractions used in rounds two and three; this protein was however identified in another size exclusion fractionation done at a later date, where it peaked perfectly in the one active fraction, number 14. NSP-4, while being found in fractions 24-29 of the anion exchange fractionation, peaked in fraction 24 rather than the active fraction 25, and in the size exclusion fractionation it was not even found in the active fractions 14 and 15. Rather, it was found in fractions 7-12, peaking in fraction 9. Similarly, VAL-4, while peaking in the active anion exchange fraction 25, was found only in fractions 11-13 of the size exclusion fractionation. This does replicate the results obtained by Kara Filbey, who showed that VAL-4 was found in gel filtration fractions 12 and 13 (Filbey, 2013). ShK-707 was, similar to L529, neither found in the gel filtration fractions used to generate the sequential fractions, nor in the anion exchange fractionation. It was found in the later size exclusion fractionation, but unlike L529 it peaked in fractions 5-6. NSP-42 was found in the fractions adjacent to the active fractions, being identified only in fraction 13 of the size exclusion fractionation and fraction 24 of the anion exchange fractionation.

In addition, the abundance profiles of previously described DC modulators could be investigated as well. The protease inhibitor cystatin (which has the accession number Hp_I02126_IG00179_L738 in our in-house database), shown by Sun et al. to impair CpG induced DC maturation (Sun et al., 2013), was eluted in fraction 24 of the anion exchange fractionation, a fraction that partially inhibited LPS induced DC activation. However, it was not identified in fraction 25, the one completely abolishing IL-12p70 production. In addition, it eluted in fraction 11 of the size exclusion fractionation, a fraction that was not able to inhibit LPS induced DC activation. Finally, it was not identified in the sequential fractionation of HES (Fig. 4.22).

TGM similarly eluted in fraction 24 of the anion exchange fractionation, but was not found at all in the active fraction 25. As expected from previous experiments (Filbey, 2013), it eluted in fraction 9 of the size exclusion fractionation and was not found in any of the other fractions. Again, it was not identified in the sequential fractionation (Fig. 4.23).

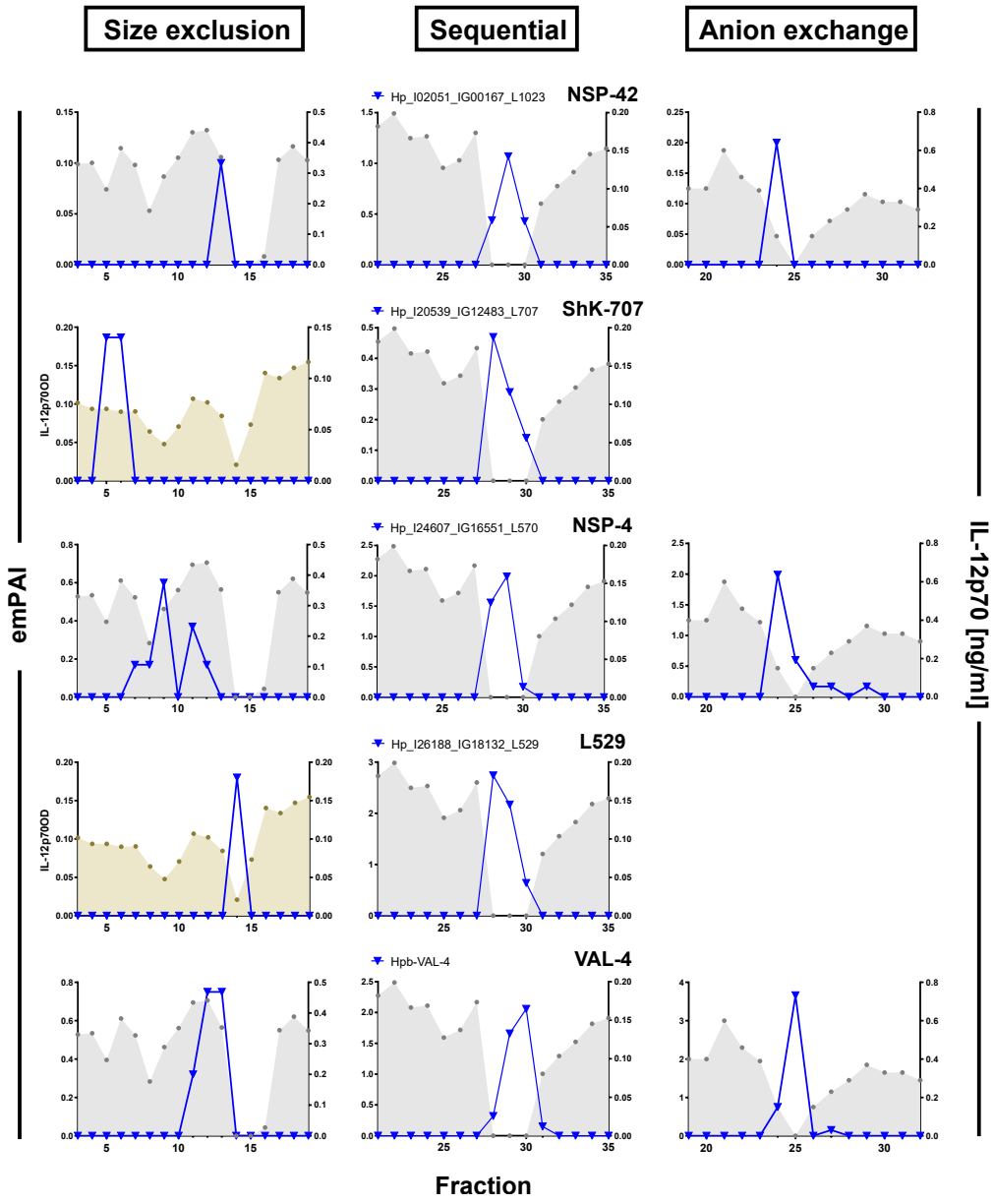

Figure 4.21: Abundance profiles of second round candidates in all three fractionation approaches. HES was fractionated using size exclusion fractionation followed by fractionation of the active fractions by anion exchange fractionation. All sequential fractions were analysed by mass spectrometry. Proteins with emPAI values peaking in the active fractions were subjected to further selection comparing their emPAI profiles to activity across the fractions, excluding housekeeping, egg or larval stage proteins and those that have been identified falsely or with only one peptide. This resulted in the shown five proteins as final candidates for expression. Shown here are their emPAI values across the fractions on the left y axis and the concentration of IL-12p70 produced by GM-CSF BMDC treated with LPS (1μg/ml) and the respective fraction on the right y axis, for the sequential fractionation and subsequent analysis of two different size exclusion fractionations (marked by distinct colours of the IL-12p70 profiles) and one anion exchange fractionation.

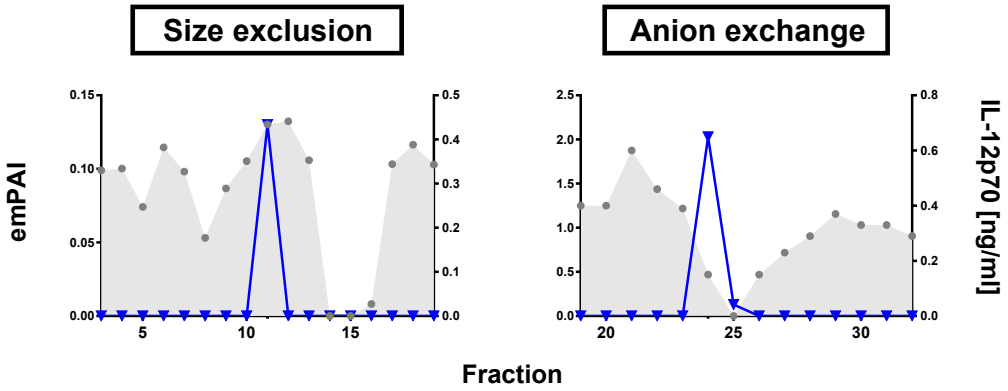

Figure 4.22: Abundance profiles of cystatin. HES was fractionated using size exclusion, sequential and anion exchange fractionation. All fractions were analysed by mass spectrometry. Cystatin's emPAI values across the fractions are shown on the left y axis and the concentration of IL-12p70 produced by GM-CSF BMDC treated with LPS ($1\mu g/ml$) and the respective fraction on the right y axis. Sequential fractionation emPAI values are not shown, as cystatin was not identified in these fractions.

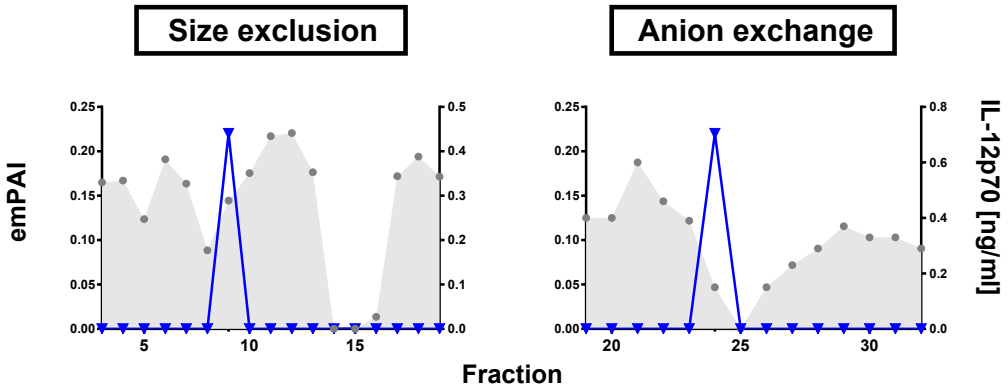

Figure 4.23: Abundance profiles of TGM. HES was fractionated using size exclusion, sequential and anion exchange fractionation. All fractions were analysed by mass spectrometry. TGM's emPAI values across the fractions are shown on the left y axis and the concentration of IL-12p70 produced by GM-CSF BMDC treated with LPS ($1\mu g/ml$) and the respective fraction on the right y axis. Sequential fractionation emPAI values are not shown, as TGM was not identified in these fractions.

4.3 Discussion

The fractionation experiments presented in this chapter resulted in some interesting findings, including that the principal inhibitor of DC activation is a previously undescribed molecule. Thus, the recently described TGM only partially inhibits LPS induced DC activation, and cannot account for the full effects of HES on cytokine and surface marker expression; in addition, its abundance profile does not fit the activity profile of the fractions (Fig. 4.23). Furthermore, the cystatin in HES that was found to also have some ability to modulate DC responses (Sun et al., 2013) did not segregate into the active fractions identified here (Fig. 4.22). We can therefore conclude that there is indeed another protein with the ability to inhibit DC activation that still remains to be found.

A number of new candidates have been identified. In the first round of fractionations, four proteins were shared between all active fractions, but none presented a plausible case (Tab. 4.1). In the second round, HES was sequentially fractionated by size exclusion and then anion exchange fractionation; in this round five candidate proteins were identified, none of which were identified in the first round, but which included a range of interesting gene family members (Tab. 4.4). Two second-round candidates were novel secreted proteins (NSPs), which are part of a group of proteins in HES that do not have any similarity to any other proteins; several of these proteins are currently being investigated but so far nothing is known about their possible functions. A third protein, L529, had never been found in HES before, and similar to the NSPs it did not have any conserved domains. It did however show some slight blastx similarities to trypsin inhibitor like cysteine rich domain containing proteins and ubiquitin-conjugating enzymes, both of which could hint to a role in regulating immune reactions. ShK-707 is another novel protein, the only conserved domain identified in this protein is the ShK-like domain. With this domain, it belongs to one of the three main protein families in HES, named according to the stichodactyla toxin that was found to block specific voltage-gated potassium channels and thereby inhibit proliferation of subsets of B and T cells (Wulff et al., 2003, 2004). Thanks to this domain ShK-707 also shows some small blastx similarities to numerous other ShK domain containing proteins, including many metalloproteinases. The last candidate protein identified in this round was VAL-4. This protein is a member of the venom allergen-like protein family which has been identified with 25 members in HES and with this was both the largest and most abundant protein family (Hewitson et al., 2011b). Several members of this family, including VAL-4, have been shown to elicit dominant antibody responses in mice (Hewitson et al., 2011a). A common feature of

these proteins and their many homologs in other species is their sperm coating protein (SCP) domain; however, little is known about their functions so far. *H. polygyrus* VAL-4 has previously been expressed in bacteria and insect cells and has been found to colocalize with goblet cells in the intestine of infected mice (Murray et al., manuscript in preparation). Its effect on DCs had not previously been investigated.

However, none of these candidates had an effect on LPS-induced DC activation (Fig. 4.13). These five proteins were selected after mass spectrometric analysis of the active sequential fractions. At a later date, all protein containing fractions of the first gel filtration step of the sequential fractionation, and all fractions from the anion exchange fractionation of HES were analysed as well, and the emPAI profiles for the first five candidates in these fractionations were then obtained. This revealed that four of these proteins had poor fits of emPAI profiles against activity profiles in the new fraction analyses (Fig. 4.21). In hindsight, these results make it clear that, apart from perhaps L529, the proteins were not convincing candidates for the DC modulatory protein, and show just how important the inclusion of further fractionations to compare abundance profiles was.

After this inclusion of further fractionations into the comparison, four more candidates were identified that had good fits of their abundance profiles against the activity profiles of all fractionations, with the exception of L452 which was not found in the anion exchange fractionation (Tab. 4.11). Both this protein and NSP-19 had no conserved domains, making it impossible to speculate on their functions. This is similarly difficult for SXCL-4, although it being a previously identified member of the ShK-like domain containing family containing barely more than a single of these domains indicates that it might act in a similar manner to the ShK toxin itself. The last candidate protein, TTR-10, belongs to the transthyretin-like family. While transthyretin itself is a protein in vertebrates that is responsible for transport of thyroid hormones through the blood stream from the thyroid gland to sites throughout the body, it is thought to have evolved by gene duplication of a transthyretin-like protein (TLP). TLPs have been found even in bacteria, and appear to have a variety of different functions; it was described that it plays an important role in uric acid degradation but only a few point mutations were needed to change this function to binding of thyroid hormones (Richardson, 2015). A TLP from *C. elegans*, TTR-52, has been described to be secreted and mediate binding between an apoptosis signal and phagocyte receptors, thereby supporting the phagocytosis of apoptotic cells (Wang et al., 2010). However, the function of the TTR-10 identified here remains to be determined.

In the end, none of the expressed proteins were able to influence LPS induced DC maturation (Fig. 4.20). The failure to identify the molecule responsible for the DC modulatory effect shown by HES could have a number of reasons. Firstly, it is possible

that this was due to a technical problem with the mass spectrometric analysis in the sense that the wanted protein might be, while very efficient at inhibiting DCs, very dilute in HES and not easily picked up by mass spectrometry. In this way it might be absent in especially the sequential fractionation, where the protein concentration of the fractions was generally fairly low. It would then not have been identified as a protein shared by the active fractions. There are very significant differences in protein identification capabilities of mass spectrometers and it is evident that they can miss numerous proteins when comparing the lists of proteins identified by analysis of the size exclusion fractions in the two different facilities, assuming that different batches of HES do not vary much in their protein composition, as has been tested by John Grainger (Grainger, 2009). As mentioned above, in the first analysis 26 proteins were identified in fraction 14 and 38 in fraction 15. The second analysis on the other hand identified 206 proteins in fraction 14 and 105 in fraction 15, with the ranks being quite different compared to analysis one. Furthermore, about half of the proteins identified in the first analysis are not found in the second (tables B.1, B.2, B.9 and B.10).

Secondly, the selection criteria, especially the step of excluding proteins with an ill fitting abundance profile by hand, were - though carefully implemented - still quite subjective. The real DC inhibitor could easily have been missed. Furthermore, it is possible that it could have been identified with only one peptide, which would have meant it would have been excluded as the probability of it being an artefact was deemed to be too high. One example where this already happened in the analysis is L452, which had been on the shortlist for candidate proteins in the sequential fractionation round (Tab. 4.3), but was excluded as it was identified by one peptide only. When all fractionation approaches were compared, more peptides of this protein were found and it was included in the list of candidates. Also the exclusion of housekeeping proteins from the list of prioritised candidates should be reconsidered, especially considering the findings presented in the next chapter, with HES influencing DC metabolism.

Thirdly, it might well be that the protein of interest does not act as a single protein, but indeed a protein complex is responsible. This is however quite unlikely, considering the very distinct activity profiles of the fractions. Proteins in a putative complex would have to be around the same size and have a very similar charge, or the complex be very stable to always be eluted as a functional unit. Another potential issue with the protein itself could be post-translational modifications. While the heat-lability of the inhibitory molecule indicates a protein component, it might well be heavily glycosylated to name just one possibility, and those post-translational modifications could have an important role in the regulation of DC activation. One example where this is the case is ω-1, the RNase found in SEA, which is bound and

internalized by the mannose receptor and can only then act on the RNAs within the cell (Everts et al., 2012a). The fact that all the recombinant proteins were larger than predicted (Fig 4.12B and Fig. 4.19B) does indicate that they were indeed modified and - especially considering the fact that there were several bands visible for a number of them - might either form protein complexes or be not properly folded and aggregate. By expression of the proteins in a mammalian cell line we tried to increase the probability of proper folding and post-translational modifications, but it is possible that this failed. Furthermore, protein production by the transfected cells was very low, so that for all candidates the purified protein had to be pooled and concentrated down. It is possible that this process was detrimental to the proteins; testing a new batch of protein that is less dilute and does not require further concentrating might be worthwhile. To address the issue of proper folding and modification, it is planned to raise polyclonal antibodies against the expressed proteins and an active fraction as a positive control. These will then be used to try and neutralize the inhibitory effect of total HES, to see if the native proteins, unlike the recombinants, are able to modulate DC activation.

In addition to this, it will however probably be necessary to address issues raised with the selection criteria described above. In addition to careful evaluation of previously excluded proteins, taking proteins with abundance profiles peaking in only two of the three fractionation approaches into consideration might be useful. Alternatively, it might be worthwhile to include a third fractionation approach, to be able to objectively choose proteins with well fitting abundance profiles while keeping the number of candidates small without having to subjectively select proteins with promising looking profiles from a larger list. One possibility could be hydrophobic interaction chromatography to separate proteins according to their polarity.

In summary, while the DC modulator in HES has not been identified yet, not all of the tested proteins can be completely excluded, and several data sets of fraction activities and protein contents have been produced that can be used in future selection of candidates.

CHAPTER 5

Effects of HES on LPS induced signalling pathways and DC metabolism

ABSTRACT

In addition to finding the molecule in HES responsible for the inhibition of TLR ligand-induced DC maturation, the identification of its mechanism of action is an important step towards its use as a potential therapeutic. Analysis of the activation of the NF-κB and MAPK signalling pathways and the production and inhibition time courses of IL-12, TNF, IL-6 and CD40 showed that HES did not affect the immediate-early phase of LPS-induced BMDC activation. Rather, it seemed to interfere with the ability of the cells to sustain the activation, and could do so even if added several hours after LPS treatment. Analysis of the transcriptome of LPS- and LPS+HES-treated BMDC at eight hours post stimulation revealed numerous changes that may contribute to the observed inhibition of maturation, the most promising being the downregulation of IRAK2 and the upregulation of ATF3 by HES. Furthermore, the detected increase in HIF-1α transcript levels and differences in transcript levels of glycolytic enzymes indicate an even higher increase of aerobic glycolysis in LPS+HES-stimulated BMDC compared to LPS-treated cells. In addition, HES treatment of LPS-stimulated cells appears to induce or increase the cellular oxidative and ER stress responses. In conclusion, the work presented here gives an insight into how HES might affect LPS-induced DC activation and identifies several promising candidates for further study.

5.1 Introduction

When DCs encounter PAMPs such as LPS, a number of signalling pathways are activated to induce the maturation of these cells. A schematic of the most important ones can be found in Fig. 5.1.

TLR4 in concert with CD14 binds LPS on the cell surface. Both MyD88 and TRIF are adaptor proteins associated with TLR4 and induce several interconnected signalling pathways upon activation. Their signalling pathways converge with the activation of TRAF6; while TRIF can directly activate TRAF6, MyD88 does so via IRAK1/2 and 4. Activation of TRAF6 is due to ubiquitination of K63, and can be inhibited by the ubiquitin ligase A20 working in concert with ABIN molecules (reviewed in Verstrepen et al., 2009). TRAF6 in turn, once activated, induces the activation of NF-κB, the MAPK cascade and several IRFs (reviewed in Brown et al., 2011).

For NF-κB induction, activation of IKKs leads to phosphorylation of IκBs, targeting them for proteasomal degradation. This frees previously bound NF-κB to translocate to the nucleus and induce transcription of target genes. NF-κB itself is a dimer composed of combinations of the five subunits c-Rel, RelA (or p65), Rel-B, p52 (after cleavage of the inhibitory p100) or p50 (after cleavage of p105) (reviewed in Kawai and Akira, 2007).

The MAPK cascade involves sequential phosphorylation of target proteins by several kinases, with the three branches named after the final kinases in the cascades, p38, ERK and JNK. Activation of these leads to phosphorylation of components of the AP-1 transcription factor and therefore its activation. AP-1 contains proteins like Jun, Fos and members of the ATF family of transcription factors. In addition to direct binding to elements in promoters of target genes, AP-1 can interact with other transcription factors. One example are members of the ETS family of transcription factors, which are regulated by MAPK signalling as well. Heterodimers of AP-1 consisting of a BATF member and a Jun protein are able to interact with both IRF4 or IRF8, enabling them to bind to elements called AICEs (AP-1–IRF composite elements). IRF4 and 8 can also interact with members of the ETS family, which enables them to bind to EICEs (ETS-IRF composite elements). These factors and their interactions are reviewed in Wasylyk et al., 1998 and Murphy et al., 2013.

Furthermore, CD14 is able to activate a signalling cascade as well. This signalling pathway causes an increase in intracellular Ca^{2+}, which activates calcineurin. Calcineurin in turn dephosphorylates NFAT, leading to its nuclear translocation.

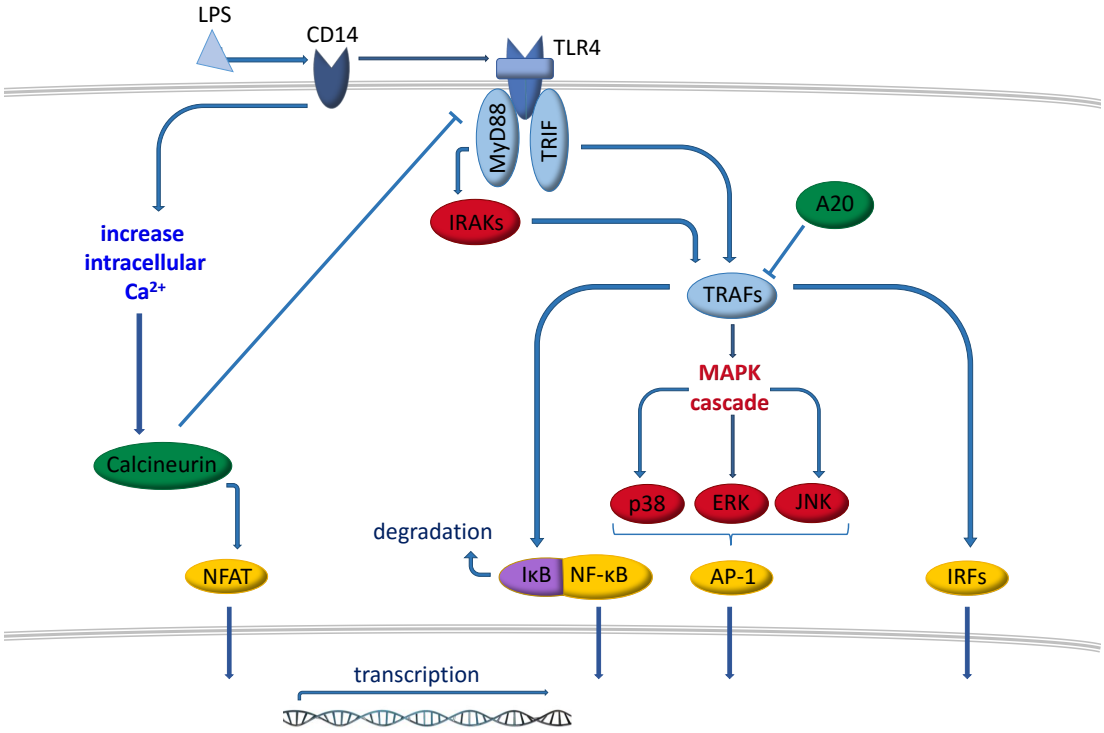

Figure 5.1: Signalling pathways in LPS-induced DC activation. CD14 and TLR4 on DCs bind to LPS. TLR4 associated MyD88 and TRIF induce activation of NF-κB, MAPKs and IRFs through various interconnected pathways. CD14 induces activation of NFAT. For a more detailed description please see the main text. AP-1: Activator protein 1; ERK: Extracellular-signal-regulated kinases; IκB: NF-κB inhibitor; IKKs: IκB kinases; IRF: Interferon regulatory factor; JNK: c-Jun N-terminal kinases; LPS: lipopolysaccharide; MAPK: mitogen-activated protein kinase; MyD88: Myeloid differentiation primary response gene 88; NFAT: nuclear factor of activated T-cells; NF-κB: Nuclear factor κ-light-chain-enhancer of activated B cells; TLR4: toll like receptor 4; TRAF: tumour necrosis factor receptor associated factor; TRIF: Toll/Interleukin-1 receptor-domain-containing adapter-inducing interferon-β

There, NFAT interacts with other transcription factors to form active complexes. In addition, calcineurin has been reported to inhibit TLR signalling pathways. Another, CD14 independent pathway for NFAT activation by LPS seems to exist as well (reviewed in Zanoni and Granucci, 2012).

All of these transcription factor families have been shown to play roles in the regulation of DC maturation. The TNF promoter alone contains binding sites for transcription factors of the NF-κB, AP-1, ETS, NFAT and IRF families (Falvo et

al., 2010). Regulation of IL-12 production is more complicated, thanks to it being composed of two separately regulated subunits, but members of all the above-mentioned families have been shown to be involved in its regulation as well.

STAT proteins are another set of transcription factors that have been found to be involved in DC signalling upon activation. STAT1 for example can be activated by p38 and increase expression of TNF, IL-6 and IL-12p40 (Gautier et al., 2005; Schroder et al., 2007), while STAT3 seems to inhibit NF-κB binding to some promoters (Nefedova et al., 2005; Wagner et al., 2015).

Another factor that can influence DC activation is their metabolism (see Fig. 1.7 and Fig. 1.8 in the Introduction for schematics). Upon activation, DCs increase glycolysis to produce more pyruvate to feed into the TCA cycle, where it is converted into citrate. The increased amount of citrate in turn is used to feed the increased fatty acid synthesis without impairing the TCA cycle and subsequent oxidative phosphorylation to generate ATP; in parallel to that, the activity of the pentose phosphate pathway is increased as well, to provide the NADPH required. These changes in DC metabolism provide the phospholipids needed to expand both endoplasmatic reticulum and Golgi apparatus. If any step of this process was disrupted, DC maturation in response to LPS was inhibited, with decreased protein levels of CD40, CD86, TNF, IL-12 and IL-6. Interestingly, mRNA levels remained the same as in DCs normally activated with LPS. These findings demonstrated just how crucial the early change in DC metabolism and expansion of ER and Golgi are to support the increased protein synthesis during DC activation (Everts et al., 2014).

Changes in DC metabolism in later stages of activation have been investigated as well. BMDC differentiated with GM-CSF express iNOS upon activation; the produced NO was found to inhibit the electron transport chain and so prevent activated BMDC to generate their ATP through oxidative phosphorylation (Everts et al., 2012b). Instead, they have to rely on regenerating NAD^+ for glycolysis by producing lactate even though oxygen is available, which is called aerobic glycolysis or Warburg metabolism, and can be found in activated macrophages as well (Krawczyk et al., 2010). An important inducer for this increase in glycolysis is the transcription factor HIF-1, and knockdown of its α subunit impaired LPS induced DC maturation (Jantsch et al., 2008).

Considering the complex machinery that is at work to induce and regulate the activation of DCs, there are plenty of points that HES could target. Previous work in our group showed that the effect of HES is not dependent on either MyD88 or TRIF, as activation of BMDC from $MyD88^{-/-}TRIF^{-/-}$ mice by ligation of CD40 was inhibited as well. Furthermore, HES does not act via PI3K, as inhibition was intact upon treatment with an inhibitor of this kinase. Signalling through the C-type lectin

receptors dectin-1 and dectin-2 is also not involved in HES mediated DC modulation, as neither blocking these receptors with antibodies nor inhibiting signalling through Syk, the kinase downstream of them, had an effect on DC inhibition (Dayer, 2011). So far, neither NF-κB nor MAPK signalling have been investigated. Therefore, to shed more light on a possible mechanism behind the DC modulation by HES, the activation of these signalling pathways was analysed. Furthermore, the timing of the effects on IL-12, TNF, IL-6 and CD40 was investigated. Finally, to create an overview of the expression changes in LPS and LPS + HES treated BMDCs, mRNA levels of cells eight hours post stimulation were analysed with a microarray; proteins involved in the described metabolic pathways and transcription factors implicated in DC activation were investigated.

5.2 Results

5.2.1 HES increases ERK1/2 phosphorylation, but inhibition of BMDC activation is independent of ERK.

The first signalling pathway investigated was one of the three branches of the MAPK cascade. GM-CSF BMDC were stimulated with LPS and HES, following which ERK1/2 phosphorylation levels during the early phase of activation were analysed by flow cytometry.

While both treatments rapidly induced phosphorylation of ERK1/2, LPS+HES treated BMDC seemed to react slightly faster leading to somewhat elevated percentage of p-ERK1/2$^+$ cells at ten minutes post stimulation. Following this, ERK1/2 phosphorylation levels rose sharply with percentages of p-ERK1/2$^+$ cells again being significantly elevated among LPS+HES treated CD11c$^+$ cells at 20 and 30 minutes post stimulation. After this early increase in activation, the percentage of p-ERK1/2$^+$ cells declined and was comparable between both groups one hour after their stimulation (Fig. 5.2A).

To ascertain whether this increase in ERK activity was relevant for the inhibition of LPS induced DC activation by HES, cells were treated with an inhibitor of the kinase phosphorylating ERK1/2, the MEK1/2 inhibitor U0126. Fig. 5.2B demonstrates that this inhibitor indeed completely abolished the phosphorylation of ERK1/2 induced by LPS. IL-12p70 secretion by LPS-stimulated BMDC was only slightly attenuated by pre-treatment with U0126, while HES inhibited secretion of this cytokine irrespective of treatment (Fig. 5.2C). Expression of the costimulatory molecules CD40 and CD80 was also inhibited by HES in the presence of U0126 (Fig. 5.2D). The increased activation of the ERK pathway is therefore dispensable for the inhibition of LPS-induced DC activation by HES.

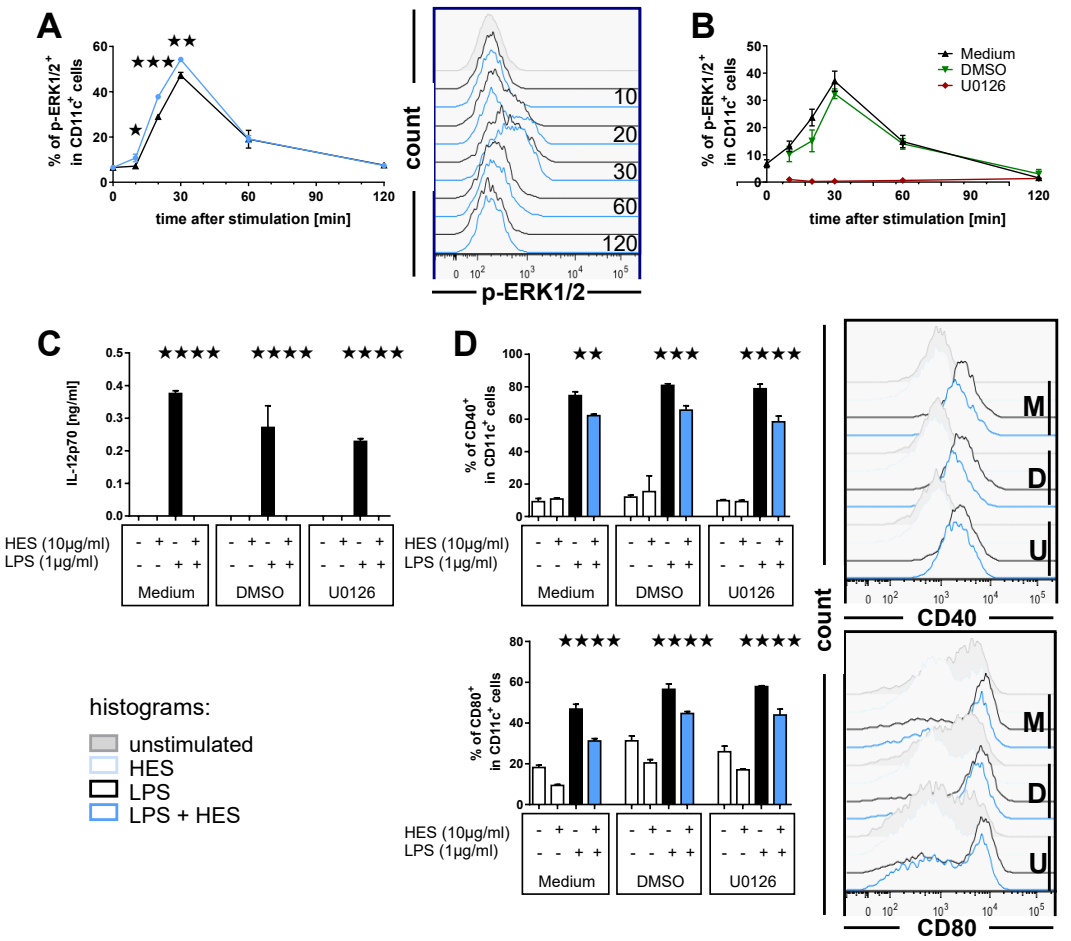

Figure 5.2: HES increases ERK1/2 phosphorylation, but inhibition of DC activation is independent of ERK. BMDC were differentiated with GM-CSF for ten days before stimulation with LPS and HES as indicated. For inhibitor experiments, BMDC were pre-incubated for 60-90 minutes with cRPMI alone, DMSO in RPMI or 10μM U0126 in cRPMI before stimulation. **(A + B)** At indicated time points after stimulation, cells were fixed and the phosphorylation status of ERK1/2 determined by intracellular flow cytometry. **(C)** Concentrations of IL-12p70 in the supernatants of cells after 18h of stimulation were determined by ELISA. **(D)** At 18h post stimultion, expression of costimulatory molecules on CD11c$^+$ cells were determined by flow cytometry. **(A and D)** Left: percentages of p-ERK1/2$^+$, CD40$^+$ or CD80$^+$ cells in the CD11c$^+$ population; Right: histograms showing p-ERK1/2 in or the expression of CD40 or CD80 on CD11c$^+$ cells - # HES alone histogram not in all panels. All results are representative data of at least three independent experiments, except for (B), control of phosphorylation status of ERK1/2 after treatment with U0126, which was performed once. Data represent mean ± SD, n = 3; Results from multiple t-tests comparing LPS and LPS+HES treated samples, analysing each row individually using the Holm-Sidak method or one-way ANOVA and Tukey's multiple comparison test are indicated as $*$: $p \leq 0.05$; $**$: $p \leq 0.01$; $***$: $p \leq 0.001$; $****$: $p \leq 0.0001$. M: Medium; D: DMSO; U: U0126.

5.2.2 HES inhibits p38 and JNK phosphorylation only after the immediate-early phase of BMDC activation.

Next, the activity of the other two branches of the MAPK cascade was investigated. Again, GM-CSF BMDC were stimulated with LPS and HES and then phosphorylation levels of p38 and JNK were measured by flow cytometry.

The percentage of cells positive for phosphorylated p38 rapidly increased after stimulation, with over 80% of cells staining positive after 30 minutes. This did not change over the next half hour, as at one hour post-stimulation around 80% of $CD11c^+$ cells remained p-$p38^+$. There was no difference between LPS- and LPS+HES-treated groups in this first hour (Fig. 5.3A). As time progressed however, the percentage of $CD11c^+$ cells with phosphorylated p38 decreased to a greater extent in the cells treated with HES; at 2.5 hours post stimulation a trend towards a lower percentage of p-$p38^+$ cells was already visible, which became significant at the following time points. While the percentage of p-$p38^+$ LPS treated cells declined to pre-stimulation levels only gradually over 15 hours, when HES was added cells returned to baseline by five hours post stimulation (Fig. 5.3B).

Similar observations can be made about phosphorylation of JNK. While it was activated slightly later than ERK1/2 or p38 with barely any cells p-JNK^+ at 15 minutes post stimulation, this rapidly changed over the following 30 minutes before the percentage of p-JNK^+ cells declined again at one hour post stimulation. During these early time points, no difference was visible between LPS- and LPS+HES-treated cells (Fig. 5.4A). Just as with p-p38 however, the percentage of p-JNK^+ LPS+HES-treated $CD11c^+$ cells declined faster than in the LPS-treated group. In LPS-treated cells, JNK phosphorylation decreased slowly over the next few hours until they dropped to pre-stimulation levels around 12 hours post LPS. LPS+HES-treated cells on the other hand showed a much steeper loss of JNK phosphorylation; at 5 hours post stimulation they had already almost returned to pre-stimulation levels of p-JNK^+ cells (Fig. 5.4B).

This timing is quite intriguing, as in both cases HES blocked the late phase duration of phosphorylation, bringing the percentage of p-$MAPK^+$ cells to near pre-stimulation levels in the samples taken five hours post stimulation, while LPS-treated cells were much slower in returning to the pre-stimulation status.

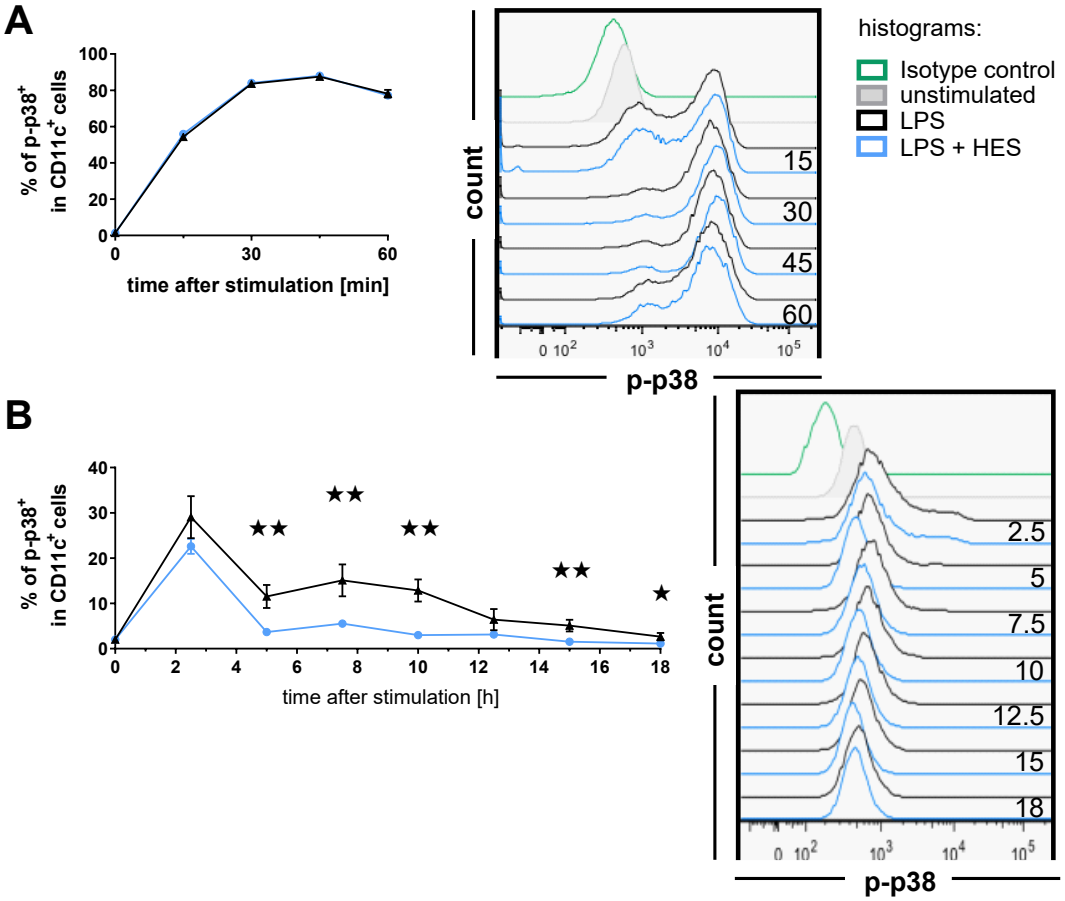

Figure 5.3: HES does not alter p38 phosphorylation during the early phase of LPS-induced BMDC maturation but reduces it at later time points. BMDC were differentiated with GM-CSF for ten days before stimulation with LPS and HES as indicated. At indicated time points after stimulation, **(A)** in minutes for the early phase of activation and **(B)** in hours for the later time points, cells were fixed and the phosphorylation status of p38 determined by intracellular flow cytometry. Left: Percentages of p-p38$^+$ cells in the CD11c$^+$ population; Right: histograms of p-p38 within CD11c$^+$ cells at the indicated time points after stimulation. Results for early time points are representative data of five, later time points of two independent experiments. Data represent mean ± SD, n = 3; Results from multiple t-tests comparing LPS- and LPS+HES-treated samples, analysing each row individually using the Holm-Sidak method are indicated as $*$: $p \leq 0.05$; $**$: $p \leq 0.01$; $***$: $p \leq 0.001$; $****$: $p \leq 0.0001$.

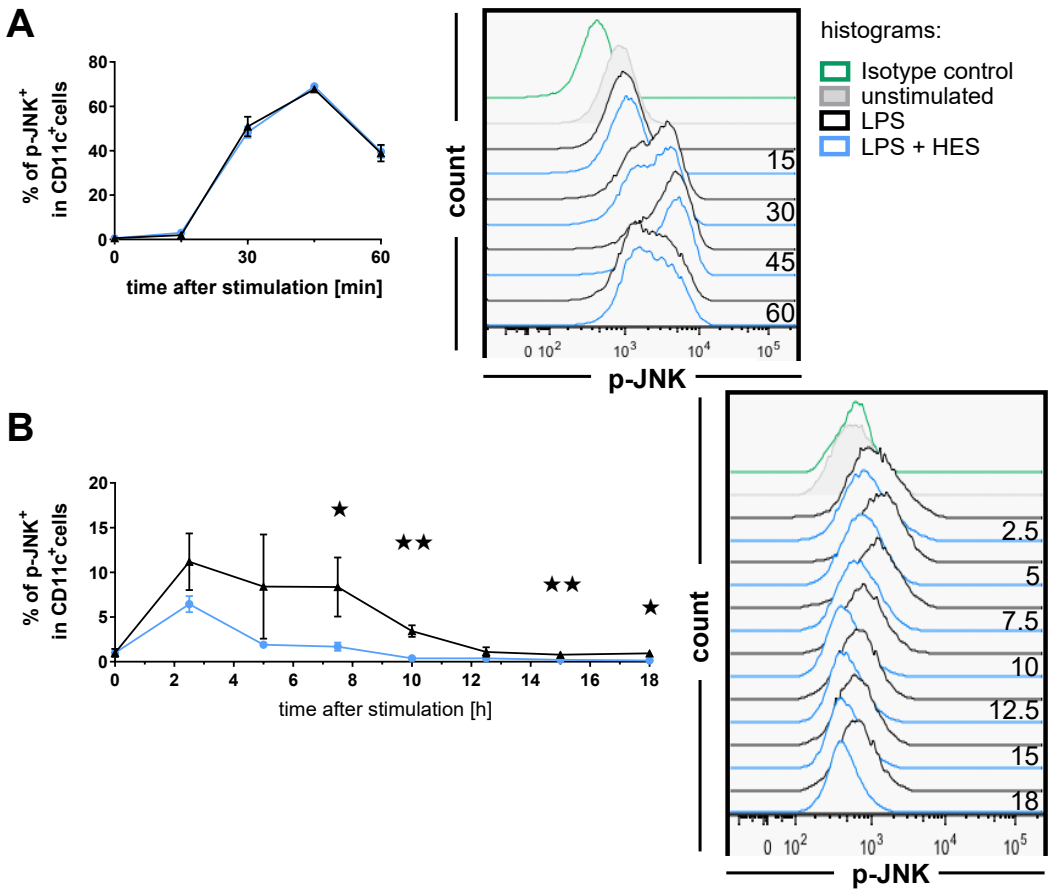

Figure 5.4: HES does not alter JNK phosphorylation during the early phase of LPS-induced BMDC maturation but reduces it at later time points. BMDC were differentiated with GM-CSF for ten days before stimulation with LPS and HES as indicated. At indicated time points after stimulation, **(A)** in minutes for the early phase of activation and **(B)** in hours for the later time points, cells were fixed and the phosphorylation status of JNK determined by intracellular flow cytometry. Left: Percentages of p-JNK$^+$ cells in the CD11c$^+$ population; Right: histograms of p-JNK within CD11c$^+$ cells at the indicated time points after stimulation. Shown are representative data of two independent experiments. Data represent mean ± SD, n = 3; Results from multiple t-tests comparing LPS- and LPS+HES-treated samples, analysing each row individually using the Holm-Sidak method are indicated as $*$: $p \leq 0.05$; $**$: $p \leq 0.01$; $***$: $p \leq 0.001$; $****$: $p \leq 0.0001$.

5.2.3 HES inhibits phosphorylation of IκBα and reduces A20 expression in LPS-stimulated BMDC.

In addition to the MAPK pathway, NF-κB signalling is crucial for the activation of DCs and was therefore the next to be investigated. As described above, NF-κB gets activated when IKKs phosphorylate IκB, targeting it for degradation and thereby releasing NF-κB to translocate to the nucleus. Phosphorylated IκB, specifically IκBα, is therefore a measure for NF-κB activation (Kawai and Akira, 2007). To analyse this, GM-CSF BMDC were stimulated with LPS and HES as before followed by determination of the phosphorylation status of IκBα by flow cytometry.

The earliest analysed time point post stimulation was at 2.5 hours, and analogous to the results for p-p38 and p-JNK, the percentage of p-IκBα$^+$ cells, even though increased compared to pre-stimulation levels, was lower in LPS+HES-treated CD11c$^+$ cells compared to the LPS-treated group. That remained the case during the whole course of the stimulation, and while the percentage of cells that were positive for p-IκBα returned to pre-stimulation levels in the LPS-treated group, it sank below that in the HES-treated group (Fig 5.5).

One important inhibitor of NF-κB activation is A20, which acts as a feedback regulator for NF-κB signalling. To check if HES inhibits the phosphorylation of IκBα by changing the expression of A20, levels of this protein in LPS- and HES-treated GM-CSF BMDC were measured by flow cytometry.

In both groups the expression of A20 increased 30 minutes after stimulation and percentages of A20$^+$ cells kept rising over the first hour of stimulation. During this early phase of DC maturation, percentages of A20$^+$ cells were comparable in both groups (Fig. 5.6A). At 2.5 hours post stimulation, the percentage of A20$^+$ cells was even higher in LPS-stimulated BMDC; this was in contrast to the LPS+HES-treated group, where it was slightly lower than at 60 minutes post stimulation. While the percentage of A20$^+$ LPS-stimulated BMDC did remain fairly constant over the next few hours, it dropped to below pre-stimulation levels in LPS+HES-treated cells at 5 hours post stimulation and remained fairly constant for the rest of the stimulation (Fig. 5.6B).

Of note, the percentage of cells positive for p-IκBα or A20 is low, especially compared to the MAP kinase phosphorylation. This might be due to technical issues, for example the sensitivity of the antibodies used, which might additionally be influenced by the fixation protocol used.

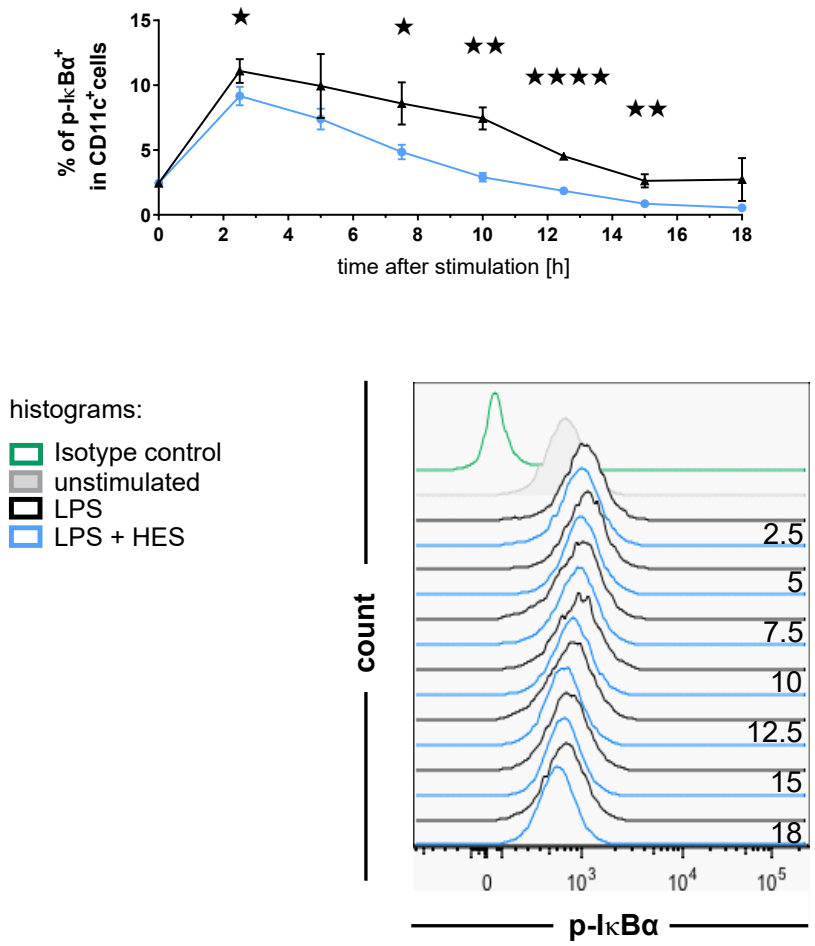

Figure 5.5: HES reduces phosphorylation of IκBα in the intermediate and late phase of LPS-induced BMDC maturation. BMDC were differentiated with GM-CSF for ten days before stimulation with LPS and HES as indicated. At indicated time points after stimulation (in hours), cells were fixed and the phosphorylation status of IκBα determined by intracellular flow cytometry. Left: Percentages of p-IκBα^+ cells in the CD11c$^+$ population; Right: histograms of p-IκBα within CD11c$^+$ cells at the indicated time points after stimulation. This experiment was performed once. Data represent mean ± SD, n = 3; Results from multiple t-tests comparing LPS and LPS+HES treated samples, analysing each row individually using the Holm-Sidak method are indicated as $*$: $p \leq 0.05$; $**$: $p \leq 0.01$; $***$: $p \leq 0.001$; $****$: $p \leq 0.0001$.

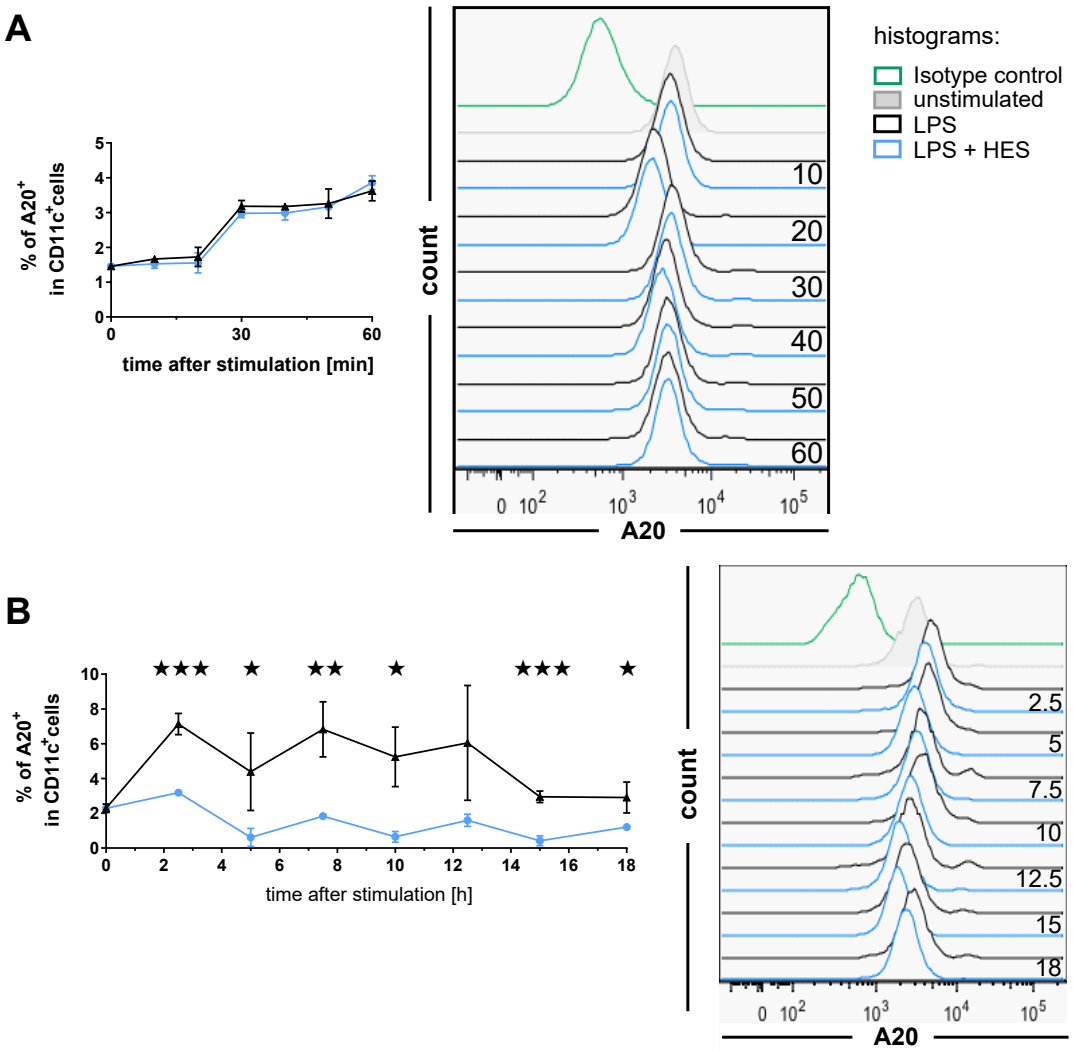

Figure 5.6: HES does not alter A20 expression during the early phase of LPS-induced BMDC maturation but reduces it at later time points. BMDC were differentiated with GM-CSF for ten days before stimulation with LPS and HES as indicated. At indicated time points after stimulation, **(A)** in minutes for the early phase of activation and **(B)** in hours for the later time points, cells were fixed and the expression levels of A20 determined by intracellular flow cytometry. Left: Percentages of $A20^+$ cells in the $CD11c^+$ population; Right: histograms of A20 within $CD11c^+$ cells at the indicated time points after stimulation. These experiments were performed once. Data represent mean ± SD, n = 3; Results from multiple t-tests comparing LPS- and LPS+HES-treated samples, analysing each row individually using the Holm-Sidak method are indicated as $* : p \leq 0.05$; $** : p \leq 0.01$; $*** : p \leq 0.001$; $**** : p \leq 0.0001$.

5.2.4 Differential dynamics of cytokine and activation marker expression and their inhibition by HES.

To put the collected data of inhibition of MAPK and NF-κB signalling at the intermediate and late phases of activation into context regarding the actual inhibition of cytokine secretion and costimulatory molecule expression from LPS-stimulated BMDC by HES, supernatants and cells were collected at different time points during the stimulation. Concentrations of IL-12p70, TNF and IL-6 in the supernatants and expression of costimulatory molecules were measured. In this way, a timeline could be created for the production of these markers and the onset and extent of inhibition.

LPS-stimulated BMDC started secreting IL-12p70 quite late, between eight and ten hours post stimulation. The concentration of this cytokine in the culture supernatant increased over the next four to six hours, before reaching a plateau until the end of the stimulation at 18 hours. No detectable IL-12p70 was produced by LPS+HES-treated BMDC at any point during the stimulation (Fig 5.7A, top).

In contrast, the release of TNF was induced from quite early time points. Unstimulated BMDC did not express any detectable amount of this cytokine (measured at 18h post-stimulation), but at two hours post stimulation both LPS- and LPS+HES-treated BMDC had started to secrete it. While the concentration of TNF steadily increased in BMDCs treated with LPS, in the presence of HES little further increase was observed and indeed levels trended downwards as the experiment progressed (Fig 5.7A, middle).

In the case of IL-6, secretion started slightly later compared to TNF, with only small amounts detectable at four hours post stimulation. At that point, both LPS- and LPS+HES-treated BMDC secreted comparable amounts of IL-6. While the concentrations of this cytokine increased in the supernatants of both groups in the following hours, the LPS-treated cells soon surpassed their LPS+HES-treated counterparts, which were only very slightly increasing the IL-6 concentration. In both groups, IL-6 concentrations in the supernatants reached a plateau at around 12 hours post stimulation (Fig 5.7A, bottom).

The expression of CD40 on $CD11c^+$ cells followed a similar dynamic as IL-6 secretion. While cells at three hours post stimulation had barely changed their expression of this costimulatory molecule, the percentage of $CD40^+$ cells had started increasing at six hours post stimulation with a trend towards higher percentages of $CD40^+$ cells in the LPS-treated group already visible. In both groups the expression of this marker increased over the next hours, but LPS+HES-treated cells started having a significantly lower percentage of $CD40^+$ cells at nine hours post stimulation. This difference continued over the remainder of the stimulation period, and within the

last two hours the LPS+HES-treated group even seemed to decrease the expression of CD40 again.

Following the investigation of the activation time course at the protein level, the expression of the two IL-12 subunits and IL-6 was examined at the mRNA level as well. As before, GM-CSF BMDC were stimulated with LPS and HES, but now RNA was extracted at various time points after stimulation and mRNA levels of p35, p40 and IL-6 analysed by real time PCR.

Notably, the mRNA for both IL-12 subunits was induced several hours before the protein could be measured in the supernatants of the cells. Furthermore, HES inhibition of IL-12 mRNA transcription was not as profound as its suppression of protein secretion. While p35 mRNA could be measured at five hours post LPS-stimulation in cells with of without added HES, it was significantly diminished in the LPS+HES-treated cells. Following this, mRNA levels of p35 stayed constant until the last measured time point at 12 hours post stimulation (Fig. 5.8, top). The p40 subunit was induced slightly earlier and was just detectable in some of the LPS-stimulated samples at three hours post stimulation. In the LPS+HES-treated group no p40 mRNA was detectable at that point. At five hours post stimulation however, p40 mRNA could be measured in both groups, albeit at a much lower level in LPS+HES-treated cells compared to the LPS-treated group. As observed for p35, p40 mRNA levels remained fairly stable after this point until 12 hours post stimulation (Fig. 5.8, middle).

IL-6 mRNA was detectable at three hours post stimulation in the LPS-treated group as well, and at a slightly higher level compared to p40. Again, LPS+HES-treated samples expressed no measurable IL-6 mRNA at this time point, and again it could be found at five hours post stimulation in cells of both groups with levels in LPS-treated BMDC surpassing those of LPS+HES-treated cells. For IL-6, this difference was not as marked as for the IL-12 subunits and did not reach significance at most of the measured time points (Fig. 5.8, bottom).

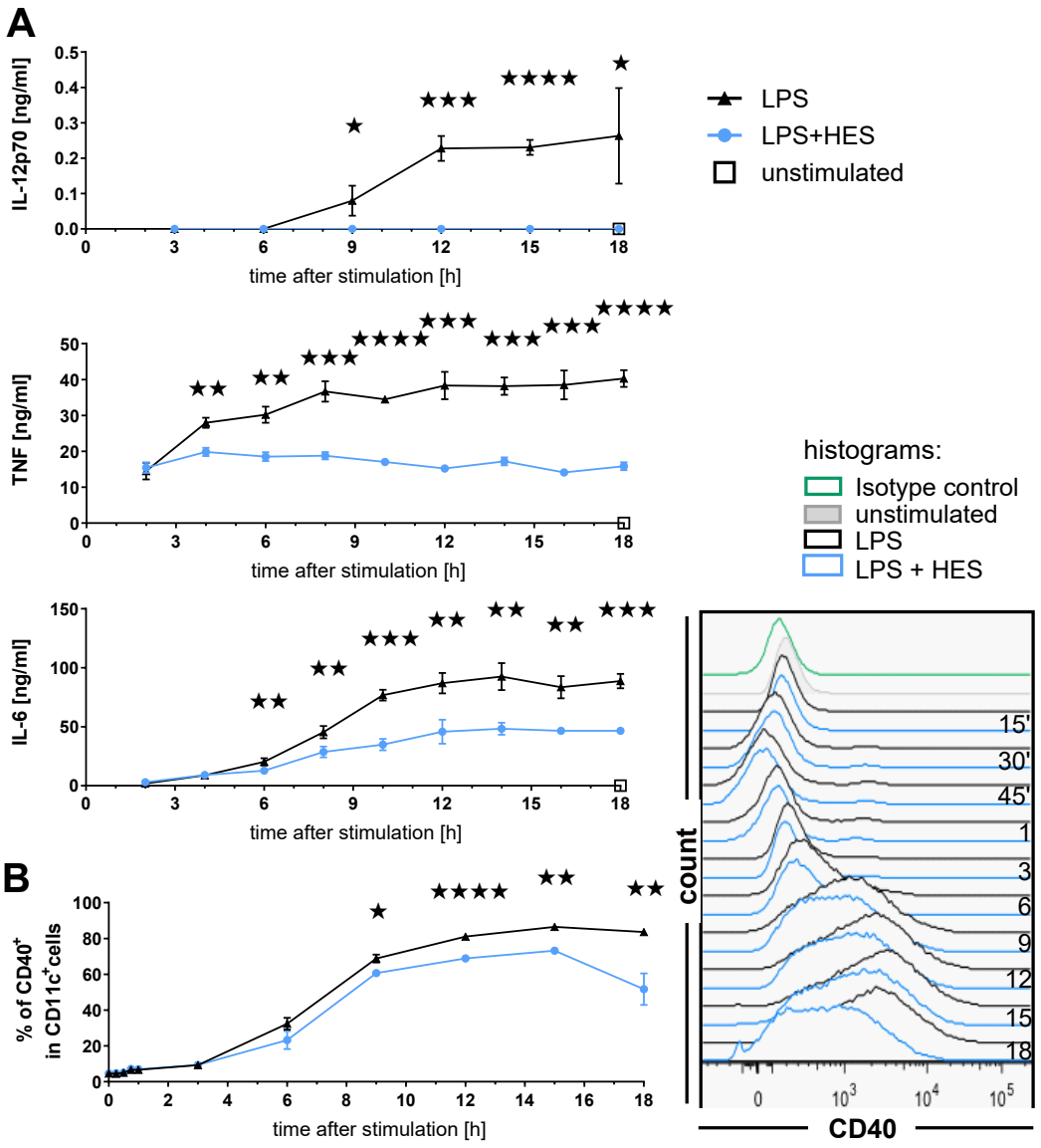

Figure 5.7: Differential dynamics of cytokine and activation marker expression and their inhibition by HES. BMDC were differentiated with GM-CSF for ten days before stimulation with LPS and HES as indicated. At indicated time points after stimulation (in hours) samples were harvested and **(A)** concentrations of IL-12p70, TNF and IL-6 were determined by ELISA and **(B)** expression levels of CD40 determined by flow cytometry. Left: Percentages of $CD40^+$ cells and Right: histograms of CD40 expression on $CD11c^+$ cells at the indicated time points after stimulation. Data for IL-12p70 are representative of 3, IL-6 and CD40 of two independent experiments. TNF was measured once. Data represent mean ± SD, n = 3; Results from multiple t-tests comparing LPS- and LPS+HES-treated samples, analysing each row individually using the Holm-Sidak method are indicated as $* : p \leq 0.05$; $** : p \leq 0.01$; $*** : p \leq 0.001$; $**** : p \leq 0.0001$.

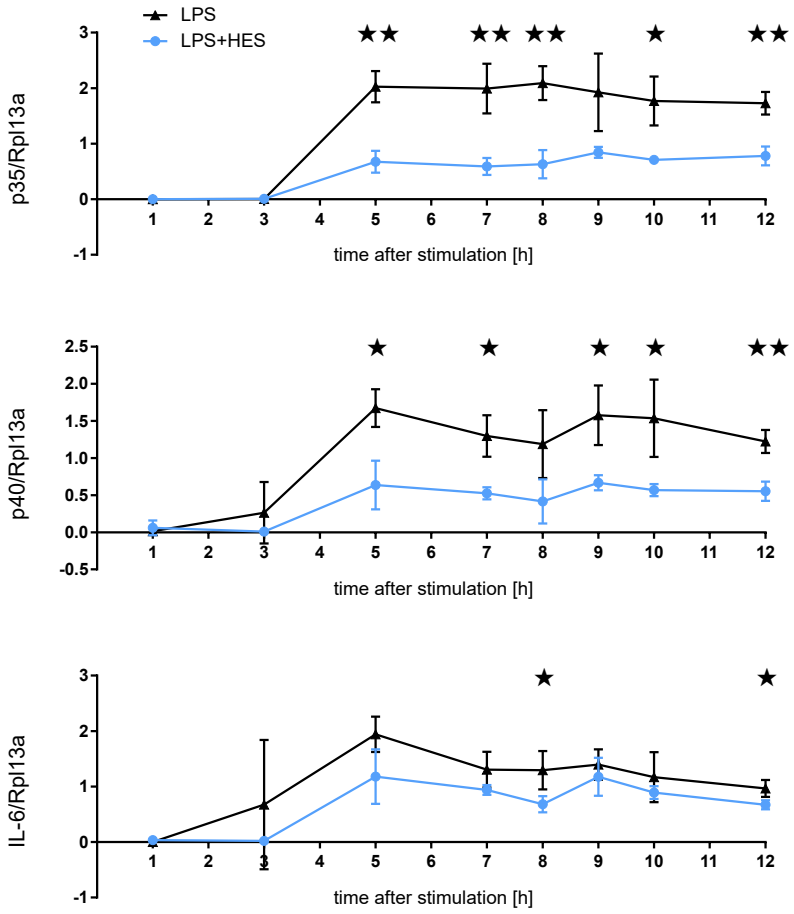

Figure 5.8: Differential dynamics of cytokine expression and their inhibition by HES. BMDC were differentiated with GM-CSF for ten days before stimulation with LPS and HES as indicated. Cells were harvested and treated with Trizol at indicated time points after stimulation. RNA was extracted, reverse transcribed and mRNA levels of p35, p40 and IL-6 determined by qPCR and normalized to Rpl13a mRNA. This experiment was performed once. Data represent mean ± SD, n = 3; Results from multiple t-tests comparing LPS and LPS+HES treated samples, analysing each row individually using the Holm-Sidak method are indicated as $* : p \leq 0.05$; $** : p \leq 0.01$; $*** : p \leq 0.001$; $**** : p \leq 0.0001$.

5.2.5 HES inhibits cytokine secretion and activation marker expression even if added hours after LPS.

In previous experiments, Blaise Dayer found that HES can inhibit LPS-induced IL-12p70 production by BMDC even if added hours after the stimulation started (Dayer, 2011). To further investigate this phenomenon, GM-CSF BMDC were stimulated with LPS and received HES at various time points after stimulation. Concentrations of IL-12p70 and TNF in the cell supernatants were determined, as was the expression of costimulatory molecules.

Just as before, IL-12p70 expression was induced by LPS alone but concentrations in cell supernatants were below the detection threshold if HES was added even up to eight hours post LPS. The inhibition of TNF secretion was not quite as efficient but still very distinct, with cells that received HES up to three hours post LPS secreting barely more TNF than those that received both at the same time. After this, TNF concentrations further increased the later HES was added, and while there was still a trend towards lower concentrations of this cytokine if HES was added seven to twelve hours after LPS, it was not significant (Fig. 5.9A).

The expression of costimulatory molecules was similarly affected. The expression of CD40 on cells that received HES up to 12 hours post LPS was still comparable to that of cells that had received both at the same time. CD80 expression on the other hand followed a similar pattern as TNF. If HES was added one or two hours post LPS, CD80 levels on the cells were comparable to those on cells that received HES with the LPS, but then the percentage of $CD80^+$ cells increased, even though it was still significantly lower compared to the LPS-stimulated cells if HES was added six hours post LPS (Fig. 5.9B).

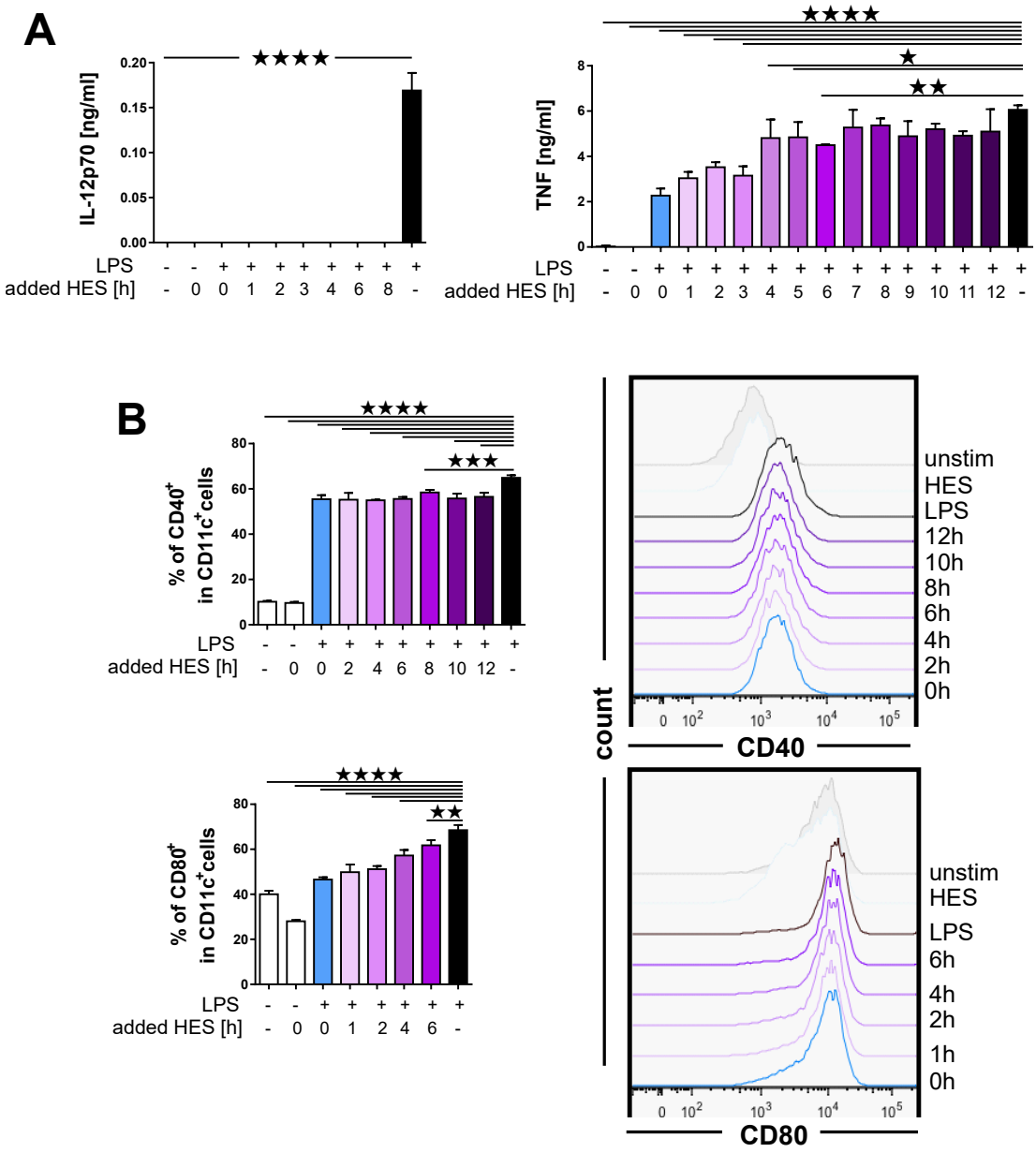

Figure 5.9: HES inhibits cytokine secretion and activation marker expression even if added hours after LPS. BMDC were differentiated with GM-CSF for ten days before stimulation with LPS. 10μg of HES were added at indicated time points after the start of the stimulation. **(A)** Concentrations of IL-12p70 and TNF in supernatants of BMDC were determined by ELISA. **(B)** Expression levels of costimulatory molecules on $CD11c^+$ cells was determined by flow cytometry. Left: percentages of $CD40^+$ and $CD80^+$ cells in the $CD11c^+$ population; Right: histograms showing the expression of CD40 or CD80 on $CD11c^+$ cells that received HES at the indicated time points after stimulation. Data are representative from at least three independent experiments. Data represent mean ± SD, n = 3; Results from 1way ANOVA and Dunnett's multiple comparison test are indicated as $*$: $p \leq 0.05$; $**$: $p \leq 0.01$; $***$: $p \leq 0.001$; $****$: $p \leq 0.0001$.

5.2.6 HES affects mRNA levels of signalling pathway components, transcription factors and enzymes involved in cell metabolism in BMDC eight hours post LPS stimulation.

As a complement to investigating cell signalling pathways involved in DC activation directly, it was decided to compare the transcriptome of LPS- and HES-treated BMDC, in order to identify potential upstream regulators of differentially expressed genes or to even directly identify regulated genes that might play a role in DC activation was a promising approach to shed light on the mechanism of DC inhibition by HES. Eight hours post stimulation was chosen as a promising time point for this analysis, as the inhibitory effect of HES on protein and, more importantly, mRNA levels was already well measurable at this point (Fig. 5.7 and 5.8), while it was also still able to change the outcome of stimulation when added at this time (Fig. 5.9). Two sets of analyses were undertaken, a preliminary array comparing only LPS- and LPS+HES-stimulated BMDC described below, and a more comprehensive dataset for which results are still awaited. This latter analysis includes important additional groups including unstimulated controls and samples treated with HES alone or active size exclusion fractions of HES.

The preliminary array investigated the effects of HES on LPS-stimulated cells. In this array, some 164 features were significantly up- or downregulated by HES ((Fig. 5.10A and B.3). Only 20 in total, not distinguishing between significant and non-significant values, were upregulated more than 1.5 fold, and only twelve were downregulated by that much. Even if looking at all transcripts with fold changes of at least 1.25 only 108 were upregulated, with only 84 downregulated by this amount. The transcripts with a fold change of $\pm$ 1.25 or more are shown in more detail in Fig. 5.10B, features with a fold change of 1.4 or more were labelled in both graphs. Only 20 features corresponding to 16 different transcripts were downregulated more than 1.4 fold in LPS+HES treated BMDC compared to the LPS treated group, with two of those features not reaching the significance threshold of 0.05. Slightly more features were upregulated, with 32 features corresponding to 25 distinct transcripts, four of which did not reach significance.

The transcript with the highest fold change was *Tgfbi*, a gene induced by TGF-β which reduces cell adhesion (Skonier et al., 1994), demonstrating the importance of the groups treated with the active fractions from gel filtration separation in the main array analysis, as these do not contain the TGF-β mimic molecule. The full list presented in tables C.1 and C.2 includes a wide range of transcripts for proteins without any immediate link to immune responses, as well as a number of

more obviously relevant ones. Among the downregulated transcripts were several peptidase inhibitors like Serpin A3F and G and the protease inhibitor Cystatin F, or a regulator of G-protein signalling (Rgs1); the list of upregulated transcripts contained both a metalloprotease (Adam8) and metalloproteinase inhibitor with anti-apoptotic function (Timp), a vascular endothelial growth factor (Vegfa) and the alarmin, IL-33.

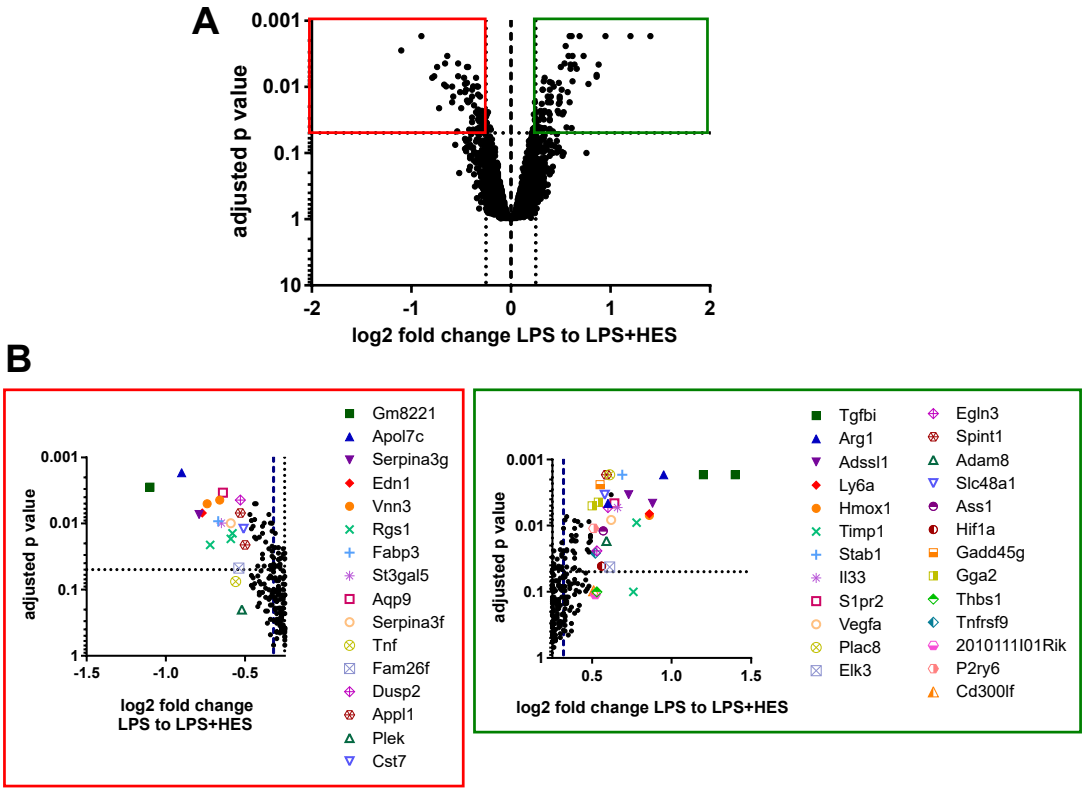

Figure 5.10: HES affects DC mRNA levels at 8h after stimulation. BMDC were differentiated with GM-CSF for ten days before stimulation with LPS and HES as indicated. At eight hours after stimulation, cells were treated with Trizol, RNA extracted and labelled for analysis on an Illumina MouseWG-6 v2.0 Expression BeadChip microarray. Statistical analysis of the data was performed by Dr. Alasdair Ivens. Data are presented as log2 fold change from mRNA levels in LPS-stimulated cells to levels in LPS+HES-stimulated cells for (A) all measured transcripts and (B) transcripts with greater than log2 fold change of $\pm$ 0.25 ($\pm$ 1.19 fold) from LPS- to LPS+HES-stimulated cells. Red indicates decreased, green indicates increased transcript levels in LPS+HES-treated cells. Dashed lines indicate log2 fold change of $\pm$ 0.32 ($\pm$ 1.25 fold). Labelled transcripts are those that reached a log2 fold change of $\pm$ 0.5 ($\pm$ 1.4 fold). The transcripts below the dotted line did not reach the significance threshold of $p \leq 0.05$. This experiment was performed once with samples in triplicates.

Fold changes of transcript levels of markers that have been analysed in Chapter 3 are shown in Fig. 5.11.

Mostly, they correlate with the expression of these markers measured before. Both Arg1 and TNF were among the transcripts most changed between the groups, with Arg1 being upregulated and TNF downregulated in LPS+HES-treated cells as shown before (see Fig. 3.6 for Arg1 and Fig. 3.1 for TNF protein, Fig. 3.4B and Fig. 5.8 for TNF mRNA levels). At least one feature corresponding to the transcripts for IL-12p35 (Il12a), IL-6, CD40, CD80 and to a lesser extent CD86 were reduced in LPS+HES-treated cells compared to LPS-treated cells as well (see Fig. 3.1 and 3.2 for protein levels and Fig. 3.4B and 5.8 for mRNA levels of the cytokines). However, most of these changes were not very extensive, in fact most of the markers were just barely more than 1.25 fold downregulated despite mRNA levels measured by RT-PCR differing to a much greater degree at this time point (see Fig. 3.4B). In addition, most did not reach

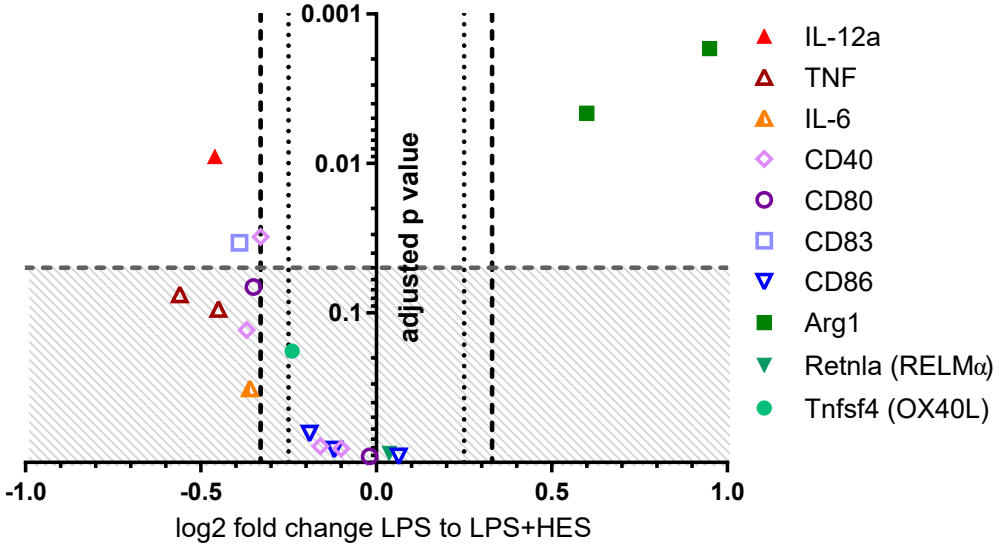

Figure 5.11: Activation marker mRNA levels are regulated by HES at 8h after stimulation. BMDC were differentiated with GM-CSF for ten days before stimulation with LPS and HES as indicated. At eight hours after stimulation, cells were treated with Trizol, RNA extracted and labelled for analysis on an Illumina MouseWG-6 v2.0 Expression BeadChip microarray. Statistical analysis of the data was performed by Dr. Alasdair Ivens. Data are presented as log2 fold change from expression levels in LPS stimulated cells to levels in LPS+HES stimulated cells for cytokines and costimulatory molecules investigated in chapter 1. Dotted lines indicate log2 fold change of ± 0.25 (± 1.19 fold); Dashed lines indicate log2 fold change of ± 0.32 (± 1.25 fold). The grey shaded area contains transcripts that did not reach the significance threshold of $p \leq 0.05$. This experiment was performed once with samples in triplicates.

significance, as indicated by the values being located in the grey shaded area beneath the dashed line, probably owing to the fact that this was only the preliminary array comparing two groups of only three samples each. In addition, transcript levels for RELMα (Retlna) were unchanged, supporting the previous results on its expression in LPS-treated BMDC (see Fig. 3.6A).

CD83, a costimulatory molecule measured on the human moDC which was - just like the other markers measured - not differentially expressed with HES treatment on the human cells, was actually downregulated on mouse cells. Surprisingly, RNA levels of OX40L (Tnfsf4) were lower in LPS+HES-treated cells compared to LPS-treated cells as well, even though it was only a non-significant 1.18 fold change.

Using the fold changes of DC activation markers as a guide for the identification of further proteins of interest and, at least for this preliminary array, not excluding the values that did not reach significance, transcripts of proteins involved in DC activation signalling pathways were inspected more closely. Several phosphatases responsible for the dephosphorylation of all three MAPKs were in fact downregulated. DUSP2, a phosphatase acting on ERK1/2 and p38, was among the most regulated transcripts shown in Fig. 5.10B, with a fold change of -1.44 for one of its features. DUSP16, responsible for the dephosphorylation of JNK, was greatly downregulated as well, with one of its features showing a fold change of -1.33 from LPS- to LPS+HES-treated cells. DUSP14, acting on all three MAPKs, was downregulated to a lesser degree, with a fold change of -1.18. On the other hand, there were upregulated transcripts involved with MAPK signalling as well. Another phosphatase of ERK2 for example, DUSP6, had one feature with a fold change of 1.22, and a target of ERK1/2, the kinase MNK2 (Mknk2) was upregulated by 1.33 fold in LPS+HES-treated cells (Fig. 5.12A).

The fold changes for the regulatory proteins A20 (Tnfaip2) and ABIN1 to 3 (Tnip1-3) are shown in Fig 5.12B. As demonstrated in Fig. 5.6, the expression of A20 in LPS+HES-treated BMDC was actually decreased compared to the LPS-stimulated group at eight hours. Only a barely detectable decrease of the transcript level of this protein could be measured here, with a fold change of only -1.07. Two of the proteins associated with its function, ABIN-1 and ABIN-3 showed a slightly larger decrease in expression with fold changes of -1.11. ABIN-2, with a fold change of -1.04 did not appear to be regulated by HES.

A variety of other factors involved in DC activation was regulated as well and their fold changes are shown in Fig. 5.12C. With a fold change of -1.3, the leucine rich repeat containing protein LRRC33, a negative regulator of TLR signalling, was significantly downregulated in LPS+HES-treated cells compared to the LPS-stimulated group. CISH, a negative regulator of STAT5, was downregulated as well with a fold change of -1.21. Another downregulated protein involved in TLR

signalling was IRAK2, with one of its features exhibiting a fold change of -1.2.

On the other side of the spectrum, MARCH1, an E3 ubiquitin ligase known to reduce cell surface CD86 by targeting it for degradation (Baravalle et al., 2011; Corcoran et al., 2011), was upregulated by 1.28 fold in LPS+HES-treated cells. In addition, the Ras-related protein Rab-7b, another negative regulator of TLR signalling which functions by trafficking TLR4 to the degradative lysosome (Wang et al., 2007), displayed a fold change of 1.24.

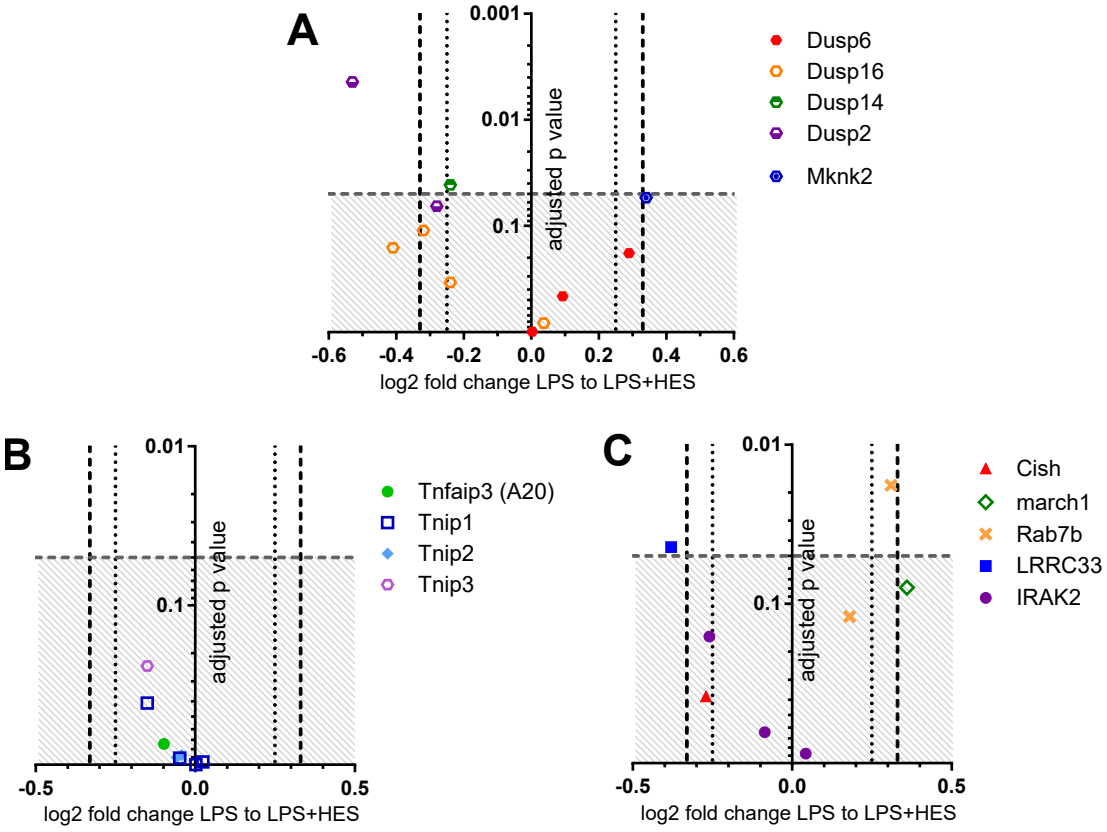

Figure 5.12: HES affects mRNA levels of some proteins relevant in DC activation signalling pathways at 8h after stimulation. GM-CSF BMDC were stimulated with LPS and HES as indicated. At eight hours after stimulation, cells were treated with Trizol, RNA extracted and labelled for analysis on an Illumina MouseWG-6 v2.0 Expression BeadChip microarray. Statistical analysis of the data was performed by Dr. Alasdair Ivens. Data are presented as log2 fold change from mRNA levels in LPS-stimulated cells to levels in LPS+HES-stimulated cells for (A) proteins involved in the MAPK signalling cascade, (B) A20 and ABINs and (C) other proteins involved in DC signalling that showed altered mRNA levels. Dotted lines indicate log2 fold change of $\pm$ 0.25 ($\pm$ 1.19 fold); Dashed lines indicate log2 fold change of $\pm$ 0.32 ($\pm$ 1.25 fold). The grey shaded area contains transcripts that did not reach the significance threshold of $p \leq 0.05$. This experiment was performed once with samples in triplicates.

Next, the expression levels of various transcription factor families previously known to be involved in the activation of DCs were investigated (Fig. 5.13). The majority of the known DC-associated transcription factors studied were unchanged between LPS- and LPS+HES-treated cells; there were however some notable members of their families that were regulated to some degree. NF-κB was an exception, with all of its subunits except RelB appearing slightly reduced in LPS+HES-treated BMDC (small black dots).

Among the most changed transcripts were those encoding members of the ETS family, and with a fold change of +1.53, ELK-3 was the transcript with the highest fold change among these transcription factors. The second highest fold change was measured for another ETS member, as expression of one of the Spi-C features was the most reduced among these transcription factors in LPS+HES-treated cells, with a fold change of -1.38. ETS-2 was the second most downregulated of these transcription factors, with a fold change of -1.23. On the other hand, transcript levels of ETS-1 were increased with a 1.27 fold change from LPS- to LPS+HES-treated BMDC.

Members of the ATF family were also among the most regulated of the investigated transcription factors. The transcript for BATF for example exhibited a fold change of -1.23 in LPS+HES-treated cells. The decrease in transcript levels of BATF2 was less distinct, this transcription factor only showed a fold change of -1.11. Conversely, among those upregulated were ATF3, with a fold change of +1.34 in LPS+HES-treated BMDC and ATF4 as another less distinctly elevated transcription factor with a fold change of +1.11. Transcript levels of the AP-1 subunit c-Jun were significantly elevated in LPS+HES-treated cells as well, with a fold change of +1.31 compared to LPS-stimulated BMDC.

Of the other transcription factor families, one feature of IRF1 displayed a fold change of -1.18 compared to LPS-stimulated cells, several more also had negative fold changes. IRF2 and its co-repressor IRF2-BP2 on the other hand were upregulated in HES-treated cells, with IRF2 only having a small fold change of +1.08, while IRF2-BP2 was increased 1.14 fold. None of the calcium dependent NFAT transcription factors were affected by HES; the transcript of the calcium independent NFAT5 on the other hand was downregulated in LPS+HES-treated cells, with a fold change of -1.16 compared to the LPS-stimulated cells. Similarly, of the STAT family only STAT5 was regulated, its transcripts reduced in LPS+HES-treated cells with fold changes of -1.23 and -1.14 for the two features. Two more transcription factors of interest were upregulated in LPS+HES treated BMDC. The transcript for C/EBPβ was somewhat increased with a fold change of +1.12, as was one of the features of the transcriptional repressor LRRFIP1, which was increased 1.2 fold in LPS+HES-treated cells.

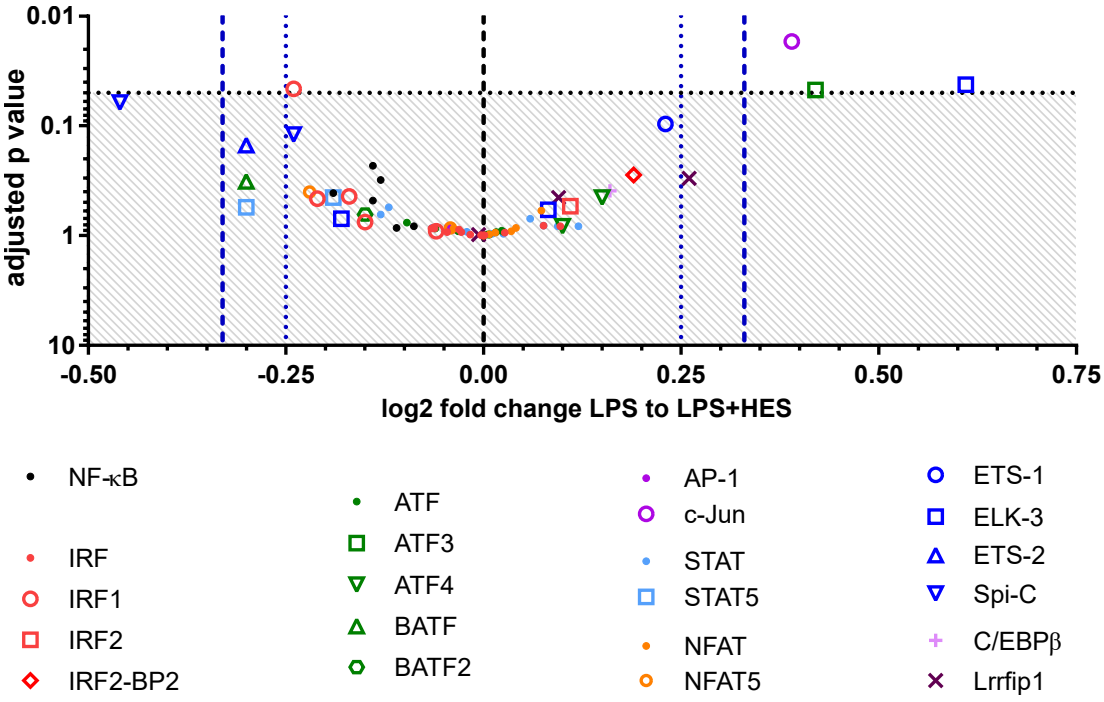

Figure 5.13: HES affects mRNA levels of some transcription factors relevant for DC activation at 8h after stimulation. BMDC were differentiated with GM-CSF for ten days before stimulation with LPS and HES as indicated. At eight hours after stimulation, cells were treated with Trizol, RNA extracted and labelled for analysis on an Illumina MouseWG-6 v2.0 Expression BeadChip microarray. Statistical analysis of the data was performed by Dr. Alasdair Ivens. Data are presented as log2 fold change from mRNA levels in LPS stimulated cells to levels in LPS+HES stimulated cells. Dotted lines indicate log2 fold change of ± 0.25 (± 1.19 fold); Dashed lines indicate log2 fold change of ± 0.32 (± 1.25 fold). The grey shaded area contains transcripts that did not reach the significance threshold of $p \leq 0.05$. This experiment was performed once with samples in triplicates.

Finally, considering the increasingly recognized importance of metabolism regulation in the activation of immune cells, including DCs, transcript levels of proteins involved in this process were analysed as well.

While the transcripts for most enzymes important for energy metabolism were not particularly different between the two groups, those involved in the shift towards aerobic glycolysis were noticeably altered. In fact, a general shift towards increased expression of glycolytic enzymes seemed to occur. More specifically, the tightly regulated α-subunit of the transcription factor regulating the increased usage of

the glycolytic pathway, HIF-1 (Jantsch et al., 2008; Pearce and Everts, 2015), was among the transcripts with the highest increase in LPS+HES-treated cells with an increase by 1.47 fold in this group, even though another one of its features appeared slightly reduced with a fold change of -1.06 in LPS+HES-treated cells. Several of its targets were also highly upregulated, such as the glucose transporter GLUT1 (Slc2a1) with a 1.39 fold increase in its transcript levels, or the two glycolytic enzymes glucose phosphate isomerase, which was increased by 1.19 fold, and an isoform of the phosphofructokinase, increased by 1.16 fold (Krawczyk et al., 2010; Minchenko et al., 2003). Another target of HIF-1 is lactate dehydrogenase A (LDHA1), which is responsible for the conversion of pyruvate into lactate to regenerate NAD^+ and depriving the TCA cycle from its carbon source (Palsson-Mcdermott and O'Neill, 2013; Pearce and Everts, 2015; Semenza et al., 1996). The transcript for this enzyme was somewhat upregulated as well, with a fold change of +1.1 in LPS+HES-treated cells. A further factor inhibiting the TCA cycle, and also a target of HIF-1, is the pyruvate dehydrogenase kinase 1, which inactivates the enzyme catalysing the conversion of pyruvate to acetyl-CoA (Kim et al., 2006; Papandreou et al., 2006). Transcript levels for PDK1 were increased by 1.08 fold (Fig. 5.14A).

In LPS activated BMDC, the main reason for the switch to aerobic glycolysis is thought to be increased production of NO by iNOS, which inhibits the electron transport chain and therefore prevents the generation of ATP by oxidative phosphorylation (Everts et al., 2012b). In contrast to the other inflammatory mediators induced by LPS described above, transcript levels of Nos2, encoding for iNOS, were actually increased 1.38 fold upon treatment of the cells with HES.

Interestingly, numerous proteins involved in cellular stress responses were upregulated by HES as well. Chief among those was heme oxidase 1 (HO-1 encoded by Hmox1), another of the most highly regulated transcripts found in this analysis. This enzyme, catalysing the degradation of heme to CO, biliverdin and iron (Hull et al., 2014; Naito et al., 2014), was upregulated by 1.82 fold in LPS+HES-treated cells. A transporter responsible for the regulation of intracellular heme availability, HRG1 (Slc48a1) (Delaby et al., 2012; White et al., 2013) was upregulated by 1.5 fold as well. Iron is subsequently bound by ferritin (Hull et al., 2014), the light chain subunit of which was slightly increased as well with transcript levels that were 1.12 fold higher in cells treated with HES.

Another HIF-1 responsive gene encodes Ddit4, a protein involved in stress responses after both oxidative and ER stress (Jin et al., 2009; Shoshani et al., 2002; Whitney et al., 2009). Expression of this protein was increased by HES as well, as its transcript levels were increased by 1.32 fold. Interestingly, the transcript levels of CIC (Slc25a1), responsible for the transport of citrate from the mitochondria into

the cytoplasm (Infantino et al., 2011) for generation of NADPH via the isocitrate dehydrogenase 1 (IDH1) (Itsumi et al., 2015) or de novo fatty acid synthesis, needed in DCs to alleviate ER stress during activation (Everts et al., 2014), were 1.12 fold reduced in cells treated with HES. Transcript levels of IDH1 on the other hand were upregulated in HES-treated cells, with a fold change of +1.26 compared to cells stimulated with LPS alone. An enzyme involved in the NADPH producing pentose phosphate pathway, transaldolase 1 (Taldo1) (Perl et al., 2011), was also increased 1.26 fold in LPS+HES-treated cells.

Several proteins involved in the production and regeneration of glutathione and therefore important in the protection of cells from oxidative stress (Rahman, 2005), were upregulated in LPS+HES-treated cells. Slc7a11, a transporter for cystine that therefore provides the cysteine needed for the production of glutathione (D'Angelo et al., 2010), was increased 1.23 fold. The first enzyme involved in the biosynthesis of glutathione, glutamate-cysteine ligase (Gclm) was even increased by 1.4 fold. Expression of glutaredoxin (Glrx) seemed increased as well, with its transcript levels being 1.34 and 1.26 fold higher after HES treatment. The microsomal glutathione S-transferase is also involved in the oxidative stress response, and showed increased expression in LPS+HES-treated cells with 1.3 and 1.27 fold increases of transcript levels compared to LPS-stimulated cells. On the other hand, also the expression of TXNIP, a protein suppressing the activity of thioredoxin (Nishiyama et al., 1999), was increased by 1.26 and 1.21 fold in cells treated with HES.

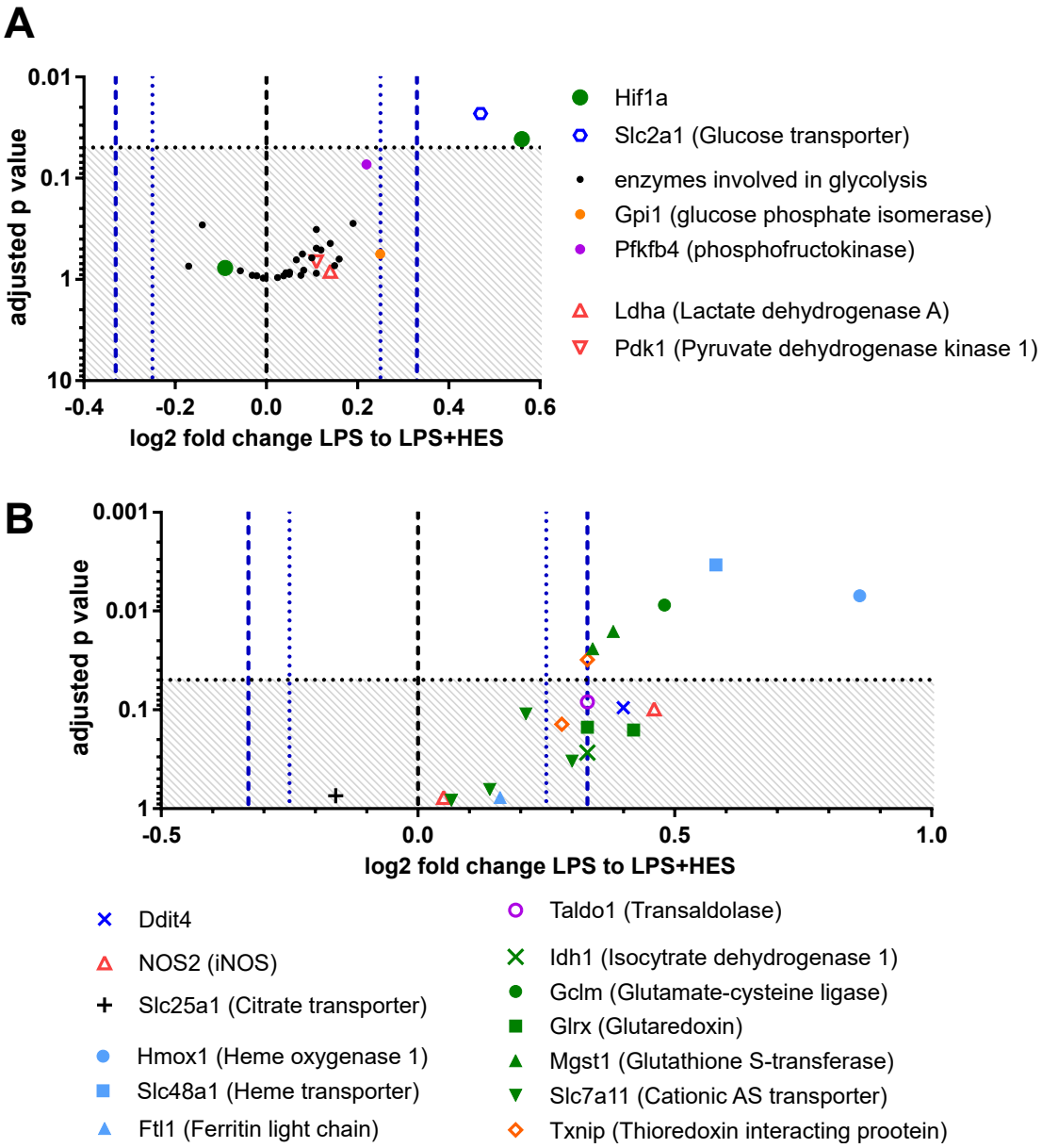

Figure 5.14: HES affects mRNA levels of proteins relevant for DC metabolism at 8h after stimulation. BMDC were differentiated with GM-CSF for ten days before stimulation with LPS and HES as indicated. At eight hours after stimulation, cells were treated with Trizol, RNA extracted and labelled for analysis on an Illumina MouseWG-6 v2.0 Expression BeadChip microarray. (A) Proteins involved in aerobic glycolysis. (B) Proteins involved in cellular stress responses. Statistical analysis of the data was performed by Dr. Alasdair Ivens. Data are presented as log2 fold change from mRNA levels in LPS-stimulated cells to levels in LPS+HES-stimulated cells. Dotted blue lines indicate log2 fold change of $\pm$ 0.25 ($\pm$ 1.19 fold); Dashed blue lines indicate log2 fold change of $\pm$ 0.32 ($\pm$ 1.25 fold). The grey shaded area or area underneath dotted black lines contains transcripts that did not reach the significance threshold of $p \leq 0.05$. This experiment was performed once with samples in triplicates.

5.3 Discussion

In addition to the search for the modulatory molecule in HES, the identification of the mechanism underlying the modulation of DC activation was the second major task in this project. This is especially important considering potential therapeutic applications of the DC modulator(s) in HES, or the exploit of the mechanism employed by it via other means. The main findings and suggested targets for future study are summarized in Fig.5.15.

In previous experiments, some signalling pathways or their components have already been ruled out as the targets of HES (Dayer, 2011). These experiments showed that HES does not act via pathways utilizing the kinase Syk, like many C-

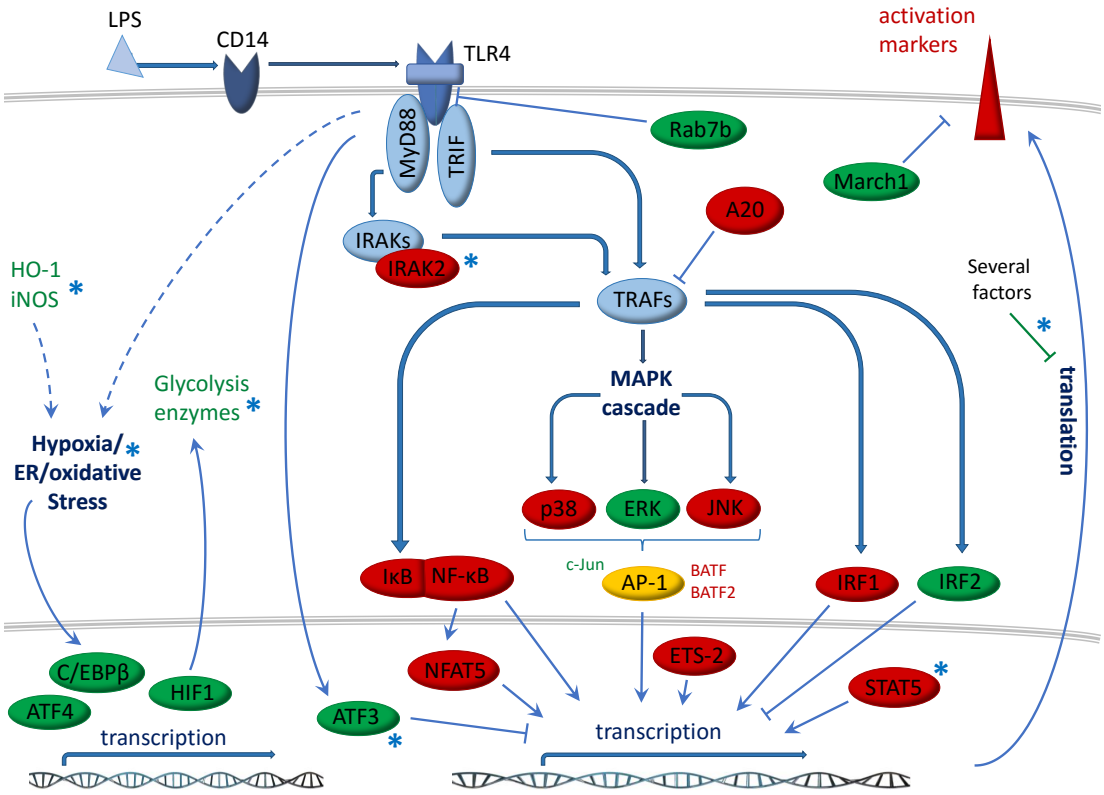

Figure 5.15: Schematic detailing changes in signalling and metabolism between LPS- and LPS+HES-treated BMDC. Activation of MAPK and NF-κB cascades in LPS- and LPS+HES-treated GM-CSF BMDC were analysed by flow cytometry; transcriptome changes at eight hours post stimulation were analysied using an Illumina MouseWG-6 v2.0 Expression BeadChip microarray. Depicted here are the most relevant changes in cell signalling and metabolism discussed in this chapter. Red: Downregulated or inhibited components; Green: Upregulated components; Asterisks denote suggested targets of future research.

type lectin receptors including Dectin-1 and 2, or PI3K, and that it does not act on or upstream of MyD88 and TRIF. Whether HES has an effect on the activity of two of the main signalling pathways involved in DC activation, NF-κB signalling and the MAPK cascade, has however not previously been investigated. The first MAP kinase investigated here was ERK. Unexpectedly, HES increased the phosphorylation of ERK1/2 during the first half hour after stimulation with LPS. This finding is less surprising considering work by Agrawal et al., showing that in human moDC, the induction of ERK1/2 phosphorylation by the TLR2 ligand Pam3cys actually results in an inhibition of IL-12p70 production which is restored upon inhibition of ERK1/2 activation (Agrawal et al., 2003). It was therefore an interesting possibility that HES inhibits DC activation via increased activation of ERK1/2. However, HES was still able to inhibit DC activation when cells were treated with an inhibitor of MEK1/2, the kinases that phosphorylate ERK1/2, demonstrating that this is not its mechanism of action (Fig. 5.2). In contrast to ERK1/2, both p38 and JNK have been shown to be important for the maturation of DCs. Inhibition of either MAP kinase resulted in a reduced upregulation of costimulatory molecules and impaired expression of IL-12p70 and TNF by human moDCs after LPS stimulation (Agrawal et al., 2003; Nakahara et al., 2004). Here, these two branches of the MAPK cascade were not affected in the first hour post stimulation, as phosphorylation of p38 and JNK was comparable in cells stimulated with LPS and LPS+HES. When looking at later time points however, it became clear that HES actually has an effect on these signalling pathways, as in cells treated with HES the phosphorylation levels of both p38 and JNK returned to pre-stimulation levels at five hours post stimulation, which was several hours before the LPS-treated cells reached that point again (Fig. 5.3 and 5.4).

Investigation of the phosphorylation status of IκBα led to a similar result. IκBα is one of the proteins bound to NF-κB, keeping it cytoplasmic by masking its nuclear translocation signal. Phosphorylation marks IκBα for degradation, leading to activation and nuclear translocation of NF-κB. Interfering with this process, for example by inhibiting this degradation of IκBα, has been shown to inhibit DC maturation (Rescigno et al., 1998). While no data is currently available on the early time points after activation, HES does seem to induce an earlier and more profound loss of IκBα phosphorylation (Fig. 5.5). Another possibility considered was that HES might increase the expression of A20, as that has been shown to be involved in the termination of TLR responses by deubiquitinating and thereby inhibiting central players in the signalling cascades like TRAF6 (Boone et al., 2004) and RIP1 (Wertz et al., 2004). While during the first hour of stimulation both LPS and LPS+HES treatment induced comparable amounts of A20, this had changed at 2.5 hours post stimulation. In contrast to the expected effect, HES actually inhibited the LPS-induced expression

of this protein (Fig. 5.6).

These results were quite puzzling, and hinted to an effect of HES not on the initial early phase of activation but on the ability of DCs to sustain the LPS-induced activation. This was further supported by the data gathered from the expression time course experiments with IL-12, TNF, IL-6 and CD40 (Fig. 5.7). Those of these proteins that were induced early on, which were IL-6, CD40 and especially TNF, were induced to the same extent in the first three to four hours of stimulation, at least considering their protein levels. Then HES seemed to have slightly different effects on the protein levels, as, while it completely stopped any further increase in secreted TNF, the concentration of IL-6 and the expression of CD40 continued rising, albeit to a lesser extent than in cells stimulated with LPS alone. IL-12p70 on the other hand, which was detectable in the cell supernatants only at a much later time than the other two cytokines, was immediately suppressed by HES. Looking at the mRNA levels of IL-12 and IL-6 however, things look slightly different again (Fig. 5.8). The two subunits of IL-12, p35 and p40 were induced hours before p70 could be detected in the cell supernatants. While mRNA levels of this cytokine were reduced by HES right away, probably owing to the fact that they were only induced at three to four hours post stimulation, which coincided with the regulatory effects taking hold on the protein expression of IL-6, TNF and CD40, they did also measurably increase in the LPS+HES-treated group. For IL-6 the discrepancy between mRNA and protein levels was quite distinct as well, as HES barely reduced the mRNA levels of this cytokine. This hints that, while HES clearly affects either transcription or mRNA stability, it might also control translation or influence protein expression at a post-translational level, for example altering protein secretion or degradation.

The hypothesis that HES inhibits the maintenance rather than the induction of DC activation is further supported by the results showing its ability to impact LPS-induced secretion of IL-12p70 and TNF, and the upregulation of both CD40 and CD80 even if added hours after the start of the stimulation (Fig. 5.9). In fact, it seems as if the effect of HES on TNF begins to wane if administration is delayed past three to four hours of LPS stimulation, which is around the same time the protein levels in the expression time course start showing the inhibitory effect of HES. Around eight hours after stimulation, when protein levels barely increase any further in the expression time course experiments, the addition of HES was almost completely unable to reduce secretion of TNF.

To gain more insights into transcriptional changes induced by HES in BMDCs, a microarray analysis of the BMDC transcriptome at eight hours post stimulation was performed. At this point only the data from the preliminary array are available, which compares only LPS- and LPS+HES-treated cells. Expression changes measured by

this array were not very notable and often did not reach significance, as indicated by the results for markers previously shown to be regulated (Fig. 5.11 compared to Fig 3.1, Fig. 3.2, Fig. 3.4 and Fig. 5.8). Furthermore, as total HES was used, effects of TGM can not be distinguished from effects caused by the putative DC modulator, a fact underscored by the finding that the highest regulated transcript is of a protein induced by TGFβ (Fig. 5.10). However, this analysis should still be a valuable tool to gain an insight into transcriptional changes induced by HES and determine potential candidates for further experiments which can be further validated once the results of the currently running array experiments comparing unstimulated BMDC and those treated with HES, LPS+HES, the active size exclusion fraction 14 and LPS+fraction 14 are available.

Indeed, there were a number of interesting changes in transcription levels of proteins between LPS- and LPS+HES-treated groups. Some were the opposite of what would have been expected.

LRRC33 for example was downregulated in LPS+HES-treated cells; this factor has been implicated as a negative regulator of TLR signalling, interacting with TLRs and blocking their interaction with downstream mediators like MyD88. Its deletion led to increased activation of MAPK and NF-κB signalling in the first hour after stimulation and a subsequent increase in TNF and IL-6 production by various TLR ligands in both macrophages and DCs (Su et al., 2014). However, as reported, HES does not change the activation of these pathways in the early phase of DC activation. Furthermore, Su et al. could show that LRRC33 expression is inhibited by TLR ligands during the course of the stimulation, so it would be possible that an accelerated downregulation of this protein is a side effect of the changes induced in DCs by HES via a different mechanism and after the early phase of activation.

The impaired induction of A20 expression in LPS+HES-treated cells was another puzzling result, as described above. Furthermore, even though at eight hours post stimulation A20 protein expression was clearly impaired in LPS+HES-treated cells, transcript levels at that point were barely reduced. This might either indicate an underestimation of fold changes by the array, or be another indication of the potential involvement of regulatory mechanisms on the translation or post-translation level. What is interesting however, is that transcript levels of A20, ABIN1 and ABIN3 seem reduced by HES treatment of cells, while ABIN2 does not seem affected. ABIN2 is, unlike ABIN1 and 3, independent of stimulation as it does not have NF-κB sites in its promoter (Verstrepen et al., 2009). Hence, the reduced transcript levels of these activation dependent proteins could be caused by the impaired NF-κB activation in HES-treated cells.

Even more surprising is the quite distinct increase in c-Jun transcript levels upon

HES treatment. This transcription factor, activated by JNK, has been shown to increase the expression of p40 in cooperation with C/EBPβ, which is also slightly increased by HES (Zhu et al., 2001), and to increase expression of TNF and IL-6 in cooperation with another slightly increased transcription factor, ATF4 (Zhang et al., 2013). However, the activity of c-Jun is dependent upon phosphorylation by JNK. As HES also impairs the activity of these kinases, it stands to reason that, while c-Jun expression is increased, this might not have any functional consequences as it can not be activated.

An effect of HES on the transcript levels of several DUSPs, enzymes dephosphorylating MAP kinases, is not at first glance surprising. However, of the four members of this family that were affected to a noticeable degree, three were downregulated in HES-treated cells, DUSP2, 14 and 16, none of which are specifically responsible for the dephosphorylation of ERK. Indeed, DUSP2 acts on both ERK and p38 (Chu et al., 1996; Zhang et al., 2005), DUSP14 on all three types of MAP kinases (Marti et al., 2001), and DUSP16 is specific for JNK (Matsuguchi et al., 2001). DUSP6 on the other hand, which is upregulated in HES treated cells, has been shown to be specific for ERK2 (Groom et al., 1996; Muda et al., 1996). In the case of DUSP2, this could be explained by the fact that its expression has been shown to be inhibited by HIF-1 (Lin et al., 2011; Wu et al., 2011), a transcription factor that seems to be expressed to a higher degree in LPS+HES- compared to LPS-treated cells. Taken together, these findings indicate that the change in expression of DUSPs is not responsible for the effect of HES.

Other regulated proteins do not seem to have an immediately apparent role in DC maturation, chief among them two of the transcription factors belonging to the ETS family. Spi-C for example has so far only been implicated in the development of splenic red pulp macrophages in response to heme (Haldar et al., 2014), or in B cells for both differentiation and function, as it inhibited the expression of components of the B cell receptor signalling pathway (Zhu et al., 2008). The increased expression of heme oxygenase in HES treated BMDC might be an explanation for the decrease in Spi-C transcript levels in these cells, considering that Haldar et al. showed that Spi-C expression is induced by heme. The role of this transcription factor in DCs is unclear however, especially as it previously has been reported to not be expressed in these cells (Kohyama et al., 2009). The other ETS member with an unclear role in DC activation is Elk-3, due to the fact that this transcription factor can apparently either suppress or activate gene transcription, depending on the involvement of the Ras signalling pathway (Giovane et al., 1994). It has however been shown to be downregulated in macrophages within six hours after stimulation with LPS, a change that could be reversed with TGFβ (Chen et al., 2003). It therefore stands to reason that TGM might be responsible for the higher transcript level of Elk-3 in LPS+HES-treated cells.

There are however also many other changes apparent that might contribute to the inhibition of DC activation by HES, these are summarized in Fig. 5.15.

Two proteins with increased transcript levels have been reported to negatively regulate DC activation by promoting protein degradation. MARCH1, an E3 ubiquitin-protein ligase, has been reported to ubiquitinate CD86 and promote its lysosomal degradation (Baravalle et al., 2011; Corcoran et al., 2011). The second protein, Rab7b, has been shown to negatively regulate production of various LPS induced inflammatory mediators including TNF and IL-6 in macrophages, probably by inducing degradation of TLR4 (Wang et al., 2007). It has later been described to do the same with TLR9 (Yao et al., 2009). In addition, it was shown to be increased in DCs treated with *Trichuris suis* ES, which does, just like HES, inhibit LPS-induced DC maturation (Klaver et al., 2015a).

CISH was another protein downregulated by HES that is involved in the regulation of a signalling pathway. More specifically, CISH both blocks the activation of STAT5 and is a target gene of this transcription factor, the transcript levels of which were also reduced in LPS+HES-treated cells (Matsumoto et al., 1999). Knockdown of CISH during the differentiation period of BMDC was shown to reduce their base expression of CD40, CD80 and CD86 and lead to reduced secretion of IL-12, TNF and IL-6 after stimulation with LPS (Miah et al., 2012). While the authors show that STAT5 activity is regulated by CISH, they do not ascertain whether the inhibition of DC maturation after CISH knockdown is mediated by STAT5. In fact, STAT5 itself has been demonstrated to increase the expression of CD80, CD86 and MHC II on both unstimulated and LPS-stimulated DCs (Zhong et al., 2010). Especially interesting in this setting is the regulation of costimulatory molecules on unstimulated cells, as this can be observed on HES-treated unstimulated DCs as well.

NFAT5 is another transcription factor that seems downregulated by HES. In macrophages it played a role in inducing the expression of TNF and IL-6 after stimulation with very low concentrations of LPS, but this effect was lost upon increase of the LPS concentration. Furthermore, its transcription was shown to be increased by NF-κB during the immediate early phase of activation after LPS stimulation; its transcript levels rose at around four hours post stimulation (Buxadé et al., 2012). It stands to reason that the inhibition of NF-κB activation by that time prevents the increase of NFAT5 expression in HES-treated BMDC.

Two more transcription factors that are induced after LPS stimulation and exhibit reduced transcript levels in HES-treated cells are BATF and BATF2. Both of these proteins heterodimerize with Jun proteins to form AP-1; they can then cooperate with ETS family members to bind to EICEs or with IRF4 or IRF8 to bind to AICEs to induce transcription of target genes (Murphy et al., 2013). BATF2 has also been shown to

cooperate with IRF1, to increase expression of TNF and iNOS (Roy et al., 2015). IRF1 was in fact another transcription factor with reduced transcript levels in LPS+HES-treated cells compared to cells stimulated with LPS alone. IRF1 has also been reported to induce transcription of both IL-12 subunits (Gabriele et al., 2006; Salkowski et al., 1999). Transcript levels of IRF2 on the other hand were slightly increased upon treatment with HES. IRF2 has been described as a competitive suppressor of IRF1-dependent gene transcription (Harada et al., 1989), although there are also reports that it suppresses TNF production but increases the expression of IL-12 and IL-6 (Cuesta et al., 2003). The fact the transcript levels of its co-repressor IRF2-BP2 (Childs and Goodbourn, 2003) are slightly increased in LPS+HES-treated DCs as well might be an indication for the prevalence of its inhibitory functions in this case.

Another transcription factor shown to interact with IRF1 is the equally downregulated ETS-2. In macrophages, ETS-2 expression is rapidly induced after LPS stimulation (Boulukos et al., 1990); at eight hours post stimulation it was found to form a complex with IRF1 and c-Rel, one of the NF-κB members, amongst others; this complex was shown to bind the p40 promoter and induce transcription of this gene (Ma et al., 1997).

Two of the most interesting regulated factors, considering the working hypothesis that HES affects the maintenance rather than the induction of DC activation, are IRAK2 and ATF3. IRAK2, which is reduced in HES-treated cells, has been shown to be necessary for sustained activation of NF-κB. In macrophages, the kinase activity of IRAK2 was induced only after two to four hours and peaked at eight hours post stimulation. In IRAK2$^{-/-}$ cells, the initial activation of NF-κB after MALP-2 stimulation (TLR2/6) was comparable to that of their wild-type counterparts, but at four hours post stimulation active NF-κB was greatly reduced in IRAK2 deficient cells and this remained the case for the rest of the stimulation period. Furthermore, expression of TNF and IL-6 was similar in both wild-type and IRAK2$^{-/-}$ macrophages at two hours post stimulation, but while mRNA levels of these cytokines increased further in wild-type cells they declined in the knock out cells at four hours post stimulation and had returned to undetectable quantities at eight hours after stimulation with MALP-2. Finally, the authors demonstrated that after a 24 hour stimulation, macrophages from IRAK2 deficient mice produced significantly less IL-6 and TNF in response to not only MALP-2 but also LPS, R848 and CpG (Kawagoe et al., 2008). Using mice expressing a mutant version of IRAK2 that was not able to bind TRAF6, Pauls et al. showed that the disruption of this signalling event decreased the phosphorylation of ERK, JNK and p38 at two hours post stimulation, and furthermore also decreased the mRNA levels of A20 (Pauls et al., 2013). Furthermore, IRAK2 deficient LPS stimulated macrophages have also

been shown to have both reduced mRNA stability and a reduced translational activity through phosphorylation of eIF4E, effectively inhibiting this translation elongation factor (Wan et al., 2009).

ATF3 on the other hand is significantly upregulated in HES treated cells. The expression of this transcription factor was induced by LPS in macrophages; after stimulation c-Rel induced its expression, which lead to an increase of ATF3-binding to promoter regions. At four hours post stimulation, ATF3-binding reached its maximum and remained constant. Binding of ATF3 to promoter regions lead to a recruitment of HDAC1, followed by deacetylation of histones which closed off the chromatin structure and inhibited transcription. In ATF3 deficient cells mRNA levels of IL-12p40, IL-6 and TNF were increased at four hours post stimulation, as were their protein levels (Gilchrist et al., 2006). This mechanism has further been shown to be active in DCs as well, and to regulate stimulation by CpG and poly(I:C) in addition to LPS (Whitmore et al., 2007).

As described before, maturation of DCs is accompanied by profound changes in their metabolism (for schematics, see Fig. 1.7 and 1.8). While they initially increase their glycolytic rate and TCA cycle to provide material for de novo fatty acid synthesis to expand their ER and Golgi apparatus and support the increased protein synthesis (Everts et al., 2014), they later commit to glycolysis as the source of ATP (Krawczyk et al., 2010). This has been shown to be due to the increased expression of iNOS; the produced NO inhibits the electron transport chain and therefore prevents oxidative phosphorylation, which is the ATP source in resting DCs (Everts et al., 2012b). The transcription factor HIF-1, which is induced in DCs by LPS stimulation even in the presence of oxygen (Spirig et al., 2010), is integral in this increase of the activity of the glycolytic pathway. Under hypoxic conditions, which prevent cells from using oxidative phosphorylation for ATP generation, knockdown of HIF-1 has been shown to lead to a reduced consumption of glucose and inhibited DC maturation (Jantsch et al., 2008). In addition to being induced by LPS its expression is also increased by NO, as demonstrated by overexpression of iNOS in macrophages (Sandau et al., 2001). As HES inhibits DC activation, it would be reasonable to assume that these metabolism changes might not be induced. However, HIF-1α, the highly regulated subunit of HIF-1, is among the most upregulated transcripts in LPS+HES-treated cells. Indeed, transcripts of enzymes involved in glycolysis appear to tend towards being slightly upregulated, including many of the reported targets of HIF-1. Furthermore, the increase in transcript levels of the HIF-1 targets LDHA and PDK1 in HES-treated cells indicate that pyruvate indeed does not continue into the TCA cycle, as the enzyme needed to convert it to acetyl-CoA is inhibited by PDK1, but gets removed from the system by LDHA which produces lactate and regenerates NAD^+ for use in glycolysis.

Considering the important role iNOS plays in inhibiting OXPHOS and forcing DCs to adopt aerobic glycolysis as method of ATP generation, the fact that its transcript levels are greatly increased in LPS+HES-treated compared to LPS-stimulated cells should fit the picture well. However, many of the factors contributing to iNOS induction, like IRF1 (Roy et al., 2015), NFAT5 (Buxadé et al., 2012) and ETS-2 (Chen et al., 2003) are downregulated by HES while transcript levels of factors that should inhibit its production, like ATF3 (Gilchrist et al., 2006) and Elk-3 (Chen et al., 2003) are increased; the increase in iNOS is therefore another puzzling finding. The substrate used by iNOS for the production of NO is L-arginine, which is also the substrate of the equally upregulated Arg1. This could indicate a mechanism to regulate NO production; however, it appears the recycling of arginine from citrullin might be boosted in HES treated cells as argininosuccinate synthetase 1 (Ass1), an enzyme involved in this reaction, is among the most increased transcripts as well. In addition, the surprising finding that both Arg1 and iNOS appear to be upregulated by HES could also be due to differential expression of these two enzymes by the too distinct populations of $CD11c^{+}$ cells found in GM-CSF derived BMDC that were described by Helft et al., 2015.

Another target of HIF-1 is very high on the list of the most regulated proteins. Heme oxygenase 1 (HO-1), the enzyme responsible for the NADPH dependent degradation of heme to Fe^{2+}, CO and biliverdin has been shown to be induced by both HIF-1 and NO (see Hull et al., 2014 and Naito et al., 2014). Transcript levels of the protein transporting heme into the cell cytoplasm where it can be degraded by HO-1 (Delaby et al., 2012; White et al., 2013) and one of the subunits of the Fe^{2+} binding protein ferritin are increased in HES treated cells as well. Whether this is due to an increase in heme - many intracellular proteins contain heme, including cytochromes, peroxidases and iNOS, so this could potentially indicate the increased degradation of these proteins, perhaps even of misfolded versions, considering the increase in ER stress response factors described below - or simply to increase the production of the mediators CO, biliverdin and its degradation product bilirubin, which have been shown to have antioxidant and anti-inflammatory effects, remains to be seen. Of these mediators, especially the production of CO is of note, as this gas increases the production of NO by iNOS; just like NO it also interferes with the electron transport chain leading to inhibition of OXPHOS. It also induces the generation of reactive oxygen species, ROS (see Bilban et al., 2008).

That HES treated cells might be under increased oxidative stress is further supported by the fact that many transcripts encoding proteins involved in the cellular oxidative stress response are increased in LPS+HES-treated BMDC. In addition to that, transcript levels of the enzyme catalysing the reversible reaction balancing the two

branches of the pentose phosphate pathway are increased in LPS+HES-treated cells. The effect of this enzyme, transaldolase, seems to depend on the cell type, as in some cell types overexpression of it limits the production of NADPH and subsequently the regeneration of glutathione and therefore increases oxidative stress, while in other cell types it has the opposite effect (reviewed in Perl et al., 2011). The authors of this review propose that the effect might be dependent on whether the forward or reverse reaction is dominant in a cell. Interestingly, the transcription factor ETS-1 that increases the expression of components of the glutathione system in an ovarian cancer cell line (Verschoor and Singh, 2013) is induced by ROS in alveolar macrophages (Song et al., 2012) and is co-expressed with HIF-1α in hypoxic smooth muscle cells (Erdozain et al., 2011) is increased by HES as well. This transcription factor has also been shown to play a role in TGFβ/Smad induced transcription (Koinuma et al., 2009), and to induce the transcription of Nos2 to a modest degree (Chen et al., 2003), in addition to being an activator of TNF transcription during the early phase of activation. However, the latter might be counterbalanced be the increased expression of LRRFIP1, which binds to the same site on the TNF promoter as ETS-1; if this site has LRRFIP1 rather than ETS-1 bound, TNF transcription is suppressed (Suriano et al., 2005).

A further cellular stress response seems to be activated in LPS+HES-treated BMDC as well, as the transcript levels of two transcription factors involved in the induction of ER stress response gene expression, ATF4 and C/EBPβ, are increased. Both of these can, as mentioned earlier, interact with c-Jun to increase the expression of pro-inflammatory cytokines. However, in the case of ATF4 this is dependent on activation of c-Jun via JNK (Zhang et al., 2013). The accumulation of unfolded proteins was shown to induce C/EBPβ expression; this lead to induction of ATF4 expression and subsequently induction of ATF4 target genes (Li et al., 2008). In a DC-like cell line treatment with the skin sensitizer DNFB lead to ER stress induced ATF4 induction, which on the one hand resulted in increased production of HO-1 and on the other hand in the inhibition of CD86 and IL-12p40 transcription (Luís et al., 2014). Everts et al. showed that early after activation DCs go through a phase of ER stress as their protein production increases and surpasses the capacity of both ER and Golgi apparatus, which leads to the increase in glycolytic flux observed in early DC activation. Unlike later in DC activation, in this early phase pyruvate gets converted into acetyl-CoA and enters the TCA cycle, which it leaves again as citrate to be transported back into the cytoplasm and used as substrate for de novo fatty acid synthesis (Everts et al., 2014). Although at eight hours this should long have occurred, the fact that the transcript levels of CIC, the transporter necessary for import of citrate from the mitochondria, is slightly reduced might be a hint towards a potential cause of ER stress. Both ATF4 and C/EBPβ, as well as HIF-1 have been shown to induce the

expression of Ddit4 (also called REDD1) after hypoxia and oxidative or ER stress (Jin et al., 2009; Shoshani et al., 2002; Whitney et al., 2009). Not surprisingly, the transcript levels of this protein were elevated in HES-treated cells as well. Overexpression of Ddit4 in mouse embryonic fibroblasts was sufficient for inhibition of mTOR which lead to the activation of 4E-BP1, an inhibitor of the translation elongation factor eIF4e and therefore a general inhibition of translation (Brugarolas et al., 2004).

The inhibition of eIF4e by its phosphorylation is also the result of the activation of another protein upregulated in LPS+HES-treated cells, Mnk2 (Mknk2), which has been shown to inhibit translation after its activation by ERK or p38 (Knauf et al., 2001; Scheper et al., 2001). Together with the inactivation of this factor observed in IRAK2 deficient macrophages mentioned above, this indicates there might be at least three different mechanisms at work that lead to inhibition of translation.

Taken together, the findings presented in this chapter show that HES induces a variety of changes that may or may not contribute to the inhibition of DC activation in response to LPS, but a few discoveries specifically stand out. The fact that the early phase of activation seems unchanged by HES and only after this initial response to stimulation the BMDC treated with HES start showing the inhibition, and that treatment of the cells with HES at this point is still enough to inhibit activation is a key finding. In light of this, the discovery of the reduction in transcript levels of IRAK2 and the increase of ATF3 transcript levels seems very promising. In addition, the potential inhibition of translation could be important, especially considering the mentioned slight discrepancies between mRNA levels and protein production. Finally, the described changes in transcript levels of proteins with important roles in cell metabolism could give some valuable insight into the effects HES has on DCs.

However, as mentioned before, at the moment it is not possible to distinguish between the effects of TGM and the putative DC modulator; the lack of unstimulated cells or cells treated with HES without LPS stimulation to serve as a baseline for the interpretation of the microarray results is another drawback. It will be important to validate the findings discussed here with the array that is currently in progress, and the inclusion of groups treated with the active size exclusion fraction 14, which should not contain TGM, will help to further narrow down the potentially interesting results.

Provided these findings can be repeated and are not due to TGM, it would be interesting to further investigate the DC metabolism changes. The production of ROS could be visualized by using oxidation sensitive dyes and its involvement in DC modulation could be investigated by treating cells with antioxidants and comparing their response to LPS stimulation. Furthermore, the role NO plays in DC maturation could be determined by measuring nitrate levels in the cell supernatants to ascertain the increase in iNOS transcript levels actually translates to increased production of

NO, followed by manipulation of the system by either adding NO donors or reducing it by knockdown of iNOS or by using Nos2$^{-/-}$ cells. The cells' energy metabolism could be investigated by measuring the consumption of glucose and production of lactate by BMDCs stimulated with LPS and LPS+HES, determining the concentrations of these molecules in the supernatants before and after stimulation. Provided the findings presented here do indeed translate into an increased glycolysis in HES treated DCs it would be interesting to see if this is due to an increase in NO production, or whether HES increases glycolytic flux even if cells can use OXPHOS to generate their ATP, which could indicate a potentially interesting mechanism for DC modulation by HES. The induction of ER stress was another potential effect of HES; Thioflavin T has been described to efficiently stain protein aggregates and be a valuable tool to directly visualize ER stress by confocal microscopy (Beriault and Werstuck, 2013).

Investigating the potential inhibition of translation by HES would also be another set of follow up experiments. In their work describing the effect of Mnk2 activation on translation, Knauf et al. used a luciferase reporter construct to measure both cap-dependent and independent translation (Knauf et al., 2001). For a more detailed analysis of translation rates of specific mRNAs the method used by Wan et al. could be employed; they separated cytoplasmic extracts using a sucrose gradient followed by fractionation of the gradient. As translation of mRNA results in the formation of a polysome, mRNAs that are being translated can be distinguished from those that are not with this method (Wan et al., 2009).

More important than these experiments however, will be to determine if the reduction of IRAK2 expression and the increased induction of ATF3 could be the cause of the inhibition of TLR ligand induced DC activation. The importance of ATF3 could easily be determined by comparing the effect HES has on LPS induced DC maturation on wild-type and ATF3$^{-/-}$ cells, or by knockdown of ATF3 by RNAi. The role IRAK2 plays would be more difficult to analyse. One possibility could be to test if HES is still able to suppress DC activation if cells were transfected with a plasmid encoding constitutively active IRAK2 so that the expression level of this kinase is constant throughout the activation period.

In addition to this, it would be interesting to see what effect HES has on STAT5 signalling, which could be done by staining for phosphorylated STAT5. If it inhibits this pathway as indicated by the array results, the comparison of inhibition profiles of LPS- and LPS+HES-stimulated cells after inhibition of STAT5 signalling might provide some useful information.

In summary, the results presented here shed some light on how HES is able to affect DC activation, but more work is needed to determine the exact mechanism involved.

CHAPTER 6

Final Discussion

The murine intestinal nematode *Heligmosomoides polygyrus* is known to influence the host's immune system in various ways, establishing chronic infections in many mouse strains (Behnke et al., 2009; Filbey et al., 2014) and alleviates symptoms or even protects mice in a number of models for conditions like EAE (Wilson et al., 2010), colitis (Blum et al., 2012; Hang et al., 2013, 2010) and allergic asthma (Wilson et al., 2005). These effects are thought to mainly be mediated by the excretory/secretory products of the parasite (HES), which have been shown to protect mice from allergic airway inflammation through both TGF-β dependent and independent mechanisms (Grainger et al., 2010; McSorley et al., 2014; McSorley et al., 2015; McSorley et al., 2012), and to inhibit TLR ligand induced DC maturation (Segura et al., 2007). While the molecules responsible for the former have recently been identified - the TGF-β mimic TGM that induces protective regulatory T cells (Johnston et al., manuscript in preparation), the alarmin release inhibitor ARI responsible for the TGF-β independent effects (Osbourne et al., manuscript in preparation) and miRNA-containing exosomes (Buck et al., 2014) - the molecule acting on DCs or its mechanism of action are still unknown.

The aim of the work described here was to shed light on these two questions. First, the phenotype of HES treated DCs was described in considerably more detail than before. HES was able to inhibit DC maturation induced by a variety of TLR ligands acting on TLR1/2, TLR3, TLR4, TLR7 and TLR9, by impairing the upregulation of costimulatory molecules and the production of IL-12p70, TNF and IL-6. This corroborated previous findings, as HES was for example able to inhibit DC activation induced by bacterial extracts acting on several TLR ligands like Pa (Grainger, 2009), and had already been shown to inhibit LPS, CpG or Poly(I:C) induced DC maturation (Segura et al., 2007). Here, the inhibition of LPS induced DC maturation was not only visible on protein level, but also on mRNA level as measured by qPCR over the course of the stimulation and by analysis of the transcriptome of LPS and LPS+HES treated BMDC eight hours after stimulation with LPS. However,

the reduction in RNA levels was only found for specific transcripts; unlike described for the RNase foung in SEA, ω-1, which was found to non-specifically degrade intracellular RNAs (Everts et al., 2012a).

HES was also able to inhibit LPS induced production of TNF and IL-6 from splenic cells enriched for CD11c, and the activation of all three populations described in BMDCs differentiated with Flt3-L (FLDC). This was an important finding, as it has recently been found that GM-CSF differentiated BMDC contain two distinct populations, one of which the authors classified as being macrophage-like cells (Helft et al., 2015); the fact that the effect of HES on FLDC is comparable to that on GM-CSF BMDC confirms that HES indeed acts on DCs.

In addition, HES had different effects on the alternative activation of DCs of two different mouse strains. In BMDC from C57BL/6 mice, which are susceptible to infection with *H. polygyrus*, HES inhibited the production of RELMα induced by IL-4 treatment, while in cells from the more restistant BALB/c strain the production of RELMα was comparable between HES treated and untreated cells. This is in line with findings in vivo, as *H. polygyrus* infected BALB/c mice expressed higher levels of RELMα than infected C57BL/6 mice (Filbey et al., 2014). In BMDC from BABL/c mice, HES also increased the expression of Arg1 and OX40L, two additional markers of alternatively activated DCs (Ekkens et al., 2003; Esser-von Bieren et al., 2013; Jenkins et al., 2007), which potentially gives an insight into how HES activates DCs to induce T_H2 responses (shown by Grainger, 2009). Interestingly, while Arg1 transcripts were elevated at eight hours post-LPS stimulation in C57BL/6 BMDC, the OX40L transcript levels seemed slightly reduced in these cells. It remains to be seen if this can be validated by qPCR and, more importantly, by measuring the protein expression of OX40L on BMDC from C57BL/6 mice.

The discovery of small vesicles secreted by helminths, including *H. polygyrus*, which were shown to be able to modulate immune responses, for example in the setting of allergic airway inflammation (Buck et al., 2014; Coakley et al., 2015), introduced these exosomes as new ES components that might act on DCs. In fact, exosomes are able to inhibit LPS induced activation of BM-macrophages (Coakley, manuscript in preparation). Contrary to these findings however, exosomes (provided by Gillian Coakley) were not able to impair LPS induced maturation of BMDCs, unlike the exosome depleted HES. In addition to the fact that the inhibitory effect was heat labile, this indicated a molecule with a protein component responsible for the impairment of DC activation.

Based on this reasoning, the strategy chosen to identify the regulatory molecule was fractionation of HES followed by mass spectrometric analysis of the fractions. Blaise Dayer already found that size exclusion fractionation of HES produced two

distinct fractions with the ability to inhibit LPS induced IL-12p70 production (Dayer, 2011), which was repeated here. In addition, the fractionation of HES by anion exchange fractionation resulted in a similar outcome; however, the comparison of the mass spectrometry results for these inhibitory fractions did not identify any plausible candidates. The method was therefore refined, with a sequential fractionation of HES by size exclusion fractionation followed by the fractionation of the active fractions by anion exchange. As before, the inhibitory activity of HES was found in distinct fractions; the analysis of all fractions by mass spectrometry enabled the creation of abundance profiles for the proteins identified. These could be compared to the activity profile of the fractions, and proteins that were found mainly in the active, inhibitory fractions could be selected. Five proteins were chosen as candidates for expression, but none of the recombinants were able to inhibit DC activation. Following this, all of the gel filtration fractions, including the active fractions used for the sequential fractionation, in addition to a new anion exchange fractionation of HES were analysed by mass spectrometry as well. Now, the abundance profiles for proteins could be established for three different fractionation approaches, which improved the selection process. For example, four of the five previously found candidates would have been excluded according to their abundance profiles in the size exclusion and anion exchange fractionations. In this new comparison, another four candidates were chosen for expression, but again none of the recombinants was able to inhibit LPS induced DC maturation. This could be due to their expression in mammalian cells instead of *H. polygyrus*, as they might be misfolded or lacking important post-translational modifications. The expression of the recombinant proteins will however enable us to raise antibodies to see if neutralizing the native proteins in HES might abolish its DC modulatory effects, to test this possibility. In addition, only the top priority proteins were expressed, with a number of candidates that seemed less likely due to for example less clear cut abundance profiles, their resemblance to housekeeping proteins or their categorization as dedicated egg or larval stage proteins still untested.

The availability of protein emPAI values across all fractions of the three fractionation approaches furthermore enabled the comparison of already established proteins modulating DC activity to the activity profiles of the fractions. This showed that the abundance profile of the protease inhibitor cystatin, which was shown to inhibit CpG induced DC activation (Sun et al., 2013), did not match the fractions' activity profiles. TGM, in addition to only partially inhibiting DC activation by LPS, did also not segregate into the active fractions. The inhibitory effects of HES on DC maturation were also previously shown to not be mediated via the TGF-β receptor, as blocking signalling through it did not impair the activity of HES (Dayer, 2011).

The further characterization of the effects HES has on LPS induced DC

maturation also allowed the establishment of a timeline for its effects. Firstly, treatment with HES for only one hour affected unstimulated DCs in such a way that subsequent stimulation is inhibited, even if HES itself is removed. This effect is transient; in experiments where unstimulated DCs were incubated with HES for 18 hours, no effect on IL-12p70 secretion could be seen if LPS was added one day after removal of HES (Grainger, 2009). Secondly, HES did not have an effect on expression of TNF, IL-6 or CD40 in the immediate-early phase of stimulation, only starting to inhibit their expression around three to four hours post stimulation. IL-12p70 only became detectable between 8-10 hours post-stimulation; accordingly, it was not detectable in the supernatants of LPS+HES treated cells at any time point. Thirdly, HES was able to inhibit LPS induced DC maturation even if added hours after the stimulation; in fact, its ability to inhibit TNF expression for example weakened around three hours post-stimulation, around the same time its effects on the concentration of this cytokine in the expression time course started to be visible, and was barely noticeable at eight hours post-stimulation, when the TNF expression reached a plateau.

These findings shed some light on results obtained when analysing the activation of signalling pathways involved in DC maturation. Previously, it was established that HES does not signal through MyD88, TRIF, Syk or PI3K dependent pathways (Dayer, 2011). Now, the MAPK and NF-κB pathways were investigated as well. Their activation in the immediate-early phase of DC maturation was not impaired, and while HES increased the phosphorylation of ERK, the activity of this kinase was dispensable for the inhibition of DC maturation. However, at later time points HES treated BMDC exhibited lower levels of p38, JNK and IκB phosphorylation, in fact coinciding with the manifestation of the inhibitory effects on activation marker expression. HES treatment reduced the levels of A20 protein at these time points as well, possibly reflecting an impaired induction of its expression due to the inhibition of NF-κB signalling.

Taken together, these results indicate that HES impairs the maintenance rather than the induction of signalling after stimulation by TLR ligands, which distinguishes it from most of the described DC modulators from other helminth species.

This also allows a better interpretation of the transcriptome comparison between LPS and LPS+HES treated cells. HES induced some changes in the expression levels of transcription factors involved in the production of pro-inflammatory molecules, for example reducing the transcript levels of IRF1, ETS-2, BATF and BATF2 as well as STAT5 and most NF-κB members. It also increased the expression of March1 and Rab7b, both involved in targeting proteins for degradation. March1 has been shown to induce the proteasomal degradation of CD86 (Baravalle et al., 2011; Corcoran et

al., 2011), while Rab7b impairs signalling through TLR4 and TLR9 by promoting their degradation (Wang et al., 2007; Yao et al., 2009), and has in fact been shown to play a role in immune modulation by *Trichuris suis* (Klaver et al., 2015a). In addition to this, HES also affected transcript levels of factors that became especially relevant considering the established inhibition timeline. Foremost, it increased the expression of ATF3 and decreased the level of IRAK2 transcript. ATF3 has been shown to be induced by TLR ligation and alter the chromatin state of gene promoter regions, especially those with NF-κB sites, thereby switching off transcription of target genes (Gilchrist et al., 2006; Whitmore et al., 2007). IRAK2 on the other hand has been described as necessary to maintain signalling after TLR ligation, without which classical activation of macrophages was significantly impaired (Kawagoe et al., 2008; Pauls et al., 2013).

Additionally, the results from the microarray experiment revealed unexpected effects of HES on DC metabolism. As described previously, DCs commit to aerobic glycolysis upon classical activation, which, at least in BMDC, is due to the fact that they start expressing iNOS, and the produced NO inhibits the electron transport chain and therefore oxidative phosphorylation (Everts et al., 2012b; Krawczyk et al., 2010). It could be expected that, since HES inhibits DC activation, this might not be the case in HES treated DCs. Contrary to this assumption, the transcript levels of iNOS were actually increased in LPS+HES treated compared to LPS stimulated cells, as were those for the tightly regulated subunit of the transcription factor responsible for the increased expression of glycolysis enzymes, HIF-1α, and many of its target genes. Furthermore, the increased transcript levels of factors involved in both ER and oxidative stress responses is intriguing as well, although it is impossible to say if these effects are a cause or an effect of the changes HES induces in DCs without further experiments.

While all of these effects still have to be verified and, most importantly, their importance for the HES induced DC modulation established, these findings do provide valuable insights into potential mechanisms.

Finally, the results presented here demonstrate that HES is also able to impair LPS induced maturation of human monocyte derived DCs. This shows that the pathway targeted by HES is conserved between mice and humans, and indicates that the modulatory molecule, once found, and its mechanism of action could well be exploited in the development of new treatment strategies for conditions that would benefit from the inhibition of DC activation.

References

Abbott, D. W., A. Wilkins, J. M. Asara, and L. C. Cantley (2004). "The Crohn's Disease Protein, NOD2, Requires RIP2 in Order to Induce Ubiquitinylation of a Novel Site on NEMO". In: *Current Biology* 14, pp. 2217–2227. DOI: 10.1016/j.

Abreu, M. T. (2010). "Toll-like receptor signalling in the intestinal epithelium: how bacterial recognition shapes intestinal function". In: *Nat Rev Immunol* 10 (2), pp. 131–144. DOI: 10.1038/nri2707.

Agrawal, S., A. Agrawal, B. Doughty, A. Gerwitz, J. Blenis, T. Van Dyke, and B. Pulendran (2003). "Cutting edge: different Toll-like receptor agonists instruct dendritic cells to induce distinct Th responses via differential modulation of extracellular signal-regulated kinase-mitogen-activated protein kinase and c-Fos." In: *Journal of immunology (Baltimore, Md. : 1950)* 171 (10), pp. 4984–9. DOI: 10.4049/jimmunol.171.10.4984.

Ahmed, S., A. Maratha, a. Q. Butt, E. Shevlin, and S. M. Miggin (2013). "TRIF-Mediated TLR3 and TLR4 Signaling Is Negatively Regulated by ADAM15". In: *The Journal of Immunology* 190 (5), pp. 2217–2228. DOI: 10.4049/jimmunol.1201630.

Alessi, D. R., S. R. James, C. P. Downes, A. B. Holmes, P. R. Gaffney, C. B. Reese, and P. Cohen (1997). "Characterization of a 3-phosphoinositide-dependent protein kinase which phosphorylates and activates protein kinase Bα." In: *Current Biology* 7 (4), pp. 261–9.

Alexopoulou, L., A. Czopik Holt, R. Medzhitov, and R. A. Flavell (2001). "Recognition of double-stranded RNA and activation of NF-kappa B by Toll-like receptor 3". In: *Nature* 413 (6857), pp. 732–738. DOI: 10.1038/35099560.

Allen, J. E. and R. M. Maizels (2011). "Diversity and dialogue in immunity to helminths." In: *Nature Reviews Immunology* 11 (6), pp. 375–88. DOI: 10.1038/nri2992.

An, H., J. Hou, J. Zhou, W. Zhao, H. Xu, Y. Zheng, Y. Yu, S. Liu, and X. Cao (2008). "Phosphatase SHP-1 promotes TLR- and RIG-I-activated production of type I interferon by inhibiting the kinase IRAK1." In: *Nature immunology* 9 (5), pp. 542–550. DOI: 10.1038/ni0311-271e.

An, H., W. Zhao, J. Hou, Y. Zhang, Y. Xie, Y. Zheng, H. Xu, C. Qian, J. Zhou, Y. Yu, S. Liu, G. Feng, and X. Cao (2006). "SHP-2 Phosphatase Negatively Regulates the TRIF Adaptor Protein-Dependent Type I Interferon and Proinflammatory Cytokine Production". In: *Immunity* 25 (6), pp. 919–928. DOI: 10.1016/j.immuni.2006.10.014.

Andrejeva, J., K. S. Childs, D. F. Young, T. S. Carlos, N. Stock, S. Goodbourn, and R. E. Randall (2004). "The V proteins of paramyxoviruses bind the IFN-inducible RNA helicase, mda-5, and inhibit its activation of the IFN-beta promoter". In: *PNAS* 101 (49), pp. 17264–17269. DOI: 10.1073/pnas.0407639101.

Anthony, R. M., J. F. Urban, F. Alem, H. a. Hamed, C. T. Rozo, J.-L. Boucher, N. Van Rooijen, and W. C. Gause (2006). "Memory T(H)2 cells induce alternatively activated macrophages to mediate protection against nematode parasites." In: *Nature medicine* 12 (8), pp. 955–60. DOI: 10.1038/nm1451.

Aranzamendi, C., F. Fransen, M. Langelaar, F. Franssen, P. van der Ley, J. P. M. van Putten, V. Rutten, and E. Pinelli (2012). "Trichinella spiralis-secreted products modulate DC functionality and expand regulatory T cells in vitro." In: *Parasite immunology* 34 (4), pp. 210–23. DOI: 10.1111/j.1365-3024.2012.01353.x.

Artis, D. (2008). "Epithelial-cell recognition of commensal bacteria and maintenance of immune homeostasis in the gut." In: *Nature reviews. Immunology* 8 (6), pp. 411–20. DOI: 10.1038/nri2316.

Artis, D., M. L. Wang, S. a. Keilbaugh, W. He, M. Brenes, G. P. Swain, P. a. Knight, D. D. Donaldson, M. a. Lazar, H. R. P. Miller, G. a. Schad, P. Scott, and G. D. Wu (2004). "RELMbeta/FIZZ2 is a goblet cell-specific immune-effector molecule in the gastrointestinal tract." In: *Proceedings of the National Academy of Sciences of the United States of America* 101 (37), pp. 13596–600. DOI: 10.1073/pnas.0404034101.

Babu, S., S. Q. Bhat, N. P. Kumar, R. Anuradha, P. Kumaran, P. G. Gopi, C. Kolappan, V. Kumaraswami, and T. B. Nutman (2009). "Attenuation of toll-like receptor expression and function in latent tuberculosis by coexistent filarial infection with restoration following antifilarial chemotherapy". In: *PLoS Neglected Tropical Diseases* 3 (7). DOI: 10.1371/journal.pntd.0000489.

Balic, A., Y. Harcus, M. J. Holland, and R. M. Maizels (2004). "Selective maturation of dendritic cells by Nippostrongylus brasiliensis-secreted proteins drives Th2 immune responses." In: *European Journal of Immunology* 34 (11), pp. 3047–59. DOI: 10.1002/eji.200425167.

Balic, A., K. A. Smith, Y. Harcus, and R. M. Maizels (2009). "Dynamics of CD11c(+) dendritic cell subsets in lymph nodes draining the site of intestinal nematode infection." In: *Immunology Letters* 127 (1), pp. 68–75. DOI: 10.1016/j.imlet.2009.09.001.

Banchereau, J., F. Briere, C. Caux, J. Davoust, S. Lebecque, Y. J. Liu, B. Pulendran, and K. Palucka (2000). "Immunobiology of dendritic cells". In: *Annual review of ...* 18 (Figure 1), pp. 767–811. DOI: 10.1146/annurev.immunol.18.1.767.

Bansemir, A. D. and M. V. Sukhedo (1994). "The food resource of adult Heligmosomoides polygyrus in the small intestine." In: *The Journal of Parasitology* 80 (1), pp. 24–8.

Baravalle, G., H. Park, M. McSweeney, M. Ohmura-Hoshino, Y. Matsuki, S. Ishido, and J.-S. Shin (2011). "Ubiquitination of CD86 is a key mechanism in regulating antigen presentation by dendritic cells." In: *Journal of Immunology* 187 (6), pp. 2966–73. DOI: 10.4049/jimmunol.1101643.

Beg, A. A., S. M. Ruben, R. I. Scheinman, S. Haskill, C. A. Rosen, and A. Baldwin (1992). "IkappaB Interacts With the Nuclear Localization Signal of the Subunits of NF-kappaB: a mechanism for cytoplasmic retention". In: *Genes & Development* 6, pp. 1899–1913.

Behnke, J. M., D. M. Menge, and H. Noyes (2009). "Heligmosomoides bakeri: a model for exploring the biology and genetics of resistance to chronic gastrointestinal nematode infections." In: *Parasitology* 136, pp. 1565–1580. DOI: 10.1017/S0031182009006003.

Bekiaris, V., E. K. Persson, and W. W. Agace (2014). "Intestinal dendritic cells in the regulation of mucosal immunity". In: *Immunological Reviews* 260 (1), pp. 86–101. DOI: 10.1111/imr.12194.

Beriault, D. R. and G. H. Werstuck (2013). "Detection and quantification of endoplasmic reticulum stress in living cells using the fluorescent compound, Thioflavin T." In: *Biochimica et biophysica acta* 1833 (10), pp. 2293–301. DOI: 10.1016/j.bbamcr.2013.05.020.

Biggelaar, A. H. J. van den, L. C. Rodrigues, R. van Ree, J. S. van Der Zee, Y. C. M. Hoeksma-Kruize, J. H. M. Souverijn, M. A. Missinou, S. Borrmann, P. G. Kremsner, and M. Yazdanbakhsh (2004). "Long-term treatment of intestinal helminths increases mite skin-test reactivity in Gabonese schoolchildren." In: *The Journal of infectious diseases* 189 (5), pp. 892–900. DOI: 10.1086/381767.

Bilban, M., A. Haschemi, B. Wegiel, B. Y. Chin, O. Wagner, and L. E. Otterbein (2008). "Heme oxygenase and carbon monoxide initiate homeostatic signaling". In: *Journal of Molecular Medicine* 86 (3), pp. 267–279. DOI: 10.1007/s00109-007-0276-0.

Blum, A. M., L. Hang, T. Setiawan, J. P. Urban, K. M. Stoyanoff, J. Leung, and J. V. Weinstock (2012). "Heligmosomoides polygyrus bakeri induces tolerogenic dendritic cells that block colitis and prevent antigen-specific gut T cell responses." In: *Journal of immunology (Baltimore, Md. : 1950)* 189 (5), pp. 2512–20. DOI: 10.4049/jimmunol.1102892.

Boone, D. L., E. E. Turer, E. G. Lee, R. C. Ahmad, M. T. Wheeler, C. Tsui, P. Hurley, M. Chien, S. Chai, O. Hitotsumatsu, E. McNally, C. Pickart, and A. Ma (2004). "The ubiquitin-modifying enzyme A20 is required for termination of Toll-like receptor responses". In: *Nat Immunol* 5 (10), pp. 1052–1060. DOI: 10.1038/ni1110.

Boonstra, A., C. Asselin-Paturel, M. Gilliet, C. Crain, G. Trinchieri, Y.-J. Liu, and A. O'Garra (2003). "Flexibility of mouse classical and plasmacytoid-derived dendritic cells in directing T helper type 1 and 2 cell development: dependency on antigen dose and differential toll-like receptor ligation." In: *The Journal of experimental medicine* 197 (1), pp. 101–9. DOI: 10.1084/jem.20021908.

Boulukos, K. E., P. Pognonec, E. Sariban, M. Bailly, C. Lagrou, and J. Ghysdael (1990). "Rapid and transient expression of Ets2 in mature macrophages following stimulation with cMGF, LPS, and PKC activators". In: *Genes and Development* 4 (3), pp. 401–409.

Brown, J., H. Wang, G. N. Hajishengallis, and M. Martin (2011). "TLR-signaling networks: an integration of adaptor molecules, kinases, and cross-talk." In: *Journal of Dental Research* 90 (4), pp. 417–27. DOI: 10.1177/0022034510381264.

Brugarolas, J., K. Lei, R. L. Hurley, B. D. Manning, J. H. Reiling, E. Hafen, L. a. Witters, L. W. Ellisen, and W. G. K. Jr (2004). "Regulation of mTOR function in response to hypoxia by REDD1 and the TSC1 / TSC2 tumor suppressor complex". In: *Genes & Development*, pp. 1–12. DOI: 10.1101/gad.1256804.(mTOR).

Brunda, M. J. (1994). "Interleukin-12." In: *Journal of Leukocyte Biology* 55 (2), pp. 280–288.

Brunner, B. T., C. H. Heusser, and C. A. Dahinden (1993). "Human Peripheral Blood Basophils Primed by Interleukin 3 (IL-3) Produce IL-4 in Response to Immunoglobulin E Reveptor Stimulation". In: *Journal of Experimental Medicine* 177 (March), pp. 605–611.

Buck, A. H., G. Coakley, F. Simbari, H. J. McSorley, J. F. Quintana, T. Le Bihan, S. Kumar, C. Abreu-Goodger, M. Lear, Y. Harcus, A. Ceroni, S. A. Babayan, M. Blaxter, A. Ivens, and R. M. Maizels (2014). "Exosomes secreted by nematode parasites transfer small RNAs to

mammalian cells and modulate innate immunity". In: *Nature Communications* 5, p. 5488. DOI: 10.1038/ncomms6488.

Burns, K., S. Janssens, B. Brissoni, N. Olivos, R. Beyaert, and J. Tschopp (2003). "Inhibition of interleukin 1 receptor/Toll-like receptor signaling through the alternatively spliced, short form of MyD88 is due to its failure to recruit IRAK-4." In: *The Journal of experimental medicine* 197 (2), pp. 263–8.

Buxadé, M., G. Lunazzi, J. Minguillón, S. Iborra, R. Berga-Bolaños, M. del Val, J. Aramburu, and C. López-Rodríguez (2012). "Gene expression induced by Toll-like receptors in macrophages requires the transcription factor NFAT5". In: *The Journal of Experimental Medicine* 209 (2), pp. 379–393. DOI: 10.1084/jem.20111569.

Cao, Z., W. J. Henzel, and X. Gao (1996). "IRAK: a kinase associated with the interleukin-1 receptor." In: *Science* 271 (5252), pp. 1128–31.

Carty, M., R. Goodbody, M. Schröder, J. Stack, P. N. Moynagh, and A. G. Bowie (2006). "The human adaptor SARM negatively regulates adaptor protein TRIF-dependent Toll-like receptor signaling." In: *Nature immunology* 7 (10), pp. 1074–81. DOI: 10.1038/ni1382.

Ceppi, M., P. M. Pereira, I. Dunand-Sauthier, E. Barras, W. Reith, M. A. Santos, and P. Pierre (2009). *MicroRNA-155 modulates the interleukin-1 signaling pathway in activated human monocyte-derived dendritic cells*. Vol. 106. 1091-6490 (Electronic), pp. 2735–2740.

Cerovic, V., S. a. Houston, C. L. Scott, A. Aumeunier, U. Yrlid, a. M. Mowat, and S. W. F. Milling (2013). "Intestinal CD103(-) dendritic cells migrate in lymph and prime effector T cells." In: *Mucosal Immunology* 6 (1), pp. 104–113. DOI: 10.1038/mi.2012.53.

Cervi, L. and A. MacDonald (2004). "Cutting edge: dendritic cells copulsed with microbial and helminth antigens undergo modified maturation, segregate the antigens to distinct intracellular compartments". In: *The Journal of ...* 172, pp. 2016–2020.

Chang, J., S. Thangamani, M. H. Kim, B. Ulrich, S. M. Morris, and C. H. Kim (2013). "Retinoic acid promotes the development of Arg1-expressing dendritic cells for the regulation of T-cell differentiation". In: *European Journal of Immunology* 43 (4), pp. 967–978. DOI: 10.1002/eji.201242772.

Chen, G., S. H. Wang, J. C. Jang, J. I. Odegaard, and M. G. Nair (2016). "Comparison of RELMalpha and RELMbeta Single- and Double-Gene-Deficient Mice Reveals that RELMalpha Expression Dictates Inflammation and Worm Expulsion in Hookworm Infection". In: *Infection and Immunity* 84 (4), pp. 1100–1111. DOI: 10.1128/IAI.01479-15.Editor.

Chen, Y.-L. and B.-L. Chiang (2016). "Targeting TSLP With shRNA Alleviates Airway Inflammation and Decreases Epithelial CCL17 in a Murine Model of Asthma". In: *Molecular Therapy—Nucleic Acids* 5 (5), e316. DOI: 10.1038/mtna.2016.29.

Chen, Y. H., M. D. Layne, S. W. Chung, K. Ejima, R. M. Baron, S. F. Yet, and M. A. Perrella (2003). "Elk-3 is a transcriptional repressor of nitric-oxide synthase 2". In: *J Biol Chem* 278 (41), pp. 39572–39577. DOI: 10.1074/jbc.M308179200.

Chen, Z., J. Hagler, V. J. Palombella, F. Melandri, D. Seherer, D. Ballard, and T. Maniatis (1995). "Phosphorylation targets IKB x to the ubiquitin-proteasome pathway". In: *Genes and Development* 9, pp. 1586–1598. DOI: 10.1101/gad.9.13.1586.

Chi, H., S. P. Barry, R. J. Roth, J. J. Wu, E. a. Jones, A. M. Bennett, and R. a. Flavell (2006). "Dynamic regulation of pro- and anti-inflammatory cytokines by MAPK phosphatase 1 (MKP-1) in innate immune responses." In: *Proceedings of the National Academy of Sciences of the United States of America* 103 (7), pp. 2274–9. DOI: 10.1073/pnas.0510965103.

Childs, K. S. and S. Goodbourn (2003). "Identification of novel co-repressor molecules for Interferon Regulatory Factor-2". In: *Nucleic Acids Research* 31 (12), pp. 3016–3026. DOI: 10.1093/nar/gkg431.

Chiu, L.-L., D.-w. Perng, C.-H. Yu, S.-N. Su, L.-P. Chow, and E. Alerts (2007). "Mold allergen, pen C 13, induces IL-8 expression in human airway epithelial cells by activating protease-activated receptor 1 and 2." In: *Journal of immunology (Baltimore, Md. : 1950)* 178 (8), pp. 5237–44. DOI: 10.4049/jimmunol.178.8.5237.

Christian, P., S. K. Khatry, and P. K. P. West (2004). "Antenatal anthelmintic treatment, birthweight, and infant survival in rural Nepal". In: *Lancet* 364 (9438), pp. 981–983. DOI: 10.1016/S0140-6736(04)17023-2.

Chu, Y., P. a. Solski, R. Khosravi-Far, C. J. Der, and K. Kelly (1996). "The mitogen-activated protein kinase phosphatases PAC1,MKP-1, and MKP-2 have unique substrate specificities and reduced activity in vivo toward the ERK2 sevenmarker mutation". In: *Journal of Biological Chemistry* 271(11) (11), pp. 6497–6501. DOI: 10.1074/jbc.271.11.6497.

Coakley, G., R. M. Maizels, and A. H. Buck (2015). "Exosomes and Other Extracellular Vesicles: The New Communicators in Parasite Infections". In: *Trends in Parasitology* 31 (10), pp. 477–489. DOI: 10.1016/j.pt.2015.06.009.

Coffman, R. L., B. W. Seymour, S. Hudak, J. Jackson, and D. Rennick (1989). "Antibody to interleukin-5 inhibits helminth-induced eosinophilia in mice." In: *Science (New York, N.Y.)* 245 (4915), pp. 308–310. DOI: 10.1126/science.2787531.

Cook, P. C., L. H. Jones, S. J. Jenkins, T. A. Wynn, J. E. Allen, and A. S. MacDonald (2012). "Alternatively activated dendritic cells regulate CD4+ T-cell polarization in vitro and in vivo." In: *Proceedings of the National Academy of Sciences of the United States of America* 109 (25), pp. 9977–82. DOI: 10.1073/pnas.1121231109.

Cooper, P. J., M. E. Chico, G. Losonsky, C. Sandoval, I. Espinel, R. Sridhara, M. Aguilar, A. Guevara, R. H. Guderian, M. M. Levine, G. E. Griffin, and T. B. Nutman (2000). "Albendazole treatment of children with ascariasis enhances the vibriocidal antibody response to the live attenuated oral cholera vaccine CVD 103-HgR." In: *The Journal of infectious diseases* 182 (4), pp. 1199–1206. DOI: 10.1086/315837.

Corcoran, K., M. Jabbour, C. Bhagwandin, M. J. Deymier, D. L. Theisen, and L. Lybarger (2011). "Ubiquitin-mediated regulation of CD86 protein expression by the ubiquitin ligase membrane-associated RING-CH-1 (MARCH1)". In: *Journal of Biological Chemistry* 286 (43), pp. 37168–37180. DOI: 10.1074/jbc.M110.204040.

Correale, J. and M. Farez (2007). "Association between parasite infection and immune responses in multiple sclerosis." In: *Annals of Neurology* 61 (2), pp. 97–108. DOI: 10.1002/ana.21067.

Correale, J. and M. Farez (2009). "Helminth antigens modulate immune responses in cells from multiple sclerosis patients through TLR2-dependent mechanisms." In: *Journal of Immunology* 183 (9), pp. 5999–6012. DOI: 10.4049/jimmunol.0900897.

Correale, J. and M. F. Farez (2013). "Parasite Infections in Multiple Sclerosis Modulate Immune Responses through a Retinoic Acid–Dependent Pathway". In: *The Journal of Immunology* 191, pp. 3827–3837. DOI: 10.4049/jimmunol.1301110.

Correale, J. and M. F. Farez (2011). "The impact of parasite infections on the course of multiple sclerosis". In: *Journal of Neuroimmunology* 233 (1-2), pp. 6–11. DOI: 10.1016/j.jneuroim.2011.01.002.

Crompton, D. T. and M. C. Nesheim (2002). "Nutritional Impact of Intestinal Helminthiasis During the Human Life Cycle". In: *Annual Review of Nutrition* 22, pp. 35–59. DOI: 10.1146/annurev.immunol.20.081501.130710.

Cuesta, N., C. a. Salkowski, K. E. Thomas, and S. N. Vogel (2003). "Regulation of lipopolysaccharide sensitivity by IFN regulatory factor-2." In: *Journal of Immunology* 170 (11), pp. 5739–5747. DOI: 10.4049/jimmunol.170.11.5739.

Cusson-Hermance, N., S. Khurana, T. H. Lee, K. A. Fitzgerald, and M. A. Kelliher (2005). "Rip1 mediates the Trif-dependent toll-like receptor 3- and 4-induced NF-{kappa}B activation but does not contribute to interferon regulatory factor 3 activation." In: *The Journal of Biological Chemistry* 280 (44), pp. 36560–6. DOI: 10.1074/jbc.M506831200.

D'Angelo, J. A., E. Dehlink, B. Platzer, P. Dwyer, M. L. Circu, J. Garay, T. Y. Aw, E. Fiebiger, and B. L. Dickinson (2010). "The cystine/glutamate antiporter regulates dendritic cell differentiation and antigen presentation". In: *J Immunol* 185 (6), pp. 3217–3226. DOI: 10.4049/jimmunol.1001199.

Dayer, B. (2011). "Modulation of Dendritic Cells Function by H. polygyrus Products". Master's Thesis. Ecole Polytechnique Federale de Lausanne.

De Smedt, T., B. Pajak, E. Muraille, L. Lespagnard, E. Heinen, P. De Baetselier, J. Urbain, O. Leo, and M. Moser (1996). "Regulation of dendritic cell numbers and maturation by lipopolysaccharide in vivo." In: *The Journal of Experimental Medicine* 184 (4), pp. 1413–24.

Degarege, A., A. Animut, M. Legesse, and B. Erko (2009). "Malaria severity status in patients with soil-transmitted helminth infections". In: *Acta Tropica* 112 (1), pp. 8–11. DOI: 10.1016/j.actatropica.2009.05.019.

Delaby, C., C. Rondeau, C. Pouzet, A. Willemetz, N. Pilard, M. Desjardins, and F. Canonne-Hergaux (2012). "Subcellular localization of iron and heme metabolism related proteins at early stages of erythrophagocytosis". In: *PLoS ONE* 7 (7). DOI: 10.1371/journal.pone.0042199.

DiDonato, J. A., M. Hayakawa, D. M. Rothwarf, E. Zandi, and M. Karin (1997). "A cytokine-responsive IkappaB kinase that activates the transcription factor NF-kappaB." In: *Nature* 388 (6642), pp. 548–54. DOI: 10.1038/41493.

DiDonato, J., F. Mercurio, C. Rosette, J. Wu-Li, H. Suyang, S. Ghosh, and M. Karin (1996). "Mapping of the inducible IkappaB phosphorylation sites that signal its ubiquitination and degradation." In: *Molecular and cellular biology* 16 (4), pp. 1295–304.

Diebold, S. S., T. Kaisho, H. Hemmi, S. Akira, and C. Reis e Souza (2004). "Innate Antiviral Responses by Means of TLR7-Mediated Recognition of Single-Stranded RNA". In: *Science* 303 (5663), pp. 1529–1531. DOI: 10.1126/science.1093616.

Dillon, S., A. Agrawal, T. Van Dyke, G. Landreth, M. Laurie, A. Koh, C. Maliszewski, S. Akira, and B. Pulendran (2004). "A Toll-Like Receptor 2 ligand stimulates Th2 responses in vivo, via induction of extracellular signal-regulated kinase mitogen-activated protein kinase and c-Fos in dendritic cells". In: *The Journal of Immunology* 172 (8), pp. 4733–4743.

Dowling, D. J., C. M. Noone, P. N. Adams, K. V. Vukman, S. F. Molloy, J. Forde, S. Asaolu, and S. M. O'Neill (2011). "Ascaris lumbricoides pseudocoelomic body fluid induces a partially activated dendritic cell phenotype with Th2 promoting ability in vivo". In: *International Journal for Parasitology* 41 (2), pp. 255–261. DOI: 10.1016/j.ijpara.2010.09.007.

Downs, J. A., C. Mguta, G. M. Kaatano, K. B. Mitchell, H. Bang, H. Simplice, S. E. Kalluvya, J. M. Changalucha, W. D. Johnson, and D. W. Fitzgerald (2011). "Urogenital schistosomiasis in women of reproductive age in Tanzania's Lake Victoria region". In: *American Journal of Tropical Medicine and Hygiene* 84 (3), pp. 364–369. DOI: 10.4269/ajtmh.2011.10-0585.

Ehrenford, F. A. (1954). "The Life Cycle of Nematospiroides dubius Baylis (Nematoda: Heligmosomidae)". In: *The Journal of Parasitology* 40 (4), pp. 480–481.

Eisenbarth, S. C., D. A. Piggott, J. W. Huleatt, I. Visintin, C. A. Herrick, and K. Bottomly (2002). "Lipopolysaccharide-enhanced, toll-like receptor 4-dependent T helper cell type 2 responses to inhaled antigen." In: *The Journal of experimental medicine* 196 (12), pp. 1645–51. DOI: 10.1084/jem.20021340.

Ekkens, M. J., Z. Liu, Q. Liu, J. Whitmire, S. Xiao, A. Foster, J. Pesce, J. VanNoy, A. H. Sharpe, J. F. Urban, and W. C. Gause (2003). "The role of OX40 ligand interactions in the development of the Th2 response to the gastrointestinal nematode parasite Heligmosomoides polygyrus." In: *Journal of immunology (Baltimore, Md. : 1950)* 170 (1), pp. 384–93.

Elias, D., D. Wolday, H. Akuffo, B. Petros, U. Bronner, and S. Britton (2001). "Effect of deworming on human T cell responses to mycobacterial antigens in helminth-exposed individuals before and after bacille Calmette-Guerin (BCG) vaccination". In: *Clinical and Experimental Immunology* 123, pp. 219–225.

Elloumi, H. Z., N. Maharshak, K. N. Rao, T. Kobayashi, H. S. Ryu, M. Mühlbauer, F. Li, C. Jobin, and S. E. Plevy (2012). "A cell permeable peptide inhibitor of NFAT inhibits macrophage cytokine expression and ameliorates experimental colitis." In: *PloS one* 7 (3), e34172. DOI: 10.1371/journal.pone.0034172.

Erdozain, O. J., S. Pegrum, V. R. Winrow, M. Horrocks, and C. R. Stevens (2011). "Hypoxia in abdominal aortic aneurysm supports a role for HIF-1?? and Ets-1 as drivers of matrix metalloproteinase upregulation in human aortic smooth muscle cells". In: *Journal of Vascular Research* 48 (2), pp. 163–170. DOI: 10.1159/000318806.

Esser-von Bieren, J., I. Mosconi, R. Guiet, A. Piersgilli, B. Volpe, F. Chen, W. C. Gause, A. Seitz, J. S. Verbeek, and N. L. Harris (2013). "Antibodies Trap Tissue Migrating Helminth Larvae

and Prevent Tissue Damage by Driving IL-4R??-Independent Alternative Differentiation of Macrophages". In: *PLoS Pathogens* 9 (11). DOI: 10.1371/journal.ppat.1003771.

Esser-von Bieren, J., B. Volpe, M. Kulagin, D. B. Sutherland, R. Guiet, A. Seitz, B. J. Marsland, J. S. Verbeek, and N. L. Harris (2015). "Antibody-mediated trapping of helminth larvae requires CD11b and Fcγ receptor I." In: *Journal of immunology (Baltimore, Md. : 1950)* 194 (3), pp. 1154–63. DOI: 10.4049/jimmunol.1401645.

Everts, B., L. Hussaarts, N. N. Driessen, M. H. J. Meevissen, G. Schramm, A. J. van der Ham, B. van der Hoeven, T. Scholzen, S. Burgdorf, M. Mohrs, E. J. Pearce, C. H. Hokke, H. Haas, H. H. Smits, and M. Yazdanbakhsh (2012a). "Schistosome-derived omega-1 drives Th2 polarization by suppressing protein synthesis following internalization by the mannose receptor". In: *Journal of Experimental Medicine* 209 (10), pp. 1753–1767. DOI: 10.1084/jem.20111381.

Everts, B., A. a. Adegnika, Y. C. M. Kruize, H. H. Smits, P. G. Kremsner, and M. Yazdanbakhsh (2010). "Functional impairment of human myeloid dendritic cells during Schistosoma haematobium infection." In: *PLoS neglected tropical diseases* 4 (4), e667. DOI: 10.1371/journal.pntd.0000667.

Everts, B., E. Amiel, S. C.-C. Huang, A. M. Smith, C.-H. Chang, W. Y. Lam, V. Redmann, T. C. Freitas, J. Blagih, G. J. W. van der Windt, M. N. Artyomov, R. G. Jones, E. L. Pearce, and E. J. Pearce (2014). "TLR-driven early glycolytic reprogramming via the kinases TBK1-IKKe supports the anabolic demands of dendritic cell activation." In: *Nature immunology* 15 (4). DOI: 10.1038/ni.2833.

Everts, B., E. Amiel, G. J. W. Van Der Windt, T. C. Freitas, R. Chott, K. E. Yarasheski, E. L. Pearce, and E. J. Pearce (2012b). "Commitment to glycolysis sustains survival of NO-producing inflammatory dendritic cells". In: *Blood* 120 (7), pp. 1422–1431. DOI: 10.1182/blood-2012-03-419747.

Everts, B. and E. J. Pearce (2014). "Metabolic control of dendritic cell activation and function: Recent advances and clinical implications". In: *Frontiers in Immunology* 5 (MAY), pp. 1–7. DOI: 10.3389/fimmu.2014.00203.

Everts, B., G. Perona-Wright, H. H. Smits, C. H. Hokke, A. J. van der Ham, C. M. Fitzsimmons, M. J. Doenhoff, J. van der Bosch, K. Mohrs, H. Haas, M. Mohrs, M. Yazdanbakhsh, and G. Schramm (2009). "Omega-1, a glycoprotein secreted by Schistosoma mansoni eggs, drives Th2 responses." In: *The Journal of Experimental Medicine* 206 (8), pp. 1673–80. DOI: 10.1084/jem.20082460.

Falcon, C. R., D. Masih, G. Gatti, M. C. Sanchez, C. C. Motran, and L. Cervi (2014). "Fasciola hepatica Kunitz type molecule decreases dendritic cell activation and their ability to induce inflammatory responses". In: *PLoS ONE* 9 (12), pp. 1–18. DOI: 10.1371/journal.pone.0114505.

Falcon, C., F. Carranza, F. F. Martinez, C. P. Knubel, D. T. Masih, C. C. Motran, and L. Cervi (2010). "Excretory-secretory products (ESP) from Fasciola hepatica induce tolerogenic properties in myeloid dendritic cells". In: *Veterinary Immunology and Immunopathology* 137 (1-2), pp. 36–46. DOI: 10.1016/j.vetimm.2010.04.007.

Fallon, P. G., S. J. Ballantyne, N. E. Mangan, J. L. Barlow, A. Dasvarma, D. R. Hewett, A. McIlgorm, H. E. Jolin, and A. N. J. McKenzie (2006). "Identification of an interleukin (IL)-25-dependent cell population that provides IL-4, IL-5, and IL-13 at the onset of helminth expulsion." In: *The Journal of experimental medicine* 203 (4), pp. 1105–16. DOI: 10.1084/jem.20051615.

Falvo, J. V., A. V. Tsytsykova, and A. E. Goldfeld (2010). "Transcriptional Control of the TNF Gene". In: *Current Directions in Autoimmunity* 11. DOI: 10.1016/j.pediatrneurol.2014.10.004.Tuberous.

Fan, Y.-H., Y. Yu, R.-F. Mao, X.-J. Tan, G.-F. Xu, H. Zhang, X.-B. Lu, S.-B. Fu, and J. Yang (2011). "USP4 targets TAK1 to downregulate TNFα-induced NF-κB activation." In: *Cell death and differentiation* 18 (10), pp. 1547–60. DOI: 10.1038/cdd.2011.11.

Favoretto, B. C., S. R. Silva, J. F. Jacysyn, N. O. S. Câmara, and E. L. Faquim-Mauro (2014). "TLR2- and 4-independent immunomodulatory effect of high molecular weight components from Ascaris suum." In: *Molecular immunology* 58 (1), pp. 17–26. DOI: 10.1016/j.molimm.2013.10.011.

Filbey, K. J., J. R. Grainger, K. A. Smith, L. Boon, N. van Rooijen, Y. Harcus, S. Jenkins, J. P. Hewitson, and R. M. Maizels (2014). "Innate and adaptive type 2 immune cell responses in genetically controlled resistance to intestinal helminth infection." In: *Immunology and cell biology* 92 (5), pp. 436–48. DOI: 10.1038/icb.2013.109.

Filbey, K. J. (2013). "Mediators and modulators of immunity to helminths". PhD thesis. University of Edinburgh.

Finkelman, F. D. (2009). "Basophils as TH2-inducing APCs: the dog can sing but is it a diva?" in: *Immunology and Cell Biology* 87 (8), pp. 568–570. DOI: 10.1038/icb.2009.67.

Fitzgerald, K. a., E. M. Palsson-McDermott, a. G. Bowie, C. a. Jefferies, a. S. Mansell, G. Brady, E. Brint, a. Dunne, P. Gray, M. T. Harte, D. McMurray, D. E. Smith, J. E. Sims, T. a. Bird, and L. a. O'Neill (2001). "Mal (MyD88-adapter-like) is required for Toll-like receptor-4 signal transduction." In: *Nature* 413 (6851), pp. 78–83. DOI: 10.1038/35092578.

Fitzgerald, K. a., D. C. Rowe, B. J. Barnes, D. R. Caffrey, A. Visintin, E. Latz, B. Monks, P. M. Pitha, and D. T. Golenbock (2003). "LPS-TLR4 signaling to IRF-3/7 and NF-kappaB involves the toll adapters TRAM and TRIF." In: *The Journal of Experimental Medicine* 198 (7), pp. 1043–55. DOI: 10.1084/jem.20031023.

Fleming, J. O. and J. V. Weinstock (2015). "Clinical trials of helminth therapy in autoimmune diseases: Rationale and findings". In: *Parasite Immunology* 37 (6), pp. 277–292. DOI: 10.1111/pim.12175.

Frobøse, H., S. G. Rønn, P. E. Heding, H. Mendoza, P. Cohen, T. Mandrup-Poulsen, and N. Billestrup (2006). "Suppressor of cytokine Signaling-3 inhibits interleukin-1 signaling by targeting the TRAF-6/TAK1 complex." In: *Molecular endocrinology (Baltimore, Md.)* 20 (March), pp. 1587–1596. DOI: 10.1210/me.2005-0301.

Fukao, T., M. Tanabe, Y. Terauchi, T. Ota, S. Matsuda, T. Asano, T. Kadowaki, T. Takeuchi, and S. Koyasu (2002). "PI3K-mediated negative feedback regulation of IL-12 production in DCs." In: *Nature immunology* 3 (9), pp. 875–81. DOI: 10.1038/ni825.

Gabriele, L., A. Fragale, P. Borghi, P. Sestili, E. Stellacci, M. Venditti, G. Schiavoni, M. Sanchez, F. Belardelli, A. Battistini, and I. Superiore (2006). "IRF-1 deficiency skews the differentiation of dendritic cells toward plasmacytoid and tolerogenic features". In: *Journal of Leukocyte Biology* 80, pp. 1500–1511. DOI: 10.1189/jlb.0406246.1.

Ganchi, P. A., S.-C. Sun, W. C. Greene, and D. W. Ballard (1992). "IkB/MAD-3 masks the nuclear localization signal of NF-kB p65 and requires the transactivation domain to inhibit NF-kB p65 DNA binding". In: *Molecular Biology of the Cell* 3 (December), pp. 1339–1352.

Gantner, B. N., R. M. Simmons, S. J. Canavera, S. Akira, and D. M. Underhill (2003). "Collaborative induction of inflammatory responses by dectin-1 and Toll-like receptor 2." In: *The Journal of experimental medicine* 197 (9), pp. 1107–17. DOI: 10.1084/jem.20021787.

Garside, P., E. Ingulli, R. R. Merica, J. C. Johnson, R. J. Noelle, and M. K. Jenkins (1998). "Visualization of Specific B and T Lymphocyte lnteracti ˜ ns in the Lymph Node". In: *Science* 281, pp. 96–99. DOI: 10.1126/science.281.5373.96.

Gautier, G., M. Humbert, F. Deauvieau, M. Scuiller, J. Hiscott, E. E. M. Bates, G. Trinchieri, C. Caux, and P. Garrone (2005). "A type I interferon autocrine-paracrine loop is involved in Toll-like receptor-induced interleukin-12p70 secretion by dendritic cells." In: *The Journal of experimental medicine* 201 (9), pp. 1435–46. DOI: 10.1084/jem.20041964.

Geijtenbeek, T. B. H. and S. I. Gringhuis (2009). "Signalling through C-type lectin receptors: shaping immune responses." In: *Nature Reviews Immunology* 9 (7), pp. 465–79. DOI: 10.1038/nri2569.

George, P. J., R. Anuradha, P. P. Kumaran, V. Chandrasekaran, T. B. Nutman, and S. Babu (2013). "Modulation of Mycobacterial-Specific Th1 and Th17 Cells in Latent Tuberculosis by Coincident Hookworm Infection." In: *Journal of immunology (Baltimore, Md. : 1950)*. DOI: 10.4049/jimmunol.1203311.

Gilchrist, M., V. Thorsson, B. Li, A. Rust, M. Korb, J. Roach, K. Kennedy, T. Hai, H. Bolouri, and A. Aderem (2006). "Systems biology approaches identify ATF3 as a negative regulator of Toll-like receptor 4". In: *Nature* 441 (7090), pp. 173–178. DOI: 10.1038/nature04768.

Giovane, A., A. Pintzas, S. M. Maira, P. Sobieszczuk, and B. Wasylyk (1994). "Net, a new ets transcription factor that is activated by Ras". In: *Genes and Development* 8 (13), pp. 1502–1513. DOI: 10.1101/gad.8.13.1502.

Girardin, S. E., R. Tournebize, M. Mavris, a. L. Page, X. Li, G. R. Stark, J. Bertin, P. S. DiStefano, M. Yaniv, P. J. Sansonetti, and D. J. Philpott (2001). "CARD4/Nod1 mediates NF-kappaB and JNK activation by invasive Shigella flexneri." In: *EMBO reports* 2 (8), pp. 736–742. DOI: 10.1093/embo-reports/kve155.

Goodridge, H. S., S. McGuiness, K. M. Houston, C. A. Egan, L. Al-Riyami, M. J. C. Alcocer, M. M. Harnett, and W. Harnett (2007). "Phosphorylcholine mimics the effects of ES-62 on macrophages and dendritic cells." In: *Parasite Immunology* 29 (3), pp. 127–37. DOI: 10.1111/j.1365-3024.2006.00926.x.

Goodridge, H. S., M. R. Deehan, W. Harnett, and M. M. Harnett (2005a). "Subversion of immunological signalling by a filarial nematode phosphorylcholine-containing secreted product". In: *Cellular Signalling* 17 (1), pp. 11–16. DOI: 10.1016/j.cellsig.2004.05.014.

Goodridge, H. S., W. Harnett, F. Y. Liew, and M. M. Harnett (2003). "Differential regulation of interleukin-12 p40 and p35 induction via Erk mitogen-activated protein kinase-dependent and -independent mechanisms and the implications for bioactive IL-12 and IL-23 responses". In: *Immunology* 109 (3), pp. 415–425. DOI: 10.1046/j.1365-2567.2003.01689.x.

Goodridge, H. S., F. A. Marshall, K. J. Else, K. M. Houston, C. Egan, L. Al-Riyami, F.-Y. Liew, W. Harnett, and M. M. Harnett (2005b). "Immunomodulation via novel use of TLR4 by the filarial nematode phosphorylcholine-containing secreted product, ES-62." In: *Journal of Immunology* 174 (1), pp. 284–93.

Goodridge, H. S., F. A. Marshall, E. H. Wilson, K. M. Houston, F. Y. Liew, M. M. Harnett, and W. Harnett (2004). "In vivo exposure of murine dendritic cell and macrophage bone marrow progenitors to the phosphorylcholine-containing filarial nematode glycoprotein ES-62 polarizes their differentiation to an anti-inflammatory phenotype". In: *Immunology* 113 (4), pp. 491–498. DOI: 10.1111/j.1365-2567.2004.01993.x.

Goriely, S., C. Molle, M. Nguyen, V. Albarani, N. O. Haddou, R. Lin, D. De Wit, V. Flamand, F. Willems, and M. Goldman (2006). "Interferon regulatory factor 3 is involved in Toll-like receptor 4 (TLR4)- and TLR3-induced IL-12p35 gene activation." In: *Blood* 107 (3), pp. 1078–84. DOI: 10.1182/blood-2005-06-2416.

Grainger, J. R., K. A. Smith, J. P. Hewitson, H. J. McSorley, Y. Harcus, K. J. Filbey, C. A. M. Finney, E. J. D. Greenwood, D. P. Knox, M. S. Wilson, Y. Belkaid, A. Y. Rudensky, and R. M. Maizels (2010). "Helminth secretions induce de novo T cell Foxp3 expression and regulatory function through the TGF-β pathway." In: *The Journal of Experimental Medicine* 207 (11), pp. 2331–41. DOI: 10.1084/jem.20101074.

Grainger, J. R. (2009). "Immune modulation by parasitic nematodes". PhD Thesis. University of Edinburgh.

Gray, P., K. S. Michelsen, C. M. Sirois, E. Lowe, K. Shimada, T. R. Crother, S. Chen, C. Brikos, Y. Bulut, E. Latz, D. Underhill, and M. Arditi (2010). "Identification of a novel human MD-2 splice variant that negatively regulates Lipopolysaccharide-induced TLR4 signaling." In: *Journal of immunology (Baltimore, Md. : 1950)* 184 (11), pp. 6359–66. DOI: 10.4049/jimmunol.0903543.

Gringhuis, S. I., J. den Dunnen, M. Litjens, B. van Het Hof, Y. van Kooyk, and T. B. H. Geijtenbeek (2007). "C-type lectin DC-SIGN modulates Toll-like receptor signaling via Raf-1 kinase-dependent acetylation of transcription factor NF-kappaB." In: *Immunity* 26 (5), pp. 605–16. DOI: 10.1016/j.immuni.2007.03.012.

Gringhuis, S. I., J. den Dunnen, M. Litjens, M. van der Vlist, B. Wevers, S. C. M. Bruijns, and T. B. H. Geijtenbeek (2009). "Dectin-1 directs T helper cell differentiation by controlling noncanonical NF-kappaB activation through Raf-1 and Syk." In: *Nature immunology* 10 (2), pp. 203–13. DOI: 10.1038/ni.1692.

Groom, L. A., A. A. Sneddon, D. R. Alessi, S. Dowd, and S. M. Keyse (1996). "Differential regulation of the MAP, SAP and RK/p38 kinases by Pyst1, a novel cytosolic dual-specificity phosphatase." In: *The EMBO journal* 15 (14), pp. 3621–32.

Gross, O., A. Gewies, K. Finger, M. Schäfer, T. Sparwasser, C. Peschel, I. Förster, and J. Ruland (2006). "Card9 controls a non-TLR signalling pathway for innate anti-fungal immunity." In: *Nature* 442 (7103), pp. 651–656. DOI: 10.1038/nature04926.

Gu, L., H. Ning, X. Qian, Q. Huang, R. Hou, R. Almourani, M. Fu, P. J. Blackshear, and J. Liu (2013). "Suppression of IL-12 Production by Tristetraprolin through Blocking NF-kcyB Nuclear Translocation." In: *Journal of immunology (Baltimore, Md. : 1950)* 191 (7), pp. 3922–30. DOI: 10.4049/jimmunol.1300126.

Guha, M. and N. Mackman (2002). "The phosphatidylinositol 3-kinase-Akt pathway limits lipopolysaccharide activation of signaling pathways and expression of inflammatory mediators in human monocytic cells." In: *The Journal of biological chemistry* 277 (35), pp. 32124–32. DOI: 10.1074/jbc.M203298200.

Haan, J. M. M. den, R. Arens, and M. C. van Zelm (2014). "The activation of the adaptive immune system: Cross-talk between antigen-presenting cells, T cells and B cells". In: *Immunology Letters* 162 (2), pp. 103–112. DOI: 10.1016/j.imlet.2014.10.011.

Häcker, H., V. Redecke, B. Blagoev, I. Kratchmarova, L.-C. Hsu, G. G. Wang, M. P. Kamps, E. Raz, H. Wagner, G. Häcker, M. Mann, and M. Karin (2006). "Specificity in Toll-like receptor signalling through distinct effector functions of TRAF3 and TRAF6." In: *Nature* 439 (7073), pp. 204–7. DOI: 10.1038/nature04369.

Haldar, M., M. Kohyama, A. Y. L. So, W. Kc, X. Wu, C. G. Briseño, A. T. Satpathy, N. M. Kretzer, H. Arase, N. S. Rajasekaran, L. Wang, T. Egawa, K. Igarashi, D. Baltimore, T. L. Murphy, and K. M. Murphy (2014). "Heme-mediated SPI-C induction promotes monocyte differentiation into iron-recycling macrophages". In: *Cell* 156 (6), pp. 1323–1334. DOI: 10.1016/j.cell.2014.01.069. arXiv: NIHMS150003.

Hamilton, C. M., D. J. Dowling, C. E. Loscher, R. M. Morphew, P. M. Brophy, and S. M. O'Neill (2009). "The Fasciola hepatica tegumental antigen suppresses dendritic cell maturation and function". In: *Infection and Immunity* 77 (6), pp. 2488–2498. DOI: 10.1128/IAI.00919-08.

Hammad, H., M. Chieppa, F. Perros, M. A. Willart, R. N. Germain, and B. N. Lambrecht (2009). "House dust mite allergen induces asthma via Toll-like receptor 4 triggering of airway structural cells." In: *Nature medicine* 15 (4), pp. 410–6. DOI: 10.1038/nm.1946.

Hammad, H. and B. N. Lambrecht (2015). "Barrier Epithelial Cells and the Control of Type 2 Immunity". In: *Immunity* 43 (1), pp. 29–40. DOI: 10.1016/j.immuni.2015.07.007.

Hammer, G. E. and A. Ma (2013). "Molecular control of steady-state dendritic cell maturation and immune homeostasis." In: *Annual review of immunology* 31, pp. 743–91. DOI: 10.1146/annurev-immunol-020711-074929.

Hang, L., A. M. Blum, T. Setiawan, J. P. Urban, K. M. Stoyanoff, and J. V. Weinstock (2013). "Heligmosomoides polygyrus bakeri Infection Activates Colonic Foxp3+ T Cells Enhancing Their Capacity To Prevent Colitis." In: *Journal of Immunology* 191 (4), pp. 1927–34. DOI: 10.4049/jimmunol.1201457.

Hang, L., T. Setiawan, A. M. Blum, J. Urban, K. Stoyanoff, S. Arihiro, H.-C. Reinecker, and J. V. Weinstock (2010). "Heligmosomoides polygyrus infection can inhibit colitis through

direct interaction with innate immunity." In: *Journal of Immunology* 185 (6), pp. 3184–9. DOI: 10.4049/jimmunol.1000941.

Hara, K., K. Iijima, M. K. Elias, S. Seno, I. Tojima, T. Kobayashi, G. M. Kephart, M. Kurabayashi, and H. Kita (2014). "Airway uric acid is a sensor of inhaled protease allergens and initiates type 2 immune responses in respiratory mucosa." In: *Journal of immunology (Baltimore, Md. : 1950)* 192 (9), pp. 4032–42. DOI: 10.4049/jimmunol.1400110.

Harada, H., T. Fujita, M. Miyamoto, Y. Kimura, M. Maruyama, A. Furia, T. Miyata, and T. Taniguchi (1989). "Structurally similar but functionally distinct factors, IRF-1 and IRF-2, bind to the same regulatory elements of IFN and IFN-inducible genes". In: *Cell* 58 (4), pp. 729–739. DOI: 10.1016/0092-8674(89)90107-4.

Hardy, M. P. and L. A. J. O'Neill (2004). "The murine Irak2 gene encodes four alternatively spliced isoforms, two of which are inhibitory". In: *Journal of Biological Chemistry* 279 (26), pp. 27699–27708. DOI: 10.1074/jbc.M403068200.

Harnett, W., M. J. Worms, a. Kapil, M. Grainger, and R. M. Parkhouse (1989). "Origin, kinetics of circulation and fate in vivo of the major excretory-secretory product of Acanthocheilonema viteae." In: *Parasitology* 99 Pt 2, pp. 229–39.

Hayashi, F., K. D. Smith, A. Ozinsky, T. R. Hawn, E. C. Yi, D. R. Goodlett, J. K. Eng, S. Akira, D. M. Underhill, and A. Aderem (2001). "The innate immune response to bacterial flagellin is mediated by Toll- like receptor 5". In: *Nature* 410 (6832), pp. 1099–103. DOI: 10.1038/35074106.

Hazeki, K., K. Nigorikawa, and O. Hazeki (2007). "Role of phosphoinositide 3-kinase in innate immunity." In: *Biological & pharmaceutical bulletin* 30 (September), pp. 1617–1623. DOI: 10.1248/bpb.30.1617.

Heil, F., H. Hemmi, H. Hochrein, F. Ampenberger, C. Kirschning, S. Akira, G. Lipford, H. Wagner, and S. Bauer (2004). "Species-Specific Recognition of Single-Stranded RNA via Toll-like Receptor 7 and 8". In: *Science* 303 (March), pp. 1526–1529.

Helft, J., J. Böttcher, P. Chakravarty, S. Zelenay, J. Huotari, B. U. Schraml, D. Goubau, and C. Reis e Sousa (2015). "GM-CSF Mouse Bone Marrow Cultures Comprise a Heterogeneous Population of CD11c+MHCII+ Macrophages and Dendritic Cells". In: *Immunity* 42 (6), pp. 1197–1211. DOI: 10.1016/j.immuni.2015.05.018.

Hemmi, H., O. Takeuchi, T. Kawai, T. Kaisho, S. Sato, H. Sanjo, M. Matsumoto, K. Hoshino, H. Wagner, K. Takeda, and S. Akira (2000). "A Toll-like receptor recognizes bacterial DNA". In: *Nature* 408 (6813), pp. 740–745. DOI: 10.1038/35047123.

Hemmi, H., T. Kaisho, O. Takeuchi, S. Sato, H. Sanjo, K. Hoshino, T. Horiuchi, H. Tomizawa, K. Takeda, and S. Akira (2002). "Small anti-viral compounds activate immune cells via the TLR7 MyD88-dependent signaling pathway." In: *Nature immunology* 3 (2), pp. 196–200. DOI: 10.1038/ni758.

Herbst, T., J. Esser, M. Prati, M. Kulagin, R. Stettler, M. M. Zaiss, J. P. Hewitson, P. Merky, J. S. Verbeek, C. Bourquin, M. Camberis, M. Prout, R. M. Maizels, G. Le Gros, and N. L. Harris (2012). "Antibodies and IL-3 support helminth-induced basophil expansion." In: *Proceedings of the National Academy of Sciences of the United States of America* 109 (37), pp. 14954–9. DOI: 10.1073/pnas.1117584109.

Hewitson, J. P., K. J. Filbey, J. Esser-von Bieren, M. Camberis, C. Schwartz, J. Murray, L. A. Reynolds, N. Blair, E. Robertson, Y. Harcus, L. Boon, S. C. C. Huang, L. Yang, Y. Tu, M. J. Miller, D. Voehringer, G. Le Gros, N. Harris, and R. M. Maizels (2015). "Concerted Activity of IgG1 Antibodies and IL-4/IL-25-Dependent Effector Cells Trap Helminth Larvae in the Tissues following Vaccination with Defined Secreted Antigens, Providing Sterile Immunity to Challenge Infection". In: *PLoS Pathogens* 11 (3), pp. 1–22. DOI: 10.1371/journal.ppat.1004676.

Hewitson, J. P., K. J. Filbey, J. R. Grainger, A. A. Dowle, M. Pearson, J. Murray, Y. Harcus, and R. M. Maizels (2011a). "Heligmosomoides polygyrus Elicits a Dominant Nonprotective Antibody Response Directed against Restricted Glycan and Peptide Epitopes". In: *The Journal of Immunology* 187 (9), pp. 4764–77. DOI: 10.4049/jimmunol.1004140.

Hewitson, J. P., Y. Harcus, J. Murray, M. van Agtmaal, K. J. Filbey, J. R. Grainger, S. Bridgett, M. L. Blaxter, P. D. Ashton, D. A. Ashford, R. S. Curwen, R. A. Wilson, A. A. Dowle, and R. M. Maizels (2011b). "Proteomic analysis of secretory products from the model gastrointestinal nematode Heligmosomoides polygyrus reveals dominance of Venom Allergen-Like (VAL) proteins." In: *Journal of Proteomics* 74 (9), pp. 1573–94. DOI: 10.1016/j.jprot.2011.06.002.

Hewitson, J. P. and R. M. Maizels (2014). "Vaccination against helminth parasite infections." In: *Expert review of vaccines* 13 (4), pp. 473–87. DOI: 10.1586/14760584.2014.893195.

Heyninck, K. and R. Beyaert (1999). "The cytokine-inducible zinc finger protein A20 inhibits IL-1-induced NF-kappaB activation at the level of TRAF6." In: *FEBS letters* 442 (2-3), pp. 147–50.

Heyninck, K., M. M. Kreike, and R. Beyaert (2003). "Structure-function analysis of the A20-binding inhibitor of NF-??B activation, ABIN-1". In: *FEBS Letters* 536 (1-3), pp. 135–140. DOI: 10.1016/S0014-5793(03)00041-3.

Horng, T., G. M. Barton, R. a. Flavell, and R. Medzhitov (2002). "The adaptor molecule TIRAP provides signalling specificity for Toll-like receptors." In: *Nature* 420 (6913), pp. 329–33. DOI: 10.1038/nature01180.

Hoshino, K., T. Kaisho, T. Iwabe, O. Takeuchi, and S. Akira (2002). "Differential involvement of IFN-beta in Toll-like receptor-stimulated dendritic cell activation." In: *International immunology* 14 (10), pp. 1225–31. DOI: 10.1093/intimm/dxf089.

Hoshino, K., O. Takeuchi, T. Kawai, T. Ogawa, Y. Takeda, S. Akira, and E. Alerts (1999). "Cutting Edge: Toll-Like Receptor 4 (TLR4)-Deficient Mice Are Hyporesponsive to Lipopolysaccharide: Evidence for TLR4 as the Lps Gene Product". In: *The Journal of Immunology* 162, pp. 3749–3752.

Hotez, P. J., P. J. Brindley, J. M. Bethony, C. H. King, E. J. Pearce, and J. Jacobson (2008). "Helminth infections: the great neglected tropical diseases". In: *The Journal of CLinical Investigation* 118 (4), pp. 1311–1321. DOI: 10.1172/JCI34261.tion.

Hu, M.-M., Q. Yang, J. Zhang, S.-M. Liu, Y. Zhang, H. Lin, Z.-F. Huang, Y.-Y. Wang, X.-D. Zhang, B. Zhong, and H.-B. Shu (2014). "TRIM38 inhibits TNFα- and IL-1β-triggered NF-κB activation by mediating lysosome-dependent degradation of TAB2/3." In: *Proceedings*

of the National Academy of Sciences of the United States of America 111 (4), pp. 1509–1514. DOI: 10.1073/pnas.1318227111.

Hu, M.-M., X.-Q. Xie, Q. Yang, C.-Y. Liao, W. Ye, H. Lin, and H.-B. Shu (2015). "TRIM38 Negatively Regulates TLR3/4-Mediated Innate Immune and Inflammatory Responses by Two Sequential and Distinct Mechanisms". In: *The Journal of Immunology* 195 (9), pp. 4415–4425. DOI: 10.4049/jimmunol.1500859.

Hull, T. D., A. Agarwal, and J. F. George (2014). "The mononuclear phagocyte system in homeostasis and disease: a role for heme oxygenase-1." In: *Antioxidants & redox signaling* 20 (11), pp. 1770–88. DOI: 10.1089/ars.2013.5673.

Husebye, H., Ø. Halaas, H. Stenmark, G. Tunheim, Ø. Sandanger, B. Bogen, A. Brech, E. Latz, and T. Espevik (2006). "Endocytic pathways regulate Toll-like receptor 4 signaling and link innate and adaptive immunity." In: *The EMBO journal* 25 (4), pp. 683–92. DOI: 10.1038/sj.emboj.7600991.

Iha, H., J.-M. Peloponese, L. Verstrepen, G. Zapart, F. Ikeda, C. D. Smith, M. F. Starost, V. Yedavalli, K. Heyninck, I. Dikic, R. Beyaert, and K.-T. Jeang (2008). "Inflammatory cardiac valvulitis in TAX1BP1-deficient mice through selective NF-kappaB activation." In: *The EMBO journal* 27 (4), pp. 629–41. DOI: 10.1038/emboj.2008.5.

Iliev, I. D., I. Spadoni, E. Mileti, G. Matteoli, a. Sonzogni, G. M. Sampietro, D. Foschi, F. Caprioli, G. Viale, and M. Rescigno (2009). "Human intestinal epithelial cells promote the differentiation of tolerogenic dendritic cells." In: *Gut* 58 (11), pp. 1481–1489. DOI: 10.1136/gut.2008.175166.

Inaba, K., M. Inaba, N. Romani, H. Aya, M. Deguchi, S. Ikehara, S. Muramatsu, and R. M. Steinman (1992). "Generation of large numbers of dendritic cells from mouse bone marrow cultures supplemented with granulocyte/macrophage colony-stimulating factor." In: *The Journal of experimental medicine* 176 (6), pp. 1693–702.

Infantino, V., P. Convertini, L. Cucci, M. A. Panaro, M. A. Di Noia, R. Calvello, F. Palmieri, and V. Iacobazzi (2011). "The mitochondrial citrate carrier: a new player in inflammation." In: *The Biochemical journal* 438 (3), pp. 433–6. DOI: 10.1042/BJ20111275.

Ishihama, Y., Y. Oda, T. Tabata, T. Sato, T. Nagasu, J. Rappsilber, and M. Mann (2005). "Exponentially modified protein abundance index (emPAI) for estimation of absolute protein amount in proteomics by the number of sequenced peptides per protein." In: *Molecular & cellular proteomics : MCP* 4 (9), pp. 1265–72. DOI: 10.1074/mcp.M500061-MCP200.

Itsumi, M., S. Inoue, a. J. Elia, K. Murakami, M. Sasaki, E. F. Lind, D. Brenner, I. S. Harris, I. I. C. Chio, S. Afzal, R. a. Cairns, D. W. Cescon, a. R. Elford, J. Ye, P. a. Lang, W. Y. Li, a. Wakeham, G. S. Duncan, J. Haight, a. You-Ten, B. Snow, K. Yamamoto, P. S. Ohashi, and T. W. Mak (2015). "Idh1 protects murine hepatocytes from endotoxin-induced oxidative stress by regulating the intracellular NADP+/NADPH ratio". In: *Cell Death and Differentiation* (October), pp. 1–9. DOI: 10.1038/cdd.2015.38.

Iwami, K.-i., T. Matsuguchi, A. Masuda, T. Kikuchi, T. Musikacharoen, and Y. Yoshikai (2000). "Cutting Edge: Naturally Occurring Soluble Form of Mouse Toll-Like Receptor 4 Inhibits

Lipopolysaccharide Signaling". In: *The Journal of Immunology* 165 (12), pp. 6682–6686. DOI: 10.4049/jimmunol.165.12.6682.

Jacobsen, E. a., S. I. Ochkur, R. S. Pero, A. G. Taranova, C. a. Protheroe, D. C. Colbert, N. a. Lee, and J. J. Lee (2008). "Allergic pulmonary inflammation in mice is dependent on eosinophil-induced recruitment of effector T cells." In: *The Journal of experimental medicine* 205 (3), pp. 699–710. DOI: 10.1084/jem.20071840.

Janssens, S., K. Burns, J. Tschopp, and R. Beyaert (2002). "Regulation of interleukin-1- and lipopolysaccharide-induced NF-kB activation by alternative splicing of MyD88". In: *Current Biology* 12 (6), pp. 467–471. DOI: 10.1016/S0960-9822(02)00712-1.

Janssens, S., K. Burns, E. Vercammen, J. Tschopp, and R. Beyaert (2003). "MyD88S, a splice variant of MyD88, differentially modulates NF-kappaB- and AP-1-dependent gene expression." In: *FEBS letters* 548 (1-3), pp. 103–7.

Jantsch, J., D. Chakravortty, N. Turza, a. T. Prechtel, B. Buchholz, R. G. Gerlach, M. Volke, J. Glasner, C. Warnecke, M. S. Wiesener, K.-U. Eckardt, a. Steinkasserer, M. Hensel, and C. Willam (2008). "Hypoxia and Hypoxia-Inducible Factor-1 Modulate Lipopolysaccharide-Induced Dendritic Cell Activation and Function". In: *The Journal of Immunology* 180 (7), pp. 4697–4705. DOI: 10.4049/jimmunol.180.7.4697.

Jeffrey, K. L., T. Brummer, M. S. Rolph, S. M. Liu, N. A. Callejas, R. J. Grumont, C. Gillieron, F. Mackay, S. Grey, M. Camps, C. Rommel, S. D. Gerondakis, and C. R. Mackay (2006). "Positive regulation of immune cell function and inflammatory responses by phosphatase PAC-1". In: *Nat Immunol* 7 (3), pp. 274–283. DOI: 10.1038/ni1310.

Jenkins, S. J., G. Perona-Wright, A. G. F. Worsley, N. Ishii, and A. S. MacDonald (2007). "Dendritic cell expression of OX40 ligand acts as a costimulatory, not polarizing, signal for optimal Th2 priming and memory induction in vivo." In: *Journal of immunology (Baltimore, Md. : 1950)* 179 (6), pp. 3515–23. DOI: 10.4049/jimmunol.179.6.3515.

Jiang, Z., P. Georgel, X. Du, L. Shamel, S. Sovath, S. Mudd, M. Huber, C. Kalis, S. Keck, C. Galanos, M. Freudenberg, and B. Beutler (2005). "CD14 is required for MyD88-independent LPS signaling." In: *Nature immunology* 6 (6), pp. 565–570. DOI: 10.1038/ni1207.

Jiang, Z., T. W. Mak, G. Sen, and X. Li (2004). "Toll-like receptor 3-mediated activation of NF-kappaB and IRF3 diverges at Toll-IL-1 receptor domain-containing adapter inducing IFN-beta." In: *Proceedings of the National Academy of Sciences of the United States of America* 101 (10), pp. 3533–3538. DOI: 10.1073/pnas.0308496101.

Jin, H.-O., S.-K. Seo, S.-H. Woo, E.-S. Kim, H.-C. Lee, D.-H. Yoo, S. An, T.-B. Choe, S.-J. Lee, S.-I. Hong, C.-H. Rhee, J.-I. Kim, and I.-C. Park (2009). "Activating transcription factor 4 and CCAAT/enhancer-binding protein-beta negatively regulate the mammalian target of rapamycin via Redd1 expression in response to oxidative and endoplasmic reticulum stress." In: *Free radical biology & medicine* 46 (8), pp. 1158–67. DOI: 10.1016/j.freeradbiomed.2009.01.015.

Johansson-Lindbom, B., M. Svensson, O. Pabst, C. Palmqvist, G. Marquez, R. Förster, and W. W. Agace (2005). "Functional specialization of gut CD103+ dendritic cells in the

regulation of tissue-selective T cell homing." In: *The Journal of experimental medicine* 202 (8), pp. 1063–73. DOI: 10.1084/jem.20051100.

Johnston, C. J. C., E. Robertson, Y. Harcus, J. R. Grainger, G. Coakley, D. J. Smyth, H. J. McSorley, and R. Maizels (2015). "Cultivation of Heligmosomoides polygyrus: an immunomodulatory nematode parasite and its secreted products." In: *Journal of visualized experiments : JoVE* (98), e52412. DOI: 10.3791/52412.

Jourdan, P. M., S. D. Holmen, S. G. Gundersen, B. Roald, and E. F. Kjetland (2011). "HIV target cells in Schistosoma haematobium-infected female genital mucosa". In: *American Journal of Tropical Medicine and Hygiene* 85 (6), pp. 1060–1064. DOI: 10.4269/ajtmh.2011.11-0135.

Kagan, J. C., T. Su, T. Horng, A. Chow, S. Akira, and R. Medzhitov (2008). "TRAM couples endocytosis of Toll-like receptor 4 to the induction of interferon-beta." In: *Nature immunology* 9 (4), pp. 361–8. DOI: 10.1038/ni1569. arXiv: NIHMS150003.

Kaisho, T. and T. Tanaka (2008). "Turning NF-kappaB and IRFs on and off in DC." In: *Trends in Immunology* 29 (7), pp. 329–36. DOI: 10.1016/j.it.2008.03.005.

Kane, C. M., L. Cervi, J. Sun, A. S. McKee, K. S. Masek, S. Shapira, C. a. Hunter, and E. J. Pearce (2004). "Helminth antigens modulate TLR-initiated dendritic cell activation." In: *Journal of immunology (Baltimore, Md. : 1950)* 173 (12), pp. 7454–61.

Kane, C. M., E. Jung, and E. J. Pearce (2008). "Schistosoma mansoni egg antigen-mediated modulation of Toll-like receptor (TLR)-induced activation occurs independently of TLR2, TLR4, and MyD88." In: *Infection and immunity* 76 (12), pp. 5754–9. DOI: 10.1128/IAI.00497-08.

Kang, Y. J., B. Kusler, M. Otsuka, M. Hughes, N. Suzuki, S. Suzuki, W.-C. Yeh, S. Akira, J. Han, and P. P. Jones (2007). "Calcineurin negatively regulates TLR-mediated activation pathways." In: *Journal of Immunology* 179 (7), pp. 4598–607.

Kato, H., S. Sato, M. Yoneyama, M. Yamamoto, S. Uematsu, K. Matsui, T. Tsujimura, K. Takeda, T. Fujita, O. Takeuchi, and S. Akira (2005). "Cell type-specific involvement of RIG-I in antiviral response". In: *Immunity* 23 (1), pp. 19–28. DOI: 10.1016/j.immuni.2005.04.010.

Kawagoe, T., S. Sato, K. Matsushita, H. Kato, K. Matsui, Y. Kumagai, T. Saitoh, T. Kawai, O. Takeuchi, and S. Akira (2008). "Sequential control of Toll-like receptor-dependent responses by IRAK1 and IRAK2." In: *Nature immunology* 9 (6), pp. 684–691. DOI: 10.1038/ni.1606.

Kawagoe, T., O. Takeuchi, Y. Takabatake, H. Kato, Y. Isaka, T. Tsujimura, and S. Akira (2009). "TANK is a negative regulator of Toll-like receptor signaling and is critical for the prevention of autoimmune nephritis." In: *Nature immunology* 10 (9), pp. 965–972. DOI: 10.1038/ni.1771.

Kawai, T., K. Takahashi, S. Sato, C. Coban, H. Kumar, H. Kato, K. J. Ishii, O. Takeuchi, and S. Akira (2005). "IPS-1, an adaptor triggering RIG-I- and Mda5-mediated type I interferon induction". In: *Nat Immunol* 6 (10), pp. 981–988. DOI: 10.1038/ni1243.

Kawai, T. and S. Akira (2007). "Signaling to NF-kappaB by Toll-like receptors." In: *Trends in Molecular Medicine* 13 (11), pp. 460–9. DOI: 10.1016/j.molmed.2007.09.002.

Kayagaki, N., Q. Phung, S. Chan, R. Chaudhari, C. Quan, K. M. O'Rourke, M. Eby, E. Pietras, G. Cheng, J. F. Bazan, Z. Zhang, D. Arnott, and V. M. Dixit (2007). "DUBA:

A Deubiquitinase That Regulates Type I Interferon Production". In: *Science* 318 (5856), pp. 1628–1632. DOI: 10.1126/science.1145918.

Kikuchi, K., Y. Yanagawa, K. Iwabuchi, and K. Onoé (2003). "Differential role of mitogen-activated protein kinases in CD40-mediated IL-12 production by immature and mature dendritic cells." In: *Immunology letters* 89 (2-3), pp. 149–54.

Kim, A., G. Khursigara, and X. Sun (2001). "Akt phosphorylates and negatively regulates apoptosis signal-regulating kinase 1". In: *Science ...* DOI: 10.1128/MCB.21.3.893.

Kim, J. W., I. Tchernyshyov, G. L. Semenza, and C. V. Dang (2006). "HIF-1-mediated expression of pyruvate dehydrogenase kinase: A metabolic switch required for cellular adaptation to hypoxia". In: *Cell Metabolism* 3 (3), pp. 177–185. DOI: 10.1016/j.cmet.2006.02.002.

Kita, H., D. A. Weiler, R. Abu-Ghazaleh, C. J. Sanderson, and G. J. Gleich (1992). "Release of granule proteins from eosinophils cultured with IL-5." In: *Journal of immunology (Baltimore, Md. : 1950)* 149 (2), pp. 629–35.

Kjetland, E. F., P. D. Ndhlovu, E. Gomo, T. Mduluza, N. Midzi, L. Gwanzura, P. R. Mason, L. Sandvik, H. Friis, S. G. Gundersen, R. Peter, L. Sandvik, H. Friis, S. Gunnar, P. R. Mason, L. Sandvik, H. Friis, and S. G. Gundersen (2006). "Association between genital schistosomiasis and HIV in rural Zimbabwean women." In: *AIDS (London, England)* 20 (4), pp. 593–600. DOI: 10.1097/01.aids.0000210614.45212.0a.

Klaver, E. J., T. C. T. M. Van Der Pouw Kraan, L. C. Laan, H. Kringel, R. D. Cummings, G. Bouma, G. Kraal, and I. Van Die (2015a). "Trichuris suis soluble products induce Rab7b expression and limit TLR4 responses in human dendritic cells". In: *Genes and Immunity* 16 (6), pp. 378–387. DOI: 10.1038/gene.2015.18.

Klaver, E. J., L. M. Kuijk, L. C. Laan, H. Kringel, S. J. van Vliet, G. Bouma, R. D. Cummings, G. Kraal, and I. van Die (2013). "Trichuris suis-induced modulation of human dendritic cell function is glycan-mediated." In: *International journal for parasitology* 43 (3-4), pp. 191–200. DOI: 10.1016/j.ijpara.2012.10.021.

Klaver, E. J., L. M. Kuijk, T. K. Lindhorst, R. D. Cummings, and I. Van Die (2015b). "Schistosoma mansoni soluble egg antigens induce expression of the negative regulators SOCS1 and SHP1 in human dendritic cells via interaction with the mannose receptor". In: *PLoS ONE* 10 (4), pp. 1–17. DOI: 10.1371/journal.pone.0124089.

Klion, A. D. and T. B. Nutman (2004). "The role of eosinophils in host defense against helminth parasites". In: *Journal of Allergy and Clinical Immunology* 113 (1), pp. 30–37. DOI: 10.1016/j.jaci.2003.10.050.

Knauf, U., C. Tschopp, and H. Gram (2001). "Negative Regulation of Protein Translation by Mitogen-Activated Protein Negative Regulation of Protein Translation by Mitogen-Activated Protein Kinase-Interacting Kinases 1 and 2". In: *Mol.Cell Biol.* 21 (16), pp. 5500–5511. DOI: 10.1128/MCB.21.16.5500.

Knott, M. L., K. I. Matthaei, P. R. Giacomin, H. Wang, P. S. Foster, and L. A. Dent (2007). "Impaired resistance in early secondary Nippostrongylus brasiliensis infections in mice with defective eosinophilopoeisis". In: *International Journal for Parasitology* 37 (12), pp. 1367–1378. DOI: 10.1016/j.ijpara.2007.04.006.

Kobayashi, K. S., M. Chamaillard, Y. Ogura, O. Henegariu, N. Inohara, G. Nuñez, and R. a. Flavell (2005). "Nod2-dependent regulation of innate and adaptive immunity in the intestinal tract." In: *Science* 307 (5710), pp. 731–4. DOI: 10.1126/science.1104911.

Kobayashi, K., L. D. Hernandez, J. E. Galán, C. a. Janeway, R. Medzhitov, and R. a. Flavell (2002). "IRAK-M is a negative regulator of Toll-like receptor signaling." In: *Cell* 110 (2), pp. 191–202.

Kohyama, M., W. Ise, B. T. Edelson, P. R. Wilker, K. Hildner, C. Mejia, W. A. Frazier, T. L. Murphy, and K. M. Murphy (2009). "Role for Spi-C in the development of red pulp macrophages and splenic iron homeostasis." In: *Nature* 457 (7227), pp. 318–21. DOI: 10.1038/nature07472.

Koinuma, D., S. Tsutsumi, N. Kamimura, H. Taniguchi, K. Miyazawa, M. Sunamura, T. Imamura, K. Miyazono, and H. Aburatani (2009). "Chromatin immunoprecipitation on microarray analysis of Smad2/3 binding sites reveals roles of ETS1 and TFAP2A in transforming growth factor beta signaling." In: *Molecular and cellular biology* 29 (1), pp. 172–86. DOI: 10.1128/MCB.01038-08.

Kool, M., M. A. M. Willart, M. van Nimwegen, I. Bergen, P. Pouliot, J. C. Virchow, N. Rogers, F. Osorio, C. Reis e Sousa, H. Hammad, and B. N. Lambrecht (2011). "An Unexpected Role for Uric Acid as an Inducer of T Helper 2 Cell Immunity to Inhaled Antigens and Inflammatory Mediator of Allergic Asthma". In: *Immunity* 34 (4), pp. 527–540. DOI: 10.1016/j.immuni.2011.03.015.

Krämer, U., J. Heinrich, M. Wjst, and H. E. Wichmann (1999). "Age of entry to day nursery and allergy in later childhood". In: *Lancet* 353 (9151), pp. 450–454. DOI: 10.1016/S0140-6736(98)06329-6.

Krawczyk, C. M., T. Holowka, J. Sun, J. Blagih, E. Amiel, R. J. Deberardinis, J. R. Cross, E. Jung, C. B. Thompson, R. G. Jones, E. J. Pearce, and W. Dc (2010). "Toll-like receptor – induced changes in glycolytic metabolism regulate dendritic cell activation". In: *Blood* 115 (23), pp. 4742–4749. DOI: 10.1182/blood-2009-10-249540.

Kuijk, L. M., E. J. Klaver, G. Kooij, S. M. a. van der Pol, P. Heijnen, S. C. M. Bruijns, H. Kringel, E. Pinelli, G. Kraal, H. E. de Vries, C. D. Dijkstra, G. Bouma, and I. van Die (2012). "Soluble helminth products suppress clinical signs in murine experimental autoimmune encephalomyelitis and differentially modulate human dendritic cell activation." In: *Molecular immunology* 51 (2), pp. 210–8. DOI: 10.1016/j.molimm.2012.03.020.

Kuwata, H., M. Matsumoto, K. Atarashi, H. Morishita, T. Hirotani, R. Koga, and K. Takeda (2006). "IkappaBNS inhibits induction of a subset of Toll-like receptor-dependent genes and limits inflammation." In: *Immunity* 24 (1), pp. 41–51. DOI: 10.1016/j.immuni.2005.11.004.

Langelaar, M., C. Aranzamendi, F. Franssen, J. Van Der Giessen, V. Rutten, P. van der Ley, and E. Pinelli (2009). "Suppression of dendritic cell maturation by Trichinella spiralis excretory/secretory products." In: *Parasite immunology* 31 (10), pp. 641–5. DOI: 10.1111/j.1365-3024.2009.01136.x.

Le Hesran, J.-Y., J. Akiana, E. H. M. Ndiaye, M. Dia, P. Senghor, and L. Konata (2004). "Severe malaria attack is associated with high prevalence of Ascaris lumbricoides infection among

children in rural Senegal". In: *Transactions of the Royal Society of Tropical Medicine and Hygiene* 98, pp. 397–399. DOI: 10.1016/j.trstmh.2004.09.003.

Lee, H. K., S. Dunzendorfer, K. Soldau, and P. S. Tobias (2006). "Double-stranded RNA-mediated TLR3 activation is enhanced by CD14". In: *Immunity* 24 (2), pp. 153–163. DOI: 10.1016/j.immuni.2005.12.012.

Lee, M. S. and Y.-J. Kim (2007). "Signaling pathways downstream of pattern-recognition receptors and their cross talk." In: *Annual review of biochemistry* 76 (Il), pp. 447–80. DOI: 10.1146/annurev.biochem.76.060605.122847.

Leynaert, B., C. Neukirch, D. Jarvis, S. Chinn, P. Burney, and F. Neukirch (2001). "Does living on a farm during childhood protect against asthma, allergic rhinitis, and atopy in adulthood?" In: *American Journal of Respiratory and Critical Care Medicine* 164 (10 I), pp. 1829–1834. DOI: 10.1164/ajrccm.164.10.2103137.

Li, S., A. Strelow, E. J. Fontana, and H. Wesche (2002). "IRAK-4: a novel member of the IRAK family with the properties of an IRAK-kinase." In: *Proceedings of the National Academy of Sciences of the United States of America* 99 (8), pp. 5567–72. DOI: 10.1073/pnas.082100399.

Li, T., M. J. Morgan, S. Choksi, Y. Zhang, Y.-S. Kim, and Z.-g. Liu (2010). "MicroRNAs modulate the noncanonical transcription factor NF-kappaB pathway by regulating expression of the kinase IKKalpha during macrophage differentiation." In: *Nature immunology* 11 (9), pp. 799–805. DOI: 10.1038/ni.1918.

Li, Y., E. Bevilacqua, C.-B. Chiribau, M. Majumder, C. Wang, C. M. Croniger, M. D. Snider, P. F. Johnson, and M. Hatzoglou (2008). "Differential control of the CCAAT/enhancer-binding protein beta (C/EBPbeta) products liver-enriched transcriptional activating protein (LAP) and liver-enriched transcriptional inhibitory protein (LIP) and the regulation of gene expression during the respo". In: *The Journal of biological chemistry* 283 (33), pp. 22443–56. DOI: 10.1074/jbc.M801046200.

Li, Z., G. Liu, Y. Chen, Y. Liu, B. Liu, and Z. Su (2011). "The phenotype and function of naturally existing regulatory dendritic cells in nematode-infected mice." In: *International journal for parasitology* 41 (11), pp. 1129–37. DOI: 10.1016/j.ijpara.2011.06.008.

Liempt, E. van, S. J. van Vliet, A. Engering, J. J. García Vallejo, C. M. C. Bank, M. Sanchez-Hernandez, Y. van Kooyk, and I. van Die (2007). "Schistosoma mansoni soluble egg antigens are internalized by human dendritic cells through multiple C-type lectins and suppress TLR-induced dendritic cell activation." In: *Molecular immunology* 44 (10), pp. 2605–15. DOI: 10.1016/j.molimm.2006.12.012.

Lin, S.-c., C.-w. Chien, J.-c. Lee, Y.-c. Yeh, K.-f. Hsu, Y.-y. Lai, S.-c. Lin, and S.-j. Tsai (2011). "Suppression of dual-specificity phosphatase – 2 by hypoxia increases chemoresistance and malignancy in human cancer cells". In: 121 (5). DOI: 10.1172/JCI44362DS1.

Lombardi, V. C. and S. F. Khaiboullina (2014). "Plasmacytoid dendritic cells of the gut: Relevance to immunity and pathology". In: *Clinical Immunology* 153 (1), pp. 165–177. DOI: 10.1016/j.clim.2014.04.007. arXiv: NIHMS150003.

Luís, A., J. D. Martins, A. Silva, I. Ferreira, M. T. Cruz, and B. M. Neves (2014). "Oxidative stress-dependent activation of the eIF2α-ATFr unfolded protein response branch by skin sensitizer 1-fluoro-2,4-dinitrobenzene modulates dendritic-like cell maturation and

inflammatory status in a biphasic manner". In: *Free Radical Biology and Medicine* 77, pp. 217–229. DOI: 10.1016/j.freeradbiomed.2014.09.008.

Lyke, K. E., A. Dicko, A. Dabo, L. Sangare, A. Kone, D. Coulibaly, A. Guindo, K. Traore, M. Daou, I. Diarra, M. B. Sztein, C. V. Plowe, and O. K. Doumbo (2005). "Association of Schistosoma haematobium infection with protection against acute Plasmodium falciparum malaria in Malian children". In: *American Journal of Tropical Medicine and Hygiene* 73 (6), pp. 1124–1130.

Lynch, N. R., I. Hagel, M. Perez, M. C. Di Prisco, R. Lopez, and N. Alvarez (1993). "Effect of anthelmintic treatment on the allergic reactivity of children in a tropical slum". In: *The Journal of Allergy and Clinical Immunology* 92 (3), pp. 404–411. DOI: 10.1016/0091-6749(93)90119-Z.

Ma, W., K. Gee, W. Lim, K. Chambers, J. B. Angel, M. Kozlowski, and A. Kumar (2004). "Dexamethasone inhibits IL-12p40 production in lipopolysaccharide-stimulated human monocytic cells by down-regulating the activity of c-Jun N-terminal kinase, the activation protein-1, and NF-kappa B transcription factors." In: *Journal of Immunology* 172 (1), pp. 318–30.

Ma, X., M. Neurath, G. Gri, and G. Trinchieri (1997). "Identification and characterization of a novel Ets-2-related nuclear complex implicated in the activation of the human interleukin-12 p40 gene promoter". In: *Journal of Biological Chemistry* 272 (16), pp. 10389–10395. DOI: 10.1074/jbc.272.16.10389.

Macatonia, S. E., N. a. Hosken, M. Litton, P. Vieira, C. S. Hsieh, J. a. Culpepper, M. Wysocka, G. Trinchieri, K. M. Murphy, and a. O'Garra (1995). "Dendritic cells produce IL-12 and direct the development of Th1 cells from naive CD4+ T cells." In: *Journal of immunology (Baltimore, Md. : 1950)* 154 (10), pp. 5071–5079.

MacDonald, A. S., A. D. Straw, N. M. Dalton, and E. J. Pearce (2002). "Cutting edge: Th2 response induction by dendritic cells: a role for CD40." In: *Journal of immunology (Baltimore, Md. : 1950)* 168 (2), pp. 537–40.

Maizels, R. M., A. Balic, N. Gomez-Escobar, M. G. Nair, M. D. Taylor, and J. E. Allen (2004). "Helminth parasites – masters of regulation". In: *Immunological Reviews* 201, pp. 89–116.

Maizels, R. M., J. P. Hewitson, J. Murray, Y. M. Harcus, B. Dayer, K. J. Filbey, J. R. Grainger, H. J. McSorley, L. a. Reynolds, and K. A. Smith (2012). "Immune modulation and modulators in Heligmosomoides polygyrus infection." In: *Experimental Parasitology* 132 (1), pp. 76–89. DOI: 10.1016/j.exppara.2011.08.011.

Maizels, R. M., H. J. McSorley, and D. J. Smyth (2014). "Helminths in the Hygiene Hypothesis - Sooner or Later ?" In: *Clinical and experimental immunology*, pp. 38–46. DOI: 10.1111/cei.12353.

Maizels, R. M. and M. Yazdanbakhsh (2003). "Immune regulation by helminth parasites: cellular and molecular mechanisms." In: *Nature reviews. Immunology* 3 (9), pp. 733–44. DOI: 10.1038/nri1183.

Maldonado-López, R., T. De Smedt, P. Michel, J. Godfroid, B. Pajak, C. Heirman, K. Thielemans, O. Leo, J. Urbain, and M. Moser (1999). "CD8alpha+ and CD8alpha-

subclasses of dendritic cells direct the development of distinct T helper cells in vivo." In: *The Journal of experimental medicine* 189 (3), pp. 587–592. DOI: 10.1084/jem.189.3.587.

Mansell, A., R. Smith, S. L. Doyle, P. Gray, J. E. Fenner, P. J. Crack, S. E. Nicholson, D. J. Hilton, L. A. J. O'Neill, and P. J. Hertzog (2006). "Suppressor of cytokine signaling 1 negatively regulates Toll-like receptor signaling by mediating Mal degradation." In: *Nature immunology* 7 (2), pp. 148–55. DOI: 10.1038/ni1299.

Marti, F., a. Krause, N. H. Post, C. Lyddane, B. Dupont, M. Sadelain, and P. D. King (2001). "Negative-feedback regulation of CD28 costimulation by a novel mitogen-activated protein kinase phosphatase, MKP6." In: *Journal of immunology (Baltimore, Md. : 1950)* 166 (1), pp. 197–206. DOI: 10.4049/jimmunol.166.1.197.

Martin, M., R. E. Schifferle, N. Cuesta, S. N. Vogel, J. Katz, and S. M. Michalek (2003). "Role of the Phosphatidylinositol 3 Kinase-Akt Pathway in the Regulation of IL-10 and IL-12 by Porphyromonas gingivalis Lipopolysaccharide". In: *The Journal of Immunology* 171, pp. 717–725. DOI: 10.4049/jimmunol.171.2.717.

Martin, M., K. Rehani, R. S. Jope, and S. M. Michalek (2005). "Toll-like receptor-mediated cytokine production is differentially regulated by glycogen synthase kinase 3." In: *Nature immunology* 6 (8), pp. 777–84. DOI: 10.1038/ni1221.

Matsuguchi, T., T. Musikacharoen, T. Johnson, A. Kraft, and Y. Yoshikai (2001). "A novel mitogen-activated protein kinase phosphatase is an important negative regulator of lipopolysaccharide-mediated c-Jun N-terminal kinase activation in mouse macrophage cell lines". In: *Molecular and cellular biology* 21 (20), p. 6999. DOI: 10.1128/MCB.21.20.6999.

Matsumoto, A., Y. Seki, M. Kubo, S. Ohtsuka, A. Suzuki, I. Hayashi, K. Tsuji, T. Nakahata, M. Okabe, S. Yamada, and A. Yoshimura (1999). "Suppression of STAT5 functions in liver, mammary glands, and T cells in cytokine-inducible SH2-containing protein 1 transgenic mice". In: *Mol Cell Biol* 19 (9), pp. 6396–6407. DOI: 10.1128/MCB.19.9.6396.

Matsushita, K., O. Takeuchi, D. M. Standley, Y. Kumagai, T. Kawagoe, T. Miyake, T. Satoh, H. Kato, T. Tsujimura, H. Nakamura, and S. Akira (2009). "Zc3h12a is an RNase essential for controlling immune responses by regulating mRNA decay." In: *Nature* 458 (7242), pp. 1185–1190. DOI: 10.1038/nature07924.

Mauro, C., F. Pacifico, A. Lavorgna, S. Mellone, A. Iannetti, R. Acquaviva, S. Formisano, P. Vito, and A. Leonardi (2006). "ABIN-1 binds to NEMO/IKK?? and co-operates with A20 in inhibiting NF-??B". In: *Journal of Biological Chemistry* 281 (27), pp. 18482–18488. DOI: 10.1074/jbc.M601502200.

McBerry, C., R. M. S. Gonzalez, N. Shryock, A. Dias, and J. Aliberti (2012). "SOCS2-induced proteasome-dependent TRAF6 degradation: A common anti-inflammatory pathway for control of innate immune responses". In: *PLoS ONE* 7 (6). DOI: 10.1371/journal.pone.0038384.

McConchie, B. W., H. H. Norris, V. G. Bundoc, S. Trivedi, A. Boesen, J. F. Urban, and A. M. Keane-Myers (2006). "Ascaris suum-derived products suppress mucosal allergic inflammation in an interleukin-10-independent manner via interference with dendritic cell function". In: *Infection and Immunity* 74 (12), pp. 6632–6641. DOI: 10.1128/IAI.00720-06.

McSorley, H. J., N. F. Blair, K. a. Smith, a. N. J. McKenzie, and R. M. Maizels (2014). "Blockade of IL-33 release and suppression of type 2 innate lymphoid cell responses by helminth secreted products in airway allergy." In: *Mucosal Immunology* 7 (5), pp. 1068–78. DOI: 10.1038/mi.2013.123.

McSorley, H. J., N. F. Blair, E. Robertson, and R. M. Maizels (2015). "Suppression of OVA-alum induced allergy by Heligmosomoides polygyrus products is MyD88-, TRIF-, regulatory T- and B cell-independent, but is associated with reduced innate lymphoid cell activation". In: *Experimental Parasitology* 158, pp. 8–17. DOI: 10.1016/j.exppara.2015.02.009.

McSorley, H. J., M. T. O'Gorman, N. Blair, T. E. Sutherland, K. J. Filbey, and R. M. Maizels (2012). "Suppression of type 2 immunity and allergic airway inflammation by secreted products of the helminth Heligmosomoides polygyrus." In: *European journal of immunology* 42 (10), pp. 2667–82. DOI: 10.1002/eji.201142161.

Mejri, N., J. Müller, and B. Gottstein (2011). "Intraperitoneal murine Echinococcus multilocularis infection induces differentiation of TGF-β-expressing DCs that remain immature". In: *Parasite Immunology* 33 (9), pp. 471–482. DOI: 10.1111/j.1365-3024.2011.01303.x.

Mercurio, F., H. Zhu, B. W. Murray, A. Shevchenko, B. L. Bennett, J. Li, D. B. Young, M. Barbosa, M. Mann, A. Manning, and A. Rao (1997). "IKK-1 and IKK-2: cytokine-activated IkappaB kinases essential for NF-kappaB activation." In: *Science* 278 (5339), pp. 860–6.

Metenou, S., M. Kovacs, B. Dembele, Y. I. Coulibaly, A. D. Klion, and T. B. Nutman (2012). "Interferon regulatory factor modulation underlies the bystander suppression of malaria antigen-driven IL-12 and IFN-γ in filaria-malaria co-infection." In: *European journal of immunology* 42 (3), pp. 641–50. DOI: 10.1002/eji.201141991.

Miah, M. A., C. H. Yoon, J. Kim, J. Jang, Y. R. Seong, and Y. S. Bae (2012). "CISH is induced during DC development and regulates DC-mediated CTL activation". In: *European Journal of Immunology* 42, pp. 58–68. DOI: 10.1002/eji.201141846.

Miller, J. E. and D. W. Horohov (2006). "Immunological aspects of nematode parasite control in sheep". In: *Journal of Animal Science* 84, pp. 124–132.

Minchenko, O., I. Opentanova, and J. Caro (2003). "Hypoxic regulation of the 6-phosphofructo-2-kinase/fructose-2,6- bisphosphatase gene family (PFKFB-1-4) expression in vivo". In: *FEBS Letters* 554 (3), pp. 264–270. DOI: 10.1016/S0014-5793(03)01179-7.

Moon, G., J. Kim, Y. Min, S. M. Wi, J. H. Shim, E. Chun, and K. Y. Lee (2015). "Phosphoinositide-dependent kinase-1 inhibits TRAF6 ubiquitination by interrupting the formation of TAK1-TAB2 complex in TLR4 signaling". In: *Cellular Signalling* 27 (12), pp. 2524–2533. DOI: 10.1016/j.cellsig.2015.09.018.

Muda, M., U. Boschert, R. Dickinson, J.-C. Martinou, I. Martinou, M. Camps, W. Schlegel, and S. Arkinstall (1996). "MKP-3, a novel cytosolic protein-tyrosine phosphatase that examplifies a new class of mitogen-activated protein kinase phosphatase". In: *J. Biol. Chem.* 271 (8), pp. 4319–4326.

Mulu, A., M. Legesse, B. Erko, Y. Belyhun, D. Nugussie, T. Shimelis, A. Kassu, D. Elias, and B. Moges (2013a). "Epidemiological and clinical correlates of malaria-helminth co-infections in Southern Ethiopia." In: *Malaria journal* 12 (1), p. 227. DOI: 10.1186/1475-2875-12-227.

Mulu, A., M. Maier, and U. G. Liebert (2013b). "Deworming of intestinal helminths reduces HIV-1 subtype C viremia in chronically co-infected individuals". In: *International Journal of Infectious Diseases* 17 (10), e897–e901. DOI: 10.1016/j.ijid.2013.03.022.

Murphy, T. L., R. Tussiwand, and K. M. Murphy (2013). "Specificity through cooperation: BATF–IRF interactions control immune-regulatory networks". In: *Nature Reviews Immunology* 13 (7), pp. 499–509. DOI: 10.1038/nri3470.

Murphy, T. L., M. G. Cleveland, P. Kulesza, J. Magram, and K. M. Murphy (1995). "Regulation of interleukin 12 p40 expression through an NF-kappa B half-site." In: *Molecular and cellular biology* 15 (10), pp. 5258–5267. DOI: 10.1016/1357-4310(96)88750-8.

Muta, T. and K. Takeshige (2001). "Essential roles of CD14 and lipopolysaccharide-binding protein for activation of toll-like receptor (TLR)2 as well as TLR4 Reconstitution of TLR2- and TLR4-activation by distinguishable ligands in LPS preparations." In: *European Journal of Biochemistry / FEBS* 268 (16), pp. 4580–9.

Mutius, E. von and D. Vercelli (2010). "Farm living: effects on childhood asthma and allergy." In: *Nature reviews. Immunology* 10 (12), pp. 861–8. DOI: 10.1038/nri2871.

Na, H., M. Cho, and Y. Chung (2016). "Regulation of Th2 Cell Immunity by Dendritic Cells." In: *Immune network* 16 (1), pp. 1–12. DOI: 10.4110/in.2016.16.1.1.

Naik, S. H., A. I. Proietto, N. S. Wilson, A. Dakic, P. Schnorrer, M. Fuchsberger, M. H. Lahoud, M. O'Keeffe, Q.-x. Shao, W.-f. Chen, J. a. Villadangos, K. Shortman, and L. Wu (2005). "Cutting edge: generation of splenic CD8+ and CD8- dendritic cell equivalents in Fms-like tyrosine kinase 3 ligand bone marrow cultures." In: *Journal of immunology (Baltimore, Md. : 1950)* 174 (11), pp. 6592–6597. DOI: 174/11/6592[pii].

Nair, M. G., Y. Du, J. G. Perrigoue, C. Zaph, J. J. Taylor, M. Goldschmidt, G. P. Swain, G. D. Yancopoulos, D. M. Valenzuela, A. Murphy, M. Karow, S. Stevens, E. J. Pearce, and D. Artis (2009). "Alternatively activated macrophage-derived RELM-{alpha} is a negative regulator of type 2 inflammation in the lung." In: *The Journal of experimental medicine* 206 (4), pp. 937–52. DOI: 10.1084/jem.20082048.

Naito, Y., T. Takagi, and Y. Higashimura (2014). "Heme oxygenase-1 and anti-inflammatory M2 macrophages". In: *Archives of Biochemistry and Biophysics* 564, pp. 83–88. DOI: 10.1016/j.abb.2014.09.005.

Nakahara, T., H. Uchi, K. Urabe, Q. Chen, M. Furue, and Y. Moroi (2004). "Role of c-Jun N-terminal kinase on lipopolysaccharide induced maturation of human monocyte-derived dendritic cells." In: *International immunology* 16 (12), pp. 1701–9. DOI: 10.1093/intimm/dxh171.

Nefedova, Y., P. Cheng, D. Gilkes, M. Blaskovich, A. A. Beg, S. M. Sebti, and D. I. Gabrilovich (2005). "Activation of dendritic cells via inhibition of Jak2/STAT3 signaling." In: *Journal of immunology (Baltimore, Md. : 1950)* 175 (7), pp. 4338–46. DOI: 10.4049/jimmunol.175.7.4338.

Negishi, H., Y. Fujita, H. Yanai, S. Sakaguchi, X. Ouyang, M. Shinohara, H. Takayanagi, Y. Ohba, T. Taniguchi, and K. Honda (2006). "Evidence for licensing of IFN-gamma-induced IFN regulatory factor 1 transcription factor by MyD88 in Toll-like receptor-dependent gene

induction program." In: *Proceedings of the National Academy of Sciences of the United States of America* 103 (41), pp. 15136–41. DOI: 10.1073/pnas.0607181103.

Negishi, H., Y. Ohba, H. Yanai, A. Takaoka, K. Honma, K. Yui, T. Matsuyama, T. Taniguchi, and K. Honda (2005). "Negative regulation of Toll-like-receptor signaling by IRF-4." In: *Proceedings of the National Academy of Sciences of the United States of America* 102 (44), pp. 15989–94. DOI: 10.1073/pnas.0508327102.

Nishiyama, A., M. Matsui, K. Hirota, H. Masutani, H. Nakamura, Y. Takagi, Y. Gon, and J. Yodoi (1999). "Identification of Thioredoxin-binding Protein-2/Vitamin D3 Up-regulated Protein 1 as a Negative Regulator of Thioredoxin Function and Expression". In: *The Journal of Biological Chemistry* 274 (31), pp. 21645–21650. DOI: 10.1074/jbc.274.31.21645.

Nono, J. K., K. Pletinckx, M. B. Lutz, and K. Brehm (2012). "Excretory/secretory-products of echinococcus multilocularis larvae induce apoptosis and tolerogenic properties in dendritic cells in vitro". In: *PLoS Neglected Tropical Diseases* 6 (2). DOI: 10.1371/journal.pntd.0001516.

Oganesyan, G., S. K. Saha, B. Guo, J. Q. He, A. Shahangian, B. Zarnegar, A. Perry, and G. Cheng (2006). "Critical role of TRAF3 in the Toll-like receptor-dependent and -independent antiviral response." In: *Nature* 439 (7073), pp. 208–211. DOI: 10.1038/nature04374.

O'Grady, S. M., N. Patil, T. Melkamu, P. J. Maniak, C. Lancto, and H. Kita (2013). "ATP release and Ca2+ signalling by human bronchial epithelial cells following Alternaria aeroallergen exposure." In: *The Journal of physiology* 591 (Pt 18), pp. 4595–609. DOI: 10.1113/jphysiol.2013.254649.

Ohtani, M., S. Nagai, S. Kondo, S. Mizuno, K. Nakamura, M. Tanabe, T. Takeuchi, S. Matsuda, and S. Koyasu (2008). "Mammalian target of rapamycin and glycogen synthase kinase 3 differentially regulate lipopolysaccharide-induced interleukin-12 production in dendritic cells." In: *Blood* 112 (3), pp. 635–43. DOI: 10.1182/blood-2008-02-137430.

Oliphant, C. J., Y. Y. Hwang, J. A. Walker, M. Salimi, S. H. Wong, J. M. Brewer, A. Englezakis, J. L. Barlow, E. Hams, S. T. Scanlon, G. S. Ogg, P. G. Fallon, and A. N. J. McKenzie (2014). "MHCII-mediated dialog between group 2 innate lymphoid cells and CD4+ T cells potentiates type 2 immunity and promotes parasitic helminth expulsion". In: *Immunity* 41 (2), pp. 283–295. DOI: 10.1016/j.immuni.2014.06.016.

O'Neill, L. A., F. J. Sheedy, and C. E. Mccoy (2011). "MicroRNAs: the fine-tuners of Toll-like receptor signalling". In: *Nature Reviews Immunology* 268, pp. 163–175. DOI: 10.1038/nri29.

Palsson-McDermott, E. M., S. L. Doyle, A. F. McGettrick, M. Hardy, H. Husebye, K. Banahan, M. Gong, D. Golenbock, T. Espevik, and L. A. J. O'Neill (2009). "TAG, a splice variant of the adaptor TRAM, negatively regulates the adaptor MyD88-independent TLR4 pathway." In: *Nature immunology* 10 (6), pp. 579–86. DOI: 10.1038/ni.1727.

Palsson-Mcdermott, E. M. and L. A. J. O'Neill (2013). "The Warburg effect then and now: From cancer to inflammatory diseases". In: *BioEssays* 35 (11), pp. 965–973. DOI: 10.1002/bies.201300084.

Panhuys, N. van, S.-C. Tang, M. Prout, M. Camberis, D. Scarlett, J. Roberts, J. Hu-Li, W. E. Paul, and G. Le Gros (2008). "In vivo studies fail to reveal a role for IL-4 or STAT6 signaling in

Th2 lymphocyte differentiation." In: *Proceedings of the National Academy of Sciences of the United States of America* 105 (34), pp. 12423–12428. DOI: 10.1073/pnas.0806372105.

Papandreou, I., R. A. Cairns, L. Fontana, A. L. Lim, and N. C. Denko (2006). "HIF-1 mediates adaptation to hypoxia by actively downregulating mitochondrial oxygen consumption". In: *Cell Metabolism* 3 (3), pp. 187–197. DOI: 10.1016/j.cmet.2006.01.012.

Park, M. K., M. K. Cho, S. A. Kang, H. K. Park, Y. S. Kim, K. U. Kim, S. C. Ahn, D. H. Kim, and H. S. Yu (2011). "Protease-activated receptor 2 is involved in Th2 responses against Trichinella spiralis infection". In: *Korean Journal of Parasitology* 49 (3), pp. 235–243. DOI: 10.3347/kjp.2011.49.3.235.

Patterson, K. I., T. Brummer, P. M. O'brien, and R. J. Daly (2009). "Dual-specificity phosphatases: critical regulators with diverse cellular targets". In: *Biochemical Journal* 418 (3), pp. 475–489. DOI: 10.1042/BJ20082234.

Paul, W. E. (2010). "What determines Th2 differentiation, in vitro and in vivo?" In: *Immunology and cell biology* 88 (3), pp. 236–9. DOI: 10.1038/icb.2010.2.

Paul, W. E. and J. Zhu (2010). "How are T(H)2-type immune responses initiated and amplified?" In: *Nature reviews. Immunology* 10 (4), pp. 225–35. DOI: 10.1038/nri2735.

Pauls, E., S. K. Nanda, H. Smith, R. Toth, J. S. C. Arthur, and P. Cohen (2013). "Two Phases of Inflammatory Mediator Production Defined by the Study of IRAK2 and IRAK1 Knock-in Mice." In: *Journal of immunology (Baltimore, Md. : 1950)* 191 (5), pp. 2717–30. DOI: 10.4049/jimmunol.1203268.

Pearce, E. J. and B. Everts (2015). "Dendritic cell metabolism". In: *Nature Reviews Immunology* 15 (1), pp. 18–29. DOI: 10.1038/nri3771.

Peng, J., Q. Yuan, B. Lin, P. Panneerselvam, X. Wang, X. L. Luan, S. K. Lim, B. P. Leung, B. Ho, and J. L. Ding (2010). "SARM inhibits both TRIF- and MyD88-mediated AP-1 activation". In: *European Journal of Immunology* 40 (6), pp. 1738–1747. DOI: 10.1002/eji.200940034.

Perl, A., R. Hanczko, T. Telarico, Z. Oaks, and S. Landas (2011). "Oxidative stress, inflammation and carcinogenesis are controlled through the pentose phosphate pathway by transaldolase". In: *Trends in Molecular Medicine* 17 (7), pp. 395–403. DOI: 10.1016/j.molmed.2011.01.014.

Perrigoue, J. G., F. A. Marshall, and D. Artis (2008). "On the hunt for helminths: Innate immune cells in the recognition and response to helminth parasites". In: *Cellular Microbiology* 10 (9), pp. 1757–1764. DOI: 10.1111/j.1462-5822.2008.01174.x.

Perrigoue, J. G., S. A. Saenz, M. C. Siracusa, E. J. Allenspach, B. C. Taylor, P. R. Giacomin, M. G. Nair, Y. Du, C. Zaph, N. van Rooijen, M. R. Comeau, E. J. Pearce, T. M. Laufer, and D. Artis (2009). "MHC class II–dependent basophil–CD4+ T cell interactions promote TH2 cytokine–dependent immunity". In: *Nature immunology* 10 (7), pp. 697–705. DOI: 10.1038/ni.1740. arXiv: 138.

Pesce, J. T., T. R. Ramalingam, M. M. Mentink-Kane, M. S. Wilson, K. C. E. Kasmi, A. M. Smith, R. W. Thompson, A. W. Cheever, P. J. Murray, and T. A. Wynn (2009a). "Arginase-1-expressing macrophages suppress Th2 cytokine-driven inflammation and fibrosis". In: *PLoS Pathogens* 5 (4). DOI: 10.1371/journal.ppat.1000371.

Pesce, J. T., T. R. Ramalingam, M. S. Wilson, M. M. Mentink-Kane, R. W. Thompson, A. W. Cheever, J. F. Urban, and T. A. Wynn (2009b). "Retnla (Relma/Fizz1) suppresses helminth-induced Th2- type immunity". In: *PLoS Pathogens* 5 (4), pp. 1–15. DOI: 10.1371/journal.ppat.1000393.

Phythian-Adams, A. T., P. C. Cook, R. J. Lundie, L. H. Jones, K. A. Smith, T. A. Barr, K. Hochweller, S. M. Anderton, G. J. Hämmerling, R. M. Maizels, and A. S. MacDonald (2010). "CD11c depletion severely disrupts Th2 induction and development in vivo." In: *The Journal of Experimental Medicine* 207 (10), pp. 2089–96. DOI: 10.1084/jem.20100734.

Plociennikowska, A., A. Hromada-Judycka, K. Borzecka, and K. Kwiatkowska (2015). "Co-operation of TLR4 and raft proteins in LPS-induced pro-inflammatory signaling". In: *Cellular and Molecular Life Sciences* 72 (3), pp. 557–581. DOI: 10.1007/s00018-014-1762-5.

Pulendran, B., J. Lingappa, M. K. Kennedy, J. Smith, M. Teepe, A. Rudensky, C. R. Maliszewski, and E. Maraskovsky (1997). "Developmental pathways of dendritic cells in vivo: distinct function, phenotype, and localization of dendritic cell subsets in FLT3 ligand-treated mice". In: *J Immunol* 159 (5), pp. 2222–2231.

Pulendran, B., J. L. Smith, G. Caspary, K. Brasel, D. Pettit, E. Maraskovsky, and C. R. Maliszewski (1999). "Distinct dendritic cell subsets differentially regulate the class of immune response in vivo." In: *Proceedings of the National Academy of Sciences of the United States of America* 96 (3), pp. 1036–1041.

Pulendran, B. (2005). "Variegation of the Immune Response with Dendritic Cells and Pathogen Recognitin Receptors". In: *Journal of immunology* 174, pp. 2457–65. DOI: 10.4049/jimmunol.174.5.2457.

Pulendran, B., P. Kumar, C. W. Cutler, M. Mohamadzadeh, T. Van Dyke, and J. Banchereau (2001). "Lipopolysaccharides from Distinct Pathogens Induce Different Classes of Immune Responses In Vivo". In: *The Journal of Immunology* 167 (9), pp. 5067–5076. DOI: 10.4049/jimmunol.167.9.5067. arXiv: NIHMS150003.

Pulendran, B., H. Tang, and S. Manicassamy (2010). "Programming dendritic cells to induce TH2 and tolerogenic responses". In: *Nature Immunology* 11 (8), pp. 647–655. DOI: 10.1038/ni.1894.

Rahman, I. (2005). "Regulation of glutathione in inflammation and chronic lung diseases". In: *Mutation Research* 579, pp. 58–80. DOI: 10.1016/j.mrfmmm.2005.02.025.

Rescigno, M., M. Martino, C. L. Sutherland, M. R. Gold, and P. Ricciardi-Castagnoli (1998). "Dendritic cell survival and maturation are regulated by different signaling pathways." In: *The Journal of experimental medicine* 188 (11), pp. 2175–80.

Resende Co, T., C. S. Hirsch, Z. Toossi, R. Dietze, and R. Ribeiro-Rodrigues (2006). "Intestinal helminth co-infection has a negative impact on both anti-Mycobacterium tuberculosis immunity and clinical response to tuberculosis therapy". In: *Clinical and Experimental Immunology* 147 (1), pp. 45–52. DOI: 10.1111/j.1365-2249.2006.03247.x.

Reyes, J. L., C. a. Terrazas, L. Vera-Arias, and L. I. Terrazas (2009). "Differential response of antigen presenting cells from susceptible and resistant strains of mice to Taenia crassiceps infection." In: *Infection, genetics and evolution : journal of molecular epidemiology*

and evolutionary genetics in infectious diseases 9 (6), pp. 1115–27. DOI: 10.1016/j.meegid.2009.05.011.

Richardson, S. J. (2015). "Tweaking the structure to radically change the function: The evolution of transthyretin from 5-hydroxyisourate hydrolase to triiodothyronine distributor to thyroxine distributor". In: *Frontiers in Endocrinology* 6 (FEB), pp. 1–9. DOI: 10.3389/fendo.2014.00245.

Riganò, R., B. Buttari, E. Profumo, E. Ortona, F. Delunardo, P. Margutti, V. Mattei, A. Teggi, M. Sorice, and A. Siracusano (2007). "Echinococcus granulosus antigen B impairs human dendritic cell differentiation and polarizes immature dendritic cell maturation towards a Th2 cell response". In: *Infection and Immunity* 75 (4), pp. 1667–1678. DOI: 10.1128/IAI.01156-06.

Rijt, L. S. van, S. Jung, A. Kleinjan, N. Vos, M. Willart, C. Duez, H. C. Hoogsteden, and B. N. Lambrecht (2005). "In vivo depletion of lung CD11c+ dendritic cells during allergen challenge abrogates the characteristic features of asthma". In: *The Journal of Experimental Medicine* 201 (6), pp. 981–991. DOI: 10.1084/jem.20042311.

Al-Riyami, L. and W. Harnett (2012). "Immunomodulatory properties of ES-62, a phosphorylcholine-containing glycoprotein secreted by Acanthocheilonema viteae." In: *Endocrine, metabolic & immune disorders drug targets* 12 (1), pp. 45–52.

Rodriguez, E., V. Noya, L. Cervi, M. L. Chiribao, N. Brossard, C. Chiale, C. Carmona, C. Giacomini, and T. Freire (2015). "Glycans from Fasciola hepatica Modulate the Host Immune Response and TLR-Induced Maturation of Dendritic Cells." In: *PLoS neglected tropical diseases* 9 (12), e0004234. DOI: 10.1371/journal.pntd.0004234.

Roy, S., R. Guler, S. P. Parihar, S. Schmeier, B. Kaczkowski, H. Nishimura, J. W. Shin, Y. Negishi, M. Ozturk, R. Hurdayal, a. Kubosaki, Y. Kimura, M. J. L. de Hoon, Y. Hayashizaki, F. Brombacher, and H. Suzuki (2015). "Batf2/Irf1 Induces Inflammatory Responses in Classically Activated Macrophages, Lipopolysaccharides, and Mycobacterial Infection". In: *The Journal of Immunology* 5 (14). DOI: 10.4049/jimmunol.1402521.

Rzepecka, J., S. Rausch, C. Klotz, C. Schnöller, T. Kornprobst, J. Hagen, R. Ignatius, R. Lucius, and S. Hartmann (2009). "Calreticulin from the intestinal nematode Heligmosomoides polygyrus is a Th2-skewing protein and interacts with murine scavenger receptor-A." In: *Molecular immunology* 46 (6), pp. 1109–19. DOI: 10.1016/j.molimm.2008.10.032.

Sabin, E. A., M. I. Araujo, E. M. Carvalho, and E. J. Pearce (1996). "Impairment of Tetanus Toxoid-Specific Th1-like Immune Responses in Humans Infected with Schistosoma mansoni". In: *The Journal of Infectious Diseases* 173 (1), pp. 269–272.

Saitoh, T., A. Tun-Kyi, A. Ryo, M. Yamamoto, G. Finn, T. Fujita, S. Akira, N. Yamamoto, K. P. Lu, and S. Yamaoka (2006). "Negative regulation of interferon-regulatory factor 3–dependent innate antiviral response by the prolyl isomerase Pin1". In: *Nature Immunology* 7 (6), pp. 598–605. DOI: 10.1038/ni1347.

Salgame, P., G. S. Yap, and W. C. Gause (2013). "Effect of helminth-induced immunity on infections with microbial pathogens." In: *Nature immunology* 14 (11), pp. 1118–26. DOI: 10.1038/ni.2736.

Salkowski, C. a., K. Kopydlowski, J. Blanco, M. J. Cody, R. McNally, and S. N. Vogel (1999). "IL-12 is dysregulated in macrophages from IRF-1 and IRF-2 knockout mice." In: *Journal of immunology (Baltimore, Md. : 1950)* 163 (3), pp. 1529–36.

Sandau, K. B., J. Fandrey, and B. Brüne (2001). "Accumulation of HIF-1alpha under the influence of nitric oxide." In: *Blood* 97 (4), pp. 1009–1015. DOI: 10.1182/blood.V97.4.1009.

Scheper, G. C., N. a. Morrice, M. Kleijn, and C. G. Proud (2001). "The Mitogen-Activated Protein Kinase Signal-Integrating Kinase Mnk2 Is a Eukaryotic Initiation Factor 4E Kinase with High Levels of Basal Activity in Mammalian Cells The Mitogen-Activated Protein Kinase Signal-Integrating Kinase Mnk2 Is a Eukaryotic Initi". In: *Molecular and Cellular Biology* 21 (3), pp. 743–754. DOI: 10.1128/MCB.21.3.743.

Schneider, M., A. G. Zimmermann, R. a. Roberts, L. Zhang, K. V. Swanson, H. Wen, B. K. Davis, I. C. Allen, E. K. Holl, Z. Ye, A. H. Rahman, B. J. Conti, T. K. Eitas, B. H. Koller, and J. P.-Y. Ting (2012). "The innate immune sensor NLRC3 attenuates Toll-like receptor signaling via modification of the signaling adaptor TRAF6 and transcription factor NF-κB". In: *Nature Immunology* 13 (9), pp. 823–31. DOI: 10.1038/ni.2378.

Schoenhaut, D. S., a. O. Chua, a. G. Wolitzky, P. M. Quinn, C. M. Dwyer, W. McComas, P. C. Familletti, M. K. Gately, and U. Gubler (1992). "Cloning and expression of murine IL-12." In: *Journal of immunology (Baltimore, Md. : 1950)* 148 (11), pp. 3433–40.

Schraml, B. U. and C. Reis e Sousa (2015). "Defining dendritic cells". In: *Current Opinion in Immunology* 32, pp. 13–20. DOI: 10.1016/j.coi.2014.11.001.

Schroder, K., M. Spille, A. Pilz, J. Lattin, K. A. Bode, K. M. Irvine, A. D. Burrows, T. Ravasi, H. Weighardt, K. J. Stacey, T. Decker, D. A. Hume, A. H. Dalpke, and M. J. Sweet (2007). "Differential Effects of CpG DNA on IFN- Induction and STAT1 Activation in Murine Macrophages versus Dendritic Cells: Alternatively Activated STAT1 Negatively Regulates TLR Signaling in Macrophages". In: *The Journal of Immunology* 179 (6), pp. 3495–3503. DOI: 10.4049/jimmunol.179.6.3495.

Schulz, O., E. Jaensson, E. K. Persson, X. Liu, T. Worbs, W. W. Agace, and O. Pabst (2009). "Intestinal CD103+, but not CX3CR1+, antigen sampling cells migrate in lymph and serve classical dendritic cell functions." In: *The Journal of experimental medicine* 206 (13), pp. 3101–14. DOI: 10.1084/jem.20091925.

Schwartz, C., A. Turqueti-Neves, S. Hartmann, P. Yu, F. Nimmerjahn, and D. Voehringer (2014). "Basophil-mediated protection against gastrointestinal helminths requires IgE-induced cytokine secretion." In: *Proceedings of the National Academy of Sciences of the United States of America* 111 (48), E5169–77. DOI: 10.1073/pnas.1412663111.

Segura, M., Z. Su, C. Piccirillo, and M. M. Stevenson (2007). "Impairment of dendritic cell function by excretory-secretory products: a potential mechanism for nematode-induced immunosuppression." In: *European Journal of Immunology* 37 (7), pp. 1887–904. DOI: 10.1002/eji.200636553.

Semenza, G., B. Jiang, S. Leung, R. Passantino, J. Concordet, P. Maire, and A. Giallongo (1996). "Hypoxia Response Elements in the Aldolase A, Enolase 1,and Lactate Dehydrogenase A Gene Promoters Contain Essential Binding Sites for Hypoxia-inducible Factor 1". In: *Journal of Biological Chemistry* 271 (51), pp. 32529–32537. DOI: 10.1074/jbc.271.51.32529.

Semnani, R. T., M. Law, J. Kubofcik, and T. B. Nutman (2004). "Filaria-induced immune evasion: suppression by the infective stage of Brugia malayi at the earliest host-parasite interface." In: *Journal of immunology (Baltimore, Md. : 1950)* 172 (10), pp. 6229–38.

Semnani, R. T., A. Y. Liu, H. Sabzevari, J. Kubofcik, J. Zhou, J. K. Gilden, and T. B. Nutman (2003). "Brugia malayi Microfilariae Induce Cell Death in Human Dendritic Cels, Inhibit Their Ability to Make IL-12 and IL-10, and Reduce Their Capacity to Activate CD4+ T Cells". In: *The Journal of Immunology* 171 (4), pp. 1950–1960.

Semnani, R. T., L. Mahapatra, B. Dembele, S. Konate, S. Metenou, H. Dolo, M. E. Coulibaly, L. Soumaoro, S. Y. Coulibaly, D. Sanogo, S. Seriba Doumbia, A. a. Diallo, S. F. Traoré, A. Klion, T. B. Nutman, and S. Mahanty (2010). "Expanded numbers of circulating myeloid dendritic cells in patent human filarial infection reflect lower CCR1 expression." In: *Journal of immunology (Baltimore, Md. : 1950)* 185 (10), pp. 6364–72. DOI: 10.4049/jimmunol.1001605.

Semnani, R. T., P. G. Venugopal, C. a. Leifer, S. Mostböck, H. Sabzevari, and T. B. Nutman (2008a). "Inhibition of TLR3 and TLR4 function and expression in human dendritic cells by helminth parasites." In: *Blood* 112 (4), pp. 1290–8. DOI: 10.1182/blood-2008-04-149856.

Semnani, R. T., P. G. Venugopal, L. Mahapatra, J. a. Skinner, F. Meylan, D. Chien, D. W. Dorward, D. Chaussabel, R. M. Siegel, and T. B. Nutman (2008b). "Induction of TRAIL- and TNF-alpha-dependent apoptosis in human monocyte-derived dendritic cells by microfilariae of Brugia malayi." In: *Journal of immunology (Baltimore, Md. : 1950)* 181 (10), pp. 7081–9.

Shembade, N., A. Ma, and E. W. Harhaj (2010). "Inhibition of NF-kappaB signaling by A20 through disruption of ubiquitin enzyme complexes." In: *Science (New York, N.Y.)* 327 (5969), pp. 1135–9. DOI: 10.1126/science.1182364. arXiv: 0036-8075.

Sher, A., E. Pearce, and P. Kaye (2003). "Shaping the immune response to parasites: Role of dendritic cells". In: *Current Opinion in Immunology* 15 (4), pp. 421–429. DOI: 10.1016/S0952-7915(03)00072-4.

Shi, M., W. Deng, E. Bi, K. Mao, Y. Ji, G. Lin, X. Wu, Z. Tao, Z. Li, X. Cai, S. Sun, C. Xiang, and B. Sun (2008). "TRIM30 alpha negatively regulates TLR-mediated NF-kappa B activation by targeting TAB2 and TAB3 for degradation." In: *Nature immunology* 9 (4), pp. 369–377. DOI: 10.1038/ni1577.

Shimazu, R., S. Akashi, H. Ogata, Y. Nagai, K. Fukudome, K. Miyake, and M. Kimoto (1999). "MD-2, a molecule that confers lipopolysaccharide responsiveness on Toll-like receptor 4." In: *The Journal of experimental medicine* 189 (11), pp. 1777–82.

Shinohara, H., A. Inoue, N. Toyama-Sorimachi, Y. Nagai, T. Yasuda, H. Suzuki, R. Horai, Y. Iwakura, T. Yamamoto, H. Karasuyama, K. Miyake, and Y. Yamanashi (2005). "Dok-1 and Dok-2 are negative regulators of T cell receptor signaling". In: *Journal of Experimental Medicine* 201 (3), pp. 333–339.

Shoshani, T., A. Faerman, I. Mett, E. Zelin, T. Tenne, S. Gorodin, Y. Moshel, S. Elbaz, A. Budanov, A. Chajut, H. Kalinski, I. Kamer, A. Rozen, O. Mor, E. Keshet, D. Leshkowitz, P. Einat, R. Skaliter, and E. Feinstein (2002). "Identification of a novel hypoxia-inducible

factor 1-responsive gene, RTP801, involved in apoptosis." In: *Molecular and cellular biology* 22 (7), pp. 2283–93. DOI: 10.1128/MCB.22.7.2283.

Silva, S. R., J. F. Jacysyn, M. S. Macedo, and E. L. Faquin-Mauro (2006). "Immunosuppressive components of Ascaris suum down-regulate expression of costimulatory molecules and function of antigen-presenting cells via an IL-10-mediated mechanism". In: *European Journal of Immunology* 36 (12), pp. 3227–3237. DOI: 10.1002/eji.200636110.

Skaug, B., J. Chen, F. Du, J. He, A. Ma, and Z. J. Chen (2011). "Direct, Noncatalytic Mechanism of IKK Inhibition by A20". In: *Molecular Cell* 44 (4), pp. 559–571. DOI: 10.1016/j.molcel.2011.09.015.

Skonier, J., K. Bennett, V. Rothwell, S. Kosowski, G. Plowman, P. Wallace, S. Edelhoff, C. Disteche, M. Neubauer, and H. Marquardt (1994). "beta ig-h3: a transforming growth factor-beta-responsive gene encoding a secreted protein that inhibits cell attachment in vitro and suppresses the growth of CHO cells in nude mice." In: *DNA and cell biology* 13 (6), pp. 571–584.

Smith, K. A., Y. Harcus, N. Garbi, A. S. Macdonald, and R. M. Maizels (2012). "Type 2 Innate Immunity in Helminth Infection Is Induced Redundantly and Acts Autonomously following CD11c + Cell Depletion". In: *Infection and Immunity* 80, pp. 3481–3489. DOI: 10.1128/IAI.00436-12.

Smith, K. a., K. Hochweller, G. J. Hämmerling, L. Boon, A. S. MacDonald, and R. M. Maizels (2011). "Chronic helminth infection promotes immune regulation in vivo through dominance of CD11cloCD103- dendritic cells." In: *Journal of immunology (Baltimore, Md. : 1950)* 186 (12), pp. 7098–109. DOI: 10.4049/jimmunol.1003636.

Song, K. S., J. H. Yoon, K. S. Kim, and D. W. Ahn (2012). "c-Ets1 inhibits the interaction of NF-kappaB and CREB, and downregulates IL-1beta-induced MUC5AC overproduction during airway inflammation". In: *Mucosal Immunol* 5 (2), pp. 207–215. DOI: 10.1038/mi.2011.67.

Spirig, R., S. Djafarzadeh, T. Regueira, S. G. Shaw, C. von Garnier, J. Takala, S. M. Jakob, R. Rieben, and P. M. Lepper (2010). "Effects of TLR agonists on the hypoxia-regulated transcription factor HIF-1?? and dendritic cell maturation under normoxic conditions". In: *PLoS ONE* 5 (6), pp. 1–12. DOI: 10.1371/journal.pone.0010983.

Steenhard, N. R., G. Jungersen, B. Kokotovic, E. Beshah, H. D. Dawson, J. F. Urban, A. Roepstorff, and S. M. Thamsborg (2009). "Ascaris suum infection negatively affects the response to a Mycoplasma hyopneumoniae vaccination and subsequent challenge infection in pigs". In: *Vaccine* 27 (37), pp. 5161–5169. DOI: 10.1016/j.vaccine.2009.05.075.

Steinfelder, S., J. F. Andersen, J. L. Cannons, C. G. Feng, M. Joshi, D. Dwyer, P. Caspar, P. L. Schwartzberg, A. Sher, and D. Jankovic (2009). "The major component in schistosome eggs responsible for conditioning dendritic cells for Th2 polarization is a T2 ribonuclease (omega-1)." In: *The Journal of experimental medicine* 206 (8), pp. 1681–90. DOI: 10.1084/jem.20082462.

Steinman, R. M. and M. D. Witmer (1978). "Lymphoid dendritic cells are potent stimulators of the primary mixed leukocyte reaction in mice." In: *Proceedings of the National Academy of Sciences of the United States of America* 75 (10), pp. 5132–6. DOI: 10.1084/jem.157.2.613.

Steinman, R. M. and Z. A. Cohn (1973). "Identification of a novel cell type in peripheral lymphoid organs of mice". In: *Journal of Experimental Medicine* 137, pp. 1142–1162. DOI: 10.1084/jem.137.5.1142.

Strachan, D. P. (1989). "Hayfever, hygiene, and household size". In: *BMJ : British Medical Journal* 299 (November), pp. 1259–1260. DOI: 10.1136/bmj.299.6710.1259.

Su, X., S. Mei, X. Liang, S. Wang, J. Liu, Y. Zhang, Y. Bao, Y. Chen, Y. Che, R. Chunhua Zhao, Z. Zhang, and R. Yang (2014). "Epigenetically modulated LRRC33 acts as a negative physiological regulator for multiple Toll-like receptors." In: *Journal of leukocyte biology* 95 (July), pp. 1–10. DOI: 10.1189/jlb.0813457.

Su, Z., M. Segura, K. Morgan, J. Concepcion, M. M. Stevenson, and J. C. Loredo-osti (2005). "Impairment of Protective Immunity to Blood-Stage Malaria by Concurrent Nematode Infection Impairment of Protective Immunity to Blood-Stage Malaria by Concurrent Nematode Infection". In: *Society* 73 (6), pp. 3531–3539. DOI: 10.1128/IAI.73.6.3531.

Sun, Y., G. Liu, Z. Li, Y. Chen, Y. Liu, B. Liu, and Z. Su (2013). "Modulation of dendritic cell function and immune response by cysteine protease inhibitor from murine nematode parasite Heligmosomoides polygyrus." In: *Immunology* 138 (4), pp. 370–81. DOI: 10.1111/imm.12049.

Suriano, A., an Sanford, and N. Kim (2005). "GCF2/LRRFIP1 represses tumor necrosis factor alpha expression". In: *Molecular and Cellular Biology* 25 (20), pp. 9073–81. DOI: 10.1128/MCB.25.20.9073.

Sutherland, T. E., R. M. Maizels, and J. E. Allen (2009). "Chitinases and chitinase-like proteins: Potential therapeutic targets for the treatment of T-helper type 2 allergies". In: *Clinical and Experimental Allergy* 39 (7), pp. 943–955. DOI: 10.1111/j.1365-2222.2009.03243.x.

Sutherland, T. E., N. Logan, D. Ruckerl, A. A. Humbles, S. M. Allan, V. Papayannopoulos, B. Stockinger, R. M. Maizels, and J. E. Allen (2014). "Chitinase-like proteins promote IL-17-mediated neutrophilia in a tradeoff between nematode killing and host damage." In: *Nature immunology* 15 (12), pp. 1116–1125. DOI: 10.1038/ni.3023.

Takaoka, A., H. Yanai, S. Kondo, G. Duncan, H. Negishi, T. Mizutani, S.-I. Kano, K. Honda, Y. Ohba, T. W. Mak, and T. Taniguchi (2005). "Integral role of IRF-5 in the gene induction programme activated by Toll-like receptors." In: *Nature* 434 (7030), pp. 243–9. DOI: 10.1038/nature03308.

Takeda, K., T. Kaisho, and S. Akira (2003). "Toll-Like Receptors". In: *Annual Review of Immunology* 21 (1), pp. 335–376. DOI: 10.1146/annurev.immunol.21.120601.141126.

Takeuchi, O., T. Kawai, P. F. Mühlradt, M. Morr, J. D. Radolf, a. Zychlinsky, K. Takeda, and S. Akira (2001). "Discrimination of bacterial lipoproteins by Toll-like receptor 6." In: *International immunology* 13 (7), pp. 933–940. DOI: 10.1093/intimm/13.7.933.

Takeuchi, O., S. Sato, T. Horiuchi, K. Hoshino, K. Takeda, Z. Dong, R. L. Modlin, and S. Akira (2002). "Cutting edge: role of Toll-like receptor 1 in mediating immune response

to microbial lipoproteins". In: *Journal of Immunology* 169 (1), pp. 10–14. DOI: 10.4049/jimmunol.169.1.10.

Takeuchi, O., K. Hoshino, T. Kawai, H. Sanjo, H. Takada, T. Ogawa, K. Takeda, and S. Akira (1999). "Differential roles of TLR2 and TLR4 in recognition of gram-negative and gram-positive bacterial cell wall components". In: *Immunity* 11 (4), pp. 443–451. DOI: 10.1016/S1074-7613(00)80119-3.

Tanaka, T., M. J. Grusby, and T. Kaisho (2007). "PDLIM2-mediated termination of transcription factor NF-kappaB activation by intranuclear sequestration and degradation of the p65 subunit." In: *Nature immunology* 8 (6), pp. 584–91. DOI: 10.1038/ni1464.

Tanaka, T., A. Shibazaki, R. Ono, and T. Kaisho (2014). "HSP70 mediates degradation of the p65 subunit of nuclear factor κB to inhibit inflammatory signaling." In: *Science signaling* 7 (356), ra119. DOI: 10.1126/scisignal.2005533.

Tang, B., B. Xiao, Z. Liu, N. Li, E. D. Zhu, B. S. Li, Q. H. Xie, Y. Zhuang, Q. M. Zou, and X. H. Mao (2010). "Identification of MyD88 as a novel target of miR-155, involved in negative regulation of Helicobacter pylori-induced inflammation". In: *FEBS Letters* 584 (8), pp. 1481–1486. DOI: 10.1016/j.febslet.2010.02.063.

Terrazas, C., L. Gómez-García, and L. Terrazas (2010). "Impaired pro-inflammatory cytokine production and increased Th2-biasing ability of dendritic cells exposed to Taenia excreted/secreted antigens: A critical role". In: *International Journal for ...* 40, pp. 1051–1062. DOI: 10.1016/j.ijpara.2010.02.016.

Terrazas, C. a., M. Alcántara-Hernández, L. Bonifaz, L. I. Terrazas, and A. R. Satoskar (2013). "Helminth-excreted/secreted products are recognized by multiple receptors on DCs to block the TLR response and bias Th2 polarization in a cRAF dependent pathway." In: *FASEB journal : official publication of the Federation of American Societies for Experimental Biology* 27 (11), pp. 1–14. DOI: 10.1096/fj.13-228932.

Terrazas, C. A., F. Sánchez-Muñoz, A. M. Mejía-Domínguez, L. M. Amezcua-Guerra, L. I. Terrazas, R. Bojalil, and L. Gómez-García (2011). "Cestode antigens induce a tolerogenic-like phenotype and inhibit LPS in-flammatory responses in human dendritic cells". In: *International Journal of Biological Sciences* 7 (9), pp. 1391–1400. DOI: 10.7150/ijbs.7.1391.

Thomas, P. G., M. R. Carter, O. Atochina, A. A. Da'Dara, D. Piskorska, E. McGuire, and D. A. Harn (2003). "Maturation of dendritic cell 2 phenotype by a helminth glycan uses a Toll-like receptor 4-dependent mechanism." In: *Journal of immunology (Baltimore, Md. : 1950)* 171 (11), pp. 5837–41. DOI: 10.4049/jimmunol.171.11.5837.

Thomas, P. G., M. R. Carter, A. A. Da, T. M. Desimone, and D. A. Harn (2005). "A Helminth Glycan Induces APC Maturation via Alternative NF-kB Activation Independent of I kBa Degradation". In: *The Journal of Immunology* 175 (4), pp. 2082–2090.

Tili, E., J.-J. Michaille, A. Cimino, S. Costinean, C. D. Dumitru, B. Adair, M. Fabbri, H. Alder, C. G. Liu, G. A. Calin, and C. M. Croce (2007). "Modulation of miR-155 and miR-125b levels following lipopolysaccharide/TNF-alpha stimulation and their possible roles in regulating the response to endotoxin shock." In: *Journal of immunology (Baltimore, Md. : 1950)* 179 (8), pp. 5082–9. DOI: 10.4049/jimmunol.179.8.5082.

Trinchieri, G., M. Wysocka, a. D'Andrea, M. Rengaraju, M. Aste-Amezaga, M. Kubin, N. M. Valiante, and J. Chehimi (1992). "Natural killer cell stimulatory factor (NKSF) or interleukin-12 is a key regulator of immune response and inflammation." In: *Progress in growth factor research* 4 (4), pp. 355–68.

Turer, E. E., R. M. Tavares, E. Mortier, O. Hitotsumatsu, R. Advincula, B. Lee, N. Shifrin, B. A. Malynn, and A. Ma (2008). "Homeostatic MyD88-dependent signals cause lethal inflamMation in the absence of A20." In: *The Journal of experimental medicine* 205 (2), pp. 451–64. DOI: 10.1084/jem.20071108.

Ullah, M. A., Z. Loh, W. J. Gan, V. Zhang, H. Yang, J. H. Li, Y. Yamamoto, A. M. Schmidt, C. L. Armour, J. M. Hughes, S. Phipps, and M. B. Sukkar (2014). "Receptor for advanced glycation end products and its ligand high-mobility group box-1 mediate allergic airway sensitization and airway inflammation". In: *Journal of Allergy and Clinical Immunology* 134 (2), 440–450.e3. DOI: 10.1016/j.jaci.2013.12.1035.

Urb, M. and D. C. Sheppard (2012). "The role of mast cells in the defence against pathogens". In: *PLoS Pathogens* 8 (4), pp. 2–4. DOI: 10.1371/journal.ppat.1002619.

Van der Kleij, D., E. Latz, J. F. H. M. Brouwers, Y. C. M. Kruize, M. Schmitz, E. A. Kurt-Jones, T. Espevik, E. C. De Jong, M. L. Kapsenberg, D. T. Golenbock, A. G. M. Tielens, and M. Yazdanbakhsh (2002). "A novel host-parasite lipid cross-talk. Schistosomal lyso-phosphatidylserine activates toll-like receptor 2 and affects immune polarization". In: *Journal of Biological Chemistry* 277 (50), pp. 48122–48129. DOI: 10.1074/jbc.M206941200.

Verhagen, L. M., P. W. M. Hermans, A. Warris, R. De Groot, M. Maes, J. A. Villalba, B. Del Nogal, S. Van Den Hof, L. Mughini Gras, D. Van Soolingen, E. Pinelli, and J. H. De Waard (2012). "Helminths and skewed cytokine profiles increase tuberculin skin test positivity in Warao Amerindians". In: *Tuberculosis* 92 (6), pp. 505–512. DOI: 10.1016/j.tube.2012.07.004.

Verschoor, M. L. and G. Singh (2013). "Ets-1 regulates intracellular glutathione levels: key target for resistant ovarian cancer." In: *Molecular cancer* 12 (1), p. 138. DOI: 10.1186/1476-4598-12-138.

Verstrepen, L., I. Carpentier, K. Verhelst, and R. Beyaert (2009). "ABINs: A20 binding inhibitors of NF-kB and apoptosis signaling". In: *Biochemical Pharmacology* 78 (2), pp. 105–114. DOI: 10.1016/j.bcp.2009.02.009.

Vliet, S. J. van, J. den Dunnen, S. I. Gringhuis, T. B. Geijtenbeek, and Y. van Kooyk (2007). "Innate signaling and regulation of Dendritic cell immunity." In: *Current opinion in immunology* 19 (4), pp. 435–40. DOI: 10.1016/j.coi.2007.05.006.

Vukman, K. V., P. N. Adams, and S. M. O'Neill (2013). "Fasciola hepatica tegumental coat antigen suppresses MAPK signalling in dendritic cells and up-regulates the expression of SOCS3." In: *Parasite immunology* (January), pp. 234–238. DOI: 10.1111/pim.12033.

Wagner, A. H., M. Conzelmann, F. Fitzer, T. Giese, K. G??low, C. S. Falk, O. H. Kr??mer, S. Dietrich, M. Hecker, and T. Luft (2015). "JAK1/STAT3 activation directly inhibits IL-12 production in dendritic cells by preventing CDK9/P-TEFb recruitment to the p35 promoter". In: *Biochemical Pharmacology* 96, pp. 52–64. DOI: 10.1016/j.bcp.2015.04.019.

Wagner, S., I. Carpentier, V. Rogov, M. Kreike, F. Ikeda, F. Löhr, C.-J. Wu, J. D. Ashwell, V. Dötsch, I. Dikic, and R. Beyaert (2008). "Ubiquitin binding mediates the NF-kappaB inhibitory potential of ABIN proteins." In: *Oncogene* 27 (26), pp. 3739–45. DOI: 10.1038/sj.onc.1211042.

Walker, J. a., J. L. Barlow, and A. N. J. McKenzie (2013). "Innate lymphoid cells - how did we miss them?" In: *Nature reviews. Immunology* 13 (2), pp. 75–87. DOI: 10.1038/nri3349.

Walsh, E. R., N. Sahu, J. Kearley, E. Benjamin, B. H. Kang, A. Humbles, and A. August (2008). "Strain-specific requirement for eosinophils in the recruitment of T cells to the lung during the development of allergic asthma." In: *The Journal of experimental medicine* 205 (6), pp. 1285–92. DOI: 10.1084/jem.20071836.

Wammes, L. J., F. Hamid, A. E. Wiria, B. De Gier, E. Sartono, R. M. Maizels, A. J. F. Luty, Y. Fillié, G. T. Brice, T. Supali, H. H. Smits, and M. Yazdanbakhsh (2010). "Regulatory T cells in human geohelminth infection suppress immune responses to BCG and Plasmodium falciparum". In: *European Journal of Immunology* 40 (2), pp. 437–442. DOI: 10.1002/eji.200939699.

Wan, Y., H. Xiao, J. Affolter, T. W. Kim, K. Bulek, S. Chaudhuri, D. Carlson, T. Hamilton, B. Mazumder, G. R. Stark, J. Thomas, and X. Li (2009). "Interleukin-1 receptor-associated kinase 2 is critical for lipopolysaccharide-mediated post-transcriptional control". In: *Journal of Biological Chemistry* 284 (16), pp. 10367–10375. DOI: 10.1074/jbc.M807822200.

Wang, C., L. Deng, M. Hong, G. R. Akkaraju, J. Inoue, and Z. J. Chen (2001). "TAK1 is a ubiquitin-dependent kinase of MKK and IKK." In: *Nature* 412 (6844), pp. 346–51. DOI: 10.1038/35085597.

Wang, H., Z. Su, and J. Schwarze (2009). "Healthy but not RSV-infected lung epithelial cells profoundly inhibit T cell activation". In: *Thorax* 64 (4), pp. 283–290. DOI: 10.1136/thx.2007.094870.

Wang, H., C. Zhao, M. Zhang, C. M. Lee, E. P. Reddy, and S. K. P. Kung (2013). "A novel role of the scaffolding protein JLP in tuning CD40-induced activation of dendritic cells." In: *Immunobiology* 218 (6), pp. 835–43. DOI: 10.1016/j.imbio.2012.10.002.

Wang, X., W. Li, D. Zhao, B. Liu, Y. Shi, H. Yang, P. Guo, X. Geng, Z. Shang, E. Peden, S. Mitani, and D. Xue (2010). "C. elegans transthyretin-like protein TTR-52 mediates recognition of apoptotic cells by the CED-1 phagocyte receptor". In: *Nature Cell Biology* 12 (7), pp. 655–664. DOI: 10.1038/ncb2068.C..

Wang, Y., Y. Tang, L. Teng, Y. Wu, X. Zhao, and G. Pei (2006). "Association of beta-arrestin and TRAF6 negatively regulates Toll-like receptor-interleukin 1 receptor signaling." In: *Nature immunology* 7 (2), pp. 139–147. DOI: 10.1038/ni1294.

Wang, Y., H. Zhou, Y. Shen, Y. Wang, W. Wu, H. Liu, Z. Yuan, Y. Xu, Y. Hu, and J. Cao (2015). "Impairment of dendritic cell function and induction of CD4(+)CD25(+)Foxp3(+) T cells by excretory-secretory products: a potential mechanism of immune evasion adopted by Echinococcus granulosus." In: *BMC immunology* 16, p. 44. DOI: 10.1186/s12865-015-0110-3.

Wang, Y., T. Chen, C. Han, D. He, H. Liu, H. An, Z. Cai, and X. Cao (2007). "Lysosome-associated small Rab GTPase Rab7b negatively regulates TLR4 signaling in macrophages

by promoting lysosomal degradation of TLR4". In: *Blood* 110 (3), pp. 962–971. DOI: 10.1182/blood-2007-01-066027.

Wasylyk, B., J. Hagman, and A. Gutierrez-Hartmann (1998). "Ets transcription factors: Nuclear effectors of the Ras-MAP-kinase signaling pathway". In: *Trends in Biochemical Sciences* 23 (6), pp. 213–216. DOI: 10.1016/S0968-0004(98)01211-0.

Weller, C. L., S. J. Collington, T. Williams, and J. R. Lamb (2011). "Mast cells in health and disease." In: *Clinical Science* 120 (11), pp. 473–484. DOI: 10.1042/CS20100459.

Wertz, I. E., K. M. O'Rourke, H. Zhou, M. Eby, L. Aravind, S. Seshagiri, P. Wu, C. Wiesmann, R. Baker, D. L. Boone, A. Ma, E. V. Koonin, and V. M. Dixit (2004). "De-ubiquitination and ubiquitin ligase domains of A20 downregulate NF-kB signalling". In: *Nature* 430 (7000), pp. 694–699. DOI: 10.1038/nature02794.

Wesche, H., W. J. Henzel, W. Shillinglaw, S. Li, Z. Cao, and E. Alerts (1997). "MyD88: An Adapter That Recruits IRAK to the IL-1 Receptor Complex". In: *Immunity* 7, pp. 837–847.

Whelan, M., M. M. Harnett, K. M. Houston, V. Patel, W. Harnett, and K. P. Rigley (2000). "A filarial nematode-secreted product signals dendritic cells to acquire a phenotype that drives development of Th2 cells." In: *Journal of immunology (Baltimore, Md. : 1950)* 164, pp. 6453–6460. DOI: 10.4049/jimmunol.164.12.6453.

White, C., X. Yuan, P. J. Schmidt, E. Bresciani, T. K. Samuel, D. Campagna, C. Hall, K. Bishop, M. L. Calicchio, A. Lapierre, D. M. Ward, P. Liu, M. D. Fleming, and I. Hamza (2013). "HRG1 is essential for heme transport from the phagolysosome of macrophages during erythrophagocytosis". In: *Cell Metabolism* 17 (2), pp. 261–270. DOI: 10.1016/j.cmet.2013.01.005. arXiv: NIHMS150003.

Whitmore, M. M., A. Iparraguirre, L. Kubelka, W. Weninger, T. Hai, and B. R. G. Williams (2007). "Negative regulation of TLR-signaling pathways by activating transcription factor-3." In: *Journal of immunology (Baltimore, Md. : 1950)* 179 (6), pp. 3622–30.

Whitney, M. L., L. S. Jefferson, and S. R. Kimball (2009). "ATF4 is necessary and sufficient for ER stress-induced upregulation of REDD1 expression". In: *Biochemical and Biophysical Research Communications* 379 (2), pp. 451–455. DOI: 10.1016/j.bbrc.2008.12.079.

Williams, J. W., M. Y. Tjota, B. S. Clay, B. Vander Lugt, H. S. Bandukwala, C. L. Hrusch, D. C. Decker, K. M. Blaine, B. R. Fixsen, H. Singh, R. Sciammas, and A. I. Sperling (2013). "Transcription factor IRF4 drives dendritic cells to promote Th2 differentiation." In: *Nature communications* 4 (May), p. 2990. DOI: 10.1038/ncomms3990.

Wilson, M. S. and R. M. Maizels (2004). "Regulation of allergy and autoimmunity in helminth infection." In: *Clinical Reviews in Allergy & Immunology* 26 (1), pp. 35–50. DOI: 10.1385/CRIAI:26:1:35.

Wilson, M. S., M. D. Taylor, A. Balic, C. A. M. Finney, J. R. Lamb, and R. M. Maizels (2005). "Suppression of allergic airway inflammation by helminth-induced regulatory T cells." In: *The Journal of Experimental Medicine* 202 (9), pp. 1199–212. DOI: 10.1084/jem.20042572.

Wilson, M. S., M. D. Taylor, M. T. O'Gorman, A. Balic, T. A. Barr, K. Filbey, S. M. Anderton, and R. M. Maizels (2010). "Helminth-induced CD19+CD23hi B cells modulate experimental allergic and autoimmune inflammation." In: *European Journal of Immunology* 40 (6), pp. 1682–96. DOI: 10.1002/eji.200939721.

Witte, M. B. and A. Barbul (2003). "Arginine physiology and its implication for wound healing". In: *Wound Repair and Regeneration* 11 (6), pp. 419–423. DOI: 10.1046/j.1524-475X.2003.11605.x.

Wolday, D., S. Mayaan, Z. G. Mariam, N. Berhe, T. Seboxa, S. Britton, N. Galai, A. Landay, and Z. Bentwich (2002). "Treatment of intestinal worms is associated with decreased HIV plasma viral load." In: *Journal of Acquired Immune Deficiency Syndromes* 31 (1), pp. 56–62. DOI: 10.1097/00126334-200209010-00008.

Worbs, T. (2006). "Oral tolerance originates in the intestinal immune system and relies on antigen carriage by dendritic cells". In: *Journal of Experimental Medicine* 203 (3), pp. 519–527. DOI: 10.1084/jem.20052016. arXiv: 177.

Wu, M. H., S. C. Lin, K. Y. Hsiao, and S. J. Tsai (2011). "Hypoxia-inhibited dual-specificity phosphatase-2 expression in endometriotic cells regulates cyclooxygenase-2 expression". In: *Journal of Pathology* 225 (3), pp. 390–400. DOI: 10.1002/path.2963.

Wu, W., C. He, C. Liu, A. T. Cao, X. Xue, H. L. Evans-marin, M. Sun, L. Fang, S. Yao, I. V. Pinchuk, D. W. Powell, Z. Liu, and Y. Cong (2015). "miR-10a inhibits dendritic cell activation and Th1 / Th17 cell immune responses in IBD". In: *Gut* 64, pp. 1755–1764. DOI: 10.1136/gutjnl-2014-307980.

Wulff, H., P. Calabresi, and R. Allie (2003). "The voltage-gated Kv1. 3 K+ channel in effector memory T cells as new target for MS". In: *Journal of Clinical ...* 111 (11), pp. 1703–1713. DOI: 10.1172/JCI200316921.Introduction.

Wulff, H., H.-G. Knaus, M. Pennington, and K. G. Chandy (2004). "K+ channel expression during B cell differentiation: implications for immunomodulation and autoimmunity." In: *Journal of immunology (Baltimore, Md. : 1950)* 173 (2), pp. 776–86.

Wullaert, A., L. Verstrepen, S. Van Huffel, M. Adib-Conquy, S. Cornelis, M. Kreike, M. Haegman, K. El Bakkouri, M. Sanders, K. Verhelst, I. Carpentier, J. M. Cavaillon, K. Heyninck, and R. Beyaert (2007). "LIND/ABIN-3 is a novel lipopolysaccharide-inducible inhibitor of NF-??B activation". In: *Journal of Biological Chemistry* 282 (1), pp. 81–90. DOI: 10.1074/jbc.M607481200.

Xiao, N., H. Li, J. Luo, R. Wang, H. Chen, J. Chen, and P. Wang (2012). "Ubiquitin-specific protease 4 (USP4) targets TRAF2 and TRAF6 for deubiquitination and inhibits TNFα-induced cancer cell migration." In: *The Biochemical journal* 441 (3), pp. 979–86. DOI: 10.1042/BJ20111358.

Xu, S., J. Huo, K.-G. Lee, T. Kurosaki, and K.-P. Lam (2009). "Phospholipase Cgamma2 is critical for Dectin-1-mediated Ca2+ flux and cytokine production in dendritic cells." In: *The Journal of biological chemistry* 284 (11), pp. 7038–46. DOI: 10.1074/jbc.M806650200.

Xu, Z., H. Zan, E. J. Pone, T. Mai, and P. Casali (2012). "Immunoglobulin class-switch DNA recombination: induction, targeting and beyond." In: *Nature reviews. Immunology* 12 (7), pp. 517–31. DOI: 10.1038/nri3216.

Xue, X., T. Feng, S. Yao, K. J. Wolf, C. G. Liu, X. Liu, C. O. Elson, and Y. Cong (2011). "Microbiota downregulates dendritic cell expression of miR-10a, which targets IL-12/IL-23p40". In: *Journal of Immunology* 187 (11), pp. 5879–5886. DOI: jimmunol.1100535[pii]\r10.4049/jimmunol.1100535.

Xue, X., A. T. Cao, X. Cao, S. Yao, E. D. Carlsen, L. Soong, C. G. Liu, X. Liu, Z. Liu, L. W. Duck, C. O. Elson, and Y. Cong (2014). "Downregulation of microRNA-107 in intestinal CD11c+ myeloid cells in response to microbiota and proinflammatory cytokines increases IL-23p19 expression". In: *European Journal of Immunology* 44 (3), pp. 673–682. DOI: 10.1002/eji.201343717.

Yamamoto, M., S. Sato, H. Hemmi, and H. Sanjo (2002). "Essential role for TIRAP in activation of the signalling cascade shared by TLR2 and TLR4". In: *Nature* 420 (November), pp. 324–329. DOI: 10.1038/nature01190.1..

Yamamoto, M., S. Sato, H. Hemmi, K. Hoshino, T. Kaisho, H. Sanjo, O. Takeuchi, M. Sugiyama, M. Okabe, K. Takeda, and S. Akira (2003a). "Role of adaptor TRIF in the MyD88-independent toll-like receptor signaling pathway." In: *Science* 301 (5633), pp. 640–3. DOI: 10.1126/science.1087262.

Yamamoto, M., S. Sato, H. Hemmi, S. Uematsu, K. Hoshino, T. Kaisho, O. Takeuchi, K. Takeda, and S. Akira (2003b). "TRAM is specifically involved in the Toll-like receptor 4-mediated MyD88-independent signaling pathway." In: *Nature immunology* 4 (11), pp. 1144–50. DOI: 10.1038/ni986.

Yao, M., X. Liu, D. Li, T. Chen, Z. Cai, and X. Cao (2009). "Late endosome/lysosome-localized Rab7b suppresses TLR9-initiated proinflammatory cytokine and type I IFN production in macrophages." In: *Journal of Immunology* 183 (3), pp. 1751–1758. DOI: 10.4049/jimmunol.0900249.

Yazdanbakhsh, M., P. G. Kremsner, and R. van Ree (2002). "Allergy , Parasites , and the Hygiene Hypothesis". In: *Science* 296, pp. 490–495. DOI: 10.1126/science.296.5567.490.

Yemaneberhan, H., Z. Bekele, A. Venn, S. Lewis, E. Parry, and J. Britton (1997). "Prevalence of wheeze and asthma and relation to atopy in urban and rural Ethiopia". In: *Lancet* 350 (9071), pp. 85–90. DOI: 10.1016/S0140-6736(97)01151-3.

Yoneyama, M., M. Kikuchi, T. Natsukawa, N. Shinobu, T. Imaizumi, M. Miyagishi, K. Taira, S. Akira, and T. Fujita (2004). "The RNA helicase RIG-I has an essential function in double-stranded RNA-induced innate antiviral responses." In: *Nature immunology* 5 (7), pp. 730–737. DOI: 10.1038/ni1087.

Yoshida, H., H. Jono, H. Kai, and J. D. Li (2005a). "The tumor suppressor cylindromatosis (CYLD) acts as a negative regulator for toll-like receptor 2 signaling via negative cross-talk with TRAF6 and TRAF7". In: *Journal of Biological Chemistry* 280 (49), pp. 41111–41121. DOI: 10.1074/jbc.M509526200.

Yoshida, K., K. Yamamoto, T. Kohno, N. Hironaka, K. Yasui, C. Kojima, H. Mukae, J. I. Kadota, S. Suzuki, K. Honma, S. Kohno, and T. Matsuyama (2005b). "Active repression of IFN regulatory factor-1-mediated transactivation by IFN regulatory factor-4". In: *International Immunology* 17 (11), pp. 1463–1471. DOI: 10.1093/intimm/dxh324.

Yu, Y. and G. S. Hayward (2010). "The Ubiquitin E3 Ligase RAUL Negatively Regulates Type I Interferon through Ubiquitination of the Transcription Factors IRF7 and IRF3". In: *Immunity* 33 (6), pp. 863–877. DOI: 10.1016/j.immuni.2010.11.027.

Yuk, J.-M., D.-M. Shin, H.-M. Lee, J.-J. Kim, S.-W. Kim, H. S. Jin, C.-S. Yang, K. A. Park, D. Chanda, D.-K. Kim, S. M. Huang, S. K. Lee, C.-H. Lee, J.-M. Kim, C.-H. Song, S. Y. Lee,

G. M. Hur, D. D. Moore, H.-S. Choi, and E.-K. Jo (2011). "The orphan nuclear receptor SHP acts as a negative regulator in inflammatory signaling triggered by Toll-like receptors." In: *Nature immunology* 12 (8), pp. 742–751. DOI: 10.1038/ni.2064.

Zabel, U., T. Henkel, M. S. Silva, and P. A. Baeuerle (1993). "Nuclear uptake control of NF-kappa B by MAD-3, an I kappa B protein present in the nucleus." In: *The EMBO journal* 12 (1), pp. 201–11.

Zanoni, I. and F. Granucci (2012). "Regulation and dysregulation of innate immunity by NFAT signaling downstream of pattern recognition receptors (PRRs)". In: *European Journal of Immunology* 42 (8), pp. 1924–1931. DOI: 10.1002/eji.201242580.

Zanoni, I., R. Ostuni, G. Capuano, M. Collini, M. Caccia, A. E. Ronchi, M. Rocchetti, F. Mingozzi, M. Foti, G. Chirico, B. Costa, A. Zaza, P. Ricciardi-Castagnoli, and F. Granucci (2009). "CD14 regulates the dendritic cell life cycle after LPS exposure through NFAT activation." In: *Nature* 460 (7252), pp. 264–8. DOI: 10.1038/nature08118.

Zanoni, I., R. Ostuni, L. R. Marek, S. Barresi, R. Barbalat, G. M. Barton, F. Granucci, and J. C. Kagan (2011). "CD14 controls the LPS-induced endocytosis of Toll-like receptor 4." In: *Cell* 147 (4), pp. 868–80. DOI: 10.1016/j.cell.2011.09.051.

Zhang, C., N. Bai, A. Chang, Z. Zhang, J. Yin, W. Shen, Y. Tian, R. Xiang, and C. Liu (2013). "ATF4 is directly recruited by TLR4 signaling and positively regulates TLR4-trigged cytokine production in human monocytes." In: *Cellular & molecular immunology* 10 (1), pp. 84–94. DOI: 10.1038/cmi.2012.57.

Zhang, F. X., C. J. Kirschning, R. Mancinelli, X. P. Xu, Y. Jin, E. Faure, A. Mantovani, M. Rothe, M. Muzio, and M. Arditi (1999). "Bacterial lipopolysaccharide activates nuclear factor-kappaB through interleukin-1 signaling mediators in cultured human dermal endothelial cells and mononuclear phagocytes." In: *The Journal of biological chemistry* 274 (12), pp. 7611–4.

Zhang, G. and S. Ghosh (2002). "Negative regulation of toll-like receptor-mediated signaling by Tollip". In: *Journal of Biological Chemistry* 277 (9), pp. 7059–7065. DOI: 10.1074/jbc.M109537200.

Zhang, H., H. Hu, N. Greeley, J. Jin, A. J. Matthews, E. Ohashi, M. S. Caetano, H. S. Li, X. Wu, P. K. Mandal, J. S. McMurray, S. J. Moghaddam, S.-C. Sun, and S. S. Watowich (2014). "STAT3 restrains RANK- and TLR4-mediated signalling by suppressing expression of the E2 ubiquitin-conjugating enzyme Ubc13". In: *Nature Communications* 5, p. 5798. DOI: 10.1038/ncomms6798.

Zhang, Q., M. Muller, C. H. Chen, L. Zeng, A. Farooq, and M. M. Zhou (2005). "New insights into the catalytic activation of the MAPK phosphatase PAC-1 induced by its substrate MAPK ERK2 binding". In: *Journal of Molecular Biology* 354 (4), pp. 777–788. DOI: 10.1016/j.jmb.2005.10.006.

Zhao, A., J. F. Urban, R. M. Anthony, R. Sun, J. Stiltz, N. van Rooijen, T. A. Wynn, W. C. Gause, and T. Shea-Donohue (2008). "Th2 Cytokine-Induced Alterations in Intestinal Smooth Muscle Function Depend on Alternatively Activated Macrophages". In: *Gastroenterology* 135 (1), pp. 217–225. DOI: 10.1053/j.gastro.2008.03.077. arXiv: NIHMS150003.

Zhao, Q., E. G. Shepherd, M. E. Manson, L. D. Nelin, A. Sorokin, and Y. Liu (2005). "The role of mitogen-activated protein kinase phosphatase-1 in the response of alveolar macrophages to lipopolysaccharide: attenuation of proinflammatory cytokine biosynthesis via feedback control of p38." In: *The Journal of biological chemistry* 280 (9), pp. 8101–8. DOI: 10.1074/jbc.M411760200.

Zhao, Q., X. Wang, L. D. Nelin, Y. Yao, R. Matta, M. E. Manson, R. S. Baliga, X. Meng, C. V. Smith, J. a. Bauer, C.-H. Chang, and Y. Liu (2006). "MAP kinase phosphatase 1 controls innate immune responses and suppresses endotoxic shock." In: *The Journal of experimental medicine* 203 (1), pp. 131–40. DOI: 10.1084/jem.20051794.

Zhao, W., L. Wang, M. Zhang, C. Yuan, and C. Gao (2012). "E3 ubiquitin ligase tripartite motif 38 negatively regulates TLR-mediated immune responses by proteasomal degradation of TNF receptor-associated factor 6 in macrophages." In: *Journal of immunology (Baltimore, Md. : 1950)* 188 (6), pp. 2567–74. DOI: 10.4049/jimmunol.1103255.

Zhong, J., P. Yang, K. Muta, R. Dong, M. Marrero, F. Gong, and C. Y. Wang (2010). "Loss of Jak2 selectively suppresses DC-mediated innate immune response and protects mice from lethal dose of LPS-induced septic shock". In: *PLoS ONE* 5 (3). DOI: 10.1371/journal.pone.0009593.

Zhou, F., X. Zhang, H. Van Dams, P. Ten Dijkes, H. Huang, and L. Zhangs (2012). "Ubiquitin-specific protease 4 mitigates toll-like/interleukin-1 receptor signaling and regulates innate immune activation". In: *Journal of Biological Chemistry* 287 (14), pp. 11002–11010. DOI: 10.1074/jbc.M111.328187.

Zhou, H., J. Xiao, N. Wu, C. Liu, J. Xu, F. Liu, and L. Wu (2015). "MicroRNA-223 Regulates the Differentiation and Function of Intestinal Dendritic Cells and Macrophages by Targeting C/EBP??" In: *Cell Reports* 13 (6), pp. 1149–1160. DOI: 10.1016/j.celrep.2015.09.073.

Zhu, C., K. Gagnidze, J. H. Gemberling, and S. E. Plevy (2001). "Characterization of an activation protein-1-binding site in the murine interleukin-12 p40 promoter. Demonstration of novel functional elements by a reductionist approach." In: *The Journal of biological chemistry* 276 (21), pp. 18519–28. DOI: 10.1074/jbc.M100440200.

Zhu, C., K. Rao, H. Xiong, K. Gagnidze, F. Li, C. Horvath, and S. Plevy (2003). "Activation of the murine interleukin-12 p40 promoter by functional interactions between NFAT and ICSBP." In: *The Journal of biological chemistry* 278 (41), pp. 39372–82. DOI: 10.1074/jbc.M306441200.

Zhu, X., B. L. Schweitzer, E. J. Romer, C. E. W. Sulentic, and R. P. DeKoter (2008). "Transgenic expression of Spi-C impairs B-cell development and function by affecting genes associated with BCR signaling". In: *European Journal of Immunology* 38 (9), pp. 2587–2599. DOI: 10.1002/eji.200838323.

Appendices

A. Scripts written for data analysis

A.1 Sorting flow cytometry data

```
#! /usr/bin/python

InFileName = raw_input("Name of file: ")
NumberOfReplicates = input("How many replicates: ")
if NumberOfReplicates == 3:
    NumberOfSingleStainings = input("How many single
       stainings: ")
    OutFileName = InFileName + '_sorted.txt'

    InFilePath = "/home/drea/Dropbox/PhD/toGraphUp/
       TablesForScripts/" + InFileName # add path to file
       name
    OutFilePath = "/home/drea/Dropbox/PhD/toGraphUp/
       TablesForScripts/OutFolder/" + OutFileName

    InFile = open(InFilePath, 'rU')
    OutFile = open(OutFilePath, 'w')

    ListOfLines = []
    ListOfEntries = []
    ListOfDataEntries = []


    for Line in InFile:# add lines in the file to a list
       and strip line endings
        Line = Line.strip()
        ListOfLines.append(str(Line))

    for Entry in ListOfLines:# separate the values in the
```

```
        lines using the tab as separator
25          ListOfEntries = Entry.split("\t")
26          ListOfDataEntries.append(ListOfEntries)# save lines
                as list of lists of values
27
28      ShortenedListOfDataEntries = ListOfDataEntries[
            NumberOfSingleStainings + 1 : -2] # delete header,
            single stainings and mean, stddev
29
30      Run = 0
31      ListOfRow = []
32      ListOfLOR = []
33
34      while Run <= len(ListOfEntries) - 1:# sort columns into
            rows
35          for List in ShortenedListOfDataEntries:
36              Entry = List[Run]# take same entry from each
                    list (= corresponding columns)
37              ListOfRow.append(Entry)# write it in new list
38          ListOfLOR.append(ListOfRow)
39          ListOfRow = []
40          Run += 1
41
42      ListNumber = 0
43      Headers = ListOfDataEntries[0]
44
45      for List in ListOfLOR:# sort the rows of data in triple
            blocks - works only on Triplicates!
46          Run = 1
47          ListFirst = []
48          ListSecond = []
49          ListThird = []
50          while Run <= len(ShortenedListOfDataEntries):
51              if Run % 3 == 0:
52                  ListThird.append(List[Run-1])
53              elif (Run + 1) % 3 == 0:
54                  ListSecond.append(List[Run-1])
55              else:
```

```
56                  ListFirst.append(List[Run-1])
57              Run += 1
58          ConvertThird = "\t".join(ListThird) + "\n"#
               converts sorted lists into strings with tabs
               between single data points and line endings
59          ConvertSecond = "\t".join(ListSecond) + "\n"
60          ConvertFirst = "\t".join(ListFirst) + "\n"
61          ConvertHeader = str(Headers[ListNumber]) + "\n"#
               add gate name to block of data
62          OutFile.write(ConvertHeader)
63          OutFile.write(ConvertFirst)# writes strings into
               OutFile
64          OutFile.write(ConvertSecond)
65          OutFile.write(ConvertThird)
66          OutFile.write("\n")
67          ListNumber += 1
68
69      InFile.close()
70      OutFile.close()
71
72
73
74  elif NumberOfReplicates == 2:
75      NumberOfSingleStainings = input("How many single
           stainings: ")
76      OutFileName = raw_input("Name of the resulting file: ")
77
78      InFilePath = "/Users/andreakemter/Data/TablesForScripts
           /" + InFileName # add path to file name
79      OutFilePath = "/Users/andreakemter/Data/Scripts/
           OutFolder/" + OutFileName
80
81      InFile = open(InFilePath, 'rU')
82      OutFile = open(OutFilePath, 'w')
83
84      ListOfLines = []
85      ListOfEntries = []
86      ListOfDataEntries = []
```

```
87
88
89      for Line in InFile:# add lines in the file to a list
            and strip line endings
90          Line = Line.strip()
91          ListOfLines.append(str(Line))
92
93      for Entry in ListOfLines:# separate the values in the
            lines using the tab as separator
94          ListOfEntries = Entry.split("\t")
95          ListOfDataEntries.append(ListOfEntries)# save lines
                as list of lists of values
96
97      ShortenedListOfDataEntries = ListOfDataEntries[
            NumberOfSingleStainings + 1 : -2] # delete header,
            single stainings and mean, stddev
98
99      Run = 0
100     ListOfRow = []
101     ListOfLOR = []
102
103     while Run <= len(ListOfEntries) - 1:# sort columns into
            rows
104         for List in ShortenedListOfDataEntries:
105             Entry = List[Run]# take same entry from each
                    list (= corresponding columns)
106             ListOfRow.append(Entry)# write it in new list
107         ListOfLOR.append(ListOfRow)
108         ListOfRow = []
109         Run += 1
110
111     ListNumber = 0
112     Headers = ListOfDataEntries[0]
113
114     for List in ListOfLOR:# sort the rows of data in triple
            blocks - works only on Duplicates!
115         Run = 1
116         ListFirst = []
```

```
117         ListSecond = []
118         ListThird = []
119         while Run <= len(ShortenedListOfDataEntries):
120             if Run % 2 == 0:
121                 ListSecond.append(List[Run-1])
122             else:
123                 ListFirst.append(List[Run-1])
124             Run += 1
125         ConvertSecond = "\t".join(ListSecond) + "\n"#
               converts sorted lists into strings with tabs
               between single data points and line endings
126         ConvertFirst = "\t".join(ListFirst) + "\n"
127         ConvertHeader = str(Headers[ListNumber]) + "\n"#
               add gate name to block of data
128         OutFile.write(ConvertHeader)
129         OutFile.write(ConvertFirst)# writes strings into
               OutFile
130         OutFile.write(ConvertSecond)
131         OutFile.write("\n")
132         ListNumber += 1
133
134     InFile.close()
135     OutFile.close()
136
137
138 else:
139     print "Error!"
140     print "Script needs duplicates or triplicates; please
           adjust script in sort-block."
```

A.2 Sorting ELISA data

```
#! usr/bin/env python

print "File names must be ELISA_plateNumber.txt (example:
    IL12_3.txt), with continuous plate numbers, and script
    needs 3 replicates per group! \n \n"
ELISA = raw_input("What ELISA do you want to sort? ")
NumberOfPlates = input("How many plates? ")

for Plate in range(1, NumberOfPlates + 1):
    InFileName = ELISA + "_" + str(Plate)
    OutFileName = "/home/drea/Dropbox/PhD/toGraphUp/160305-
       ELISAs/read2/sorted/" + InFileName + ".csv"
    InFilePath = "/home/drea/Dropbox/PhD/toGraphUp/160305-
       ELISAs/read2/txt/" + InFileName + ".txt" # add path
       to file name

    InFile = open(InFilePath, 'rU')
    OutFile = open(OutFileName, 'w')

    ListOfLines = []
    ListOfSamples = []
    ListOfEntries = []
    ListOfDataEntries = []
    ListOfMeans = []
    ListForPrism = []

    for Line in InFile:# add lines in the file to a list
       and strip line endings
        Line = Line.strip()
        ListOfLines.append(str(Line))

    for Entry in ListOfLines:
        if Entry != "":#ignore all empty entrys
            if Entry[0]=="U" and Entry[1]=="n" and Entry
               [4]=="\t": # take only lines with sample
```

```
                readings in them, those start with Un\d\d\t
29                ListOfSamples.append(Entry)
30
31      for Entry in ListOfSamples:# separate the values in the
            lines using the tab as separator
32          ListOfEntries = Entry.split("\t")
33          ListOfDataEntries.append(ListOfEntries)# save lines
                as list of lists of values
34
35      for Entry in ListOfDataEntries:
36          Mean = Entry[5]
37          if Mean == "Range?":# find the samples that were
               below detection limit and set concentration to 0
                (caution with values over!)
38              Mean = 0
39          ListForPrism.append(Mean)# creating a list with the
                mean concentrations
40          Mean = str(Mean) + "\n"
41          ListOfMeans.append(Mean)
42
43      StringOfListOfMeans = ''.join(ListOfMeans)
44
45      OutFile.write(StringOfListOfMeans)#writing all the
           means into one column, just in case different
           sorting is needed...
46      OutFile.write("\n")
47
48      Run = 1# sorting values into blocks of three, for the
           triplicates per group
49      ListOfThird = []
50      ListOfSecond = []
51      ListOfFirst = []
52
53      for Entry in ListForPrism:
54          if Run % 3 == 0:
55              ListOfThird.append(Entry)
56          elif (Run + 1) % 3 == 0:
57              ListOfSecond.append(Entry)
```

```
58          else:
59              ListOfFirst.append(Entry)
60          Run += 1
61
62      StringFirst = str(ListOfFirst) + "\n"
63      StringSecond = str(ListOfSecond) + "\n"
64      StringThird = str(ListOfThird) + "\n"
65      OutFile.write(StringFirst)
66      OutFile.write(StringSecond)
67      OutFile.write(StringThird)
68
69      InFile.close()
70      OutFile.close()
71
72
73  print "\n \n Done!"
```

A.3 Comparing fraction protein content

```
1  #! /usr/bin/python
2
3  UserName = 'drea'
4  ListOfFileNames = ['14.txt', '15.txt', '39.txt', '40.txt']
                #these files need to contain the accession
       numbers as >...\n
5  OutFileName = 'SharedHits.txt'
6  DatabaseFileName = 'Database.txt'
7  InFilePath = '/home/' + UserName + '/Dropbox/PhD/CP/
       HESproteomics/DCMod-S2AnEx1_Glasgow/'
8  OutFilePath = InFilePath + 'Results/'
9
10
11 #To load the database into a dictionary, so shared hits can
        later be looked up in database and all info printed in
       file automatically:
12 DicOfDatabase = {}
```

```
13
14 DatabaseFile = open(InFilePath + DatabaseFileName, 'rU')
15
16 for Line in DatabaseFile:
17     ListOfLine = Line.split(' ')
18     Description = ' '.join(ListOfLine[1: -1])
                    #to get accession number, blast info and
        sequence in different entries
19     ListOfDescription = Description.split(',')
20     Description = ';'.join(ListOfDescription)
                    #getting rid of , in description so file
        can be saved as .csv
21     Sequence = ListOfLine[-1]
                    #getting rid of \n
22     DicOfDatabase[ListOfLine[0]] = [Description, Sequence
       [:-1]]     #store database in dictionary with
       accession numbers as keys and blast info and
       sequences stored as nested lists
23
24 DatabaseFile.close()
25
26
27 #make a list of all the protein hits and store fraction
    contents in dictionary
28 ListOfLines = []
29 DicOfFractions = {}
30
31 for File in ListOfFileNames:
32     InFile = open(InFilePath + File, 'rU')
33     DicOfFractions[File] = []
                    #fraction number is key of dictionary
34     for Line in InFile:
35         ListOfLines.append(Line)
36         DicOfFractions[File].append(Line)
                        #with protein accession number as
           value
37     InFile.close()
38
```

```
39
40 SetOfLines = set(ListOfLines)
41 ListOfHits = list(SetOfLines)
                #make sure list contains each accession
    number only once
42
43
44 #make a dictionary with protein accession number as key and
     fractions as values
45 DicOfHits = {}
46
47 for Hit in ListOfHits:
48     DicOfHits[Hit] = []
49     for Fraction in ListOfFileNames:
50         if Hit in DicOfFractions[Fraction]:
51             DicOfHits[Hit].append(Fraction)
52
53 #check how many fractions each protein was found in and
    which, and store accession number in appropriate list
54 ListOfShared = []
55 ListOf141539 = []
56 ListOf141540 = []
57 ListOf143940 = []
58 ListOf153940 = []
59 ListOf2 = []
60 ListOf1 = []
61
62 for Hit in ListOfHits:
63     if Hit in DicOfHits:
64         if len(DicOfHits[Hit]) == 4:
65             ListOfShared.append(Hit)
66         elif len(DicOfHits[Hit]) == 3:
67             if '14.txt' in DicOfHits[Hit]:
68                 if '15.txt' in DicOfHits[Hit]:
69                     if '39.txt' in DicOfHits[Hit]:
70                         ListOf141539.append(Hit)
71                     else:
72                         ListOf141540.append(Hit)
```

```
73                  elif '39.txt' in DicOfHits[Hit]:
74                      ListOf143940.append(Hit)
75              else:
76                  ListOf153940.append(Hit)
77          elif len(DicOfHits[Hit]) == 2:
78              ListOf2.append(Hit)
79          else:
80              ListOf1.append(Hit)
81
82
83  #and write those lists into files
84  OutFileShared = open(OutFilePath + 'All4.csv', 'w')
85  for Entry in ListOfShared:
86      OutFileShared.write(Entry[:-1] + ',' + str(
           DicOfDatabase[Entry[:-1]]) + '\n')
87  OutFileShared.close()
88
89  OutFile141539 = open(OutFilePath + '14-15-39.csv', 'w')
90  for Entry in ListOf141539:
91      OutFile141539.write(Entry[:-1] + ',' + str(
           DicOfDatabase[Entry[:-1]]) + '\n')
92  OutFile141539.close()
93
94  OutFile141540 = open(OutFilePath + '14-15-40.csv', 'w')
95  for Entry in ListOf141540:
96      OutFile141540.write(Entry[:-1] + ',' + str(
           DicOfDatabase[Entry[:-1]]) + '\n')
97  OutFile141540.close()
98
99  OutFile143940 = open(OutFilePath + '14-39-40.csv', 'w')
100 for Entry in ListOf143940:
101     OutFile143940.write(Entry[:-1] + ',' + str(
           DicOfDatabase[Entry[:-1]]) + '\n')
102 OutFile143940.close()
103
104 OutFile153940 = open(OutFilePath + '15-39-40.csv', 'w')
105 for Entry in ListOf153940:
106     OutFile153940.write(Entry[:-1] + ',' + str(
```

```
        DicOfDatabase[Entry[:-1]]) + '\n')
OutFile153940.close()

OutFileTwo = open(OutFilePath + 'In2.csv', 'w')
for Entry in ListOf2:
    if Entry[:-1] in DicOfDatabase:
        OutFileTwo.write(Entry[:-1] + ',' + str(DicOfHits[
            Entry]) + ',' + str(DicOfDatabase[Entry[:-1]]) +
             '\n')
    else:
        OutFileTwo.write(Entry[:-1] + ',' + str(DicOfHits[
            Entry]) + '\n')
OutFileTwo.close()

OutFileOne = open(OutFilePath + 'In1.csv', 'w')
for Entry in ListOf1:
    if Entry[:-1] in DicOfDatabase:
        OutFileOne.write(Entry[:-1] + ',' + str(DicOfHits[
            Entry]) + ',' + str(DicOfDatabase[Entry[:-1]]) +
             '\n')
    else:
        OutFileOne.write(Entry[:-1] + ',' + str(DicOfHits[
            Entry]) + '\n')
OutFileOne.close()
```

A.4 Extraction of emPAI values

```
#! /usr/bin/python

class AutoVivification(dict):
    """Implementation of perl's autovivification feature.
       """
    def __getitem__(self, item):
        try:
            return dict.__getitem__(self, item)
        except KeyError:
            value = self[item] = type(self)()
            return value


UserName = 'XXX'
FileNames = ['XXX', 'XXX', 'XXX', '....']
SetOfFileNames = set(FileNames)
SetOfActive = set(ListOfActive)
InFilePath = '/Users/' + UserName + '/Desktop/MS_Comparison
    /'
OutFilePath = InFilePath + 'Results/'


"""To get all the lines with results in them (they start at
     line 70), then split them at the comma and grab columns
     containing accession numbers, descriptions and emPAI
    values:"""
DicOfemPAI = AutoVivification()
ListOfAllHits = []

for File in FileNames: #
                loop to open all the files specified before,
     get the names of protein hits and store a list of
    single hits for each one
    InFile = open(InFilePath + File + '.csv', 'rU')
    SetFile = open(OutFilePath + File + '.txt', 'w') #
```

```
                to get a result file with the list of
    single hits for one fraction
28
29      ListOfLines = []
30      Run = 1
31      for Line in InFile:
32          if Run > 69:
33              ListOfLines.append(Line) #
                            make a list of all lines with
                results
34          Run += 1
35
36      ListOfEntries = []
37
38      for Line in ListOfLines:
39          ListOfEntries = Line.split(',')
40          ListOfAllHits.append(ListOfEntries[2]) #
                        grab column with name of hit and put
            it in List for later use
41          if "emPAI" in ListOfEntries: #
                        if Hit comes with an emPAI value,
            grab it
42              DicOfemPAI[File][ListOfEntries[2]] =
                    ListOfEntries[-1]# and write it into
                    dictionary
43              del ListOfEntries[-27:-1]#
                            delete all entries in the list
                    between description and emPAI
44              del ListOfEntries[1]#
                            delete the second column as well
45              StringOfDescription = ''.join(ListOfEntries
                    [2:-1])#     in case there were some commas
                    in the description, put it back together
46              StremPAIHits = str(ListOfEntries[0]) + ',' +
                    str(ListOfEntries[1]) + ',' + str(
                    StringOfDescription) + ',' + str(
                    ListOfEntries[-1])
47              ListOfemPAIs.append(StremPAIHits)#
```

```
                                and put the line of group, hit,
                description, emPAI into a list to write in a
                 file
48
49      for Entry in ListOfemPAIs:
50          SetFile.write(Entry + '\n')#
                            write all the entries into a .txt
              file called like the fraction in the result
              folder
51
52
53  SetOfAllHits = set(ListOfAllHits)#
                create a list with all hits in it to loop
     through dictionaries
54  ListOfAllHits = list(SetOfAllHits)
55
56  '''Now sort through all the hits to get the emPAI profiles
     per hit and write them into a file'''
57  DicOfHitemPAIList = {}
58
59  for Hit in ListOfAllHits:#
                loop through all hits in every fraction
60      DicOfHitemPAIList[Hit] = []#
                    make list for the hit being processed
61      DicOfHitemPAIList['Header'] = []#
                    create entry in the list for the header
           of the table, saying which fractions
62      for Fraction in FileNames:#
                    to loop through all the fractions in the
            dictionary (by looping through list)
63          DicOfHitemPAIList['Header'].append(Fraction)#
                            write the name of the fraction into
              the list for the table header
64          if Hit in DicOfemPAI[Fraction]:#
                            if the hit has an emPAI in this
              fraction
65              DicOfHitemPAIList[Hit].append(DicOfemPAI[
                   Fraction][Hit][:-1])# append it to the list
```

```
66          else:#
                        if not
67              DicOfHitemPAIList[Hit].append('0')#
                            put a 0 into the list as
                   placeholder
68
69  emPAIfile = open(OutFilePath + 'emPAIs.csv', 'w')#
                   open the emPAI file and write the sorted
      emPAIs in
70  emPAIfile.write('All Hits with their emPAIs in the order in
       which you gave the filenames: \n')
71  emPAIfile.write('\n')
72  emPAIfile.write(',' + str(DicOfHitemPAIList['Header']) + '\
      n')
73
74  for Hit in ListOfAllHits:
75      emPAIfile.write(Hit + ',' + str(DicOfHitemPAIList[Hit])
            + '\n')
76
77  emPAIfile.close()
```

A.5 Comparing protein emPAI peaks

```
1  #! /usr/bin/python
2
3  class AutoVivification(dict):
4      """Implementation of perl's autovivification feature.
           """
5      def __getitem__(self, item):
6          try:
7              return dict.__getitem__(self, item)
8          except KeyError:
9              value = self[item] = type(self)()
10             return value
11
12 UserName = 'XXX'
```

```
13 FileNames = ['XXX', 'XXX', 'XXX']# fill in username of the
       account on your computer and the file names of your
       emPAI peaks .txt file
14 OutFileName = 'SharedHits.txt'
15 DatabaseFileName = 'Database.txt'
16 InFilePath = '/Users/' + UserName + '/Desktop/MS_Comparison
       /'
17 OutFilePath = InFilePath + 'Results/'
18
19
20 '''To load the database into a dictionary, so shared hits
       can later be looked up in database and all info printed
       in file automatically:'''
21 DicOfDatabase = {}
22
23 DatabaseFile = open(InFilePath + DatabaseFileName, 'rU')
24
25 for Line in DatabaseFile:
26     ListOfLine = Line.split(' ')
27     Description = ' '.join(ListOfLine[1: -1])
28     ListOfDescription = Description.split(',')
29     Description = ';'.join(ListOfDescription)
30     Sequence = ListOfLine[-1]
31     DicOfDatabase[ListOfLine[0]] = [Description, Sequence
           [:-1]]
32
33 DatabaseFile.close()
34
35
36 '''Loading all the accession numbers found into one list
       and make a set of it, plus make dictionary with [
       Fractionation][Hit][Peak]'''
37 ListOfAccessionNumbers = []
38 DicOfPeaks = AutoVivification()
39
40 for File in FileNames:
41     PeakFile = open(InFilePath + File, 'rU')
42     for Line in PeakFile:
```

```
43          ListOfLine = Line.split('\t')
44          ListOfAccessionNumbers.append(ListOfLine[0])
45          DicOfPeaks[File][ListOfLine[0]] = ListOfLine[-1]
46      PeakFile.close()
47
48  SetOfAccessionNumbers = set(ListOfAccessionNumbers)
49  ListOfAccessionNumbers = list(SetOfAccessionNumbers)
50
51  '''For every Hit, look up if peak is in active fractions
        for each fractionation and write that into dictionary'''
52  DicOfHits = AutoVivification()
53
54  for Hit in ListOfAccessionNumbers:
55      DicOfHits[Hit] = []
56      Fractionation = 'SizePeaks.txt'
57      if DicOfPeaks[Fractionation][Hit] == '14\n' or
           DicOfPeaks[Fractionation][Hit] == '15\n':
58          DicOfHits[Hit].append(Fractionation[:-9])
59      Fractionation = 'AnEx3Peaks.txt'
60      if DicOfPeaks[Fractionation][Hit] == '25\n':
61          DicOfHits[Hit].append(Fractionation[:-9])
62      Fractionation = 'SequentialPeaks.txt'
63      if DicOfPeaks[Fractionation][Hit] == '28\n' or
           DicOfPeaks[Fractionation][Hit] == '29\n' or
           DicOfPeaks[Fractionation][Hit] == '30\n':
64          DicOfHits[Hit].append(Fractionation[:-9])
65
66
67
68  '''And then make Lists for Hits shared in the different
        approaches and print them to files'''
69  ListSiSeAn = []
70  ListSiAn = []
71  ListSiSe = []
72  ListAnSe = []
73  ListSize = []
74  ListAnion = []
75  ListSequential = []
```

```
76
77 for Hit in ListOfAccessionNumbers:
78     if Hit in DicOfHits:
79         if len(DicOfHits[Hit]) == 3:
80             ListSiSeAn.append(Hit)
81         elif len(DicOfHits[Hit]) == 2:
82             if 'Size' in DicOfHits[Hit]:
83                 if 'AnEx' in DicOfHits[Hit]:
84                     ListSiAn.append(Hit)
85                 else:
86                     ListSiSe.append(Hit)
87             else:
88                 ListAnSe.append(Hit)
89         elif len(DicOfHits[Hit]) == 1:
90             if 'Size' in DicOfHits[Hit]:
91                 ListSize.append(Hit)
92             elif 'AnEx' in DicOfHits[Hit]:
93                 ListAnion.append(Hit)
94                 else:
95                 ListSequential.append(Hit)
96
97
98
99 OutFile3SiSeAn = open(OutFilePath + 'SizeSequentialAnion.
    csv', 'w')
100 for Entry in ListSiSeAn:
101     OutFile3SiSeAn.write(Entry + ',' + str(DicOfDatabase['>
        ' + Entry]) + '\n')
102 OutFile3SiSeAn.close()
103
104 OutFile2SiAn = open(OutFilePath + 'SizeAnion.csv', 'w')
105 for Entry in ListSiAn:
106     OutFile2SiAn.write(Entry + ',' + str(DicOfDatabase['>'
        + Entry]) + '\n')
107 OutFile2SiAn.close()
108
109 OutFile2SiSe = open(OutFilePath + 'SizeSequential.csv', 'w'
    )
```

```
110 for Entry in ListSiSe:
111     OutFile2SiSe.write(Entry + ',' + str(DicOfDatabase['>'
            + Entry]) + '\n')
112 OutFile2SiSe.close()
113
114 OutFile2AnSe = open(OutFilePath + 'SequentialAnion.csv', 'w
        ')
115 for Entry in ListAnSe:
116     OutFile2AnSe.write(Entry + ',' + str(DicOfDatabase['>'
            + Entry]) + '\n')
117 OutFile2AnSe.close()
118
119 OutFile1Si = open(OutFilePath + 'Size.csv', 'w')
120 for Entry in ListSize:
121     OutFile1Si.write(Entry + ',' + str(DicOfDatabase['>' +
            Entry]) + '\n')
122 OutFile1Si.close()
123
124 OutFile1Se = open(OutFilePath + 'Sequential.csv', 'w')
125 for Entry in ListSequential:
126     OutFile1Se.write(Entry + ',' + str(DicOfDatabase['>' +
            Entry]) + '\n')
127 OutFile1Se.close()
128
129 OutFile1An = open(OutFilePath + 'Anion.csv', 'w')
130 for Entry in ListAnion:
131     OutFile1An.write(Entry + ',' + str(DicOfDatabase['>' +
            Entry]) + '\n')
132 OutFile1An.close()
```

B. Supplementary material for the proteomics analysis of HES

B.1 Mass spectrometry results for active size exclusion and anion exchange fractions from the first round of fractionations

Table B.1: Proteins identified in fraction 14 of the first size exclusion fractionation of HES. 0.476mg HES were fractionated by size exclusion fractionation and fractions tested for their inhibitory activity on LPS-stimulated GM-CSF BMDC. Fraction 14 showed the ability to completely inhibit IL-12p70 production; it was analysed by mass spectrometry in the facility in Glasgow, using an Orbitrap mass spectrometer and using Mascot and the in-house *H. polygyrus* transcriptomic database. The significance threshold for consideration of proteins was $p<0.05$; no minimum cutoff score was set. Listed are ranks of the proteins in the mass spectrometric analysis, their accession numbers, their Mascot scores, the number of peptide hits for the respective protein and their emPAI values, in addition to their rank in the subsequent second analysis in Edinburgh. Green: Proteins found in later re-analysis.

Rank	Protein accession number	Protein score	Protein matches	emPAI	Rank in 2. MS
1	Hp_I22388_IG14332_L637	108	4	0.34	198
2	Hp_I08959_IG02564_L1212	90	2	0.08	18
3	Hp_I22261_IG14205_L639	85	2	0.16	111
4	Hp_I21617_IG13561_L662	82	2	0.17	49
5	Hp_I05325_IG00908_L1903	82	3	0.11	31
6	Hp_I20768_IG12712_L696	67	2	0.14	91
7	Hp_I21133_IG13077_L683	63	2	0.15	77
8	FL8UM6J01A0LLF	51	1	1.01	64
9	Hp_I05364_IG00921_L2082	51	5	0.05	
10	Hp_I05355_IG00918_L1570	50	1	0.06	180
11	Hp_I02849_IG00289_L1962	47	5	0.1	4

Table B.1: Proteins identified in fraction 14 of the first size exclusion fractionation of HES (continued).

Rank	Protein accession number	Protein score	Protein matches	emPAI	Rank in 2. MS
12	Hp_I14513_IG06457_L1354	42	1	0.07	
13	HICN8C105F5IW6	40	2	0.47	
14	Hp_I09081_IG02625_L1173	37	1	0.08	
15	Hp_I06193_IG01201_L3148	37	2	0.03	
16	Hp_I23836_IG15780_L590	27	1	0.17	148
17	Hp_I01065_IG00070_L5127	27	3	0.04	
18	HICN8C106G4WQS	26	2	0.28	
19	Hp_I19157_IG11101_L778	24	1	0.13	10
20	Hp_I14783_IG06727_L1293	24	2	0.08	
21	Hp_I13080_IG05024_L1939	22	2	0.05	
22	HICN8C106HKUXG	22	2	0.21	
23	Hp_I12524_IG04468_L2585	21	2	0.04	
24	Hp_I06583_IG01353_L2360	19	1	0.04	
25	Hp_I08941_IG02555_L1722	17	1	0.06	
26	Hp_I05999_IG01134_L555	16	2	0.19	120

Table B.2: Proteins identified in fraction 15 of the first size exclusion fractionation of HES. 0.476mg HES were fractionated by size exclusion fractionation and fractions tested for their inhibitory activity on LPS-stimulated GM-CSF BMDC. Fraction 15 showed the ability to completely inhibit IL-12p70 production; it was analysed by mass spectrometry in the facility in Glasgow, using an Orbitrap mass spectrometer and using Mascot and the in-house *H. polygyrus* transcriptomic database. The significance threshold for consideration of proteins was $p<0.05$; no minimum cutoff score was set. Listed are ranks of the proteins in the mass spectrometric analysis, their accession numbers, their Mascot scores, the number of peptide hits for the respective protein and their emPAI values, in addition to their rank in the subsequent second analysis in Edinburgh. Green: Proteins found in later re-analysis. Red: expressed proteins.

Rank	Protein accession number	Protein score	Protein matches	emPAI	Rank in 2. MS
1	Hp_I12336_IG04280_L5030	190	6	0.02	43
2	Hp_I20188_IG12132_L723	148	4	0.3	
3	Hp_I21133_IG13077_L683	148	4	0.32	21
4	Hp_I03893_IG00508_L677	105	2	0.15	11
5	Hp_I21565_IG13509_L658	102	7	0.56	22
6	Hp_I01077_IG00070_L5125	85	9	0.04	

Table B.2: Proteins identified in fraction 15 of the first size exclusion fractionation of HES (continued).

Rank	Protein accession number	Protein score	Protein matches	emPAI	Rank in 2. MS
7	Hp_I32194_IG24138_L452	61	2	0.23	
8	Hp_I13832_IG05776_L1555	59	4	0.13	
9	Hp_I05565_IG00988_L1210	58	2	0.08	103
10	Hp_I05355_IG00918_L1570	54	2	0.06	
11	Hp_I26601_IG18545_L528	53	2	0.21	4
12	Hp_I06193_IG01201_L3148	52	2	0.03	
13	Hp_I22851_IG14795_L620	52	2	0.16	18
14	Hp_I02849_IG00289_L1962	51	2	0.05	1
15	Hp_I10419_IG03294_L714	47	4	0.31	10
16	HICN8C104EIKTM	44	2	0.49	
17	FL8UM6J01A0LLF	43	1	1.01	
18	Hp_I08791_IG02480_L1486	42	2	0.07	52
19	Hp_I13472_IG05416_L1706	41	3	0.06	
20	Hp_I05364_IG00921_L2082	40	2	0.05	
21	Hp_I40801_IG32745_L368	39	3	0.29	40
22	Hp_I05273_IG00890_L1799	39	5	0.05	
23	Hp_I14053_IG05997_L1482	36	2	0.07	
24	Hp_I01010_IG00065_L2171	25	2	0.05	
25	Hp_C00098_IG00001_L1007	24	2	0.1	
26	Hp_I05325_IG00908_L1903	23	1	0.05	
27	Hp_I23836_IG15780_L590	23	1	0.17	
28	HICN8C106G4WQS	22	2	0.28	
29	GP9KNTD03GFT8V	22	2	1.01	
30	Hp_I30299_IG22243_L471	21	1	0.23	
31	Hp_I08941_IG02555_L1722	19	2	0.06	
32	Hp_I18212_IG10156_L840	18	1	0.13	
33	GP9KNTD03F2GRS	18	2	0.33	
34	Hp_I41761_IG33705_L357	17	3	0.29	
35	Hp_I20831_IG12775_L695	16	2	0.15	
36	Hp_I35940_IG27884_L415	16	2	0.27	
37	Hp_I23746_IG15690_L590	14	2	0.18	
38	GNK0QLK03GAMLD	14	2	0.22	

Table B.3: Proteins identified in fraction 39 of the first anion exchange fractionation of HES. 0.751mg HES were fractionated by anion exchange fractionation and fractions tested for their inhibitory activity on LPS-stimulated GM-CSF BMDC. Fraction 39 showed the ability to completely inhibit IL-12p70 production; it was analysed by mass spectrometry in the facility in Glasgow, using an Orbitrap mass spectrometer and using Mascot and the in-house *H. polygyrus* transcriptomic database. The significance threshold for consideration of proteins was p<0.05; no minimum cutoff score was set. Listed are ranks of the proteins in the mass spectrometric analysis, their accession numbers, their Mascot scores, the number of peptide hits for the respective protein and their emPAI values, in addition to their rank in fraction 25 of the subsequent second analysis in Edinburgh. Green: Proteins found in the active fraction 25 of a more recent anion exchange fractionation. Red: expressed proteins.

Rank	Protein accession number	Protein score	Protein matches	emPAI	Rank in 2. MS
1	Hp_I03894_IG00508_L604	378	24	7.88	57
2	Hp_I20188_IG12132_L723	361	21	2.26	57
3	Hp_I21133_IG13077_L683	358	23	2.44	57
4	Hp_I08665_IG02417_L1321	321	12	0.54	27
5	Hp_I10155_IG03162_L783	277	15	1.28	80
6	Hp_I03895_IG00508_L600	226	22	5.56	
7	Hp_I13201_IG05145_L1858	208	5	0.17	180
8	Hp_C00053_IG00001_L722	192	9	0.73	57
9	Hp_I15488_IG07432_L1169	186	10	0.49	
10	Hp_I01065_IG00070_L5127	178	12	0.08	3
11	Hp_I19940_IG11884_L726	170	5	0.46	
12	Hp_I05693_IG01031_L1691	168	15	0.34	17
13	Hp_I06559_IG01341_L2453	156	6	0.09	
14	Hp_I10817_IG03493_L822	141	9	0.79	
15	Hpb-VAL-3	140	2	0.07	2
16	Hpb-VAL2.2	133	6	0.24	1
17	Hp_I13874_IG05818_L1547	117	5	0.21	11
18	Hp_I22851_IG14795_L620	116	2	0.16	116
19	Hp_I24607_IG16551_L570	114	5	0.18	41
20	Hp_I25311_IG17255_L555	111	6	0.67	21
21	Hp_I15133_IG07077_L1218	105	2	0.08	
22	Hp_I24705_IG16649_L569	104	2	0.19	
23	Hp_I48980_IG40924_L272	97	1	0.42	2
24	Hp_I02849_IG00289_L1962	97	2	0.05	19
25	Hp_C00215_IG00001_L710	87	6	0.5	35
26	Hp_I13832_IG05776_L1555	80	6	0.2	40
27	Hp_I15536_IG07480_L1158	73	6	0.27	79

Table B.3: Proteins identified in fraction 39 of the first anion exchange fractionation of HES (continued).

Rank	Protein accession number	Protein score	Protein matches	emPAI	Rank in 2. MS
28	Hp_I05325_IG00908_L1903	72	1	0.05	190
29	Hp_I13312_IG05256_L1794	71	6	0.11	69
30	Hp_I16083_IG08027_L1071	70	2	0.09	
31	GP9KNTD03FMXAA	69	2	0.38	
32	Hp_I24525_IG16469_L572	69	5	0.4	
33	Hp_I20153_IG12097_L724	66	1	0.14	
34	Hp_I15874_IG07818_L1106	65	2	0.09	103
35	Hp_I21073_IG13017_L680	61	3	0.15	26
36	Hp_I36714_IG28658_L408	54	4	0.65	134
37	Hp_I12754_IG04698_L2228	52	2	0.04	238
38	Hp_I22470_IG14414_L621	47	4	0.37	33
39	Hp_I14513_IG06457_L1354	46	1	0.07	
40	Hp_I12932_IG04876_L2052	44	1	0.05	
41	Hp_I05364_IG00921_L2082	43	2	0.05	
42	Hp_I04525_IG00683_L718	43	4	0.15	
43	Hp_I09124_IG02646_L958	40	3	0.1	
44	Hp_I12336_IG04280_L5030	39	6	0.02	59
45	Hp_I25374_IG17318_L554	38	2	0.18	
46	Hp_I05565_IG00988_L1210	37	2	0.08	
47	HELDS7W07IPGTM	35	1	0.38	
48	Hp_I10156_IG03162_L593	35	3	0.35	88
49	Hp_I14762_IG06706_L1297	32	1	0.08	
50	Hp_I04570_IG00700_L4683	32	3	0.02	13
51	Hp_I03306_IG00378_L1606	30	2	0.06	
52	Hp_I26703_IG18647_L521	30	1	0.06	
53	Hp_I07426_IG01797_L2216	27	2	0.05	
54	Hp_I14231_IG06175_L1432	26	1	0.07	
55	Hp_I24175_IG16119_L582	26	4	0.4	33
56	Hp_I08811_IG02490_L1739	25	3	0.06	
57	Hp_C00282_IG00001_L564	25	2	0.18	
58	Hp_I07672_IG01920_L1701	24	3	0.06	
59	Hp_I36005_IG27949_L411	22	2	0.25	
60	Hp_I12350_IG04294_L3967	21	6	0.02	
61	Hp_I23528_IG15472_L598	21	1	0.18	
62	Hp_I45134_IG37078_L322	21	3	0.35	
63	HICN8C104EAO7Z	17	2	0.22	

Table B.3: Proteins identified in fraction 39 of the first anion exchange fractionation of HES (continued).

Rank	Protein accession number	Protein score	Protein matches	emPAI	Rank in 2. MS
64	Hp_I14354_IG06298_L1401	16	1	0.07	
65	Hp_I21313_IG13257_L675	16	1	0.15	31
66	GNK0QLK03GDDOW	16	1	0.3	
67	Hp_I21920_IG13864_L651	15	1	0.15	
68	Hp_I14352_IG06296_L1401	15	3	0.07	
69	Hp_I07682_IG01925_L1479	15	2	0.07	12
70	Hp_I24000_IG15944_L579	13	1	0.18	

Table B.4: Proteins identified in fraction 40 of the first anion exchange fractionation of HES. 0.751mg HES were fractionated by anion exchange fractionation and fractions tested for their inhibitory activity on LPS-stimulated GM-CSF BMDC. Fraction 40 showed the ability to completely inhibit IL-12p70 production; it was analysed by mass spectrometry in the facility in Glasgow, using an Orbitrap mass spectrometer and using Mascot and the in-house *H. polygyrus* transcriptomic database. The significance threshold for consideration of proteins was $p<0.05$; no minimum cutoff score was set. Listed are ranks of the proteins in the mass spectrometric analysis, their accession numbers, their Mascot scores, the number of peptide hits for the respective protein and their emPAI values, in addition to their rank in fraction 25 of the subsequent second analysis in Edinburgh. Green: Proteins found in the active fraction 25 of a more recent anion exchange fractionation. Red: expressed proteins.

Rank	Protein accession number	Protein score	Protein matches	emPAI	Rank in 2. MS
1	Hp_I01066_IG00070_L5129	677	42	0.45	
2	Hp_I08665_IG02417_L1321	556	19	1.06	27
3	Hp_I03894_IG00508_L604	462	17	3.76	57
4	Hp_I05693_IG01031_L1691	434	26	0.79	17
5	Hp_I10155_IG03162_L783	419	14	1.28	80
6	Hp_I03893_IG00508_L677	382	16	2.45	57
7	FL8UM6J01DGLOO	248	10	24.11	
8	Hp_I04629_IG00719_L1853	307	15	0.53	4
9	Hp_I22851_IG14795_L620	271	8	0.57	116
10	Hp_I20188_IG12132_L723	254	16	1.2	57
11	Hp_I23736_IG15680_L595	239	10	1.25	74
12	Hp_I15710_IG07654_L1132	231	10	0.52	14
13	Hp_I21073_IG13017_L680	230	13	2.04	26

Table B.4: Proteins identified in fraction 40 of the first anion exchange fractionation of HES (continued).

Rank	Protein accession number	Protein score	Protein matches	emPAI	Rank in 2. MS
14	Hp_I12624_IG04568_L2400	208	11	0.23	94
15	Hp_I21133_IG13077_L683	195	16	1.28	57
16	Hp_I05355_IG00918_L1570	194	6	0.2	48
17	Hp_I19157_IG11101_L778	190	6	0.27	
18	Hp_I07682_IG01925_L1479	176	7	0.31	12
19	Hp_I05746_IG01049_L1033	171	4	0.32	
20	Hp_I25311_IG17255_L555	169	10	0.98	21
21	Hp_I24607_IG16551_L570	161	9	0.92	41
22	Hp_I15874_IG07818_L1106	159	7	0.3	103
23	FL8UM6J01BCVJW	157	4	1.03	34
24	Hp_I13874_IG05818_L1547	153	6	0.28	11
25	Hp_I04280_IG00603_L1135	152	3	0.19	
26	Hp_I14314_IG06258_L1412	147	3	0.14	117
27	Hp_I06753_IG01438_L1571	147	8	0.2	
28	Hp_C00215_IG00001_L710	140	6	0.72	35
29	Hp_I20153_IG12097_L724	133	4	0.29	29
30	Hp_I22261_IG14205_L639	129	12	1.12	97
31	Hp_I02849_IG00289_L1962	124	2	0.05	19
32	Hp_I32194_IG24138_L452	124	2	0.23	
33	Hp_I22470_IG14414_L621	121	3	0.37	33
34	Hp_C00318_IG00001_L1664	120	5	0.12	65
35	Hp_I05758_IG01053_L926	118	3	0.23	
36	Hp_I15488_IG07432_L1169	116	5	0.17	
37	Hp_I24441_IG16385_L572	113	7	0.61	
38	Hp_I12336_IG04280_L5030	112	5	0.04	59
39	Hp_I24525_IG16469_L572	111	6	0.4	
40	Hp_I10817_IG03493_L822	110	6	0.26	
41	Hp_I19958_IG11902_L735	108	13	0.46	152
42	Hp_I15089_IG07033_L1228	108	9	0.26	30
43	Hp_I05472_IG00957_L1361	105	3	0.16	45
44	Hp_I24175_IG16119_L582	101	3	0.4	33
45	Hp_I16213_IG08157_L1054	98	2	0.1	1
46	Hp_I07953_IG02060_L1482	94	4	0.15	
47	Hpb-VAL-2.3	94	4	0.15	
48	Hp_I15157_IG07101_L1223	89	2	0.08	28
49	Hp_I25440_IG17384_L551	80	8	0.39	56

Table B.4: Proteins identified in fraction 40 of the first anion exchange fractionation of HES (continued).

Rank	Protein accession number	Protein score	Protein matches	emPAI	Rank in 2. MS
50	Hp_I23528_IG15472_L598	78	2	0.18	
51	Hp_I08791_IG02480_L1486	77	6	0.15	8
52	Hp_I12337_IG04281_L4997	73	10	0.08	9
53	Hp_I09123_IG02646_L960	72	3	0.22	106
54	Hp_C02597_IG00028_L1734	72	2	0.06	
55	Hp_I07274_IG01721_L3765	70	4	0.05	
56	Hp_I01131_IG00073_L2163	66	3	0.05	
57	Hp_I16239_IG08183_L1050	63	3	0.2	43
58	Hp_I07875_IG02021_L1389	60	3	0.07	
59	Hp_C00053_IG00001_L722	59	4	0.3	57
60	GKYPR1L02BZ2HH	57	6	1.7	
61	FL8UM6J01DGCZI	57	3	1.43	
62	Hp_I13832_IG05776_L1555	56	4	0.06	40
63	Hp_I05326_IG00908_L1911	51	2	0.05	
64	Hp_I05325_IG00908_L1903	51	4	0.05	190
65	Hp_I05364_IG00921_L2082	51	2	0.05	
66	Hp_I24705_IG16649_L569	49	1	0.19	
67	Hp_I02212_IG00191_L3366	47	2	0.03	
68	Hp_I16723_IG08667_L984	46	2	0.1	68
69	Hp_I40812_IG32756_L369	42	1	0.28	
70	HICN8C105F5IW6	41	2	0.47	
71	Hp_I25889_IG17833_L540	39	1	0.19	
72	Hp_I12819_IG04763_L2150	38	1	0.05	76
73	Hp_I12518_IG04462_L2600	38	3	0.04	163
74	Hp_I25825_IG17769_L543	38	5	0.69	
75	Hp_I10156_IG03162_L593	37	3	0.16	88
76	GSXTT4C06GU61M	36	2	0.26	
77	Hp_I14119_IG06063_L1461	35	3	0.07	154
78	Hp_I26703_IG18647_L521	34	2	0.06	
79	Hp_I25374_IG17318_L554	34	2	0.18	
80	GWDWRH002CDF07	34	4	0.3	
81	Hp_I06750_IG01437_L1569	33	1	0.06	
82	Hp_I15536_IG07480_L1158	33	4	0.08	79
83	Hp_I13897_IG05841_L1536	32	7	0.06	91
84	Hp_I04010_IG00535_L4397	31	1	0.02	109
85	Hp_I40131_IG32075_L375	31	1	0.28	

Table B.4: Proteins identified in fraction 40 of the first anion exchange fractionation of HES (continued).

Rank	Protein accession number	Protein score	Protein matches	emPAI	Rank in 2. MS
86	Hp_C00282_IG00001_L564	30	2	0.18	
87	Hp_I36714_IG28658_L408	29	1	0.29	134
88	Hp_I15169_IG07113_L1216	28	1	0.08	
89	Hp_I20875_IG12819_L687	28	1	0.15	
90	Hp_I04798_IG00762_L1055	26	3	0.1	
91	Hp_I23863_IG15807_L590	25	3	0.17	
92	Hp_I16609_IG08553_L1004	25	2	0.03	
93	Hp_I04378_IG00631_L1589	24	5	0.06	
94	Hp_I34696_IG26640_L421	23	1	0.25	
95	Hp_I04874_IG00782_L1023	20	2	0.1	250
96	GP9KNTD03FQWQK	19	1	0.95	
97	Hp_I03120_IG00339_L546	19	4	0.19	
98	Hp_I04570_IG00700_L4683	19	5	0.02	13
99	Hp_I10589_IG03379_L596	19	1	0.17	174
100	Hp_I15617_IG07561_L1141	19	3	0.09	
101	Hp_I19530_IG11474_L758	17	2	0.14	
102	Hp_I12466_IG04410_L2780	17	2	0.04	
103	Hp_I12856_IG04800_L2123	16	1	0.05	171
104	Hp_I50094_IG42038_L253	14	2	0.44	
105	GNK0QLK03GBGV9	14	1	0.22	

B.2 Mass spectrometry and content comparison of sequential fractions

Table B.5: Proteins identified in fraction 28 of the sequential fractionation of HES. HES was fractionated by size exclusion followed by anion exchange fractionation. All fractions were analysed by mass spectrometry and tested for their inhibitory activity on GM-CSF BMDC. Fraction 28 showed the ability to completely inhibit IL-12p70 production. Listed are ranks of the proteins in the mass spectrometric analysis, their accession numbers, the number of peptide hits for the respective protein and their emPAI values. Red: expressed proteins.

Rank	Protein accession number	Protein score	Protein matches	emPAI
1	Hp_I04570_IG00700_L4683	1796	72	2.68
2	HICN8C106HP9PI_length=274	997	37	3.46
3	Hp_I21313_IG13257_L675	679	24	4.47
4	Hp_I08665_IG02417_L1321	660	19	2.73
5	Hp_I10419_IG03294_L714	630	24	3.16
6	Hp_I18858_IG10802_L799	516	14	3.39
7	Hp_I22486_IG14430_L629	444	13	3.36
7	Hp_I08791_IG02480_L1486	395	16	1.66
7	GSXTT4C07IB13H_length=463	198	7	2.58
7	Hp_I13898_IG05842_L1539	162	4	0.29
7	Hp_I04202_IG00583_L1521	58	3	0.21
7	Hpb-VAL-1.1	139	3	
7	Hp_I08792_IG02480_L662	95	5	
7	Hp_I04671_IG00730_L1535	63	2	
7	Hp_I19246_IG11190_L772	60	4	
7	GNK0QLK03HBAHW_length=398	46	1	
7	HICN8C104EUPYS_length=127	41	1	
7	Hp_I20083_IG12027_L726	39	1	
7	GS66ZV202BRKI2_length=193	31	2	
7	GS66ZV202CFXAN_length=237	23	1	
8	Hp_I28744_IG20688_L490	409	13	9.36
9	Hp_I07157_IG01645_L560	389	17	12.23
9	Hp_I07158_IG01645_L560	357	16	10.26
10	Hp_I13810_IG05754_L1566	379	14	1.02

Table B.5: Proteins identified in fraction 28 of the sequential fractionation of HES (continued).

Rank	Protein accession number	Protein score	Protein matches	emPAI
11	Hp_C00269_IG00001_L1007	370	8	1.07
11	FL8UM6J01B6ULB_length=156	129	2	
11	FL3BO7401ASYIS_length=170	123	2	
12	Hp_I26188_IG18132_L529	370	8	2.74
13	Hp_I07312_IG01740_L4913	343	12	0.26
13	Hp_I07313_IG01740_L570	81	1	
13	Hp_I30910_IG22854_L463	60	2	
14	Hp_I13075_IG05019_L1949	328	10	0.57
14	Hp_I28606_IG20550_L493	66	1	
15	Hp_I19378_IG11322_L765	297	6	1.07
16	Hp_I19157_IG11101_L778	294	11	2.14
17	Hp_I23293_IG15237_L606	293	6	1.4
18	Hp_I01063_IG00070_L5127	274	12	0.25
18	Hp_I01077_IG00070_L5125	273	11	0.22
18	FL8UM6J01CURPT_length=239	34	1	
18	FL8UM6J01AP92T_length=187	30	1	
19	Hp_I50492_IG42436_L247	274	11	15.24
19	Hp_I50368_IG42312_L251	212	6	
20	Hp_I07496_IG01832_L2183	262	6	0.29
20	Hp_I07497_IG01832_L1722	235	6	0.37
21	Hp_I10590_IG03379_L588	261	10	3.54
22	Hp_I27122_IG19066_L517	256	6	1.43
23	Hp_I24512_IG16456_L570	236	7	2.04
23	GNK0QLK03F82AT_length=271	120	2	
24	Hp_I21565_IG13509_L658	214	6	1.03
25	Hp_I05758_IG01053_L926	205	6	0.83
25	Hp_I05759_IG01053_L914	76	2	
26	GNK0QLK03GQOZO_length=396	188	6	1.41
26	GS66ZV203C3717_length=247	119	3	
26	GS66ZV203DJXOH_length=245	92	2	
26	GWDWRH002CES3N_length=67	85	3	
27	Hp_I21133_IG13077_L683	188	6	1.2
27	Hp_I08959_IG02564_L1212	76	2	0.17
27	Hp_C00053_IG00001_L722	64	3	0.3
27	Hp_I45702_IG37646_L317	72	1	
27	Hp_I20188_IG12132_L723	71	3	

Table B.5: Proteins identified in fraction 28 of the sequential fractionation of HES (continued).

Rank	Protein accession number	Protein score	Protein matches	emPAI
27	Hp_I03894_IG00508_L604	61	1	
27	Hp_I06559_IG01341_L2453	60	2	
27	Hp_I02590_IG00245_L1152	32	1	
28	Hp_I15528_IG07472_L1156	184	8	0.74
29	Hp_I23776_IG15720_L592	179	8	1.89
30	Hp_I02849_IG00289_L1962	176	7	0.27
31	Hp_I25974_IG17918_L541	172	6	1.67
32	Hp_I12336_IG04280_L5030	165	5	0.1
33	Hp_I15488_IG07432_L1169	160	4	0.36
34	Hp_I22470_IG14414_L621	159	8	2.32
34	Hp_I24175_IG16119_L582	114	7	2.08
35	Hp_I15133_IG07077_L1218	158	5	0.45
36	Hp_I05659_IG01019_L943	158	2	0.22
37	FL8UM6J01B7CV6_length=228	157	3	2.29
38	Hp_I04541_IG00689_L698	154	4	0.68
38	Hp_I04543_IG00689_L522	49	2	
38	Hp_I09370_IG02769_L634	48	1	
39	Hp_I00798_IG00050_L1759	154	4	0.23
39	Hp_I00796_IG00050_L1763	117	2	
39	Hp_I00800_IG00050_L1766	25	1	
40	Hp_I45709_IG37653_L316	149	3	1.29
41	Hp_I02051_IG00167_L1023	148	4	0.44
41	GS66ZV202BZOD1_length=219	104	2	
41	HELDS7W07H029J_length=253	65	2	
41	GSXTT4C08I82OC_length=200	49	1	
41	GS66ZV202B0XRC_length=246	37	1	
42	Hp_I12624_IG04568_L2400	145	5	0.22
42	FL8UM6J01C5SEG_length=170	72	2	
43	Hp_I17933_IG09877_L867	143	4	0.55
44	Hp_I07995_IG02081_L699	143	4	0.69
45	Hpb-VAL-4	141	2	0.32
45	FL8UM6J01BH6HY_length=236	98	1	
46	Hp_I18845_IG10789_L800	139	4	0.4
47	Hp_I40999_IG32943_L364	139	2	0.65
48	Hp_I01023_IG00066_L1337	132	3	0.23
48	FL8UM6J01B19RE_length=231	94	2	

Table B.5: Proteins identified in fraction 28 of the sequential fractionation of HES (continued).

Rank	Protein accession number	Protein score	Protein matches	emPAI
48	GSXTT4C07H11X2_length=416	62	1	
49	Hp_I24965_IG16909_L566	132	5	0.89
50	Hp_I25311_IG17255_L555	130	4	0.93
51	Hp_I12337_IG04281_L4997	126	7	0.11
51	FL8UM6J01B4I85_length=259	43	1	
51	FL8UM6J01BGCU6_length=234	43	1	
51	FL3BO7403BPZG6_length=114	35	1	
52	Hp_I06078_IG01161_L583	124	3	0.6
53	Hp_I27254_IG19198_L516	124	2	0.41
54	Hp_I23528_IG15472_L598	122	4	0.87
55	Hp_I20654_IG12598_L702	122	3	0.47
56	Hp_I22064_IG14008_L644	122	3	0.51
57	Hp_I10517_IG03343_L655	120	5	1
57	Hp_I10518_IG03343_L562	114	5	
58	Hp_I07202_IG01671_L440	119	2	0.5
59	Hp_I13122_IG05066_L1913	119	5	0.28
60	Hp_I15168_IG07112_L1217	118	4	0.27
61	Hp_I22851_IG14795_L620	118	6	1.38
62	Hpb-VAL-14	109	5	0.43
63	Hp_I12776_IG04720_L2202	109	3	0.13
64	Hp_I32194_IG24138_L452	108	2	0.48
65	HELDS7W08JQN3O_length=274	108	1	0.39
66	Hp_I05325_IG00908_L1903	107	2	0.11
67	Hp_I08941_IG02555_L1722	107	3	0.17
68	Hp_I36714_IG28658_L408	105	2	0.62
69	Hp_I24607_IG16551_L570	105	7	1.56
69	Hp_I49814_IG41758_L259	87	5	
70	Hp_I13832_IG05776_L1555	103	2	0.12
71	Hp_I07249_IG01697_L637	102	3	0.52
72	Hp_I03893_IG00508_L677	100	2	0.3
73	Hp_I16226_IG08170_L1053	99	5	0.56
74	Hp_I11144_IG03656_L469	96	4	1.16
75	Hp_I10155_IG03162_L783	96	3	0.25
75	Hp_I10156_IG03162_L593	37	2	
76	Hp_I25374_IG17318_L554	96	2	0.38
77	Hp_I05827_IG01076_L1116	95	5	0.5

Table B.5: Proteins identified in fraction 28 of the sequential fractionation of HES (continued).

Rank	Protein accession number	Protein score	Protein matches	emPAI
77	Hp_I40994_IG32938_L367	62	2	
78	Hp_I03611_IG00436_L810	95	4	0.38
78	HELDS7W08JC1EG_length=251	67	1	
79	Hp_I14314_IG06258_L1412	92	1	0.07
80	Hp_I15760_IG07704_L1122	91	1	0.09
81	Hp_I22173_IG14117_L645	90	2	0.32
82	Hp_I23836_IG15780_L590	88	1	0.16
83	Hp_I06589_IG01356_L2259	88	1	0.04
84	Hp_I08227_IG02198_L1357	87	1	0.07
85	Hp_I32832_IG24776_L445	86	1	0.22
86	Hp_I34129_IG26073_L426	85	1	0.23
87	Hp_I09863_IG03016_L798	84	1	0.13
88	Hp_I42666_IG34610_L339	83	1	0.29
89	Hp_I21725_IG13669_L658	82	1	0.15
90	Hp_I00695_IG00044_L591	82	1	0.16
91	Hp_I14119_IG06063_L1461	81	3	0.21
92	Hpb-VAL-3	80	3	0.22
93	Hp_I05407_IG00935_L1040	79	1	0.09
94	Hp_I14795_IG06739_L1291	79	1	0.07
95	Hp_I42038_IG33982_L358	78	4	1.76
95	Hp_I44775_IG36719_L318	43	2	
96	Hp_I20539_IG12483_L707	78	4	0.47
97	FL8UM6J01BC1ZN_length=62	77	2	7.27
98	Hp_I40417_IG32361_L370	77	2	0.6
99	Hp_I12734_IG04678_L2250	76	1	0.04
100	Hp_I07155_IG01644_L585	76	1	0.17
101	GSXTT4C05GBC4L_length=430	76	1	0.24
102	Hp_I04083_IG00553_L1755	75	1	0.05
103	Hp_C00031_IG00001_L1071	74	1	0.09
104	Hp_I08175_IG02172_L1570	74	3	0.13
104	Hp_I19423_IG11367_L741	47	1	
105	Hp_I38626_IG30570_L389	72	2	0.59
106	Hp_I06748_IG01436_L1580	71	1	0.06
107	Hp_I44112_IG36056_L331	71	2	0.7
108	Hp_I12350_IG04294_L3967	71	1	0.02
109	Hp_I05355_IG00918_L1570	70	3	0.19

Table B.5: Proteins identified in fraction 28 of the sequential fractionation of HES (continued).

Rank	Protein accession number	Protein score	Protein matches	emPAI
110	Hp_I14116_IG06060_L1462	70	1	0.07
111	Hp_I30585_IG22529_L470	70	1	0.21
112	GS66ZV203DFM3U_length=95	70	1	1.31
113	Hp_I08946_IG02557_L754	68	3	0.42
113	Hp_I28711_IG20655_L493	44	1	
114	Hp_I07378_IG01773_L2592	68	2	0.08
114	Hp_I07379_IG01773_L2104	59	1	
115	Hp_I07172_IG01652_L523	67	3	0.68
115	Hp_I07171_IG01652_L539	55	2	
115	Hp_I10719_IG03444_L597	28	1	
116	Hpb-CRT	67	1	0.08
117	Hp_I02283_IG00202_L1498	67	2	0.14
117	Hp_I02285_IG00202_L1064	63	1	
117	Hp_I02287_IG00202_L850	25	1	
118	Hp_I29394_IG21338_L484	67	1	0.21
119	FL8UM6J01CI46H_length=220	66	1	0.45
120	Hp_I23615_IG15559_L596	66	2	0.36
120	GKYPR1L02BZNH0_length=404	48	1	
121	Hp_I00841_IG00053_L616	65	2	0.37
122	Hp_I13416_IG05360_L1738	64	2	0.12
123	GSXTT4C06GQDI1_length=169	64	1	0.66
124	Hp_I21746_IG13690_L653	64	2	0.33
125	Hp_I54277_IG46221_L174	64	2	1.74
126	Hp_I24441_IG16385_L572	63	1	0.17
127	Hp_I38988_IG30932_L386	63	2	0.58
128	Hp_I16824_IG08768_L974	63	2	0.2
129	Hp_I22261_IG14205_L639	63	1	0.16
130	Hp_I44260_IG36204_L332	63	1	0.31
131	FL8UM6J01BH6V1_length=59	62	1	2.43
132	Hp_I22350_IG14294_L635	61	2	0.32
133	Hp_I08475_IG02322_L1881	61	1	0.05
134	Hp_I10751_IG03460_L637	61	1	0.15
135	Hp_I03369_IG00388_L681	58	1	0.14
136	Hp_I38698_IG30642_L388	58	2	0.59
137	Hp_I49935_IG41879_L259	57	2	0.99
138	Hp_I43851_IG35795_L337	57	1	0.29

Table B.5: Proteins identified in fraction 28 of the sequential fractionation of HES (continued).

Rank	Protein accession number	Protein score	Protein matches	emPAI
139	Hp_I05472_IG00957_L1361	56	1	0.07
140	Hp_I15237_IG07181_L1208	56	1	0.08
141	Hp_I01036_IG00067_L1461	56	1	0.07
142	Hp_I07334_IG01751_L2741	54	1	0.04
143	Hp_I03099_IG00335_L808	54	1	0.12
144	Hp_I07274_IG01721_L3765	54	1	0.03
145	Hp_I12608_IG04552_L2437	54	1	0.04
146	Hp_I02136_IG00181_L1019	54	2	0.2
146	Hp_I15620_IG07564_L1137	25	1	
147	Hp_I14444_IG06388_L1373	53	1	0.07
148	Hp_I17541_IG09485_L897	51	1	0.1
149	FL8UM6J01DXUGS_length=253	50	2	1.07
150	Hp_I34113_IG26057_L428	49	2	0.25
151	Hp_I12568_IG04512_L2492	48	1	0.04
152	Hp_I00697_IG00045_L2819	47	1	0.03
153	GW6977U05FJ9VT_length=110	47	2	2.88
153	GS66ZV202CF40B_length=221	32	1	
154	Hp_I06838_IG01481_L1319	46	1	0.08
155	Hp_I23280_IG15224_L606	46	1	0.15
156	GSXTT4C07H9V8V_length=405	46	2	0.24
157	GP9KNTD03FMXAA_length=261	46	1	0.36
158	Hp_I49433_IG41377_L267	45	1	0.37
159	Hp_I43570_IG35514_L336	45	1	0.29
160	HICN8C104EH4N8_length=157	45	1	0.68
161	Hp_I09769_IG02969_L1009	45	3	0.2
162	Hp_C00065_IG00001_L1348	44	1	0.07
163	Hp_I14135_IG06079_L1458	44	1	0.07
164	Hp_I05755_IG01052_L1113	43	1	0.09
165	Hp_I17380_IG09324_L905	42	2	0.22
166	Hp_I03228_IG00366_L2337	41	2	0.04
167	Hp_I12932_IG04876_L2052	41	1	0.05
168	Hp_I06271_IG01234_L1502	40	1	0.06
169	Hp_I09474_IG02821_L795	40	1	0.12
170	Hp_I26307_IG18251_L531	40	1	0.18
171	GSXTT4C07H1SRT_length=291	40	1	0.36
172	Hp_C00282_IG00001_L564	39	1	0.17

Table B.5: Proteins identified in fraction 28 of the sequential fractionation of HES (continued).

Rank	Protein accession number	Protein score	Protein matches	emPAI
173	FL8UM6J01D4QX3_length=59	39	1	2.43
174	Hp_I13588_IG05532_L1650	38	1	0.06
175	Hp_I05809_IG01070_L1113	38	1	0.09
176	Hp_I18874_IG10818_L798	38	1	0.12
177	Hp_I44884_IG36828_L326	38	1	0.3
178	Hpb-VAL-8	38	3	0.24
178	Hp_I08945_IG02557_L1281	26	2	
179	Hp_I45843_IG37787_L315	38	1	0.33
180	Hp_I14711_IG06655_L1305	38	1	0.08
181	Hp_I10507_IG03338_L686	37	1	0.14
182	HELDS7W07IETUG_length=224	37	1	0.47
183	Hp_I38562_IG30506_L390	36	1	0.27
184	Hp_I20989_IG12933_L687	36	2	0.3
185	Hp_I22770_IG14714_L618	35	1	0.16
186	Hp_I16462_IG08406_L1016	35	1	0.09
187	Hp_I00739_IG00047_L2586	35	2	0.07
188	Hp_I38111_IG30055_L394	35	1	0.25
189	Hp_I14044_IG05988_L1484	35	1	0.06
190	Hp_I27304_IG19248_L514	34	1	0.19
191	Hpb-APY-1.1	34	1	0.09
192	Hp_I01422_IG00100_L1076	33	1	0.09
193	Hp_I42165_IG34109_L355	33	1	0.3
194	Hp_I26227_IG18171_L535	33	2	0.19
195	GP9KNTD03GRXA0_length=393	32	1	0.24
196	Hp_I00806_IG00050_L1112	32	1	0.09
197	GKYPR1L02CFV8D_length=134	32	1	0.87
198	Hp_I12342_IG04286_L4223	32	1	0.02
199	Hp_I13426_IG05370_L1731	31	1	0.06
200	Hp_I07527_IG01847_L1908	30	2	0.05
201	HELDS7W07IJKS4_length=381	30	1	0.27
202	Hp_I48105_IG40049_L286	30	1	0.36
203	Hp_I39892_IG31836_L376	29	1	0.26
204	GSXTT4C05FNWZW_length=206	29	1	0.52
205	Hp_I34646_IG26590_L427	29	2	0.24
206	Hp_I38850_IG30794_L366	29	1	0.28
207	GP9KNTD03FLCRS_length=301	29	1	0.33

Table B.5: Proteins identified in fraction 28 of the sequential fractionation of HES (continued).

Rank	Protein accession number	Protein score	Protein matches	emPAI
208	Hp_I45671_IG37615_L316	28	1	0.34
209	Hp_I47440_IG39384_L295	28	1	0.33
210	Hp_I16449_IG08393_L1019	27	1	0.09
211	Hp_I24623_IG16567_L570	27	2	0.17
212	Hp_I09575_IG02872_L1199	27	1	0.08
213	Hp_I05780_IG01060_L750	27	1	0.13
214	Hp_I15783_IG07727_L1116	27	1	0.09
215	Hp_I10670_IG03419_L511	27	1	0.19
216	Hp_I11951_IG04060_L390	27	1	0.24
217	Hp_I04874_IG00782_L1023	27	1	0.1
218	Hp_I16723_IG08667_L984	26	1	0.1
219	HICN8C104EF9L9_length=388	26	1	0.27
220	Hp_I49529_IG41473_L265	26	2	0.37
221	Hp_I14250_IG06194_L1431	26	1	0.07
222	Hp_I13952_IG05896_L1510	25	1	0.07
223	Hp_I16505_IG08449_L1014	25	1	0.09
224	Hp_I48880_IG40824_L273	25	1	0.38
225	Hp_I16562_IG08506_L1005	25	2	0.21
226	Hp_I43395_IG35339_L341	25	1	0.32
227	Hp_I13874_IG05818_L1547	25	1	0.06
228	Hp_I12527_IG04471_L2582	25	1	0.04
229	Hp_I01453_IG00104_L978	24	1	0.1
230	Hp_I05565_IG00988_L1210	24	1	0.08
231	GS66ZV208JGIBQ_length=382	24	1	0.27
232	Hp_I15587_IG07531_L1141	23	1	0.08
233	Hp_I03365_IG00388_L986	23	1	0.1
234	Hp_I15089_IG07033_L1228	23	1	0.08
235	Hp_I32435_IG24379_L441	22	1	0.22
236	Hp_I04266_IG00599_L823	22	1	0.12
237	Hp_I04581_IG00707_L1760	22	1	0.06
238	Hp_I29599_IG21543_L474	22	1	0.21
239	Hp_I22123_IG14067_L644	22	1	0.15
240	Hp_I08219_IG02194_L2089	21	1	0.05
241	GLSD98I04EIBBZ_length=463	20	1	0.23
242	Hp_I17525_IG09469_L900	20	1	0.1

Table B.6: Proteins identified in fraction 29 of the sequential fractionation of HES. HES was fractionated by size exclusion followed by anion exchange fractionation. All fractions were analysed by mass spectrometry and tested for their inhibitory activity on GM-CSF BMDC. Fraction 29 showed the ability to completely inhibit IL-12p70 production. Listed are ranks of the proteins in the mass spectrometric analysis, their accession numbers, the number of peptide hits for the respective protein and their emPAI values. Red: expressed proteins.

Rank	Protein accession number	Protein score	Protein matches	emPAI
1	Hp_I04570_IG00700_L4683	1336	52	1.59
1	HICN8C105F2ANR_length=463	39	1	
2	GNK0QLK03GQOZO_length=396	1062	29	2.74
2	GS66ZV203C3717_length=247	907	23	
2	GS66ZV203DJXOH_length=245	863	20	
2	GWDWRH002CES3N_length=67	171	6	
3	Hp_I10419_IG03294_L714	813	25	5.14
4	Hp_I01079_IG00070_L5124	798	31	0.67
4	Hp_I01061_IG00070_L5128	767	31	0.67
4	FL8UM6J01BC1ZN_length=62	94	2	7.27
4	FL8UM6J01AP92T_length=187	71	2	
5	HICN8C106HP9PI_length=274	779	30	12.66
5	Hp_I10288_IG03228_L610	752	29	
6	Hp_I10590_IG03379_L588	707	17	8.68
6	Hp_I10589_IG03379_L596	181	7	1.46
7	Hp_I19157_IG11101_L778	622	19	6.86
8	Hp_I08791_IG02480_L1486	525	14	1.05
8	Hp_I22486_IG14430_L629	364	11	3.36
8	GSXTT4C07IB13H_length=463	172	5	1.34
8	Hpb-VAL-1.2	161	6	0.39
8	Hp_I13898_IG05842_L1539	158	5	
8	Hpb-VAL-1.1	140	4	
8	Hp_I08792_IG02480_L662	79	3	
8	Hp_I04671_IG00730_L1535	52	3	
8	HICN8C104EUPYS_length=127	33	1	
8	Hp_I20083_IG12027_L726	31	1	
8	Hp_I19246_IG11190_L772	25	2	
9	Hp_I21313_IG13257_L675	518	17	2.24
10	Hp_I18858_IG10802_L799	468	12	2.49
11	Hp_I08665_IG02417_L1321	455	14	1.46
11	Hp_I08666_IG02417_L925	109	2	

Table B.6: Proteins identified in fraction 29 of the sequential fractionation of HES (continued).

Rank	Protein accession number	Protein score	Protein matches	emPAI
12	Hp_I07157_IG01645_L560	378	14	7.15
12	Hp_I07158_IG01645_L560	314	13	5.94
12	Hp_I10997_IG03583_L513	36	2	
13	Hp_I13075_IG05019_L1949	378	11	0.64
13	Hp_I28606_IG20550_L493	56	1	
14	Hp_I26188_IG18132_L529	363	7	2.17
15	Hp_I19378_IG11322_L765	329	6	1.07
16	Hp_I13810_IG05754_L1566	322	8	0.6
17	Hp_I43851_IG35795_L337	307	10	12.13
18	Hp_I40999_IG32943_L364	282	5	2.48
19	HELDS7W08JQN3O_length=274	281	4	0.39
20	Hp_I07312_IG01740_L4913	279	10	0.19
20	Hp_I07313_IG01740_L570	85	1	
20	Hp_I30910_IG22854_L463	81	2	
21	Hpb-VAL-4	270	7	1.66
21	FL8UM6J01BXB62_length=190	193	3	
21	FL8UM6J01BH6HY_length=236	147	2	
22	Hp_I02051_IG00167_L1023	257	8	1.07
22	GS66ZV203C3ECE_length=216	105	2	
22	GS66ZV202BZOD1_length=219	105	2	
22	HELDS7W07H029J_length=253	93	4	
22	GSXTT4C08I82OC_length=200	74	3	
22	Hp_I48914_IG40858_L269	46	1	
22	GS66ZV202B0XRC_length=246	34	1	
23	Hp_I24512_IG16456_L570	245	7	1.6
23	GNK0QLK03F82AT_length=271	177	4	
24	Hp_I05758_IG01053_L926	226	6	0.83
24	Hp_I05759_IG01053_L914	98	2	
25	Hp_I28744_IG20688_L490	223	9	4.04
26	Hp_I24607_IG16551_L570	220	8	1.99
26	Hp_I49814_IG41758_L259	74	4	
27	Hp_I50492_IG42436_L247	208	11	15.24
27	Hp_I50368_IG42312_L251	166	7	
27	Hp_I48105_IG40049_L286	31	1	
28	Hp_I02849_IG00289_L1962	198	7	0.4
28	Hp_I02853_IG00289_L1028	128	3	

Table B.6: Proteins identified in fraction 29 of the sequential fractionation of HES (continued).

Rank	Protein accession number	Protein score	Protein matches	emPAI
28	Hp_I02850_IG00289_L1486	93	4	
29	Hp_I29394_IG21338_L484	196	5	1.61
30	Hp_I04541_IG00689_L698	193	6	1.18
30	Hp_I04543_IG00689_L522	50	3	
30	Hp_I09370_IG02769_L634	39	1	
31	Hp_I25311_IG17255_L555	187	5	1.27
31	FL8UM6J01EH57D_length=239	53	1	
32	Hp_I07497_IG01832_L1722	184	5	0.3
32	Hp_I07496_IG01832_L2183	183	5	0.23
33	Hp_I21565_IG13509_L658	182	7	1.34
34	Hp_I17933_IG09877_L867	174	6	0.92
35	Hp_I12624_IG04568_L2400	163	5	0.22
35	GP9KNTD03F5ENS_length=137	63	1	
35	FL8UM6J01C5SEG_length=170	59	1	
36	Hp_I24965_IG16909_L566	162	5	1.21
37	Hp_I00798_IG00050_L1759	155	5	0.23
37	Hp_I00806_IG00050_L1112	59	2	0.18
37	Hp_I00796_IG00050_L1763	118	3	
37	Hp_I00809_IG00050_L1090	104	2	
37	Hp_I00811_IG00050_L794	40	2	
38	Hp_I23776_IG15720_L592	153	6	1.13
39	Hp_I26601_IG18545_L528	144	2	0.44
39	GSXTT4C05GBC4L_length=430	100	1	
40	Hp_I16226_IG08170_L1053	142	6	0.7
41	Hp_I27254_IG19198_L516	134	2	0.41
42	Hp_I23863_IG15807_L590	132	4	0.83
43	Hp_I23528_IG15472_L598	129	3	0.6
44	Hp_I15133_IG07077_L1218	128	4	0.35
45	Hp_C00269_IG00001_L1007	127	4	0.44
45	FL8UM6J01B6ULB_length=156	67	1	
45	FL3BO7401ASYIS_length=170	41	1	
46	Hp_I08941_IG02555_L1722	126	3	0.17
47	Hp_I22851_IG14795_L620	124	5	0.78
48	Hp_I15488_IG07432_L1169	124	4	0.36
49	Hp_I26227_IG18171_L535	121	3	0.42
50	Hp_I14250_IG06194_L1431	116	2	0.14

Table B.6: Proteins identified in fraction 29 of the sequential fractionation of HES (continued).

Rank	Protein accession number	Protein score	Protein matches	emPAI
51	Hp_I12336_IG04280_L5030	115	4	0.06
51	Hp_I05631_IG01010_L1108	40	1	
52	Hp_I24441_IG16385_L572	113	4	0.85
53	Hp_I38698_IG30642_L388	111	3	0.59
54	FL8UM6J01B7CV6_length=228	109	3	2.29
55	Hp_I36714_IG28658_L408	109	2	0.62
56	Hp_I08175_IG02172_L1570	107	7	0.52
56	Hp_I32820_IG24764_L439	76	2	
56	Hp_I19423_IG11367_L741	58	1	
56	GKYPR1L02BXFPQ_length=335	22	1	
57	Hp_I28140_IG20084_L502	104	2	0.43
58	Hp_I14513_IG06457_L1354	100	2	0.15
59	Hp_I23615_IG15559_L596	99	3	0.59
59	GKYPR1L02BZNH0_length=404	37	1	
60	Hp_I18845_IG10789_L800	97	2	0.25
61	Hp_I25374_IG17318_L554	97	1	0.17
62	Hp_I38988_IG30932_L386	96	5	2.12
63	Hp_I12337_IG04281_L4997	96	5	0.09
63	FL3BO7403BPZG6_length=114	52	1	
63	FL8UM6J01B4I85_length=259	47	1	
64	Hp_I10517_IG03343_L655	95	4	0.74
64	Hp_I10518_IG03343_L562	84	4	0.91
65	Hp_I14314_IG06258_L1412	94	2	0.14
66	Hp_I03750_IG00471_L768	94	3	0.42
67	Hp_I11671_IG03920_L408	91	2	0.55
68	Hp_C00053_IG00001_L722	91	2	0.3
68	Hp_I21133_IG13077_L683	66	3	0.48
68	Hp_I06559_IG01341_L2453	88	1	
68	Hp_I08959_IG02564_L1212	50	2	
68	Hp_I45702_IG37646_L317	47	1	
68	Hp_I20188_IG12132_L723	32	2	
68	Hp_I02590_IG00245_L1152	30	1	
69	Hp_I07314_IG01741_L2856	90	2	0.07
70	Hp_I08946_IG02557_L754	87	4	0.42
71	Hp_I27122_IG19066_L517	86	2	0.43
72	Hp_I22064_IG14008_L644	86	1	0.15

Table B.6: Proteins identified in fraction 29 of the sequential fractionation of HES (continued).

Rank	Protein accession number	Protein score	Protein matches	emPAI
73	Hp_I32194_IG24138_L452	85	1	0.22
74	Hp_I15587_IG07531_L1141	85	4	0.37
75	Hp_I01036_IG00067_L1461	85	4	0.29
75	FL8UM6J01CLAA6_length=170	70	3	
75	Hp_I13955_IG05899_L1513	65	3	
75	Hp_I14843_IG06787_L1280	42	1	
76	Hp_I22470_IG14414_L621	85	5	1.12
76	Hp_I01045_IG00068_L1382	50	3	0.22
76	Hp_I24175_IG16119_L582	60	3	
77	Hp_I15760_IG07704_L1122	85	2	0.18
78	Hp_I07995_IG02081_L699	84	2	0.3
79	Hp_I05999_IG01134_L555	84	1	0.18
80	Hp_I21825_IG13769_L655	84	1	0.15
81	Hp_I07249_IG01697_L637	84	2	0.32
82	Hp_I05325_IG00908_L1903	83	2	0.11
82	Hp_I05327_IG00908_L1147	80	1	
83	Hp_I03369_IG00388_L681	83	2	0.3
84	Hp_I38626_IG30570_L389	82	1	0.26
85	Hp_I21725_IG13669_L658	82	1	0.15
86	Hp_I00695_IG00044_L591	82	2	0.35
87	Hp_I38562_IG30506_L390	82	3	1.05
88	Hp_I05659_IG01019_L943	80	1	0.11
89	Hp_I03611_IG00436_L810	79	4	0.38
89	HELDS7W08JC1EG_length=251	49	1	
90	Hp_I20654_IG12598_L702	77	2	0.29
91	Hp_I10522_IG03345_L588	76	2	0.15
92	GS66ZV203DFM3U_length=95	75	1	1.31
93	Hp_I23836_IG15780_L590	74	1	0.16
94	Hp_I15528_IG07472_L1156	73	3	0.17
95	Hp_I07334_IG01751_L2741	73	1	0.04
96	Hp_I06078_IG01161_L583	72	2	0.37
97	Hp_I13122_IG05066_L1913	71	2	0.1
98	Hp_I24705_IG16649_L569	71	1	0.18
99	Hp_I14119_IG06063_L1461	69	3	0.14
100	Hp_I05827_IG01076_L1116	68	4	0.4
100	Hp_I40994_IG32938_L367	67	3	1.07

Table B.6: Proteins identified in fraction 29 of the sequential fractionation of HES (continued).

Rank	Protein accession number	Protein score	Protein matches	emPAI
101	Hpb-VAL-14	67	3	0.24
102	Hp_I15710_IG07654_L1132	67	1	0.08
103	Hp_I35779_IG27723_L416	67	2	0.53
104	Hp_C00031_IG00001_L1071	66	1	0.09
105	Hpb-TRP	64	1	0.11
106	Hp_I44260_IG36204_L332	64	1	0.31
107	Hp_I17476_IG09420_L907	62	2	0.22
108	Hp_I06750_IG01437_L1569	61	2	0.13
109	Hp_I07527_IG01847_L1908	60	1	0.05
110	Hp_I13066_IG05010_L1961	59	2	0.1
111	Hp_I06838_IG01481_L1319	59	2	0.08
112	Hp_I03893_IG00508_L677	57	1	0.14
113	Hp_I05472_IG00957_L1361	56	2	0.15
114	Hp_I09071_IG02620_L1210	56	1	0.08
115	Hp_I34129_IG26073_L426	56	2	0.51
116	Hp_I22350_IG14294_L635	55	1	0.15
117	Hp_I32832_IG24776_L445	53	1	0.22
118	Hp_C00282_IG00001_L564	53	1	0.17
119	Hp_I34646_IG26590_L427	53	3	0.53
120	Hp_I17450_IG09394_L904	53	1	0.1
121	Hp_I12608_IG04552_L2437	52	1	0.04
122	Hp_I07171_IG01652_L539	51	2	0.4
123	Hp_I22261_IG14205_L639	51	1	0.16
124	Hp_I25974_IG17918_L541	50	2	0.39
125	Hp_I16083_IG08027_L1071	49	1	0.09
126	Hp_I32811_IG24755_L446	49	1	0.22
127	Hp_I20539_IG12483_L707	48	2	0.29
128	Hp_I45281_IG37225_L323	47	2	0.73
128	GS66ZV208IXGIJ_length=214	46	1	
129	Hp_I07274_IG01721_L3765	46	2	0.05
130	Hp_I17541_IG09485_L897	46	1	0.1
131	Hp_I14584_IG06528_L1336	45	2	0.15
132	Hp_I19958_IG11902_L735	44	2	0.28
133	Hp_I30926_IG22870_L465	44	1	0.21
134	Hp_I43395_IG35339_L341	44	1	0.32
135	Hp_I49433_IG41377_L267	44	1	0.37

Table B.6: Proteins identified in fraction 29 of the sequential fractionation of HES (continued).

Rank	Protein accession number	Protein score	Protein matches	emPAI
136	Hp_I15237_IG07181_L1208	44	1	0.08
137	Hp_I54277_IG46221_L174	44	1	0.66
138	Hp_I42038_IG33982_L358	43	2	0.66
139	Hp_I28260_IG20204_L501	43	1	0.22
140	Hp_I05355_IG00918_L1570	43	1	0.06
141	Hp_I13874_IG05818_L1547	43	1	0.07
142	Hp_I19711_IG11655_L743	43	1	0.13
143	Hpb-VAL-8	42	3	0.24
144	Hp_I32108_IG24052_L453	42	2	0.22
145	Hp_I03099_IG00335_L808	42	1	0.12
146	Hp_I01422_IG00100_L1076	42	1	0.09
147	Hp_I14757_IG06701_L1297	41	1	0.07
148	HICN8C105FSWIS_length=222	41	1	0.48
149	HELDS7W07IETUG_length=224	41	1	0.47
150	Hp_I13588_IG05532_L1650	41	1	0.06
151	Hp_I32912_IG24856_L446	40	1	0.22
152	Hp_I05397_IG00932_L1799	40	1	0.05
153	Hp_I15168_IG07112_L1217	40	2	0.08
154	Hp_I27637_IG19581_L511	40	2	0.41
155	Hp_I12977_IG04921_L2010	38	1	0.05
156	Hp_I22248_IG14192_L638	38	1	0.15
157	Hp_I02801_IG00283_L2030	37	1	0.05
158	GSXTT4C06GQDI1_length=169	37	1	0.66
159	Hp_I16562_IG08506_L1005	37	3	0.21
160	Hp_I12444_IG04388_L2875	37	1	0.03
161	Hp_I31855_IG23799_L456	37	2	0.47
162	Hp_I05809_IG01070_L1113	36	1	0.09
163	Hp_I13666_IG05610_L1621	36	1	0.06
164	Hp_I05482_IG00960_L1223	36	1	0.08
165	Hp_I11144_IG03656_L469	36	2	0.21
166	Hp_I14323_IG06267_L1413	35	1	0.07
167	GSXTT4C06GZXXX_length=291	35	1	0.36
168	Hp_I43570_IG35514_L336	35	1	0.29
169	GP9KNTD03FPOC6_length=206	35	1	0.53
170	Hp_I13752_IG05696_L1585	35	1	0.06
171	Hp_I36380_IG28324_L410	35	1	0.24

Table B.6: Proteins identified in fraction 29 of the sequential fractionation of HES (continued).

Rank	Protein accession number	Protein score	Protein matches	emPAI
172	Hp_I25825_IG17769_L543	35	1	0.18
173	Hp_I17216_IG09160_L933	34	1	0.1
174	GNK0QLK03FM4KR_length=324	34	1	0.32
175	Hp_I48638_IG40582_L276	34	1	0.36
176	Hp_I13426_IG05370_L1731	34	1	0.06
177	Hpb-VAL-3	34	3	0.22
177	Hp_I05548_IG00982_L1432	22	1	
177	Hp_I19215_IG11159_L774	21	1	
178	Hp_I26494_IG18438_L527	33	1	0.18
179	Hp_I05927_IG01110_L916	33	1	0.1
180	Hp_I47440_IG39384_L295	33	1	0.33
181	Hp_I24494_IG16438_L573	33	1	0.17
182	Hp_I27407_IG19351_L514	33	1	0.2
183	Hp_I22123_IG14067_L644	33	1	0.15
184	Hp_I29233_IG21177_L488	32	1	0.19
185	HICN8C106HC28H_length=166	32	1	0.64
186	Hp_I45671_IG37615_L316	31	1	0.34
187	GSXTT4C07H9V8V_length=405	31	3	0.24
188	Hp_I13843_IG05787_L1552	31	1	0.06
189	Hp_I12776_IG04720_L2202	30	1	0.04
190	Hp_I35665_IG27609_L418	30	1	0.24
191	HELDS7W07IJKS4_length=381	30	1	0.27
192	Hp_I12342_IG04286_L4223	29	1	0.02
193	HICN8C105F8RGF_length=429	29	1	0.24
194	Hp_I24623_IG16567_L570	28	2	0.17
195	Hp_I10916_IG03542_L519	28	1	0.19
196	Hp_I00739_IG00047_L2586	28	2	0.07
197	Hp_I06001_IG01134_L530	27	1	0.19
198	Hp_I01453_IG00104_L978	27	1	0.1
199	Hp_I22685_IG14629_L621	27	1	0.16
200	Hp_I18969_IG10913_L793	27	2	0.26
201	Hp_I17168_IG09112_L939	26	1	0.11
202	Hp_I38243_IG30187_L393	26	1	0.26
203	Hp_I14648_IG06592_L1319	26	1	0.07
204	Hp_I12442_IG04386_L2881	26	1	0.03
205	Hp_I09519_IG02844_L954	26	1	0.11

Table B.6: Proteins identified in fraction 29 of the sequential fractionation of HES (continued).

Rank	Protein accession number	Protein score	Protein matches	emPAI
206	Hp_I09018_IG02593_L883	26	1	0.11
207	Hp_I30585_IG22529_L470	25	1	0.21
208	Hp_I40421_IG32365_L372	25	1	0.26
209	Hp_I13527_IG05471_L1682	25	1	0.06
210	Hp_I09575_IG02872_L1199	25	1	0.08
211	Hp_I08844_IG02506_L1048	25	1	0.09
212	Hp_I08219_IG02194_L2089	25	1	0.05
213	Hp_I45709_IG37653_L316	24	1	0.32
214	Hp_I26246_IG18190_L526	24	1	0.18
215	Hp_I18874_IG10818_L798	24	1	0.12
216	FL8UM6J01DWGTH_length=207	24	1	0.49
217	Hp_I04010_IG00535_L4397	24	1	0.02
218	GSXTT4C05FSGQ4_length=438	23	1	0.25
219	Hp_I17380_IG09324_L905	23	1	0.11
220	Hp_I16462_IG08406_L1016	23	1	0.09
221	Hp_I16505_IG08449_L1014	23	1	0.09
222	Hp_I40256_IG32200_L371	22	1	0.26
223	Hp_I12485_IG04429_L2697	22	1	0.04
224	Hp_I23359_IG15303_L605	22	1	0.16
225	Hp_I12350_IG04294_L3967	21	1	0.02
226	Hp_I51114_IG43058_L239	21	1	0.47
227	Hp_I07482_IG01825_L2043	21	1	0.05
228	Hp_I04378_IG00631_L1589	20	1	0.06

Table B.7: Proteins identified in fraction 30 of the sequential fractionation of HES. HES was fractionated by size exclusion followed by anion exchange fractionation. All fractions were analysed by mass spectrometry and tested for their inhibitory activity on GM-CSF BMDC. Fraction 30 showed the ability to completely inhibit IL-12p70 production. Listed are ranks of the proteins in the mass spectrometric analysis, their accession numbers, the number of peptide hits for the respective protein and their emPAI values. Red: expressed proteins.

Rank	Protein accession number	Protein score	Protein matches	emPAI
1	HICN8C106HP9PI_length=274	911	32	8.85
1	Hp_I10288_IG03228_L610	851	29	
2	GNK0QLK03GQOZO_length=396	836	24	2.74
2	GS66ZV203C3717_length=247	731	20	
2	GS66ZV203DJXOH_length=245	692	18	
2	GWDWRH002CES3N_length=67	122	4	
3	Hp_I04570_IG00700_L4683	764	37	0.94
4	Hp_I10419_IG03294_L714	742	23	5.14
5	Hp_I19157_IG11101_L778	679	17	4.58
6	Hp_I02849_IG00289_L1962	664	18	0.2
6	Hp_I02850_IG00289_L1486	614	17	
6	Hp_I02853_IG00289_L1028	77	1	
7	Hp_I35779_IG27723_L416	633	18	28.95
8	Hp_I08665_IG02417_L1321	464	14	1.46
8	Hp_I08666_IG02417_L925	81	1	
8	Hp_I32943_IG24887_L443	37	1	
9	Hp_I10590_IG03379_L588	420	13	6.15
9	Hp_I10589_IG03379_L596	149	4	
10	Hp_I21313_IG13257_L675	377	11	2.24
11	Hp_I01065_IG00070_L5127	376	25	0.42
11	FL8UM6J01BC1ZN_length=62	125	4	67.44
11	Hp_I01061_IG00070_L5128	370	24	
11	Hp_I01081_IG00070_L5124	359	24	
11	Hp_I01077_IG00070_L5125	352	23	
11	FL8UM6J01AP92T_length=187	56	2	
11	FL8UM6J01C588R_length=58	33	1	
12	Hpb-VAL-4	370	8	2.06
12	FL8UM6J01BXB62_length=190	297	5	
12	FL8UM6J01BH6HY_length=236	128	2	
13	Hp_I40421_IG32365_L372	369	7	4.17
14	Hp_I07157_IG01645_L560	326	16	12.23

Table B.7: Proteins identified in fraction 30 of the sequential fractionation of HES (continued).

Rank	Protein accession number	Protein score	Protein matches	emPAI
14	Hp_I07158_IG01645_L560	228	13	7.15
15	Hp_I22851_IG14795_L620	315	13	3.9
16	Hp_I05758_IG01053_L926	283	5	0.65
16	Hp_I05759_IG01053_L914	122	1	
17	Hp_I22486_IG14430_L629	272	7	1.42
17	GSXTT4C07IB13H_length=463	197	6	1.89
17	Hp_I08791_IG02480_L1486	186	10	0.68
17	Hp_I13898_IG05842_L1539	54	3	0.21
17	Hp_I08792_IG02480_L662	59	4	
17	Hp_I19246_IG11190_L772	43	3	
17	Hpb-VAL-1.1	42	2	
17	Hp_I04671_IG00730_L1535	39	2	
17	Hp_I20083_IG12027_L726	30	1	
17	HICN8C104EUPYS_length=127	26	1	
18	Hp_I14119_IG06063_L1461	264	4	0.29
19	Hp_I24512_IG16456_L570	257	9	3.18
19	GNK0QLK03F82AT_length=271	150	3	
20	Hpb-VAL-3	251	8	0.69
20	Hp_I05548_IG00982_L1432	147	3	
20	Hp_I19215_IG11159_L774	57	1	
20	Hp_I48980_IG40924_L272	50	1	
21	HELDS7W08JQN3O_length=274	235	5	0.94
22	Hp_I28744_IG20688_L490	226	8	3.21
23	Hp_I19378_IG11322_L765	225	5	0.83
24	Hp_I13075_IG05019_L1949	225	10	0.43
24	Hp_I28606_IG20550_L493	52	1	
25	Hp_I25889_IG17833_L540	223	5	1.31
26	Hp_I26601_IG18545_L528	208	6	1.96
26	GSXTT4C05GBC4L_length=430	72	1	
27	Hp_I18858_IG10802_L799	203	6	0.98
28	Hp_I23776_IG15720_L592	203	7	1.48
29	Hp_I03750_IG00471_L768	198	4	0.59
30	Hp_I36380_IG28324_L410	189	7	3.52
31	Hp_I13810_IG05754_L1566	188	6	0.42
32	Hp_I40999_IG32943_L364	187	4	1.71
33	Hp_I07314_IG01741_L2856	184	4	0.14

Table B.7: Proteins identified in fraction 30 of the sequential fractionation of HES (continued).

Rank	Protein accession number	Protein score	Protein matches	emPAI
34	Hp_I02051_IG00167_L1023	183	4	0.43
34	GS66ZV202BZOD1_length=219	104	2	
34	GS66ZV203C3ECE_length=216	100	2	
34	Hp_I48914_IG40858_L269	35	1	
35	Hp_I25374_IG17318_L554	178	3	0.62
36	Hp_I05999_IG01134_L555	166	3	0.64
37	Hp_I10136_IG03152_L609	165	4	0.79
38	Hp_I43851_IG35795_L337	164	4	1.8
39	Hp_I50492_IG42436_L247	161	8	10.46
39	Hp_I50368_IG42312_L251	128	5	
40	Hp_I07496_IG01832_L2183	161	4	0.18
40	Hp_I07497_IG01832_L1722	154	4	0.24
41	Hp_I28140_IG20084_L502	160	4	1.04
42	Hp_I24965_IG16909_L566	152	5	1.21
43	Hp_I15710_IG07654_L1132	148	3	0.27
43	Hp_I25323_IG17267_L551	90	1	
44	Hp_I29394_IG21338_L484	147	4	1.15
45	Hp_I23528_IG15472_L598	143	3	0.6
46	Hp_I00798_IG00050_L1759	131	3	0.17
46	Hp_I00806_IG00050_L1112	40	2	0.18
46	Hp_I00796_IG00050_L1763	96	2	
46	Hp_I00809_IG00050_L1090	90	1	
46	Hp_I00811_IG00050_L794	28	1	
47	Hp_I04541_IG00689_L698	131	5	0.68
47	Hp_I04543_IG00689_L522	67	3	
47	Hp_I02360_IG00213_L980	64	1	
48	Hp_I10518_IG03343_L562	129	5	0.91
48	Hp_I10517_IG03343_L655	107	5	0.74
49	Hp_I12337_IG04281_L4997	129	7	0.11
49	FL8UM6J01BGCU6_length=234	50	2	
49	FL3BO7403BPZG6_length=114	49	1	
50	Hp_I21565_IG13509_L658	128	4	0.73
51	Hp_I12705_IG04649_L2285	125	2	0.08
51	FL8UM6J01CI46H_length=220	86	1	
52	Hp_I17933_IG09877_L867	123	3	0.39
53	Hp_C00031_IG00001_L1071	121	3	0.3

Table B.7: Proteins identified in fraction 30 of the sequential fractionation of HES (continued).

Rank	Protein accession number	Protein score	Protein matches	emPAI
54	Hp_I07312_IG01740_L4913	119	5	0.1
54	Hp_I30910_IG22854_L463	31	2	
55	Hp_I12336_IG04280_L5030	117	3	0.06
56	Hp_I12624_IG04568_L2400	115	5	0.22
56	FL8UM6J01C5SEG_length=170	79	2	
57	Hp_I34581_IG26525_L426	113	3	0.93
58	Hp_I00801_IG00050_L1766	110	2	0.11
58	Hp_I00800_IG00050_L1766	82	1	
59	Hp_I15587_IG07531_L1141	110	4	0.37
60	Hp_I08475_IG02322_L1881	108	1	0.05
61	Hp_I12776_IG04720_L2202	108	3	0.13
62	Hp_I15760_IG07704_L1122	106	2	0.18
63	Hp_I34129_IG26073_L426	106	2	0.51
64	Hp_I13527_IG05471_L1682	105	3	0.18
65	Hp_I26188_IG18132_L529	101	3	0.64
66	Hp_I14513_IG06457_L1354	100	2	0.15
67	Hp_I22064_IG14008_L644	95	3	0.51
67	Hp_I21699_IG13643_L657	36	1	
68	Hp_I11671_IG03920_L408	95	3	0.93
69	Hp_I10155_IG03162_L783	92	2	0.25
69	Hp_I10156_IG03162_L593	37	1	
70	Hp_I27122_IG19066_L517	90	3	0.7
71	Hp_I38626_IG30570_L389	89	1	0.26
72	Hp_I21725_IG13669_L658	87	1	0.15
73	Hp_C00053_IG00001_L722	86	1	0.14
74	Hp_I27254_IG19198_L516	84	2	0.41
75	Hp_I32194_IG24138_L452	82	2	0.48
76	Hp_I05827_IG01076_L1116	82	5	0.52
76	Hp_I40994_IG32938_L367	33	2	
77	Hp_I07995_IG02081_L699	81	2	0.3
78	Hp_I19711_IG11655_L743	81	1	0.13
79	Hp_I30926_IG22870_L465	80	2	0.47
80	Hp_I36714_IG28658_L408	80	3	0.62
81	Hp_I30337_IG22281_L473	80	1	0.22
82	FL8UM6J01B7CV6_length=228	80	2	1.21
83	Hp_I05355_IG00918_L1570	79	2	0.12

Table B.7: Proteins identified in fraction 30 of the sequential fractionation of HES (continued).

Rank	Protein accession number	Protein score	Protein matches	emPAI
84	Hp_I13494_IG05438_L1681	79	1	0.06
85	Hp_I20654_IG12598_L702	74	2	0.29
86	Hp_I05472_IG00957_L1361	74	1	0.07
87	Hp_I08175_IG02172_L1570	73	6	0.35
87	Hp_I32820_IG24764_L439	61	2	
87	Hp_I19423_IG11367_L741	20	1	
88	Hp_I38698_IG30642_L388	73	3	1
89	Hp_I24441_IG16385_L572	73	2	0.36
90	Hpb-VAL7.1	70	2	0.29
91	Hp_I19958_IG11902_L735	69	2	0.28
92	Hp_I14250_IG06194_L1431	69	1	0.07
93	Hp_I05407_IG00935_L1040	69	1	0.09
94	Hp_I52412_IG44356_L216	68	2	1.13
95	Hp_I03893_IG00508_L677	68	1	0.14
96	Hp_I30585_IG22529_L470	67	1	0.21
97	Hp_I05648_IG01016_L1943	65	1	0.05
98	Hp_I07249_IG01697_L637	65	1	0.15
99	Hp_I07334_IG01751_L2741	64	1	0.04
100	Hp_I14314_IG06258_L1412	64	2	0.14
101	Hp_I18845_IG10789_L800	64	1	0.12
102	Hp_I24607_IG16551_L570	63	1	0.17
103	Hp_I44260_IG36204_L332	63	1	0.31
104	Hp_I53318_IG45262_L197	62	2	1.66
104	Hp_I15769_IG07713_L1115	48	1	
105	Hp_I21133_IG13077_L683	62	2	0.3
105	Hp_I20188_IG12132_L723	21	1	
106	Hp_I15237_IG07181_L1208	61	1	0.08
107	GSXTT4C07H11X2_length=416	61	2	0.54
107	GSXTT4C08I6F9R_length=269	54	1	
108	Hp_I15133_IG07077_L1218	59	1	0.08
109	Hp_I13832_IG05776_L1555	59	1	0.06
110	Hpb-VAL-7.3	56	1	0.14
111	Hp_I00747_IG00047_L1129	56	2	0.18
112	Hp_I42038_IG33982_L358	54	2	0.66
113	Hp_I17476_IG09420_L907	54	2	0.22
114	Hp_I06001_IG01134_L530	54	1	0.19

Table B.7: Proteins identified in fraction 30 of the sequential fractionation of HES (continued).

Rank	Protein accession number	Protein score	Protein matches	emPAI
115	Hp_I06838_IG01481_L1319	51	1	0.08
116	HELDS7W07H0BVM_length=251	50	1	0.41
117	Hp_I15528_IG07472_L1156	50	2	0.17
118	Hp_I13752_IG05696_L1585	49	1	0.06
119	Hp_I05190_IG00863_L3474	49	1	0.03
120	Hpb-TRP	49	1	0.11
121	Hp_I27637_IG19581_L511	49	1	0.19
122	Hp_I01036_IG00067_L1461	48	2	0.14
122	Hp_I14843_IG06787_L1280	38	1	
122	FL8UM6J01CLAA6_length=170	29	1	
123	HICN8C105FSWIS_length=222	48	1	0.48
124	Hp_I45281_IG37225_L323	47	2	0.32
125	Hp_I49433_IG41377_L267	47	1	0.37
126	Hp_I03099_IG00335_L808	47	1	0.12
127	Hp_I35665_IG27609_L418	46	2	0.24
128	Hp_I12342_IG04286_L4223	46	1	0.02
129	Hp_I34646_IG26590_L427	46	3	0.89
130	Hp_I05927_IG01110_L916	46	1	0.1
131	Hp_I23863_IG15807_L590	46	1	0.16
132	Hp_I08946_IG02557_L754	44	2	0.27
132	Hp_I28711_IG20655_L493	31	1	
133	Hp_I26937_IG18881_L522	44	1	0.19
134	Hp_I04148_IG00569_L936	43	1	0.1
135	Hp_I05565_IG00988_L1210	43	1	0.08
136	Hp_I16781_IG08725_L979	43	1	0.1
137	Hp_I19989_IG11933_L735	42	1	0.14
138	Hp_I14795_IG06739_L1291	42	1	0.07
139	Hp_I27407_IG19351_L514	42	1	0.2
140	Hp_I13122_IG05066_L1913	42	1	0.05
141	Hp_I02136_IG00181_L1019	41	2	0.2
142	Hp_I54277_IG46221_L174	41	1	0.66
143	Hp_I10087_IG03128_L706	40	1	0.13
144	Hp_I38111_IG30055_L394	40	1	0.25
145	Hp_I32912_IG24856_L446	39	1	0.22
146	Hp_I12356_IG04300_L3770	39	2	0.05
147	Hp_I20633_IG12577_L701	39	1	0.14

Table B.7: Proteins identified in fraction 30 of the sequential fractionation of HES (continued).

Rank	Protein accession number	Protein score	Protein matches	emPAI
148	Hpb-VAL-14	39	1	0.07
149	GSXTT4C06G5C5J_length=208	39	1	0.5
150	Hp_I22470_IG14414_L621	39	1	0.16
151	Hp_I38988_IG30932_L386	38	2	0.58
152	Hp_I43570_IG35514_L336	38	1	0.29
153	GSXTT4C07H9V8V_length=405	38	3	0.53
153	GSXTT4C07H6OEY_length=167	35	1	
153	HICN8C104EVBCL_length=374	25	2	
154	Hp_I16462_IG08406_L1016	38	1	0.09
155	Hp_I17541_IG09485_L897	37	1	0.1
156	Hp_I45709_IG37653_L316	37	1	0.32
157	Hp_I07494_IG01831_L2349	36	2	0.08
158	Hp_I40417_IG32361_L370	35	1	0.27
159	Hp_I22261_IG14205_L639	35	1	0.16
160	Hpb-VAL-8	35	1	0.08
161	Hp_I29233_IG21177_L488	35	1	0.19
162	Hp_I07286_IG01727_L3181	34	1	0.03
163	Hp_I31855_IG23799_L456	34	2	0.47
164	Hp_I11951_IG04060_L390	33	1	0.24
165	HICN8C104ETD9I_length=322	33	1	0.32
166	Hp_I14909_IG06853_L1261	33	1	0.08
167	HELDS7W07IETUG_length=224	32	1	0.47
168	Hp_I13066_IG05010_L1961	32	1	0.05
169	Hp_C00282_IG00001_L564	32	1	0.17
170	Hp_I15168_IG07112_L1217	32	1	0.08
171	Hp_I07527_IG01847_L1908	31	2	0.05
172	Hp_I01453_IG00104_L978	31	1	0.1
173	HICN8C106G3J43_length=50	30	1	2.83
174	Hp_I45843_IG37787_L315	30	1	0.33
175	Hp_I11144_IG03656_L469	30	1	0.21
176	FL8UM6J01DWGTH_length=207	30	1	0.49
177	Hp_I05468_IG00955_L951	30	1	0.1
178	Hp_I13426_IG05370_L1731	29	1	0.06
179	HICN8C105F7BX8_length=227	29	1	0.47
180	Hp_I05315_IG00904_L1277	29	1	0.08
181	Hp_I13909_IG05853_L1521	29	1	0.06

Table B.7: Proteins identified in fraction 30 of the sequential fractionation of HES (continued).

Rank	Protein accession number	Protein score	Protein matches	emPAI
182	Hp_I24096_IG16040_L584	29	1	0.18
183	GKYPR1L02BZNH0_length=404	28	1	0.24
184	Hp_I12361_IG04305_L3540	28	1	0.03
185	Hp_I40246_IG32190_L374	27	1	0.27
186	Hp_I07814_IG01991_L1596	27	1	0.06
187	Hp_I16226_IG08170_L1053	27	1	0.09
188	Hpb-VAL-12	27	1	0.07
189	Hp_I17216_IG09160_L933	26	1	0.1
190	GLSD98I05F0MGD_length=346	25	1	0.29
191	Hp_I01758_IG00132_L2863	25	1	0.03
192	Hp_I15461_IG07405_L1171	24	1	0.08
193	Hp_I30912_IG22856_L462	24	1	0.23
194	Hp_I51550_IG43494_L231	24	1	0.47
195	Hp_I45971_IG37915_L313	23	1	0.32
196	Hp_I07274_IG01721_L3765	23	1	0.03
197	Hp_I32832_IG24776_L445	23	1	0.22
198	Hp_I09016_IG02592_L604	23	1	0.16
199	Hp_I23359_IG15303_L605	23	1	0.16
200	Hp_I14323_IG06267_L1413	23	1	0.07
201	GS66ZV203DB0T9_length=193	23	1	0.55
202	Hp_I09018_IG02593_L883	22	1	0.11
203	Hp_I20539_IG12483_L707	22	1	0.14
204	Hp_I03369_IG00388_L681	21	1	0.14
205	Hp_I36389_IG28333_L409	21	1	0.23
206	Hp_I23736_IG15680_L595	21	1	0.17
207	Hp_I44251_IG36195_L332	21	1	0.31
208	Hp_I19755_IG11699_L745	21	1	0.13
209	Hp_I09809_IG02989_L788	21	1	0.13
210	Hp_I08063_IG02116_L1656	20	1	0.06
211	Hp_I09465_IG02817_L1098	20	1	0.09

Table B.8: Proteins with emPAI values peaking in active sequential fractions 28-30 with their emPAI values across the fractions. HES was fractionated by size exclusion followed by anion exchange fractionation. All fractions were analysed by mass spectrometry and tested for their inhibitory activity on GM-CSF BMDC. Proteins with emPAI values peaking in the active fractions were identified and only those considered for further selection of proteins with emPAI profiles fitting the activity profile of the fractions. Green text: Proteins with good fits that were later excluded; Red text: expressed proteins.

	21	22	23	24	25	26	27	28	29	30	31	32	33	34	35
FL8UM6J01BH6V1_length=59	0	0	0	0	0	0	0	2.43	0	0	0	0	0	0	0
FL8UM6J01CI46H_length=220	0	0	0	0	0	0	0	0.45	0	0	0	0	0	0	0
FL8UM6J01D4QX3_length=59	0	0	0	0	0	0	0	2.43	0	0	0	0	0	0	0
GKYPR1L02CFV8D_length=134	0	0	0	0	0	0	0	0.87	0	0	0	0	0	0	0
GLSD98I04EIBBZ_length=463	0	0	0	0	0	0	0	0.23	0	0	0	0	0	0	0
GNK0QLK03FM4KR_length=324	0	0	0	0	0	0	0	0	0.32	0	0	0	0	0	0
GNK0QLK03GQOZO_length=396	0	0	0	0	0.25	0.25	0.25	1.41	2.74	2.74	1.41	1.41	0.55	0.25	0.55
GP9KNTD03FLCRS_length=301	0	0	0	0	0	0	0.33	0.33	0	0	0	0	0	0	0
GP9KNTD03FMXAA_length=261	0	0	0	0	0	0.36	0	0.36	0	0	0	0	0	0	0
GP9KNTD03GRXA0_length=393	0	0	0	0	0	0	0	0.24	0	0	0	0	0	0	0
GS66ZV203DB0T9_length=193	0	0	0	0	0	0.55	0.55	0	0	0.55	0	0	0	0	0
GS66ZV208JGIBQ_length=382	0	0	0	0	0	0	0	0.27	0	0	0	0	0	0	0
GSXTT4C05FNWZW_length=206	0	0	0	0	0	0	0	0.52	0	0	0	0	0	0	0
GSXTT4C05FSGQ4_length=438	0	0	0	0	0	0	0	0	0.25	0	0	0	0	0	0
GSXTT4C06GQDI1_length=169	0	0	0	0	0	0	0	0.66	0.66	0	0	0	0	0	0
GSXTT4C06GZXXX_length=291	0	0	0	0	0	0	0	0	0.36	0	0	0	0	0	0
GSXTT4C07H1SRT_length=291	0	0	0	0	0	0	0	0.36	0	0	0	0	0	0	0
GSXTT4C07H9V8V_length=405	0	0	0	0	0	0	0.53	0.24	0.24	0.53	0	0	0	0	0
GSXTT4C07IB13H_length=463	0	0	0	0.53	0.89	1.34	0.89	2.58	1.34	1.89	1.34	1.34	0.24	0.53	0.89

Table B.8: Proteins with emPAI values peaking in active sequential fractions 28-30 with their emPAI values across the fractions (continued).

	21	22	23	24	25	26	27	28	29	30	31	32	33	34	35
GW6977U05FJ9VT_length=110	0	0	0	2.88	0	2.88	0	2.88	0	0	0	0	0	0	0
HELDS7W07IETUG_length=224	0	0	0	0	0	0	0	0.47	0.47	0.47	0	0	0	0	0
HELDS7W07IJKS4_length=381	0	0	0	0	0	0	0	0.27	0.27	0	0	0	0	0	0
HICN8C104EF9L9_length=388	0	0	0	0	0	0	0	0.27	0	0	0	0	0	0	0
HICN8C104EH4N8_length=157	0	0	0	0	0	0	0.68	0.68	0	0	0	0	0	0	0
HICN8C104ETD9I_length=322	0	0	0	0	0	0	0	0	0	0.32	0	0	0	0	0
HICN8C105F7BX8_length=227	0	0	0	0	0	0	0	0	0	0.47	0	0	0	0	0
HICN8C105F8RGF_length=429	0	0	0	0	0	0	0	0	0.24	0	0	0	0	0	0
HICN8C106G3J43_length=50	0	0	0	0	0	0	0	0	0	2.83	0	0	0	0	0
HICN8C106HC28H_length=166	0	0	0	0	0	0	0	0	0.64	0	0	0	0	0	0
HICN8C106HP9PI_length=274	0	0	0.35	0	0.35	1.45	0.82	3.46	12.66	8.85	6.11	8.85	7.11	5.01	8.85
Hp_C00031_IG00001_L1071	0	0	0	0	0	0.09	0.19	0.09	0.09	0.3	0.09	0.19	0	0.09	0
Hp_C00065_IG00001_L1348	0	0	0	0	0	0.07	0	0.07	0	0	0	0	0	0	0
Hp_C00269_IG00001_L1007	0	0	0	0	0	0.31	0.89	1.07	0.44	0	0	0	0	0	0
Hp_I00695_IG00044_L591	0	0	0.35	0.35	0	0.16	0.16	0.16	0.35	0	0	0	0	0	0
Hp_I00747_IG00047_L1129	0	0	0	0	0	0	0	0	0	0.18	0	0	0	0	0
Hp_I00806_IG00050_L1112	0	0	0	0	0	0	0.18	0.09	0.18	0.18	0	0	0	0	0
Hp_I01036_IG00067_L1461	0	0.07	0.07	0.14	0.14	0.07	0.07	0.07	0.29	0.14	0.07	0	0	0	0
Hp_I01045_IG00068_L1382	0	0	0	0	0	0	0	0	0.22	0	0	0	0	0	0
Hp_I01061_IG00070_L5128	0	0	0	0.02	0	0.18	0.31	0	0.67	0	0.31	0	0	0.06	0.02
Hp_I01063_IG00070_L5127	0	0	0	0	0	0	0	0.25	0	0	0	0	0	0	0
Hp_I01065_IG00070_L5127	0	0	0	0	0	0	0	0	0	0.42	0	0	0	0	0

Table B.8: Proteins with emPAI values peaking in active sequential fractions 28-30 with their emPAI values across the fractions (continued).

	21	22	23	24	25	26	27	28	29	30	31	32	33	34	35
Hp_I01077_IG00070_L5125	0	0	0	0	0	0	0	0.22	0	0	0	0	0	0	0
Hp_I01079_IG00070_L5124	0	0	0	0	0	0	0	0	0.67	0	0	0.24	0	0	0
Hp_I01422_IG00100_L1076	0	0	0	0.09	0	0.09	0.09	0.09	0.09	0	0	0	0	0	0
Hp_I01758_IG00132_L2863	0	0	0	0	0	0	0	0	0	0.03	0	0	0	0	0
Hp_I02051_IG00167_L1023	0	0	0	0	0	0	0	0.44	1.07	0.43	0	0	0	0	0
Hp_I02136_IG00181_L1019	0	0	0	0	0	0	0	0.2	0	0.2	0	0	0	0	0
Hp_I02849_IG00289_L1962	0	0	0	0.2	0.2	0.32	0.26	0.27	0.4	0.2	0.2	0.2	0.15	0.15	0.15
Hp_I03228_IG00366_L2337	0	0	0	0	0	0	0	0.04	0	0	0	0	0	0	0
Hp_I03611_IG00436_L810	0	0	0	0	0	0	0	0.38	0.38	0	0	0	0	0	0
Hp_I03750_IG00471_L768	0	0	0	0	0	0	0	0	0.42	0.59	0.42	0.26	0	0	0.26
Hp_I04010_IG00535_L4397	0	0	0	0	0	0	0	0	0.02	0	0	0	0	0	0
Hp_I04083_IG00553_L1755	0	0	0	0	0	0	0.05	0.05	0	0	0	0	0	0	0
Hp_I04541_IG00689_L698	0	0	0.48	0.68	0.3	1.18	0.92	0.68	1.18	0.68	0.68	0.68	0.3	0.3	0.14
Hp_I04570_IG00700_L4683	0	0	0.02	0.06	0.12	0.53	1.45	2.68	1.59	0.94	0.66	0.53	0.04	0.04	0.06
Hp_I04581_IG00707_L1760	0	0	0	0	0	0	0	0.06	0	0	0	0	0	0	0
Hp_I04874_IG00782_L1023	0	0	0	0	0	0	0	0.1	0	0	0	0	0	0	0
Hp_I05407_IG00935_L1040	0	0	0	0	0	0	0.09	0.09	0	0.09	0	0	0	0	0
Hp_I05468_IG00955_L951	0	0	0	0	0	0	0	0	0	0.1	0	0	0	0	0
Hp_I05472_IG00957_L1361	0	0	0	0	0	0	0	0.07	0.15	0.07	0.07	0.07	0	0	0
Hp_I05482_IG00960_L1223	0	0	0	0	0	0	0	0	0.08	0	0	0	0	0	0
Hp_I05755_IG01052_L1113	0	0	0	0.09	0.09	0.09	0.09	0.09	0	0	0	0	0	0	0
Hp_I05780_IG01060_L750	0	0	0	0	0	0	0	0.13	0	0	0	0	0	0	0

Table B.8: Proteins with emPAI values peaking in active sequential fractions 28-30 with their emPAI values across the fractions (continued).

	21	22	23	24	25	26	27	28	29	30	31	32	33	34	35
Hp_I05827_IG01076_L1116	0	0	0.18	0.52	0.18	0.38	0.38	0.5	0.4	0.52	0.27	0.18	0.18	0.27	0.18
Hp_I05999_IG01134_L555	0	0	0	0	0	0	0	0	0.18	0.64	0.39	0.39	0	0	0.18
Hp_I06271_IG01234_L1502	0	0	0	0	0	0	0	0.06	0	0	0	0	0	0	0
Hp_I06589_IG01356_L2259	0	0	0	0	0	0	0.04	0.04	0	0	0	0	0	0	0
Hp_I06750_IG01437_L1569	0	0	0	0	0	0	0	0	0.13	0	0	0	0	0	0
Hp_I07155_IG01644_L585	0	0	0	0	0	0	0	0.17	0	0	0	0	0	0	0
Hp_I07171_IG01652_L539	0	0	0	0	0	0.18	0	0	0.4	0	0	0	0	0	0
Hp_I07286_IG01727_L3181	0	0	0	0	0	0	0	0	0	0.03	0	0	0	0	0
Hp_I07312_IG01740_L4913	0	0	0.08	0.14	0.14	0.16	0.14	0.26	0.19	0.1	0.12	0.06	0	0	0
Hp_I07334_IG01751_L2741	0	0	0	0	0	0	0	0.04	0.04	0.04	0	0	0	0	0
Hp_I07378_IG01773_L2592	0	0	0	0	0	0.04	0.04	0.08	0	0	0	0	0	0	0
Hp_I07482_IG01825_L2043	0	0	0	0	0	0	0	0	0.05	0	0	0	0	0	0
Hp_I07496_IG01832_L2183	0	0	0	0.04	0	0.04	0.18	0.29	0.23	0.18	0.18	0	0.04	0	0.04
Hp_I07497_IG01832_L1722	0	0	0	0	0	0	0.24	0.37	0.3	0.24	0.24	0.3	0	0	0
Hp_I08063_IG02116_L1656	0	0	0	0	0	0	0	0	0	0.06	0	0	0	0	0
Hp_I08175_IG02172_L1570	0	0	0	0	0	0.06	0.27	0.13	0.52	0.35	0.2	0.06	0	0	0
Hp_I08227_IG02198_L1357	0	0	0	0	0	0	0	0.07	0	0	0	0	0	0	0
Hp_I08475_IG02322_L1881	0	0	0	0	0	0	0	0.05	0	0.05	0	0	0	0	0
Hp_I08791_IG02480_L1486	0	0	0	0	0	0.68	1.05	1.66	1.05	0.68	0.58	0.48	0.22	0.3	0.3
Hp_I08844_IG02506_L1048	0	0	0	0	0	0	0	0	0.09	0	0	0	0	0	0
Hp_I08941_IG02555_L1722	0	0	0.12	0	0.06	0.06	0.11	0.17	0.17	0	0	0	0	0	0
Hp_I09016_IG02592_L604	0	0	0	0	0	0	0.16	0	0	0.16	0	0	0	0	0

Table B.8: Proteins with emPAI values peaking in active sequential fractions 28-30 with their emPAI values across the fractions (continued).

	21	22	23	24	25	26	27	28	29	30	31	32	33	34	35
Hp_I09071_IG02620_L1210	0	0	0	0	0	0	0	0	0.08	0	0	0	0	0	0
Hp_I09474_IG02821_L795	0	0	0	0	0	0	0	0.12	0	0	0	0	0	0	0
Hp_I09519_IG02844_L954	0	0	0	0	0	0	0	0	0.11	0	0	0	0	0	0
Hp_I09769_IG02969_L1009	0	0	0	0	0	0	0	0.2	0	0	0	0	0.1	0	0
Hp_I09809_IG02989_L788	0	0	0	0	0	0	0	0	0	0.13	0	0	0	0	0
Hp_I10136_IG03152_L609	0	0	0	0	0	0	0	0	0	0.79	0.55	0	0	0	0
Hp_I10419_IG03294_L714	0.3	0.48	0.48	0.68	0.91	1.82	2.66	3.16	5.14	5.14	3.74	1.48	1.82	1.48	0.91
Hp_I10507_IG03338_L686	0	0	0	0	0	0	0	0.14	0	0	0	0	0	0	0
Hp_I10522_IG03345_L588	0	0	0	0	0	0	0	0	0.15	0	0	0	0	0	0
Hp_I10589_IG03379_L596	0	0	0	0	0	0	0.35	0	1.46	0	0	0	0	0	0
Hp_I10590_IG03379_L588	0	0	0	0	0	0	0	3.54	8.68	6.15	2.91	0.57	0	0	0
Hp_I10670_IG03419_L511	0	0	0	0	0	0	0	0.19	0	0	0	0	0	0	0
Hp_I11671_IG03920_L408	0	0	0	0	0	0	0	0	0.55	0.93	0	0	0	0	0
Hp_I11951_IG04060_L390	0	0	0	0.24	0	0	0	0.24	0	0.24	0	0	0	0	0
Hp_I12336_IG04280_L5030	0	0	0	0.04	0.06	0.06	0.1	0.1	0.06	0.06	0.06	0	0	0	0
Hp_I12342_IG04286_L4223	0	0	0	0	0	0	0	0.02	0.02	0.02	0	0	0	0	0
Hp_I12361_IG04305_L3540	0	0	0	0	0	0	0	0	0	0.03	0	0	0	0	0
Hp_I12442_IG04386_L2881	0	0	0	0	0	0	0	0	0.03	0	0	0	0	0	0
Hp_I12444_IG04388_L2875	0	0	0	0	0	0	0	0	0.03	0	0	0	0	0	0
Hp_I12485_IG04429_L2697	0	0	0	0	0	0	0	0	0.04	0	0	0	0	0	0
Hp_I12527_IG04471_L2582	0	0	0	0	0	0	0	0.04	0	0	0	0	0	0	0
Hp_I12568_IG04512_L2492	0	0	0	0	0	0	0	0.04	0	0	0	0	0	0	0

Table B.8: Proteins with emPAI values peaking in active sequential fractions 28-30 with their emPAI values across the fractions (continued).

	21	22	23	24	25	26	27	28	29	30	31	32	33	34	35
Hp_I12608_IG04552_L2437	0	0	0	0	0	0.04	0	0.04	0.04	0	0	0	0	0	0
Hp_I12624_IG04568_L2400	0	0	0.04	0.04	0	0.04	0	0.22	0.22	0.22	0	0.04	0	0	0
Hp_I12734_IG04678_L2250	0	0	0	0	0	0	0	0.04	0	0	0	0	0	0	0
Hp_I12776_IG04720_L2202	0	0	0	0.09	0	0	0.09	0.13	0.04	0.13	0.04	0	0	0	0
Hp_I12977_IG04921_L2010	0	0	0	0	0	0	0	0	0.05	0	0	0	0	0	0
Hp_I13066_IG05010_L1961	0	0	0	0	0	0	0.1	0	0.1	0.05	0.05	0.05	0	0	0
Hp_I13122_IG05066_L1913	0	0	0.05	0.05	0	0.1	0.22	0.28	0.1	0.05	0.1	0.1	0	0	0
Hp_I13416_IG05360_L1738	0	0	0	0	0	0.06	0.06	0.12	0	0	0	0	0	0	0
Hp_I13527_IG05471_L1682	0	0	0	0	0	0	0	0	0.06	0.18	0	0	0	0	0
Hp_I13666_IG05610_L1621	0	0	0	0	0	0	0	0	0.06	0	0	0	0	0	0
Hp_I13843_IG05787_L1552	0	0	0	0	0	0	0	0	0.06	0	0	0	0	0	0
Hp_I13874_IG05818_L1547	0	0	0	0	0	0	0	0.06	0.07	0	0	0	0	0	0
Hp_I13952_IG05896_L1510	0	0	0	0	0	0	0	0.07	0	0	0	0	0	0	0
Hp_I14044_IG05988_L1484	0	0	0	0	0	0	0	0.06	0	0	0	0	0	0	0
Hp_I14116_IG06060_L1462	0	0	0	0	0	0	0	0.07	0	0	0	0	0	0	0
Hp_I14135_IG06079_L1458	0	0	0	0	0	0	0.07	0.07	0	0	0	0	0	0	0
Hp_I14250_IG06194_L1431	0	0	0	0	0	0	0	0.07	0.14	0.07	0.07	0	0	0	0
Hp_I14314_IG06258_L1412	0	0.07	0.07	0.14	0.07	0.07	0.07	0.07	0.14	0.14	0	0	0	0	0
Hp_I14444_IG06388_L1373	0	0	0	0.07	0	0	0	0.07	0	0	0	0	0	0	0
Hp_I14513_IG06457_L1354	0	0	0	0	0	0.07	0	0	0.15	0.15	0.07	0.07	0	0	0
Hp_I14584_IG06528_L1336	0	0	0	0	0	0	0.07	0	0.15	0	0	0	0.07	0	0
Hp_I14711_IG06655_L1305	0	0	0	0	0	0	0	0.08	0	0	0	0	0	0	0

Table B.8: Proteins with emPAI values peaking in active sequential fractions 28-30 with their emPAI values across the fractions (continued).

	21	22	23	24	25	26	27	28	29	30	31	32	33	34	35
Hp_I14909_IG06853_L1261	0	0	0	0	0	0	0	0	0	0.08	0	0	0	0	0
Hp_I15133_IG07077_L1218	0	0	0	0	0	0	0	0.45	0.35	0.08	0.16	0.08	0	0	0.08
Hp_I15168_IG07112_L1217	0	0	0	0	0	0	0.17	0.27	0.08	0.08	0	0	0	0	0
Hp_I15461_IG07405_L1171	0	0	0	0	0	0	0	0	0	0.08	0	0	0	0	0
Hp_I15760_IG07704_L1122	0	0	0	0	0	0	0	0.09	0.18	0.18	0.09	0.09	0	0	0
Hp_I15783_IG07727_L1116	0	0	0	0	0.09	0	0.09	0.09	0	0	0	0	0	0	0
Hp_I16226_IG08170_L1053	0	0	0	0	0	0	0	0.56	0.7	0.09	0.09	0.09	0	0.09	0
Hp_I16562_IG08506_L1005	0	0	0	0	0	0	0	0.21	0.21	0	0	0	0	0	0
Hp_I16723_IG08667_L984	0	0	0	0.1	0.1	0.1	0.1	0.1	0	0	0	0	0	0	0
Hp_I16824_IG08768_L974	0	0	0	0	0	0	0	0.2	0	0	0	0	0	0	0
Hp_I17168_IG09112_L939	0	0	0	0	0	0	0	0	0.11	0	0	0	0	0	0
Hp_I17933_IG09877_L867	0	0	0.12	0	0.39	0.72	0.72	0.55	0.92	0.39	0.39	0.39	0.12	0.24	0.39
Hp_I18969_IG10913_L793	0	0	0	0	0	0	0.12	0	0.26	0	0	0	0	0	0.12
Hp_I19157_IG11101_L778	0	0	0	0.26	0	0	0.58	2.14	6.86	4.58	2.53	2.95	0.41	0	0.12
Hp_I19755_IG11699_L745	0	0	0	0	0	0	0	0	0	0.13	0	0	0	0	0
Hp_I19958_IG11902_L735	0	0	0	0	0	0	0	0	0.28	0.28	0.13	0	0	0	0
Hp_I19989_IG11933_L735	0	0	0	0.14	0	0	0	0	0	0.14	0	0	0	0	0
Hp_I20539_IG12483_L707	0	0	0	0	0	0	0	0.47	0.29	0.14	0	0	0	0	0
Hp_I20654_IG12598_L702	0	0	0	0	0	0	0.14	0.47	0.29	0.29	0	0	0	0	0
Hp_I21313_IG13257_L675	0	0	0.14	0.15	0.3	0.69	2.24	4.47	2.24	2.24	2.69	0.92	0.48	0.3	0.69
Hp_I22173_IG14117_L645	0	0	0	0	0	0	0	0.32	0	0	0	0	0	0	0
Hp_I22248_IG14192_L638	0	0	0	0	0	0	0	0	0.15	0	0	0	0	0	0

Table B.8: Proteins with emPAI values peaking in active sequential fractions 28-30 with their emPAI values across the fractions (continued).

	21	22	23	24	25	26	27	28	29	30	31	32	33	34	35
Hp_I22350_IG14294_L635	0	0	0	0	0	0	0.32	0.32	0.15	0	0	0	0	0.15	0
Hp_I22470_IG14414_L621	0	0	0	0.16	0	0.16	0.35	2.32	1.12	0.16	0.16	0	0	0	0
Hp_I22685_IG14629_L621	0	0	0	0	0	0	0	0	0.16	0	0	0	0	0	0
Hp_I22770_IG14714_L618	0	0	0	0	0	0	0	0.16	0	0	0	0	0	0	0
Hp_I22851_IG14795_L620	0	0	0	0.16	0.33	0.78	1.38	1.38	0.78	3.9	3.24	2.67	1.06	0.54	1.38
Hp_I23280_IG15224_L606	0	0	0.15	0.15	0	0	0.15	0.15	0	0	0	0	0	0	0
Hp_I23293_IG15237_L606	0	0	0	0	0	0	0	1.4	0	0	0	0	0	0	0
Hp_I23736_IG15680_L595	0	0	0	0	0	0	0	0	0	0.17	0	0	0	0	0
Hp_I23863_IG15807_L590	0	0	0	0	0	0	0	0	0.83	0.16	0	0.17	0	0	0
Hp_I24096_IG16040_L584	0	0	0	0.18	0.18	0.18	0.18	0	0	0.18	0	0	0	0	0
Hp_I24175_IG16119_L582	0	0	0	0.17	0	0	0	2.08	0	0	0	0	0	0	0
Hp_I24441_IG16385_L572	0	0	0.17	0	0	0.17	0	0.17	0.85	0.36	0.36	0.36	0	0	0
Hp_I24512_IG16456_L570	0	0	0	0.37	0.61	0.37	2.57	2.04	1.6	3.18	0.89	0.37	0	0	0
Hp_I24607_IG16551_L570	0	0	0	0	0	0	0	1.56	1.99	0.17	0	0	0	0	0
Hp_I25311_IG17255_L555	0	0	0	0	0	0.39	0.64	0.93	1.27	0	0	0	0	0	0
Hp_I25825_IG17769_L543	0	0	0	0	0	0	0	0	0.18	0	0	0	0	0	0
Hp_I25889_IG17833_L540	0	0	0	0	0	0	0	0	0	1.31	0.4	0.65	0	0.18	0
Hp_I25974_IG17918_L541	0	0	0	0	0	0	0	1.67	0.39	0	0	0	0	0	0
Hp_I26188_IG18132_L529	0	0	0	0	0	0	0	2.74	2.17	0.64	0	0	0	0	0
Hp_I26227_IG18171_L535	0	0	0	0	0	0	0	0.19	0.42	0	0	0	0	0	0
Hp_I26307_IG18251_L531	0	0	0	0	0	0	0	0.18	0	0	0	0	0	0	0
Hp_I26494_IG18438_L527	0	0	0	0	0	0	0	0	0.18	0	0	0	0	0	0

Table B.8: Proteins with emPAI values peaking in active sequential fractions 28-30 with their emPAI values across the fractions (continued).

	21	22	23	24	25	26	27	28	29	30	31	32	33	34	35
Hp_I26601_IG18545_L528	0	0	0.2	0.72	1.47	0.72	1.06	0	0.44	1.96	0.72	0.44	0	0	0
Hp_I27122_IG19066_L517	0	0	0	0.19	0	0.43	1.41	1.43	0.43	0.7	0	0	0	0	0
Hp_I27304_IG19248_L514	0	0	0	0.19	0	0.19	0	0.19	0	0	0	0	0	0	0
Hp_I27407_IG19351_L514	0	0	0	0	0	0	0	0	0.2	0.2	0	0	0	0	0
Hp_I28260_IG20204_L501	0	0	0	0	0	0	0	0	0.22	0	0	0	0	0	0
Hp_I29394_IG21338_L484	0	0	0	0	0	0	0	0.21	1.61	1.15	1.15	0.21	0	0	0
Hp_I29599_IG21543_L474	0	0	0	0	0	0	0	0.21	0	0	0	0	0	0	0
Hp_I30585_IG22529_L470	0	0	0.21	0.21	0	0	0.21	0.21	0.21	0.21	0	0	0	0	0
Hp_I31855_IG23799_L456	0	0.21	0	0.47	0.21	0.21	0.47	0	0.47	0.47	0.21	0.21	0	0.21	0
Hp_I32108_IG24052_L453	0	0	0	0	0	0	0	0	0.22	0	0	0	0	0	0
Hp_I32194_IG24138_L452	0	0	0	0	0	0	0.22	0.48	0.22	0.48	0.22	0	0	0	0
Hp_I32435_IG24379_L441	0	0	0	0	0	0	0	0.22	0	0	0	0	0	0	0
Hp_I34646_IG26590_L427	0	0	0.53	0.53	0.89	0.53	0.89	0.24	0.53	0.89	0.24	0.53	0	0	0.24
Hp_I35665_IG27609_L418	0	0	0	0	0	0	0	0	0.24	0.24	0	0	0	0	0
Hp_I35779_IG27723_L416	0	0	0	0	0	0	0	0	0.53	28.95	18.58	5.77	0.89	0.89	0.24
Hp_I36380_IG28324_L410	0	0	0	0	0	0	0	0	0.24	3.52	0	0	0	0	0
Hp_I38243_IG30187_L393	0	0	0	0	0	0	0	0	0.26	0	0	0	0	0	0
Hp_I38562_IG30506_L390	0	0	0	0	0	0.27	0.27	0.27	1.05	0	0	0	0	0	0
Hp_I38626_IG30570_L389	0	0	0	0.28	0	0.26	0.26	0.59	0.26	0.26	0.26	0	0	0	0
Hp_I38698_IG30642_L388	0	0	0	0	0	0	0	0.59	0.59	1	0.59	0.26	0	0	0
Hp_I38850_IG30794_L366	0	0	0.28	0	0	0	0.28	0.28	0	0	0	0	0	0	0
Hp_I38988_IG30932_L386	0	0	2.12	1.49	0.98	0.98	0.58	0.58	2.12	0.58	0.98	0.58	0.26	0.58	0.58

Table B.8: Proteins with emPAI values peaking in active sequential fractions 28-30 with their emPAI values across the fractions (continued).

	21	22	23	24	25	26	27	28	29	30	31	32	33	34	35
Hp_I39892_IG31836_L376	0	0	0	0.26	0	0	0	0.26	0	0	0	0	0	0	0
Hp_I40246_IG32190_L374	0	0	0	0	0	0	0	0	0	0.27	0	0	0	0	0
Hp_I40256_IG32200_L371	0	0	0	0	0	0	0	0	0.26	0	0	0	0	0	0
Hp_I40999_IG32943_L364	0	0	0.65	1.71	0.65	2.48	1.11	0.65	2.48	1.71	0.28	0	0	0.28	0.28
Hp_I42165_IG34109_L355	0	0	0	0	0	0	0	0.3	0	0	0	0	0	0	0
Hp_I43395_IG35339_L341	0	0	0	0	0	0	0.32	0.32	0.32	0	0	0	0	0	0
Hp_I43851_IG35795_L337	0	0	0	0	0	0	0	0.29	12.13	1.8	0	0	0	0	0
Hp_I44884_IG36828_L326	0	0	0	0	0	0.3	0.3	0.3	0	0	0	0	0	0	0
Hp_I45281_IG37225_L323	0	0	0	0	0	0	0	0	0.73	0.32	0	0	0	0	0
Hp_I45671_IG37615_L316	0	0	0.34	0	0.34	0.34	0.34	0.34	0.34	0	0	0	0	0	0
Hp_I45709_IG37653_L316	0	0	0	0.73	0	0.73	1.29	1.29	0.32	0.32	0.73	0.32	0	0	0
Hp_I45843_IG37787_L315	0	0	0	0.33	0	0.33	0.33	0.33	0	0.33	0	0	0	0	0
Hp_I45971_IG37915_L313	0	0	0	0	0	0	0	0	0	0.32	0	0	0	0	0
Hp_I48638_IG40582_L276	0	0	0	0	0	0	0.36	0	0.36	0	0	0	0	0	0
Hp_I48880_IG40824_L273	0	0	0	0	0	0	0	0.38	0	0	0	0	0	0	0
Hp_I49529_IG41473_L265	0	0	0	0	0	0	0	0.37	0	0	0	0	0	0	0
Hp_I51114_IG43058_L239	0	0	0	0	0.47	0	0	0	0.47	0	0	0	0	0	0
Hp_I51550_IG43494_L231	0	0	0	0	0	0	0	0	0	0.47	0	0	0	0	0
Hp_I52412_IG44356_L216	0	0	0	0	0	0	0	0	0	1.13	0	0	0	0	0
Hp_I53318_IG45262_L197	0	0	0	0	0	0	0	0	0	1.66	0	0	0	0	0
Hp_I54277_IG46221_L174	0	0	0	0	0	0	0	1.74	0.66	0.66	0	0	0	0	0
Hpb-APY-1.1	0	0	0	0	0	0.09	0	0.09	0	0	0	0	0	0	0

Table B.8: Proteins with emPAI values peaking in active sequential fractions 28-30 with their emPAI values across the fractions (continued).

	21	22	23	24	25	26	27	28	29	30	31	32	33	34	35
Hpb-TRP	0	0	0	0	0.11	0.11	0.11	0	0.11	0.11	0	0	0	0	0
Hpb-VAL-3	0	0	0	0	0	0.14	0.58	0.22	0.22	0.69	0.58	0.07	0	0	0
Hpb-VAL-4	0	0	0	0	0	0	0	0.32	1.66	2.06	0.15	0	0	0	0
Hpb-VAL7.1	0	0	0	0	0	0	0	0	0	0.29	0.14	0	0	0	0
Hpb-VAL-8	0	0	0	0	0	0	0	0.24	0.24	0.08	0.16	0.08	0.08	0.16	0

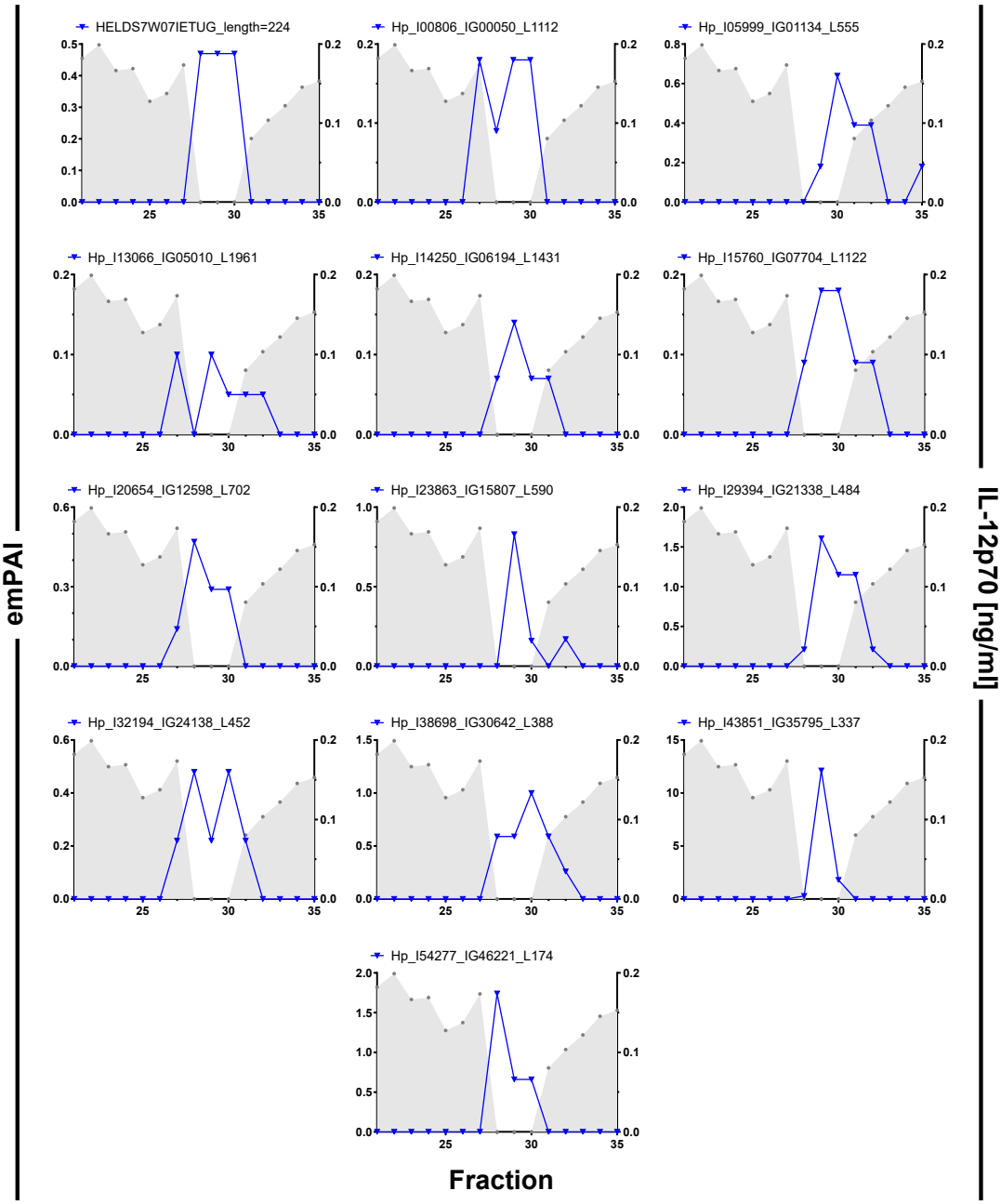

Figure B.1: Rejected candidates from the sequential fractionation. HES was fractionated using size exclusion fractionation followed by fractionation of the active fractions by anion exchange fractionation. All sequential fractions were analysed by mass spectrometry. Proteins with emPAI values peaking in the active fractions were subjected to further selection comparing their emPAI profiles to activity across the fractions, excluding housekeeping, egg or larval stage proteins and those that have been identified falsely or with only one peptide. These excluded proteins are shown here with their emPAI values across the fractions on the left y axis and the concentration of IL-12p70 produced by GM-CSF BMDC treated with LPS (1μg/ml) and the respective fraction on the right y axis.

B.3 Mass spectrometry and analysis of all fractions

Table B.9: Proteins identified in fraction 14 of the second size exclusion fractionation of HES. 1.244mg HES were fractionated by size exclusion fractionation and all fractions were analysed by mass spectrometry in the facility in Edinburgh, using an Orbitrap mass spectrometer and using Mascot and the in-house *H. polygyrus* transcriptomic database. The significance threshold for consideration of proteins was $p<0.05$; a minimum cutoff score of 20 was set. Fractions were tested for their inhibitory activity on GM-CSF BMDC; fraction 14 showed the ability to completely inhibit IL-12p70 production. Listed are ranks of the proteins, their accession numbers, the number of peptide hits for the respective protein, their emPAI values and their ranks in the earlier size exclusion fractionation analysed in Glasgow. Green: proteins identified in the previous analysis of a size exclusion fraction 14; Red: expressed proteins.

Rank	Protein accession number	Protein score	Protein matches	emPAI	Rank in 1. MS
1	Hp_I07157_IG01645_L560	643	46	106.92	
1	Hp_I07158_IG01645_L560	497	42	65.49	
1	Hp_I10997_IG03583_L513	35	6		
2	Hp_I06078_IG01161_L583	351	22	9.48	
2	Hp_I06079_IG01161_L526	86	4		
3	HICN8C106HP9PI_length=274	348	13	2.31	
4	Hp_I02849_IG00289_L1962	339	11	0.45	11
5	Hp_I26601_IG18545_L528	324	11	6.31	
5	GSXTT4C05GBC4L_length=430	53	1		
6	Hp_I10419_IG03294_L714	307	14	3.74	
7	Hp_I21313_IG13257_L675	290	10	2.69	
8	Hp_I15588_IG07532_L1149	261	8	0.93	
9	Hp_I13075_IG05019_L1949	256	9	0.5	
10	Hp_I19157_IG11101_L778	253	7	1.23	19
11	Hp_I28744_IG20688_L490	237	10	5.04	
12	Hp_I23776_IG15720_L592	227	11	2.91	
13	Hp_I21565_IG13509_L658	217	11	2.11	
14	Hp_I38325_IG30269_L391	177	6	3.09	
15	Hp_I22851_IG14795_L620	174	11	2.67	
16	Hp_I04570_IG00700_L4683	170	12	0.19	
17	Hp_I15528_IG07472_L1156	168	6	0.61	
18	Hp_C00053_IG00001_L722	168	5	0.69	
18	Hp_I10817_IG03493_L822	154	6	0.74	

Table B.9: Proteins identified in fraction 14 of the second size exclusion fractionation of HES (continued).

Rank	Protein accession number	Protein score	Protein matches	emPAI	Rank in 1. MS
18	Hp_I06559_IG01341_L2453	81	2		
18	Hp_I08959_IG02564_L1212	69	4		2
19	Hp_I04266_IG00599_L823	166	5	0.76	
19	GSXTT4C06HF8RX_length=190	62	1		
20	Hp_I00798_IG00050_L1759	165	7	0.44	
20	Hp_I00801_IG00050_L1766	117	4	0.17	
20	Hp_I00803_IG00050_L1749	150	6		
20	Hp_I00800_IG00050_L1766	113	4		
20	Hp_I00796_IG00050_L1763	106	4		
20	Hp_I00799_IG00050_L1753	92	3		
20	Hp_I00811_IG00050_L794	85	4		
20	Hp_I00809_IG00050_L1090	82	2		
20	Hp_I00806_IG00050_L1112	44	2		
20	Hp_I22699_IG14643_L627	38	1		
20	Hp_I00808_IG00050_L1102	34	1		
21	GNK0QLK03GQOZO_length=396	155	6	1.41	
21	GS66ZV203C3717_length=247	150	5		
21	GS66ZV203DJXOH_length=245	136	4		
21	GWDWRH002CES3N_length=67	22	1		
22	HICN8C105FSWIS_length=222	155	6	1.19	
23	Hp_I10517_IG03343_L655	125	7	1.3	
23	Hp_I10518_IG03343_L562	110	7	1.25	
24	Hp_I00841_IG00053_L616	124	4	0.88	
24	HICN8C105GB60T_length=201	33	1		
25	Hp_I34892_IG26836_L422	122	3	0.91	
26	Hp_I34646_IG26590_L427	120	8	4.47	
27	Hp_I19989_IG11933_L735	118	8	1.46	
28	Hp_I15778_IG07722_L1118	118	3	0.29	
29	Hp_I00843_IG00054_L964	117	6	0.63	
29	Hp_I24240_IG16184_L580	82	5	0.88	
29	Hp_I00850_IG00054_L907	69	4	0.51	
29	GS66ZV202BO7NU_length=145	108	5		
29	GS66ZV203DM0PP_length=226	82	4		
29	GS66ZV203CUYIB_length=146	71	3		
29	GS66ZV203C4QVV_length=191	36	2		
30	Hp_I23615_IG15559_L596	110	4	0.85	

Table B.9: Proteins identified in fraction 14 of the second size exclusion fractionation of HES (continued).

Rank	Protein accession number	Protein score	Protein matches	emPAI	Rank in 1. MS
30	GKYPR1L02BZNH0_length=404	48	1		
31	Hp_I05325_IG00908_L1903	108	1	0.05	5
32	Hp_I40444_IG32388_L371	106	3	1.19	
33	Hp_I25374_IG17318_L554	99	3	0.62	
34	Hp_I38933_IG30877_L384	98	2	0.59	
35	Hp_I24512_IG16456_L570	98	4	0.89	
35	GNK0QLK03F82AT_length=271	50	2		
36	Hp_I22123_IG14067_L644	97	3	0.52	
37	Hp_I38988_IG30932_L386	96	3	0.98	
38	Hp_I05659_IG01019_L943	95	2	0.22	
39	Hp_I16449_IG08393_L1019	91	5	0.42	
39	HICN8C104D48FA_length=165	52	1		
40	Hpb-Sequence-14	88	2	0.67	
40	HICN8C104ELA3K_length=239	75	1		
40	GNK0QLK03FSOQA_length=163	28	1		
41	Hp_I27637_IG19581_L511	88	3	0.68	
42	Hp_I18845_IG10789_L800	88	3	0.4	
43	Hp_I07249_IG01697_L637	86	4	0.75	
44	Hp_I26246_IG18190_L526	85	4	0.66	
45	Hp_I50368_IG42312_L251	85	3	1.81	
46	Hp_I41819_IG33763_L358	85	3	1.17	
47	Hp_I12336_IG04280_L5030	84	7	0.12	
48	Hp_I40999_IG32943_L364	84	1	0.28	
49	Hp_I21617_IG13561_L662	83	1	0.16	4
50	Hp_I35779_IG27723_L416	83	4	1.34	
51	GS66ZV203DFM3U_length=95	80	2	4.36	
52	Hp_I40421_IG32365_L372	77	2	0.6	
53	HELDS7W07H0BVM_length=251	76	3	1.78	
53	GS66ZV203DAUV3_length=283	68	2		
53	HELDS7W08JC1EG_length=251	47	1		
53	GSXTT4C08JOHGR_length=153	24	1		
54	Hp_I24881_IG16825_L563	76	2	0.41	
55	Hp_I25622_IG17566_L549	75	2	0.39	
56	Hp_I08946_IG02557_L754	75	4	0.6	
56	Hp_I28711_IG20655_L493	38	1		
57	Hp_I23324_IG15268_L606	75	4	0.79	

Table B.9: Proteins identified in fraction 14 of the second size exclusion fractionation of HES (continued).

Rank	Protein accession number	Protein score	Protein matches	emPAI	Rank in 1. MS
58	Hp_I07490_IG01829_L2288	75	1	0.04	
59	Hpb-VAL-2.2	74	2	0.15	
59	Hp_I07952_IG02060_L1493	58	1		
60	Hp_I19992_IG11936_L730	73	2	0.28	
61	Hp_I07497_IG01832_L1722	72	4	0.24	
61	Hp_I07496_IG01832_L2183	45	3		
62	Hp_I39181_IG31125_L382	71	2	0.58	
63	Hp_I14119_IG06063_L1461	70	1	0.07	
64	Hp_I12776_IG04720_L2202	69	2	0.09	
64	FL8UM6J01A0LLF_length=129	50	1		8
65	Hp_I12337_IG04281_L4997	69	6	0.09	
65	FL3BO7403BPZG6_length=114	41	2		
65	FL8UM6J01BGCU6_length=234	35	1		
65	FL8UM6J01CKHCK_length=278	32	1		
66	Hp_I28724_IG20668_L494	68	1	0.2	
67	Hp_I13832_IG05776_L1555	67	2	0.12	
68	Hp_I42607_IG34551_L347	66	1	0.29	
69	Hp_I15783_IG07727_L1116	66	1	0.09	
70	Hp_I44251_IG36195_L332	65	4	1.98	
71	Hp_I32194_IG24138_L452	65	2	0.48	
72	Hp_I01061_IG00070_L5128	65	5	0.08	
72	FL8UM6J01AP92T_length=187	36	1		
73	Hp_I05809_IG01070_L1113	63	2	0.18	
74	Hp_I12624_IG04568_L2400	63	2	0.08	
74	FL8UM6J01C5SEG_length=170	40	1		
75	Hp_I06001_IG01134_L530	63	1	0.19	
76	Hp_I49594_IG41538_L265	63	3	1.64	
76	Hp_I49433_IG41377_L267	42	2	0.89	
77	Hp_I21133_IG13077_L683	62	5	0.48	7
77	Hp_I20188_IG12132_L723	60	3		
77	Hp_I03894_IG00508_L604	54	1		
78	Hp_C02597_IG00028_L1734	61	4	0.24	
79	Hp_I30337_IG22281_L473	60	1	0.22	
80	Hp_I13743_IG05687_L1584	59	1	0.06	
81	Hp_I26937_IG18881_L522	59	2	0.41	
82	Hp_I02548_IG00238_L1779	58	2	0.11	

Table B.9: Proteins identified in fraction 14 of the second size exclusion fractionation of HES (continued).

Rank	Protein accession number	Protein score	Protein matches	emPAI	Rank in 1. MS
83	Hp_I07527_IG01847_L1908	58	3	0.05	
84	Hp_I15760_IG07704_L1122	58	1	0.09	
85	Hp_I29394_IG21338_L484	56	2	0.47	
86	Hp_I01036_IG00067_L1461	55	2	0.14	
86	Hp_I13955_IG05899_L1513	53	1		
86	FL8UM6J01CLAA6_length=170	27	1		
87	Hp_I05758_IG01053_L926	55	1	0.11	
88	Hp_I22064_IG14008_L644	54	2	0.32	
88	Hp_I21699_IG13643_L657	24	1		
89	Hp_I36714_IG28658_L408	54	1	0.27	
90	Hp_I15194_IG07138_L1211	53	2	0.16	
91	Hp_I20768_IG12712_L696	52	2	0.29	6
91	GSXTT4C05FZBSU_length=163	27	1		
92	Hp_I07995_IG02081_L699	52	2	0.3	
93	Hp_I05407_IG00935_L1040	51	1	0.09	
94	Hp_I05827_IG01076_L1116	51	4	0.38	
94	Hp_I40994_IG32938_L367	38	2	0.62	
95	Hp_I14371_IG06315_L1386	51	1	0.07	
96	Hp_I15587_IG07531_L1141	50	3	0.27	
97	Hp_I08665_IG02417_L1321	49	2	0.15	
97	Hp_I08666_IG02417_L925	45	1		
98	Hp_I30585_IG22529_L470	48	1	0.21	
99	Hp_C08742_IG00702_L613	48	2	0.35	
100	Hp_C00179_IG00001_L1163	48	1	0.09	
101	Hp_I03893_IG00508_L677	48	1	0.14	
102	Hp_I03750_IG00471_L768	47	2	0.26	
103	Hp_I22350_IG14294_L635	47	1	0.15	
104	Hp_I14314_IG06258_L1412	47	1	0.07	
105	Hp_I40801_IG32745_L368	47	2	0.62	
106	Hp_C00031_IG00001_L1071	47	1	0.09	
107	Hp_I18253_IG10197_L840	47	1	0.11	
108	Hpb-VAL-7.3	46	1	0.14	
109	Hp_I23528_IG15472_L598	46	2	0.37	
110	Hp_I09383_IG02776_L925	46	1	0.11	
111	Hp_I22261_IG14205_L639	45	1	0.16	3
112	Hp_I38111_IG30055_L394	45	2	0.56	

Table B.9: Proteins identified in fraction 14 of the second size exclusion fractionation of HES (continued).

Rank	Protein accession number	Protein score	Protein matches	emPAI	Rank in 1. MS
113	Hp_I35752_IG27696_L420	45	3	0.57	
114	Hp_I06096_IG01167_L557	45	1	0.18	
115	Hpb-VAL-1.1	44	2	0.15	
115	Hp_I04671_IG00730_L1535	38	1		
115	Hp_I08791_IG02480_L1486	25	1		
116	Hp_I25949_IG17893_L538	44	3	0.39	
117	Hp_I06509_IG01316_L615	44	1	0.16	
118	Hp_I22275_IG14219_L639	44	1	0.15	
119	Hp_I02965_IG00308_L1259	43	1	0.08	
120	Hp_I05999_IG01134_L555	43	1	0.18	26
121	GNK0QLK03FHM83_length=50	43	1	2.83	
122	Hp_I40392_IG32336_L373	43	1	0.28	
123	HICN8C105F7BX8_length=227	43	1	0.47	
124	Hp_I19711_IG11655_L743	43	1	0.13	
125	Hp_I21746_IG13690_L653	43	1	0.15	
126	Hp_I56769_IG48713_L107	43	1	1.18	
127	Hp_I13332_IG05276_L1776	43	1	0.05	
128	Hp_I38850_IG30794_L366	42	2	0.65	
129	Hpb-VAL7.1	42	1	0.14	
130	Hp_I15488_IG07432_L1169	42	2	0.17	
131	Hp_I19958_IG11902_L735	41	1	0.13	
132	GQ6YEYD07H2LVG_length=277	40	2	0.38	
133	Hp_I24623_IG16567_L570	40	2	0.36	
134	Hp_I08415_IG02292_L1231	39	1	0.08	
135	Hp_I24430_IG16374_L575	38	1	0.17	
136	Hp_I00695_IG00044_L591	38	1	0.16	
137	Hp_C00282_IG00001_L564	38	3	0.37	
138	GLSD98I04D6NC8_length=454	37	1	0.21	
139	Hp_I24705_IG16649_L569	37	1	0.18	
140	HICN8C105F4XWC_length=461	37	2	0.47	
140	GSXTT4C07H11X2_length=416	33	1		
140	FL8UM6J01CZ23X_length=243	22	1		
141	GSXTT4C06GXMIV_length=179	37	2	0.58	
142	Hp_I12932_IG04876_L2052	36	1	0.05	
143	Hp_I03228_IG00366_L2337	36	1	0.04	
144	Hp_I18333_IG10277_L834	36	2	0.25	

Table B.9: Proteins identified in fraction 14 of the second size exclusion fractionation of HES (continued).

Rank	Protein accession number	Protein score	Protein matches	emPAI	Rank in 1. MS
144	Hp_I23692_IG15636_L593	26	1		
145	Hp_I03365_IG00388_L986	36	1	0.1	
146	Hp_I24096_IG16040_L584	36	2	0.38	
147	Hp_I05755_IG01052_L1113	35	1	0.09	
148	Hp_I23836_IG15780_L590	35	2	0.35	16
149	Hp_I24997_IG16941_L561	35	1	0.17	
150	Hp_I24494_IG16438_L573	35	1	0.17	
151	Hp_I25184_IG17128_L557	35	1	0.18	
152	Hp_I30636_IG22580_L471	34	1	0.21	
153	Hp_I15168_IG07112_L1217	34	1	0.08	
154	GSXTT4C07IOOUR_length=396	34	1	0.27	
155	Hp_I21268_IG13212_L674	33	1	0.14	
156	Hp_I14639_IG06583_L1320	33	1	0.07	
157	Hp_I09863_IG03016_L798	33	1	0.13	
158	Hp_I11144_IG03656_L469	33	1	0.21	
159	Hp_I23863_IG15807_L590	33	1	0.16	
160	Hp_I06838_IG01481_L1319	33	1	0.08	
161	Hp_I31855_IG23799_L456	33	1	0.21	
162	Hp_I05565_IG00988_L1210	33	2	0.16	
163	Hp_I07274_IG01721_L3765	32	2	0.03	
164	Hp_I13494_IG05438_L1681	32	1	0.06	
165	Hp_I05058_IG00828_L787	32	1	0.13	
166	Hp_I19378_IG11322_L765	32	1	0.13	
167	Hp_I30926_IG22870_L465	32	1	0.21	
168	Hp_I11447_IG03808_L449	32	1	0.22	
169	Hp_I12456_IG04400_L2825	31	1	0.03	
170	Hp_I44137_IG36081_L328	31	1	0.31	
171	Hp_I25725_IG17669_L542	31	2	0.38	
172	Hp_I43570_IG35514_L336	31	1	0.29	
173	Hp_I02234_IG00194_L1318	31	1	0.07	
174	Hp_I12705_IG04649_L2285	31	1	0.04	
175	Hp_I23530_IG15474_L600	31	3	0.35	
176	GS66ZV203DB0T9_length=193	30	1	0.55	
177	Hp_I20989_IG12933_L687	30	1	0.14	
178	GLSD98I05F6IT3_length=173	28	1	0.6	
179	Hp_I07334_IG01751_L2741	28	1	0.04	

Table B.9: Proteins identified in fraction 14 of the second size exclusion fractionation of HES (continued).

Rank	Protein accession number	Protein score	Protein matches	emPAI	Rank in 1. MS
180	Hp_I05355_IG00918_L1570	28	1	0.06	10
181	Hp_I43185_IG35129_L337	28	1	0.31	
182	Hp_I26844_IG18788_L525	27	1	0.18	
183	Hpb-TRP	27	1	0.11	
184	Hp_I07526_IG01847_L1909	27	2	0.05	
185	Hp_I14584_IG06528_L1336	26	1	0.07	
186	Hp_I17383_IG09327_L916	25	1	0.11	
187	Hp_I16638_IG08582_L998	25	1	0.1	
188	Hp_I15353_IG07297_L1178	25	1	0.08	
189	Hp_I25677_IG17621_L546	25	1	0.18	
190	Hp_I16723_IG08667_L984	25	1	0.1	
191	Hp_I40417_IG32361_L370	25	1	0.27	
192	Hp_I45671_IG37615_L316	25	1	0.34	
193	Hp_I22320_IG14264_L638	24	1	0.15	
194	Hp_I08175_IG02172_L1570	24	1	0.06	
195	Hp_I36017_IG27961_L415	24	1	0.23	
196	Hp_I26504_IG18448_L528	23	1	0.19	
197	GSXTT4C06GUNT5_length=342	23	1	0.3	
198	Hp_I22388_IG14332_L637	23	1	0.15	1
199	Hp_I06335_IG01256_L998	23	1	0.1	
200	Hp_I15133_IG07077_L1218	22	1	0.08	
201	FL8UM6J01BC1ZN_length=62	21	1	1.88	
202	Hp_I13122_IG05066_L1913	21	1	0.05	
203	Hp_I18045_IG09989_L856	21	1	0.11	
204	Hp_I44112_IG36056_L331	20	1	0.3	
205	Hp_I27930_IG19874_L505	20	1	0.2	
206	Hp_I38451_IG30395_L390	20	1	0.26	

Table B.10: Proteins identified in fraction 15 of the second size exclusion fractionation of HES. 1.244mg HES were fractionated by size exclusion fractionation and all fractions were analysed by mass spectrometry in the facility in Edinburgh, using an Orbitrap mass spectrometer and using Mascot and the in-house *H. polygyrus* transcriptomic database. The significance threshold for consideration of proteins was $p<0.05$; a minimum cutoff score of 20 was set. Fractions were tested for their inhibitory activity on GM-CSF BMDC; fraction 15 showed the ability to completely inhibit IL-12p70 production. Listed are ranks of the proteins, their accession numbers, the number of peptide hits for the respective protein, their emPAI values and their ranks in the earlier size exclusion fractionation analysed in Glasgow Green: proteins identified in the previous analysis of a size exclusion fraction 15; Red: expressed proteins.

Rank	Protein accession number	Protein score	Protein matches	emPAI	Rank in 1. MS
1	Hp_I02849_IG00289_L1962	154	4	0.15	14
2	Hp_I13075_IG05019_L1949	151	5	0.25	
2	Hp_I28606_IG20550_L493	57	1		
3	Hp_I07157_IG01645_L560	134	14	2.64	
3	Hp_I10997_IG03583_L513	34	3		
4	Hp_I26601_IG18545_L528	111	2	0.44	11
4	GSXTT4C05GBC4L_length=430	79	1		
5	Hp_I31855_IG23799_L456	104	6	0.21	
6	Hp_I38325_IG30269_L391	95	3	1.02	
6	Hp_I38451_IG30395_L390	72	3	1.05	
7	Hp_C00053_IG00001_L722	91	3	0.3	
8	Hp_I05057_IG00828_L820	89	3	0.4	
9	GNK0QLK03GQOZO_length=396	78	2	0.55	
10	Hp_I10419_IG03294_L714	76	4	0.68	15
11	Hp_I03893_IG00508_L677	74	2	0.3	4
11	Hp_I03895_IG00508_L600	54	1		
12	Hp_I08946_IG02557_L754	73	3	0.42	
12	Hp_I28711_IG20655_L493	43	1		
13	Hp_I32811_IG24755_L446	68	1	0.22	
14	Hp_I42607_IG34551_L347	66	2	0.67	
15	Hp_I15194_IG07138_L1211	64	3	0.26	
16	Hp_I12337_IG04281_L4997	63	8	0.07	
16	FL8UM6J01BANI8_length=60	55	1		
16	FL3BO7403BPZG6_length=114	33	1		
16	FL8UM6J01BGCU6_length=234	22	1		
17	Hp_I07527_IG01847_L1908	63	2	0.05	
18	Hp_I22851_IG14795_L620	60	2	0.33	13
19	Hp_I10855_IG03512_L534	59	2	0.4	

Table B.10: Proteins identified in fraction 15 of the second size exclusion fractionation of HES (continued).

Rank	Protein accession number	Protein score	Protein matches	emPAI	Rank in 1. MS
20	HICN8C106HP9PI_length=274	57	1	0.35	
21	Hp_I21133_IG13077_L683	54	5	0.3	3
21	Hp_I03894_IG00508_L604	23	2		
22	Hp_I21565_IG13509_L658	53	4	0.53	5
23	Hp_I16449_IG08393_L1019	52	1	0.09	
24	HICN8C105FSWIS_length=222	52	3	1.19	
25	Hp_I56769_IG48713_L107	52	1	1.18	
26	GSXTT4C05FPGBC_length=392	52	1	0.25	
27	Hp_I22064_IG14008_L644	52	2	0.15	
28	Hp_I10518_IG03343_L562	51	2	0.38	
28	Hp_I10517_IG03343_L655	44	1		
29	Hp_I43395_IG35339_L341	51	1	0.32	
30	Hp_I14584_IG06528_L1336	50	1	0.07	
31	Hp_I06838_IG01481_L1319	50	1	0.08	
32	GS66ZV202BO7NU_length=145	49	2	2.25	
33	Hp_I01036_IG00067_L1461	48	3	0.21	
33	Hp_I14843_IG06787_L1280	45	1		
34	Hp_I19992_IG11936_L730	47	1	0.13	
35	Hp_I25725_IG17669_L542	47	1	0.18	
36	Hp_I07274_IG01721_L3765	46	1	0.03	
37	FL8UM6J01B7CV6_length=228	46	1	0.49	
38	Hp_I31577_IG23521_L459	45	1	0.22	
39	Hp_I18845_IG10789_L800	45	1	0.12	
40	Hp_I40801_IG32745_L368	43	1	0.27	21
41	Hp_I14371_IG06315_L1386	43	1	0.07	
42	Hp_I00796_IG00050_L1763	42	2	0.11	
42	Hp_I00806_IG00050_L1112	40	1		
42	Hp_I00800_IG00050_L1766	28	1		
43	Hp_I12336_IG04280_L5030	41	6	0.08	1
44	Hp_I23615_IG15559_L596	39	1	0.17	
45	Hp_I16462_IG08406_L1016	38	2	0.19	
46	Hp_I20768_IG12712_L696	37	1	0.14	
47	Hp_I14119_IG06063_L1461	37	1	0.07	
48	Hp_I05758_IG01053_L926	36	1	0.11	
49	Hp_I15778_IG07722_L1118	36	1	0.09	
50	Hp_I34892_IG26836_L422	36	1	0.24	

Table B.10: Proteins identified in fraction 15 of the second size exclusion fractionation of HES (continued).

Rank	Protein accession number	Protein score	Protein matches	emPAI	Rank in 1. MS
51	Hp_I19378_IG11322_L765	36	1	0.13	
52	Hp_I08791_IG02480_L1486	36	1	0.07	18
53	Hp_I27940_IG19884_L505	35	1	0.19	
54	Hp_I22261_IG14205_L639	35	1	0.16	
55	Hp_I10601_IG03385_L624	35	1	0.16	
56	Hp_I18384_IG10328_L830	34	1	0.12	
57	Hp_C00318_IG00001_L1664	34	1	0.06	
58	Hp_I05827_IG01076_L1116	34	1	0.08	
59	Hp_I35726_IG27670_L415	34	1	0.24	
60	HICN8C104EH4N8_length=157	34	1	0.68	
61	Hp_I21726_IG13670_L658	33	1	0.14	
62	Hp_I23324_IG15268_L606	33	1	0.16	
63	Hp_I01061_IG00070_L5128	33	3	0.04	
63	FL8UM6J01AUO3H_length=165	30	1		
63	FL8UM6J01DHE8P_length=68	24	1		
64	Hp_I14639_IG06583_L1320	33	1	0.07	
65	GLSD98I05F0MGD_length=346	32	1	0.29	
66	Hp_I13810_IG05754_L1566	32	1	0.06	
67	Hp_I12624_IG04568_L2400	32	3	0.08	
67	FL8UM6J01C5SEG_length=170	28	1		
67	FL8UM6J01BLY7J_length=177	22	2		
68	Hp_I16083_IG08027_L1071	32	2	0.09	
69	FL8UM6J01EFBYL_length=63	32	1	1.88	
70	Hp_I29233_IG21177_L488	31	1	0.19	
71	Hp_I21825_IG13769_L655	31	1	0.15	
72	GNK0QLK03G3KHF_length=294	31	1	0.34	
73	Hp_I07249_IG01697_L637	30	1	0.15	
74	Hp_I00695_IG00044_L591	30	1	0.16	
75	Hp_I45710_IG37654_L317	29	1	0.33	
76	Hp_I03099_IG00335_L808	28	1	0.12	
77	Hpb-APY-2	28	2	0.09	
78	Hp_I23736_IG15680_L595	28	1	0.17	
79	Hpb-VAL-1.1	28	1	0.07	
80	Hp_I13874_IG05818_L1547	28	1	0.06	
81	Hp_I15133_IG07077_L1218	28	1	0.08	
82	Hp_C02597_IG00028_L1734	28	1	0.06	

Table B.10: Proteins identified in fraction 15 of the second size exclusion fractionation of HES (continued).

Rank	Protein accession number	Protein score	Protein matches	emPAI	Rank in 1. MS
83	Hp_I30075_IG22019_L477	28	2	0.21	
84	GNK0QLK03F82AT_length=271	27	2	0.38	
85	Hp_I43570_IG35514_L336	27	1	0.29	
86	Hp_I12936_IG04880_L2046	26	1	0.05	
87	Hp_I40558_IG32502_L371	26	1	0.27	
88	Hp_I16860_IG08804_L972	26	1	0.11	
89	Hp_I04332_IG00616_L354	26	1	0.28	
90	Hp_I50368_IG42312_L251	26	1	0.41	
91	Hp_I45709_IG37653_L316	26	1	0.32	
92	Hp_I05268_IG00889_L2671	25	2	0.04	
93	Hp_I13122_IG05066_L1913	25	1	0.05	
94	Hp_I20875_IG12819_L687	25	1	0.14	
95	Hp_I01383_IG00095_L656	24	1	0.16	
96	Hp_I28625_IG20569_L494	24	1	0.2	
97	GLSD98I04EBL7F_length=389	23	1	0.26	
98	Hp_I04525_IG00683_L718	23	1	0.14	
99	Hp_I32491_IG24435_L448	23	1	0.23	
100	Hp_I28383_IG20327_L491	22	1	0.21	
101	Hp_I27958_IG19902_L502	22	1	0.19	
102	Hp_I16854_IG08798_L973	21	1	0.1	
103	Hp_I05565_IG00988_L1210	21	1	0.08	9
104	Hp_I34113_IG26057_L428	20	1	0.25	
105	Hp_I14323_IG06267_L1413	20	1	0.07	

Table B.11: Proteins identified in the active fraction 25 of the second anion exchange fractionation of HES. 1mg HES was fractionated by anion exchange fractionation and all fractions were analysed by mass spectrometry in the facility in Edinburgh, using an Orbitrap mass spectrometer and using Mascot and the in-house *H. polygyrus* transcriptomic database. The significance threshold for consideration of proteins was $p<0.05$; a minimum cutoff score of 20 was set. Fractions were tested for their inhibitory activity on GM-CSF BMDC; fraction 25 showed the ability to completely inhibit IL-12p70 production. Listed are ranks of the proteins, their accession numbers, the number of peptide hits for the respective protein, their emPAI values and their ranks in the earlier size exclusion fractionation analysed in Glasgow. Green: proteins identified in the two active fractions 39 and 40 of the previous anion exchange fractionation of HES; Red: expressed proteins.

Rank	Protein accession number	Protein score	Protein matches	emPAI	Rank in 1. MS fr. 39	Rank in 1. MS fr. 40
1	Hpb-VAL-2.2	1007	42	1.46	16	
1	Hp_I07952_IG02060_L1493	884	38			
1	Hp_I16213_IG08157_L1054	651	28			45
2	Hpb-VAL-3	752	23	2.04	15	
2	Hp_I48980_IG40924_L272	262	7	9.6	23	
2	Hp_I05548_IG00982_L1432	482	13			
2	Hp_I19215_IG11159_L774	71	3			
3	Hp_I01077_IG00070_L5125	689	35	0.78		
3	Hp_I01065_IG00070_L5127	682	34	0.71	10	
3	Hp_I01085_IG00070_L5126	698	35			
3	Hp_I01061_IG00070_L5128	672	34			
3	FL8UM6J01DHE8P_length=68	53	1			
3	FL8UM6J01CURPT_length=239	50	2			
3	FL8UM6J01B6EWE_length=223	44	2			
3	FL8UM6J01C588R_length=58	42	1			
3	FL8UM6J01AP92T_length=187	35	1			
3	FL3BO7402A3GMD_length=78	33	1			
3	FL8UM6J01D3AZE_length=56	32	1			
3	FL8UM6J01AF8W5_length=111	30	1			
3	FL8UM6J01BNPTC_length=64	25	1			
4	Hp_I04627_IG00719_L1926	349	13	0.79		
4	Hp_I04629_IG00719_L1853	294	12	0.75		8
5	Hpb-VAL-4	341	12	3.66		
5	FL8UM6J01BXB62_length=190	246	7			
5	HELDS7W07IOFZZ_length=285	158	3			
5	FL8UM6J01BH6HY_length=236	88	2			

Table B.11: Proteins identified in the active fraction 25 of the second anion exchange fractionation of HES (continued).

Rank	Protein accession number	Protein score	Protein matches	emPAI	Rank in 1. MS fr. 39	Rank in 1. MS fr. 40
6	Hpb-VAL-12	304	15	1.15		
6	HICN8C105F8RGF_length=429	36	1			
7	Hpb-VAL-5	298	14	0.91		
7	Hp_I07899_IG02033_L1514	232	12			
7	Hp_I50804_IG42748_L243	26	1			
8	Hp_I22486_IG14430_L629	276	9	1.42		
8	Hp_I08791_IG02480_L1486	187	8	0.48		51
8	Hp_I04202_IG00583_L1521	154	4	0.29		
8	Hp_I13898_IG05842_L1539	140	4	0.29		
8	GNK0QLK03HBAHW_length=398	70	2	0.59		
8	Hpb-VAL-1.2	107	3			
8	Hp_I08792_IG02480_L662	35	1			
8	Hp_I04671_IG00730_L1535	22	1			
9	Hp_I12337_IG04281_L4997	254	18	0.35		52
9	Hp_I17241_IG09185_L930	44	1			
9	FL3BO7403BPZG6_length=114	38	1			
9	FL8UM6J01C5UK3_length=170	27	1			
9	FL8UM6J01BANI8_length=60	25	1			
9	HICN8C106HRUG1_length=372	22	1			
10	Hp_I12803_IG04747_L2174	249	10	0.41		
10	Hp_I34273_IG26217_L428	22	1			
11	Hp_I13874_IG05818_L1547	247	11	0.82	17	24
12	Hp_I07682_IG01925_L1479	227	10	0.58	69	18
13	Hp_I04570_IG00700_L4683	224	15	0.34	50	98
14	Hp_I15710_IG07654_L1132	194	8	0.9		12
14	Hp_I25323_IG17267_L551	90	4	0.95		
14	Hp_I16723_IG08667_L984	36	2	0.2		68
15	Hp_I07836_IG02002_L1957	190	6	0.33		
16	Hp_I13075_IG05019_L1949	189	11	0.64		
17	Hp_I05693_IG01031_L1691	186	9	0.65	12	4
17	GSXTT4C06GWJRB_length=411	65	2			
17	GSXTT4C06GPQYK_length=226	33	1			
18	Hp_I13043_IG04987_L1979	185	7	0.39		
18	Hp_I12998_IG04942_L2000	107	4			
19	Hp_I02849_IG00289_L1962	181	5	0.21	24	31

Table B.11: Proteins identified in the active fraction 25 of the second anion exchange fractionation of HES (continued).

Rank	Protein accession number	Protein score	Protein matches	emPAI	Rank in 1. MS fr. 39	Rank in 1. MS fr. 40
19	Hp_I02853_IG00289_L1028	149	4			
19	Hp_I02850_IG00289_L1486	49	1			
20	Hp_I14221_IG06165_L1437	174	8	0.67		
20	FL8UM6J01A9TLT_length=238	101	3			
20	FL8UM6J01DWOYY_length=214	67	2			
21	Hp_I25311_IG17255_L555	171	7	2.15	20	20
21	Hp_I06127_IG01177_L423	80	2			
21	FL8UM6J01EH57D_length=239	68	2			
21	Hp_I06126_IG01177_L442	64	1			
21	Hp_I46145_IG38089_L308	35	1			
22	Hp_I01207_IG00080_L1679	171	7	0.42		
22	Hp_I01209_IG00080_L442	83	2			
22	Hp_I45924_IG37868_L314	57	2			
23	Hpb-VAL-8	165	11	1.22		
23	Hp_I08945_IG02557_L1281	151	9			
24	Hp_I07468_IG01818_L2128	163	7	0.29		
24	Hp_I20319_IG12263_L706	82	1			
25	GS66ZV203CYBIS_length=408	159	5	0.95		
25	GS66ZV202B7UAH_length=375	94	2			
25	GLSD98I04EAT7X_length=285	85	3			
26	Hp_I21073_IG13017_L680	156	6	0.95	35	13
27	Hp_I08665_IG02417_L1321	155	4	0.32	4	2
28	Hp_I15157_IG07101_L1223	144	4	0.36		48
29	Hp_I20153_IG12097_L724	143	6	0.63		29
30	Hp_I15089_IG07033_L1228	129	4	0.35		42
31	Hp_I21313_IG13257_L675	127	5	0.92	65	
32	Hp_I01451_IG00104_L976	117	8	0.94		
32	Hp_I01449_IG00104_L991	116	6	0.58		
32	Hp_I01453_IG00104_L978	112	6	0.59		
32	Hp_I01454_IG00104_L794	127	7			
32	GS66ZV202B64CW_length=211	65	4			
32	GS66ZV202B0Y18_length=222	54	2			
32	GNK0QLK03FJQ4Z_length=212	33	1			
33	Hp_I24175_IG16119_L582	125	6	1.62	55	44
33	Hp_I01045_IG00068_L1382	73	2	0.14		

Table B.11: Proteins identified in the active fraction 25 of the second anion exchange fractionation of HES (continued).

Rank	Protein accession number	Protein score	Protein matches	emPAI	Rank in 1. MS fr. 39	Rank in 1. MS fr. 40
33	Hp_I22470_IG14414_L621	94	5		38	33
33	Hp_I07148_IG01640_L579	50	1			
34	FL8UM6J01BCVJW_length=245	125	5	2.91		23
35	Hp_C00215_IG00001_L710	122	7	0.92	25	28
35	GSXTT4C07HZK7K_length=132	100	5			
36	Hp_I03085_IG00332_L1160	122	5	0.49		
36	Hp_I03086_IG00332_L1160	106	5	0.49		
37	Hp_I12673_IG04617_L2333	120	4	0.18		
38	Hp_I13332_IG05276_L1776	119	4	0.23		
39	Hp_I06752_IG01438_L1571	119	5	0.34		
40	Hp_I13832_IG05776_L1555	112	4	0.26	26	62
41	Hp_I24607_IG16551_L570	112	4	0.6	19	21
42	Hp_I04148_IG00569_L936	110	3	0.21		
43	Hp_I16239_IG08183_L1050	109	4	0.41		57
43	Hp_I17228_IG09172_L931	58	2	0.21		
43	HICN8C106HGHGB_length=348	48	1			
44	Hp_I15767_IG07711_L1120	107	2	0.19		
45	Hp_I05472_IG00957_L1361	105	5	0.23		43
46	Hp_I00798_IG00050_L1759	103	4	0.24		
46	Hp_I00806_IG00050_L1112	60	2	0.18		
46	Hp_I00796_IG00050_L1763	80	3			
46	Hp_I00803_IG00050_L1749	66	3			
46	Hp_I00811_IG00050_L794	53	1			
46	Hp_I00799_IG00050_L1753	44	2			
46	Hp_I00808_IG00050_L1102	23	1			
47	Hp_I13626_IG05570_L1638	102	4	0.18		
48	Hp_I05355_IG00918_L1570	102	6	0.42		16
48	Hp_I05356_IG00918_L1571	92	6	0.42		
49	Hp_I12444_IG04388_L2875	100	5	0.18		
50	Hp_I28140_IG20084_L502	97	3	0.7		
51	Hp_I12757_IG04701_L2227	95	4	0.19		
52	Hp_I26227_IG18171_L535	94	3	0.69		
53	Hp_I45281_IG37225_L323	94	3	1.29		
53	GS66ZV208IXGIJ_length=214	56	1			
54	Hp_I09305_IG02737_L997	91	1	0.09		

Table B.11: Proteins identified in the active fraction 25 of the second anion exchange fractionation of HES (continued).

Rank	Protein accession number	Protein score	Protein matches	emPAI	Rank in 1. MS fr. 39	Rank in 1. MS fr. 40
55	Hp_I05659_IG01019_L943	91	6	0.66		
55	Hp_I05657_IG01019_L1010	75	4	0.34		
55	Hp_I13122_IG05066_L1913	49	2	0.1		
55	HICN8C104EOX41_length=346	41	1			
55	GS66ZV202BPLMJ_length=260	28	2			
56	Hp_I25440_IG17384_L551	88	3	0.61		49
57	Hp_I21133_IG13077_L683	87	4	0.69	3	15
57	Hp_I08959_IG02564_L1212	54	2	0.17		
57	Hp_I03894_IG00508_L604	50	3	0.57	1	3
57	Hp_I20188_IG12132_L723	63	4		2	10
57	Hp_I45702_IG37646_L317	41	1			
57	Hp_C00053_IG00001_L722	31	1		8	
57	Hp_I03893_IG00508_L677	31	2			6
57	HICN8C104EH4N8_length=157	25	1			
58	Hp_I24965_IG16909_L566	85	4	0.89		
59	Hp_I12336_IG04280_L5030	84	5	0.08	44	38
59	Hp_I22411_IG14355_L634	38	1			
60	Hp_I07874_IG02021_L1689	83	2	0.12		
61	Hp_I04746_IG00749_L1266	81	3	0.24		
61	Hp_I04744_IG00749_L1308	48	2			
62	Hp_I17476_IG09420_L907	81	2	0.22		
63	Hp_I28347_IG20291_L499	81	3	0.73		
64	Hp_I14662_IG06606_L1314	81	2	0.15		
65	Hp_C00318_IG00001_L1664	79	3	0.18		34
66	Hp_I14323_IG06267_L1413	79	2	0.15		
67	Hp_I14909_IG06853_L1261	78	5	0.44		
68	Hp_I10136_IG03152_L609	76	2	0.34		
69	Hp_I13312_IG05256_L1794	75	2	0.11	29	
70	Hp_I12670_IG04614_L2338	72	2	0.08		
71	Hp_I08289_IG02229_L1998	72	2	0.1		
72	Hp_I14447_IG06391_L1373	72	1	0.07		
73	Hp_I10517_IG03343_L655	71	3	0.52		
73	Hp_I10518_IG03343_L562	57	2			
74	Hp_I23736_IG15680_L595	71	4	0.37		11
75	Hp_I24007_IG15951_L583	71	3	0.36		

Table B.11: Proteins identified in the active fraction 25 of the second anion exchange fractionation of HES (continued).

Rank	Protein accession number	Protein score	Protein matches	emPAI	Rank in 1. MS fr. 39	Rank in 1. MS fr. 40
76	Hp_I12819_IG04763_L2150	70	1	0.04		72
77	Hp_I05927_IG01110_L916	70	3	0.34		
77	Hp_I40602_IG32546_L371	50	1			
77	Hp_I05928_IG01110_L497	35	1			
78	Hp_I37752_IG29696_L390	69	2	0.6		
79	Hp_I15536_IG07480_L1158	69	6	0.47	27	82
80	Hp_I10155_IG03162_L783	67	2	0.25	5	5
81	GNK0QLK03GQOZO_length=396	67	2	0.55		
82	Hp_I27254_IG19198_L516	67	3	0.68		
83	Hp_I15902_IG07846_L1103	67	1	0.09		
84	Hp_I17933_IG09877_L867	67	2	0.24		
85	Hp_I15775_IG07719_L1120	66	1	0.09		
86	Hp_I20989_IG12933_L687	66	2	0.3		
86	Hp_I19992_IG11936_L730	56	1			
87	Hpb-APY-1.1	65	2	0.2		
88	Hp_I10156_IG03162_L593	65	2	0.34	48	75
89	Hp_I21746_IG13690_L653	65	1	0.15		
90	Hp_I18845_IG10789_L800	65	2	0.25		
91	Hp_I13897_IG05841_L1536	65	1	0.06		83
92	Hp_I04070_IG00550_L1810	65	2	0.11		
93	Hp_I12485_IG04429_L2697	64	2	0.07		
94	Hp_I12624_IG04568_L2400	63	2	0.08	14	
94	GP9KNTD03F5ENS_length=137	32	1			
95	GSXTT4C07IIS51_length=389	61	1	0.29		
96	Hp_I21182_IG13126_L679	61	5	0.69		
97	Hp_I22261_IG14205_L639	61	1	0.16		30
98	Hp_I03099_IG00335_L808	60	1	0.12		
99	Hp_I08747_IG02458_L1084	59	3	0.19		
100	Hp_I02742_IG00275_L749	59	1	0.13		
101	Hp_I06715_IG01419_L1709	58	1	0.06		
102	Hp_I31041_IG22985_L459	57	1	0.21		
103	Hp_I15874_IG07818_L1106	57	2	0.18	34	22
104	Hp_I16107_IG08051_L1068	57	1	0.09		
105	Hp_I11897_IG04033_L376	55	1	0.27		
106	Hp_I09123_IG02646_L960	54	2	0.21		53

Table B.11: Proteins identified in the active fraction 25 of the second anion exchange fractionation of HES (continued).

Rank	Protein accession number	Protein score	Protein matches	emPAI	Rank in 1. MS fr. 39	Rank in 1. MS fr. 40
107	Hp_I07312_IG01740_L4913	54	4	0.08		
107	Hp_I30910_IG22854_L463	28	2			
108	Hp_I18045_IG09989_L856	54	1	0.11		
109	Hp_I04010_IG00535_L4397	54	2	0.02		84
110	Hp_I07157_IG01645_L560	53	2	0.38		
111	Hp_I24623_IG16567_L570	53	3	0.59		
112	Hp_I03648_IG00446_L2680	53	1	0.03		
113	HICN8C104EI0NY_length=231	52	1	0.43		
114	Hp_I18857_IG10801_L798	52	4	0.4		
115	Hp_I17367_IG09311_L916	52	2	0.21		
116	Hp_I22851_IG14795_L620	52	4	0.78	18	9
117	Hp_I14314_IG06258_L1412	52	1	0.07		26
118	Hp_I13967_IG05911_L1505	52	1	0.06		
119	HICN8C104D48FA_length=165	51	1	0.7		
120	Hp_I10419_IG03294_L714	51	2	0.3		
121	Hp_I50524_IG42468_L249	51	2	1.04		
122	Hp_I44062_IG36006_L335	50	1	0.31		
123	Hp_I03163_IG00349_L1163	50	1	0.08		
124	Hp_I24997_IG16941_L561	49	1	0.17		
125	Hp_I21919_IG13863_L649	49	1	0.15		
126	Hp_I54342_IG46286_L172	49	1	0.67		
127	Hp_I14477_IG06421_L1364	49	1	0.07		
128	Hp_I15720_IG07664_L1128	48	1	0.09		
129	Hp_I03703_IG00460_L2193	47	1	0.04		
130	HELDS7W07HYSKQ_length=134	46	1	0.84		
131	Hp_I34129_IG26073_L426	46	2	0.51		
132	Hp_I06164_IG01191_L389	45	2	0.59		
133	Hp_I14129_IG06073_L1461	45	2	0.14		
134	Hp_I36714_IG28658_L408	44	1	0.27	36	87
135	Hp_I22937_IG14881_L616	44	1	0.16		
136	Hp_I22552_IG14496_L630	44	1	0.16		
137	Hp_I21076_IG13020_L685	44	1	0.14		
138	FL8UM6J01B2BCH_length=241	43	1	0.45		
139	GP9KNTD03FPOC6_length=206	43	1	0.53		
140	Hp_I13644_IG05588_L1625	43	2	0.12		

Table B.11: Proteins identified in the active fraction 25 of the second anion exchange fractionation of HES (continued).

Rank	Protein accession number	Protein score	Protein matches	emPAI	Rank in 1. MS fr. 39	Rank in 1. MS fr. 40
141	Hp_I09609_IG02889_L890	43	1	0.11		
142	Hp_I05463_IG00954_L1399	43	1	0.07		
143	Hp_I20654_IG12598_L702	42	1	0.14		
144	Hpb-VAL-20	42	1	0.07		
145	Hp_I08941_IG02555_L1722	42	2	0.11		
145	Hp_I12877_IG04821_L2113	29	1			
146	HICN8C106G240C_length=375	42	1	0.28		
147	Hp_I17588_IG09532_L899	42	1	0.11		
148	Hp_I38698_IG30642_L388	42	1	0.26		
149	Hp_I17130_IG09074_L942	41	1	0.11		
150	Hp_I18672_IG10616_L814	41	2	0.26		
151	Hp_I30926_IG22870_L465	41	1	0.21		
152	Hp_I19958_IG11902_L735	40	1	0.13		41
153	Hp_I08021_IG02095_L2057	40	3	0.14		
154	Hp_I14119_IG06063_L1461	40	2	0.14		77
155	Hp_I07837_IG02002_L1154	40	1	0.09		
156	Hp_I16083_IG08027_L1071	40	2	0.19		
157	Hp_I09191_IG02680_L1307	40	1	0.07		
158	Hp_I13437_IG05381_L1722	40	3	0.11		
159	Hp_I24512_IG16456_L570	40	2	0.17		
160	Hpb-APY-3	39	2	0.2		
160	Hp_I34250_IG26194_L432	28	1			
161	Hp_I12989_IG04933_L2009	39	2	0.05		
162	Hp_I07528_IG01848_L2299	39	1	0.04		
163	Hp_I12518_IG04462_L2600	39	1	0.04		73
164	Hp_I08161_IG02165_L1513	38	1	0.06		
165	Hp_I06748_IG01436_L1580	38	1	0.06		
166	Hp_I16357_IG08301_L1032	38	1	0.09		
167	Hp_I47440_IG39384_L295	38	1	0.33		
168	Hp_I18903_IG10847_L800	38	1	0.11		
169	Hp_I11671_IG03920_L408	37	1	0.24		
170	Hp_I20106_IG12050_L727	37	1	0.13		
171	Hp_I12856_IG04800_L2123	37	1	0.05		103
172	GSXTT4C07H1KXM_length=433	36	1	0.24		
173	GLSD98I05F6IT3_length=173	36	3	1.54		

Table B.11: Proteins identified in the active fraction 25 of the second anion exchange fractionation of HES (continued).

Rank	Protein accession number	Protein score	Protein matches	emPAI	Rank in 1. MS fr. 39	Rank in 1. MS fr. 40
174	Hp_I10589_IG03379_L596	36	1	0.16		99
175	Hp_I14819_IG06763_L1285	35	1	0.08		
176	Hp_I35779_IG27723_L416	35	1	0.24		
177	GQ6YEYD07IH8NV_length=254	35	1	0.45		
178	GNK0QLK03GEF2E_length=349	34	1	0.29		
179	Hp_I15275_IG07219_L1202	33	1	0.08		
180	Hp_I13201_IG05145_L1858	33	3	0.05	7	
181	Hp_I45109_IG37053_L322	33	1	0.33		
182	Hp_I22184_IG14128_L642	33	1	0.15		
183	Hp_I06970_IG01547_L1058	33	1	0.09		
184	Hp_I26349_IG18293_L526	33	1	0.19		
185	Hp_I12307_IG04251_L678	32	1	0.15		
186	Hp_I12356_IG04300_L3770	32	1	0.02		
187	Hp_I15761_IG07705_L1121	32	1	0.09		
188	Hp_I30640_IG22584_L466	32	1	0.21		
189	Hp_I17533_IG09477_L904	32	1	0.11		
190	Hp_I05325_IG00908_L1903	32	1	0.05	28	64
191	GP9KNTD03HEYKX_length=353	32	1	0.29		
192	Hp_I08946_IG02557_L754	31	2	0.13		
193	Hp_I02260_IG00198_L2283	31	1	0.04		
194	Hp_I20186_IG12130_L717	31	1	0.14		
195	Hp_I12594_IG04538_L2461	31	2	0.08		
196	Hp_I20314_IG12258_L716	30	2	0.28		
197	Hp_I16694_IG08638_L992	30	1	0.1		
198	Hp_I21825_IG13769_L655	30	1	0.15		
199	Hp_I13398_IG05342_L1737	30	1	0.06		
200	Hp_I14921_IG06865_L1261	29	2	0.08		
201	Hp_I20393_IG12337_L714	29	1	0.13		
202	Hp_I11929_IG04049_L398	29	1	0.25		
203	Hp_I23293_IG15237_L606	29	1	0.16		
204	Hp_I03094_IG00334_L1829	29	1	0.05		
205	Hp_I14648_IG06592_L1319	29	1	0.07		
206	Hp_I38562_IG30506_L390	29	1	0.27		
207	GLSD98I05F5ITC_length=415	29	1	0.22		
208	Hp_I08139_IG02154_L1715	28	1	0.06		

Table B.11: Proteins identified in the active fraction 25 of the second anion exchange fractionation of HES (continued).

Rank	Protein accession number	Protein score	Protein matches	emPAI	Rank in 1. MS fr. 39	Rank in 1. MS fr. 40
209	Hp_I15010_IG06954_L1245	28	1	0.08		
210	Hp_I12776_IG04720_L2202	28	1	0.04		
211	Hp_I20274_IG12218_L717	28	1	0.13		
212	Hp_I02126_IG00179_L738	27	2	0.13		
213	Hp_I13865_IG05809_L1545	27	1	0.06		
214	Hp_I07286_IG01727_L3181	27	1	0.03		
215	Hp_I23615_IG15559_L596	27	1	0.17		
216	Hp_I12527_IG04471_L2582	27	1	0.04		
217	Hp_I18858_IG10802_L799	27	1	0.12		
218	GLSD98I05F0MGD_length=346	26	1	0.29		
219	Hp_I20884_IG12828_L690	26	1	0.14		
220	Hp_I03660_IG00449_L3044	26	1	0.03		
221	Hp_I06986_IG01555_L958	26	1	0.1		
222	Hp_I07318_IG01743_L3042	26	1	0.03		
223	Hp_I03499_IG00413_L1865	26	1	0.05		
224	Hp_I10841_IG03505_L619	26	1	0.16		
225	HICN8C104EDEVR_length=54	26	1	2.43		
226	Hp_I10521_IG03345_L626	25	1	0.15		
227	Hp_I23374_IG15318_L597	25	1	0.17		
228	Hp_I17728_IG09672_L887	25	1	0.1		
229	Hp_I12275_IG04222_L261	25	1	0.38		
230	Hp_I20231_IG12175_L721	24	1	0.14		
231	Hp_I22655_IG14599_L627	24	1	0.16		
232	Hp_I04103_IG00558_L1245	24	1	0.08		
233	Hp_I21982_IG13926_L651	24	1	0.15		
234	Hp_I18054_IG09998_L853	23	1	0.11		
235	Hp_I13345_IG05289_L1772	23	1	0.06		
236	Hp_I08349_IG02259_L1293	23	1	0.07		
237	Hp_I20368_IG12312_L714	23	1	0.13		
238	Hp_I12754_IG04698_L2228	23	1	0.04	37	
239	Hp_C01552_IG00008_L1448	23	1	0.06		
240	Hp_I15778_IG07722_L1118	23	1	0.09		
241	GLSD98I05F32KD_length=465	23	1	0.22		
242	Hp_I25677_IG17621_L546	23	1	0.18		
243	Hpb-VAL-14	23	1	0.07		

Table B.11: Proteins identified in the active fraction 25 of the second anion exchange fractionation of HES (continued).

Rank	Protein accession number	Protein score	Protein matches	emPAI	Rank in 1. MS fr. 39	Rank in 1. MS fr. 40
244	Hp_I49935_IG41879_L259	23	1	0.41		
245	Hp_I11951_IG04060_L390	22	1	0.26		
246	Hp_I28361_IG20305_L498	22	1	0.2		
247	Hp_I22484_IG14428_L640	22	1	0.15		
248	Hp_I07496_IG01832_L2183	22	1	0.04		
249	Hp_I14665_IG06609_L1313	21	1	0.07		
250	Hp_I04874_IG00782_L1023	21	1	0.1		95
251	Hp_I08483_IG02326_L1214	21	1	0.08		
252	Hp_I10597_IG03383_L595	21	1	0.16		
253	Hp_I07666_IG01917_L1781	21	1	0.05		
254	Hp_C00910_IG00003_L2934	21	1	0.03		
255	Hp_I29394_IG21338_L484	20	1	0.21		
256	Hp_I14044_IG05988_L1484	20	1	0.06		

Table B.12: Proteins with emPAI values peaking in size exclusion fractions 14 or 15. HES was fractionated by size fractionation an all fractions analysed by mass spectrometry and tested for their inhibitory activity on GM-CSF BMDC. Proteins with emPAI values peaking in the active fractions were shortlisted for further selection to find candidate proteins for expression.

FL8UM6J01BC1ZN_length=62	GSXTT4C06GUNT5_length=342	Hp_I01383_IG00095_L656
FL8UM6J01EFBYL_length=63	GSXTT4C06GXMIV_length=179	Hp_I02234_IG00194_L1318
GLSD98I04D6NC8_length=454	GSXTT4C07IOOUR_length=396	Hp_I02548_IG00238_L1779
GLSD98I04EBL7F_length=389	HELDS7W07H0BVM_length=251	Hp_I03099_IG00335_L808
GLSD98I05F0MGD_length=346	HICN8C105F4XWC_length=461	Hp_I03228_IG00366_L2337
GLSD98I05F6IT3_length=173	HICN8C105F7BX8_length=227	Hp_I04266_IG00599_L823
GNK0QLK03F82AT_length=271	HICN8C106HP9PI_length=274	Hp_I04332_IG00616_L354
GNK0QLK03FHM83_length=50	Hp_C00179_IG00001_L1163	Hp_I05058_IG00828_L787
GNK0QLK03G3KHF_length=294	Hp_C00282_IG00001_L564	Hp_I05325_IG00908_L1903
GNK0QLK03GQOZO_length=396	Hp_C02597_IG00028_L1734	Hp_I05407_IG00935_L1040
GQ6YEYD07H2LVG_length=277	Hp_C08742_IG00702_L613	Hp_I05565_IG00988_L1210
GS66ZV202BO7NU_length=145	Hp_I00695_IG00044_L591	Hp_I05659_IG01019_L943
GS66ZV203DB0T9_length=193	Hp_I00798_IG00050_L1759	Hp_I05809_IG01070_L1113
GS66ZV203DFM3U_length=95	Hp_I00841_IG00053_L616	Hp_I05827_IG01076_L1116
GSXTT4C05FPGBC_length=392	Hp_I00850_IG00054_L907	Hp_I05999_IG01134_L555

Table B.12: Proteins with emPAI values peaking in size exclusion fractions 14 or 15 (continued).

Hp_I06001_IG01134_L530	Hp_I18333_IG10277_L834	Hp_I26844_IG18788_L525
Hp_I06335_IG01256_L998	Hp_I18384_IG10328_L830	Hp_I26937_IG18881_L522
Hp_I06509_IG01316_L615	Hp_I18845_IG10789_L800	Hp_I27637_IG19581_L511
Hp_I06838_IG01481_L1319	Hp_I19378_IG11322_L765	Hp_I27930_IG19874_L505
Hp_I07157_IG01645_L560	Hp_I19711_IG11655_L743	Hp_I27958_IG19902_L502
Hp_I07158_IG01645_L560	Hp_I19958_IG11902_L735	Hp_I28625_IG20569_L494
Hp_I07249_IG01697_L637	Hp_I19989_IG11933_L735	Hp_I28724_IG20668_L494
Hp_I07274_IG01721_L3765	Hp_I19992_IG11936_L730	Hp_I28744_IG20688_L490
Hp_I07334_IG01751_L2741	Hp_I20768_IG12712_L696	Hp_I29394_IG21338_L484
Hp_I07490_IG01829_L2288	Hp_I20875_IG12819_L687	Hp_I30337_IG22281_L473
Hp_I07995_IG02081_L699	Hp_I21268_IG13212_L674	Hp_I30585_IG22529_L470
Hp_I08415_IG02292_L1231	Hp_I21313_IG13257_L675	Hp_I30636_IG22580_L471
Hp_I09863_IG03016_L798	Hp_I21565_IG13509_L658	Hp_I30926_IG22870_L465
Hp_I10517_IG03343_L655	Hp_I21617_IG13561_L662	Hp_I31577_IG23521_L459
Hp_I10518_IG03343_L562	Hp_I21726_IG13670_L658	Hp_I32194_IG24138_L452
Hp_I10601_IG03385_L624	Hp_I21746_IG13690_L653	Hp_I32491_IG24435_L448
Hp_I10855_IG03512_L534	Hp_I22064_IG14008_L644	Hp_I34113_IG26057_L428
Hp_I11144_IG03656_L469	Hp_I22123_IG14067_L644	Hp_I34646_IG26590_L427
Hp_I11447_IG03808_L449	Hp_I22275_IG14219_L639	Hp_I34892_IG26836_L422
Hp_I12456_IG04400_L2825	Hp_I22320_IG14264_L638	Hp_I35726_IG27670_L415
Hp_I12776_IG04720_L2202	Hp_I22350_IG14294_L635	Hp_I35752_IG27696_L420
Hp_I12936_IG04880_L2046	Hp_I22388_IG14332_L637	Hp_I36017_IG27961_L415
Hp_I13494_IG05438_L1681	Hp_I23528_IG15472_L598	Hp_I38111_IG30055_L394
Hp_I13743_IG05687_L1584	Hp_I23530_IG15474_L600	Hp_I38325_IG30269_L391
Hp_I14371_IG06315_L1386	Hp_I23776_IG15720_L592	Hp_I38451_IG30395_L390
Hp_I14584_IG06528_L1336	Hp_I23836_IG15780_L590	Hp_I38850_IG30794_L366
Hp_I15194_IG07138_L1211	Hp_I23863_IG15807_L590	Hp_I38933_IG30877_L384
Hp_I15353_IG07297_L1178	Hp_I24096_IG16040_L584	Hp_I38988_IG30932_L386
Hp_I15488_IG07432_L1169	Hp_I24430_IG16374_L575	Hp_I39181_IG31125_L382
Hp_I15528_IG07472_L1156	Hp_I24512_IG16456_L570	Hp_I40392_IG32336_L373
Hp_I15587_IG07531_L1141	Hp_I24623_IG16567_L570	Hp_I40417_IG32361_L370
Hp_I15588_IG07532_L1149	Hp_I24705_IG16649_L569	Hp_I40444_IG32388_L371
Hp_I15760_IG07704_L1122	Hp_I25184_IG17128_L557	Hp_I40801_IG32745_L368
Hp_I15778_IG07722_L1118	Hp_I25374_IG17318_L554	Hp_I40994_IG32938_L367
Hp_I15783_IG07727_L1116	Hp_I25622_IG17566_L549	Hp_I40999_IG32943_L364
Hp_I16638_IG08582_L998	Hp_I25725_IG17669_L542	Hp_I41819_IG33763_L358
Hp_I16854_IG08798_L973	Hp_I26246_IG18190_L526	Hp_I42607_IG34551_L347
Hp_I16860_IG08804_L972	Hp_I26504_IG18448_L528	Hp_I43185_IG35129_L337
Hp_I17383_IG09327_L916	Hp_I26601_IG18545_L528	Hp_I44251_IG36195_L332

Table B.12: Proteins with emPAI values peaking in size exclusion fractions 14 or 15 (continued).

Hp_I45710_IG37654_L317	Hp_I50368_IG42312_L251	Hpb-VAL-1.1
Hp_I49433_IG41377_L267	Hpb-Sequence-14	Hpb-VAL-7.3
Hp_I49594_IG41538_L265		

Table B.13: Proteins with emPAI values peaking in anion exchange fraction 25. HES was fractionated by anion exchange fractionation and all fractions analysed by mass spectrometry and tested for their inhibitory activity on GM-CSF BMDC. Proteins with emPAI values peaking in the active fraction were shortlisted for further selection to find candidate proteins for expression.

FL8UM6J01BCVJW_length=245	Hp_I05693_IG01031_L1691
GLSD98I05F6IT3_length=173	Hp_I06164_IG01191_L389
GNK0QLK03GEF2E_length=349	Hp_I06752_IG01438_L1571
GNK0QLK03GQOZO_length=396	Hp_I06986_IG01555_L958
GP9KNTD03FPOC6_length=206	Hp_I07312_IG01740_L4913
GP9KNTD03HEYKX_length=353	Hp_I07468_IG01818_L2128
GQ6YEYD07IH8NV_length=254	Hp_I07682_IG01925_L1479
HICN8C104D48FA_length=165	Hp_I07837_IG02002_L1154
HICN8C104EI0NY_length=231	Hp_I08289_IG02229_L1998
Hp_C00318_IG00001_L1664	Hp_I08349_IG02259_L1293
Hp_C00910_IG00003_L2934	Hp_I08483_IG02326_L1214
Hp_I00806_IG00050_L1112	Hp_I08747_IG02458_L1084
Hp_I02260_IG00198_L2283	Hp_I09191_IG02680_L1307
Hp_I03086_IG00332_L1160	Hp_I10136_IG03152_L609
Hp_I03648_IG00446_L2680	Hp_I10517_IG03343_L655
Hp_I03703_IG00460_L2193	Hp_I10521_IG03345_L626
Hp_I03894_IG00508_L604	Hp_I10589_IG03379_L596
Hp_I04010_IG00535_L4397	Hp_I10841_IG03505_L619
Hp_I04627_IG00719_L1926	Hp_I11671_IG03920_L408
Hp_I04629_IG00719_L1853	Hp_I11951_IG04060_L390
Hp_I04746_IG00749_L1266	Hp_I12275_IG04222_L261
Hp_I04874_IG00782_L1023	Hp_I12307_IG04251_L678
Hp_I05325_IG00908_L1903	Hp_I12356_IG04300_L3770
Hp_I05355_IG00918_L1570	Hp_I12485_IG04429_L2697
Hp_I05356_IG00918_L1571	Hp_I12594_IG04538_L2461
Hp_I05463_IG00954_L1399	Hp_I12670_IG04614_L2338
Hp_I05472_IG00957_L1361	Hp_I12673_IG04617_L2333
Hp_I05659_IG01019_L943	Hp_I12757_IG04701_L2227

Table B.13: Proteins with emPAI values peaking in anion exchange fraction 25 (continued).

Hp_I12776_IG04720_L2202	Hp_I20654_IG12598_L702
Hp_I12856_IG04800_L2123	Hp_I20884_IG12828_L690
Hp_I13043_IG04987_L1979	Hp_I21073_IG13017_L680
Hp_I13626_IG05570_L1638	Hp_I21182_IG13126_L679
Hp_I13644_IG05588_L1625	Hp_I21982_IG13926_L651
Hp_I14044_IG05988_L1484	Hp_I22184_IG14128_L642
Hp_I14129_IG06073_L1461	Hp_I22484_IG14428_L640
Hp_I14221_IG06165_L1437	Hp_I22552_IG14496_L630
Hp_I14314_IG06258_L1412	Hp_I23374_IG15318_L597
Hp_I14323_IG06267_L1413	Hp_I23615_IG15559_L596
Hp_I14662_IG06606_L1314	Hp_I23736_IG15680_L595
Hp_I14665_IG06609_L1313	Hp_I24623_IG16567_L570
Hp_I14819_IG06763_L1285	Hp_I24965_IG16909_L566
Hp_I14909_IG06853_L1261	Hp_I25311_IG17255_L555
Hp_I14921_IG06865_L1261	Hp_I26227_IG18171_L535
Hp_I15157_IG07101_L1223	Hp_I26349_IG18293_L526
Hp_I15775_IG07719_L1120	Hp_I28140_IG20084_L502
Hp_I15902_IG07846_L1103	Hp_I29394_IG21338_L484
Hp_I16239_IG08183_L1050	Hp_I30926_IG22870_L465
Hp_I16357_IG08301_L1032	Hp_I35779_IG27723_L416
Hp_I16694_IG08638_L992	Hp_I36714_IG28658_L408
Hp_I17476_IG09420_L907	Hp_I38698_IG30642_L388
Hp_I17533_IG09477_L904	Hp_I44062_IG36006_L335
Hp_I17588_IG09532_L899	Hp_I45109_IG37053_L322
Hp_I17728_IG09672_L887	Hp_I50524_IG42468_L249
Hp_I18054_IG09998_L853	Hp_I54342_IG46286_L172
Hp_I18672_IG10616_L814	Hpb-APY-1.1
Hp_I19958_IG11902_L735	Hpb-VAL-12
Hp_I20106_IG12050_L727	Hpb-VAL-2.2
Hp_I20186_IG12130_L717	Hpb-VAL-3
Hp_I20231_IG12175_L721	Hpb-VAL-4
Hp_I20274_IG12218_L717	Hpb-VAL-5
Hp_I20393_IG12337_L714	

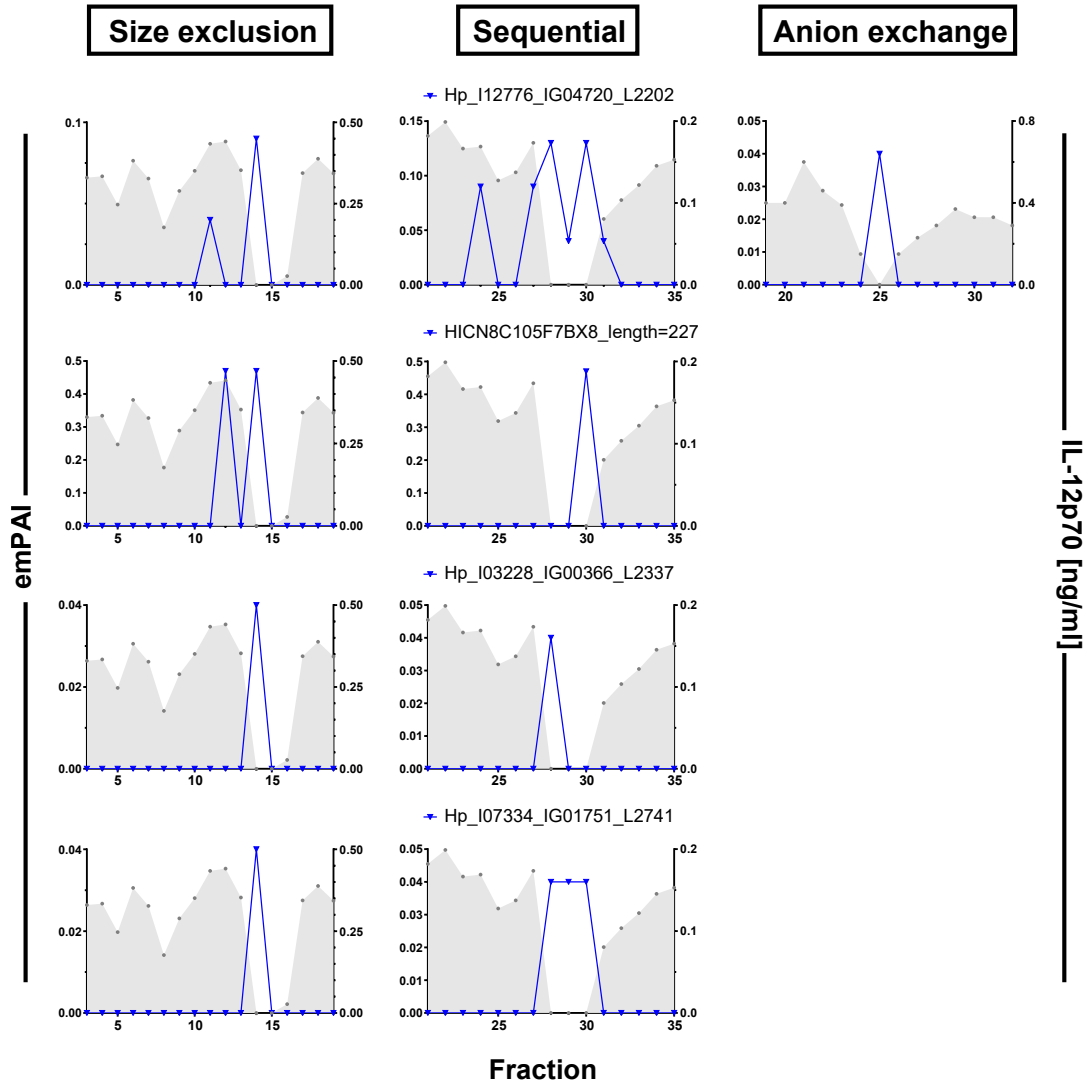

Figure B.2: Rejected candidates from third round of candidate protein identification. HES was fractionated by size exclusion, sequential and anion exchange fractionation, all fractions were analysed by mass spectrometry and their inhibitory activity tested on LPS-activated GM-CSF BMDC. Lists of proteins with emPAI values peaking in the active fractions were compiled for each fractionation approach and compared to identify shared proteins. These were subjected to further selection comparing their abundance profiles (emPAI values over the fractions) to activity (inhibition of IL-12p70 production in LPS-activated BMDC) across the fractions and excluding housekeeping proteins and those that have been identified falsely or with only one peptide. These excluded proteins are shown here with their emPAI values across the fractions on the left y axis and the concentration of IL-12p70 produced by GM-CSF BMDC treated with LPS (1μg/ml) and the respective fraction on the right y axis.

C. Supplementary material for BMDC signalling & metabolism

Table C.1: Transcripts up-regulated in LPS+HES treated compared to LPS stimulated BMDC. BMDC were differentiated with GM-CSF for ten days before stimulation with LPS and HES as indicated. At eight hours after stimulation, cells were treated with Trizol, RNA extracted and labelled for analysis on an Illumina MouseWG-6 v2.0 Expression BeadChip microarray. Statistical analysis of the data was performed by Dr. Alasdair Ivens. Listed are symbols and descriptions of the features together with their log 2 and linear fold changes and adjusted p values. Only features with a log 2 fold change of at least 0.25 (linear fold change of 1.9) are listed.

Symbol	Description	log2 FC	fold change	adjusted p value
Tgfbi	transforming growth factor, beta induced	1.4	2.64	0.0017
Tgfbi	transforming growth factor, beta induced	1.2	2.30	0.0017
Arg1	arginase, liver	0.95	1.93	0.0017
Adssl1	adenylosuccinate synthetase like 1	0.88	1.84	0.0046
Ly6a	lymphocyte antigen 6 complex, locus A	0.86	1.82	0.0066
Hmox1	heme oxygenase (decycling) 1	0.86	1.82	0.007
Timp1	tissue inhibitor of metalloproteinase 1	0.78	1.72	0.009
Timp1	tissue inhibitor of metalloproteinase 1	0.76	1.69	0.1
Adssl1	adenylosuccinate synthetase like 1	0.73	1.66	0.0034
Stab1	stabilin 1	0.69	1.61	0.0017
Il33	interleukin 33	0.66	1.58	0.0053
S1pr2	sphingosine-1-phosphate receptor 2	0.64	1.56	0.0046
NA	NA	0.62	1.54	0.0034
Vegfa	vascular endothelial growth factor A	0.62	1.54	0.0082
Plac8	placenta-specific 8	0.61	1.53	0.0017
Elk3	ELK3, member of ETS oncogene family	0.61	1.53	0.042
Arg1	arginase, liver	0.6	1.52	0.0046

Table C.1: Transcripts upregulated in LPS+HES treated compared to LPS stimulated BMDC (continued).

Symbol	Description	log2 FC	fold change	adjusted p value
Egln3	EGL nine homolog 3 (C. elegans)	0.6	1.52	0.0053
Spint1	serine protease inhibitor, Kunitz type 1	0.59	1.51	0.0017
Adam8	a disintegrin and metallopeptidase domain 8	0.59	1.51	0.017
Slc48a1	solute carrier family 48 (heme transporter), member 1	0.58	1.49	0.0034
Ass1	argininosuccinate synthetase 1	0.57	1.48	0.012
Hif1a	hypoxia inducible factor 1, alpha subunit	0.56	1.47	0.041
Gadd45g	growth arrest and DNA-damage-inducible 45 gamma	0.55	1.46	0.0024
Gga2	golgi associated, gamma adaptin ear containing, ARF BP2	0.54	1.45	0.0044
Egln3	EGL nine homolog 3 (C. elegans)	0.53	1.44	0.024
Thbs1	thrombospondin 1	0.53	1.44	0.1
Tnfrsf9	tumor necrosis factor receptor superfamily, member 9	0.52	1.43	0.026
2010111I01Rik	RIKEN cDNA 2010111I01 gene	0.52	1.43	0.11
P2ry6	pyrimidinergic receptor P2Y, G-protein coupled, 6	0.51	1.42	0.011
Cd300lf	CD300 antigen like family member F	0.51	1.42	0.096
Gga2	golgi associated, gamma adaptin ear containing, ARF BP2	0.5	1.41	0.005
Vegfa	vascular endothelial growth factor A	0.49	1.40	0.014
LOC100044439	similar to cytochrome P450 CYP4F18	0.49	1.40	0.015
LOC676420	similar to Ceramide kinase (Acylsphingosine kinase)	0.49	1.40	0.017
Gclm	glutamate-cysteine ligase, modifier subunit	0.48	1.39	0.0087
Acpp	acid phosphatase, prostate	0.48	1.39	0.018
Pdgfb	platelet derived growth factor, B polypeptide	0.48	1.39	0.025

Table C.1: Transcripts upregulated in LPS+HES treated compared to LPS stimulated BMDC (continued).

Symbol	Description	log2 FC	fold change	adjusted p value
Clec7a	C-type lectin domain family 7, member a	0.48	1.39	0.082
Slc2a1	solute carrier family 2 (facilitated glucose transporter)	0.47	1.39	0.023
Tubb6	tubulin, beta 6	0.47	1.39	0.09
Gadd45g	growth arrest and DNA-damage-inducible 45 gamma	0.46	1.38	0.052
Sdc1	syndecan 1	0.46	1.38	0.066
Nos2	nitric oxide synthase 2, inducible	0.46	1.38	0.098
Adam8	a disintegrin and metallopeptidase domain 8	0.44	1.36	0.079
Emp1	epithelial membrane protein 1	0.43	1.35	0.0099
Atf3	activating transcription factor 3	0.42	1.34	0.047
Slc11a1	solute carrier family 11 (proton-coupled divalent metal ion)	0.42	1.34	0.1
Glrx	glutaredoxin	0.42	1.34	0.16
Lpar6	lysophosphatidic acid receptor 6	0.41	1.33	0.0087
Anxa6	annexin A6	0.41	1.33	0.075
NA	NA	0.41	1.33	0.076
Emilin2	elastin microfibril interfacer 2	0.41	1.33	0.19
Spsb4	splA/ryanodine receptor domain and SOCS box containing 4	0.4	1.32	0.014
Ccnd1	cyclin D1	0.4	1.32	0.017
Ddit4	DNA-damage-inducible transcript 4	0.4	1.32	0.095
Paox	polyamine oxidase (exo-N4-amino)	0.39	1.31	0.0084
Hspa1a	heat shock protein 1A	0.39	1.31	0.011
Jun	Jun oncogene	0.39	1.31	0.017

Table C.1: Transcripts upregulated in LPS+HES treated compared to LPS stimulated BMDC (continued).

Symbol	Description	log2 FC	fold change	adjusted p value
F13a1	coagulation factor XIII, A1 subunit	0.39	1.31	0.026
Ankrd37	ankyrin repeat domain 37	0.39	1.31	0.031
Pdlim7	PDZ and LIM domain 7	0.39	1.31	0.032
LOC100047419	similar to c-Maf long form	0.39	1.31	0.043
Cyp4f18	cytochrome P450, family 4, subfamily f, polypeptide 18	0.39	1.31	0.065
Slc29a3	solute carrier family 29 (nucleoside transporters)	0.39	1.31	0.073
Rai14	retinoic acid induced 14	0.39	1.31	0.11
Osm	oncostatin M	0.39	1.31	0.11
Pqlc3	PQ loop repeat containing	0.39	1.31	0.21
Mgst1	microsomal glutathione S-transferase 1	0.38	1.30	0.016
Cxcr4	chemokine (C-X-C motif) receptor 4	0.38	1.30	0.024
Per2	period homolog 2 (Drosophila)	0.38	1.30	0.045
Tnfsf13b	tumor necrosis factor (ligand) superfamily, member 13b	0.37	1.29	0.014
Kcnn4	Na intermediate/small conductance Ca-activated channel	0.37	1.29	0.017
Casp6	caspase 6	0.37	1.29	0.076
Dnmt3l	DNA (cytosine-5-)-methyltransferase 3-like	0.37	1.29	0.17
LOC100048461	similar to dendritic cell-associated C-type lectin-1	0.37	1.29	0.3
NA	NA	0.37	1.29	0.39
march1	membrane-associated ring finger (C3HC4) 1	0.36	1.28	0.079
Emilin2	elastin microfibril interfacer 2	0.36	1.28	0.089
Echs1	enoyl Coenzyme A hydratase, short chain, 1, mitochondrial	0.36	1.28	0.19

Table C.1: Transcripts upregulated in LPS+HES treated compared to LPS stimulated BMDC (continued).

Symbol	Description	log2 FC	fold change	adjusted p value
38595	septin 9	0.35	1.27	0.07
Tmem86a	transmembrane protein 86A	0.35	1.27	0.12
Msn	moesin	0.35	1.27	0.45
Carhsp1	calcium regulated heat stable protein 1	0.34	1.27	0.0073
Srxn1	sulfiredoxin 1 homolog (S. cerevisiae)	0.34	1.27	0.023
Mgst1	microsomal glutathione S-transferase 1	0.34	1.27	0.024
Bin1	bridging integrator 1	0.34	1.27	0.042
Mknk2	MAP kinase-interacting serine/threonine kinase 2	0.34	1.27	0.054
Atp7a	ATPase, Cu++ transporting, alpha polypeptide	0.34	1.27	0.054
Slc11a1	solute carrier family 11 (proton-coupled divalent metal ion)	0.34	1.27	0.12
Ppp1r3b	protein phosphatase 1, regulatory (inhibitor) subunit 3B	0.34	1.27	0.14
Coro1c	coronin, actin binding protein 1C	0.34	1.27	0.15
Stab1	stabilin 1	0.33	1.26	0.0082
Txnip	thioredoxin interacting protein	0.33	1.26	0.031
Cyb5	cytochrome b-5	0.33	1.26	0.06
Taldo1	transaldolase 1	0.33	1.26	0.083
Cotl1	coactosin-like 1 (Dictyostelium)	0.33	1.26	0.096
Scd2	stearoyl-Coenzyme A desaturase 2	0.33	1.26	0.12
Fst	follistatin	0.33	1.26	0.13
Glrx	glutaredoxin	0.33	1.26	0.15
Pycard	PYD and CARD domain containing	0.33	1.26	0.18

Table C.1: Transcripts upregulated in LPS+HES treated compared to LPS stimulated BMDC (continued).

Symbol	Description	log2 FC	fold change	adjusted p value
Slco3a1	solute carrier organic anion transporter family, member 3a1	0.33	1.26	0.23
Anxa2	annexin A2	0.33	1.26	0.24
Idh1	isocitrate dehydrogenase 1 (NADP+), soluble	0.33	1.26	0.27
NA	NA	0.33	1.26	0.32
Apoe	apolipoprotein E	0.33	1.26	0.39
Tnfrsf9	tumor necrosis factor receptor superfamily, member 9	0.32	1.25	0.011
Nisch	nischarin	0.32	1.25	0.011
Ppap2b	phosphatidic acid phosphatase type 2B	0.32	1.25	0.024
NA	NA	0.32	1.25	0.057
Cgnl1	cingulin-like 1	0.32	1.25	0.06
Sdc1	syndecan 1	0.32	1.25	0.061
NA	NA	0.32	1.25	0.093
Acpp	acid phosphatase, prostate	0.32	1.25	0.21
B4galt1	UDP-Gal:betaGlcNAc beta 1,4- galactosyltransferase	0.32	1.25	0.38
5430435G22Rik	RIKEN cDNA 5430435G22 gene	0.31	1.24	0.018
Naip2	NLR family, apoptosis inhibitory protein 2	0.31	1.24	0.027
Hvcn1	hydrogen voltage-gated channel 1	0.31	1.24	0.029
Saa1	serum amyloid A 1	0.31	1.24	0.042
Sirpb1a	signal-regulatory protein beta 1A	0.31	1.24	0.046
1190002H23Rik	RIKEN cDNA 1190002H23 gene	0.31	1.24	0.083
Bdh2	3-hydroxybutyrate dehydrogenase, type 2	0.31	1.24	0.095

Table C.1: Transcripts upregulated in LPS+HES treated compared to LPS stimulated BMDC (continued).

Symbol	Description	log2 FC	fold change	adjusted p value
Zmiz1	zinc finger, MIZ-type containing 1	0.31	1.24	0.12
NA	NA	0.31	1.24	0.22
Actb	actin, beta	0.31	1.24	0.29
Sulf2	sulfatase 2	0.3	1.23	0.023
Phf17	PHD finger protein 17	0.3	1.23	0.042
Prkar2b	protein kinase, cAMP dependent regulatory, type II beta	0.3	1.23	0.043
Zfp532	zinc finger protein 532	0.3	1.23	0.044
Bag3	BCL2-associated athanogene 3	0.3	1.23	0.062
Pstpip1	proline-serine-threonine phosphatase-interacting protein 1	0.3	1.23	0.083
Anpep	alanyl (membrane) aminopeptidase	0.3	1.23	0.09
Tuba1a	tubulin, alpha 1A	0.3	1.23	0.16
Hvcn1	hydrogen voltage-gated channel 1	0.3	1.23	0.28
Slc7a11	solute carrier family 7 (cationic amino acid transporter, y+)	0.3	1.23	0.33
Inhba	inhibin beta-A	0.3	1.23	0.43
LOC676974	similar to Glucose-6-phosphate isomerase	0.3	1.23	0.49
Lpcat2	lysophosphatidylcholine acyltransferase 2	0.3	1.23	0.49
Areg	amphiregulin	0.29	1.22	0.041
Tubb2c	tubulin, beta 2C	0.29	1.22	0.045
Pid1	phosphotyrosine interaction domain containing 1	0.29	1.22	0.069
Ccnd1	cyclin D1	0.29	1.22	0.078
Sdcbp2	syndecan binding protein (syntenin) 2	0.29	1.22	0.078

Table C.1: Transcripts upregulated in LPS+HES treated compared to LPS stimulated BMDC (continued).

Symbol	Description	log2 FC	fold change	adjusted p value
Aldh3b1	aldehyde dehydrogenase 3 family, member B1	0.29	1.22	0.082
Srxn1	sulfiredoxin 1 homolog (S. cerevisiae)	0.29	1.22	0.13
Siva1	SIVA1, apoptosis-inducing factor	0.29	1.22	0.14
Slc6a8	solute carrier family 6 (neurotransmitter, creatine)	0.29	1.22	0.15
Nisch	nischarin	0.29	1.22	0.17
Dusp6	dual specificity phosphatase 6	0.29	1.22	0.18
Ifi30	interferon gamma inducible protein 30	0.29	1.22	0.29
Gm14446	predicted gene 14446	0.29	1.22	0.31
Gnptab	N-acetylglucosamine-1-phosphate transferase, a and b	0.29	1.22	0.35
AI314180	expressed sequence AI314180	0.28	1.21	0.032
Gpr176	G protein-coupled receptor 176	0.28	1.21	0.068
Sigmar1	sigma non-opioid intracellular receptor 1	0.28	1.21	0.14
Rassf1	Ras association (RalGDS/AF-6) domain family member 1	0.28	1.21	0.14
Tnfrsf1b	tumor necrosis factor receptor superfamily, member 1b	0.28	1.21	0.14
Txnip	thioredoxin interacting protein	0.28	1.21	0.14
Ecm1	extracellular matrix protein 1	0.28	1.21	0.16
Errfi1	ERBB receptor feedback inhibitor 1	0.28	1.21	0.18
Dcxr	dicarbonyl L-xylulose reductase	0.28	1.21	0.21
Gm5483	predicted gene 5483	0.28	1.21	0.23
Rin2	Ras and Rab interactor 2	0.28	1.21	0.25
Tnfrsf21	tumor necrosis factor receptor superfamily, member 21	0.27	1.21	0.044

Table C.1: Transcripts upregulated in LPS+HES treated compared to LPS stimulated BMDC (continued).

Symbol	Description	log2 FC	fold change	adjusted p value
Nt5e	5 nucleotidase, ecto	0.27	1.21	0.068
Havcr2	hepatitis A virus cellular receptor 2	0.27	1.21	0.096
Apbb2	amyloid beta (A4) precursor protein-binding	0.27	1.21	0.13
Rab11fip5	RAB11 family interacting protein 5 (class I)	0.27	1.21	0.15
Slc7a8	solute carrier family 7 (cationic amino acid transporter, y+)	0.27	1.21	0.15
9030425E11Rik	RIKEN cDNA 9030425E11 gene	0.27	1.21	0.26
Csf2rb	colony stimulating factor 2 receptor, beta, low-affinity (GM)	0.27	1.21	0.37
Rnpep	arginyl aminopeptidase (aminopeptidase B)	0.27	1.21	0.45
Cmtm6	CKLF-like MARVEL transmembrane domain containing 6	0.27	1.21	0.46
Selplg	selectin, platelet (p-selectin) ligand	0.27	1.21	0.5
Nisch	nischarin	0.27	1.21	0.53
P2rx4	purinergic receptor P2X, ligand-gated ion channel 4	0.27	1.21	0.55
Epb4.1l2	erythrocyte protein band 4.1-like 2	0.26	1.20	0.024
LOC100046741	similar to red-1	0.26	1.20	0.038
Agpat9	1-acylglycerol-3-phosphate O-acyltransferase 9	0.26	1.20	0.04
Adra2a	adrenergic receptor, alpha 2a	0.26	1.20	0.043
Dgkz	diacylglycerol kinase zeta	0.26	1.20	0.056
Pkp2	plakophilin 2	0.26	1.20	0.089
Tec	tec protein tyrosine kinase	0.26	1.20	0.096
Plekhg3	pleckstrin homology domain containing, family G	0.26	1.20	0.099
S1pr2	sphingosine-1-phosphate receptor 2	0.26	1.20	0.1

Table C.1: Transcripts upregulated in LPS+HES treated compared to LPS stimulated BMDC (continued).

Symbol	Description	log2 FC	fold change	adjusted p value
Slc11a1	solute carrier family 11 (proton-coupled divalent metal ion)	0.26	1.20	0.12
NA	NA	0.26	1.20	0.12
Tubb2b	tubulin, beta 2B	0.26	1.20	0.13
NA	NA	0.26	1.20	0.13
Plp2	proteolipid protein 2	0.26	1.20	0.13
Ak3	adenylate kinase 3	0.26	1.20	0.19
Adipor2	adiponectin receptor 2	0.26	1.20	0.24
Lrrfip1	leucine rich repeat (in FLII) interacting protein 1	0.26	1.20	0.3
Dnmt3l	DNA (cytosine-5-)-methyltransferase 3-like	0.26	1.20	0.31
Tmbim1	transmembrane BAX inhibitor motif containing 1	0.26	1.20	0.37
Chka	choline kinase alpha	0.26	1.20	0.41
Csf1r	colony stimulating factor 1 receptor	0.26	1.20	0.48
Cd14	CD14 antigen	0.26	1.20	0.53
Mx1	myxovirus (influenza virus) resistance 1	0.26	1.20	0.69
Esyt1	extended synaptotagmin-like protein 1	0.25	1.19	0.03
Casp6	caspase 6	0.25	1.19	0.046
Chst11	carbohydrate sulfotransferase 11	0.25	1.19	0.052
Tpcn2	two pore segment channel 2	0.25	1.19	0.068
Psd4	pleckstrin and Sec7 domain containing 4	0.25	1.19	0.078
6430527G18Rik	RIKEN cDNA 6430527G18 gene	0.25	1.19	0.082
Sepx1	selenoprotein X 1	0.25	1.19	0.083

Table C.1: Transcripts upregulated in LPS+HES treated compared to LPS stimulated BMDC (continued).

Symbol	Description	log2 FC	fold change	adjusted p value
NA	NA	0.25	1.19	0.09
Lass5	LAG1 homolog, ceramide synthase 5	0.25	1.19	0.092
Htatip2	HIV-1 tat interactive protein 2, homolog (human)	0.25	1.19	0.096
Eif4e3	eukaryotic translation initiation factor 4E member 3	0.25	1.19	0.12
Grasp	GRP1-associated scaffold protein	0.25	1.19	0.13
Aldh1a2	aldehyde dehydrogenase family 1, subfamily A2	0.25	1.19	0.13
Hmgcl	3-hydroxy-3-methylglutaryl-Coenzyme A lyase	0.25	1.19	0.14
NA	NA	0.25	1.19	0.14
Ifnar2	interferon (alpha and beta) receptor 2	0.25	1.19	0.15
Dgkz	diacylglycerol kinase zeta	0.25	1.19	0.17
Tnfsf13b	tumor necrosis factor (ligand) superfamily, member 13b	0.25	1.19	0.2
Pdzk1ip1	PDZK1 interacting protein 1	0.25	1.19	0.22
Jmjd6	jumonji domain containing 6	0.25	1.19	0.23
Lpcat3	lysophosphatidylcholine acyltransferase 3	0.25	1.19	0.28
Oasl1	2-5 oligoadenylate synthetase-like 1	0.25	1.19	0.31
NA	NA	0.25	1.19	0.31
Ccr5	chemokine (C-C motif) receptor 5	0.25	1.19	0.33
Ninj1	ninjurin 1	0.25	1.19	0.35
Tuba1b	tubulin, alpha 1B	0.25	1.19	0.4
Fbxo9	f-box protein 9	0.25	1.19	0.44
Fam102b	family with sequence similarity 102, member B	0.25	1.19	0.46

Table C.1: Transcripts upregulated in LPS+HES treated compared to LPS stimulated BMDC (continued).

Symbol	Description	log2 FC	fold change	adjusted p value
Gpi1	glucose phosphate isomerase 1	0.25	1.19	0.56
Oasl1	2-5 oligoadenylate synthetase-like 1	0.25	1.19	0.58

Table C.2: Transcripts down-regulated in LPS+HES treated compared to LPS stimulated BMDC. BMDC were differentiated with GM-CSF for ten days before stimulation with LPS and HES as indicated. At eight hours after stimulation, cells were treated with Trizol, RNA extracted and labelled for analysis on an Illumina MouseWG-6 v2.0 Expression BeadChip microarray. Statistical analysis of the data was performed by Dr. Alasdair Ivens. Listed are symbols and descriptions of the features together with their log 2 and linear fold changes and adjusted p values. Only features with a log 2 fold change of at least -0.25 (linear fold change of -1.9) are listed.

Symbol	Description	log2 FC	fold change	adjusted p value
Gm8221	apolipoprotein L, 3-like	-1.1	-2.14	0.0028
Apol7c	apolipoprotein L 7c	-0.9	-1.87	0.0017
Serpina3g	serine (or cysteine) peptidase inhibitor, clade A, 3G	-0.79	-1.73	0.0073
Edn1	endothelin 1	-0.77	-1.71	0.0069
Vnn3	vanin 3	-0.74	-1.67	0.005
Rgs1	regulator of G-protein signaling 1	-0.72	-1.65	0.021
Fabp3	fatty acid binding protein 3, muscle and heart	-0.67	-1.59	0.0092
Vnn3	vanin 3	-0.66	-1.58	0.0044
St3gal5	ST3 beta-galactoside alpha-2,3-sialyltransferase 5	-0.65	-1.57	0.0098
Aqp9	aquaporin 9	-0.64	-1.56	0.0034
Serpina3f	serine (or cysteine) peptidase inhibitor, clade A, 3F	-0.59	-1.51	0.0099
Rgs1	regulator of G-protein signaling 1	-0.59	-1.51	0.017
Rgs1	regulator of G-protein signaling 1	-0.58	-1.49	0.014
Tnf	tumor necrosis factor	-0.56	-1.47	0.075
Fam26f	family with sequence similarity 26, member F	-0.54	-1.45	0.047
Dusp2	dual specificity phosphatase 2	-0.53	-1.44	0.0044

Table C.2: Transcripts upregulated in LPS+HES treated compared to LPS stimulated BMDC (continued).

Symbol	Description	log2 FC	fold change	adjusted p value
Appl1	adaptor protein, p-Y interaction, PHD and leucine zipper	-0.53	-1.44	0.0069
Plek	pleckstrin	-0.52	-1.43	0.2
Cst7	cystatin F (leukocystatin)	-0.51	-1.42	0.012
Appl1	adaptor protein, p-Y interaction, PHD and leucine zipper	-0.5	-1.41	0.021
NA	NA	-0.47	-1.39	0.0073
Il12a	interleukin 12a	-0.46	-1.38	0.009
Tnfsf15	tumor necrosis factor (ligand) superfamily, member 15	-0.46	-1.38	0.012
Spic	Spi-C transcription factor (Spi-1/PU.1 related)	-0.46	-1.38	0.061
Cd70	CD70 antigen	-0.46	-1.38	0.086
Gpr85	G protein-coupled receptor 85	-0.45	-1.37	0.011
9030625A04Rik	RIKEN cDNA 9030625A04 gene	-0.45	-1.37	0.066
Tnf	tumor necrosis factor	-0.45	-1.37	0.094
Hmgn3	high mobility group nucleosomal binding domain 3	-0.44	-1.36	0.005
Tnfaip2	tumor necrosis factor, alpha-induced protein 2	-0.44	-1.36	0.0087
Atp2a3	ATPase, Ca++ transporting, ubiquitous	-0.44	-1.36	0.016
Fam49a	family with sequence similarity 49, member A	-0.44	-1.36	0.081
Ccrl2	chemokine (C-C motif) receptor-like 2	-0.43	-1.35	0.005
Cxcl1	chemokine (C-X-C motif) ligand 1	-0.43	-1.35	0.017
Pla1a	phospholipase A1 member A	-0.42	-1.34	0.044
NA	NA	-0.42	-1.34	0.062
Fam46a	family with sequence similarity 46, member A	-0.42	-1.34	0.18

Table C.2: Transcripts upregulated in LPS+HES treated compared to LPS stimulated BMDC (continued).

Symbol	Description	log2 FC	fold change	adjusted p value
2310014L17Rik	RIKEN cDNA 2310014L17 gene	-0.41	-1.33	0.016
Plk2	polo-like kinase 2 (Drosophila)	-0.41	-1.33	0.075
Upp1	uridine phosphorylase 1	-0.41	-1.33	0.11
Marco	macrophage receptor with collagenous structure	-0.41	-1.33	0.12
Dusp16	dual specificity phosphatase 16	-0.41	-1.33	0.16
Pkp4	plakophilin 4	-0.4	-1.32	0.052
Lmo4	LIM domain only 4	-0.4	-1.32	0.082
Atp2a3	ATPase, Ca++ transporting, ubiquitous	-0.39	-1.31	0.011
Lad1	ladinin	-0.39	-1.31	0.014
Cp	ceruloplasmin	-0.39	-1.31	0.029
Cd83	CD83 antigen	-0.39	-1.31	0.034
Pilra	paired immunoglobin-like type 2 receptor alpha	-0.39	-1.31	0.11
Hmgn3	high mobility group nucleosomal binding domain 3	-0.38	-1.30	0.0098
Lrrc33	leucine rich repeat containing 33	-0.38	-1.30	0.044
Sema7a	sema domain, Ig domain, and GPI membrane anchor, 7A	-0.38	-1.30	0.082
Hsd17b11	hydroxysteroid (17-beta) dehydrogenase 11	-0.37	-1.29	0.019
Il27	interleukin 27	-0.37	-1.29	0.095
Cd40	CD40 antigen	-0.37	-1.29	0.13
9030625A04Rik	RIKEN cDNA 9030625A04 gene	-0.37	-1.29	0.21
P2ry13	purinergic receptor P2Y, G-protein coupled 13	-0.36	-1.28	0.21
Il6	interleukin 6	-0.36	-1.28	0.32

Table C.2: Transcripts upregulated in LPS+HES treated compared to LPS stimulated BMDC (continued).

Symbol	Description	log2 FC	fold change	adjusted p value
Pvrl2	poliovirus receptor-related 2	-0.35	-1.27	0.0073
Rilpl2	Rab interacting lysosomal protein-like 2	-0.35	-1.27	0.024
Cd80	CD80 antigen	-0.35	-1.27	0.067
NA	NA	-0.35	-1.27	0.1
Upp1	uridine phosphorylase 1	-0.35	-1.27	0.14
St3gal5	ST3 beta-galactoside alpha-2,3-sialyltransferase 5	-0.34	-1.27	0.0098
Kynu	kynureninase (L-kynurenine hydrolase)	-0.34	-1.27	0.043
Slc12a6	solute carrier family 12, member 6	-0.34	-1.27	0.049
Ly9	lymphocyte antigen 9	-0.34	-1.27	0.062
Arg2	arginase type II	-0.34	-1.27	0.13
Ktelc1	KTEL (Lys-Tyr-Glu-Leu) containing 1	-0.34	-1.27	0.13
Ebi3	Epstein-Barr virus induced gene 3	-0.34	-1.27	0.17
Cxcl2	chemokine (C-X-C motif) ligand 2	-0.34	-1.27	0.28
Csrp1	cysteine and glycine-rich protein 1	-0.34	-1.27	0.48
Lta	lymphotoxin A	-0.33	-1.26	0.0099
Tlr6	toll-like receptor 6	-0.33	-1.26	0.013
BC057079	cDNA sequence BC057079	-0.33	-1.26	0.022
D16Ertd472e	DNA segment, Chr 16, ERATO Doi 472, expressed	-0.33	-1.26	0.026
Cd40	CD40 antigen	-0.33	-1.26	0.031
Fam177a	family with sequence similarity 177, member A	-0.33	-1.26	0.066
Car4	carbonic anhydrase 4	-0.33	-1.26	0.11

Table C.2: Transcripts upregulated in LPS+HES treated compared to LPS stimulated BMDC (continued).

Symbol	Description	log2 FC	fold change	adjusted p value
Cyp27a1	cytochrome P450, family 27, subfamily a, polypeptide 1	-0.33	-1.26	0.12
NA	NA	-0.33	-1.26	0.17
NA	NA	-0.32	-1.25	0.033
Nck1	non-catalytic region of tyrosine kinase adaptor protein 1	-0.32	-1.25	0.041
2310001A20Rik	RIKEN cDNA 2310001A20 gene	-0.32	-1.25	0.047
H2-M3	histocompatibility 2, M region locus 3	-0.32	-1.25	0.054
Lox	lysyl oxidase	-0.32	-1.25	0.1
Rcsd1	RCSD domain containing 1	-0.32	-1.25	0.1
Dusp16	dual specificity phosphatase 16	-0.32	-1.25	0.11
Cytip	cytohesin 1 interacting protein	-0.32	-1.25	0.29
Rpl18a	ribosomal protein L18A	-0.32	-1.25	0.69
Gpr183	G protein-coupled receptor 183	-0.31	-1.24	0.014
Il23a	interleukin 23, alpha subunit p19	-0.31	-1.24	0.023
Gbp5	guanylate binding protein 5	-0.31	-1.24	0.044
Pop5	processing of precursor 5, ribonuclease P/MRP family	-0.31	-1.24	0.066
Ppm1b	protein phosphatase 1B, magnesium dependent, beta	-0.31	-1.24	0.13
Slamf7	SLAM family member 7	-0.31	-1.24	0.14
NA	NA	-0.31	-1.24	0.14
Sbds	Shwachman-Bodian-Diamond syndrome homolog	-0.31	-1.24	0.19
Slc2a6	solute carrier family 2 (facilitated glucose transporter)	-0.31	-1.24	0.2
LOC100044376	similar to Dusp2	-0.3	-1.23	0.044

Table C.2: Transcripts upregulated in LPS+HES treated compared to LPS stimulated BMDC (continued).

Symbol	Description	log2 FC	fold change	adjusted p value
Mmp13	matrix metallopeptidase 13	-0.3	-1.23	0.073
Npm1	nucleophosmin 1	-0.3	-1.23	0.1
Swap70	SWA-70 protein	-0.3	-1.23	0.11
Ets2	E26 avian leukemia oncogene 2, 3 domain	-0.3	-1.23	0.15
Trim21	tripartite motif-containing 21	-0.3	-1.23	0.15
Agrn	agrin	-0.3	-1.23	0.23
Casp4	caspase 4, apoptosis-related cysteine peptidase	-0.3	-1.23	0.28
Batf	basic leucine zipper transcription factor, ATF-like	-0.3	-1.23	0.32
Hamp	hepcidin antimicrobial peptide	-0.3	-1.23	0.43
Il4i1	interleukin 4 induced 1	-0.3	-1.23	0.44
Stat5a	signal transducer and activator of transcription 5A	-0.3	-1.23	0.55
Tmem39a	transmembrane protein 39a	-0.29	-1.22	0.023
Gbp1	guanylate binding protein 1	-0.29	-1.22	0.028
Pde4b	phosphodiesterase 4B, cAMP specific	-0.29	-1.22	0.035
Gtpbp2	GTP binding protein 2	-0.29	-1.22	0.044
Snn	stannin	-0.29	-1.22	0.073
Nap1l1	nucleosome assembly protein 1-like 1	-0.29	-1.22	0.089
Tnfaip2	tumor necrosis factor, alpha-induced protein 2	-0.29	-1.22	0.11
Pilrb1	paired immunoglobin-like type 2 receptor beta 1	-0.29	-1.22	0.12
Irgm2	immunity-related GTPase family M member 2	-0.29	-1.22	0.19
NA	NA	-0.29	-1.22	0.29

Table C.2: Transcripts upregulated in LPS+HES treated compared to LPS stimulated BMDC (continued).

Symbol	Description	log2 FC	fold change	adjusted p value
Plagl2	pleiomorphic adenoma gene-like 2	-0.29	-1.22	0.3
Rabgef1	RAB guanine nucleotide exchange factor (GEF) 1	-0.28	-1.21	0.034
Sfxn1	sideroflexin 1	-0.28	-1.21	0.041
Lilrb4	leukocyte immunoglobulin-like receptor, subfamily B	-0.28	-1.21	0.042
Rai12	retinoic acid induced 12	-0.28	-1.21	0.046
Dusp2	dual specificity phosphatase 2	-0.28	-1.21	0.065
Mtdh	metadherin	-0.28	-1.21	0.1
Il18	interleukin 18	-0.28	-1.21	0.14
NA	NA	-0.28	-1.21	0.19
Tnfaip2	tumor necrosis factor, alpha-induced protein 2	-0.28	-1.21	0.19
Gbp3	guanylate binding protein 3	-0.28	-1.21	0.22
Wnk1	WNK lysine deficient protein kinase 1	-0.28	-1.21	0.27
Vav3	vav 3 oncogene	-0.28	-1.21	0.31
Map3k8	mitogen-activated protein kinase kinase kinase 8	-0.28	-1.21	0.35
Gp49a	glycoprotein 49 A	-0.28	-1.21	0.45
Tlr1	toll-like receptor 1	-0.27	-1.21	0.033
Mtdh	metadherin	-0.27	-1.21	0.12
BC006779	cDNA sequence BC006779	-0.27	-1.21	0.19
E130102H24Rik	RIKEN cDNA E130102H24 gene	-0.27	-1.21	0.2
Tnfsf9	tumor necrosis factor (ligand) superfamily, member 9	-0.27	-1.21	0.24
Ddhd1	DDHD domain containing 1	-0.27	-1.21	0.25

Table C.2: Transcripts upregulated in LPS+HES treated compared to LPS stimulated BMDC (continued).

Symbol	Description	log2 FC	fold change	adjusted p value
Hbp1	high mobility group box transcription factor 1	-0.27	-1.21	0.25
Ctsk	cathepsin K	-0.27	-1.21	0.27
Ccl3	chemokine (C-C motif) ligand 3	-0.27	-1.21	0.29
Cish	cytokine inducible SH2-containing protein	-0.27	-1.21	0.38
LOC100046953	similar to Rab6 interacting protein 1	-0.27	-1.21	0.4
Suz12	suppressor of zeste 12 homolog (Drosophila)	-0.27	-1.21	0.41
Klf7	Kruppel-like factor 7 (ubiquitous)	-0.26	-1.20	0.024
Sfxn1	sideroflexin 1	-0.26	-1.20	0.029
Rab33a	RAB33A, member of RAS oncogene family	-0.26	-1.20	0.052
Hbb-b1	hemoglobin, beta adult major chain	-0.26	-1.20	0.052
Rap2a	RAS related protein 2a	-0.26	-1.20	0.068
Nod1	nucleotide-binding oligomerization domain containing 1	-0.26	-1.20	0.082
Stard7	START domain containing 7	-0.26	-1.20	0.099
N4bp2l1	NEDD4 binding protein 2-like 1	-0.26	-1.20	0.12
Gbp3	guanylate binding protein 3	-0.26	-1.20	0.13
LOC100048721	similar fibronectin leucine rich transmembr. protein 3	-0.26	-1.20	0.14
Irak2	interleukin-1 receptor-associated kinase 2	-0.26	-1.20	0.16
Alcam	activated leukocyte cell adhesion molecule	-0.26	-1.20	0.19
Trps1	trichorhinophalangeal syndrome I (human)	-0.26	-1.20	0.19
Igsf9	immunoglobulin superfamily, member 9	-0.26	-1.20	0.23
Sort1	sortilin 1	-0.26	-1.20	0.34

Table C.2: Transcripts upregulated in LPS+HES treated compared to LPS stimulated BMDC (continued).

Symbol	Description	log2 FC	fold change	adjusted p value
Fscn1	fascin homolog 1, actin bundling protein	-0.26	-1.20	0.44
Mtmr14	myotubularin related protein 14	-0.25	-1.19	0.028
Glipr1	GLI pathogenesis-related 1 (glioma)	-0.25	-1.19	0.034
1110018G07Rik	RIKEN cDNA 1110018G07 gene	-0.25	-1.19	0.063
Hbb-b1	hemoglobin, beta adult major chain	-0.25	-1.19	0.083
Pvrl2	poliovirus receptor-related 2	-0.25	-1.19	0.12
Atp6v1d	ATPase, H+ transporting, lysosomal V1 subunit D	-0.25	-1.19	0.12
Hbp1	high mobility group box transcription factor 1	-0.25	-1.19	0.16
Pgap2	post-GPI attachment to proteins 2	-0.25	-1.19	0.23
Srgn	serglycin	-0.25	-1.19	0.38
Rps4x	ribosomal protein S4, X-linked	-0.25	-1.19	0.38
Rdh11	retinol dehydrogenase 11	-0.25	-1.19	0.39
1500012F01Rik	RIKEN cDNA 1500012F01 gene	-0.25	-1.19	0.41
Cd52	CD52 antigen	-0.25	-1.19	0.44
Irgm1	immunity-related GTPase family M member 1	-0.25	-1.19	0.51
Chi3l3	chitinase 3-like 3	-0.25	-1.19	0.52
Pla1a	phospholipase A1 member A	-0.25	-1.19	0.58
NA	NA	-0.25	-1.19	0.69